

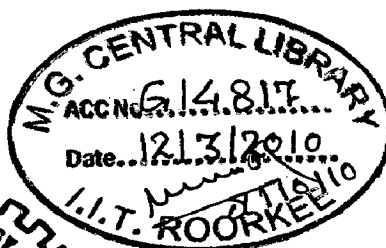
# CHARACTERIZATION AND HOT CORROSION STUDIES OF DETONATION-GUN SPRAYED COATINGS

## A THESIS

*Submitted in partial fulfilment of the  
requirements for the award of the degree  
of*  
**DOCTOR OF PHILOSOPHY**  
*in*  
**METALLURGICAL AND MATERIALS ENGINEERING**

*by*

**SUBHASH KAMAL**



**DEPARTMENT OF METALLURGICAL AND MATERIALS ENGINEERING  
INDIAN INSTITUTE OF TECHNOLOGY ROORKEE  
ROORKEE - 247 667 (INDIA)  
MARCH, 2009**

©INDIAN INSTITUTE OF TECHNOLOGY ROORKEE, ROORKEE, 2009  
ALL RIGHTS RESERVED





# INDIAN INSTITUTE OF TECHNOLOGY ROORKEE


## CANDIDATE'S DECLARATION


I hereby certify that the work which is being presented in the thesis entitled **Characterization and Hot Corrosion Studies of Detonation-Gun Sprayed Coatings** in partial fulfilment of the requirement for the award of the Degree of Doctor of Philosophy and submitted in the Department of Metallurgical and Materials Engineering of the Indian Institute of Technology Roorkee, Roorkee is an authentic record of my own work carried out during a period from August, 2005 to March, 2009 under the supervision of Dr. R. Jayaganthan, Assistant Professor and Dr. Satya Prakash, Professor, Department of Metallurgical and Materials Engineering, Indian Institute of Technology Roorkee, Roorkee.

The matter presented in this thesis has not been submitted by me for the award of any other degree of this or any other Institute.

  
(SUBHASH KAMAL)

This is to certify that the above statement made by the candidate is correct to the best of our knowledge.

  
(Satya Prakash)  
Supervisor

  
(R. Jayaganthan)  
Supervisor

Date:- 03.03.09

The Ph.D. Viva-Voice examination of **Mr. Subhash Kamal**, Research Scholar, has been held on

Signature of Supervisors

Signature of External Examiner

## ABSTRACT

---

High temperature oxidation and hot corrosion represent the most deleterious forms of surface degradation, which can lead to the loss of mechanical strength and catastrophic failure of structural and engineering components. They are routinely encountered in superalloys used in land based turbine and aero engines, which operate in high temperature and corrosive environments. Due to extensive application of the superalloys in land-based and aero gas turbine engines, the high temperature oxidation and hot corrosion behaviour of superalloys has been the subject of intense investigation for the past several years. Most of the studies have focused on the mechanism of oxidation and hot corrosion such as oxide scale growth behaviour of materials based on short-term tests. An understanding of long term high temperature oxidation and hot corrosion behaviour of coatings on superalloys is extremely important for the industrial applications. Hot corrosion may be defined as an accelerated corrosion, resulting from the presence of salt contaminants such as  $\text{Na}_2\text{SO}_4$ ,  $\text{K}_2\text{SO}_4$ ,  $\text{NaCl}$ , and  $\text{V}_2\text{O}_5$  that combine to form molten deposits, which damage the protective surface oxides. Hot corrosion occurs when metals are heated in the temperature range 700–900°C in the presence of sulphate deposits formed as a result of the reaction between sodium chloride and sulphur compounds in the gas phase surrounding the metals. At higher temperatures, deposits of  $\text{Na}_2\text{SO}_4$  are molten (m.p. 884°C) and can cause accelerated attack on Ni-, Fe- and Co-based superalloys. This type of attack is commonly called hot corrosion. For example, alloy components in gas turbines in aircraft, thermal power plants, land-based power generators, boilers, internal combustion engines, gas turbines, fluidized bed combustion and industrial waste incinerators undergo hot corrosion. It is a life-limiting form of accelerated environmental attack that can occur on vanes and blades in the hot sections of gas turbine engines. Gurrappa reported that directionally solidified superalloys are highly susceptible to hot corrosion and the life is hardly 4 hours in a 90%  $\text{Na}_2\text{SO}_4$  +10%  $\text{NaCl}$  environment and less than 2 hours in a vanadium containing environment (90%  $\text{Na}_2\text{SO}_4$  + 5%  $\text{NaCl}$  + 5%  $\text{V}_2\text{O}_5$ ) at 900 °C. During hot corrosion, a porous non-protective oxide scale is formed at the surface and sulphides in the substrate. This form of corrosion, unlike oxidation, can consume the material at an unpredictably rapid rate. Consequently, the load-carrying ability of the components reduces quickly, leading eventually to catastrophic failure. It is due to the

following reasons; for example, superalloys used for high temperature applications could not meet the requirements of both the high-temperature strength and the high-temperature erosion-corrosion resistance simultaneously. Therefore, thermal spray coatings deposited on superalloys made a significant contribution for combating high temperature oxidation and hot corrosion.

Use of inhibitors like MgO, CeO<sub>2</sub>, CaO and MnO<sub>2</sub> applied superficially have already been investigated (Gitanjaly, 2003; Gitanjaly et al., 2002) on the superalloys exposed to most aggressive environment of Na<sub>2</sub>SO<sub>4</sub>-60% V<sub>2</sub>O<sub>5</sub> at 900 °C and found the substantial reduction of damage due to hot corrosion. However, the major limitation is due to the application of these inhibitors to the hot metal surface. Hence, the viable countermeasure against the oxidation and hot corrosion constitute the use of protective coatings. The high temperature oxidation and hot corrosion of HVOF and plasma sprayed coatings on superalloys and on boiler tube steels have been investigated and the improved oxidation resistance of superalloys has been observed as reported in the literature (Prakash et al. 2005; Singh et al 2007, 2005C, 2005D; Sidhu and Prakash 2003,2005; Sidhu et al., 2006A, 2006B, 2006G, 2006H).

The oxidation and hot corrosion studies of Cr<sub>3</sub>C<sub>2</sub>-NiCr, NiCrAlY+0.4wt%CeO<sub>2</sub> and NiCoCrAlYTa coatings developed by D-gun spray is scarce in the literature. In view of that, in the present study, oxidation and hot corrosion behaviour of some superalloys designated as superni 75, superni 718 and superfer 800H as per the manufacturer's specifications, has been investigated with and without the application of D-gun sprayed Cr<sub>3</sub>C<sub>2</sub>-NiCr, NiCrAlY+0.4 wt% CeO<sub>2</sub> and NiCoCrAlYTa coatings in air, Na<sub>2</sub>SO<sub>4</sub>-60%V<sub>2</sub>O<sub>5</sub>, Na<sub>2</sub>SO<sub>4</sub>-25%K<sub>2</sub>SO<sub>4</sub>, at 900 °C, and in actual coal fired boiler environment under cyclic conditions. These superalloys are developed by Mishra Dhatu Nigam Limited, Hyderabad (India) for the high temperature applications such as boilers and gas turbine parts, heat exchangers and piping in chemical industries, jet engines, pump bodies, high temperature furnace parts and heat treatment jigs.

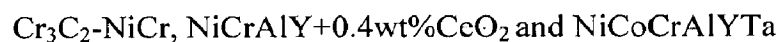
A study on the behaviour of aforementioned coatings in different environment will be helpful in choosing the suitable coating and substrate to withstand against oxidation and hot corrosion problems manifested in the gas turbine and boiler applications. The outcome of the present research work are critically analyzed and discussed in the light of existing literature to propose an insight in to the corrosion mechanism in both coated and bare superalloys. The whole thesis is presented in 9 chapters.

**Chapter 1** contains a brief introduction as to oxidation and hot corrosion effects and its deleterious impact on the various engineering equipments and components. The remedial measures to obviate this problem are also briefly discussed.

**Chapter 2** contains oxidation and hot corrosion studies reported by various researchers relevant to the current study. It has been critically reviewed particularly those conducted on similar Ni- and Fe-based alloys in air and molten salt environments. The various preventive measures have been summarised along with the description of D-gun spray process. The problem has been formulated based on the available literature on oxidation and hot corrosion behaviour of coated and bare superalloys used in high temperature applications.

**Chapter 3** presents the experimental techniques and procedures employed for applying the coating and their characterisation, oxidation studies in air, molten salt environments and in actual coal fired boiler environment. The specification of the equipments and other instruments used for the present investigation and the techniques used to analyse the corrosion products are discussed below.

The D-gun sprayed coatings were deposited at SVX Powder M Surface Engineering Pvt. Ltd, New Delhi (India) on Ni- and Fe- based superalloys. These superalloys were procured from Mishra Dhatu Nigam Ltd., Hyderabad (India). In the present work three types of coatings were formulated as given below.



The as-sprayed coatings were characterised by metallography, FE-SEM/EDS, X-ray mapping analysis, mechanical properties such as microhardness of the coatings have been evaluated. Surface roughness and porosity of the as-sprayed coatings were also measured.

The oxidation and hot corrosion behaviour of bare and D-gun coated superalloys have been studied in the air, two molten salts ( $\text{Na}_2\text{SO}_4\text{-60\%V}_2\text{O}_5$  and  $\text{Na}_2\text{SO}_4\text{-25\%K}_2\text{SO}_4$ ) in the laboratory furnace and actual coal fired boiler environments for 100 cycles under cyclic conditions. Each cycle consisted of 1 hour heating at 900 °C in a silicon carbide tube furnace followed by 20 minutes cooling at room temperature (25 °C), these studies were performed for uncoated as well as coated specimens for comparison. Whereas, in case of actual coal fired boiler environment, the specimens were exposed to the combustion environment for 10 cycles. Each cycle

consisted of 100 hours heating followed by 1 hour cooling at ambient conditions. At the end of each cycle, the specimens were critically examined regarding the colour, luster, physical changes on the samples, scale adherence/spallation and then subjected to weight change measurements. The molten salt studies were performed by applying a uniform layer ( $3\text{-}5\text{mg/cm}^2$ ) of the mixture of  $\text{Na}_2\text{SO}_4\text{-}60\%\text{V}_2\text{O}_5$  and  $\text{Na}_2\text{SO}_4\text{-}25\%\text{K}_2\text{SO}_4$  on the preheated specimens ( $250\text{ }^\circ\text{C}$ ) with the help of camel hair brush. XRD and FE-SEM/EDS analytical techniques were used to identify the phases and the elemental analysis of the surface scale, respectively. The coated samples were then cut across the cross-section for analyzing its elemental composition by X-ray mapping analysis.

**Chapter 4** deals with the detailed investigation of bare and D-sprayed  $\text{Cr}_3\text{C}_2\text{-NiCr}$  coating on Ni- and Fe-based superalloys, which include characterisation, oxidation and hot corrosion studies in air and in two molten salt ( $\text{Na}_2\text{SO}_4\text{-}60\%\text{V}_2\text{O}_5$  and  $\text{Na}_2\text{SO}_4\text{-}25\%\text{K}_2\text{SO}_4$ ) environments in the laboratory under cyclic condition at  $900\text{ }^\circ\text{C}$  for 100 cycles. The techniques such as XRD, FE-SEM/EDS and X-ray mapping were used to analyse the as-sprayed coating and the corroded specimens.

A good adhesion of the coatings to the substrate was evident from the absence of cracks and gaps at the interfaces as well as due to the uniform distribution of carbide particles along metallic binders with the porosity value around 0.69%. The microhardness of the  $\text{Cr}_3\text{C}_2\text{-}25\%\text{NiCr}$  coatings was found to be in the range of 775 –1200Hv due to high volume fraction of carbides, dispersed uniformly in the matrix. Coating thickness ranges from 221-246 $\mu\text{m}$ , where as surface roughness varies from 4.92-6.05 $\mu\text{m}$  as observed in the present work.

The D-gun sprayed  $\text{Cr}_3\text{C}_2\text{-NiCr}$  coatings on three different superalloys when subjected to cyclic oxidation in air at  $900\text{ }^\circ\text{C}$  for 100 cycles were found to be successful in maintaining its adherence with the substrate superalloys. The oxide scales were also found to be intact and there is no indication of any spalling in all the cases. A saving in overall cumulative weight gain for  $\text{Cr}_3\text{C}_2\text{-NiCr}$  coated superni 75, superni 718 and superfer 800H with respect to the bare alloys tend to be of the order of 37.3%, 26.3% and 19.6% respectively. The  $\text{Cr}_3\text{C}_2\text{-NiCr}$  coating after exposure to air oxidation showed the presence of mainly oxides of Cr in the upper region of the scale. In the subscale region, the phases revealed were oxides of Cr and Ni, and their spinels, below the subscale region, Ni-rich splats remained un-oxidised and provided protection to the superalloys against high temperature oxidation.

Hot corrosion behaviour of  $\text{Cr}_3\text{C}_2\text{-NiCr}$  coating in two different molten salt environments shows that the  $\text{Na}_2\text{SO}_4\text{-60\%V}_2\text{O}_5$  is more aggressive than the  $\text{Na}_2\text{SO}_4\text{-25\%K}_2\text{SO}_4$ . Among three superalloys, bare and coated superalloy superfer 800H have shown lower and higher resistance to hot corrosion in  $\text{Na}_2\text{SO}_4\text{-60\%V}_2\text{O}_5$  molten salt environment, respectively. The better protection of  $\text{Cr}_3\text{C}_2\text{-NiCr}$  coated superfer 800H might be attributed to the formation of dense, massive and continuous oxide scale mainly consisting of Cr in the upper most part of the scale with NiO layer in the subscale region where Cr is depleted. Where as in case of  $\text{Na}_2\text{SO}_4\text{-25\%K}_2\text{SO}_4$  molten salt environment, bare and  $\text{Cr}_3\text{C}_2\text{-NiCr}$  coated superfer 718 exhibit least and highest protections, respectively. The superior corrosion resistance of coated alloy might be ascribed to the formation of oxides of Cr, Ni and their spinel, further the scale was dense, compact and without any spallation/sputtering or peeling tendency.

**Chapter 5** contains the investigation as to characterisation, oxidation, and hot corrosion of bare and D-gun sprayed  $\text{NiCrAlY+0.4wt\%CeO}_2$  coating on Ni- and Fe-based superalloys in the laboratory under cyclic condition at  $900^\circ\text{C}$  for 100 cycles. The techniques such as XRD, FE-SEM/EDS and X-ray mapping were used to analyse the as-sprayed coating and the corroded specimens. The morphology, porosity, microhardness, roughness, and thickness of as-sprayed coating were characterized. The surface morphology depicts the formation of un-melted particles in the form of globular dendritic structure. The microhardness of the coating is found to be in the range of 697-920  $\text{H}_\text{V}$  and the average porosity is less than 0.58%. The thickness of coating ranges from 200-250  $\mu\text{m}$  and it showed a good adhesion with the substrate. The surface roughness of the coating is found to be in the range of 6.17-6.94  $\mu\text{m}$ , respectively.

Oxidation kinetic was established at  $900^\circ\text{C}$  for 100 cycles under cyclic conditions. The D-gun sprayed  $\text{NiCrAlY + 0.4 wt\% CeO}_2$  coating on superfer 800H has provided a maximum oxidation resistance. The presence of Si,  $\text{NiCr}_2\text{O}_4$ , NiO,  $\alpha\text{-Al}_2\text{O}_3$  and respective spinels might have contributed for better oxidation resistance. Further, a thick band of chromium along the coating - substrate interface, where all other elements were depleted, might have acted as a diffusion barrier to the oxygen to enter in to the substrate.

Hot corrosion kinetics was also studied on two different molten salt environments namely of  $\text{Na}_2\text{SO}_4\text{-60\%V}_2\text{O}_5$  and  $\text{Na}_2\text{SO}_4\text{-25\%K}_2\text{SO}_4$ . The bare and D-gun sprayed  $\text{NiCrAlY + 0.4 wt\% CeO}_2$  coating on superfer 800H depicts least and maximum hot corrosion resistance in both the

molten salt environments, respectively. The better hot corrosion resistance of coating might be attributed to the formation of dense oxide scale with phases like NiO, Cr<sub>2</sub>O<sub>3</sub>, Al<sub>2</sub>O<sub>3</sub>, NiCr<sub>2</sub>O<sub>4</sub> and NiAl<sub>2</sub>O<sub>4</sub>. Further, oxides along the splat boundaries and within open pores of the coating might have acted as diffusion barrier to the inward diffusion of molten salt, also a thin continuous streaks of iron and silicon oxides on the top surface of hot corroded coating contributed to enhance the hot corrosion resistance. A co-existence of cerium oxide and vanadium along the cross-section shows the possible formation of cerium vanadates (CeVO<sub>4</sub>), which might have further contributed to the better hot corrosion resistance of NiCrAlY + 0.4 wt% CeO<sub>2</sub> coated superfer 800H (Fig.5.29).

**Chapter 6** describes the detailed investigation of D-gun sprayed NiCoCrAlYTa coatings on Ni- and Fe-based superalloys. The characterisation of D-gun sprayed NiCoCrAlYTa coatings has been discussed in detail. Oxidation studies in air at 900 °C under cyclic conditions and hot corrosion studies in two different molten salt environments at 900 °C under cycle conditions are discussed. The techniques such as XRD, FE-SEM/EDS and X-ray mapping are used to analyse the corrosion product of oxidation and hot corrosion.

D-gun sprayed NiCoCrAlYTa coating exhibits dense and adherent microstructure. The thin contrast stringers which appeared in the microstructure are presumably the oxides that are believed to be formed due to the oxidation of in-flight particles. Micrograph depicts the presence of porosity; oxide stringers (Al<sub>2</sub>O<sub>3</sub>), un-melted and semi-melted particles and oxide inclusions. The average thickness of the coatings on three superalloys were found to be in the range of 200-250µm. The porosity of the coating is less than 0.48 %. Roughness was found to be in the range of 6.25- 7.48(Ra) µm, where as microhardness of the substrates is found to be in the range of 290-395 Hv and it is 385-748Hv along the cross section of the coatings.

Oxidation kinetics was established at 900 °C for 100 cycles under cyclic conditions by weight gain data. D-gun sprayed NiCoCrAlYTa coated superni 75 showed the lowest weight gain. The better protection against oxidation shown by the NiCoCrAlYTa-coated superni 75 might be ascribed to the formation of oxide of Al, Co, Cr, Ni, thereby suggesting the formation of spinel.

The coated superalloys after exposed to molten salt environments at 900 °C for 100 cycles under cyclic conditions show that the Na<sub>2</sub>SO<sub>4</sub>-60%V<sub>2</sub>O<sub>5</sub> is found to be more aggressive than the Na<sub>2</sub>SO<sub>4</sub>-25%K<sub>2</sub>SO<sub>4</sub>. It may be attributed to the penetration of oxygen little deeper in to

the coating forming thick oxide scale, further Si and Fe has diffused upwards and reached top surface of coating. There is micro-spallation of coating along the corners and edges in the coating. Where as in case of  $\text{Na}_2\text{SO}_4$ -25% $\text{K}_2\text{SO}_4$  coating across the cross-section got partially oxidised thereby restricting penetration of corrosive species. NiCoCrAlYTa coating provided maximum hot corrosion resistance to superfer 800H by reducing weight gain by 37% and 41% in  $\text{Na}_2\text{SO}_4$ -60% $\text{V}_2\text{O}_5$  and  $\text{Na}_2\text{SO}_4$ -25% $\text{K}_2\text{SO}_4$  molten salt environments, respectively, in comparison with bare superfer 800H.

**Chapter 7** deals with the study of bare and D-gun sprayed  $\text{Cr}_3\text{C}_2$ -NiCr, NiCrAlY +0.4 wt % $\text{CeO}_2$  and NiCoCrAlYTa coatings on Fe-based superalloy superfer 800H. In order to establish an understanding of the behaviour of these coatings and bare superalloy in the actual coal fired boiler environments, where these coatings are intended to be used, the specimens were exposed for 1000 hours to platen super-heater zone of coal fired boiler at Guru Nanak Dev Thermal Power Plant, Bathinda, Punjab. This zone was selected for the present study as many break downs occurred in this power plant due to the hot corrosion degradation of the platen super-heater tubes of coal fired boilers. The samples were hanged in this zone, having temperature  $900 \pm 10$  °C, with the help of stainless steel wires for 10 cycles, each cycle consisting of 1000 hours of heating followed by 1 hour of cooling in open air. At the end of each cycle, the specimens were visually examined with respect to colour, luster, spallation tendency and adherence of the scale. Thereafter, the specimens were subjected to weight change measurements but it could not be of much use for predicting hot corrosion, as there is suspected spallation and ash deposition on the samples. The hot corroded superalloys with respect to different phases and their distribution were analysed by using XRD, FE-SEM/EDS and X-ray mapping.

**Chapter 8** describes the comparative results of all the bare and D-gun coated superalloys in air, molten salt environments ( $\text{Na}_2\text{SO}_4$ -60% $\text{V}_2\text{O}_5$  and  $\text{Na}_2\text{SO}_4$ -25% $\text{K}_2\text{SO}_4$ ) and in actual coal fired boiler environment at 900 °C under cyclic conditions.

**Chapter 9** includes conclusions of the present investigation and scope for the future work.



## ACKNOWLEDGEMENTS

---

The author has great privilege and pride to express his immense sense of gratitude to **Dr. R. Jayaganthan**, Asst. Professor and **Dr. Satya Prakash**, Professor, Department of Metallurgical and Materials Engineering (MMED), Indian Institute of Technology, Roorkee for his valuable and intellectual guidance throughout the tenure of this work. They have been a motivating and driving force where targets appeared to be tough during the course of work. Without their timely help, constructive criticism, positive attitude and painstaking efforts, it would have been impossible to complete this thesis in the present form.

Deep sense of gratitude is acknowledged to Sanjay Kumar S.V.X Powder M. Surface Engineering Pvt. Ltd. New Delhi (India) for having provided a detonation-gun coating facility time to time as per the requirement of research work.

Author is highly indebted to Dr. S. K. Nath, Head, M.M.E.D for his co-operation in extending the necessary facilities and supports during the concluding phase of this work. Author wishes to record his deep sense of gratitude to Dr. Ramesh Chandra, Institute Instrumentation Centre (IIC), and Indian Institute of Technology Roorkee for extending FE-SEM/EDS facilities during the experimental and analysis work.

Author is highly obliged and wishes to owe his sincere thanks to the technical and administrative staff of the MMED, especially to Mr. Rajinder S. Sharma, Mr. Shamsheer Singh, Mr. N. K. Seth, Mr. Vidya Prakash, Mr. T. K. Sharma, Mr. R. K. Sharma, Mr. H. K. Ahuja, Mr. Shakti Gupta, Mr. Dhan Prakash, Mr. M. Pandey, Mr. B. Sharma, Mr. Jasbir Singh, Mr. V. P. Verma and Mr. M. Aslam, who helped him in all possible ways during the experimental work.

Author expresses his sincere thanks to Mr. K. Ramesh (GM) Marketing, Mr. Sridhar, Mr. I. S. N. Murthy, Mishra Dhatu Nigam Ltd. Hyderabad, INDIA, for providing the superalloys for the research work.

Author owes his sincere thanks to Vikas Chawla, Research Scholar, MMED, Er. Suresh Garg, Er. R. N. Sharma and Er. A. P. Singh for their extended help and support to carry out the experimentation work at GNDTP Bathinda, Punjab. Special thanks are due to Mr. Gurcharan Singh foreman GNDTP Bathinda for his kind co-operation and help during experimentation work.

Author wishes to thank his friends and colleagues for their moral support and camaraderie help to keep things in perspective. Thanks are due to Mr. S. K. Panigrahi, Dr. Mahesh R.A, Mr. Vipin and Amit Chawla, Dr. Harpreet singh, Dr. Buta Singh, Dr. T. S. Sidhu, Dr. D. Shivaligappa, Dr. Chennupati Vijay Kumar, Mr. D. I. Lalwani, Mr. Karunanidhi, Mr. Devakumar, Mr. Jayprakash Chadchan, Mr. H. M. Nanjunda, Mr. Shankar Murthy, Dr. Arivazaghan and Mr. Dinesh Pawar Mr. Shivanand Nayak and S. Ghanaraja. Special thanks to Mr. Adesh Sharma and my student Omkar Bembalge for their everlasting support in thesis type setting corrections.

Author is highly grateful to his wife Anita S. Kamal who co-operated her best for the duration of Ph.D work. Author would like to express his reverence and great admiration to his parents, who have always been the guiding and encouraging force for him.

**(SUBHASH KAMAL)**

# CONTENTS

---

	Page No.
<i>Abstract</i>	i
<i>Acknowledgements</i>	viii
<i>List of Figures</i>	xvii
<i>List of Tables</i>	xxxiii
<i>Research Papers Presented/Published</i>	xxxv
<i>Abbreviations</i>	xxxviii
<b>CHAPTER 1 INTRODUCTION</b>	<b>1</b>
<b>CHAPTER 2 LITERATURE REVIEW</b>	<b>5</b>
<b>2.1 HIGH TEMPERATURE OXIDATION</b>	<b>5</b>
<b>2.1.1 Fundamentals of oxidation</b>	<b>5</b>
<b>2.1.2 Formation of protective scales</b>	<b>7</b>
<b>2.1.3 Breakdown of protective scales</b>	<b>10</b>
<b>2.2 OXIDATION OF SUPERALLOYS</b>	<b>11</b>
<b>2.2.1 Oxidation of Nickel and Nickel-Based Alloys</b>	<b>14</b>
<b>2.2.2 Oxidation of Iron and Iron-Based Alloys</b>	<b>17</b>
<b>2.3 HOT CORROSION</b>	<b>19</b>
<b>2.3.1 Characteristics of hot corrosion</b>	<b>20</b>
<b>2.3.1.1 High Temperature Hot Corrosion (HTHC) Type I</b>	<b>22</b>
<b>2.3.1.2 Low Temperature Hot Corrosion (LTHC)-Type II</b>	<b>22</b>
<b>2.3.2 Degradation of the Superalloys</b>	<b>23</b>
<b>2.3.2.1 The Initiation Stage</b>	<b>23</b>

2.3.2.2	<i>The Propagation Stage</i>	23
2.3.3	<b>Mechanisms of Hot Corrosion</b>	25
2.3.4	<b>Chemistry of salts</b>	28
2.3.4.1	<i>Sulphate Chemistry</i>	28
2.3.4.2	<i>Vanadate Chemistry</i>	28
2.3.4.3	<i>Chemistry of Salts in the Combustion of Coal/Fuel Oils</i>	31
<b>2.4</b>	<b>HOT CORROSION IN THE MOLTEN SALT ENVIRONMENTS</b>	31
2.4.1	<b>Molten salt (Na<sub>2</sub>SO<sub>4</sub> - 60%V<sub>2</sub>O<sub>5</sub>) Environment-I</b>	31
2.4.2	<b>Molten salt (Na<sub>2</sub>SO<sub>4</sub> - 25%K<sub>2</sub>SO<sub>4</sub>) Environment-II</b>	34
2.4.3	<b>Hot Corrosion of the Nickel and Nickel-Based Alloys</b>	36
2.4.4	<b>Hot Corrosion of the Iron and Iron-Based Alloys</b>	42
<b>2.5</b>	<b>SOME STUDIES ON POWER PLANT ENVIRONMENTS</b>	46
<b>2.6</b>	<b>PREVENTIVE MEASURES AGAINST HOT CORROSION</b>	51
<b>2.7</b>	<b>ROLE OF COATINGS</b>	52
2.7.1	<b>Advantages of Coatings</b>	53
2.7.2	<b>Requirement of High Temperature Coatings</b>	54
2.7.3	<b>Coating-Substrate Requirements</b>	55
2.7.4	<b>Coating Deposition Techniques</b>	56
2.7.4.1	<i>Thermal Spray Techniques</i>	56
<b>2.8</b>	<b>DETONATION GUN COATING</b>	63
2.8.1	<b>Working principal of D-Gun coating</b>	64
2.8.2	<b>D-gun Coating characteristics</b>	65
2.8.3	<b>Advantages of the D-gun coating System</b>	65
<b>2.9</b>	<b>PROBLEM FORMULATION</b>	68
2.9.1	<b>Scope</b>	68
2.9.2	<b>Objectives</b>	71

<b>CHAPTER 3</b>	<b>EXPERIMENTAL TECHNIQUES AND PROCEDURES</b>	73
3.1	<b>SUBSTRATE MATERIALS</b>	73
3.2	<b>DEVELOPMENT OF COATINGS by D-Gun PROCESS</b>	73
	3.2.1 Preparation of Substrate Materials	73
	3.2.2 Feedstock Materials For The Coatings	73
	3.2.3 Formulation of Coatings	75
3.3	<b>CHARACTERISATION OF THE COATINGS</b>	76
	3.3.1 Specimen preparation	76
	3.3.2 Measurement of Coating Thickness	77
	3.3.3 Measurement of Porosity	77
	3.3.4 Metallographic Studies	77
	3.3.5 Measurement of Microhardness	78
	3.3.6 Measurement of Surface Roughness	78
	3.3.7 X-Ray Diffraction (XRD) Analysis	78
	3.3.8 Field Emission-Scanning Electron Microscopy (FE-SEM) and Energy Dispersive X-ray Spectrometry (EDS) Analysis	79
	3.3.8.1 Surface Morphology/EDS Analysis	79
	3.3.8.2 Cross sectional analysis	79
	3.3.9 X-ray mapping analysis	79
3.4	<b>HIGH TEMPERATURE OXIDATION AND HOT CORROSION STUDIES</b>	80
	3.4.1 Experimental Setup	80
	3.4.2 Oxidation Studies in Air	81
	3.4.3 Hot Corrosion Studies in Molten Salts	81
	i) ( $\text{Na}_2\text{SO}_4 - 60\%\text{V}_2\text{O}_5$ )	
	ii) ( $\text{Na}_2\text{SO}_4 - 25\%\text{K}_2\text{SO}_4$ )	
	3.4.3.1 Coating of Molten Salts	81
	3.4.3.2 Hot Corrosion Studies	81

3.4.4	Studies in coal fired Industrial boiler Environment	81
3.5	<b>ANALYSIS OF CORROSION PRODUCTS OF OXIDATION IN AIR AND MOLTEN SALTS</b>	82
3.5.1	Visual Observation	83
3.5.2	Weight change Studies	84
3.5.3	X-ray diffraction (XRD) Analysis	85
3.5.4	<b>FE-SEM/EDS Analysis</b>	85
3.5.4.1	<i>Surface Morphology</i>	85
3.5.4.2	<i>Cross-Sectional analysis</i>	85
<b>CHAPTER 4</b>	<b>Cr<sub>3</sub>C<sub>2</sub>-NiCr COATING</b>	86
4.1	<b>MICROSTRUCTURES OF THE SUBSTRATE SUPERALLOYS</b>	86
4.2	<b>CHARACTERISATION OF THE COATING</b>	87
4.2.1	Introduction	87
4.2.2	Experimental Details	88
4.2.3	Results	89
4.2.4	Discussion	96
4.2.5	Conclusions	102
4.3	<b>OXIDATION STUDIES IN AIR</b>	103
4.3.1	Introduction	103
4.3.2	Experimental Details	104
4.3.3	Results	104
4.3.4	Discussion	113
4.3.5	Conclusions	121
4.4	<b>HOT CORROSION STUDIES</b>	122
4.4.1	<b>Na<sub>2</sub>SO<sub>4</sub>-60% V<sub>2</sub>O<sub>5</sub> Molten Salt Environment-I</b>	122
4.4.1.1	Introduction	122
4.4.1.2	Experimental Details	123

4.4.1.3	Results	123
4.4.1.4	Discussion	134
4.4.1.5	Conclusions	141
4.4.2	<b>Na<sub>2</sub>SO<sub>4</sub>-25%K<sub>2</sub>SO<sub>4</sub> Molten Salt Environment-II</b>	142
4.4.2.1	Introduction	142
4.4.2.2	Experimental Details	142
4.4.2.3	Results	142
4.4.2.4	Discussion	152
4.4.2.5	Conclusion	159
<b>CHAPTER 5</b>	<b>NiCrAlY+0.4wt%CeO<sub>2</sub> COATING</b>	160
<b>5.1</b>	<b>CHARACTERISATION OF THE COATING</b>	160
5.1.1	Introduction	160
5.1.2	Experimental Details	162
5.1.3	Results	162
5.1.4	Discussion	168
5.1.5	Conclusions	174
<b>5.2</b>	<b>OXIDATION STUDIES IN AIR</b>	175
5.2.1	Introduction	175
5.2.2	Experimental details	176
5.2.3	Results	176
5.2.4	Discussion	184
5.2.5	Conclusions	189
<b>5.3</b>	<b>HOT CORROSION STUDIES</b>	191
<b>5.3.1</b>	<b>Na<sub>2</sub>SO<sub>4</sub>-60% V<sub>2</sub>O<sub>5</sub> Molten Salt Environment-I</b>	191
5.3.1.1	Introduction	191
5.3.1.2	Experimental Details	192
5.3.1.3	Results	193

5.3.1.4 Discussion	201
5.3.1.5 Conclusions	208
5.3.2 Na <sub>2</sub> SO <sub>4</sub> -25%K <sub>2</sub> SO <sub>4</sub> Molten Salt Environment-II	209
5.3.2.1 Introduction	209
5.3.2.2 Experimental details	209
5.3.2.3 Results	209
5.3.2.4 Discussion	218
5.3.2.5 Conclusions	224
<b>CHAPTER 6 NiCoCrAlYTa COATING</b>	<b>225</b>
<b>6.1 CHARACTERISATION OF THE COATING</b>	<b>225</b>
6.1.1 Introduction	225
6.1.2 Experimental Details	226
6.1.3 Results	226
6.1.4 Discussion	238
6.1.5 Conclusions	241
<b>6.2 OXIDATION STUDIES IN AIR</b>	<b>242</b>
6.2.1 Introduction	242
6.2.2 Experimental details	242
6.2.3 Results	243
6.2.4 Discussion	250
6.2.5 Conclusions	255
<b>6.3 HOT CORROSION STUDIES</b>	<b>257</b>
6.3.1 Na <sub>2</sub> SO <sub>4</sub> -60% V <sub>2</sub> O <sub>5</sub> Molten Salt Environment-I	257
6.3.1.1 Introduction	257
6.3.1.2 Experimental details	257
6.3.1.3 Results	257
6.3.1.4 Discussion	266



6.3.1.5 Conclusions	272
6.3.2 Na <sub>2</sub> SO <sub>4</sub> -25%K <sub>2</sub> SO <sub>4</sub> Molten Salt Environment-II	273
6.3.2.1 Introduction	273
6.3.2.2 Experimental details	273
6.3.2.3 Results	273
6.3.2.4 Discussion	281
6.3.2.5 Conclusions	287
<b>CHAPTER 7</b>	<b>CORROSION STUDIES IN INDUSTRIAL</b>
	<b>ENVIRONMENT OF COAL FIRED BOILER</b>
7.1 Experimental details	288
7.2 Results and Discussion	288
7.3 Summery Of Results	299
7.4 Comprehensive Discussion	299
7.4.1 Bare Superalloys	299
7.4.2 D-gun Coated Superfer 800H	305
7.4.2.1 Cr <sub>3</sub> C <sub>2</sub> -NiCr Coating	305
7.4.2.2 NiCrAlY+0.4wt%CeO <sub>2</sub> Coating	306
7.4.2.3 NiCoCrAlYT <sub>a</sub>	307
<b>CHAPTER 8</b>	<b>COMPARATIVE DISCUSSION</b>
8.1 Oxidation in Air	308
8.2 Na <sub>2</sub> SO <sub>4</sub> -60%V <sub>2</sub> O <sub>5</sub> Molten Salt Environment-I	310
8.3 Na <sub>2</sub> SO <sub>4</sub> -25%K <sub>2</sub> SO <sub>4</sub> Molten Salt Environment-II	311
8.4 Actual Industrial Coal Fired Boiler Environment	313
<b>CHAPTER 9</b>	<b>CONCLUSIONS</b>
	<b>SUGGESTIONS FOR FUTURE WORK</b>
	<b>APPENDIX</b>
	<b>REFERENCES</b>

## LIST OF FIGURE

Figure No.	Particulars	Page No.
Fig.2.1	Schematic showing the effect of chromium in Fe-Cr alloys on oxidation rate and oxide scale structure based on isothermal oxidation studies at 1000 ° C (Wright, 1987).	6
Fig.2.2	Schematic representation of the transient oxidation of Ni-Al alloys (a) containing sufficient aluminium to establish an Al <sub>2</sub> O <sub>3</sub> scale, (b) containing insufficient aluminium to establish an Al <sub>2</sub> O <sub>3</sub> scale, showing the progressive development of the scale in each case (Chattopadhyay and Wood 1970).	8
Fig.2.3	Schematic cross sections of an A-B alloy where both components form stable oxides but BO is more stable than AO. (a) Alloy dilute in B showing internal oxidation of B under an external layer of AO. (b) Alloy concentrated in B showing continuous external BO (Whittle, 1983)	9
Fig.2.4	Alloy oxidation mechanisms, with the corresponding morphologies of the oxide layers (Dieter, 2007).	11
Fig.2.5	Schematic diagram illustrating the oxidation mechanisms for Ni-Cr-Al alloys (Giggins, et al., 1971)	13
Fig. 2.6	Schematic diagram showing probable oxidation mode for the Ni <sub>3</sub> Al coated superni 601 exposed to air at 900 °C for 50 cycles (Singh et al., 2006).	17
Fig.2.7	Schematic diagram to illustrate the mechanism of hot corrosion in (a) High temperature hot corrosion and (b) Low temperature hot corrosion (Goebel, et al., 1973).	21
Fig.2.8	Schematic diagram illustrating the conditions that develop during the initiation and the propagation of hot corrosion attack and to identify the factors that determine the time at which the transition from the initiation to the propagation stage occurs (Pettit and Meier, 1985).	24
Fig.2.9	Schematic diagrams of basic and acidic fluxing mechanisms with respective typical morphology of corrosion attack (Goebel et al., 1973)	26

<b>Fig.2.10</b>	Na-Cr-S-O phase stability diagram for 1200 K (Rapp, 1986).	29
<b>Fig.2.11</b>	Phase stability diagram for Na-V-S-O system at 900 <sup>0</sup> C(Hwang and Rapp 1989).	30
<b>Fig.2.12</b>	Schematic diagram showing the possible hot corrosion mode for the NiCrBSi coated superni 718 exposed to the Na <sub>2</sub> SO <sub>4</sub> -60% V <sub>2</sub> O <sub>5</sub> environment at 900 °C for 50 cycles (Sidhu et al., 2007).	34
<b>Fig.2.13</b>	Phase Diagram for Na <sub>2</sub> SO <sub>4</sub> -V <sub>2</sub> O <sub>5</sub> System (Otero et al, 1987).	38
<b>Fig.2.14</b>	Schematic diagram showing probable hot corrosion mechanism in Na <sub>2</sub> SO <sub>4</sub> 60%V <sub>2</sub> O <sub>5</sub> after exposure for 50 cycles at 900 <sup>0</sup> C for alloys (Gitanjaly, 2003) (a) superni 75 (b) superni 601.	41
<b>Fig.2.15</b>	Phase diagram of Na <sub>2</sub> SO <sub>4</sub> and K <sub>2</sub> SO <sub>4</sub> system (Shi et al., 1992).	44
<b>Fig.2.16</b>	Schematic illustration of the growth of chromia scales in (i) the absence of oxygen active elements and with predominant outward transport of chromia through the scale, and (ii) the presence of oxygen active elements and with predominant inward transport of oxygen (Kofstad, 1990).	47
<b>Fig.2.17</b>	Coating deposition technology, (Bhushan and Gupta, 1991)	57
<b>Fig.2.18</b>	Schematic development of the thermal spray process and mechanism of coating build-up (Matthews, 2004).	59
<b>Fig.2.19</b>	Coating deposition and the oxidation process (Herman, 1988).	59
<b>Fig.2.20</b>	Comparison of various thermal spray processes in terms of particle temperature and velocity (Kuroda et al., 2008).	62
<b>Fig.2.21</b>	Schematic diagram showing a cross-section through a thermally sprayed coating (Gledhill et al., 1999)	62
<b>Fig.2.22</b>	Schematics for oxidation of particles, in-flight. (Deshpande et al., 2006)	63
<b>Fig.2.23</b>	Schematic Diagram of the D-gun Spray Process (Rao et al., 1986)	64
<b>Fig.3.1</b>	D-gun thermal spray process used in the current research work	76
<b>Fig.3.2</b>	FE-SEM morphology and EDS compositional analysis of fly ash	84
<b>Fig.4.0</b>	Optical micrographs of the substrate superalloys (a) superni 75 (b) superni 718 and (c) superfer 800H.	87
<b>Fig.4.1</b>	SEM of Cr <sub>3</sub> C <sub>2</sub> -25%NiCr powder.	89
<b>Fig.4.2</b>	BSE Image showing cross section morphology of the D-Gun sprayed Cr <sub>3</sub> C <sub>2</sub> -	90

25%NiCr on (a) superni 75, (b) superni 718 and (c) superfer 800H

- Fig.4.3** SEM micrographs showing surface morphology of Detonation gun as-sprayed  $\text{Cr}_3\text{C}_2$ -25%NiCr coating on superalloys superni 75 (a) as-sprayed surface and (b) polished surface. 91
- Fig.4.4** Microhardness profiles for Detonation-gun sprayed  $\text{Cr}_3\text{C}_2$ -25%NiCr coatings on different superalloys. 91
- Fig.4.5** FE-SEM micrographs showing surface morphology of Detonation gun as-sprayed  $\text{Cr}_3\text{C}_2$ -25%NiCr coating on superalloy superni 75 (a) at lower magnification 2000 X, (b) at higher magnification 10,000X, 93
- Fig.4.6.** FE-SEM/EDS analysis at the cross-section of as sprayed  $\text{Cr}_3\text{C}_2$ -25%NiCr coating on superalloy superni 75 94
- Fig.4.7** X-ray diffraction for the  $\text{Cr}_3\text{C}_2$ -25%NiCr powder 95
- Fig.4.8** X-ray diffraction for the  $\text{Cr}_3\text{C}_2$ -25%NiCr coating on superalloy (a) superni 718, (b) superni 75 and (c) superfer 800H 95
- Fig.4.9** Composition image (SEI) and X-ray mapping of the cross-section of the as-sprayed  $\text{Cr}_3\text{C}_2$ -25%NiCr coating on superni 75 superalloys 97
- Fig.4.10** Composition image (SEI) and X-ray mapping of the cross-section of the as-sprayed  $\text{Cr}_3\text{C}_2$ -25%NiCr coating on superni 718 superalloys 98
- Fig.4.11** Composition image (SEI) and X-ray mapping of the cross-section of the as-sprayed  $\text{Cr}_3\text{C}_2$ -25%NiCr coating on superfer 800H superalloys 99
- Fig.4.12** Surface macrograph of  $\text{Cr}_3\text{C}_2$ -NiCr coated and bare superalloys subjected to cyclic oxidation in air for 100 cycles at 900 °C, (a) Bare superni 75, (b) Coated superni 75, (c) Bare superni 718, (d) Coated superni 718, (e) Bare superfer 800H, (f) Coated superfer 800H 105
- Fig.4.13** Weight gain/area vs. number of cycles plot for  $\text{Cr}_3\text{C}_2$ -NiCr-coated and bare superalloys subjected to cyclic oxidation in air for 100 cycles at 900 °C. 105
- Fig.4.14**  $(\text{Weight gain/area})^2$  vs. number of cycles plot for  $\text{Cr}_3\text{C}_2$ -NiCr-coated and bare superalloys subjected to cyclic oxidation in air for 100 cycles at 900 °C. 106
- Fig.4.15** Bar chart showing cumulative weight gain per unit area for bare and  $\text{Cr}_3\text{C}_2$ -NiCr-coated superalloys subjected to cyclic oxidation in air for 100 cycles at 900 °C. 106

<b>Fig.4.16</b>	X-ray diffraction patterns for $\text{Cr}_2\text{C}_3$ -NiCr coated superalloys exposed to cyclic oxidation in air at 900 °C after 100 cycles	107
<b>Fig 4.17</b>	X-ray diffraction patterns for $\text{Cr}_2\text{C}_3$ -NiCr coated superalloys exposed to cyclic oxidation in air at 900 °C after 100 cycles.	109
<b>Fig.4.18</b>	FE-SEM/EDS analysis along with EDS spectrum for coated superalloys subjected to cyclic oxidation in air at 900 °C after 100 cycles: (a) coated superni 75, (b) coated superni 718 and (c) coated superfer 800H.	110
<b>Fig.4.19</b>	FE-SEM/EDS analysis along with EDS spectrum for the bare superalloys subjected to cyclic oxidation in air at 900 °C after 100 cycles: (a) bare superni 75, (b) bare sperni 718 and (c) bare sperfer 800H	111
<b>Fig.4.20</b>	Morphology of oxide scale and variation of elemental composition across the cross-section of $\text{Cr}_3\text{C}_2$ -NiCr-coated superalloys subjected to cyclic oxidation at 900 °C in air after 100 cycles: (a) superni 75, (b) superni 718 and (c) superfer 800H.	114
<b>Fig.4.21</b>	Composition image (SEI) and X-ray mapping of the cross-section of the $\text{Cr}_3\text{C}_2$ -NiCr-coated superalloy superni 75 subjected to cyclic oxidation in air at 900 °C after 100 cycles.	115
<b>Fig.4.22</b>	Composition image (SEI) and X-ray mapping of the cross-section of the $\text{Cr}_3\text{C}_2$ -NiCr-coated superalloy superni 718 subjected to cyclic oxidation in air at 900 °C after 100 cycles.	116
<b>Fig.4.23</b>	Composition image (BSEI) and X-ray mapping of the cross-section of the $\text{Cr}_3\text{C}_2$ -NiCr coated superalloy superfer 800H subjected to cyclic oxidation in air at 900 °C after 100 cycles.	117
<b>Fig.4.24</b>	Schematic of the proposed oxidation mechanism of the $\text{Cr}_3\text{C}_2$ -NiCr coated superalloy superni 75 at 900 °C in air after 100 cycles.	120
<b>Fig.4.25</b>	Surface macrograph of $\text{Cr}_3\text{C}_2$ -NiCr coated and bare superalloys subjected to hot corrosion in $\text{Na}_2\text{SO}_4$ -60% $\text{V}_2\text{O}_5$ environment at 900 °C for 100 cycles. (a) Bare superni 718, (b) Coated superni 718, (c) Bare superni 75, (d) Coated superni 75, (e) Bare superfer 800H and (f) Coated superfer 800H.	124
<b>Fig.4.26</b>	Weight gain/area vs. number of cycles plot for coated and bare superalloys	124

	subjected to cyclic oxidation for 100 cycles in Na <sub>2</sub> SO <sub>4</sub> -60% V <sub>2</sub> O <sub>5</sub> at 900 °C	
<b>Fig.4.27</b>	(weight gain/area) <sup>2</sup> vs. number of cycles plot for coated and bare superalloys subjected to cyclic oxidation for 100 cycles in Na <sub>2</sub> SO <sub>4</sub> -60% V <sub>2</sub> O <sub>5</sub> at 900 °C	125
<b>Fig.4.28</b>	Bar chart showing cumulative weight gain per unit area for coated and bare superalloys subjected to cyclic oxidation for 100 cycles in Na <sub>2</sub> SO <sub>4</sub> -60% V <sub>2</sub> O <sub>5</sub> at 900 °C.	125
<b>Fig.4.29</b>	X-ray diffraction patterns for bare superalloys exposed to cyclic oxidation in Na <sub>2</sub> SO <sub>4</sub> -60%V <sub>2</sub> O <sub>5</sub> at 900 °C after 100 cycles.	128
<b>Fig.4.30</b>	X-ray diffraction patterns for Cr <sub>2</sub> C <sub>3</sub> -NiCr coated superalloys exposed to cyclic oxidation in Na <sub>2</sub> SO <sub>4</sub> -60%V <sub>2</sub> O <sub>5</sub> at 900 °C after 100 cycles	129
<b>Fig.4.31</b>	FE-SEM/EDS analysis along with EDS spectrum for Cr <sub>2</sub> C <sub>3</sub> -NiCr coated superalloys subjected to cyclic oxidation in Na <sub>2</sub> SO <sub>4</sub> -60%V <sub>2</sub> O <sub>5</sub> at 900 °C after 100 cycles (a) superni 75, (b) superfer 800H and (c) superni 718	130
<b>Fig.4.32</b>	FE-SEM/EDS analysis along with EDS spectrum for the bare superalloys subjected to cyclic oxidation in Na <sub>2</sub> SO <sub>4</sub> -60%V <sub>2</sub> O <sub>5</sub> at 900 °C after 100 cycles: (a) superni 75 (b) superfer 800H and (c) superni 718.	131
<b>Fig.4.33</b>	Oxide scale morphology and variation of elemental composition across the cross-section of Cr <sub>3</sub> C <sub>2</sub> -NiCr coated superalloys subjected to cyclic oxidation at 900°C in Na <sub>2</sub> SO <sub>4</sub> -60%V <sub>2</sub> O <sub>5</sub> after 100 cycles (a) superni 75, (b) superni 718 and (c) superfer 800H	132
<b>Fig.4.34</b>	Composition image (SE) and X-ray mapping of the cross-section of the Cr <sub>3</sub> C <sub>2</sub> -NiCr -coated superalloy superni 75 subjected to cyclic oxidation at 900 °C in Na <sub>2</sub> SO <sub>4</sub> -60%V <sub>2</sub> O <sub>5</sub> after 100 cycles.	135
<b>Fig.4.35</b>	Composition image (SE) and X-ray mapping of the cross-section of the Cr <sub>3</sub> C <sub>2</sub> -NiCr coated superalloy superni 718 subjected to cyclic oxidation at 900°C in Na <sub>2</sub> SO <sub>4</sub> -60%V <sub>2</sub> O <sub>5</sub> after 100 cycles.	136
<b>Fig.4.36</b>	Composition image (SE) and X-ray mapping of the cross-section of the Cr <sub>3</sub> C <sub>2</sub> -NiCr coated superalloy superfer 800H subjected to cyclic oxidation at 900 °C in Na <sub>2</sub> SO <sub>4</sub> -60%V <sub>2</sub> O <sub>5</sub> after 100 cycles	137
<b>Fig.4.37</b>	Schematic of the proposed oxidation mechanism of the Cr <sub>3</sub> C <sub>2</sub> -NiCr coated	140

- superalloy superni 718 at 900 °C in  $\text{Na}_2\text{SO}_4$ -60% $\text{V}_2\text{O}_5$  after 100 cycles.
- Fig.4.38** Surface macrograph of  $\text{Cr}_3\text{C}_2$ -NiCr coated and bare superalloys subjected to hot corrosion in  $\text{Na}_2\text{SO}_4$ -25% $\text{K}_2\text{SO}_4$  environment at 900 °C for 100 cycles, (a) Coated superni 75, (b) Coated superni 718, (c) Coated superfer 800 H, (d) Bare superni 75, (e) Bare superni 718, (f) Bare superfer 800H. 143
- Fig.4.39** weight gain/area vs. number of cycles plot for  $\text{Cr}_3\text{C}_2$ -NiCr coated and bare superalloys subjected to cyclic oxidation for 100 cycles in  $\text{Na}_2\text{SO}_4$ -25%  $\text{K}_2\text{SO}_4$  at 900 °C, 143
- Fig.4.40** (weight gain/area)<sup>2</sup> vs. number of cycles plot for coated and bare superalloys subjected to cyclic oxidation for 100 cycles in  $\text{Na}_2\text{SO}_4$ -25%  $\text{K}_2\text{SO}_4$  at 900 °C 144
- Fig.4.41** Bar chart showing cumulative weight gain per unit area for coated and bare superalloys subjected to cyclic oxidation for 100 cycles in  $\text{Na}_2\text{SO}_4$ -25%  $\text{K}_2\text{SO}_4$  at 900 °C 144
- Fig.4.42** X-ray diffraction patterns for bare superalloys exposed to cyclic oxidation in  $\text{Na}_2\text{SO}_4$ -25% $\text{K}_2\text{SO}_4$  environment at 900 °C after 100 cycles, (a) superni 718, (b) superni 75 and (c) superfer 800H. 146
- Fig.4.43** X-ray diffraction patterns for  $\text{Cr}_2\text{C}_3$ -NiCr coated superalloys exposed to cyclic oxidation in  $\text{Na}_2\text{SO}_4$ -25% $\text{K}_2\text{SO}_4$  environment at 900 °C after 100 cycles, (a) Coated superni 718, (b) Coated superni 75 and (c) Coated superfer 800H. 147
- Fig.4.44** FE-SEM/EDS analysis for coated superalloys subjected to cyclic oxidation in  $\text{Na}_2\text{SO}_4$ -25% $\text{K}_2\text{SO}_4$  environment at 900 °C after 100 cycles: (a) Coated superni 75, (b) Coated superni 718 and (c) Coated superfer 800H. 148
- Fig.4.45** FE-SEM/EDS analysis for bare superalloys subjected to cyclic oxidation in  $\text{Na}_2\text{SO}_4$ -25% $\text{K}_2\text{SO}_4$  environment at 900 °C after 100 cycles: (a) superni 75, (b) superni 718 and (c) superfer 800H. 149
- Fig.4.46** Oxide scale morphology and variation of elemental composition across the cross-section of  $\text{Cr}_3\text{C}_2$ -NiCr coated superalloys subjected to cyclic oxidation at 900 °C in  $\text{Na}_2\text{SO}_4$ -25% $\text{K}_2\text{SO}_4$  environment after 100 cycles (a) superni 75, (b) superni 718 and (c) superfer 800H 150
- Fig.4.47** Composition image (SE) and X-ray mapping of the cross-section of the 153

Cr<sub>3</sub>C<sub>2</sub>-NiCr-coated superalloy superni 75 subjected to cyclic oxidation at 900 °C in Na<sub>2</sub>SO<sub>4</sub>-25%K<sub>2</sub>SO<sub>4</sub> after 100 cycles.

- Fig.4.48** Composition image (SE) and X-ray mapping of the cross-section of the Cr<sub>3</sub>C<sub>2</sub>-NiCr-coated superalloy superni 718 subjected to cyclic oxidation at 900 °C in Na<sub>2</sub>SO<sub>4</sub>-25%K<sub>2</sub>SO<sub>4</sub> after 100 cycles. 154
- Fig.4.49** Composition image (SE) and X-ray mapping of the cross-section of the Cr<sub>3</sub>C<sub>2</sub>-NiCr-coated superalloy superfer 800H subjected to cyclic oxidation at 900 °C in Na<sub>2</sub>SO<sub>4</sub>-25%K<sub>2</sub>SO<sub>4</sub> after 100 cycles. 155
- Fig.4.50** Schematic of the proposed oxidation mechanism of the Cr<sub>3</sub>C<sub>2</sub>-NiCr coated superalloy superni 718 at 900 °C in Na<sub>2</sub>SO<sub>4</sub>-25%K<sub>2</sub>SO<sub>4</sub> after 100 cycles. 158
- Fig.5.1** SEM of NiCrAlY + 0.4wt % CeO<sub>2</sub> powder 162
- Fig.5.2** SEM micrographs showing as-sprayed cross-sectional and surface morphology of Detonation gun sprayed NiCrAlY+0.4wt %CeO<sub>2</sub> coating on (a and d) superni 75, (b and e) superni 718 and (c and f) superfer 800H respectively. 163
- Fig.5.3** Microhardness profiles for Detonation-gun sprayed NiCrAlY+0.4 wt% CeO<sub>2</sub> coating on different superalloys 164
- Fig.5.4** X-ray diffraction for the NiCrAlY+0.4wt%CeO<sub>2</sub> powder and coating on different superalloys 165
- Fig.5.5** FE-SEM surface micrographs with EDS spectrum of D-gun sprayed NiCrAlY +0.4wt%CeO<sub>2</sub> coating (a) as-sprayed superfer 800H and (b) polished superni 75 166
- Fig.5.6** FE-SEM/EDS analysis at the cross-section of as sprayed NiCrAlY+0.4 wt% CeO<sub>2</sub> coating on superalloy superni 718 167
- Fig.5.7** Composition image (SEI) and X-ray mapping of the cross-section of the as sprayed NiCrAlY+ 0.4 wt%CeO<sub>2</sub> coated on superni 75 superalloys. 171
- Fig.5.8** Composition image (SEI) and X-ray mapping of the cross-section of the as sprayed NiCrAlY+0.4wt%CeO<sub>2</sub> coated on superni 718 superalloys. 172
- Fig.5.9** Composition image (SEI) and X-ray mapping of the cross-section of the as sprayed NiCrAlY+ 0.4wt%CeO<sub>2</sub> coated on superfer 800H superalloys 173
- Fig.5.10** Surface macrograph of NiCrAlY+0.4wt%CeO<sub>2</sub> coated superalloys subjected 177



to cyclic oxidation in air for 100 cycles at 900 °C, (a) superni 75, (b) superni 718 and (c) superfer 800H

- Fig.5.11** Weight gain/area vs. number of cycles plot for NiCrAlY+0.4wt%CeO<sub>2</sub> coated and bare superalloys subjected to cyclic oxidation in air for 100 cycles at 900 °C. 177
- Fig.5.12** (Weight gain/area)<sup>2</sup> vs. number of cycles plot for NiCrAlY+0.4wt%CeO<sub>2</sub> coated and bare superalloys subjected to cyclic oxidation in air for 100 cycles at 900 °C 178
- Fig.5.13** Bar chart showing cumulative weight gain per unit area for bare and NiCrAlY + 0.4Wt%CeO<sub>2</sub> -coated superalloys subjected to cyclic oxidation in air for 100 cycles at 900 °C. 178
- Fig.5.14** X-ray diffraction patterns for NiCrAlY+0.4wt%CeO<sub>2</sub> coated superalloys exposed to cyclic oxidation in air at 900 °C after 100 cycles. 180
- Fig.5.15** FE-SEM/EDS analysis along with EDS spectrum for NiCrAlY+0.4wt% CeO<sub>2</sub> coated superalloys subjected to cyclic oxidation in air at 900 °C after 100 cycles: (a) superni 75, (b) superni 718 and (c) superfer 800H. 181
- Fig.5.16** Morphology of oxide scale and variation of elemental composition across the cross-section of NiCrAlY+0.4wt%CeO<sub>2</sub>-coated superalloys subjected to cyclic oxidation at 900 °C in air after 100 cycles: (a) superni 75, (b) superni 718 and (c) superfer 800H. 183
- Fig.5.17** Composition image (SEI) and X-ray mapping of the cross-section of NiCrAlY+ 0.4 wt %CeO<sub>2</sub> -coated superalloy superni 75 subjected to cyclic oxidation in air at 900 °C after100 cycles 185
- Fig.5.18** Composition image (SEI) and X-ray mapping of the cross-section of NiCrAlY+0.4wt%CeO<sub>2</sub>-coated superalloy superni 718 subjected to cyclic oxidation in air at 900 °C after 100 cycles. 186
- Fig.5.19** Composition image (SEI) and X-ray mapping of the cross-section of NiCrAlY+0.4wt%CeO<sub>2</sub>-coated superalloy superfer 800H subjected to cyclic oxidation in air at 900 °C after100 cycles. 187
- Fig.5.20** Schematic of the proposed oxidation mechanism of the NiCrAlY+0.4wt% 190

- CeO<sub>2</sub> coated superalloy superfer 800H at 900 °C in air after 100 cycles.
- Fig.5.21** Surface macrograph of NiCrAlY+0.4wt%CeO<sub>2</sub> coated superalloys subjected to hot corrosion in Na<sub>2</sub>SO<sub>4</sub>-60%V<sub>2</sub>O<sub>5</sub> environment at 900 °C for 100 cycles, (a) superni 75, (b) superni 718, (c) superfer 800H 194
- Fig.5.22** weight gain/area vs. number of cycles plot for NiCrAlY+0.4wt%CeO<sub>2</sub> coated and bare superalloy subjected to cyclic oxidation for 100 cycles in Na<sub>2</sub>SO<sub>4</sub>-60%V<sub>2</sub>O<sub>5</sub> at 900 °C. 194
- Fig.5.23** (weight gain/area)<sup>2</sup> vs. number of cycles plot for NiCrAlY+0.4wt%CeO<sub>2</sub> coated and bare superalloys subjected to cyclic oxidation for 100 cycles in Na<sub>2</sub>SO<sub>4</sub>-60%V<sub>2</sub>O<sub>5</sub> at 900 °C. 195
- Fig.5.24** Bar chart showing cumulative weight gain per unit area for NiCrAlY+0.4 wt % CeO<sub>2</sub> coated and bare superalloys subjected to cyclic oxidation for 100 cycles in Na<sub>2</sub>SO<sub>4</sub>-60%V<sub>2</sub>O<sub>5</sub> at 900 °C. 195
- Fig.5.25** X-ray diffraction patterns for NiCrAlY+0.4wt%CeO<sub>2</sub> coated superalloys exposed to cyclic oxidation in Na<sub>2</sub>SO<sub>4</sub>-60%V<sub>2</sub>O<sub>5</sub> environment at 900 °C after 100 cycles 197
- Fig.5.26** FE-SEM/EDS analysis along with EDS spectrum for NiCrAlY+0.4wt %CeO<sub>2</sub> coated superalloys subjected to cyclic oxidation in Na<sub>2</sub>SO<sub>4</sub>-60%V<sub>2</sub>O<sub>5</sub> environment at 900 °C after 100 cycles: (a) superni 75, (b) superni 718 and (c) superfer 800H. 199
- Fig.5.27** Oxide scale morphology and variation of elemental composition across the cross-section of NiCrAlY+0.4 wt% CeO<sub>2</sub> coated superalloys subjected to cyclic oxidation at 900 °C in molten salt after 100 cycles (a) superni 75, (b) superni 718 and (c) superfer 800H. 200
- Fig.5.28** Composition image (SE) and X-ray mapping of the cross-section of the NiCrAlY + 0.4wt % CeO<sub>2</sub> coated superalloy superni 75 subjected to cyclic oxidation at 900 °C in Na<sub>2</sub>SO<sub>4</sub>-60%V<sub>2</sub>O<sub>5</sub> after 100 cycles 202
- Fig.5.29** Composition image (SE) and X-ray mapping of the cross-section of the NiCrAlY + 0.4wt % CeO<sub>2</sub> coated superalloy superni 718 subjected to cyclic oxidation at 900 °C in Na<sub>2</sub>SO<sub>4</sub>-60%V<sub>2</sub>O<sub>5</sub> after 100 cycles. 203
- Fig.5.30** Composition image (SE) and X-ray mapping of the cross-section of the 204

NiCrAlY +0.4wt % CeO<sub>2</sub> coated superalloy superfer 800H subjected to cyclic oxidation at 900 °C in Na<sub>2</sub>SO<sub>4</sub>-60%V<sub>2</sub>O<sub>5</sub> after 100 cycles.

- Fig.5.31** Schematic diagram showing proposed hot corrosion mechanism of the NiCrAlY+ 0.4wt%CeO<sub>2</sub> coated superalloy superfer 800H at 900 °C in Na<sub>2</sub>SO<sub>4</sub>-60%V<sub>2</sub>O<sub>5</sub> after 100 cycles. 207
- Fig.5.32** Surface macrograph of NiCrAlY+0.4wt%CeO<sub>2</sub> coated superalloys subjected to cyclic oxidation in Na<sub>2</sub>SO<sub>4</sub>-25%K<sub>2</sub>SO<sub>4</sub> environment at 900°C for 100 cycles, (a) superni 75, (b) superni 718 and (c) superfer 800H 210
- Fig.5.33** weight gain/area vs. number of cycles plot for NiCrAlY+0.4wt%CeO<sub>2</sub> coated and bare superalloys subjected to cyclic oxidation for 100 cycles in Na<sub>2</sub>SO<sub>4</sub> - 25% K<sub>2</sub>SO<sub>4</sub> at 900 °C. 210
- Fig.5.34** (weight gain/area)<sup>2</sup> vs. number of cycles plot for NiCrAlY+0.4wt%CeO<sub>2</sub> coated and bare superalloys subjected to cyclic oxidation for 100 cycles in Na<sub>2</sub>SO<sub>4</sub>-25% K<sub>2</sub>SO<sub>4</sub> at 900 °C. 211
- Fig.5.35** Bar chart showing cumulative weight gain per unit area for NiCrAlY+ 0.4 wt % CeO<sub>2</sub> coated and bare superalloys subjected to cyclic oxidation for 100 cycles in Na<sub>2</sub>SO<sub>4</sub>-25%K<sub>2</sub>SO<sub>4</sub> at 900 °C. 211
- Fig.5.36** X-ray diffraction patterns for Cr<sub>2</sub>C<sub>3</sub>-NiCr-coated superalloys exposed to cyclic Oxidation in Na<sub>2</sub>SO<sub>4</sub>-25%K<sub>2</sub>SO<sub>4</sub> environment at 900 °C after 100 cycles, (a) superni 718, (b) superni 75 and (c) superfer 800H. 213
- Fig.5.37** FE-SEM/EDS analysis for NiCrAlY+0.4wt%CeO<sub>2</sub> coated superalloys subjected to cyclic oxidation in Na<sub>2</sub>SO<sub>4</sub>-25%K<sub>2</sub>SO<sub>4</sub> environment at 900 °C after 100 cycles: (a) superni 75, (b) superni 718 and (c) superfer 800H. 215
- Fig.5.38** Oxide scale morphology and variation of elemental composition across the cross-section of NiCrAlY+0.4wt%CeO<sub>2</sub> coated superalloys subjected to cyclic oxidation at 900 °C in Na<sub>2</sub>SO<sub>4</sub>-25%K<sub>2</sub>SO<sub>4</sub> environment after 100 cycles (a) superni 75, (b) superni 718 and (c) superfer 800H. 216
- Fig.5.39** Composition image (SE) and X-ray mapping of the cross-section of the NiCrAlY+0.4wt%CeO<sub>2</sub> coated superalloy superni 75 subjected to cyclic oxidation at 900 °C in Na<sub>2</sub>SO<sub>4</sub>-25%K<sub>2</sub>SO<sub>4</sub> after 100 cycles. 220
- Fig.5.40** Composition image (SE) and X-ray mapping of the cross-section of the 221

NiCrAlY +0.4wt%CeO<sub>2</sub> coated superalloy superni 718 subjected to cyclic oxidation at 900 °C in Na<sub>2</sub>SO<sub>4</sub>–25%K<sub>2</sub>SO<sub>4</sub> after 100 cycles.

- Fig.5.41** Composition image (SE) and X-ray mapping of the cross-section of the NiCrAlY+0.4wt %CeO<sub>2</sub> coated superalloy superfer 800H subjected to cyclic oxidation at 900 °C in Na<sub>2</sub>SO<sub>4</sub>–25%K<sub>2</sub>SO<sub>4</sub> after 100 cycles. 222
- Fig.5.42** Schematic of the proposed oxidation mechanism of the NiCrAlY+0.4wt %CeO<sub>2</sub> coated superalloy superfer 800H at 900 °C in Na<sub>2</sub>SO<sub>4</sub>–25%K<sub>2</sub>SO<sub>4</sub> after 100 cycles. 223
- Fig.6.1** SEM of NiCoCrAlYT a powder. 227
- Fig.6.2** FE-SEM micrographs showing as-sprayed cross-sectional and surface morphology of D-gun sprayed NiCoCrAlYT a coating on (a and b) superni 75,(c and d) superni 718 and (e and f) superfer 800H respectively. 228
- Fig.6.3** Microhardness profiles for D–gun sprayed NiCoCrAlYT a coatings on three different superalloys. 229
- Fig.6.4** X-ray diffraction pattern of the NiCoCrAlYT a powder and as–sprayed NiCoCrAlYT a coating on different superalloys. 230
- Fig.6.5** FE-SEM surface micrographs with EDS spectrum along with elemental composition of D-gun sprayed NiCoCrAlYT a coatings on (a) superni 75, (b) superni 718 and (c) superfer 800H. 231
- Fig.6.6** Cross-section morphology of NiCoCrAlYT a coated superalloys in as sprayed condition and cross-section EDS line scan of superni 75. 234
- Fig.6.7** Composition image (SEI) and X-ray mapping of the cross-section of the as-sprayed NiCoCrAlYT a coated on superni 75 superalloys. 235
- Fig.6.8** Composition image (SEI) and X-ray mapping of the cross-section of the as-sprayed NiCoCrAlYT a coated on superni 718 superalloys. 236
- Fig.6.9** Composition image (SEI) and X-ray mapping of the cross-section of the as-sprayed NiCoCrAlYT a coated on superfer 800H superalloys. 237
- Fig.6.10** Surface macrograph of NiCoCrAlYT a coated superalloys subjected to cyclic oxidation in air for 100 cycles at 900 °C, (a) superni 75, (b) superni 718 and (c) superfer 800H. 244
- Fig.6.11** Weight gain/area vs. number of cycles plot for NiCoCrAlYT a coated and 244

	bare superalloys subjected to cyclic oxidation in air for 100 cycles at 900 °C.	
<b>Fig.6.12</b>	(Weight gain/area) <sup>2</sup> vs. number of cycles plot for NiCoCrAlYTa coated and bare superalloys subjected to cyclic oxidation in air for 100 cycles at 900 °C.	245
<b>Fig.6.13</b>	Bar chart showing cumulative weight gain per unit area for bare and NiCoCrAlYTa coated superalloys subjected to cyclic oxidation in air for 100 cycles at 900 °C.	245
<b>Fig.6.14</b>	X-ray diffraction patterns for NiCoCrAlYTa coated superalloys exposed to cyclic oxidation in air at 900 °C after 100 cycles.	247
<b>Fig.6.15</b>	FE-SEM/EDS analysis along with EDS spectrum for NiCoCrAlYTa coated superalloys subjected to cyclic oxidation in air at 900 °C after 100 cycles: (a) superni 75, (b) superni 718 and (c) superfer 800H.	248
<b>Fig.6.16</b>	Morphology of oxide scale and variation of elemental composition across the cross-section of NiCoCrAlYTa-coated superalloys subjected to cyclic oxidation at 900 °C in air after 100 cycles: (a) superni 75, (b) superni 718 and (c) superfer 800H.	249
<b>Fig.6.17</b>	Composition image (SEI) and X-ray mapping of the cross-section of NiCoCrAlYTa-coated superalloy superni 75 subjected to cyclic oxidation in air at 900 °C after 100 cycles.	251
<b>Fig.6.18</b>	Composition image (SEI) and X-ray mapping of the cross-section of NiCoCrAlYTa-coated superalloy superni 718 subjected to cyclic oxidation in air at 900 °C after 100 cycles.	252
<b>Fig.6.19</b>	Composition image (SEI) and X-ray mapping of the cross-section of NiCoCrAlYTa-coated superalloy superfer 800H subjected to cyclic oxidation in air at 900 °C after 100 cycles.	253
<b>Fig.6.20</b>	Schematic of the proposed oxidation mechanism of the NiCoCrAlYTa coated superalloy superni 75 at 900 °C in air after 100 cycles.	256
<b>Fig.6.21</b>	Surface macrograph of NiCoCrAlYTa coated superalloys subjected to hot corrosion in Na <sub>2</sub> SO <sub>4</sub> -60%V <sub>2</sub> O <sub>5</sub> environment at 900 °C for 100 cycles, (a) superni 75, (b) superni 718, (c) superfer 800H.	259
<b>Fig.6.22</b>	weight gain/area vs. number of cycles plot for NiCoCrAlYTa coated and un-	259

coated superalloys subjected to cyclic oxidation for 100 cycles in  $\text{Na}_2\text{SO}_4 - 60\% \text{V}_2\text{O}_5$  at  $900^\circ\text{C}$ .

- Fig.6.23** (weight gain/area)<sup>2</sup> vs. number of cycles plot for NiCoCrAlYTa coated and un-coated superalloys subjected to cyclic oxidation for 100 cycles in  $\text{Na}_2\text{SO}_4-60\%\text{V}_2\text{O}_5$  at  $900^\circ\text{C}$  260
- Fig.6.24** Bar chart showing cumulative weight gain per unit area for NiCoCrAlYTa coated and Un-coated superalloys subjected to cyclic oxidation for 100 cycles in  $\text{Na}_2\text{SO}_4-60\%\text{V}_2\text{O}_5$  at  $900^\circ\text{C}$ . 260
- Fig.6.25** X-ray diffraction patterns for NiCoCrAlYTa coated superalloys exposed to cyclic oxidation in  $\text{Na}_2\text{SO}_4-60\%\text{V}_2\text{O}_5$  environment at  $900^\circ\text{C}$  after 100 cycles. 262
- Fig.6.26** FE-SEM/EDS analysis along with EDS spectrum for NiCoCrAlYTa coated superalloys subjected to cyclic oxidation in  $\text{Na}_2\text{SO}_4-60\%\text{V}_2\text{O}_5$  environment at  $900^\circ\text{C}$  after 100 cycles: (a) superni 75, (b) superni 718 and (c) superfer 800 H. 263
- Fig.6.27** Oxide scale morphology and variation of elemental composition across the cross-section of NiCoCrAlYTa coated superalloys subjected to cyclic oxidation at  $900^\circ\text{C}$  in molten salt after 100 cycles (a) superni 75, (b) superni 718 and (c) superfer 800H. 265
- Fig.6.28** Composition image (SE) and X-ray mapping of the cross-section of the NiCoCrAlYTa coated superalloy superni 75 subjected to cyclic oxidation at  $900^\circ\text{C}$  in  $\text{Na}_2\text{SO}_4-60\%\text{V}_2\text{O}_5$  after 100 cycles. 267
- Fig.6.29** Composition image (SE) and X-ray mapping of the cross-section of the NiCoCrAlYTa coated superalloy superni 718 subjected to cyclic oxidation at  $900^\circ\text{C}$  in  $\text{Na}_2\text{SO}_4-60\%\text{V}_2\text{O}_5$  after 100 cycles. 268
- Fig.6.30** Composition image (SE) and X-ray mapping of the cross-section of the NiCoCrAlYTa coated superalloy superfer 800H subjected to cyclic oxidation at  $900^\circ\text{C}$  in  $\text{Na}_2\text{SO}_4-60\%\text{V}_2\text{O}_5$  after 100 cycles. 269
- Fig.6.31** Schematic of the proposed oxidation mechanism of the NiCoCrAlYTa coated superalloy superfer 800H at  $900^\circ\text{C}$  in  $\text{Na}_2\text{SO}_4-60\%\text{V}_2\text{O}_5$  after 100 cycles. 271
- Fig.6.32** Surface macrograph of NiCoCrAlYTa coated superalloys subjected to cyclic 274

- oxidation in  $\text{Na}_2\text{SO}_4$ -25% $\text{K}_2\text{SO}_4$  environment at 900 °C for 100 cycles, (a) superni 75, (b) superni 718 and (c) superfer 800H
- Fig.6.33** weight gain/area vs. number of cycles plot for NiCoCrAlYTa coated and uncoated superalloys subjected to cyclic oxidation for 100 cycles in  $\text{Na}_2\text{SO}_4$ -25% $\text{K}_2\text{SO}_4$  at 900 °C. 274
- Fig.6.34** (weight gain/area)<sup>2</sup> vs. number of cycles plot for NiCoCrAlYTa coated and uncoated superalloys subjected to cyclic oxidation for 100 cycles in  $\text{Na}_2\text{SO}_4$ -25% $\text{K}_2\text{SO}_4$  at 900 °C. 275
- Fig.6.35** Bar chart showing cumulative weight gain per unit area for NiCoCrAlYTa coated and uncoated superalloys subjected to cyclic oxidation for 100 cycles in  $\text{Na}_2\text{SO}_4$ -25% $\text{K}_2\text{SO}_4$  at 900 °C. 275
- Fig.6.36** X-ray diffraction patterns for NiCoCrAlYTa-coated superalloys exposed to oxidation in  $\text{Na}_2\text{SO}_4$ -25% $\text{K}_2\text{SO}_4$  environment at 900 °C after 100 cycles. 277
- Fig.6.37** FE-SEM/EDS surface analysis for NiCoCrAlYTa coated superalloys subjected to cyclic oxidation in  $\text{Na}_2\text{SO}_4$ -25% $\text{K}_2\text{SO}_4$  environment at 900 °C after 100 cycles (a) Coated superni 75, (b) Coated superni 718 and (c) Coated superfer 800H. 279
- Fig.6.38** Oxide scale morphology and variation of elemental composition across the cross -section of NiCoCrAlYTa-coated superalloys subjected to cyclic oxidation at 900 °C in  $\text{Na}_2\text{SO}_4$ -25% $\text{K}_2\text{SO}_4$  environment after 100 cycles (a) superni 75, (b) superni 718 and (c) superfer 800H. 280
- Fig.6.39** Secondary electron image (SEI) and X-ray mapping of the cross-section of the NiCoCrAlYTa-coated superalloy superni 75 subjected to cyclic oxidation at 900 °C in  $\text{Na}_2\text{SO}_4$ -25%  $\text{K}_2\text{SO}_4$  after 100 cycles. 282
- Fig.6.40** Secondary electron image (SEI) and X-ray mapping of the cross-section of the NiCoCrAlYTa-coated superalloy superni 718 subjected to cyclic oxidation at 900 °C in  $\text{Na}_2\text{SO}_4$ -25% $\text{K}_2\text{SO}_4$  after 100 cycles. 283
- Fig.6.41** Secondary electron image (SEI) and X-ray mapping of the cross-section of the NiCoCrAlYTa-coated superalloy superfer 800H subjected to cyclic oxidation at 900 °C in  $\text{Na}_2\text{SO}_4$ -25% $\text{K}_2\text{SO}_4$  after 100 cycles. 284
- Fig.6.42** Schematic of the proposed oxidation mechanism of the NiCoCrAlYTa-coated 286

superalloy superfer 800H at 900 °C in  $\text{Na}_2\text{SO}_4$ -25% $\text{K}_2\text{SO}_4$  after 100 cycles.

- Fig.7.1** Macrographs of the (a) bare and D-gun sprayed (b)  $\text{Cr}_3\text{C}_2$ -NiCr, (c) NiCoCr-AlYTa and (d) NiCoCrAlYTa coated on superfer 800H after 1000 hour's exposure to low temperature super-heater zone of the boiler at 900 °C. 289
- Fig.7.2** Weight change vs. time plots for the bare and D-gun coated superfer 800H subjected to 1000 hrs cyclic exposure to low temperature super heater zone of the coal fired boiler at 900 °C. 291
- Fig.7.3** (Weight gain/area)<sup>2</sup> vs. number of hours plots for the bare and D-gun coated superfer 800H subjected to 1000 hrs cyclic exposure to low temperature super-heater zone of the coal fired boiler at 900°C. 291
- Fig.7.4** BSE images for the bare and D-gun coated superfer 800H after 1000 hrs exposure to low temperature super-heater zone of the coal fired boiler at 900 °C : (a) Bare superalloy (b) $\text{Cr}_3\text{C}_2$ -NiCr coated (c) NiCrAlY+0.4wt% $\text{CeO}_2$  coated(d) NiCoCrAlYTa coated 292
- Fig.7.5** Bar charts indicating the extent of corrosion for the bare and D-gun coated superfer 800H after 1000 hrs exposure to the coal fired boiler at 900 °C. 292
- Fig.7.6** X-ray diffraction patterns for the (i) bare and D-gun sprayed (ii)  $\text{Cr}_3\text{C}_2$ -NiCr (iii) NiCrAlY+0.4wt% $\text{CeO}_2$  (iv) NiCoCrAlYTa coatings on superfer 800H after 1000 hrs exposure to low temperature super-heater zone of the coal fired boiler at 900 °C. 293
- Fig.7.7** FE-SEM/EDS analysis showing elemental composition (wt.%) for the bare and D-gun coated superfer 800H after 1000 hrs exposure to low temperature super heater zone of the coal fired boiler at 900 °C: (a) Bare superfer 800H (b)  $\text{Cr}_3\text{C}_2$ -NiCr coated (c)NiCrAlY+0.4wt% $\text{CeO}_2$  coated (d) NiCoCrAlYTa coated. 295
- Fig.7.8** Oxide scale morphologies and variations of elemental composition (wt%) across the cross section of (a)bare and D-gun sprayed (b)  $\text{Cr}_3\text{C}_2$ -NiCr, (c) NiCrAlY+0.4wt% $\text{CeO}_2$  and (d) NiCoCrAlYTa coating on superfer 800H after 1000 hours exposure to the coal fired boiler at 900 °C. 297
- Fig.7.9** Composition image (BSEI) and X-ray mappings across the cross-section of bare superfer 800H after 1000 hrs exposure to low temperature super-heater 301



zone of the coal fired boiler at 900 °C.

- Fig.7.10** Composition image (BSEI) and X-ray mappings across the cross-section of D-gun sprayed  $\text{Cr}_3\text{C}_2$ -NiCrcoated superfer 800H after 1000 hrs exposure to low temperature super-heater zone of the coal fired boiler at 900 °C. 302
- Fig.7.11** Composition image (BSEI) and X-ray mappings across the cross-section of D-gun sprayed NiCrAlY+0.4wt%CeO<sub>2</sub>coated superfer 800H after 1000 hrs of exposure to low temperature super-heater zone of coal fired boiler at 900 °C. 303
- Fig.7.12** Composition image (BSEI) and X-ray mappings across the cross-section of D-gun sprayed NiCoCrAlYT<sub>a</sub> coated superfer 800H after 1000 hrs exposure to low temperature super-heater zone of the coal fired boiler at 900 °C. 304
- Fig.8.1** Bar chart showing cumulative weight gain ( $\text{mg}/\text{cm}^2$ ) for the bare and coated superalloys subjected to cyclic oxidation in air at 900 °C for 100 cycles 309
- Fig.8.2** Bar chart showing cumulative weight gain ( $\text{mg}/\text{cm}^2$ ) for the bare and coated superalloys subjected to cyclic oxidation in  $\text{Na}_2\text{SO}_4$ -60% $\text{V}_2\text{O}_5$  environment at 900 °C for 100 cycles 309
- Fig.8.3** Bar chart showing cumulative weight gain ( $\text{mg}/\text{cm}^2$ ) for the bare and coated superalloys subjected to cyclic oxidation in  $\text{Na}_2\text{SO}_4$ -25% $\text{K}_2\text{SO}_4$  environment at 900 °C for 100 cycles 312
- Fig.8.4** Bar chart showing net weight change ( $\text{mg}/\text{cm}^2$ ) for the bare and coated superalloys after exposure to platen super-heater zone of the coal fired boiler at 900 °C for 1000 hours. 312

## LIST OF TABLES

Table No.	Particulars	Page No.
<b>Table 2.1</b>	Comparison of characteristics for various thermal spray processes.	61
<b>Table 3.1</b>	Chemical composition (wt.%) for various superalloys	74
<b>Table 3.2</b>	Composition of the alloy powders, shape and size of the particles.	75
<b>Table 3.3</b>	Spray parameters as employed during D-gun spraying	76
<b>Table 3.4</b>	Chemical analysis of ash and flue gases inside the boiler.	83
<b>Table 4.1</b>	Parabolic rate constant ( $k_p$ ) values for bare and D-gun sprayed $Cr_3C_2$ -Ni Cr-coated superalloys subjected to cyclic oxidation in air for 100 cycles at 900 °C	108
<b>Table 4.2</b>	parabolic rate constant ( $K_p$ ) values for D-gun sprayed $Cr_3C_2$ -NiCr-coated and bare superalloys subjected to cyclic oxidation for 100 cycles in $Na_2SO_4$ -60% $V_2O_5$ at 900 °C	127
<b>Table 4.3</b>	Parabolic rate constant ( $k_p$ ) and correlation coefficient values for coated and bare superalloys subjected to cyclic oxidation for 100 cycles in $Na_2SO_4$ -25% $K_2SO_4$ at 900 °C.	145
<b>Table 5.1</b>	The EDS elemental composition of the as-sprayed and polished NiCrAlY +0.4 wt% $CeO_2$ coating on superalloy 75	167
<b>Table 5.2</b>	Parabolic rate constant ( $k_p$ ) values for bare and D-gun sprayed NiCrAlY+0.4wt% $CeO_2$ -coated superalloys subjected to cyclic oxidation in air for 100 cycles at 900 °C	179
<b>Table 5.3</b>	Parabolic rate constant ( $k_p$ ) values for D-gun sprayed NiCrAlY+0.4wt % $CeO_2$ -coated and bare superalloys subjected to cyclic oxidation for 100 cycles in $Na_2SO_4$ -60% $V_2O_5$ at 900 °C	196
<b>Table 5.4</b>	Parabolic rate constant ( $k_p$ ) for NiCrAlY+0.4wt% $CeO_2$ coated and bare superalloys subjected to cyclic hot corrosion for 100 cycles in $Na_2SO_4$ -25% $K_2SO_4$ environment at 900 °C.	212

<b>Table 6.1</b>	Parabolic rate constant ( $k_p$ ) values for bare and D-gun-sprayed NiCoCrAlYTa-coated superalloys subjected to cyclic oxidation in air for 100 cycles at 900 °C.	246
<b>Table 6.2</b>	Parabolic rate constant ( $k_p$ ) values for D-gun sprayed NiCoCrAlYTa-coated and bare superalloys subjected to cyclic oxidation for 100 cycles in Na <sub>2</sub> SO <sub>4</sub> -60%V <sub>2</sub> O <sub>5</sub> at 900 °C	261
<b>Table 6.3</b>	Parabolic rate constant ( $k_p$ ) for NiCoCrAlYTa coated and bare superalloys subjected to cyclic hot corrosion in Na <sub>2</sub> SO <sub>4</sub> -25%K <sub>2</sub> SO <sub>4</sub> environment for 100 cycles at 900 °C.	276
<b>Table 7.1</b>	Summary of the results obtained for bare and coated superfer 800H exposed to the low temperature super-heater zone of the coal fired boiler at 900±10 °C for 1000 hours	300
<b>Table A.1</b>	Summary of oxidation of Fe-, Ni- & Co- base alloys in Air, Na <sub>2</sub> SO <sub>4</sub> and V <sub>2</sub> O <sub>5</sub> environments	321

## RESEARCH PAPERS PRESENTED/PUBLISHED

---

Research papers published out of the present investigation, in the peer-reviewed journals as well as presented/published in the conferences, are as follows

### (I) REFERRED JOURNALS

1. **Subhash Kamal**, R. Jayaganthan, S Prakash, Sanjay Kumar, Hot Corrosion Behavior of Detonation gun sprayed  $\text{Cr}_3\text{C}_2$ -NiCr coating on Ni-Fe-based superalloy in  $\text{Na}_2\text{SO}_4$ -60% $\text{V}_2\text{O}_5$  environment at 900 °C, Journal of Alloy and Compounds, Vol. 463 (2008) pp. 358-372.
2. **Subhash Kamal**, R. Jayaganthan, S Prakash, High temperature oxidation studies of Detonation-Gun sprayed  $\text{Cr}_3\text{C}_2$ -NiCr coating on Fe and Ni -Based superalloys in air under cyclic condition at 900 °C, Journal of Alloy and Compounds, 2009 (in press).
3. **Subhash Kamal**, R Jayaganthan, S Prakash, Characterisation of Detonation gun sprayed  $\text{Cr}_3\text{C}_2$  25%NiCr coatings on Ni- and Fe-based superalloys, Surface Engineering. 2008, (In press).
4. **Subhash Kamal**, Jayaganthan, R. and Prakash, S., "Evaluation of cyclic hot corrosion behaviour of detonation gun sprayed  $\text{Cr}_3\text{C}_2$ -25%NiCr coatings on nickel- and iron-based superalloys," Surf. Coat. Technol., Vol.203, (2009), pp.1004-1013.
5. **Subhash Kamal**, R Jayaganthan, S Prakash, Mechanical and Microstructural characterisation of NiCoCrAlYTaNi coatings on superalloys deposited by Detonation gun, Surface Engineering, 2008, (In press).
6. **Subhash Kamal**, R Jayaganthan, S Prakash, Mechanical and Microstructural characteristics of detonation gun sprayed NiCrAlY+0.4wt% $\text{CeO}_2$  coatings on superalloys, Journal of Thermal Spray Technology, 2009 (Under review).
7. **Subhash Kamal**, R Jayaganthan, S Prakash, Some studies on detonation-gun-sprayed NiCrAlY+0.4wt% $\text{CeO}_2$  coatings on superalloys in molten salt environment, Oxidation of Metals, 2009 (Under review).
8. **Subhash Kamal**, R Jayaganthan, S Prakash, Hot corrosion behaviour of D-gun sprayed NiCoCrAlYTaNi coated superalloys at 900 °C in molten salt environment, Journal of Thermal Spray Technology, 2009, (Communicated).

9. **Subhash Kamal**, R Jayaganthan, S Prakash, Evaluation of high temperature cyclic oxidation and hot corrosion behaviors of superalloys at 900 °C, Bulletin of Materials Science, 2008 (Under review).
10. **Subhash Kamal**, R Jayaganthan, S Prakash, High temperature oxidation studies of Detonation gun sprayed NiCrAlY+0.4wt%CeO<sub>2</sub> coating on superalloys in air at 900 °C, Tribology - Materials, Surfaces & Interfaces, 2009 (communicated).

## (II) NATIONAL/INTERNATIONAL CONFERENCES PROCEEDINGS.

11. **Subhash Kamal**, R. Jayaganthan, S. Prakash “Mechanical and Metallurgical Properties of Detonation Gun Sprayed Cr<sub>3</sub>C<sub>2</sub>-NiCr Coating on Superalloys” Global Conference on Production and Industrial Engineering (CPIE-2007), March 22-24, 2007, I.E-NIT JALANDHAR, pp.40
12. **Subhash Kamal**, R. Jayaganthan, S. Prakash “Oxidation and Hot Corrosion Behaviour of Detonation Gun Sprayed Cr<sub>3</sub>C<sub>2</sub>-NiCr Coating on Ni and Fe Based Superalloys” International Conference on Metallurgical Coatings and Thin Films, Town and Country Hotel San Diego, California, April 23-27, 2007
13. **Subhash Kamal**, R. Jayaganthan, S. Prakash, R.A. Mahesh, Vikas. K .Das, Hot Corrosion behavior of detonation gun sprayed 75Cr<sub>3</sub>C<sub>2</sub>-25(80Ni-20Cr) coating in Molten Salt Environment, CORCON 2007, International Conference on Corrosion, Organised By NACE International India Section (NIIS) at Hotel Intercontinental The Grand Mumbai Sept. 26 -28, 2007.
14. **Subhash Kamal**, R. Jayaganthan, S. Prakash, Cycle oxidation and hot corrosion behaviour of Ni and Fe based superalloy in molten salt environment at 900 °C,” 16th International Conference on: Processing and Fabrication of Advanced Materials (PFAM16), December 17-19 2007, Singapore.

15. R. A. Mahesh, **Subhash Kamal**, Ankur Modi, R Jayaganthan, S. Prakash, “Degradation Behavior of HVOF sprayed Ni-based coatings on superalloy in 40%Na<sub>2</sub>SO<sub>4</sub>-60%V<sub>2</sub>O<sub>5</sub> environment at 900 °C”, International Thermal Spray Conference-08, Maastricht, Netherlands June 02-04, 2008.
16. **Subhash Kamal**, R. A. Mahesh, R. Jayaganthan and S. Prakash, (2008), “Analytical studies on Detonation gun sprayed Cr<sub>3</sub>C<sub>2</sub>-NiCr coating on Ti-6Al-4V (Ti-31) Alloy in Air at Elevated Temperature”, for oral presentation in IISc Centenary – International Conference on Advances in Mechanical Engineering (IC-ICAME), Bangalore, India, July 02-04, 2008.

## ABBREVIATIONS

---

D-Gun	Detonation gun
Bal	Balance
BSEI	Back Scattered Electron Image
SEI	Secondary Electron Image
EDAX	Energy Dispersive X-ray Analysis
EDS	Energy Dispersive X-ray Spectroscopy
EPMA	Electron Probe Micro Analyser
hr.	Hour
HVOF	High Velocity Oxy-Fuel
$K_p$	Parabolic Rate Constant
LPPS	Low Pressure Plasma Spray
m.p.	Melting Point
min	Minute
FE-SEM	Field Emission Scanning Electron Microscopy
VPS	Vacuum Plasma Spray
Wt%	Weight Percentage
Wt. Gain	Weight Gain
XRD	X-ray Diffraction
Hv	Vickers hardness
DGS	Detonation gun spray
LTHC	Low temperature hot corrosion
HTHC	High temperature hot corrosion

# CHAPTER 1

## INTRODUCTION

---

It is said that corrosion never stops. Corrosion causes plant shut downs, waste of valuable resources, loss or contamination of products, reduction in efficiency and costly maintenance. In USA, the loss due to corrosion is around 4 per cent of GDP. In India, the corrosion losses will be around Rs. 1 lakh crore per annum. Around 80 per cent of the unscheduled shutdowns and breakdowns in industries are due to corrosion and process fouling. Out of the total loss due to corrosion, 25 per cent of loss can be easily saved with pro-active approach and protecting the system by applying protective coatings (Madhu Chittora, 2008).

In today's gas turbines, the emphasis is on saving energy and reducing the amounts of pollutants emitted. This can be attained only by designing alloys with higher melting points and the capability to retain mechanical integrity at increased temperatures. The development of nickel-based superalloys has reached its limit, as the alloys are operating at critical temperatures close to their melting points. Further increase in the operating temperatures will result in dissolution of the strengthening phases and even melting. An operation of gas turbines is usually limited by hot corrosion, which could lead to catastrophic failures. Increased temperatures have an adverse effect on the corrosion of the alloys (Maledi, 2006). Early age gas turbines were developed after the 1940s, and were designed to operate at 700 °C. Improvements in metallurgical processes, blade cooling techniques and application of coatings allowed for increased working temperatures (Eliaz et al., 2002). Coatings made a greater contribution towards increased operating temperatures and protection against environmental degradation (Stringer, 1987; Gurrappa, 2003).

Hot corrosion is one of the serious problems for high temperature application, such as aircraft, marine, utility, industrial and land-base gas turbines, boilers, oil refinery furnace and engines. The use of wide range of fuels from natural gas, kerosene, diesel oils, residual oils and gaseous fuels coupled with increased operating temperatures cause hot corrosion (Nicholls, 2002). Eliaz et al. (2002) have defined the hot corrosion as an accelerated corrosion, resulting from the presence of salt contaminants such as  $\text{Na}_2\text{SO}_4$ ,  $\text{NaCl}$ , and  $\text{V}_2\text{O}_5$  that combine to form molten deposits, which damage the protective surface oxides.

Unacceptable corrosion rates have occurred when biofuel fired boiler has been operated with steam temperature of 530°C (Salmenoja et al., 1996). However, these lower steam



temperatures drastically decrease the efficiency of electricity production. On the other hand, in order to meet the demand for more electricity, the operating temperature and pressure of pulverized coal-fired boilers have to be increased (Blum, 1997). The combination of such high-temperatures with contaminants of environment and low grade fuels necessitate special attentions to the phenomenon of hot corrosion.

Hot corrosion has been observed in boilers, internal combustion engines, gas turbines, fluidized bed combustion and industrial waste incinerators since 1940's. However, it became a topic of importance and popular interest in the late 1960's when gas turbine engines of military aircrafts suffered severe corrosion attacks while operating over and near sea water during the Vietnam conflict (Rapp, 1986 and 2002).

Corrosion occurs when molten compounds ( $\text{Na}_2\text{SO}_4$  melting point  $884^\circ\text{C}$ ) dissolve the protective oxide layers, which naturally form on materials during boiler/gas turbine operation. Moreover, the vanadium compounds are also good oxidation catalysts and allow oxygen and other gases in the combustion atmosphere to diffuse rapidly to the metal surface and cause further oxidation. As soon as the metal is oxidized, the cycle starts over again resulting into high corrosion rates (Natesan, 1976; Sharma, 1996).

In energy generation processes the mechanism of hot corrosion is dependent on the formation of a liquid phase that is predominantly  $\text{Na}_2\text{SO}_4$  or  $\text{K}_2\text{SO}_4$ . The sulphur released from the coal, forms  $\text{SO}_2$  with a minor amount of  $\text{SO}_3$  and reacts with the volatilised alkalis to form  $\text{Na}_2\text{SO}_4$  vapour, which then condenses together with fly ash on the super-heater and reheater tubes in the boiler. Such a liquid phase dissolves the chromium oxide in the protective coating, which allows the base metal to react with sulphate ions to form sulphide ions and non-protective oxides (Natesan, 1976 and Rapp et al, 1981).

Among high temperature alloys, the promising alloys are "superalloys" namely Nickel, Cobalt and Iron based superalloys, which show high temperature mechanical properties and moderate resistance to hot corrosion.

One of the viable solutions, therefore, is to develop alloys with optimum mechanical properties, then to confer resistance to oxidation and hot corrosion using appropriate high temperature coatings. Considerable efforts are now being made to produce high temperature degradation resistant thermal spray coatings process by various means such as vacuum plasma spraying (VPS), chemical vapor deposition (CVD), (Blackwood et al., 2000), low

pressure plasma spray (LPPS) processes (Du et al., 1996; Mobarra et al., 2006), HVOF and D-gun Spraying (Ren and Wang, 2006).

Thermally sprayed  $\text{Cr}_3\text{C}_2\text{-NiCr}$  coatings are used in applications that demand protection against surface degradation due to oxidation, wear and corrosion under severe conditions of excessive heat and load up to  $850\text{ }^\circ\text{C}$  (Staia et al., 2001). Whereas  $\text{NiCoCrAlYT}$ a overlay coatings provide excellent oxidation and corrosion resistance at high temperature, and are potential bond coats for thermal barrier coatings (TBC) on gas turbines and diesel engine components (Lima and Guilemany, 2007). Recently it has been reported that the presence of 0.4%  $\text{CeO}_2$  in  $\text{MCrAlY}$  coating can considerably improve both wear and corrosion resistance (Tian et al., 2006).

Investigations in the area of inhibitors like  $\text{MgO}$ ,  $\text{CeO}_2$ ,  $\text{CaO}$ ,  $\text{MnO}_2$ , etc. have already been done and the decrease in the extent of hot corrosion in the most aggressive environment of  $\text{Na}_2\text{SO}_4\text{-60}\%\text{V}_2\text{O}_5$  at  $900\text{ }^\circ\text{C}$  has been achieved. However the major problem being faced is how to inject these inhibitors along with the fuel in the combustion chamber in actual industrial environment (Tiwari and Prakash, 1998 and Gitanjaly et al, 2002).

Abrasion and corrosion resistance of components can be greatly increased by protective coatings and this is a growing industry of considerable economic importance. Coatings are used in both aqueous and high temperature applications such as diesel and gas turbine engines. Coal gasification electric power generation and waste incineration involves severe conditions and therefore thick coatings have been proved effective (Hocking, 1993).

Better understanding of the degradation and failure mechanisms of high-temperature coatings in the field need to be achieved, particularly with respect to the effects of engine operation and environment on the coating performance (e.g., thermal cycling) (National Materials Advisory Board, 1996).

Detonation-Gun is capable of producing the highest pressure, velocity, and density in the gas flow, which is not achievable by all other spraying techniques. As a result, the detonation coatings are characterized by extremely high density, low oxide content, high bond strength, high impact velocity and low porosity, which are suitable for applications requiring very high standards, such as aircraft engine components (Saravanan et al., 2000; Murthy et al., 2006).

D-gun coating is a new technology ejecting the melting or semi-melting state powder heated by the combustion of acetylene and oxygen to the surface of working piece (Hao Du

et al., 2007; Jia et al, 1999) at a high speed 800–1200 m/s (Semenov et al., 2002; Wu et al., 2003).

D-gun sprayed coatings have relatively higher bond strength than the plasma sprayed coating owing to the higher kinetic energy of the powder particles. Also, the density of D-gun sprayed coatings is significantly higher than that of plasma sprayed coatings. D-gun sprayed coatings are usually much harder and stronger than plasma sprayed coatings due to higher density and cohesive strength (Rajasekaran et al., 2008). Furthermore as compared to other thermal spraying process the impact velocity of D-gun type spraying is at least 2–3 times larger resulting in smaller splat thicknesses (Venkataraman et al., 2006).

Good mechanical performance of D-gun coating is determined mainly by the effect of mechanical interlocking between flattened particles. This may take place more effectively owing to the micro-rough features of the splat surface. In addition, a high particle velocity assist for better interlocking of flattened particles (Li and Ohmori, 1996)

In the present investigation, D-gun sprayed  $\text{Cr}_3\text{C}_2\text{-NiCr}$ ,  $\text{NiCrAlY+0.4wt\%CeO}_2$  and  $\text{NiCoCrAlYTaNi}$  alloys on Ni- and Fe-based superalloys have been selected to evaluate their oxidation and hot corrosion behaviour in the laboratory as well as in the actual coal fired boiler environments, for application of these coatings on the hot section components of turbine engines.

# CHAPTER 2

## LITERATURE REVIEW

---

*This chapter deals with a comprehensive review of the literature with reference to oxidation, hot corrosion of nickel- and iron-based superalloys in different molten salt and boiler environments. D-gun process has been described in detail. The problem has been formulated after critical analysis of the literature towards the end of this chapter.*

### 2.1 HIGH TEMPERATURE OXIDATION

Oxidation is an environmental phenomenon in which metals and alloys (and other materials) exposed to oxygen or oxygen-containing gases at elevated temperatures convert some or all of the metallic elements to their oxides. The oxide can form as a protective scale if it remains adherent, and reduces further oxidation, or may continually spall off, exposing fresh metal. The latter case results in progressive metal loss. Additionally, internal oxidation may also occur. The technological implications of oxidation lie in the loss of load-bearing capability of the original metal or alloy component, eventually resulting in component failure. Resistance to oxidation at high temperatures is a requisite for superalloys whether used in the coated or uncoated conditions. Therefore, a better understanding of the superalloy oxidation and how it is influenced by the alloy characteristics and exposure conditions are essential for effective design and application of superalloys.

#### 2.1.1 Fundamentals of oxidation

Oxide products have also been found to be more effective in limiting further reaction between the metal or alloy and the high temperature gaseous environment than nitrides and sulfides (Pettit, 1969). Pure chromium and alloys of Fe, Co, and Ni containing significant amounts of chromium form  $\text{Cr}_2\text{O}_3$  scales on oxidation at elevated temperatures. At the lower temperatures in this range, which in practice means below 1200 °C or so, the rate of thickening of the scale, or the overall weight gain of the specimen, effectively follows a parabolic rate law :

$$w^2 \text{ (or } x^2) = k_p t \quad (2.1)$$

However, at higher temperatures, or at very long times, deviations from this become apparent. Eventually, the weight of the specimen reaches a maximum and starts to diminish, the rate of weight loss tending asymptotically to a constant value (linear rate law) and the scale thickness also approaching a constant value asymptotically. This is due to the oxidation of the  $\text{Cr}_2\text{O}_3$  to the volatile species  $\text{CrO}_3$  (Stringer 1972).

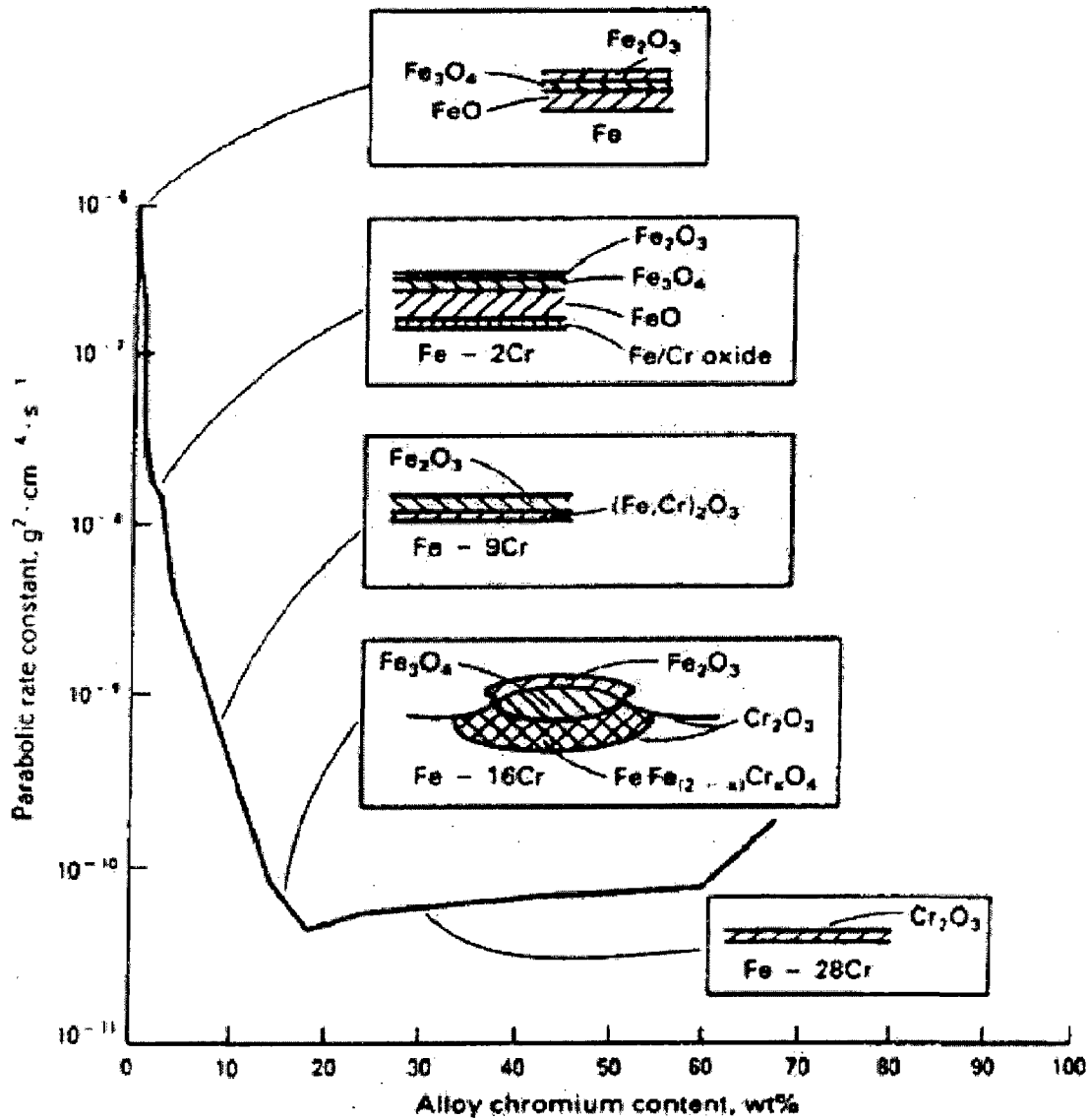


Fig. 2.1 Schematic showing the effect of chromium in Fe-Cr alloys on oxidation rate and oxide scale structure based on isothermal oxidation studies at  $1000^\circ\text{C}$  (Wright, 1987)

Most metals and alloys react with oxygen to oxidise to some extent in gaseous atmospheres. Oxides are generally more thermodynamically stable than reaction products from these species (like N and S) which may be present in the environment. It is therefore common for oxides to form at gas-metal interface (Pettit, 1977).

According to Wright (1987) the development of oxidation resistance of alloys is based on the addition of an element, usually chromium, aluminum or silicon, which will oxidize selectively and produce a protective surface oxide. He has explained the effect of chromium in Fe-Cr alloys on oxidation rate and oxide scale structure based on isothermal oxidation studies at 1000 °C. This has been shown schematically in Fig. 2.1.

### 2.1.2 Formation of protective scale

Thermodynamically, an oxide is likely to form on a metal surface when the oxygen potential in the environment is greater than the oxygen partial pressure in equilibrium with the oxide (Kofstad, 1966). However, according to Kofstad (1966), initially, the metal-oxygen reaction involves the adsorption of gas on the metal surface. As the reaction proceeds, oxygen may dissolve in the metal, resulting in the formation of oxide on the surface either as a film or as separate oxide nuclei, the surface oxide then separates the metal and the gas. When a compact film covers the surface, the reaction may proceed only through a solid-state diffusion of the reactants through the film. For thin films, the driving force for this transport of reactants may be due to the electric fields in or across the film, whereas for thick film or scales it is determined by the chemical potential gradient across the scale. Metals may also form porous oxide scales, which as such do not serve as a solid-state diffusion barrier between the reactants. In such cases, the reaction may be limited by processes occurring at phase boundaries. Further, at high temperatures, the oxide may also be liquid or volatile (Kofstad, 1966).

Chattopadhyay and Wood (1970) illustrated the transient oxidation of a Ni-Al alloy (Fig.2.2a) where  $Al_2O_3$  becomes the steady-state scale; the possible oxides are NiO (doped with  $Al^{3+}$  ions),  $NiAl_2O_4$  and the thermodynamically favoured oxide,  $Al_2O_3$ . Both NiO and  $Al_2O_3$  develop but the NiO nuclei tend to overgrow and undercut the  $Al_2O_3$  because the NiO is the faster-growing oxide. However, for aluminium-rich alloys,  $Al_2O_3$  soon attempts to establish itself as a complete layer at the scale base by direct entry into the scale, in principle at least by

reduction of initially formed NiO and, particularly, by producing a sufficient population density of  $\text{Al}_2\text{O}_3$  internal oxide particles that they impinge to produce a full layer which then continues to thicken alone. The NiO residues are left outside the completed steady-state  $\text{Al}_2\text{O}_3$  scale. For alloys containing insufficient aluminium to establish an  $\text{Al}_2\text{O}_3$  scale, internal  $\text{Al}_2\text{O}_3$  precipitates continue to propagate into the alloy and the steady-state scale is essentially NiO into which  $\text{Al}_2\text{O}_3$  is incorporated and converted into  $\text{NiAl}_2\text{O}_4$  when the NiO scale encroaches on the subscale in the internal-oxidation zone (Fig.2.2b).

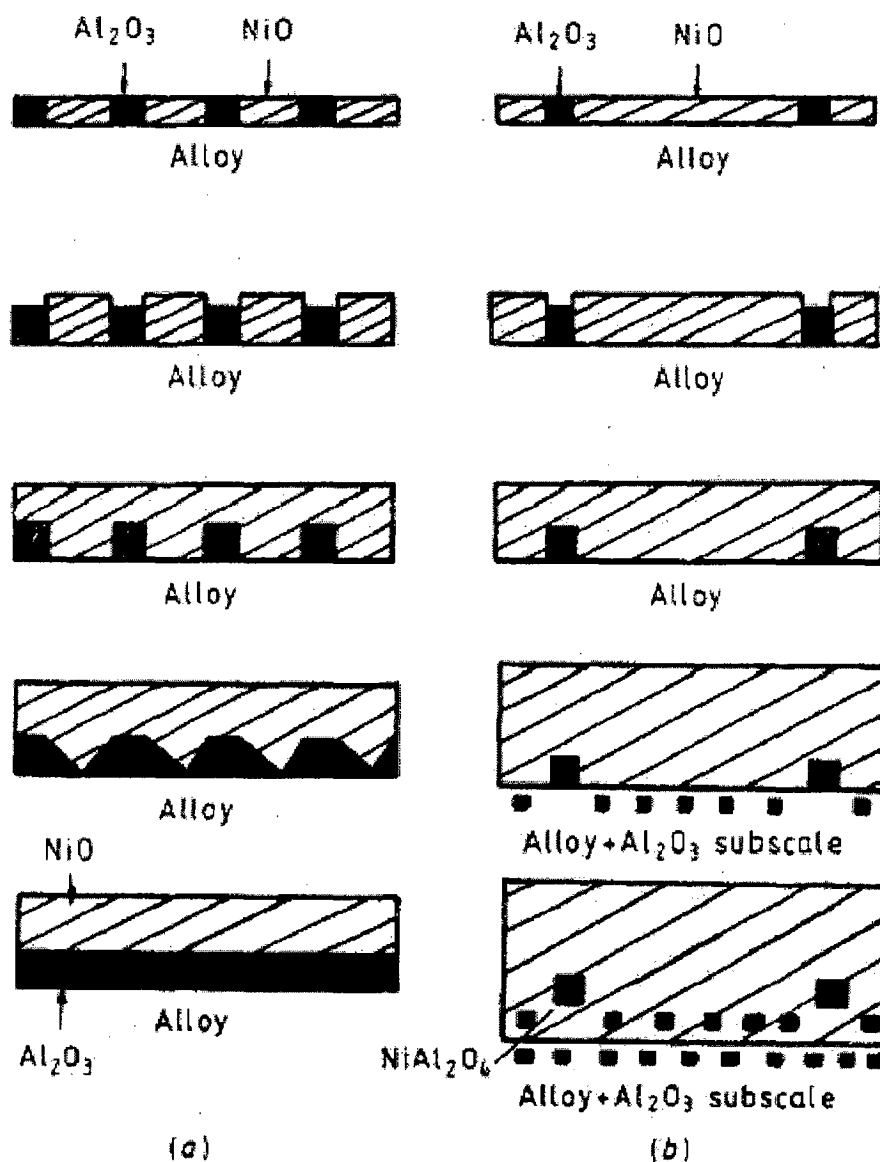


**Fig. 2.2** Schematic representation of the transient oxidation of Ni-Al alloys (a) containing sufficient aluminium to establish an  $\text{Al}_2\text{O}_3$  scale, (b) containing insufficient aluminium to establish an  $\text{Al}_2\text{O}_3$  scale, showing the progressive development of the scale in each case (Chattopadhyay and Wood 1970).

Whittle (1983) explained the typical oxidation process of binary alloy where the oxides of both A and B are stable in the gas but BO is more stable than AO (in superalloys, A generally represents Ni or Co and B represents Cr, Al etc) as shown in Fig. 2.3. Thus, the alloying element B, which forms a very stable and slow growing oxide, is added in the superalloy in sufficient quantity to form a protective surface layer by selective oxidation. The selective oxidation process is very important because it allows the most thermodynamically stable oxide to cover the entire alloy surface. It is the primary method used to develop oxidation resistance on the structural alloys presently in use.

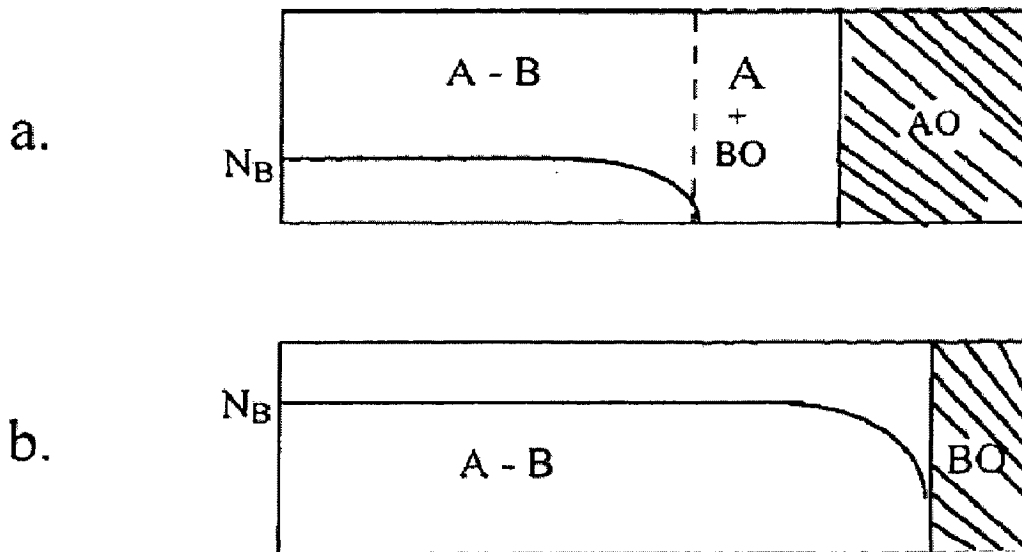


**Fig. 2.3** Schematic cross sections of an A-B alloy where both components form stable oxides but BO is more stable than AO. (a) Alloy dilute in B showing internal oxidation of B under an external layer of AO. (b) Alloy concentrated in B showing continuous external BO (Whittle, 1983)

The formation of a stable and slowly growing protective oxide scale such as  $Al_2O_3$ ,  $Cr_2O_3$ , or  $SiO_2$  is essential for alloys used at high temperatures. However, the protective  $Al_2O_3$  scales formed at high temperatures may be prone to crack and spall during thermal cycling. Therefore, a suitable technique to enhance adhesion of  $Al_2O_3$  scales, so that alloys and coatings can resist high temperatures, has become a major focus of high-temperature materials research. To date, the most successful technique has been to add a small amount of reactive elements such as Y, Ce, Hf, etc., or their oxides to the alloy (Wang 1997).



The development of oxidation resistance in alloys is based on the addition of an element, usually chromium, aluminum or silicon, which will oxidize selectively and produce a protective surface oxide (Sibi, 2003; Kai, 1998). Therefore, the factors which influence the development of the protective oxide and those which can render it non-protective are of prime importance.

Haugsrud (2003) has reported the oxidation properties of nickel. According to him, nickel above 1100 °C, oxidizes and follows a parabolic rate law and the oxidation rate is governed by the outward lattice diffusion of Ni via either singly or doubly charged Ni vacancies. The dominating outward growth was observed and with decrease in temperature, the oxidation mechanism of Ni was found to be more complex as reported in their work.

Li et al (2003A) have opined that although considerable insight has been accumulated on mechanisms of high temperature oxidation, from both engineering and more fundamental studies, reaction mechanisms are often not fully understood. They further stated that the degradation by oxidation is one of the main failure modes of hot-section components in the gas turbines, so an understanding of the oxidation phenomenon is very necessary, particularly for the superalloys (Li et al, 2003A). Abundance of literature is available on the high temperature oxidation of metals and alloys, which is difficult to review in a sensible manner in such a short space. As an alternative, it is proposed to overview the high temperature phenomenon in context with some current studies conducted by various researchers in the field, which may form a basis for the formulation the problem.

According to Dieter (2007), the study of the oxidation behaviour of binary alloys AB highlights the most important oxidation mechanisms of multi-component alloys. The two components of a binary alloy in general do not have the same affinity for oxygen and therefore do not oxidise at the same rate. Two distinct types of behaviour are observed: (i) if the affinity for oxygen of A is much greater than that of B, A will undergo selective oxidation; (ii) if A and B have comparable affinities for oxygen, they undergo simultaneous oxidation. The alloy oxidation mechanism has been depicted in Fig 2.4.

### **2.1.3 Breakdown of protective scales**

The formation of a protective scale on an alloy by selective oxidation necessarily depletes the scale-forming element from the underlying alloy. The depletion must eventually result in the protective scale becoming un-stable; degradation of high-temperature alloys is generally more

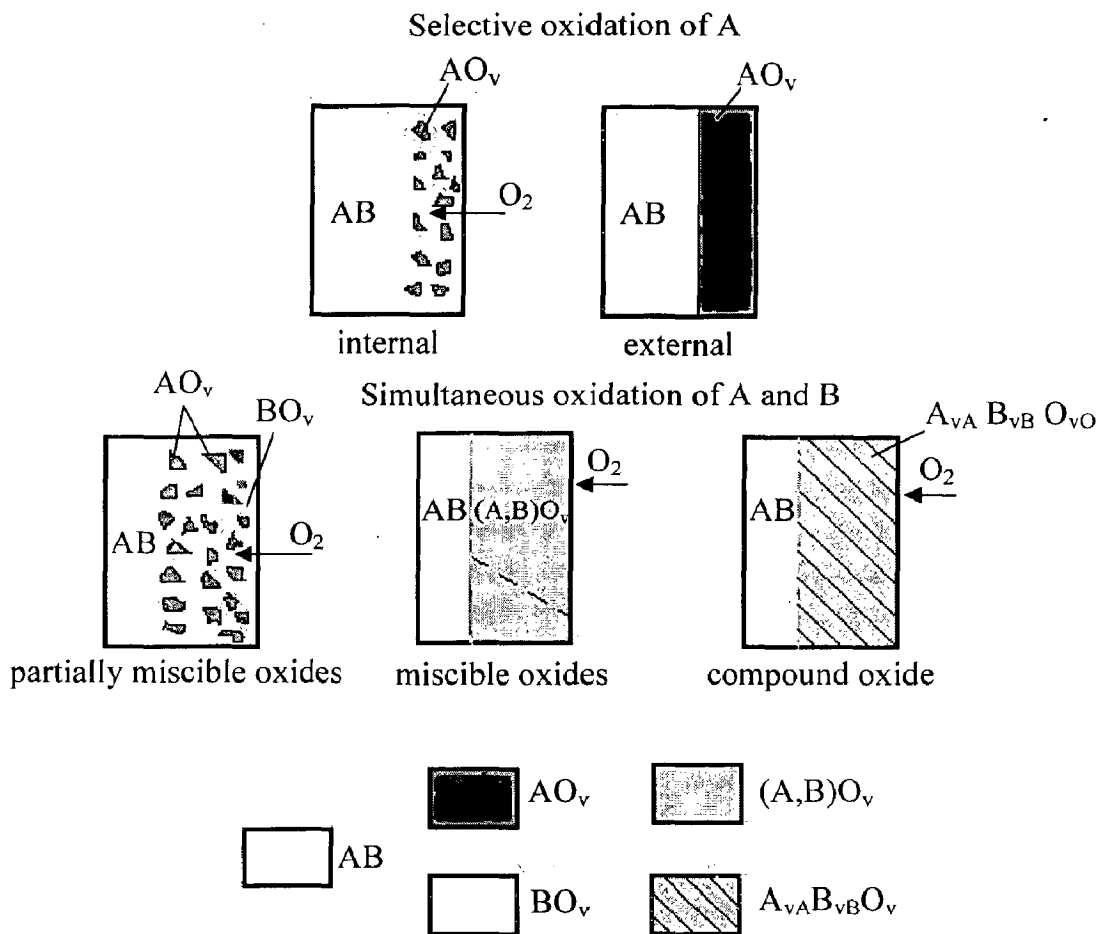


**Fig. 2.4** Alloy oxidation mechanisms, with the corresponding morphologies of the oxide layers (Dieter, 2007).

rapid under thermal cycling conditions because of cracking and spalling of the protective oxide scale. The cause is stress generation arising from thermal expansion mismatch between the scale and alloy (thermal stresses) which may be superposed on stresses generated by scale growth (growth stresses) (Meier, 1989). The breakdown of chromia and alumina in high sulfur pressure atmospheres is associated with the development of sulfide channels through the scales Stott et al. (1985).

## 2.2 OXIDATION OF SUPERALLOYS

Giggins and Pettit, (1971) reported the oxidation mechanism of Ni-Cr-Al alloys in Fig. 2.5, the results obtained by them are as follows. In the beginning, for any alloys, the rapid uptake of oxygen, converts the surface layer of the alloy into an oxide, as illustrated in Fig.2.5 (a), this layer is predominantly Ni (Cr, Al)<sub>2</sub>O<sub>4</sub> and NiO. However, the exact composition of this layer

varies with starting composition of the alloy, a significant amount of  $\text{Cr}_2\text{O}_3$ ,  $\text{Al}_2\text{O}_3$  would be present on alloy surface with sufficiently high Cr or Al contents. As the reaction continues, diffusional processes in the alloys begin to affect the oxidation reaction. Since the oxygen activity required to oxidise Cr and Al in the alloy is less than that established over the alloy by NiO or spinel in the external oxide scale, it moves in to the alloy and precipitate  $\text{Cr}_2\text{O}_3$  and  $\text{Al}_2\text{O}_3$  (Fig.2.5b). The activity of oxygen required to oxidise the Al in the alloy is smaller than that required for oxidising of the Cr. Thus, the particles of  $\text{Al}_2\text{O}_3$  extended deeper in to the alloy than the particles of  $\text{Cr}_2\text{O}_3$ . The diffusion of Cr and Al from the interior of the alloy results in the precipitation of additional  $\text{Cr}_2\text{O}_3$  and  $\text{Al}_2\text{O}_3$  in the subscale zone, afterwards a continuous layer of  $\text{Cr}_2\text{O}_3$  or  $\text{Al}_2\text{O}_3$  scales are formed beneath the external oxide layer (Fig.2.5c). The formation of continuous, duplex layer of oxide further reduces the flux of the oxygen in to the alloy since it establishes a low oxygen activity over the alloy. For the  $\text{Cr}_2\text{O}_3$  -former alloys (Group I), the flux of oxygen from the duplex scale in to the alloy is still sufficient to oxidise the Al internally but not the Cr, therefore Cr diffuses from the alloy through the duplex scale to form  $\text{Cr}_2\text{O}_3$  above the duplex scale (Fig.2.5d). In the case of the  $\text{Al}_2\text{O}_3$  -former alloys (Group II), the volume fraction of precipitated  $\text{Al}_2\text{O}_3$  is sufficient to form a continuous layer beneath the duplex zone as shown in Fig.2.5e. Steady state conditions are reached when the  $\text{Cr}_2\text{O}_3$  and  $\text{Al}_2\text{O}_3$  layer becomes continuous and the oxidation reaction is controlled by transport through the  $\text{Al}_2\text{O}_3$  scale (Giggins and Pettit, 1971).

Superalloys are now widely used in a variety of applications at temperatures ranging from 923 to 1373 K in aggressive atmospheres such as the combustion products of fuel and air, high temperature catalytic reactors etc. (Jena, 1984). In order to function satisfactorily in such a severe environment, superalloys must possess properties such as outstanding high temperature strength, creep and fatigue resistance, excellent ductility, good impact resistance and adequate resistance to hot-corrosion (Jena, 1984).

Superalloys are used extensively in oxidizing environments; for example, as disks in turbine engines. The superalloys have been developed to achieve oxidation resistance by utilising the concept of selective oxidation. The selective oxidation approach to obtain oxidation resistance in superalloys consists of oxidising essentially only one element in the superalloy and

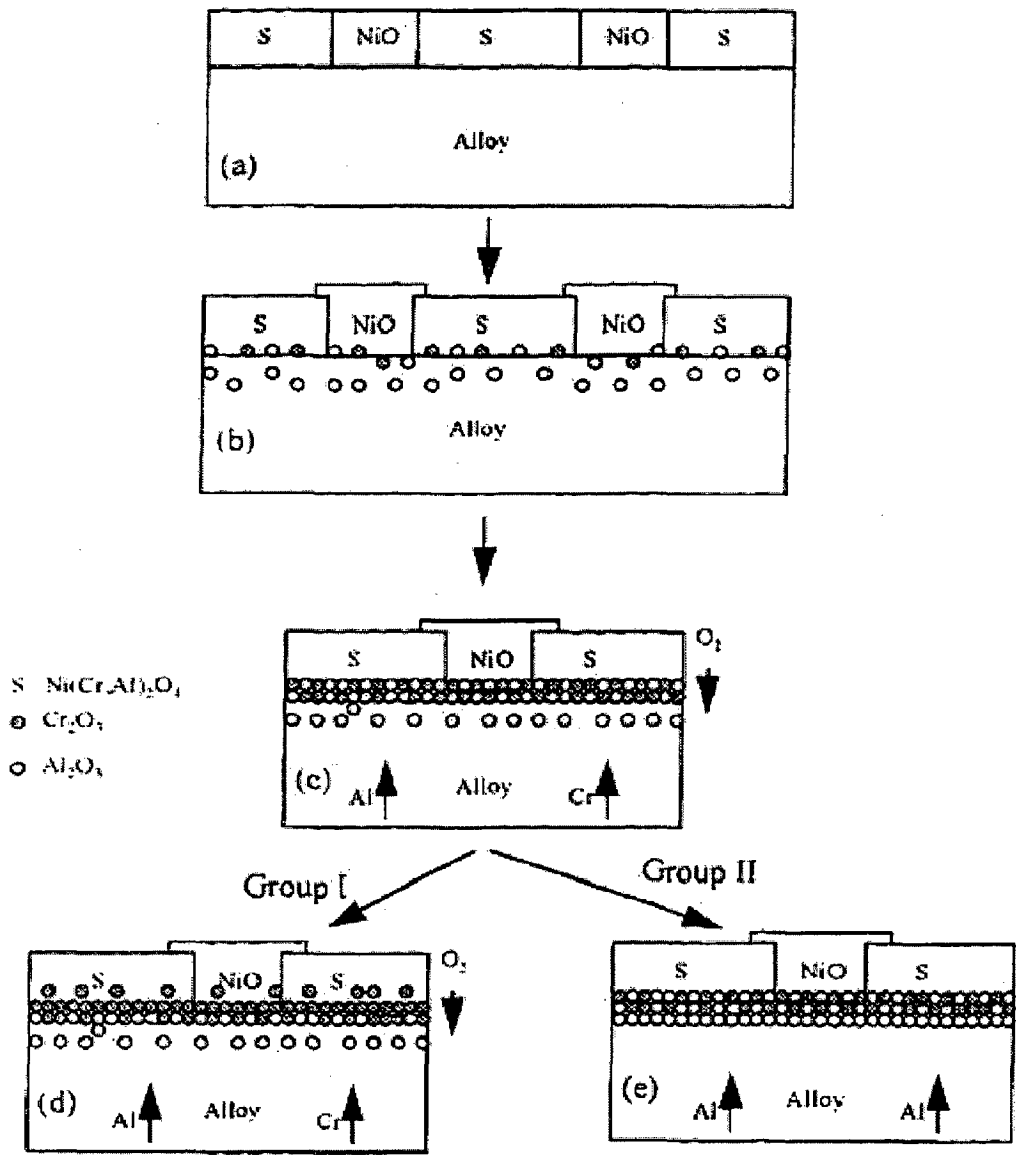


**Fig.2.5** Schematic diagram illustrating the oxidation mechanisms for Ni-Cr-Al alloys (Giggins, et al., 1971)

relying upon this element's oxide for protection. For effective protection, it is anticipated that the oxide should cover the whole surface of the alloy and it must be an oxide through which the diffusion of the reactants takes place at comparatively slow rate. Nickel-, cobalt- and iron-base superalloys make use of the selective oxidation of the aluminium or chromium to develop oxidation resistance (Pettit and Meier, 1985). Further, Pettit and Meier (1985) have reported that the selective oxidation processes are affected by a number of factors such as alloy composition,

alloy surface conditions, gas environment and cracking of the oxide scale. Cyclic oxidation conditions whereby the oxide scales crack and spall, as well as certain phases present in the superalloys, both affect the capability to selectively oxidise aluminium or chromium in the superalloys. For example, Co- and Fe-based superalloys cannot be made to contain enough aluminium to permit them to be alumina formers as it will have detrimental effect on their mechanical properties. Therefore, the Co- and Fe-base superalloys have to rely on the chromia scales for oxidation resistance. Consequently the oxidation resistance of Co- and Fe-base superalloys is inferior to that of Ni-base superalloys. Furthermore, even when considering the Ni-base superalloys that are chromia formers, as degradation begins i.e. the chromia scales are damaged, the less protective oxides formed on the Ni-base alloys contain significant amount of nickel oxide as compared to cobalt and iron oxides on the cobalt and iron-base superalloys, respectively. Since nickel oxides are more protective than cobalt and iron oxides, the oxidation resistance drop-off is more abrupt in the case of the Co- and Fe-base superalloys. Further, the oxidation resistance of the Co- and Fe-base superalloys usually increases with the chromium concentrations and the oxidation resistance of the alloys with less than about 20% chromium is comparatively poor (Pettit and Meier, 1985).

The superalloys exhibit outstanding strength and surface stability at temperature up to 85% of their melting points. Usually the superalloys are used at temperatures above 540 °C (Metal Handbook, 1990). However, compared with steels, corrosion resistance of the superalloys is relatively less known (Smith et al., 1999; Castello et al. 2000). The superalloys are broadly classified as nickel-, cobalt- and iron-based alloys.

### **2.2.1 Oxidation of Nickel and Nickel-Based Alloys**

Pettit and Meier (1985) opined that during isothermal oxidation of Ni-base superalloys,  $\text{Cr}_2\text{O}_3$  and  $\text{Al}_2\text{O}_3$  scales are expected to be formed. Whereas, under cyclic conditions, depletion of chromium and aluminium leads to the formation of NiO scale, some alloys move toward the NiO scale formation much more rapidly than others. They further concluded that the application of aluminide coatings to two nickel based superalloys B-1900 and Mar M200 makes them remain in alumina scale formation range for even longer times than obtained for the uncoated. The time

over which nickel base superalloys can maintain protective, external scales of alumina or chromia is affected by temperature, the gas environment and alloy composition.

Superalloys contains a number of significant alloying elements in addition to Cr and Al, including Mn, Ti, Si, and the refractory elements, Mo, W, Ta, Zr, and Hf. In many cases, these elements exert significant influence on the oxidation resistance of  $\text{Cr}_2\text{O}_3$  and  $\text{Al}_2\text{O}_3$  forming alloy. Some alloying elements are beneficial and some are deleterious to superalloy oxidation resistance depending upon their amount and working condition. A number of studies have been carried out on the effect of their additions on the oxidation behaviour of different alloys. Smialek et al. (1987) has given an extensive review of this behaviour.

Levy et al (1989) reported studies on the cyclic oxidation resistance of three single-crystal nickel base superalloys and DS Mar M 200 at 1093 °C using a tube furnace and burner rig. The same ranking of the alloys was reported in both tests with the single-crystal superalloys having better oxidation resistance than the directionally solidified alloy DS Mar M 200. They further opined that tube furnace tests can be used in place of burner-rig tests to rank alloys. Oxidation tests at 900°C using the tube furnace produced a ranking of the alloys consistent with the 1093 °C results.

The effects of thin surface applied  $\text{Y}_2\text{O}_3$ ,  $\text{Al}_2\text{O}_3$  and  $\text{Cr}_2\text{O}_3$  coatings or films on the selective oxidation of chromium for Ni-15Cr and Ni-10Cr alloys in air at 1000°C have been studied by Yedong and Stott (1994). The oxide films were deposited by an electrochemical method. They observed the establishment of chromia scale which was promoted effectively by the presence of an  $\text{Y}_2\text{O}_3$  film on Ni-15Cr and at least locally on Ni-10Cr. In comparison with the cases of surface deposited  $\text{Al}_2\text{O}_3$  and  $\text{Cr}_2\text{O}_3$  oxide films, the additional beneficial effect of the  $\text{Y}_2\text{O}_3$  film in maintaining the selective oxidation of chromium reportedly attributed to its ability to improve the mechanical integrity and adhesion of the chromium scale.

Whereas from the mass-gain measurements, Greene and Finfrock (2001) identified three regimes of oxidation for Inconel 718, a low-temperature regime in which the alloy behaved as if passivated after an initial period of transient oxidation, an intermediate-temperature regime in which the rate of oxidation was limited by diffusion and exhibited a constant parabolic rate dependence, and a high-temperature regime in which material deformation and damage accompanied an accelerated oxidation rate above the parabolic regime.

Blackwood et al. (2001) investigated the two types of nickel coatings on the surface of Nd<sub>2</sub>Fe<sub>14</sub>B substrates, The corrosion characteristics of both coatings were evaluated both by electrochemical potentiodynamic polarisation and by physical exposure to high-humidity environments. The results showed that both coatings enhanced the corrosion resistance of substrate. Studies of the protective alumina scales which formed on NiCrAlY-alloys after isothermal oxidation in the temperature range of 950-1100<sup>0</sup>C with Si addition showed that the Si additions upto 2 mass% have only a minor effect on the scale growth of Ni-20Cr-10Al-Y (Nickel et al, 2002). Similarly they concluded that the small additions of Ti (around 0.4 mass-%) can improve the scale adherence.

The oxidation behaviour of a single-crystal Ni-base superalloy has been studied using discontinuous thermogravimetric analysis and prolonged exposure in air at 800 and 900<sup>0</sup>C by Li et al (2003A), and over the temperature range from 1000–1150<sup>0</sup>C by Li et al (2003B). They observed that the mass gain at 900<sup>0</sup>C was lower than that at 800<sup>0</sup>C due to the formation of a protective inner  $\alpha$ -Al<sub>2</sub>O<sub>3</sub> layer at 900<sup>0</sup>C. The scale formed at 900<sup>0</sup>C was found to be more uniform than that formed at 800<sup>0</sup>C, which consisted of several layers: an NiO outer layer, spinel-rich sub-layer, a CrTaO<sub>4</sub>-rich layer and an  $\alpha$ -Al<sub>2</sub>O<sub>3</sub> inner layer. Whereas in the temperature range of 1000–1150<sup>0</sup>C, the outer NiO layer was observed to be replaced by an outer layer of spinel, a sub-layer of mainly  $\alpha$ -Al<sub>2</sub>O<sub>3</sub>, with unchanged composition of inner layers of the scale. Further, no internal oxides or nitrides were observed below the inner  $\alpha$ -Al<sub>2</sub>O<sub>3</sub> layer after 1000 hours at 1000<sup>0</sup>C, and after 200 hours at 1100 and 1150<sup>0</sup>C.

Li et al., (2003C) studied the oxidation kinetics and oxidation layer of a cast Ni-base superalloy K35 at 800<sup>0</sup>C by still TGA method. The results showed that oxidation kinetics of the superalloy obeyed the parabolic law. They further observed that oxidation rate of the superalloy was dependent on the growth dynamics of Cr<sub>2</sub>O<sub>3</sub>. Moreover, the oxide layer was found to be thin and, consisted of Cr<sub>2</sub>O<sub>3</sub> mainly with a bit of NiCr<sub>2</sub>O<sub>4</sub> and TiO.TiO<sub>2</sub>. Internal oxidation of the alloy was also observed.

Zhao et al (2005A) investigated the oxidation behaviour of a new nickel-based superalloy in air at 950<sup>0</sup>C and 1000<sup>0</sup>C for 140 hours and reported that the alloy obeyed the parabolic rate law at 950<sup>0</sup>C, whereas small deviations were observed at 1000<sup>0</sup>C. No oxide spallation was observed at 950<sup>0</sup>C, while minor spallation was seen at 1000<sup>0</sup>C. The oxide scale was found to be consisted

of  $\text{Cr}_2\text{O}_3$ ,  $(\text{Ni}, \text{Co}) \text{Cr}_2\text{O}_4$ ,  $\text{TiO}_2$ ,  $\text{SiO}_2$ ,  $\text{TiO}_2$  and  $\text{Al}_2\text{O}_3$ . Internal oxidation of the superalloy was also indicated at both the temperatures of the investigation.

Singh et al., (2006) has conducted high temperature oxidation behaviour of plasma sprayed  $\text{Ni}_3\text{Al}$  coatings on superalloys 600, 601 and 718 and, one Fe-base superalloy, Inconel 800H in air at  $900^\circ\text{C}$  under cyclic conditions for 50 cycles.  $\text{Ni}_3\text{Al}$  coating was found to be successful in maintaining its adherence to the superalloy substrates, oxide scales were also found to be intact and spallation-free in all the cases. The probable oxidation mode for  $\text{Ni}_3\text{Al}$  coated superalloy 601, have been schematically shown in Fig. 2.6.

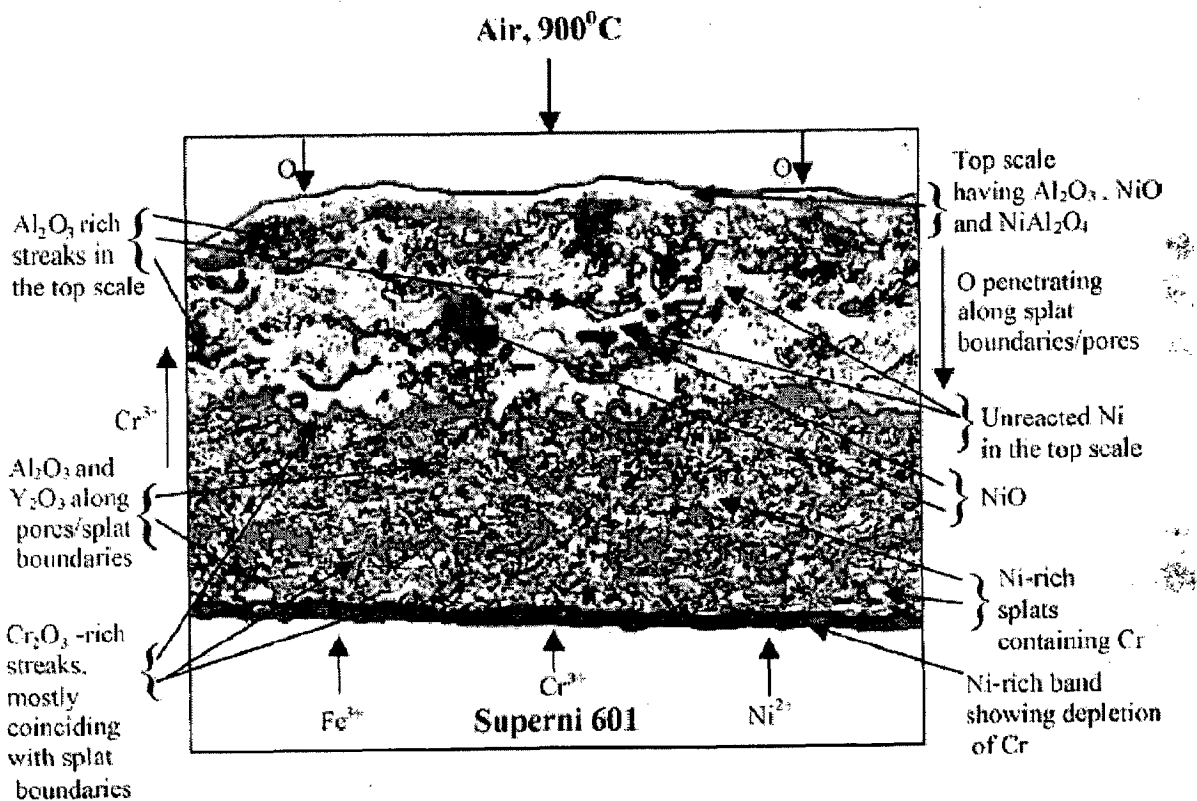


**Fig.2.6** Schematic diagram showing probable oxidation mode for the  $\text{Ni}_3\text{Al}$  coated superalloy 601 exposed to air at  $900^\circ\text{C}$  for 50 cycles (Singh et al., 2006).

## 2.2.2 Oxidation of Iron and Iron-Based Alloys

Hussain et al. (1994) shown the comparison of the oxidation kinetics of four commercial heat-resisting alloys namely Hastelloy C-4, SS 304L, Incoloy 800H and Incoloy 825 in air from  $600$  to  $1200^\circ\text{C}$ . Hastelloy C-4 was found to be the most resistant to oxidation for temperatures upto  $1000^\circ\text{C}$  following a cubic-rate law SS 304L was reported to be oxidised in the form of



stratified nodules of two distinct layers, which grow in opposite directions at the metal-oxide interface irrespective of time and temperature of oxidation. Incoloy 800H and Incoloy 825 showed similar kinetics, following parabolic-rate law at 1000 °C and 1200 °C. They also observed the deleterious effect of Mo on the oxidation resistance of Incoloy 825.

Khalid et al (1999) conducted similar studies for comparison of high temperature oxidation behaviour of Incoloy 800H and Incoloy 825 at 1000 and 1200 °C. Incoloy 800H exhibited compact, dense and adherent oxide layer, whereas the Incoloy 825 decomposed completely into the oxide. They attributed the comparatively less oxidation resistance of the Incoloy 825 to the presence of coarse Ti-rich inclusions, which showed less dissolution of Ti in the alloy.

Sadique et al (2000) showed that aluminium additions have marked effects on the oxidation characteristics of Fe-10Cr at all temperatures. They observed reduction in rate of oxidation in terms of specific weight gain with increasing aluminium content. The amount of spallation of the oxide scale was also found to decrease with increasing Al content. Al content was shown to help in enhancing the adhesion of Cr<sub>2</sub>O<sub>3</sub>. Failure of the protective scale was inhibited either through the immediate reformation of an external protective scale or through the internal oxidation and subsequent formation of a sub-scale layer. It was concluded that a minimum level of aluminium exists for the formation of a complete protective scale on the alloy surface depending upon the temperature.

Haugrud (2001) reviewed some studies on the oxidation of binary alloys, A-B, such as those based on Fe, Co, Ni or Cu and containing 0-30% of a higher valent, less noble metal, B. He reported that the oxidation essentially follows parabolic kinetics and the rate constant reaches a maximum with additions of B around 5-10%. The oxygen pressure and temperature dependencies of the parabolic rate constants are stronger than for the unalloyed metal, A. He further suggested that the oxide scale morphology for the binary alloys is considerably more complex than for unalloyed A and the oxide usually comprises an outer region consisting of AO and an inner two-phase region containing dispersed BO-particles and pores in a matrix of AO.

Sidhu (2003) carried out high temperature oxidation studies on the GrA1, T11 and T22 boiler steels in air at 900<sup>0</sup>C. He observed that the Mo containing T22 steel showed least oxidation resistance. He attributed this to the formation of a low melting point MoO<sub>3</sub> phase. This low melting point phase (795<sup>0</sup>C) was reported to cause the disruption and dissolution of the

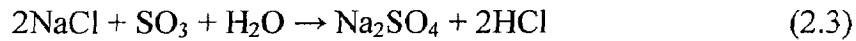
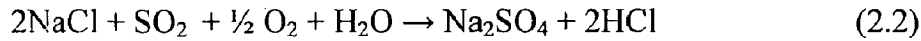
protective oxide scale, resulting in accelerated oxidation of the steel. Some other oxidation studies which may be relevant to the present work are summarised in Appendix A1.

## 2.3 HOT CORROSION

The first technical publication on hot corrosion was reported by Simons et al. (1955); he suggested that hot corrosion is an electrochemical process in which the molten salt acts as an electrolyte. Seybolt (1968) attributed  $\text{Na}_2\text{SO}_4$  induced hot corrosion of Ni–Cr alloys to accelerated oxidation of the Cr-depleted alloy following preferential internal sulfidation of Cr. Bornstein and DeCrescente (1969) reported that accelerated kinetics were not observed during the oxidation of three different presulfidised superalloys and proposed a hot corrosion mechanism based on the (basic) dissolution of the protective oxide scale by a reaction involving  $\text{Na}_2\text{O}$ , the basic minority component of the fused salt. Goebel and Pettit (1970A) and Goebel et al. (1973) extended this mechanism to include acidic fluxing and oxide reprecipitation to account for the catastrophic oxidation caused by  $\text{Na}_2\text{SO}_4$  for alloys containing strong acidic components, such as V or Mo. These mechanisms are still accepted today, and some quantitative aspects of oxide solubility and electrochemical reaction steps have been added in the literature. Accelerated corrosion can also be caused by other salts, viz. vanadate or sulphates-vanadate mixtures and in the presence of solid or gaseous salts such as chlorides (Bornstein et al., 1973). However, turbine manufacturers and users became aware of hot corrosion in late 1960's, (Stringer, 1977) have conducted experimental as well as field tests to identify the nature of attack and explained its temperature dependence and the corresponding morphologies. Hot corrosion was first associated with  $\text{Na}_2\text{SO}_4$  in mid 1950's (Luthra and shores, 1980). Hot corrosion became a topic of importance and popular interest in the late 1960s when gas turbine engines in military aircraft suffered severe corrosion during the Vietnam conflict while operating over sea water (Rapp, 1986). When metals are heated in the temperature range 700–900 °C, sulphates deposits are formed as a result of the reaction between sodium chloride and sulphur compounds in the gas phase surrounding the metals (Hancock, 1987).

According to Shih et al. (1989) metals and alloys often experience an accelerated oxidation in high-temperature gas environments when covered with a thin layer of molten salt deposit, usually alkali sulphates. This type of oxidation is commonly called hot corrosion.

Hot corrosion is a degradation of metals and /or an alloy owing to the oxidation processes which are affected by liquid salt deposits, predominantly Na<sub>2</sub>SO<sub>4</sub>. The primary source of Na<sub>2</sub>SO<sub>4</sub>, in marine and aircraft engines, is due to reaction between NaCl in ingested air and sulfur in fuel according to the following reactions (Khajavi, 2004)



To protect the turbine engines from the high temperature corrosion attack facilitated by impurities, thermal sprayed coatings are to be deposited over the hot section components of turbine engines and boiler tubes. The thermal sprayed coatings consist of oxides and voids originating from spraying process are found at the splat boundaries, through which the coatings were mainly attacked (Uusitalo et al., 2004).

### 2.3.1 Characteristics of hot corrosion

Goebel, et al., (1973) schematically shown the mechanism of high and low temperature hot corrosion in Fig. 2.7. High temperature hot corrosion (Type-I) is the form of hot corrosion that usually occurs above the melting point of sodium sulfate (884 °C), where the salt is clearly a liquid state. Goebel et al., (1973) extended the fluxing theory to explain the acidic fluxing of protective scale in Cr<sub>2</sub>O<sub>3</sub> and Al<sub>2</sub>O<sub>3</sub> forming alloys which contain Mo, W and V. Fig.2.7a shows that Al<sub>2</sub>O<sub>3</sub> can be fluxed as cationic species attached to the metal surface, which is acidified by refractory metal oxides, such as MoO<sub>3</sub>, WO<sub>3</sub> and V<sub>2</sub>O<sub>5</sub>. Further a continuous layer of Al<sub>2</sub>O<sub>3</sub> forms on the alloy surface by using the oxygen present in the salt. This increases the sulfur activity in the salt, it increases to such an extent that the sulfides of aluminum are formed as particles in the metal substrate. Due to the formation of sulfides of aluminum in the substrate, the key element (Al) for protecting the alloy surface gets depleted in the alloy, once sulfur is removed from the salt, the oxygen activity in the salt increases, the local basicity of salt increases to such an extent that Al<sub>2</sub>O<sub>3</sub> dissolves in the basic salt at the oxide/salt interface and get reprecipitated at the salt/gas interface. This reaction continues until the sodium sulfate remains on the alloy surface and increases the rate of hot corrosion due to fluxing of protective oxide scale. Low temperature hot corrosion (type-II) (Fig. 2.7b) is one of the forms of hot corrosion that occurs below the m.p of Na<sub>2</sub>SO<sub>4</sub>, where the salt is supposed to be a solid. High corrosion rate

during the initial stages were attributed to the rapid sulfation of cobalt oxide or Co (at scale/metal interface) which forms liquid eutectic melt followed by the dissolution and precipitation of cobalt oxide at the gas /salt interface by counter transport of  $\text{Co}^{2+} / \text{Co}^{3+}$  ions during the

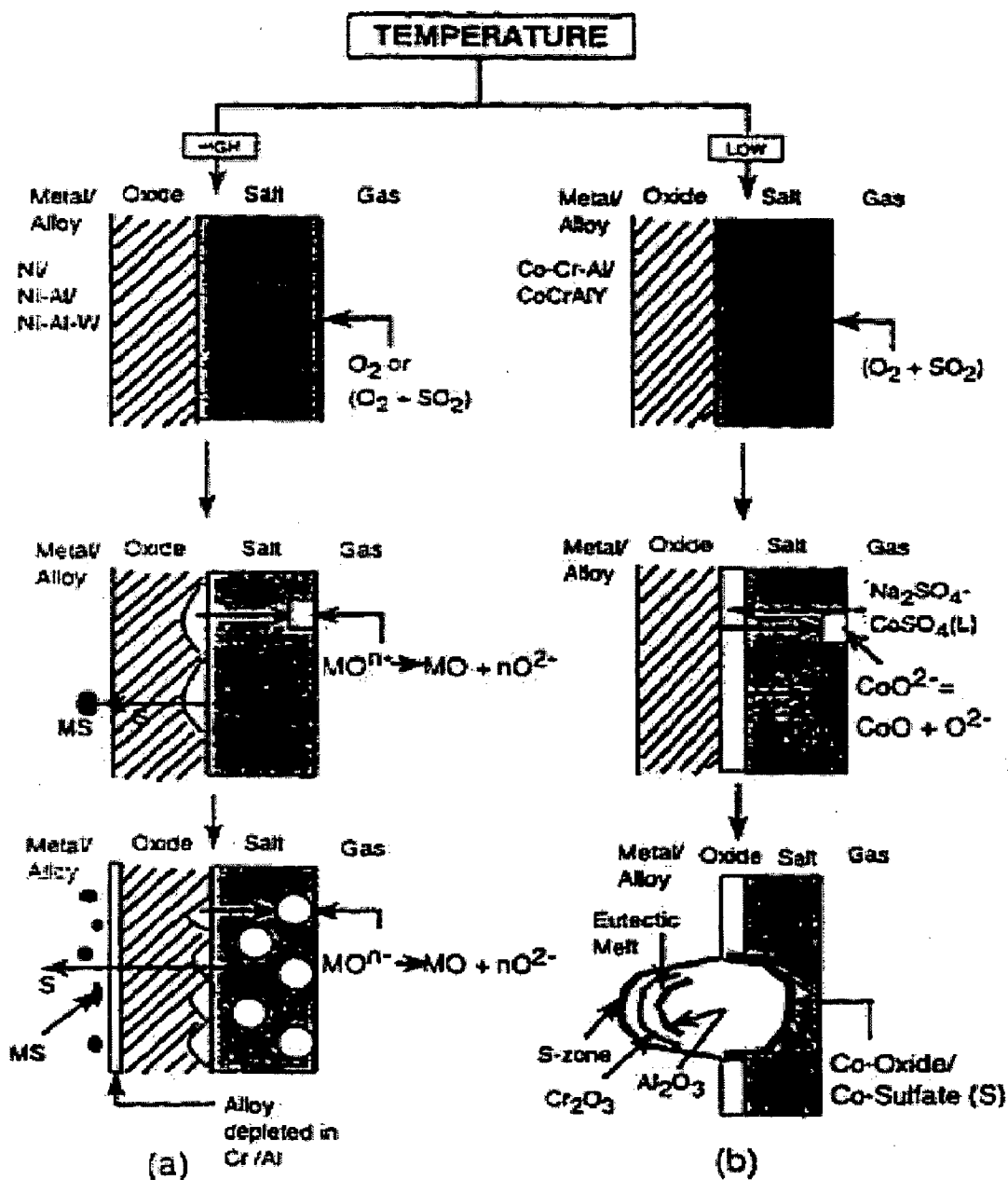


Fig. 2.7 Schematic diagram to illustrate the mechanism of hot corrosion in (a) High Temperature hot corrosion and (b) Low temperature hot corrosion (Goebel, et al., 1973),

propagation stage. Thus, fluxing action of cobalt oxide prevents the formation of protective layer of Cr<sub>2</sub>O<sub>3</sub>, as the temperature increase the partial pressure of SO<sub>3</sub> decreases, which is not sufficient to form liquid eutectic mixture. Hence, the corrosion rate at high temperature is much less than at low temperatures (Goebel et al., 1973).

### **2.3.1.1 High Temperature Hot Corrosion (HTHC)-Type I**

It has been known since the 1950s and it is an extremely rapid form of oxidation that takes place at temperatures between 815 °C and 926 °C in the presence of pure Na<sub>2</sub>SO<sub>4</sub> (m.p 886 °C) (Khajavi, 2004). HTHC starts with the condensation of fused alkali salts (Na<sub>2</sub>SO<sub>4</sub>) on the surface of the component; the most significant source of sodium is marine, industrial atmosphere as well as fuel. During combustion of fuels, sodium from air and sulfur from the fuel combine to form a sodium sulphate (Eliaz et al., 2002). Na<sub>2</sub>SO<sub>4</sub> formation lies basically in the reaction



Type I, or high-temperature hot corrosion, is characterized by a macroscopically uniform corrosion front, which involves an internal layer of internal oxidation, which may also contain internal sulfides and carbides. The external oxide is not protective, and is composed of the oxides of the base metal (nickel or cobalt); and the oxides of the other constituents, particularly chromium and aluminum (Stringer 1998).

Sidhu et al., (2006J) reported that the macroscopic appearance of HTHC is characterized in many cases by severe peeling of metal and by significant colour changes. For instance, a greenish tone appears on the surface of metals and alloys due to the formation of NiO in the area of accelerated attack. Microscopically, the morphology of Type I is characterized by a sulphidation and depletion region beneath the porous, non-protective scale.

### **2.3.1.2 Low Temperature Hot Corrosion (LTHC) Type II**

Low temperature hot corrosion (LTHC) was recognized in the mid-1970s as a separate mechanism of corrosion attack (Khajavi, 2004). Low temperature hot corrosion mainly observed within the temperature range 650-800 °C and requires a significant high partial pressure of SO<sub>3</sub>, for cobalt-based superalloys. The formation of low melting eutectic compounds occurs due to the combination of sodium sulfate and cobalt sulfate (melting temperature of the Na<sub>2</sub>SO<sub>4</sub> ± CoSO<sub>4</sub> eutectic is 540 °C) (Eliaz et al., 2002). The formation of Na<sub>2</sub>SO<sub>4</sub> + NiSO<sub>4</sub> eutectics 671 °C has

been reported for nickel-based superalloys, the morphology of attack is pitting when the LTHC takes place, low temperature corrosion characteristically shows no denuded zone, no or little inter-granular attack, and a layered type of corrosion scale and also no subscale sulfide particles (Misra, 1986). Chromium (25-40%) and silicon are particularly beneficial in coatings for protection against Type II corrosion. It should be noted that the classification of the form of the attack (type I or type II) is primarily based on the morphology of the attack, and not the temperature. Type II, or low-temperature hot corrosion is characterized by a pitting attack (Stringer, 1998).

### **2.3.2 Degradation of the Superalloys**

The hot corrosion degradation of superalloys usually involves two distinct stages of attack (Pettit and Meier, 1985; Pettit and Giggins, 1987), namely, an initiation (incubation) stage and propagation stage. Such conditions are depicted schematically in Fig.2.8.

#### **2.3.2.1 The Initiation Stage**

No alloy is immune to hot corrosion attack indefinitely although there are some alloy compositions that require a long initiation times before the hot corrosion process moves from the initiation stage to the propagation stage. During the initiation stage of hot corrosion, superalloys are being degraded at rates similar to those that would have prevailed in the absence of the deposits. Elements in the alloy are oxidised and electrons are transferred from metallic atoms to the reducible substances in the deposit. Consequently, the reaction product barrier that forms beneath the deposit on the alloy surface usually exhibits primarily those features resulting from the gas-alloy reaction (Pettit and Giggins, 1987). Numerous factors affect the time at which the hot corrosion process moves from the initiation stage into the propagation stage as shown in Fig. 2.2. These factors also play the dominant role in determining the type of reaction product that is formed in the propagation stage. This fact is responsible for variety of hot corrosion processes that have been observed when superalloys are exposed to different environments (Pettit and Meier, 1985).

#### **2.3.2.2 The Propagation Stage**

The propagation stage of the hot corrosion sequence is the stage for which the superalloy must be removed from service since this stage always has much larger corrosion rates than for

the same superalloy in the initiation stage (Pettit and Meier, 1985 and Pettit and Giggins, 1987). Since superalloys always contain elements that have high affinities for oxygen, an oxygen gradient is established across the deposit. Hence, an important effect of the deposit is to separate

## HOT CORROSION CHRONOLOGY

### Initiation Stage

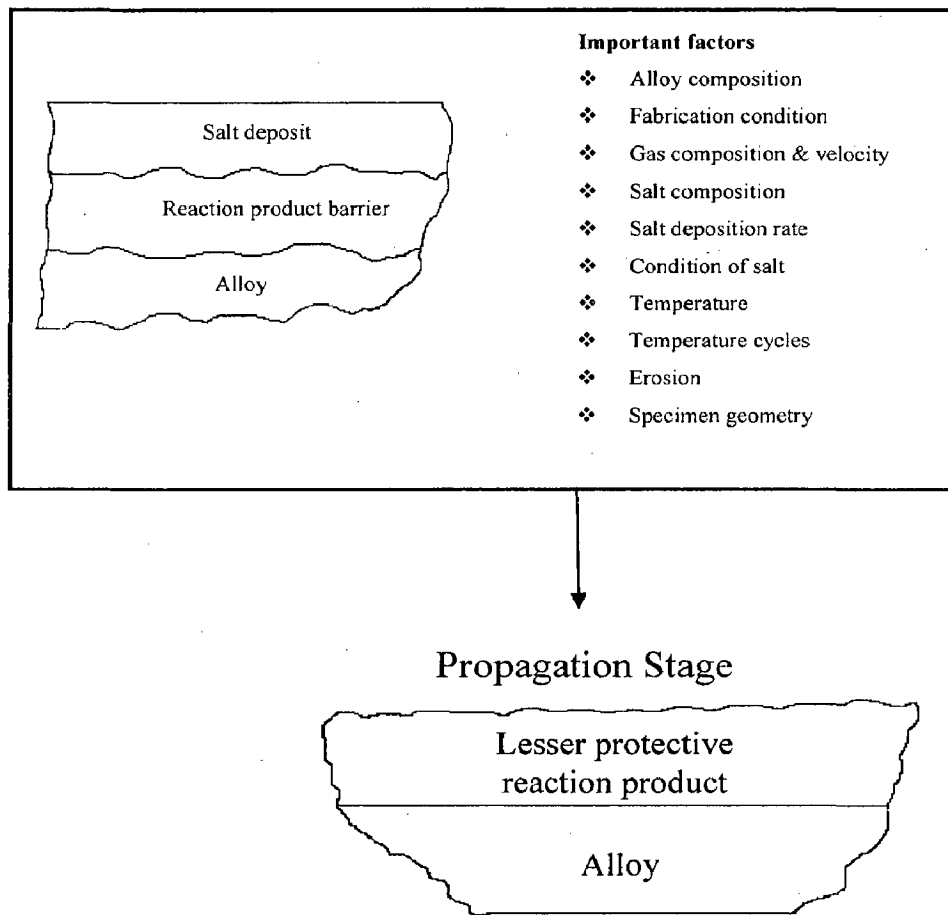


**Fig. 2.8** Schematic diagram illustrating the conditions that develop during the initiation and the propagation of hot corrosion attack and to identify the factors that determine the time at which the transition from the initiation to the propagation stage occurs (Pettit and Meier, 1985).

the superalloy from the gas environment. This situation usually results in a lower oxygen activity over the surface of the alloy than what would have been established in the absence of a deposit (Pettit and Meier, 1984; Pettit and Giggins, 1987).

### 2.3.3 Mechanisms of Hot Corrosion

From the literature review, it has been observed that there are varieties of conditions which can be considered for hot corrosion degradation of the superalloys. Researchers have proposed number of mechanisms for this type of degradation such as failure of oxide scale, sulphidation-oxidation and salt fluxing, oxide solubility, and effect of vanadium (Goebel and Pettit, 1970A; Goebel and Pettit, 1970B; Beltran and Shores, 1972; Rapp and Goto, 1981; Pettit and Meier, 1985; Rapp, 1986; Stringer, 1987; Otsuka and Rapp, 1990; Zhang et al., 1993; Eliaz et al., 2002).

These mechanisms can be considered in relation to each other rather than as completely different and unrelated corrosion process. The salt fluxing mechanism was firstly proposed by Goebel and Petit (1970A and 1970B). According to this model, the protection efficiency of the surface oxide layer might be lost as a result of fluxing of this layer in the molten salt. This fluxing may be either due to combination of oxides with  $O^{2-}$  to form anions (basic fluxing) or by decomposition of the oxides into the corresponding cations and  $O^{2-}$  (acidic fluxing). Fig.2.9 schematically illustrates oxide solubility with the superposition of four different sets of basicities at the salt/gas interface II, and at the oxide/metal interface I (Goebel et al., 1973).

As compared to basic fluxing, acidic fluxing causes more severe oxidation. The acidic fluxing takes place when the  $O^{2-}$  activity in the molten salt is markedly lowered. In contrast to basic fluxing, the acidic fluxing can be self-sustaining because the displacement of the salt from the stoichiometry does not become progressively more difficult as the reaction proceeds (Stringer, 1987).

It is important to notice that the concentration of oxygen ions available for basic fluxing is limited by the amount of deposit present upon the surface of the superalloy. Hence basic fluxing reactions are not self-sustaining but require a continuous source of  $Na_2SO_4$  in order to precede this type of degradation indefinitely. As opposed to the basic fluxing, the acidic fluxing can be self-sustaining, since the displacement of the salt from stoichiometry does not become progressively more difficult as the reaction proceeds (Stringer, 1987; Pettit and Meier, 1985). Therefore, acidic fluxing is more severe as compared to basic fluxing. In general, the hot corrosion of the superalloys with high contents of aluminium and chromium is often reported to occur according to the basic fluxing mechanism. On the other hand, the hot corrosion of alloys with high contents of tungsten, molybdenum and vanadium is often reported to follow the acidic



fluxing mechanism (Eliaz et al., 2002) and these elements, when oxidised in the presence of  $\text{Na}_2\text{SO}_4$ , deposit on superalloys causing catastrophic self-sustaining hot corrosion (Pettit and Meier, 1985).

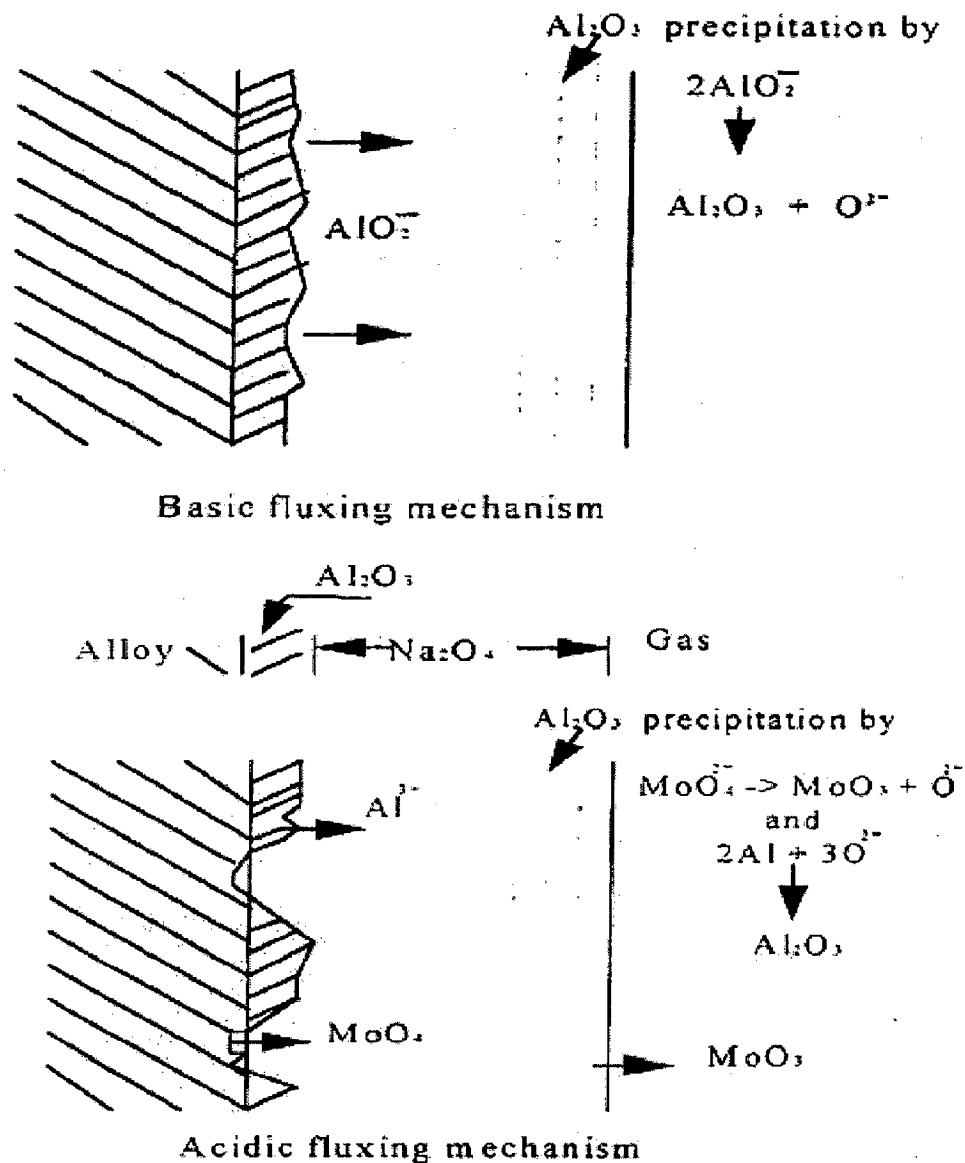


**Fig.2.9** Schematic diagrams of basic and acidic fluxing mechanisms with respective typical morphology of corrosion attack (Goebel et al., 1973)

Stott et al. (1994) proposed that sulphur-containing species, penetrating through localized short-circuit paths in the oxide, develop sulphide ducts from the scale-metal interface to the scale-gas interface. The sulphide ducts provide easier diffusion paths for the base-metal ions through the oxide to the surface, and eventually allow more rapid growth of

sulphide nodules above the oxide. However, Natesan (1985) reported that no transport of sulphur into the oxide, or sulphide duct formation was necessary to form massive mixed iron and chromium sulphides at the oxide–gas interface. Based on the experimental results of sulphidation–oxidation of Incoloy 800, he reported that adsorption of sulphur by the oxide scale accelerates the transport of cations such as Fe and Ni from the substrate to the gas/scale interface and if the sulphur partial pressure in the gas is above that needed for base-metal sulphidation, the transported cations react with sulphur to form sulphides as an outer scale, external to the preformed chromium oxide layer.

Hot corrosion in sulphates, chloride and vanadate environment of a cast nickel base superalloy had been reported by Deb et al. (1996) Weight gain studies were carried out in air for the uncoated samples and coated with 100% Na<sub>2</sub>SO<sub>4</sub>, 75% Na<sub>2</sub>SO<sub>4</sub>-25% NaCl and 60% Na<sub>2</sub>SO<sub>4</sub> + 30% NaVO<sub>3</sub>+10% NaCl. The presence of sulphur in the form of sulphates can cause internal sulphidation of the alloy beneath the external oxide layer. Chlorides cause the formation of volatile species, which form voids and pits at grain boundaries, thus forming an easy path for flow of corrodents. The presence of vanadate in conjunction with sulphates and chloride provides additional fluxing action. This destroys the integrity of the alloy and weakens its mechanical properties.

Rapp and Goto (1981) proposed that protective scales on alloy become non-protective when the solubility gradients of the protective oxides in the molten deposit are negative, due to possibility of continuous dissolution and re-precipitation of oxide. On the basis of oxide solubilities measurement in molten Na<sub>2</sub>SO<sub>4</sub> as a function of the acidity of the salt, they suggested that a negative gradient of the solubility of the protective oxide in the salt film at the oxide/salt interface should lead to oxide dissolution at this interface and to precipitation of a non-protective oxide away from the interface, where the solubility is lower. Fluxing arises in this case only because of the local variation of sodium oxide activity and/or oxygen partial pressure across the salt film, without any necessity of sulphide-forming reaction. This mechanism can explain a self-sustaining process of dissolution of the protective oxide to maintain an accelerated corrosion attack (Stringer, 1987).

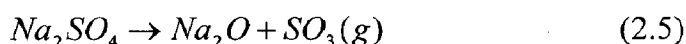
Different research workers have examined the effect of vanadium on high temperature hot corrosion of metals and alloys. Bornstein et al. (1973) and Goebel et al. (1973) suggested that a self-sustained acidic dissolution of the protective Cr<sub>2</sub>O<sub>3</sub> or Al<sub>2</sub>O<sub>3</sub> scales could take place when

the salt film contains vanadium, because  $V_2O_5$  is a strong acidic oxide. Zhang and Rapp (1987) further suggested that every oxide forms an acidic solute with much higher solubility in the presence of vanadate, which contributes to the more accelerated attack of oxides by mixed sulphate-vanadate, melts than by a pure sulphate melt. Some of hot corrosion studies conducted by various investigators in  $Na_2SO_4$  or  $V_2O_5$  environments are summarised in Appendix A.1.

## 2.3.4 Chemistry of salts

### 2.3.4.1 Sulphate Chemistry

As described by Rapp (1986 and 2002), oxy-anion melts of alkali nitrates, carbonates, hydroxides, and sulphates exhibit an acid/base character wherein the acid components may be considered as  $NO_2(g)$ ,  $CO_2(g)$ ,  $H_2O(g)$  or  $SO_3(g)$ , respectively. Although the use of the Lux-Flood selection of  $NO_3^-$ ,  $CO_3^{2-}$ ,  $OH^-$  and  $SO_4^{2-}$  as the basic components is common for such fused salts, the oxide ion can alternatively be chosen as the Lewis base in common for all of these salts. For a melt of pure  $Na_2SO_4$  (m.p.  $884^\circ C$ ), there exists an equilibrium as given below:



According to Rapp (1986), in examining the expected stability of the protective oxide  $Cr_2O_3$ , with respect to dissolution either as acidic solutes such as  $Cr_2(SO_4)_3$  or as basic solutes such as  $Na_2CrO_4$  or  $NaCrO_2$ , the phase stability diagram for the Cr-S-O system can be superimposed on that for Na-S-O, as shown in Fig. 2.10. The two abscissa scales at the bottom and top of figure provide alternate parameters for melt basicity (or acidity). Under no conditions, the metal chromium remains stable in contact with  $Na_2SO_4$  at 1200 K ( $927^\circ C$ ) (Rapp, 1986).

### 2.3.4.2 Vanadate Chemistry

Among the transition metals vanadium is unique, in that it forms a low-melting oxide  $V_2O_5$ . This low melting temperature ( $670^\circ C$  under 1 atm of oxygen) results from the peculiar crystal structure of the compound in which vanadium is 5-coordinated with oxygen and in which there occur four different vanadium-oxygen bond lengths (Suito and Gaskell, 1971). The phase stability diagram for the Na-V-S-O system at  $900^\circ C$  reported by Hwang and Rapp (1989) has been shown in Fig. 2.11. The dashed lines present the isoactivity lines for the vanadate species in the salt solution.

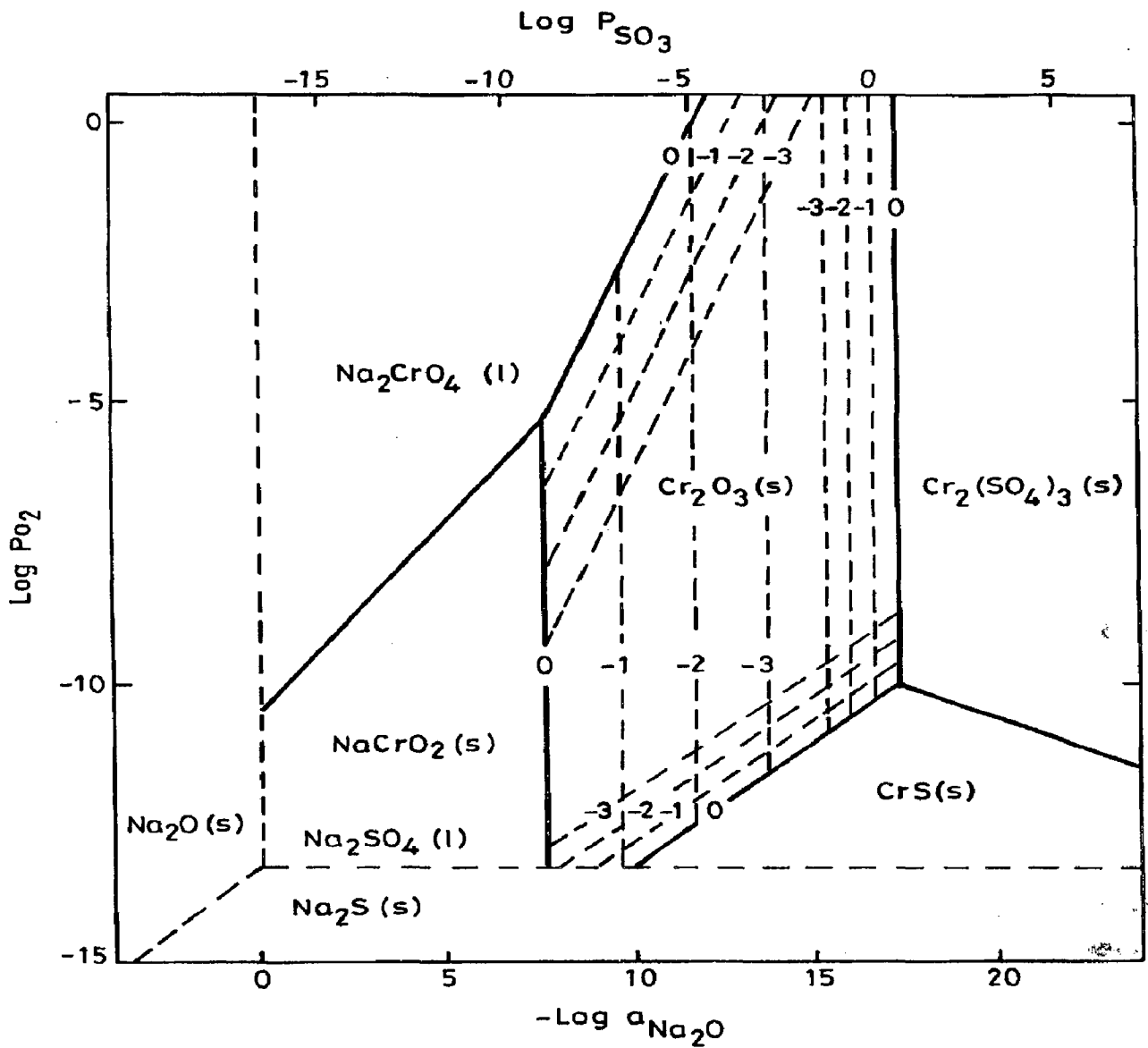


Fig. 2.10 Na-Cr-S-O phase stability diagram for 1200 K (Rapp, 1986).

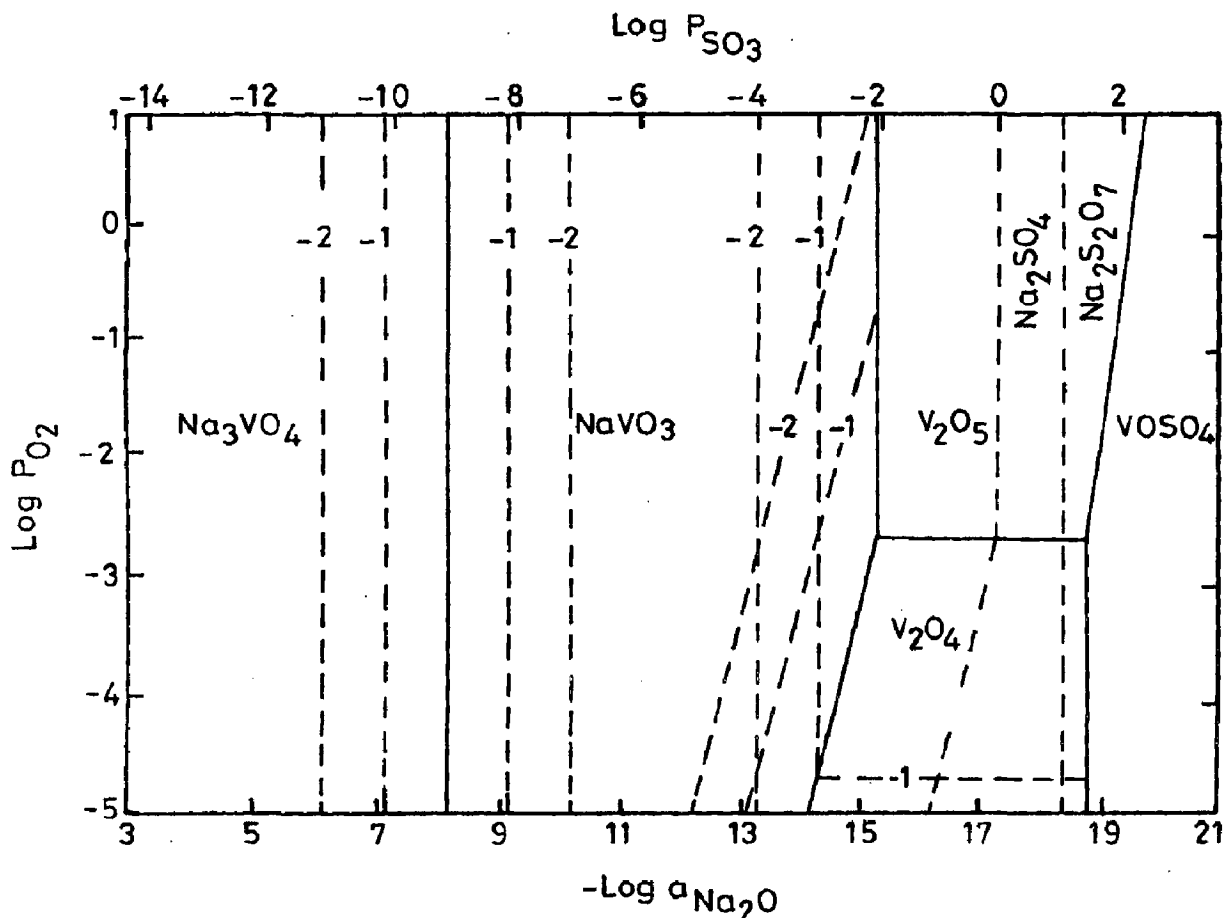
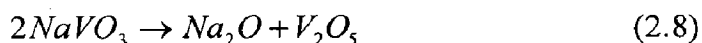
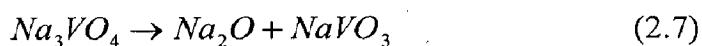
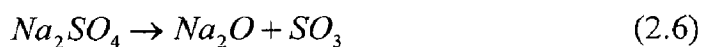


Fig. 2.11 Phase stability diagram for Na-V-S-O system at 900 °C (Hwang and Rapp, 1989).

They determined the dependence of the equilibrium concentrations of various vanadate solutes in the sodium sulphate-vanadate solutions on the melt basicity by considering following equilibrium reactions:

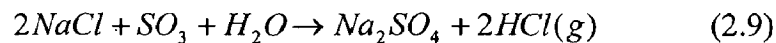


The equilibrium concentration of each vanadium compound varies continuously with melt basicity.  $\text{Na}_3\text{VO}_4$  is the dominant component in the melt at basicity less than 8.2 and  $\text{V}_2\text{O}_5$  is dominant at basicity greater than 16.3. For basicities between 8.2 and 16.3,  $\text{NaVO}_3$  is the most important vanadium solute (Hwang and Rapp, 1989).

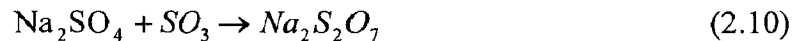
### 2.3.4.3 Chemistry of Salts in the Combustion of Coal/Fuel Oils

It is not possible to remove sulphur from coal or fuel oil completely and economically, also it is not possible to prevent the formation of SO<sub>2</sub> during combustion (Nelson et al., 1959). In the combustion system of coal fired boilers, much of the sodium and potassium is volatilised from the mineral matter in the flame to form Na<sub>2</sub>O and K<sub>2</sub>O vapours. The sulphur released from the coal forms SO<sub>2</sub> with a minor amount of SO<sub>3</sub>, reacts with the volatilised alkalies to form Na<sub>2</sub>SO<sub>4</sub> vapours. These vapours condense together with fly ash on the pendant super-heater and re-heater tubes in the boiler. Corrosion has been attributed to the fluxing action of the molten salt deposits on the oxide scales formed on the tubes, leading to rapid localised corrosion, accompanied by Sulphidation (Beltran and Shores, 1972; Rapp et al., 1981).

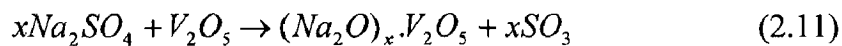
Khanna and Jha (1998) reported that the sulphur present in fuel oils yields SO<sub>2</sub> on combustion which is partially oxidised to SO<sub>3</sub>. The NaCl (either as impurities in the fuel or in the air) reacts with SO<sub>3</sub> and water vapours at combustion temperatures to yield Na<sub>2</sub>SO<sub>4</sub> as given below:



At lower temperatures, Na<sub>2</sub>SO<sub>4</sub> can further react with SO<sub>3</sub> to form sodium pyrosulphate, Na<sub>2</sub>S<sub>2</sub>O<sub>7</sub> with melting point (m. p.) of 401 °C:



Small amounts of vanadium may be present in fuel oils, which on combustion forms V<sub>2</sub>O<sub>5</sub>. This may further react with Na<sub>2</sub>SO<sub>4</sub> to form low melting sodium vanadates, which are highly corrosive.



Thus metals and alloys in combustion gases are exposed to various corrosives such as O<sub>2</sub>, SO<sub>2</sub>/SO<sub>3</sub>, molten salts, e.g. Na<sub>2</sub>SO<sub>4</sub> or sulphate mixtures, sodium vanadates, NaCl etc. (Khanna and Jha, 1998).

## 2.4 HOT CORROSION IN THE MOLTEN SALT ENVIRONMENTS

### 2.4.1 Molten salt (Na<sub>2</sub>SO<sub>4</sub>-60%V<sub>2</sub>O<sub>5</sub>) Environment-I

Kolta et al. (1972) studied the kinetics of reactions between Na<sub>2</sub>SO<sub>4</sub> and V<sub>2</sub>O<sub>5</sub>. They concluded that the rate of reaction depends both on the temperature (600-1300 °C) and the molar ratios of Na<sub>2</sub>SO<sub>4</sub> and V<sub>2</sub>O<sub>5</sub>. They further revealed that with increase in the reaction period (>30

min.), the reaction rate decreased and finally reached to zero order. They attributed this decrease in the reaction rate to the formation of vanadosulphate complexes such as  $(\text{NaV}_3\text{O}_8)_2 \cdot \text{Na}_2\text{SO}_4$  and  $(\text{NaVO}_3)_2 \cdot \text{Na}_2\text{SO}_4$ , which are decomposed at higher temperatures giving the meta- and pyrovanadates respectively.

The effect of vanadium and sodium on the accelerated oxidation of nickel base alloys has been reported by Bornstein et al (1975). They observed the initial rapid rate of oxidation between  $\text{V}_2\text{O}_5$  and metal substrate which is attributed to the reduction of  $\text{V}_2\text{O}_5$  by the substrate. Inter-metallic systems  $\text{Ni}_3\text{Al}$  and  $\text{NiAl}$  were particularly found to be susceptible to  $\text{V}_2\text{O}_5$  corrosion. According to them, the sulphidation attack alters the composition of the melt to produce more oxide ions i.e.  $M + \text{SO}_4^- = \text{MS} + \text{O}^- + 3/2\text{O}_2$ . Severity of attack is found to decrease with increase in the initial oxide ion content of the melt. Oxides such as  $\text{Cr}_2\text{O}_3$  have been suggested to react preferentially with oxide ions. Natesan (1976) reported that molten sulphate-vanadate deposits are extremely corrosive to high-temperature materials in the combustion systems.

Luthra and Spacil (1982) carried out a thermo-chemical analysis of deposits in gas turbines for liquid fuels containing Na, S and V. They observed that the predominant species in the salt deposits formed on the gas turbine surfaces were  $\text{Na}_2\text{SO}_4$ ,  $\text{V}_2\text{O}_5$  and  $\text{Na}_2\text{V}_2\text{O}_6$ . This environment is also pertinent to the boilers. According to Otero et al (1987),  $\text{Na}_2\text{SO}_4$ -60% $\text{V}_2\text{O}_5$  deposit was detected on a number of components in actual service which were operated at high temperature and were in contact with high-temperature gases from combustion of dirty fuels, containing certain amounts of impurities, i.e. Na, V, S etc. The presence of sulphur and its oxidised compounds were reported to favour the formation of isolated lobes with radial morphology having great permeability to facilitate the access of oxygen which further led to reduction in the protective nature of scale. The presence of vanadium and its oxidised products was observed to generate compounds with acicular morphology, identified to look like alkaline vanadate complexes. These acicular shapes further contribute to reduce the protective character of the scale.

Kofstad (1988) has proposed that during combustion, the vanadium contaminants are oxidized to the higher valence vanadium oxides ( $\text{V}_2\text{O}_4$  and  $\text{V}_2\text{O}_5$ ) which react with sodium salts to form low melting point sodium vanadates (lowest M.P. 535 °C) such as  $(\text{Na}_2\text{O})_x\text{V}_2\text{O}_4(\text{V}_2\text{O}_5)_{12-x}$ ,  $(\text{Na}_2\text{O})_5(\text{V}_2\text{O}_4)_x(\text{V}_2\text{O}_5)_{12-x}$ ,  $\text{NaVO}_3$ ,  $\text{Na}_4\text{V}_2\text{O}_7$  and  $\text{Na}_3\text{VO}_4$ . Metal oxides

dissolved in the vanadates may suppress the melting points and eutectic temperatures even further. He further reported that the slags developed on valves in diesel engines consist predominantly of sodium sulphate and sodium vanadates and have melting points as low as 400 °C. Hwang and Rapp (1989) studied the solubility of oxides in the mixed sodium sulphate-vanadate solution containing 30 mole% vanadates. They reported that the basicity of the melt, oxygen partial pressure and proportion of  $V^{5+}$  and  $V^{4+}$  states of vanadate in the sulphate-vanadate solution decide the solubilities of oxides. Kofstad (1988) revealed that the solubilities of metal oxides may be high and are dependent on the Na:V ratio. The solubilities of  $Cr_2O_3$  and  $Fe_2O_3$  are highest ( $\approx 50$  mol. %) at Na : V ratios close to 5 : 12. For NiO, the solubility is about 60 mol. % at Na : V = 3 : 2 which decreases to about 55 mol.% at Na : V = 5 : 12. As  $V_2O_5$  is acidic, it will react with more basic oxides to form the corresponding vanadates.

In this aggressive environment ( $Na_2SO_4$ -60% $V_2O_5$ ), the hot corrosion behaviour of superalloy IN-657 at 1000 K (727°C) has been investigated by Otero et al (1990 and 1992). They reported that corrosion rate of the alloy in contact with molten salt mixtures has been approximately reduced by one order of magnitude over exposure times of 210 hrs when the amount of molten salt is kept constant. During the initial stages of the exposures, the corrosion rate was found to be increased with increasing the temperature up to 1000 K (727°C) and further reported to have decreased at higher temperature. After 100 hours of exposure, the influence of temperature was insignificant. Zhang and Rapp (1994) measured the solubility of  $CeO_2$  as a function of melt basicity in a  $Na_2SO_4$ -10mol.% $NaVO_3$  solution at 900 °C and 1 atm. oxygen. A comparison of the solubility in  $Na_2SO_4$ -10mol.% $NaVO_3$  with the solubilities in both pure  $Na_2SO_4$  and in  $Na_2SO_4$ -30mol.% $NaVO_3$  was made. Their results indicated that  $CeO_2$  dissolves in the salt solution either as a basic or as an acidic solute.

Sidhu, (2003) studied the hot corrosion behaviour of boiler tube steels namely ASTM-SA210 grade A1, ASTM-SA213-T-11 and ASTM-SA213-T-22 in air and molten salt environments of  $Na_2SO_4$ -60% $V_2O_5$  at 900 °C. They found that all the steels show less resistance in the molten salt environment than in air. They reported that the presence of vanadium, sodium and sulphur accelerates the rate of corrosion of boiler steels in the molten salt environment. Sidhu et al., (2007) evaluated the hot corrosion behaviour of HVOF sprayed  $Cr_3C_2$ -NiCr and NiCrBSi coated superalloy 718 at 900 °C under cyclic conditions in the presence of the  $Na_2SO_4$ -60% $V_2O_5$  salt mixture. He concluded that the  $Cr_3C_2$ -NiCr coating oxidizes partially along the splat boundaries up to the



coating-substrate interface, whereas in the case of NiCrBSi coating, only the upper layer of the coating oxidizes and the remaining portion of the coating remains similar to as-sprayed coating, schematic representation of the possible hot corrosion mode for the NiCrBSi coated superni 718 is shown in Fig. 2.12

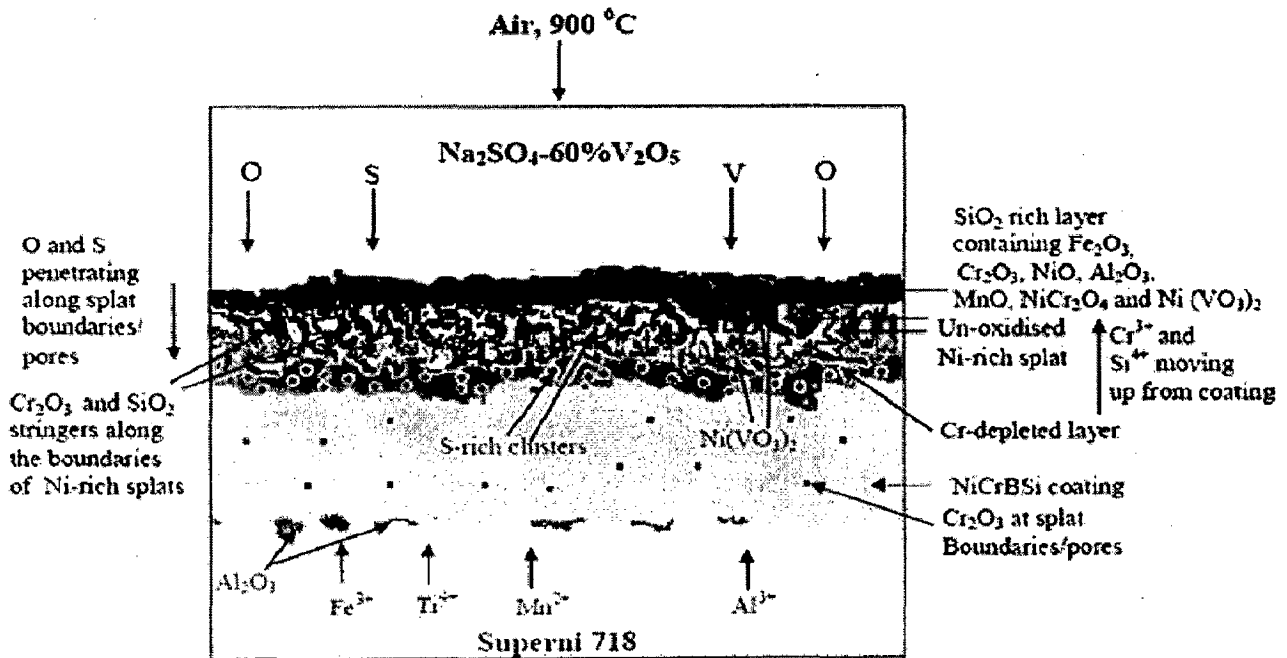


Fig. 2.12 Schematic diagram showing the possible hot corrosion mode for the NiCrBSi coated superni 718 exposed to the  $\text{Na}_2\text{SO}_4\text{-60\% V}_2\text{O}_5$  environment at  $900\text{ }^\circ\text{C}$  for 50 cycles (Sidhu et al., 2007).

#### 2.4.2 Molten salt ( $\text{Na}_2\text{SO}_4\text{-25\%K}_2\text{SO}_4$ ) Environment-II

Shih et al. (1989) studied the behaviour of  $\text{K}_2\text{SO}_4 + \text{Na}_2\text{SO}_4$ -coated aluminium diffusion coatings on a pure iron substrate with aluminium concentrations of 28%-51% at the outermost surface of the coatings at  $600\text{ }^\circ\text{C}$  in  $\text{O}_2\text{-SO}_2\text{-SO}_3$  gases. All the coatings were found to undergo sub-melting point hot corrosion although their corrosion rates were much lower than those for pure iron; and there was evidence of the formation of a liquid phase, which is believed to be a complex sulphate melt containing potassium, sodium, iron and aluminium. Uusitalo et al. (2004) also investigated the high-temperature behaviour of the same coatings in the presence of a salt environment of 40%  $\text{Na}_2\text{SO}_4\text{-40\% K}_2\text{SO}_4\text{-10\%NaCl-10\%KCl}$  in two environments viz. oxidising environment of  $\text{N}_2\text{-20H}_2\text{O-14CO}_2\text{-3O}_2\text{-500 vppm HCl}$ , reducing environment of  $\text{N}_2\text{-20H}_2\text{O-}$

5CO-0.06H<sub>2</sub>S-500 vppm HCl. They found that the corrosion was more severe in oxidising environments as compared to the corrosion in reducing environment. An active oxidation was responsible for the accelerated corrosion in oxidising environments. The coatings were prone to the chlorine attack in both the atmospheres through the interconnected oxide network at the splat boundaries. The Ni-57CrMoSiB coating was the only material forming a protective oxide layer. Whereas in reducing conditions, the materials with high chromium content were found to be able to form a protective layer containing chromium, sulphur, and sodium. The corrosion resistance of this layer increased with increasing chromium content. Further, it was concluded that the corrosion resistance of the nickel-based, high chromium coating materials was satisfactory in the test conditions.

Wang et al. (2004) tested the hot corrosion behaviour of arc ion plating NiCoCrAlY (SiB) coatings deposited on nickel base superalloys DZ 125 and DSM 11, in molten 75 Na<sub>2</sub>SO<sub>4</sub> + 25K<sub>2</sub>SO<sub>4</sub> (wt%) at 900 °C in air for 90 hours. The coating improved the hot corrosion resistance of DZ125 and DSM11 superalloys. The authors concluded that the additions of Si and B can promote the selective oxidation of the protective scale-forming elements resulting in the formation of a continuous scale in the initial corrosion stage and improve the adherence of the outer scale to the coating in the subsequent hot corrosion process.

Due to depletion of high-grade fuels and for economic reasons, use of residual fuel oil together with coal in energy generation systems in turbines, boilers, and industrial waste incinerators, is well known. These fuels contain Na, V, K and S as impurities, these impurities react together to form low melting point compounds, which deposit on the surface of materials and induce accelerated oxidation (hot corrosion), corrosion occurs when these molten compounds dissolve the protective oxide layers that naturally form on materials during boiler/gas turbine operation, the inability to either totally prevent the hot corrosion or at least detect it at an early stage has resulted in several accidents, leading to loss of life and/ or destruction of engines /infrastructures (Sidhu, 2006E).

A nanocrystalline Ni-30Cr-8Al-0.5Y coating was deposited on a Ni-base superalloy by magnetron sputtering (Ren and Wang, 2006). Post-aluminizing was performed on the sputtered coating. The isothermal oxidation behavior at 1000-1100 °C and hot-corrosion behavior in the presence of 75 wt.% Na<sub>2</sub>SO<sub>4</sub>+25 wt.% K<sub>2</sub>SO<sub>4</sub>/NaCl film at 900 °C of the sputtered coating with and without aluminizing have been investigated using TGA, SEM/EDS, XRD and EPMA,

respectively. They indicated that the sputtered NiCrAlY coating possessed excellent oxidation resistance at 1000 °C due to the presence of extensive amount of chromium and good amount of aluminum. Because of the excessive consumption of Al in the coating, it lost protection at 1100 °C. The mass gain of the aluminized NiCrAlY coating was a little higher than that of the sputtered coating due to the formation of the rapid growing  $\theta$ -Al<sub>2</sub>O<sub>3</sub> phase at 1000 °C. At 1100 °C, the oxidation resistance of the latter was better than that of the former. The sputtered coating provided a limited protection at the transient hot-corrosion stage in the molten salt film and degenerated completely with time. On the contrary, the aluminized NiCrAlY coating showed much better hot-corrosion resistance in the presence of 75 wt.% Na<sub>2</sub>SO<sub>4</sub>+K<sub>2</sub>SO<sub>4</sub>/NaCl film as a result of the formation of a continuous and protective Al<sub>2</sub>O<sub>3</sub> scale (Ren and Wang, 2006).

Zheng et al (2006) reported that a novel enamel-Al<sub>2</sub>O<sub>3</sub> composite coating with a thin NiCoCrAlY bond coat was deposited on K38G superalloy. They indicated that this composite coating exhibited excellent high temperature oxidation resistance at 900 and 1000 °C and hot corrosion resistance in molten sulfate salts (75 wt.% Na<sub>2</sub>SO<sub>4</sub>+25 wt.% K<sub>2</sub>SO<sub>4</sub>) at 900 °C, much better than solo NiCoCrAlY coating and uncoated K38G. The protection mechanism of this composite coating was different from those of traditional metallic coatings. Further, they observed that it has no longer oxidized during tests and acted as a barrier to effectively hinder the corrosive species from migrating into substrate.

Guo et al., (2006A) studied the corrosion kinetics of the specimens coated with 0.5 mg (Na<sub>2</sub>SO<sub>4</sub> + K<sub>2</sub>SO<sub>4</sub> 20 wt.% salt mixture)/cm<sup>2</sup> at 900 °C. For bare DSM 11 alloy, significant mass gain is associated with rapid hot corrosion attack of the alloy during the first 20 hours, followed by fluctuation due to the competition of oxide-scale formation and spallation. After 80 hours, the mass decreases sharply due to a great amount of oxide spallation

### **2.4.3 Hot Corrosion of the Nickel and Nickel-Based Alloys**

Bornstein et al. (1975) have studied the effect of vanadium and sodium on the accelerated oxidation of the nickel based alloys. Liquid V<sub>2</sub>O<sub>5</sub> has been proposed to be an excellent flux and easy path for oxygen diffusion. They attributed the initial rapid rate of oxidation between V<sub>2</sub>O<sub>5</sub> and metal substrate to the reduction of V<sub>2</sub>O<sub>5</sub> by the substrate. They concluded that the sulphidation attack can be attenuated if the initial oxide ion content of the melt is prevented from increasing. Oxides such as Cr<sub>2</sub>O<sub>3</sub> have been reported to react preferentially with oxide ions.

Rapp and Goto (1981) have hypothesized that presence of multivalent metal ions in vanadate-sulphates melt could greatly accelerate the hot corrosion rate either by counter diffusion of multivalent cations or else by electron hopping which provides the fast transport of charge through the deposited layer.

The mechanisms of the hot corrosion by the molten sulphate-vanadate deposits were investigated by Sidky and Hocking (1987). They studied the hot corrosion of Ni-10Cr, Ni-30Cr, Ni-20Cr-3Al, Ni-21Cr-0.3Si, Ni-20Cr-5V and IN738 superalloys. The effect of addition of Cr to Ni was found to be beneficial in the  $\text{Na}_2\text{SO}_4$  melt. However, on increasing the  $\text{VO}_3^-$  concentration in the melt, this effect diminished, and became harmful in pure  $\text{NaVO}_3$  due to the formation of the non protective  $\text{CrVO}_4$ . According to them, alloying element Al was found to be harmful in  $\text{Na}_2\text{SO}_4\text{-NaVO}_3$  melts. Cr depletion was observed in rich  $\text{VO}_3^-$  melts but internal corrosion was more obvious in the  $\text{SO}_4^{2-}$  rich melts. Corrosion in rich  $\text{VO}_3^-$  melts was aggressive due to the fluxing action of the salt, which takes place along internally sulphidised areas. According to their study, IN738 suffered tremendous internal attack due to its  $\gamma$  precipitates which became sulphidation prone areas, and were fluxed by the  $\text{VO}_3^-$  melt.

Thermogravimetric studies which delineate the conditions for simultaneous sulphate and vanadate induced corrosion at 650 to 800<sup>0</sup>C have been carried out by Seiersten and Kofstad (1987). They found that the corrosion caused by sodium sulphate/sodium vanadate mixtures have a complex mechanism. Samples coated with sodium vanadate were exposed to  $\text{O}_2 + 4\% \text{SO}_2$  and the initial reaction was observed to be same as that observed in pure oxygen. After an incubation period, the duration was found to decrease with increasing temperature and sufficient  $\text{SO}_3$  got dissolved in the molten vanadate which resulted in formation of a mixture of  $\text{NiSO}_4$  and  $\text{Na}_2\text{SO}_4$  near the metal. When a molten  $\text{NiSO}_4\text{-Na}_2\text{SO}_4$  solution containing small amounts of vanadate was formed as an intermediate layer, the reaction reportedly proceeded as sulphate-induced hot corrosion. The corrosion mechanism was observed to change from initial vanadate-induced to essentially sulphate induced hot corrosion when the sulphur trioxide pressure was high enough to form sodium sulphate.

Otero et al. (1987) investigated the hot corrosion behaviour of IN657 (46.5 Cr, 1.32 Nb, bal-Ni) at 635 °C in a molten salt environment of 60:40  $\text{V}_2\text{O}_5\text{:Na}_2\text{SO}_4$  (Mol%). They characterised the morphology and chemical compositions of the corrosion products and found that the presence of sulphur and its oxidised compounds favour the formation of isolated lobes with

radial morphology. These lobes had great permeability which facilitated the access of oxygen; therefore the protective character of the scale was reduced. They reported that the presence of vanadium and its oxidised products generate compounds with aciculate morphology, which is not very much covering and reduces the protective character of the scale. The equilibrium diagram for varying composition of  $\text{Na}_2\text{SO}_4$  is shown in Fig. 2.13 and the mixture of  $\text{Na}_2\text{SO}_4$ -60% $\text{V}_2\text{O}_5$  is seen to have the lowest eutectic temperature.

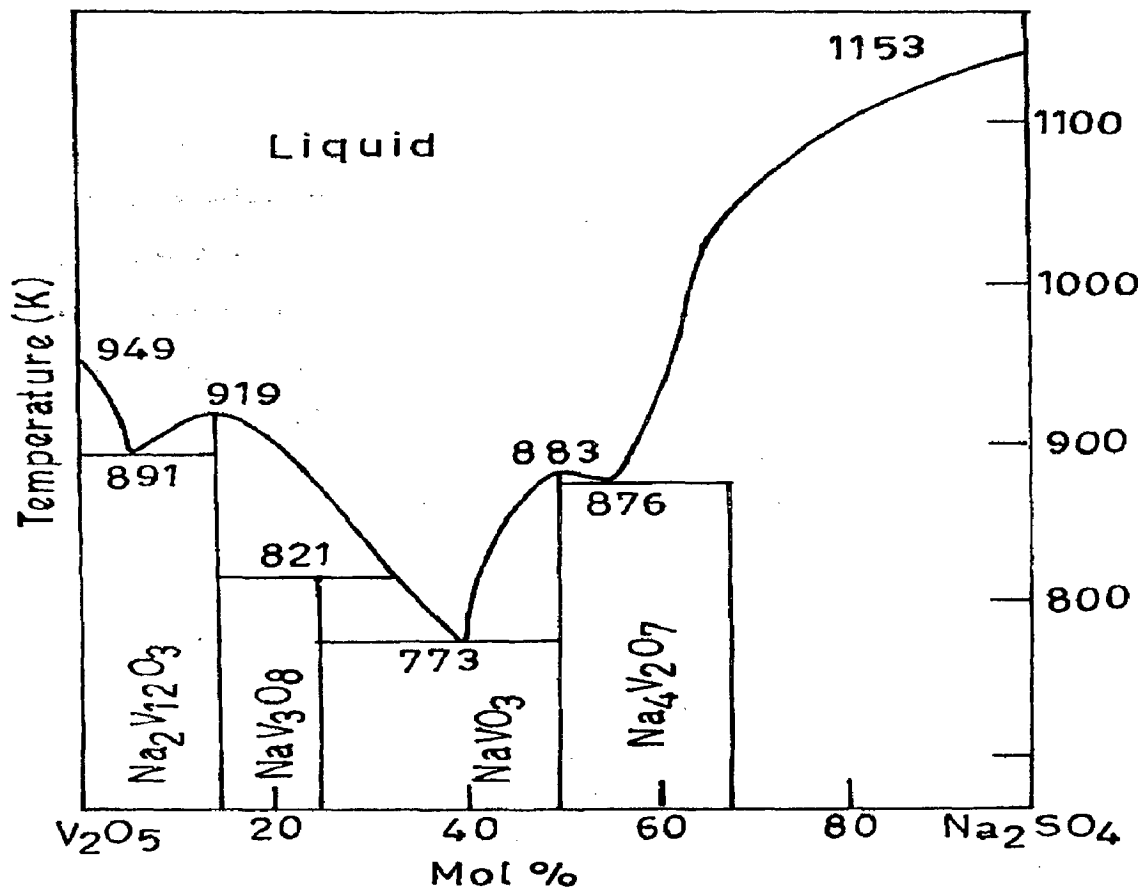


Fig. 2.13 Phase Diagram for  $\text{Na}_2\text{SO}_4$ - $\text{V}_2\text{O}_5$  System (Otero et al, 1987).

Otero et al. (1990) again studied the hot corrosion behaviour of the same alloy IN657 in same molten salt environment 60% $\text{V}_2\text{O}_5$ -40% $\text{Na}_2\text{SO}_4$ . They observed that for duration less than 100 hours, the corrosion kinetics increased with temperature when the temperature was less than 727 °C. For temperatures greater than 727 °C, corrosion rate decreased. An increase in corrosion rate with temperature observed during the initial stages of exposure was related to the higher fluidity of the molten salt mixture. At temperatures greater than 727 °C, once the appropriate fluidity was

achieved, the corrosion rate decreased due to the decrease in the oxygen solubility in the molten salt.

Otsuka and Rapp (1990) examined the effects of chromate and vanadate anions on the hot corrosion of Ni by a thin fused  $\text{Na}_2\text{SO}_4$  film in an  $\text{SO}_2\text{-O}_2$  gas atmosphere at  $900^\circ\text{C}$ . The results indicate that the inhibition of sulphidation may be due to the precipitation of solid  $\text{Cr}_2\text{O}_3$  from the melt which partially seals/plugs the crack defects and grain boundaries of the original protective oxide layer. Further, they found that vanadate anions enhanced the onset of the hot corrosion and sulphidation probably via rapid dissolution of the protective oxide scale at cracks/defects or grain boundaries.

The oxidation and hot corrosion studies of nickel based alloys in  $\text{Na}_2\text{SO}_4\text{-60\%V}_2\text{O}_5$  environment at  $700^\circ\text{C}$  were carried out by Lambert et al. (1991) to investigate the effects of Si addition. The chemical compositions (wt.%) of these alloys were Ni-17Cr-6Al-0.5Y and Ni-16Cr-5.7Al-0.47Y-5Si. They found that an outer layer of NiO developed on the surface of the standard alloy whereas a thin  $\text{Al}_2\text{O}_3$  scale formed on the Si enriched alloy. They opined that the condensed vanadates of sodium are highly corrosive and can markedly increase the rate of oxidation of nickel-based superalloys. According to them, the development of protective oxide barrier was considerably affected by the corrosive coating, particularly in the Si-enriched alloy. They detected Ni, Cr, Al and Si complex oxides in the inner oxide layer.

Swaminathan and Raghavan (1992) reported that the cracking and fluxing of the protective scales together with easier crack nucleation and growth at grain boundaries in the presence of liquid deposits of sodium metavanadate and sodium metavanadate plus 15wt% sodium sulphate at  $650\text{-}750^\circ\text{C}$  account for the enhanced creep rates and reduced rupture life for superni-600. Swaminathan and Raghavan (1994) further studied superni-C276 in the presence of  $\text{NaVO}_3$  and  $\text{NaVO}_3\text{-15\%Na}_2\text{SO}_4$  at  $650, 700$  and  $750^\circ\text{C}$ . They reported similar findings of an enhanced creep damage at all test temperatures. They opined that the degradation of the alloy in case of  $\text{NaVO}_3$  melt was due to the cracking of the protective scales under the influence of the applied stress and the fluxing action of the melt. They further reported that eutectic  $\text{NaVO}_3 + 15\text{wt\% Na}_2\text{SO}_4$  mixture was more severe in degrading the creep properties. They found that addition of sodium sulphate to sodium metavanadate increased the corrosivity of the deposit by lowering the melting point and by the formation of molten Ni-NiS<sub>2</sub> eutectic which initiates a self

sustaining hot corrosion. Further, they revealed that the additional presence of molybdenum compounds  $\text{Na}_2\text{MoO}_4\text{-MoO}_3$  enhanced the degradation.

Deb et al. (1996) in their study on the hot corrosion behaviour of a cast nickel-based superalloy coated with 60%  $\text{Na}_2\text{SO}_4\text{-30% NaVO}_3\text{-10% NaCl}$  observed a thin layer of NiO, followed by a thick layer of  $\text{Ni}_3(\text{VO}_4)_2$  and a inner porous duplex layer of oxides of Ni and Cr and CrS. They observed that the corrosion rate decreased with time, which they attributed to the formation of refractory nickel vanadate layer over the surface. The authors also conducted studies in 100%  $\text{Na}_2\text{SO}_4$  and 75%  $\text{Na}_2\text{SO}_4 + 25\% \text{NaCl}$  molten salt environment. They revealed that the presence of sulphur in the form of sulphates caused internal sulphidation of the alloy beneath the external oxide layer. Further, volatile species of chlorides led to formation of voids and pits at grain boundaries, which provide easy path for the corrodents to penetrate into the alloys. They observed that the presence of vanadate in conjunction with sulphate and chloride provided additional fluxing action, which destroyed the integrity of the alloy and weakened its mechanical properties.

Gurrappa (1999) studied the hot corrosion behaviour of Ni-base superalloy CM 247 LC in  $\text{Na}_2\text{SO}_4$  and  $\text{Na}_2\text{SO}_4\text{+NaCl}$  mixtures at 900 °C. He has observed that the superalloy CM 247 LC got severely corroded in just 4 hr, while it was completely consumed in 70 hr when tested in 90% $\text{Na}_2\text{SO}_4\text{+10%NaCl}$  at 900 °C. The life of the superalloy, however, further decreased to just 2 hours when studied in 90% $\text{Na}_2\text{SO}_4\text{+5%NaCl+5%V}_2\text{O}_5$  environment at 900 °C.

Gitanjaly (2003) studied the hot corrosion performance of some Ni-, Fe- and Co-based superalloys in an environment of  $\text{Na}_2\text{SO}_4\text{+60%V}_2\text{O}_5$  at 900 °C. In general, the author observed significant corrosion rates in all the superalloys. However, the Ni-based superalloy superni 75 showed lowest rate of corrosion compared to Co-base superalloy superco-605. The better corrosion resistance of Ni-base superalloys was attributed to the presence of refractory nickel vanadate  $\text{Ni}(\text{VO}_3)_2$  which acted as a diffusion barrier for the oxidising species. The proposed hot corrosion mechanisms of this study for the superalloys superni 75 and superni 601 have been schematically shown in Fig. 2.14.

Tzvetkoff and Gencheva (2003) reviewed the mechanism of formation of corrosion layers on nickel and nickel-based alloys in melts containing oxyanions. They reported that acidic oxides such as those of V and Mo induce rapid fluxing of the oxide scale and therefore catastrophic hot corrosion. The chromates were stated to be beneficial for the repassivation of the surfaces following fluxing of the oxide scale by the molten salt. Further, they reported that the molten

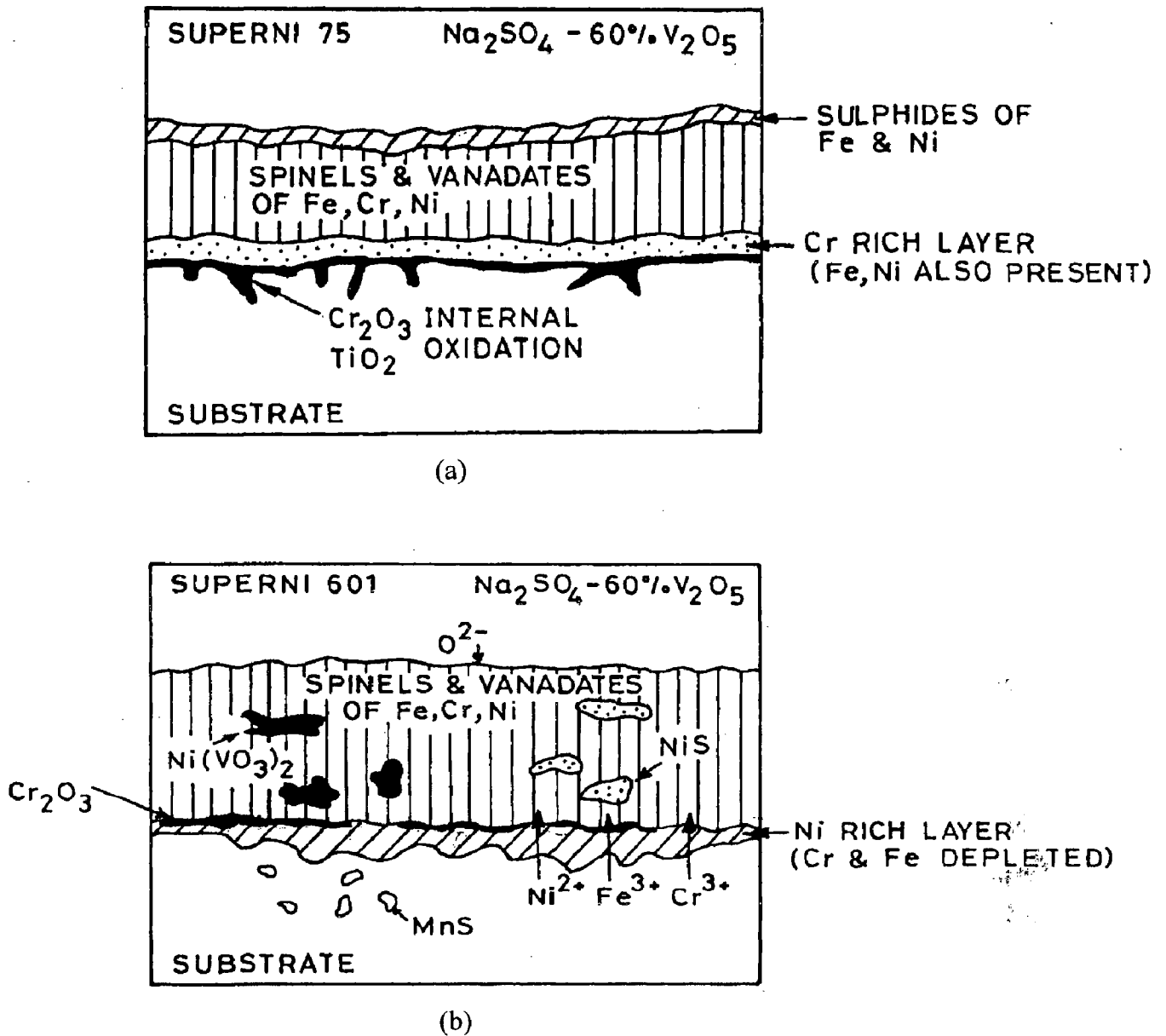


**Fig. 2.14** Schematic diagram showing probable hot corrosion mechanism in  $\text{Na}_2\text{SO}_4 - 60\% \text{V}_2\text{O}_5$  after exposure for 50 cycles at  $900^\circ\text{C}$  for alloys (Gitanjaly, 2003) (a) superni 75 (b) superni 601.

sulphate mixtures are aggressive towards Ni superalloys. In such environments, the formation of Cr-rich passive films such as spinel-type oxides could be protective to some extent. They further detected the presence of sulphides at metal/oxide interface which do not offer plausible protection except for a possible positive role of  $\text{MoS}_2$  formed on Ni alloys containing significant amounts of Mo.



Singh et al. (2005D) investigated the corrosion behaviour of a nickel-base superalloy in  $\text{Na}_2\text{SO}_4$ -60% $\text{V}_2\text{O}_5$  environment at 900 °C under cyclic conditions for 50 cycles of one hour each. They used thermogravimetric technique to establish the kinetics of corrosion. They revealed that superalloy superalloy 601 showed intense spalling of the scale and the weight gain, including the spalled scale, was enormous during hot corrosion studies in the given aggressive environment. They reported continuous increase in the weight of the superalloys, but the rate of increase was high during the initial period of exposure. They revealed that  $\text{NaVO}_3$  formed due to the reaction of  $\text{Na}_2\text{SO}_4$ -60% $\text{V}_2\text{O}_5$  acts as a catalyst and also serves as a oxygen carrier to the metal. The chromium has high affinity for oxygen to form  $\text{Cr}_2\text{O}_3$  and so in the earlier stages of hot corrosion, there was rapid increase in weight.

Prakash et al. (2005) studied the hot corrosion behaviour of another Ni-based superalloy under the same conditions and at same temperature. They reported that the superalloy suffered a catastrophic corrosion in the form of intense spalling and sputtering of the scale. They attributed this behaviour to the presence of Mo in the alloy, as oxides of Mo cause an alloy-induced acidic fluxing. Ravindra et al., (2007) also reported the hot corrosion and oxidation behaviour of a directionally solidified nickel base superalloy.

#### **2.4.4 Hot Corrosion of the Iron and Iron-Based Alloys**

Fairman (1962) reported severe corrosion of some metal specimens in an ash mixture ( $\text{V}_2\text{O}_5$  +10%  $\text{Na}_2\text{SO}_4$ ) environment in air. The corrosion attack was found to be greatest where the concentration of  $\text{O}_2$  and  $\text{V}_2\text{O}_5$  was higher, suggesting the transfer of oxygen atoms or ions by the pentoxide to the metal surface:  $2\text{V}_2\text{O}_5 \rightarrow 2\text{V}_2\text{O}_4 + 2\text{O} \downarrow$ . He reported that the accelerated oxidation is a diffusion controlled process of the incorporation of defects into the oxide scale. He further suggested that the mechanism of accelerated attack could be most satisfactorily explained by the catalytic action of  $\text{V}_2\text{O}_5$  operating with an increase in the defect concentration of the scale.

Thilkan et al. (1967) studied the hot corrosion of nickel free austenitic stainless steel, Cr-Ni stainless steel and Inconel in an oxygen atmosphere at different temperatures and in an aggressive environment of vanadium-sodium salt of varying composition. They justified the use of saturated solution of  $\text{Na}_2\text{SO}_4$  as the liquid medium because of its low gas solubility, vapour pressure and viscosity. They reported that threshold temperature lie between 700 and 800 °C. Above the threshold temperature, the extent of attack initially increased but with increasing temperature either it became

constant (as observed for Inconel) or decreased (for other alloys). Oxidation first increased and then decreased with increase in the amounts of  $\text{Na}_2\text{SO}_4$  in the mixtures of sodium sulphate-vanadium pentoxide in temperature range 820-870 °C. However, at 950 °C all  $\text{Na}_2\text{SO}_4$  additions decreased the corrosive effect of  $\text{V}_2\text{O}_5$ . They revealed that fluidity of slag was important in allowing diffusion of oxygen. At lower temperatures, the fluidity might have a marked effect in increasing the attack. At higher temperatures, however, this may not have any effect on the corrosion rate as there may be negligible difference in the fluidity of fused  $\text{V}_2\text{O}_5$  and  $\text{V}_2\text{O}_5$ - $\text{Na}_2\text{SO}_4$  mixture. They found an interesting observation that nickel free stainless steel has a high resistance to attack against  $\text{V}_2\text{O}_5$ - $\text{Na}_2\text{SO}_4$  mixture and under the experimental conditions showed a resistance superior to that of even Inconel at temperatures 850 °C specially in 70%  $\text{V}_2\text{O}_5$ -30%  $\text{Na}_2\text{SO}_4$ .

Kerby and Wilson (1972) revealed that the liquid vanadates increase the corrosion rate of metals by fluxing of the normally protective oxide layers present on the surface of the alloys and by providing a source of oxide ion for the corrosion reaction. The electrical conductivity increased with increase in temperature and with decreasing oxygen pressure. Incorporation of sodium into the  $\text{V}_2\text{O}_5$  lattice structure caused a reduction in the valency of the vanadium atoms from  $\text{V}^{5+}$  to  $\text{V}^{4+}$  due to donation of the alkali metal valence electron to a vanadium atom.

Valdes et al. (1973) studied AISI 446 stainless steel under  $\text{V}_2\text{O}_5$  and  $\text{Na}_2\text{O} \cdot 6\text{V}_2\text{O}_5$  environment in the temperature range 700-900 °C in air and found that the oxide scale was mainly  $\text{Cr}_2\text{O}_3$  with some vanadium oxide which acted as a moderate barrier to corrosion. Above 850 °C in  $\text{V}_2\text{O}_5$ , a breakaway corrosion reaction occurred. No  $\text{Cr}_2\text{O}_3$  oxide barrier was present but there was a continuous oxide scale that comprised of  $\text{Cr}_2\text{O}_3$ ,  $\text{Fe}_2\text{O}_3$  and  $\text{V}_2\text{O}_5$  at the metal/oxide interface from which a region of crystals grew. They suggested that the addition of  $\text{Na}_2\text{O}$  to  $\text{V}_2\text{O}_5$  increased the oxide ion ( $\text{O}^{2-}$ ) content of the melt and made it more aggressive to acidic oxides such as  $\text{Cr}_2\text{O}_3$ .

Shi et al., (1992) studied the effect of  $\text{K}_2\text{SO}_4$  added to a  $\text{Na}_2\text{SO}_4$  deposit on the high temperature hot corrosion behavior of iron aluminum alloys. He concluded that  $\text{K}_2\text{SO}_4$  additive accelerated the low temperature hot corrosion of Fe-Al alloys caused by  $\text{Na}_2\text{SO}_4$  deposit atmospheres containing  $\text{O}_2$ ,  $\text{SO}_2$ , and  $\text{SO}_3$  but the corrosion mechanism remained unchanged. In the early stage, dissolution/precipitation of iron oxides proceeded at a considerable rate; at a longer time, growth of a compact iron oxide dominated the accelerated hot corrosion caused by  $\text{K}_2\text{SO}_4$  additive was not attributed to the formation of complex sulfates or the stimulation of

sulfation of  $\text{Fe}_2\text{O}_3$ , but rather to the earlier appearance of a eutectic melt on the alloy surface. The equilibrium phase diagram for varying composition of  $\text{Na}_2\text{SO}_4$  and  $\text{K}_2\text{SO}_4$  is shown in Fig. 2.15.

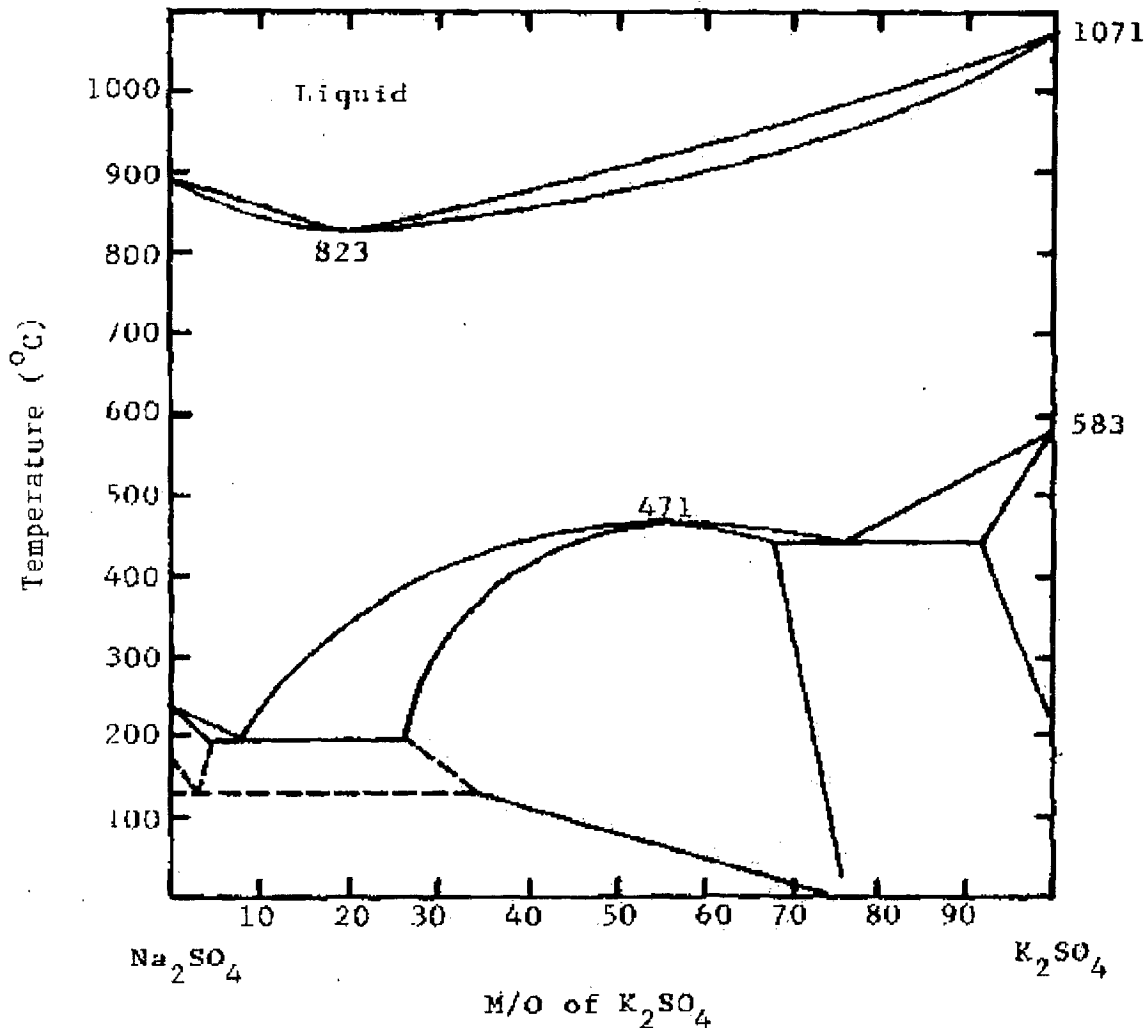


**Fig. 2.15** Phase diagram of  $\text{Na}_2\text{SO}_4$  and  $\text{K}_2\text{SO}_4$  system (Shi et al., 1992).

Tiwari and Prakash (1996 and 1997) and Tiwari (1997) have reported hot corrosion studies on some industrial superalloys in temperature range 700-900 °C in the environments comprising of pure  $\text{Na}_2\text{SO}_4$ ,  $\text{Na}_2\text{SO}_4$ -15% $\text{V}_2\text{O}_5$  and  $\text{Na}_2\text{SO}_4$ -60% $\text{V}_2\text{O}_5$ . The corrosion rates were observed to be very high in the environment having  $\text{Na}_2\text{SO}_4$ -60% $\text{V}_2\text{O}_5$  composition. The extremely corrosive nature of this composition was attributed to its low melting point i.e. 550 °C.

Tiwari and Prakash (1997) further revealed that in  $\text{Na}_2\text{SO}_4$ -60% $\text{V}_2\text{O}_5$  melt, the degradation was due to the cracking of the protective scale under the influence of the fluxing action of the melt for both Fe-base alloy superfer 800H and Co- base alloy superco 605. The enhanced degradation was reported to be due to the presence of tungsten in form of  $\text{Na}_2\text{WO}_4$ - $\text{WO}_3$  compound. No oxidation and sulphidation into the substrate was observed by them in Co-based alloy. Tewari (1997) concluded that the Co-based alloy has inferior corrosion resistance than the Ni-base alloy in  $\text{Na}_2\text{SO}_4$ -60% $\text{V}_2\text{O}_5$  environment at 900 °C.

Almeraya et al. (1998A) conducted electrochemical studies on AISI-SA-213-TP-347H steel in 80 wt%  $\text{V}_2\text{O}_5$  + 20 wt%  $\text{Na}_2\text{SO}_4$  at temperature 540 °C–680 °C and reported the corrosion rate values of around 0.58-7.14 mm/year. They found an increase in the corrosion rate with time. However, the corrosion potential was observed to be decreasing with increase in temperature from 540 °C to 680 °C. Almeraya et al. (1998B) further conducted electrochemical studies of hot corrosion of type 347H stainless steel under same environment and temperature range, and revealed that with change in temperature from 540 °C to 680 °C the corrosion potential decreased.

Cuevas-Arteaga et al. (2001) used LPR (Linear Polarisation Resistance) and weight loss techniques, in their hot corrosion study on alloy 800 in  $\text{Na}_2\text{SO}_4$ -20% $\text{V}_2\text{O}_5$ , and reported a slightly higher corrosion rate at 900 °C than at 700 °C. They further reported that in both the techniques, the corrosion rate increased in the beginning of the experiment but decreased later on until steady values reached.

Kamachi Mudali et al., (2004) reported that the stainless steels are prone to corrosion whenever they are exposed to aggressive corrosive environments, including aqueous, high temperature, stress and other service parameters. Under such circumstances, attention is paid to create entirely different surface properties by forming corrosion-resistant coatings

Singh et al. (2005C) investigated the hot corrosion behaviour of an iron-based superalloy in molten salt ( $\text{Na}_2\text{SO}_4$ -60% $\text{V}_2\text{O}_5$ ) environment at 900 °C under cyclic conditions for 50 hours and found that the superalloy underwent severe spalling and sputtering and the weight gain was enormous during the course of study.

Sidhu et al., 2006F reported that iron-base superalloy superfer 800H underwent intense spalling, sputtering (disintegration of the scale accompanied by cracking sound during cooling) and peeling of the scale in an aggressive environment of  $\text{Na}_2\text{SO}_4$ -60% $\text{V}_2\text{O}_5$  at 900 °C. During the

cyclic study for 50 hours, the mass gained by the superalloy was enormous. It was found that the mass increased continuously, although the rate of increase was high during the initial period of exposure. This rapid increase in mass gain was attributed to the formation of  $\text{NaVO}_3$  compound. This  $\text{NaVO}_3$  acts as a catalyst and also serves as an oxygen carrier to the base alloy that leads to the rapid oxidation of the basic elements of the superalloy to form the protective oxide scale. Slower increase in mass gain after initial mass gain was due to the simultaneous growth and dissolution of oxide scale in the molten salt due to the reaction



This  $\text{Na}_2\text{CrO}_4$  gets evaporated as a gas

Sidhu et al., 2006F and 2006G reported the performance of HVOF sprayed  $\text{Cr}_3\text{C}_2$ -NiCr coatings on a Fe-based superalloy in  $\text{Na}_2\text{SO}_4$ -60% $\text{V}_2\text{O}_5$  environment at 900 °C under cyclic conditions. The weight change measurements were used to study the kinetics of corrosion. The coating has successfully imparted the hot corrosion resistance to the molten salt environment. The corrosion resistance of the  $\text{Cr}_3\text{C}_2$ -NiCr coated alloys has been ascribed to the formation of phases like  $\text{Cr}_2\text{O}_3$ , NiO, and  $\text{NiCr}_2\text{O}_4$  in the oxide scales.

## 2.5 SOME STUDIES ON POWER PLANT ENVIRONMENTS

Different authors reported that accumulation /condensation of low melting-point salts from flue-gases on the boiler tubes used for super-heaters and reheaters in coal fired boilers is a root cause for the severe wastage of tube materials. These salts containing sulfates of sodium and potassium easily liquefy at the operating temperatures and causes sever hot corrosion of boiler tubes (Nelson et al., 1959; Rapp, 1986; Backman et al., 1987; Salmenoja et al., 1996).

Boilers and other steam power plant equipments are subjected to a wide variety of failures involving one or more of several mechanisms. Overheating is reported to be the main cause of failure in steam generators. A survey compiled by one laboratory over a period of 12 years, encompassing 413 investigations, listed overheating as the cause in 201 failures or 48.7% of those investigated. Fatigue and corrosion fatigue were listed as the next most common causes of failure accounting for 89 failures or 21.5%. Corrosion, stress corrosion and hydrogen embrittlement caused a total of 68 failures or 16.5%. Defective or improper material has been cited as the cause of most of the remaining failures (13.3%). Although “defective material” is often blamed for a failure but this survey indicates that statistically it is one of the least likely cause of failure in power plant equipments (Metals Handbook, 1975).

Moujahid (1987) observed severe ash corrosion, mechanical deformation and cracks on the cast iron chains of moving grate used to air burning of coal. Liquid coal ash at 1300 °C is strongly acidic, dissolves the basic wustite/spinel layers which formed on the chains at elevated temperature. The fused ash embeds coal particles and also reduces the thermal efficiency of the equipment. Drastic enhancement in ash corrosion rate has been attributed to the mechanical damages. Kofstad (1990) explained these diffusion processes with the help of neat sketches shown in Fig. 2.16 which illustrate the growth of chromia scale in the presence or absence of oxygen active elements.

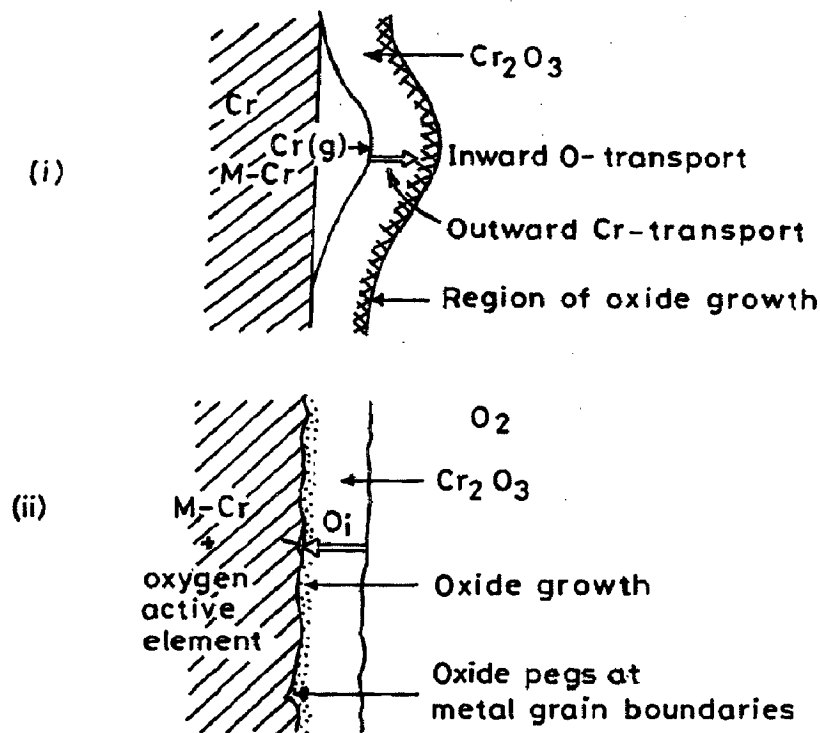


**Fig. 2.16** Schematic illustration of the growth of chromia scales in (i) the absence of oxygen active elements and with predominant outward transport of chromia through the scale, and (ii) the presence of oxygen active elements and with predominant inward transport of oxygen (Kofstad, 1990).

Iyer et al. (1987) studied the hot corrosion behaviour of Nimonic 80A under tension using combustion gases environment at 600-700 °C and reported the presence of NiO, Cr<sub>2</sub>O<sub>3</sub>, Ni(VO<sub>3</sub>)<sub>2</sub> and NiO.Cr<sub>2</sub>O<sub>3</sub> on the surface of the corroded alloy. Accelerated oxidation was observed and the scale was reported to be spongy. They observed that the lowest melting liquid was formed even at 550 °C. They suggested that the presence of stresses enhanced the damage due to spalling, allowing fresh surface to be exposed to hot corrosion. They proposed that as vanadium content increases some of the vanadium participates as vanadates and, therefore, increase in vanadium beyond a certain level is not monotonically aggressive. This critical level was found to be around 20 ppm vanadium. Also at high-temperature, the stability of V<sub>2</sub>O<sub>5</sub> would decrease resulting in critical level of V for the worst corrosion attack. Early in 1945, it was reported that both Na<sub>2</sub>SO<sub>4</sub> and K<sub>2</sub>SO<sub>4</sub> deposited on the surface of heat exchange tubes or plates in boilers, later study showed that the co-deposition of Na<sub>2</sub>SO<sub>4</sub> and K<sub>2</sub>SO<sub>4</sub> was frequently found in gas turbines operating in a coal-fired combined cycle (Shi et al., 1992).

Levy (1993) observed unacceptable levels of degradation of heat exchanger tubes in some boilers, particularly fluidized bed combustors, by a combined mechanism of erosion-corrosion. The author noticed that the extent of such degradation varied considerably, both between different boilers and within the same boiler operating on different feed-stocks. However, primarily same erosion-corrosion mechanism occurred in all cases that has integrated both chemical and mechanical behaviour of the base metal and the boiler particles. They revealed the formation of a continuous and dynamic surface layer that consists of a mechanical mixture of particles from the boiler gases and oxide scale growing from the base metal. It was constantly refurbished and removed at a rate that resulted in an essentially constant thickness of the deposit/scale layer during steady state operation of the boiler. So the loss of sound metal is related to the rate of oxidation of metal.

Colot et al. (1997) investigated the corrosion of 9 Cr-Mo (T91 and EM12) steels in synthetic environments similar to those experienced by tubes in the coal-fired boilers. They compared the effects of water vapour, SO<sub>2</sub> and ash deposits with and without alkali salts on the corrosion of steels in ambient air in the temperature range 460 -800 °C. In the synthetic atmospheres, maximum corrosion rate was observed approximately at 600 °C which they attributed to the effect of water vapour and/or SO<sub>2</sub>. They reported that the alkali silicates are responsible for high rates of corrosion as temperature reaches 800 °C.

Saunders et al. (1997) studied high-temperature corrosion behaviour of FeCr alloy and three iron aluminides alloy containing 16 and 28 at% Al with up to 5 at% Cr in simulated coal gasification conditions containing 1000 ppm HCl at 450 and 550 °C and 3283 ppm HCl at 550 °C for 1000 hrs. They used higher HCl level at 1 bar in the laboratory experiments to simulate a gasifier operating at 10 bar with a coal containing 0.3% Cl. According to them, inter-metallic alloys containing 28 at% Al and 2-5 at% Cr showed exceptional resistance to attack even in the most aggressive conditions with mass gains of generally less than  $1 \text{ g m}^{-2}$ . The corrosion resistance was somewhat reduced for the lower Cr alloy. For the most aggressive test conditions, the inter-metallic alloys were found to exhibit superior resistance to attack as compared with FeCr alloy, but a 16 at% Al inter-metallic with 5 at% Cr showed the lowest corrosion resistance among the materials investigated.

Prakash et al. (2001) reported a case study on boiler tube failure in the coal fired power plants in north-western region of India, covering a period of one year. They described that total 89 failures occurred in the study period, out of which 50 failures were attributed to the ho corrosion and erosion by ash. They further investigated five samples of failed boiler tube: selected randomly from the same installation. They found overheating as another main cause of tube failures.

Krishna and Sidhu (2002) observed severe pitting corrosion of carbon steel tube in the air-preheater of thermal power plant. They reported that corrosive species settled at the tube surface due to the extended non operation of the plant. The complete failure of the tubes occurred due to diffusion of these elements into the base metal and precipitation of potassium and chlorine compounds along the grain boundaries with subsequent dislodging of grains. Further they reported that the nonmetallic inclusions acted as nucleating sites for local pitting bursting. Non-uniform heat transfer during operation accelerated the selective corrosion of front-end tubes and relatively high heat transfer resulted in condensation of some corrosive gases and consequent corrosion. Continuous operation of the plant with some precautions during assembly of the tubes reduced the corrosion problem.

Uusitalo et al. (2003) performed high-temperature corrosion tests on ferritic and austenitic boiler steels, using simulated bio-fuel combustion conditions at 550 °C for 1000 hours. The tests were performed in oxidizing atmosphere containing 500 vppm HCl, 20% H<sub>2</sub>O, 3% O<sub>2</sub>, and Argon the balance. The author reported that the chromium oxide layer formed on the austenitic

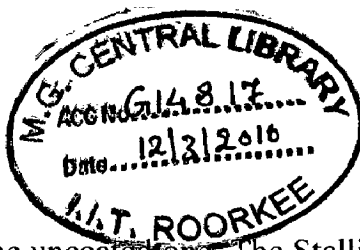


steel was more protective than the iron oxide layer on the ferritic steel. He further reported that oxides formed in presence of chlorine reduced the corrosion rate but they were not protective. The oxides on the ferritic steel spalled off. The chromium oxide layer on the austenitic steel was observed to be discontinuous and cracks in the oxide layer were also detected. Some chlorine-containing corrosion products of iron, chromium and nickel are reported to be volatile at test temperature.

Wang and Pan (2003) studied the high-temperature corrosion of a boiler material (SB450) using simulated combustion environment of an actual boiler's service conditions, at 750 and 850 °C using carbon steel with 2 mg cm<sup>-2</sup> NaCl coating. The combustion environment was produced by burning ASTM 2D diesel oil or an emulsion thereof with 10% water. The experimental results indicate that both the higher temperature and the water vapours in the atmosphere promoted metal loss. The metal loss of SB450 in the atmosphere that contained water vapours, resulting from the burning of emulsified oil, was more than that obtained by burning just the diesel oil. They reported that water vapour contributed to higher SO<sub>2</sub> concentrations in the gas produced, thus, SB450 suffers sulphidation more seriously in an atmosphere that contains water vapours than in one obtained by burning diesel oil and, therefore, it deteriorates more rapidly.

Coal is an attractive fuel owing to its low price linked to its worldwide availability and due to the future shortage of other fossil fuel reserves such as oil and gas. But combustion of coal generates very corrosive media particularly near the super-heater tubes. Hot corrosion of boiler tubes used for super-heaters and re-heaters in steam-generating systems has been recognized as a severe problem, resulting in tube wall thinning and premature failure. Attempts to decrease the maintenance costs of these components have increased interest in shielding them with protective coatings (Sidhu et al., 2006B).

Sidhu et al. (2006A, B, C, D, E) conducted experiments in an attempt to evaluate the hot corrosion behaviour of HVOF sprayed NiCrBSi and Stellite-6 coatings on a nickel-based superalloy in an actual industrial environment of a coal fired boiler. The cyclic studies were performed in the platen super-heater zone of a coal-fired boiler where the temperature was around 900 °C. Experiments were carried out for ten cycles each of 100 h duration followed by 1 h cooling at ambient temperature. Both the coatings deposited on Ni-based superalloy imparted



better hot corrosion resistance than the uncoated one. The Stellite-6 coated superalloy performed better than the NiCrBSi coated alloy in the given environment.

## 2.6 PREVENTIVE MEASURES AGAINST HOT CORROSION

The corrosion control in highly aggressive applications requires careful selection of materials. Nickel-based superalloys have good mechanical properties and superior corrosion resistance at higher temperatures and are used as base materials for hot section components in turbines. However, the hot corrosion is inevitable when these alloys are used at higher temperatures for longer periods of time in an extreme environment (Goebel et al., 1973).

Heath et al. (1997) proposed a number of countermeasures corresponding to the variety of corrosive environments including

- Proper selection of alloy,
- Optimum design of components,
- Use of chemical additives to neutralise the corrosive components in the flue gases,
- Shielding the substrate, and
- Protective coatings.

The important factors that influence hot corrosion are as follows: (a) alloy composition; (b) alloy fabrication condition; (c) deposit composition; (d) amount of deposit on superalloy; (e) gas composition and velocity; (f) temperature; (g) temperature cycles; and (h) erosion. (Gurrappa, 1999). Eliaz et al. (2002) also, in their review of hot corrosion in gas turbine components, suggested several approaches to control the hot corrosion of gas turbine components. These approaches are proper selection of structural alloys, application of coatings, washing of hot parts, air filtering, and control of both fuel cleanliness and composition.

Another method of hot corrosion prevention is to coat the alloy with a protective layer, which has been used in the current investigation. This is the preferred approach, even when relatively less hot corrosion-resistant alloys are used (Eliaz et al., 2002). For adequate corrosion protection of a metal in an aggressive environment, it is important to select materials and techniques that are compatible. For example, addition of an organic inhibitor (e.g. pyridines, pyrimidines, quinolines) is sufficient to mitigate corrosion of metals in many corrosive media. However, these inhibitors have shown only limited success due to solubility and/or thermal stability problems in high-temperature, concentrated salt solutions (Priyantha et al., 2003).

Hot corrosion preventive and control methods used in the aggressive environment can be classified as corrosion inhibitors, selection of proper alloy, cathodic protection and protective coatings (Priyantha et al., 2003; Bai et al., 2004). MCrAlYs are amongst the most important protective coating materials applied to counteract hot corrosion and high temperature oxidation. Like other coatings designed to resist oxidative environments at high temperatures, MCrAlYs should be capable of developing a thermodynamically stable, slow-growing and adherent surface oxide layer (Zhao et al., 2004B).

## 2.7 ROLE OF COATINGS

The coatings at high temperature develop a protective oxide layer on the metal surface to limit loss of metal by oxidation. Generally, these protective oxides (namely  $Al_2O_3$ ,  $Cr_2O_3$ , and  $SiO_2$ ) minimize the diffusion of gaseous or liquid species towards the component and conversely prevent elemental diffusion from the alloy towards the external surface where they could react with the substrate. Moreover, inter-diffusion effects between coating and substrates are supposed to be minimum as far as the properties of the coated component are concerned (Mevrel et al., 1989).

Early failure of the thermal power plant components frequently occurs due to the complex reactions between the metallic materials and the hostile combustion environment. It is important to clarify the degradation mechanism of the high temperature materials by typical salts, so as to reduce the tube material consumption by developing more protective structural materials and coatings, with an ultimate goal to increase the energy recovery efficiency (Li et al., 2005). Materials for high temperature service need excellent mechanical properties, including high temperature strength, good creep resistance, microstructure stability, and strong corrosion resistance. These requirements sometimes cannot be achieved by alloy development alone. An alternative approach in which mechanical strength is accomplished by alloy development and corrosion resistance by surface coating or surface treatment is often used (Tsaour et al., 2005).

Due to the increasing aggressive service environments, coatings must be applied to Ni-based superalloy gas turbine components for high temperature oxidation and hot corrosion resistance (Zheng et al., 2006).

Coatings are playing a significant role in today's aero and industrial turbine engines to extend the life or enhance the performance of components; about **75%** of all the components in jet

engines are coated (Zheng et al., 2006 and Gurrappa, 2000). The most common metallic coatings used in the hot section of turbine engines are MCrAlY type overlay coatings, which can be specifically designed and produced to meet the particular environmental operating conditions independent of substrates (Guo et al., 2006A).

### **2.7.1 Advantages of Coatings**

The demand for protective coatings has increased recently for almost all types of superalloys with improved strength, since high-temperature corrosion problem become much more significant for these alloys with increasing operating temperatures of modern heat engines (Yoshiba, 1993). Further, Porcayo-Calderon et al (1998) have reported the use of protective coatings for the super-heater/re-heater components of boiler where the material severely suffers on fireside corrosion. Coatings provide a way of extending the limits of use of materials at the upper end of their performance capabilities, by allowing the mechanical properties of the substrate materials to be maintained while protecting them against wear or corrosion (Sidky and Hocking, 1999).

Unfortunately, it is well known in the literature that it is not always possible to develop an alloy that will be resistant to hot corrosion as well as possess good high-temperature strength by the addition of alloying elements. Some alloying elements may help to improve the mechanical properties, while others may improve the hot corrosion resistance, but generally both properties are not improved simultaneously. For example, elements such as tungsten, vanadium, and molybdenum are excellent in improving mechanical properties, but their presence makes the alloy highly susceptible to hot corrosion (Gurrappa, 1999).

The desire for higher operating temperature, improved performance, extended component lives, and cleaner and more fuel-efficient power plant/processes places severe demands on the structural materials used to construct such a high-temperature plant. As a result, many components operating at high temperature within such plants are coated or surface treated (Nicholls, 2000). According to Taylor and Evans (2001), a few earlier attempts have been made on the thermal sprayed protective coatings for fossil power plants though the thermal spray process is extensively used for gas turbine applications

In addition to the development of the conventional steam-raising plant, alternative energy supply systems, such as combined cycle plants, in which a gas turbine and a steam turbine are

coupled, offer the prospect of even higher thermal efficiencies, as the gas turbine inlet temperatures are 1200 °C and above (Nickel et al, 2002). According to them, such high temperatures result in increased oxidation rates, therefore protective coatings with higher temperature capabilities are required. Therefore, an alternative is to go for protective coatings for hot corrosion resistance; it is necessary to develop appropriate coatings to enhance the operational life of the components. Although corrosion problems cannot be completely eliminated, however, 25 to 30% of annual corrosion related costs could be saved with the use of optimum corrosion preventive and control strategies (Koch et al., 2002; Priyantha et al., 2003).

Considerable efforts are now being made to produce high temperature degradation resistant coatings by various means. When these coatings exposed to an oxidizing environment, it form a dense and well-adhered oxide layer that controls both the outward diffusion of the alloying elements and the inward diffusion of the corrosive species (Shirvani, et al., 2003). Sundararajan et al (2003A and B) advocate the need for applying thermal spray coatings on the boiler components.

### **2.7.2 Requirement of High Temperature Coatings**

The demand for protective coatings has increased recently even for almost all types of superalloys, since high-temperature corrosion problem become much more significant for these alloys with increasing operating temperatures of boilers, turbines and heat engines. The necessities for higher performance and increased efficiency have resulted in the progressive increase in their operation temperatures (Yoshiba, 1993; Stott et al., 1994; Conner and Connor, 1994). Protective surface treatments are widely used at low temperature, but the use of these at elevated temperature is more recent. High-temperature applications are limited largely to the aerospace industry. An enormous challenge exists to develop and apply these techniques to other high-temperature applications (Stroosnijder et al., 1994). As a result, components operating at high-temperature within such plants are coated or surface treated (Nicholls, 2000). Superalloys have been designed for high temperature applications; however, protective coatings are applied to enhance their life for use in corrosive environments as they are not able to meet the requirement of high-temperature strength and high-temperature corrosion resistance simultaneously (Liu et al., 2001).

### 2.7.3 Coating-Substrate Requirements

In oxidising environments at high temperature, a coating in general owes its oxidation resistance to the formation of a protective oxide layer. Therefore, in selecting coating materials, it is important that the coating-substrate system meet the following requirements (Kofstad, 1966; Chatterjee, et al., 2001).

1. The coating should be chemically and thermally stable (forming an integral coating-metal/alloy system) during service life of the component.
2. It should have properties compatible with those of the metallic substrate.
3. The rate of inter-diffusion of the elements in the integral system (i.e., between coating and substrate alloy) must be slow during the desired service life.
4. The protective layer and the metallic substrate should have matching thermal expansion coefficients to avoid cracking and exfoliation of the coating during thermal cycling.
5. A protective coating should exhibit some mechanical “elasticity” under operating conditions to accommodate creep and plastic deformation.
6. A coating material should resist damage from impact, erosion and abrasion depending on the specific applications of the metallic components.
7. It should exhibit a spontaneous “self-healing” property for self-repair in case failure occurs due to cracking or spallation of the layer. So, the coating should act as a reservoir for the highly oxidisable metallic constituent/constituents for early development of a protective scale.
8. It should be relatively easy to apply the coating on substrates and the defects that may occur during handling of the component should be repairable without accompanying adverse effects on the sound neighboring areas.

Consequently, the development of a truly satisfactory coating that meets all of the above requirements is a difficult task. Accordingly, compromises are often made, depending on the specific application of the coated material in a particular environment. Moreover, because of coating-environment and coating-substrate reactions, the structures of the actual protective coating systems are complex.

## **2.7.4 Coating Deposition Techniques**

Nicoll (1984) reported that from production point of view, chemical vapour deposition (CVD), physical vapour deposition (PVD) and thermal spraying (metal spraying) are used extensively. Since CVD process is a non-line-of-site technique, proper masking and tooling are the major design considerations and it is expensive. Another shortcoming of the CVD process is the inclusion of pack particles in the coating which can lead to coating failure.

There are many coating deposition techniques available, and choosing the best process depends on the functional requirements, adaptability of the coating material to the technique intended, level of adhesion required (size, shape, and metallurgy of the substrate), and availability and cost of the equipment. The commonly employed coating deposition techniques have been enlisted in Fig.2.17 (Bhushan and Gupta, 1991). These techniques are divided into metallic and non-metallic categories. Metallic coating deposition can be considered under three categories, hard facing being the technique most important to this research (DeMasi-Marcin and Gupta, 1994). Nicholls and Stephenson (1995) revealed that overlay coatings performed better than diffusion coatings at higher temperatures. For depositing overlay coatings, thermal spray technologies are often considered.

### **2.7.4.1 Thermal Spray Techniques**

In the early nineteen hundreds, a young Swiss inventor named Dr. Max Schoop invented thermal spraying, after watching his son playing with his toy cannon. Dr. Schoop observed that the hot lead shots that were projected out of the cannon, stuck to almost any surface, the result of which gave him the idea that if metal could be melted and projected in a spray like manner, then a surface could be built up with that material. A variety of engineering problems have been solved

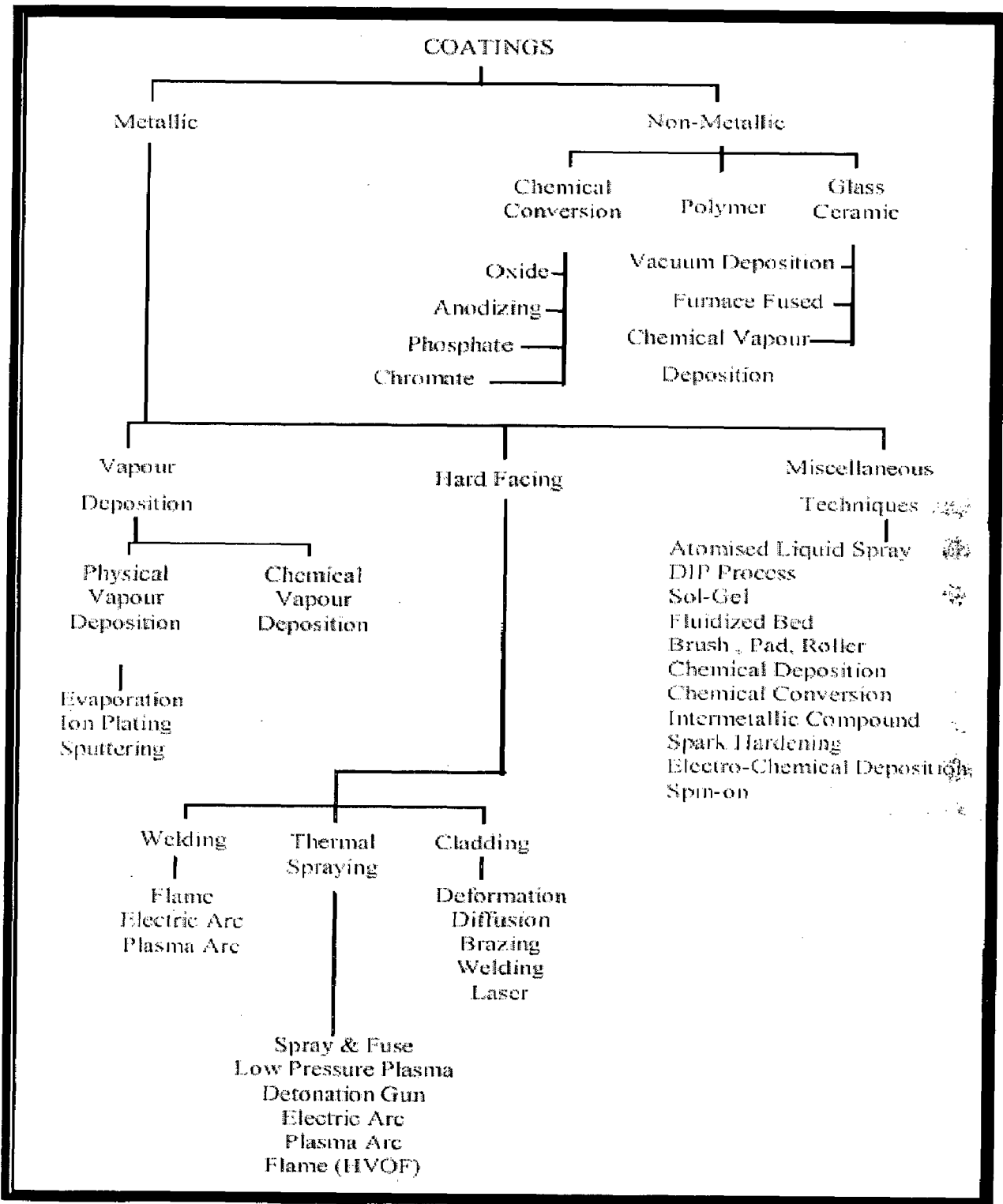


Fig.2.17 Coating deposition technology, (Bhushan and Gupta, 1991)



using thermal spraying applications. The use of thermal spraying ranges across many manufacturing processes, from the automotive to the space exploration industry (Nicoll, 1984). Thermal spraying is one of the most versatile hard facing techniques available for the application of coating materials used to protect components from abrasive wear, adhesive wear, erosive wear or surface fatigue and corrosion (such as that caused by oxidation or seawater) (Marceau and Adjorlolo, 1995).

Thermal spraying is a generic coating technique whereby droplets of molten or partially-molten material are generated and projected at a surface to form a coating. The droplets undergo little interaction with the substrate, merely adhering to the roughened surface through physical means to form an “overlay” coating. Variety of techniques has been designed for this process, varying in the manner in which they heat the material, the operating temperature and the velocity to which the droplets are accelerated. Through the range of operating conditions generated, any material that does not undergo sublimation or degradation upon heating can be applied as a coating. Materials ranging from polymers to metals, cermets and ceramics are routinely sprayed. In the generalised thermal spray process, the coating material in rod, wire or powder form, is fed into a high temperature heat source, where it is heated close to, or in excess of, its melting temperature. A high velocity accelerating gas or combustion gas stream accelerates the droplets of material to the substrate, where they impact and spread across the surface to form a “splat”, Fig. 2.18 (Matthews, 2004). The oxidation time during thermal spray coating is short (Fig. 2.19) typically less than 0.01 s, and can occur in either the solid or molten state. The oxidation of coatings is not always harmful, it is equally important to control and understand the different aspects of oxidation of coatings; therefore, it is important to find an optimum level for oxidation of coatings (Herman, 1988; Korpiola and Vuoristo, 1996; Nerz et al, 1992).

Generally, any material which does not decompose, vaporize, sublime, or dissociate on heating, can be thermally sprayed. Consequently, a large class of metallic and nonmetallic materials (metals, alloys, ceramics, cermets, and polymers) can be deposited by thermal spraying. Metals, carbides and cermets are the most widely used coating materials; however the spraying of polymers has also been investigated (Kawase and Nakano, 1996).

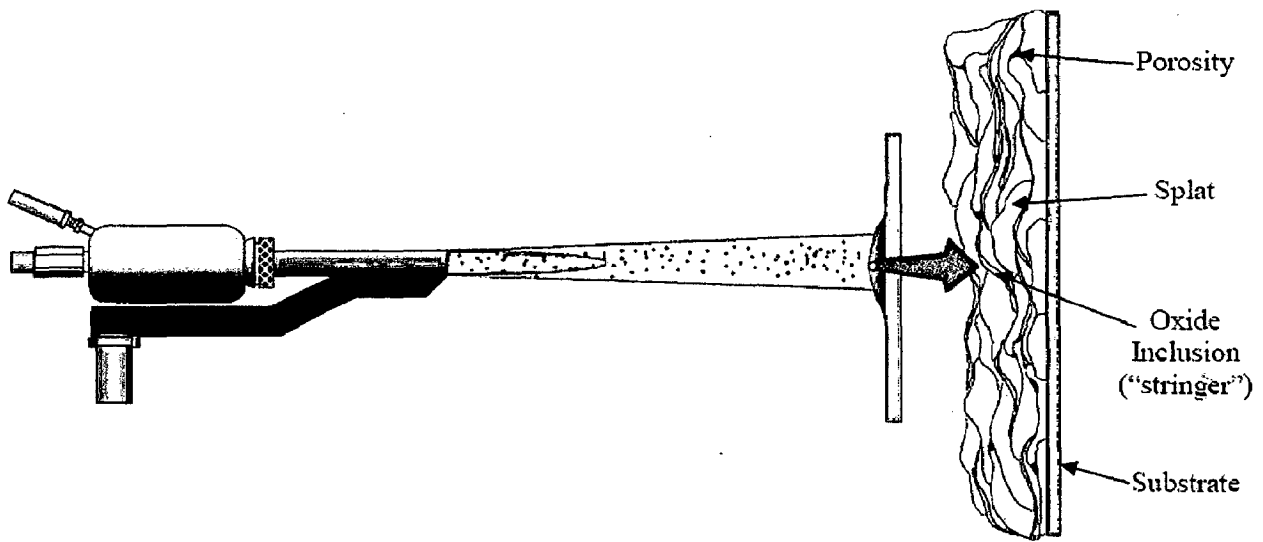


**Fig.2.18** Schematic development of the thermal spray process and mechanism of coating build-up (Matthews, 2004).

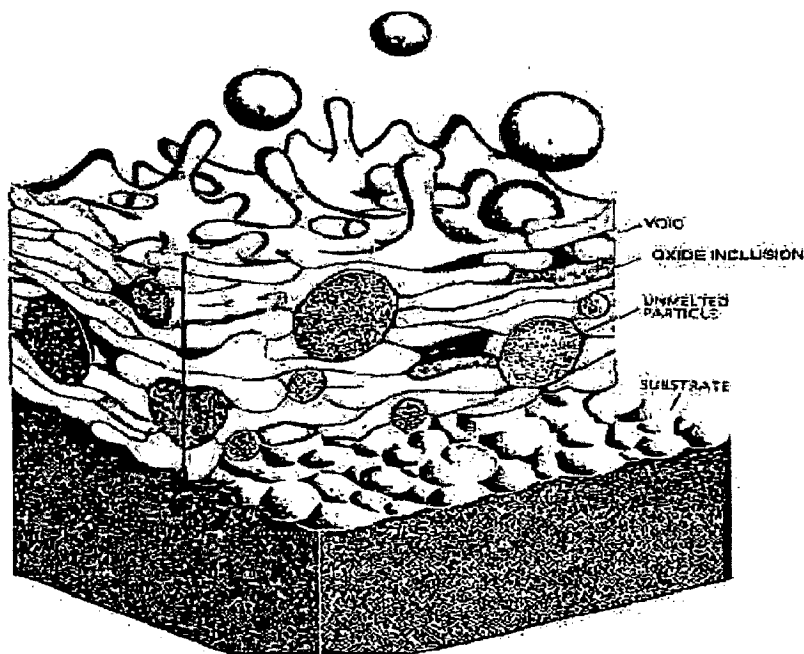


**Fig.2.19** Coating deposition and the oxidation process (Herman, 1988).

The Thermal spray processes that have been used to deposit the coatings for the protection against the high-temperature corrosion are enlisted below, summarised by Heath et al. (1997):

- Flame spraying with a powder or wire
- Electric arc wire spraying
- Plasma spraying
- Spray and fuse
- High Velocity Oxy-fuel (HVOF) spraying
- Detonation Gun

Table 2.1 shows some of the important characteristics associated with these thermal spray techniques (Bhushan and Gupta, 1991; Sobolev et al., 2004; Wagner et al., 1984). Particle speed, flame temperature and spray atmosphere are the main parameters which differentiate the various spraying techniques. Coating porosity, bond strength and oxide content are typical properties influenced by the coating procedure. Also, Kuroda et al., (2008) shown the classification of various thermal spray processes in terms of particle temperature and velocity (Fig.2.20). Similarly, Gledhill et al. (1999) proposed the schematic diagram (Fig.2.21) showing un-melted particles, splats, voids and in coming particles with un-melted core along the cross-section through a thermally sprayed coating. The technology continued, but expanded in the 70s due to development of the thermal plasmas and the increasing demand of high-temperature and wear resistant materials and coating systems (Knotek, 2001).

Deshpande et al. (2006) proposed that, during in-flight oxidation, a layer of oxide is formed on the molten particle due to chemical reactions between the surface of the liquid phase and oxygen or due to diffusion of oxygen into the liquid. The turbulent mixing of the liquid part of the powder particle during its flight destroys the surface layer of oxides and causes the oxides to be distributed more uniformly through the bulk volume of the particle. However, when temperature of the particle starts dropping during later part of the flight, these oxides tend to solidify and a thin oxide shell would form around the droplet (Fig.2.22).

Deposition Technique	Heat source	Propellant	Material feed type	Spray Gun temp. (°C)	Particle velocity m/s	Coating materials	Relative bond strength	Porosity level% volume
Electric Arc	Arc between electrodes	Air	Wire	6000	240	Ductile materials	Good	8-15
Plasma Arc Spraying	Plasma Arc	Inert Gas	Powder	16000	120-600	Metallic, ceramic, plastic and compounds	Very Good to Excellent	2-5
Low Pressure Plasma Spraying	Plasma Arc	Inert Gas	Powder	16000	900	Metallic, ceramic, plastic and compounds	Excellent	<5
Spray & Fuse	-	-	Powder	-	-	Fusible metals	Excellent	<0.5
Flame Spraying	Oxyacetylene/ Oxy hydrogen	Air	Powder	3000	30-120	Metallic and ceramics	Fair	10-20
Detonation Gun Spraying	Oxygen/ Acetylene/ Nitrogen Gas Detonation	Detonation Shock Waves	Powder	4500	800-1200*	Metallic, ceramic, plastic and compounds	Excellent	0.1 to 1
High Velocity Oxy-fuel (HVOF)	Oxy-propylene/ hydrogen/ propane/LPG	Combustion Jet	Powder/ wire	3000	800	Metallic and ceramic	Excellent	0.1-2

**Table 2.1** Comparison of characteristics for various thermal spray processes (Bhushan and Gupta, 1991; Stokes, 2003; Sobolev et al.2004 ; Wagner et al.1984\*, Hao Du et al. 2005\*).

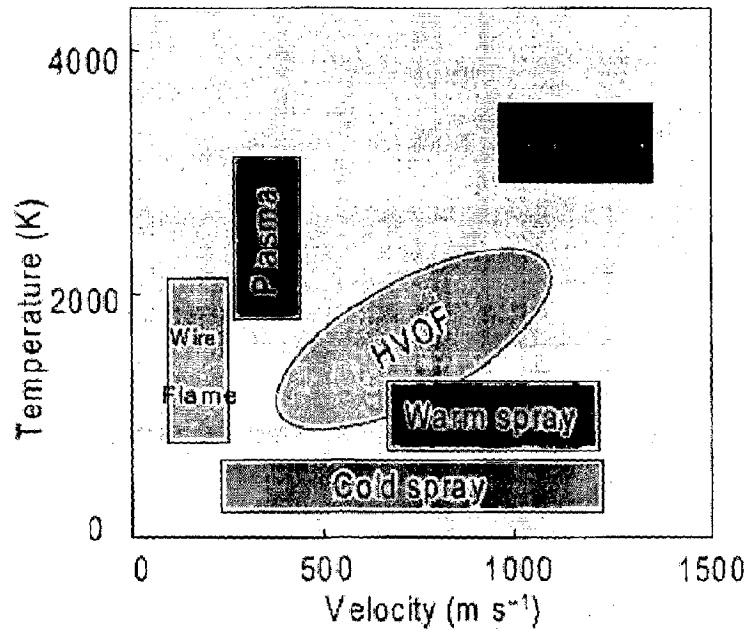


Fig. 2.20 Comparison of various thermal spray processes in terms of particle temperature and velocity (Kuroda et al., 2008).

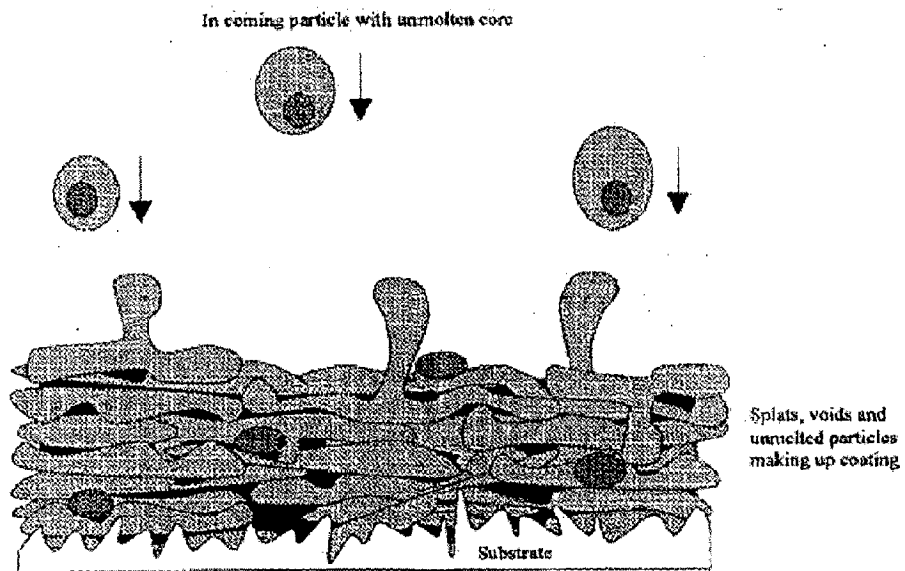


Fig.2.21 Schematic diagram showing a cross-section through a thermally sprayed coating (Gledhill et al., 1999)

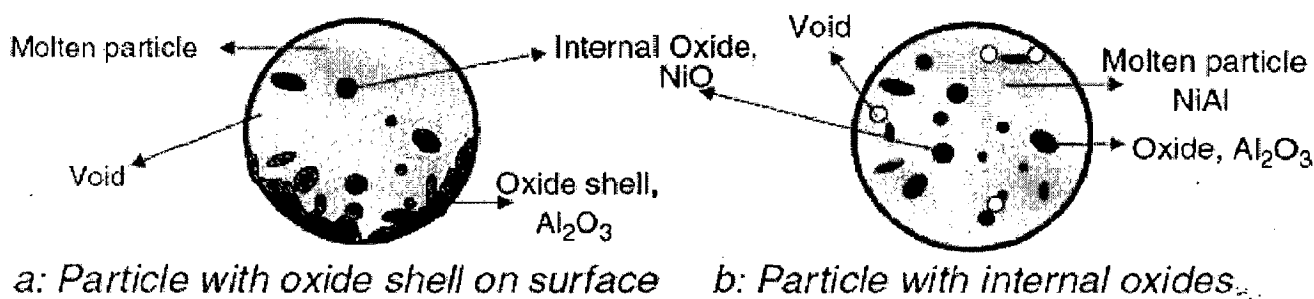


Fig. 2.22 Schematics for oxidation of particles, in-flight. (Deshpande et al., 2006)

## 2.8 DETONATION GUN COATING

D-gun spraying is one of the most promising thermal spray techniques and was originally developed and patented by Union Carbide (now Praxair) in 1955 (Kharlamov et al., 1987) and developed independently in 1969 at the Institute of Materials Science, Kiev, Ukraine. Since then, the D-gun coating process has been used for wide applications such as in the aircraft industries of the United States, Japan, and the former Soviet Union (Kharlamov, 1987; Kadyrov et al., 1995; Ma et al., 1999; Tucker, 1974). D-gun spraying is characterized by the spraying of particles that are accelerated by the detonation-wave and impact on the substrate surface at a high velocity of 800–1200 m/s (Semenov et al., 2002; Wagner et al., 1984; Wu et al., 2003), which is higher than that of High Velocity Oxyfuel spraying (HVOF) (about 550–850 m/s) (Stokes et al., 2001). Higher particle velocity during deposition provides a minimum decomposition of the feed powder, due to lower heat enthalpy and shorter duration involved in the coating process (Hao Du et al., 2007). As a result, the coatings obtained by D-gun spray process exhibit desirable morphological features such as low porosity, high density, low oxide contents and superior mechanical properties such as hardness, bond strength, and adhesion strength (Klimenko et al., 1979; Kharlamov et al., 1974; Murthy et al., 2006). The compressive residual stresses along with a fine-grained structure composed of many layers (splats) in the D-gun sprayed coatings are beneficial to improve its tribological properties (Rajasekaran et al., 2006). Therefore, D-gun technology has been widely used in many fields, such as aviation, petroleum, metallurgy, and machinery industry (Hao Du et al., 2005). The good mechanical

performance of D-gun coating is determined mainly by the effect of mechanical interlocking between flattened particles. This may take place more effectively owing to the micro-rough features of the splat surface. In addition, a high particle velocity assist for better interlocking of flattened particles (Li and Ohmori, 1996).

### 2.8.1 Working principal of D-Gun coating

A detonation gun consists of a water cooled barrel several feet long and about one inch in diameter with some associated valving for gases and powder, as shown schematically in Fig. 2.23 (Rao et al., 1986). A carefully measured mixture of gases, usually oxygen and acetylene, is fed to the barrel along with a charge of powder (usually with a particle size less than 100 microns). A spark is used to ignite the gas and the resulting detonation wave heats and

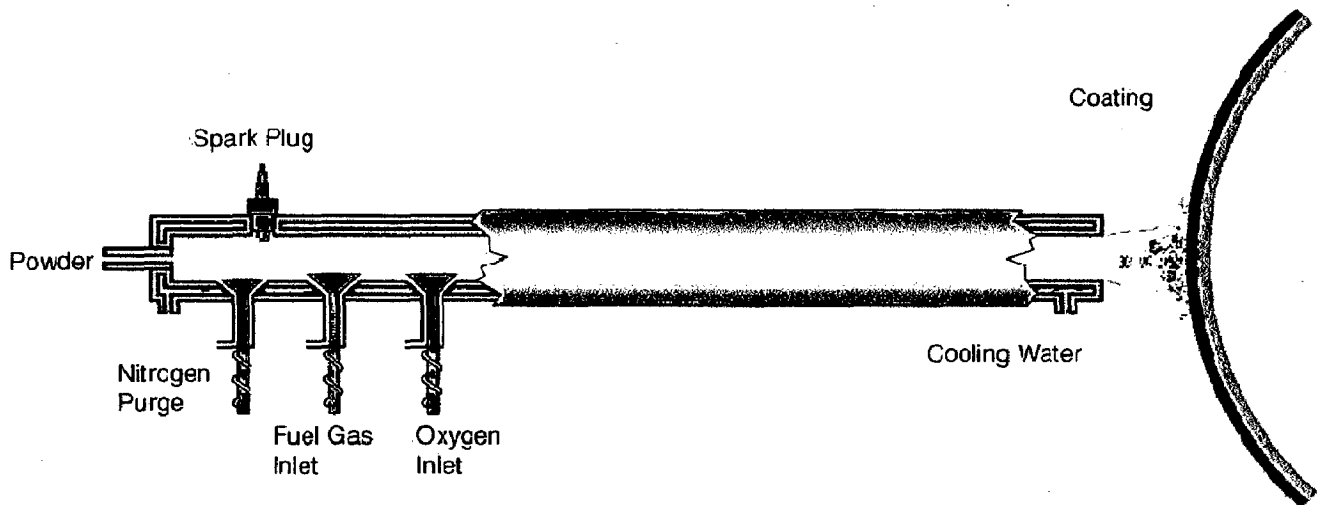


**Fig.2.23** Schematic Diagram of the D-gun Spray Process (Rao et al., 1986)

accelerates the powder as it moves down the barrel. The gas is traveling at a supersonic velocity and the powder is entrained for a sufficient distance for it to be accelerated to a supersonic velocity as well, typically about 800–1200 m/s. Instead of a continuous combustion process, it uses an intermittent series of explosions to melt and propel the particles onto the substrate. After each detonation, the barrel is purged with nitrogen gas and the process repeats itself several times per second. Each individual detonation results in the deposition of a circle (disk) of coating a few microns thick and about one inch in diameter. The coating is made of many overlapping disks.

This process is repeated to achieve the desired coating thickness. The process produces noise levels that can exceed 140 decibels and requires special sound and explosion proof rooms. The coatings produced through this process are of excellent quality. The drawback is that the process is relatively expensive to operate.

### **2.8.2 D-gun Coating characteristics**

Detonation gun coatings thus consist of multiple layers of densely packed, thin lenticular particles tightly bonded to the surface. Primarily because of their high density and high bond strength, Praxair Surface Technologies' D-Gun coatings have become the standard of excellence for thermal spray coatings. The as-deposited surface roughnesses of D-Gun coatings vary with the type of coating from about 60 to over 300 micro inches, Ra. Although for many applications the coating is used as-deposited, most are ground or ground and lapped to 1 to 10 micro inches, Ra. Typical coating thicknesses range from about 0.002 to 0.020 inch, but both thicker and thinner coatings are used depending on the specific application.

The detonation gun process is called "line-of-sight" because the end of the barrel must be able to "see" the area being coated. The best coating properties are achieved when the angle of deposition is close to 90 degrees to the surface. Because of the very high powder velocity, however, little degradation in properties is usually noted down to at least 60 degrees and useful coatings can be made at angles as low as at least 45 degrees. The size of the detonation gun makes it impractical to manipulate the gun itself inside cavities, thus cavities are only coated by firing into them at an angle. As a result, for example, the inside surface of a hollow, circular cylinder can be coated only to a depth equal to the diameter (an angle of deposition of 45 degrees).

### **2.8.3 Advantages of the D-gun coating System**

Detonation gun (D-gun) spray process can minimize decomposition of the feed powder due to a lower heat enthalpy, high velocity and shorter duration involved in the deposition as compared to plasma and HVOF thermal spray process. The higher particle velocity during deposition provides the resulting coatings several advantages, such as

- Lower porosity,
- Good adhesion between the substrate and coating,



- Higher microhardness, bond strength and
- Lower oxidation of in-flight particles (Hao Du et al., 2007)

WC-10Co-4Cr and Cr<sub>3</sub>C<sub>2</sub>-20(NiCr) coatings were deposited by HVOF and pulsed detonation spray (DS) processes and low stress abrasion wear resistance of these coatings was compared (Murthy and Venkataraman, 2006). The abrasion tests were done using a three-body solid particle rubber wheel test rig using silica grits as the abrasive medium. The results showed that the DS coating performed slightly better than the HVOF coating possibly due to the higher residual compressive stresses induced by the former process and WC-based coating has higher wear resistance in comparison to Cr<sub>3</sub>C<sub>2</sub>-based coatings. Also, the thermally sprayed carbide-based coatings were found to have excellent wear resistance with respect to the hard chrome coatings. WC-10Co-4Cr had better abrasive wear resistance compared to Cr<sub>3</sub>C<sub>2</sub>-20(NiCr) coating possibly due to the higher hardness of WC particles and better matrix properties of the CoCr binder material. The indentation fracture toughness of WC-CoCr coating was slightly better than that for Cr<sub>3</sub>C<sub>2</sub>-20(NiCr), which might also have caused the wear resistance to improve in the former. The coatings deposited by the DS process had slightly improved wear resistance compared to the HVOF process possibly due to the higher density and compressive residual stresses induced in the DS coating. Both the thermally sprayed coatings had superior wear performance in comparison to the hard chrome coating. It has been proposed that the distance from the coating surface to the coating/substrate interface along the splat boundaries has a great effect on corrosion resistance of thermally sprayed coatings (Bluni and Mardar, 1996)

Psyllaki et al. (2001) compared the microstructure and sliding wear resistance of alumina coatings prepared by atmospheric plasma spraying (APS) and D-gun spraying processes on cast iron and Hastelloy substrates. They reported that denser coatings made by D-gun spray process exhibited higher wear resistance compared with the coating deposited by APS process.

High-temperature corrosion resistance of Ni-20Cr, Ni-50Cr and Cr coated boiler tubes in an actual refuse incineration plant as well as in laboratory tests have been evaluated by Yamada et al. (2002). It was observed that detonation sprayed Ni-50Cr coating exhibit a highest corrosion resistance in the laboratory test at 600 °C, followed by the HVOF coatings among the detonation gun sprayed, plasma sprayed and HVOF sprayed coatings. The detonation sprayed Ni-50Cr coated tubes performed very well for seven years of testing in the actual plant without any problems and were expected to have a longer life. They further concluded that the Incolloy 825

and Inconel 625, having high nickel content possessed higher corrosion resistance than the stainless steels.

Isothermal oxidation behaviour of detonation sprayed  $\text{Cr}_3\text{C}_2\text{-NiCr}$  coating onto conticaster rolls made of high-temperature structural steel DIN 12CrMo44 has been studied by Wang et al. (2000). Tests were carried out in an electric muffle furnace at 750 and 850 °C in air. They revealed that the coated specimens exhibited a much better improvement in high-temperature corrosion resistance than the uncoated specimens. The total weight gain of the coated specimens was approximately 10 times and 100 times less than that of the uncoated specimens after 70 hours of oxidation at 750 and 850 °C, respectively. They concluded that the high chromium content and the dense coating protected the substrate from the inward permeation of oxygen and promoted the selective oxidation of chromium which improves the high-temperature corrosion resistance of the steel. Wang et al. (2000) further carried out in service testing of detonation sprayed  $\text{Cr}_3\text{C}_2\text{-NiCr}$  coating on the same conticaster rolls at steelmaking plant of Bao Shan Steel Company. They reported that after 3740 heats, there were many alligator cracks formed on the surfaces of the uncoated rolls, some of which had to be repaired. However, compared with the original feature, no changes were detected on the surfaces of coated ones. Their first report from the in-service test shows that the use of the coating is an efficient means of prolonging the life of the conticaster rolls.

Cyclic oxidation behaviour of NiCrAlY and CoNiCrAlY coatings was determined at a maximum temperature of 1273 K in air by Belzunce et al (2001). The authors reported that high frequency pulse detonation (HFPD) coatings were dense and exhibit interconnected porosity along droplet boundaries. Adherence of the coatings with the substrate was found to be good, which remained unaffected after the cyclic oxidation. The oxidant atmosphere penetrated into the coatings through the open porosity and internal oxidation occurred until all the accessible internal surfaces were oxidised. Subsequently, the oxidation took place only on the external surface, where a continuous and uniform layer of alumina protected the coating from further oxidation.

Isothermal oxidation behavior of D-gun sprayed NiCrAlY coatings at 1050 °C was studied by Zhang et al., (2002), after oxidation for 300 hours; the results showed that,  $\text{Al}_2\text{O}_3$  was appeared in the coating and at the coating-substrate interface, and also as Al-N compounds in the substrate. Further, he reported that the porosities of the detonation gun sprayed coating contained

the residual air, which accelerate the Al oxidation because D-gun process entraps the air during spraying and micropores acted shelters for the residual air, since the coating solidification was as rapid as enough time was not provided for the reaction to take place even if there were oxygen in the pores. The splat thickness of D-gun sprayed coating is less, as impact velocity is 2-3 times higher than that of the other thermal spray processes (Venkataraman et al., 2006). Zhang et al., (2003) reported the comparative study of Detonation gun sprayed NiCrAlY coating and low pressure plasma spray NiCrAlY coating. It is found that the surface hardness of D-gun sprayed coatings is higher than those of LPPS coating, but the oxidation resistance of D-gun coating is relatively lower.

The superalloys are subjected to high temperature oxidation and hot corrosion during service conditions in the gas turbines used for various applications such as air craft, thermal power plants, energy conversion systems, etc. D-gun-sprayed superalloy coatings have several advantages such as lower porosity, higher bond strength and hardness with fine grain structure (Murthy and Venkataraman, 2006).

## **2.9 PROBLEM FORMULATION**

### **2.9.1 Scope**

Hot corrosion is a serious problem, as steady, continuous increase in the operating temperatures of the hot sections of aero, marine and utility turbines focuses upon achieving its higher efficiency alone. This temperature rise has been met by the intelligent use of materials with high temperature stability through the use of advanced manufacturing technologies, including investment cast blades with improved cooling efficiencies and single crystal technology, and the advanced coating systems. A wide range of turbine operating conditions exists in utility turbines, which makes use of multi-fuels. The industries pose demand mainly on the design of high efficiency power plant, capable of operating on a wide range of fuels. Under these service conditions, the engine may experience high temperature oxidation, which needs to be considered seriously (Nicholls, 2002).

Modern gas turbine engines blades in aero, marine and industrial gas turbines are manufactured exclusively from nickel based superalloys and operate under the most arduous conditions of temperature and stress of many components in the engine. This is further complicated in marine applications due to the aggressive environment, which includes sulphur

and sodium from the fuel and various halides contained in seawater. These features are known to drastically reduce the superalloy component life and reliability by consuming the material at an unpredictably rapid rate, thereby reducing the load-carrying capacity and potentially leading to catastrophic failure of components (Eliaz et al., 2002; Liu et al., 2006). Thus, in order to improve an efficiency of the gas turbine engine significantly, the hot corrosion resistance of superalloys is as important as its high temperature strength. (Khajavia, 2004; Guo, 2006)

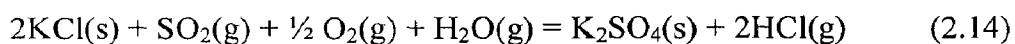
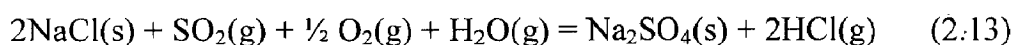
Recent studies showed that the high temperature strength materials are highly susceptible to hot corrosion and the surface engineering plays a key role in effectively combating it (Gururappa, 2006; Rocca, 2003). Therefore, the combination two materials, i.e., base and coating must be considered as an integral system and the interface between them is equally important as it can be the limiting factor. An ideal system i.e, super alloy and coating should be able to survive the harsh corrosive environment to the designed service life (Lin, 1984).

Different types of hot corrosion damages caused by vanadium have been encountered in all types of combustion equipments burning low-grade fuel oils. These include boilers, furnaces, diesel engines, and gas turbines. Indeed, petroleum crude and fuel oils can contain up to 4 percent sulfur, 500 ppm vanadium and several tens of ppm of sodium. The ash particles that result from their combustion consist of complex mixtures of vanadium pentoxide ( $V_2O_5$ ) and sodium sulfate ( $Na_2SO_4$ ) that exhibit low melting points down to  $500^\circ C$ . These compounds partly deposit on the hot gas path of the thermal equipment walls, tubes, piston/cylinder, turbine combustors. The resulting film acts as an ion-electrolyte and is conducive to fast attack of the substrate material by the oxidizing agents present in combustion gas and in the molten salt film. When the salt films ( $Na_2SO_4$ ) contain vanadium, an acidic dissolution of the protective oxide scale would take place because  $V_2O_5$  like  $MoO_3$  or  $WO_3$  acts as a strongly acidic oxide. Hence, the presence of vanadium in such molten salts causes a significant increase of the acidic solubility of the protective oxides (Hussain et al., 1994).

Owing to the aforementioned facts, there is a significant scope in understanding the reaction kinetics and the nature of the surface scales formed during oxidation, as they are important to evaluate the alloys for high temperature applications. The oxidation behavior of bare and coated complex superalloys has not been studied extensively and is not well understood. Therefore, further studies are needed on oxidation behavior of complex superalloys, particularly those used for high temperature applications (Gitanjali et al., 2002).

Several Ni- and Fe-based superalloys have been investigated to understand the effect of the composition of the substrate alloy on the oxidation/hot corrosion behaviour of a particular coating as reported in the literature (Smeggil and Bornstein, 1983; Sundararajan et al., 2004; Prakash et al., 2005). They observed the inter-diffusion of the elements between the coating and the substrate during the high temperature exposures. Shifler (2004) discovered that the high-temperature coatings on various superalloy substrates behaved differently during 1000 hours of exposure in a Type I hot corrosion environment at 899°C. He reported that differences in chemical compositions between a coating and a substrate alloy can lead to inter-diffusion between these materials that can modify the oxidation and corrosion resistance of the coating and the mechanical properties of the coating-substrate system. He further suggested that the stress state may also significantly influence and increase the magnitude of the inter-diffusion that may lead to deleterious precipitation reactions. Sundararajan et al. (2005A) reported that diffusion of elements adjacent to the coating-substrate interface induces microstructural changes.

Otsuka (2002) reported that high-temperature corrosion of boiler tubes in the coal-fired boiler results from formation of liquid phase, complex sulphates such as  $(\text{Na}, \text{K})_3 \text{Fe}(\text{SO}_4)_3$  in the deposits. He observed that  $\text{Na}_2\text{SO}_4$  and  $\text{K}_2\text{SO}_4$  compounds were vapour condensed from flue-gas on tube surfaces, while  $\text{Fe}_2\text{O}_3$  is considered to accumulate by impingement/adhesion of fly-ash particles, containing solid  $\text{Fe}_2\text{O}_3$ , onto super-heater tube surfaces. For boilers firing high-chlorine high-sulphur coal, he concluded that  $\text{Na}_2\text{SO}_4$  and  $\text{K}_2\text{SO}_4$  vapours condensed from flue-gases to form deposits on the metal surface, whereas chloride condensation was not evident. This was attributed to the high-sulphur content of coal, which changed chloride salts to sulphate salts in tube deposits, according to the following reactions:



The hot corrosion environment  $\text{Na}_2\text{SO}_4$ -60% $\text{V}_2\text{O}_5$  has been selected for the laboratory tests as the molten sulphate-vanadate deposits resulting from the condensation of combustion products of low grade fuels are extremely corrosive to the high-temperature materials (Rapp, 1986). Furthermore, sodium vanadyl vanadate ( $\text{Na}_2\text{O} \cdot \text{V}_2\text{O}_4 \cdot 5\text{V}_2\text{O}_5$ ), which melts at a relatively low temperature 550 °C is found to be the most common salt deposit on the boiler super-heaters (Barbooti et al., 1988). This environment will also be pertinent to the gas turbines as the

predominant species in the salt deposits forming on gas turbine surfaces are expected to be  $\text{Na}_2\text{SO}_4$ ,  $\text{V}_2\text{O}_5$  and  $\text{Na}_2\text{V}_2\text{O}_6$ .

The high temperature corrosion behavior of the coatings deposited by D-gun spray technique is very limited in the literature so far. Nickel and Cobalt based metallic coatings are frequently considered for the protection against oxidation, corrosion, wear and erosion at high temperatures. Therefore, the present research work is envisaged to make a detailed investigation of Detonation Gun sprayed coatings ( $75\%\text{Cr}_3\text{C}_2\text{-NiCr}$ ,  $\text{NiCrAlY}+0.4\%\text{wtCeO}_2$  and  $\text{NiCoCrAlYTaNi}$  coatings) on superalloys subjected to oxidation, hot corrosion and actual boiler environments. The Ni- and Fe based superalloys such as superni 75, superni 718 and superfer 800H developed by Mishra Dhanu Nigam Ltd., Hyderabad have been chosen for the present work. It is very essential to investigate the hot corrosion behavior of D-Gun spray coatings on these superalloys to assess its suitability for high temperature applications. Most industrial processes involve the use of metals and alloys at elevated temperature followed by cooling to room temperature numerous times. The operating conditions in such plants are mostly cyclic, rather than to isothermal processes. Therefore, oxidation under cyclic conditions constitutes a more realistic approach towards solving the problem of metal corrosion (Hocking, and Sidky, 1987). Relatively fewer studies are reported under cyclic conditions, which actually simulate the working conditions of boilers and gas turbines. Owing to the aforementioned views, the present work has been focused to address the issues as given in following section.

### **2.9.2 Objectives**

1. The objective of the present research work is aimed at studying the high temperature (900 °C) oxidation (Air), hot corrosion in  $\text{Na}_2\text{SO}_4\text{-}60\%\text{V}_2\text{O}_5$  and  $75\text{Na}_2\text{SO}_4\text{-K}_2\text{SO}_4$  environment in the laboratory tube furnace and actual coal fired boiler environment on superalloys such as superni 75, superni 718 and superfer 800H in bare conditions and after application of D-gun sprayed  $75\%\text{Cr}_3\text{C}_2\text{-NiCr}$ ,  $\text{NiCrAlY} + 0.4\%\text{wtCeO}_2$  and  $\text{NiCoCrAlYTaNi}$  coatings on the superalloys.
2. To compare the oxidation and hot corrosion performance of the D-gun coated superalloys with bare ones and assess its suitability for using it in the boiler super-heaters and re-

heaters, and for other future hot section components to be used in similar corrosive environments.

3. To understand and propose mechanisms for the high-temperature corrosion of the substrate superalloy and coated alloys, wherever possible. As far as the testing in air environment is concerned, the study could also provide useful information regarding the adhesion of the coatings and the spalling tendency of their oxide scales apart from air oxidation behaviour of the coatings.
4. In order to establish the behaviour of these coatings and bare superalloys in the actual working conditions in which they may be used, the coatings are investigated in the operational environment of the coal fired boiler at Guru Nanak Dev Thermal Plant, Bathinda, Punjab, India.
5. In both the laboratory as well in industrial environments, the experiments are planned to conduct under cyclic conditions as it provides the severest conditions for testing and represents the actual industrial environment where breakdown and shutdown occur frequently.
6. The  $75\%Cr_3C_2-NiCr$ ,  $NiCrAlY+0.4\%wtCeO_2$  and  $NiCoCrAlYTaNi$  coatings deposited on superalloys, after high temperature air oxidation and hot corrosion studies were characterized by the techniques such as XRD, FE-SEM/EDS and X-ray mapping to render an insight into the corrosion mechanisms based on the morphology of the corroded products formed on the coated superalloys. The similar characterizations studies were performed for the corroded uncoated superalloys.
7. To summarize the important contributions made in the present work on D-Gun sprayed coatings on superalloys and highlight the scope for future work in the high temperature corrosion of coatings.

# CHAPTER 3

## EXPERIMENTAL TECHNIQUES AND PROCEDURES

---

*This chapter presents the experimental techniques and procedures employed for deposition and characterisation of coatings. A detailed description of oxidation and hot corrosion studies of coated and bare superalloys in air and molten salt environments, respectively, is given in this chapter. The procedures for analyzing the corrosion products are discussed. The specifications of the equipments used are furnished.*

### 3.1 SUBSTRATE MATERIALS

The Ni-based superalloys namely, Midhani Grades superni 75 and superni 718, and Fe-based superalloy namely superfer 800H have been selected as the substrate materials for the present study. These alloys were procured from Mishra Dhatu Nigam Limited, Hyderabad (India) in the rolled sheet form, for protecting them against high temperature corrosive environment applications. The nominal chemical compositions of these alloys are given in Table 3.1. These superalloys find applications in steam boilers, heat exchangers, piping in the chemical industry, gas turbines, jet engines, furnace equipment, reformers and baffle plates/tubes in fertilizer plants.

### 3.2 DEVELOPMENT OF COATINGS by D-Gun PROCESS

#### 3.2.1 Preparation of Substrate Materials

Specimens with dimensions of approximately 20mm X 15mm X 5mm were cut from the alloy sheets. The specimens were polished using emery papers of 220, 400, 600 grit sizes and subsequently on 1/0, 2/0, 3/0 and 4/0 grades. These substrates are then grit blasted with alumina powders (Grit 45) prior to the deposition of the coatings by detonation gun thermal spray process.

#### 3.2.2 Feedstock Materials For The Coatings

Three types of commercially available alloy powders namely  $\text{Cr}_3\text{C}_2\text{-NiCr}$  (H. C. Starck),  $\text{NiCrAlY}$  (H.C.Starck - 413.3) and  $\text{NiCoCrAlYTaNi}$  (Sulzer metco) were chosen for D-gun spray



Table 3.1

Chemical composition (wt.%) for various superalloys

Alloy Midhani grade (similar grade)	Chemical composition (wt %)										
	Fe	Cr	Ti	Al	Mo	Mn	Si	Cu	Ta	C	Ni
Superni 75 (Nimonic 75)	03.00	19.50	00.30							0.10	77.10
Superni 718 (Inconel 718)	18.50	19.00	00.90	00.50	03.05	00.18	00.18	00.15	05.13	00.04	52.37
Superfer 800H (Incoloy 800H)	43.80	21.00	00.30	00.30		01.50	01.00			00.10	32.00

deposition on the three superalloy substrates. The chemical composition and particle size of all the alloy powders are reported in Table 3.2. An additive CeO<sub>2</sub> (0.4 wt %) with 99.99% purity and NiCrAlY powders were dry-ball milled in a conventional rotating ball mill with stainless steel balls as a milling/grinding medium for 8 hrs to form a uniform and homogeneous mixture. It may be mentioned here that these commercial alloy powders have been selected for depositing the coatings on the superalloy substrates as the characterisation and oxidation studies of these coated superalloy substrates are scarce in the literature.

**Table 3.2** Composition of the alloy powders, shape and size of the particles.

Alloy powders	Chemical Composition (Wt. %)	Shape	Particle Size
Cr <sub>3</sub> C <sub>2</sub> -NiCr (H.C.Starck -584.072)	75%Cr <sub>3</sub> C <sub>2</sub> -25%( 80Ni-20Cr)	Irregular	10-38μ
NiCrAlY + CeO <sub>2</sub> (H.C.Starck - 413.3)	Ni-22.1Cr-10.4Al-1.01Y-0.4CeO <sub>2</sub>	Spherical	5-45 μ
NiCoCrAlYTa Sulzer metco (Amdry 997)	Ni-23Co-20Cr-8.5Al-4Ta-0.6Y	spheroidal	5-37 μ

### 3.2.3 Formulation of Coatings

The D-gun process was used to apply coatings on the superalloys at SVX Powder M Surface Engineering Pvt. Ltd, New Delhi (India) (as shown in Fig. 3.1). Standard spray parameters were designed by the above firm for depositing the coatings in the present work. All the process parameters, including the spray distance (165 ± 2 mm), were kept constant throughout the coating process. The process parameters for the D-gun spray process employed for applying the coatings are summarised in Table 3.3

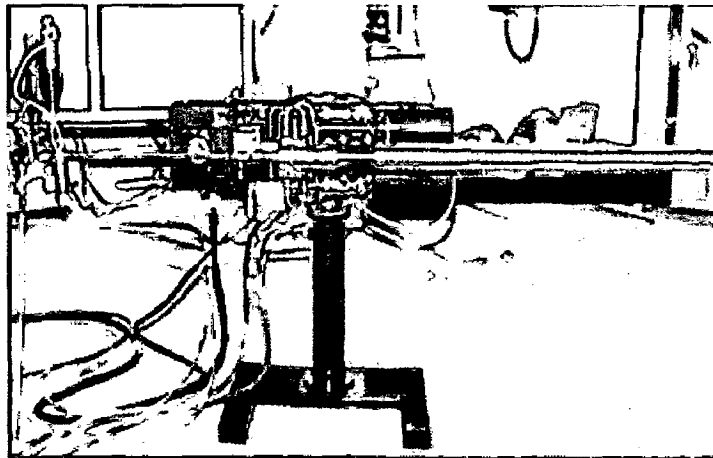


**Fig. 3.1** D-gun thermal spray process used in the current research work

**Table 3.3** Spray parameters as employed during D-gun spraying

Parameters	Cr <sub>3</sub> C <sub>2</sub> -NiCr	NiCrAlY + CeO <sub>2</sub>	NiCoCrAlYTa
Oxygen/acetylene flow rate	1:1.21	1:1.21	1:1.2
Carrier gas flow rate N <sub>2</sub> (m <sup>3</sup> /hr)	0.96	0.82	0.72
Frequency (shots/s)	3	3	3
Diameter of spot (Shot size) mm	20	20	20
Spraying distance from Nozzle(mm)	165 ± 5	165 ± 5	165 ± 5
Powder flow rate (gram/shot)	1-2	1-2	1-2

### 3.3 CHARACTERISATION OF THE COATINGS

#### 3.3.1 Specimen preparation

The as-coated superalloys were cut with a diamond cutter (Buehler's Precision Diamond Saw, Model ISOMET 1000, made in USA) across its cross-section and subsequently hot mounted in Buehler's transoptic powder (20-3400-080). Subsequently, the mounted specimens were polished manually using emery papers of 220, 400, 600 grit sizes and subsequently on 1/0, 2/0, 3/0 and 4/0 grades. Finally, the specimens were mirror polished on a cloth polishing wheel machine with 0.05 µm alumina powder suspension. The specimens were washed thoroughly with flowing water, and dried in hot air to remove any moisture.

### **3.3.2 Measurement of Coating Thickness**

The thickness was monitored during the process of D-gun spraying process with a Minitest-2000 thin film thickness gauge (made in Germany, precision  $\pm 1 \mu\text{m}$ ). Efforts were made to obtain the coatings with uniform thickness. The thickness of some of the as-sprayed specimens were further verified by cutting along the cross-section and mounted, as explained in Section 3.3.1. A Scanning Electron Microscope (LEO 435VP, Leo Electron Microscopy Ltd., Cambridge, UK) with an attached Robinson Back Scattered Detector (RBSD) was used for some of the specimens and also field emission scanning electron microscope (FE-SEM)(FEI Quanta 200F, Made in Czech Republic) was used to obtain the back scattered electron (BSE) images. The average coating thickness measured from the BSE images at different locations is reported in Chapter 4 of the present study.

### **3.3.3 Measurement of Porosity**

Porosity of the coatings was measured with an image analyser using Zeiss Axiovert 200 MAT inverted optical microscope, fitted with imaging software Zeiss Axiovision Release 4.1, (Germany) software, which was developed based on ASTM B276. The magnification was chosen such that the coating microstructure image covers the screen and allows the resolution of the voids that contributes notably to the total porosity area percentage. The process of selecting the appropriate range of light grey contrast spots was carried out methodically by stereographic imaging to ensure that only voids were selected. The analysis using image processing software determines the pore area size in the view field by converting the pore areas (grey-level areas) into a background colour such as red while the rest of the microstructure remains in its original colour. The area of one feature is numerically related to the total area of the picture, as the program counts the number of one colour type pixels (red) and sets that as a ratio of the total number of pixels in the picture (total area). About twenty (20) separate locations were selected to avoid the overlap between two locations and determine the area percent porosity and the values are reported in Chapter 4, 5 and 6.

### **3.3.4 Metallographic Studies**

The D-gun sprayed as-coated specimens were prepared as explained in Section 3.3.1 for metallographic studies. Specimens were then examined under Zeiss Axiovert 200 MAT Inverted

Optical Microscope interfaced with imaging software Zeiss AxioVision Release 4.1 to obtain surface microstructures of the coatings. The surface as well as cross-sectional microstructures of the specimens is discussed in Chapter 4, 5 and 6 of the present study.

### 3.3.5 Measurement of Microhardness

For obtaining microhardness of the D-gun sprayed coatings, the specimens were cut, mounted and polished as explained in section 3.3.1. The microhardness of the as sprayed coatings was measured by using Miniload 2 Microhardness Tester (Leitz, Germany) fitted with a Vickers pyramidal diamond indenter. A 15 g (147.1mN) load was applied to the indenter for penetration of as sprayed coatings. Hardness value was calculated from the relation  $Hv = 1854.4 \times \frac{F}{d^2}$  where 'F' is the load in grams and 'd' is the diameter of the indenter in micrometer. Each reported value of the microhardness is the average value of five measurements. These microhardness values are plotted as a function of distance from the coating/substrate interface and incorporated in Chapter 4, 5 and 6.

### 3.3.6 Measurement of Surface Roughness

The surface roughness (Ra) values of the D-gun sprayed as coated specimens were measured using Surface Roughness Tester (Mitutoyo SJ-201, Japan). Each reported value of surface roughness (Ra) is the mean of five observations taken at different locations. The centre line average (CLA) method was used to obtain the Ra values. The surface roughness values are presented in Chapter 4, 5 and 6.

### 3.3.7 X-Ray Diffraction (XRD) Analysis

XRD analysis was carried out for both the alloy powders as well as D-gun coated specimens to identify the various phases present on their surfaces. The X-ray diffraction patterns were obtained by a Bruker AXS D-8 Advance Diffractometer (Germany) with  $\text{CuK}_\alpha$  radiation and nickel filter at 30 mA under a voltage of 40 kV. The specimens were scanned with a scanning speed of 2°/min in  $2\theta$  range of 10° to 110° and the intensities were recorded. Assuming height of the most prominent peak as 100%, the relative intensities were calculated for all the peaks. The diffractometer interfaced with Bruker DIFFRAC<sup>plus</sup> X-Ray diffraction software provides 'd' values directly on the diffraction pattern. These 'd' values were then used for identification of various phases with the help of JCPDS data cards.

### **3.3.8 Field Emission-Scanning Electron Microscopy (FE-SEM) and Energy Dispersive X-ray Spectrometry (EDS) Analysis**

#### **3.3.8.1 Surface Morphology/EDS Analysis**

The surface morphologies of the alloy powders and D-gun coated specimens were studied with the help of a Scanning Electron Microscope (LEO 435VP, Leo Electron Microscopy Ltd., Cambridge, UK) and field emission scanning electron microscope (FEI Quanta 200F, Made in Czech Republic) with an aim to understand the morphology of the alloy powders and to identify inclusions, un-melted, partially melted particles and pores in the as sprayed coatings. Most of the samples are characterized using field emission scanning electron microscope (FEI Quanta 200F, Made in Czech Republic) fitted with EDAX Genesis software attachment. The EDAX genesis software directly indicates the oxides (phases) present at a point along with their compositions (weight %). Although the composition correspond to selected points on the as-sprayed surfaces it is useful to understand the formation of desired compositions in the coatings. SEM morphologies of the alloy powders and FE-SEM/EDS analysis for the D-gun coated specimens are reported in Chapter 4, 5 and 6.

#### **3.3.8.2 Cross sectional analysis**

BSEI and SEI/EDS analysis along the cross-sections of some coated specimens was carried out. The sample was prepared as explained in the section 3.3.1. The analysis was carried out using a Scanning Electron Microscope of JEOL and also using FE-SEM/EDS. The back scattered electron images were taken and the EDS analysis was performed across the cross section to ascertain elemental composition (weight %) at different points as well as to identify the presence of various elements along the cross-section of the coatings.

#### **3.3.9 X-ray mapping analysis**

To obtain cross-sectional analysis of the different elements present in the coatings, the specimens were cut along the cross-section, mounted and polished in accordance with the procedure already discussed in section 3.3.1., thereafter the specimen were silver pasted between samples and the stub in order to have conductivity, thereafter, gold coated to facilitate elemental X-ray mapping analysis of the different elements present across the coating. The selected area has three regions i.e. substrate, coating and some epoxy region. X-ray mappings were obtained for all the elements of the substrate

and the coatings, but only those mappings are reported which indicates the presence of some element. X-ray mapping analysis of the samples was done on field emission scanning electron microscope (FEI, Quanta 200F Company) for image acquisition entailed a backscattered electron image (BSEI) and secondary electron image (SEI) mode. An accelerating voltage of 20-25 kV, a working distance of 9–10 mm, and an image size of 1024\*884 pixels were used for getting quality images. Energy Dispersive X-ray Spectroscopy (EDS) and X-ray mapping were employed while imaging on FE-SEM was carried out to obtain elemental composition at different areas of the coating and surface morphology of the coatings, respectively.

### **3.4 HIGH TEMPERATURE OXIDATION AND HOT CORROSION STUDIES**

#### **3.4.1 Experimental Setup**

Oxidation and hot corrosion studies were conducted at 900 °C in a laboratory silicon carbide tube furnace, Digitech, India make. The furnace was calibrated to an accuracy of  $\pm 5$  °C using Platinum/Platinum-13% Rhodium thermocouple fitted with a temperature indicator of Electromek (Model-1551 P), India. The bare as well as the coated specimens were polished down to 1 $\mu$ m alumina wheel cloth polishing to obtain similar condition of reaction before being subjected to corrosion run. The physical dimensions of the specimens were then recorded carefully with digital vernier caliper to evaluate their surface areas. Subsequently, the specimens were washed properly with acetone and dried in hot air to remove the moisture. During experimentation, the prepared specimen was kept in an alumina boat and the weight of boat and specimen was measured. The alumina boats used for the studies were pre-heated at a constant temperature of 1200 °C for 12 hours and it was assumed that their weight would remain constant during the course of high temperature cyclic oxidation/corrosion study. Then, the boat containing the specimen was inserted into hot zone of the furnace maintained at a temperature of 900 °C. The weight of the boat loaded with the specimen was measured after each cycle during the corrosion run, the spalled scale if any was also considered during the weight change measurements. Holding time in the furnace was one hour in still air followed by cooling at the ambient temperature for 20 minutes. Following this, weight of the boat along with specimen was measured and this constituted one cycle of the oxidation study. Electronic Balance Model CB-120 (Contech, Mumbai, India) having a sensitivity of  $10^{-3}$  g was used to conduct the weight

change studies. The specimens were subjected to visual observations carefully after the end of each cycle with respect to colour or any other physical aspect of the oxide scales being formed. All oxidation and hot corrosion studies were carried out for 100 cycles. The reproducibility in the experiments was established by repeating hot corrosion experiments for three cases.

### **3.4.2 Oxidation Studies in Air**

The oxidation tests at 900 °C were performed on all three base superalloys (mirror polished) as well as D-gun spray coated superalloys in laboratory furnace up to 100 cycles as discussed in section 3.4.1.

### **3.4.3 Hot Corrosion Studies in Molten Salts**

i) ( $\text{Na}_2\text{SO}_4 - 60\%\text{V}_2\text{O}_5$ )

ii) ( $\text{Na}_2\text{SO}_4 - 25\%\text{K}_2\text{SO}_4$ )

#### **3.4.3.1 Coating of Molten Salts**

The D-gun spray coated as well as bare specimens (mirror polished) was prepared for studies as discussed in section 3.4.1. The specimens were then heated in an oven up to 250 °C and a salt mixture of  $\text{Na}_2\text{SO}_4-60\%\text{V}_2\text{O}_5$  and  $\text{Na}_2\text{SO}_4-25\%\text{K}_2\text{SO}_4$  dissolved in distilled water was coated on all the six surfaces of the warm polished specimens with the help of a camel hair brush. Amount of the salt coating was kept in the range of 3.0 -5.0 mg/cm<sup>2</sup>. The salt coated specimens as well as the alumina boats were then dried in the oven for 3 hours at 100 °C and weighed before being exposed to hot corrosion tests.

#### **3.4.3.2 Hot Corrosion Studies**

The bare as well as D-gun spray coated specimens after application of salt coating were subjected to hot corrosion in the laboratory furnace at 900 °C for 100 cycles as discussed in section 3.4.1.

### **3.4.4 Studies in coal fired Industrial boiler Environment**

The D-gun coated as well as bare superalloy specimens were exposed to the platen super-heater zone of the coal fired boiler of Stage-II at Guru Nanak Dev Thermal Plant, Bathinda, Punjab (India). This zone was selected for the present study as many breakdowns occurred in this power plant due to hot corrosion degradation of the platen super-heater tubes of the coal



fired boilers. A hole of 1.2 mm diameter was drilled in all the specimens to hang them in the boiler for experimentation. The coated as well as bare specimens were polished down to 1 $\mu$ m alumina on a cloth polishing wheel machine to obtain similar conditions of reaction on the surface of all the specimens. The physical dimensions of the specimens were measured with a Sylvac digital vernier caliper (Swiss make, resolution 0.01), to evaluate their surface areas. To measure the thickness during experimentations, the average thickness of each specimen (average of 10 measurements) was measured using Sylvac micrometer screw gauge (Swiss make, resolution 0.001), before exposing them to the boiler environment. The coated as well as bare specimens were then hanged with the help of a stainless steel wire through the soot blower dummy points at 27 m height from the base of the boiler. The specimens were exposed to the combustion environment for 10 cycles. Each cycle consisted of 100 hours heating followed by 1 hour cooling at ambient conditions. The temperature was measured at regular intervals during the study and the average temperature was about 900 °C with variation of  $\pm 10$  °C. After the end of each cycle, the specimens were visually observed for any change in the surface texture, further it has been washed by acetone and weight of the specimens were measured subsequently using an Electronic Balance Model CB-120 (Contech, Mumbai, India, and sensitivity  $10^{-3}$  g). The chemical analysis of the flue gas and ash present inside the boiler is given in Table 3.4. The FE-SEM/EDS analysis of the fly ash is shown in Fig. 3.2. After the end of each cycle, the specimens were subjected to careful visual observation for any change in the surface.

### **3.5 ANALYSIS OF CORROSION PRODUCTS OF OXIDATION IN AIR AND MOLTEN SALTS**

All the specimens subjected to oxidation, hot corrosion as well as in the boiler environments were analysed for the characterisation of corrosion products. The surface and cross-section of the corroded specimens were analysed by using various analytical techniques such as XRD, FE-SEM/EDS, and X-ray mapping analyses.

**Table 3.4:** Chemical analysis of ash and flue gases inside the boiler.

Ash		Flue Gases	
Constituent	Wt. %age	Volumetric flow = 122.44 m <sup>3</sup> /sec	
		Constituent	Value relative to flue gases
Silica	54.70	SO <sub>x</sub>	280.53 mg/m <sup>3</sup>
Fe <sub>2</sub> O <sub>3</sub>	0.18	NO <sub>x</sub>	1166.67 µg/m <sup>3</sup>
Al <sub>2</sub> O <sub>3</sub> -Fe <sub>2</sub> O <sub>3</sub> /Al <sub>2</sub> O <sub>3</sub>	29.56	CO <sub>2</sub>	12.2
CaO	1.48	O <sub>2</sub>	7.0
MgO	1.45	40% excess air was supplied to the boiler for the combustion of coal.	
SO <sub>3</sub>	0.23		
Na <sub>2</sub> O	0.34		
K <sub>2</sub> O	1.35		
Ignition loss	4.31		
others	Rest		

### 3.5.1 Visual Observation

After every oxidation and hot corrosion run, surface scale of each specimen was visually examined after each cycle for any change in colour, luster, adherence-spalling tendency, and growth of cracks in the coatings/oxide scales were recorded. After the completion of 100 cycles (each cycle of 1 hr heating and 20 minutes cooling) in laboratory and 10 cycles (each cycle of 100 hr heating and 1hr cooling) in case of industrial environment, the specimens were finally examined and their macrographs were taken. The physical conditions of the exposed specimens such as changes in the color, spallation, disintegration of the coating, cracks in the surface etc, if any, can be observed from the macrographs. The macrographs were obtained on a Stemi 2000C Stereo Microscope (Carl Zeiss Jena GmbH, Germany), fitted with a Sony Cyber-Shot DSC-S85 Digital Still Camera.

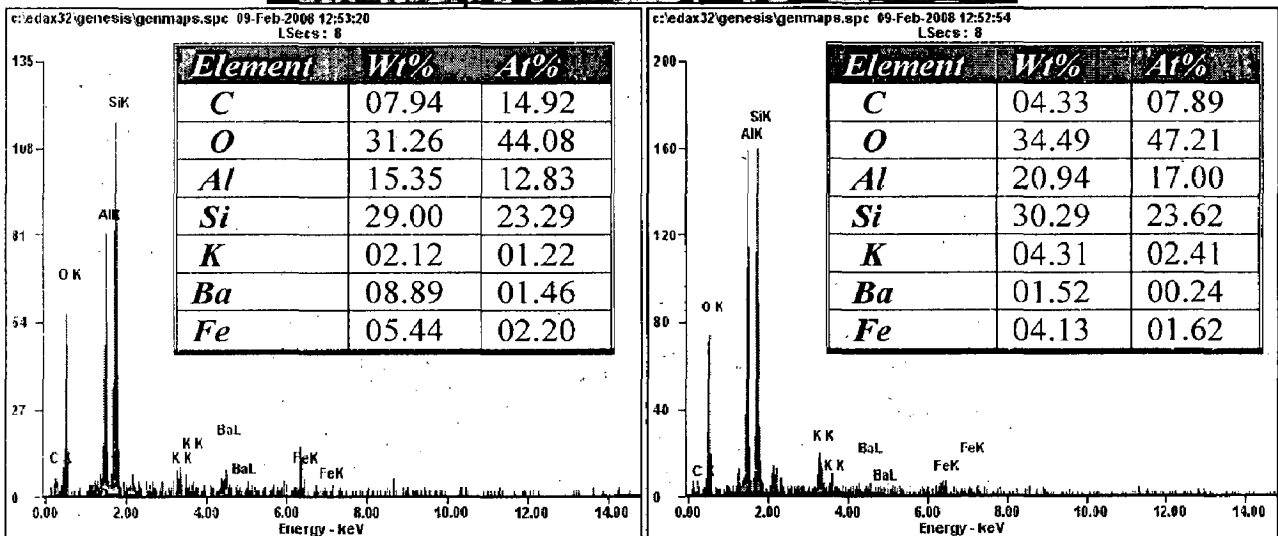
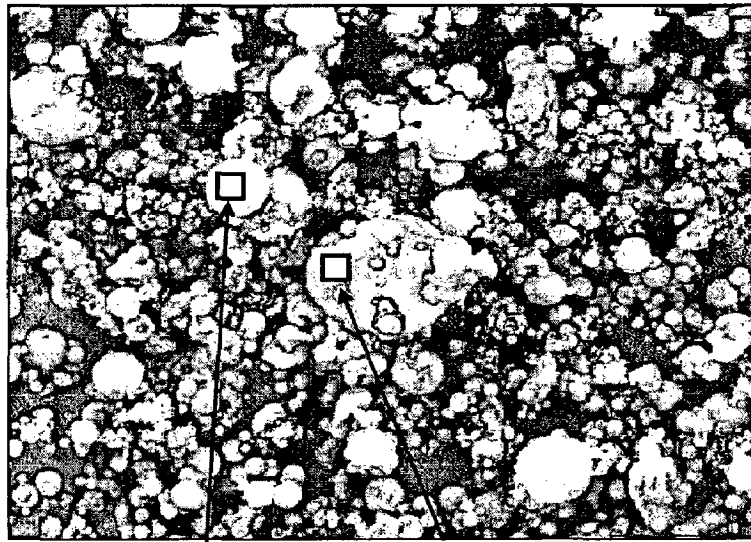


Fig. 3.2 FE-SEM morphology and EDS compositional analysis of fly ash

### 3.5.2 Weight change Studies

The weight change values were measured at the end of each cycle with the aim to establish the kinetics of oxidation and hot corrosion. The weight change data was plotted with respect to number of cycles for each specimen and the plots are given in the subsequent chapters. However, in case of the specimens exposed to the industrial environment, the actual working conditions of the coal fired boiler in a thermal power plant, the spalled scale could not be collected and incorporated in the mass change. In this case, the weight change consists of a weight gain owing to the formation of the oxide scales and a weight loss due to the suspected

spalling and fluxing of the oxide scales. Therefore, the net weight change in the industrial environment represents the combined effects of these two processes. The weight change data was plotted with respect to number of hours for each specimen and the plots are presented in subsequent chapter 7.

### **3.5.3 X-ray diffraction (XRD) Analysis**

For identification of different phases formed in the oxides scales of oxidized/hot corroded specimens after 100 cycles in the laboratory and in actual industrial environment, X-ray diffractometer has been used as described in section 3.3.8.

### **3.5.4 FE-SEM/EDS Analysis**

#### **3.5.4.1 Surface Morphology**

The surface morphology of some of the oxidized/hot corroded specimen surfaces after 100 cycles were studied with the help of a field emission scanning electron microscope (FE-SEM/EDS) (FEI Quanta 200F, Made in Czech Republic) and the details regarding the equipment are provided in section 3.3.9.1. The specimens were scanned under the microscope and the critical areas of interests were photographed with an aim to identify the micro cracks, voids, inclusions and surface morphology of the scale. Point analysis by EDS was carried out at various locations on these identified areas of interest to understand composition (weight %) of various phases in the oxide scales. Although these compositions correspond to selected points on the surfaces, the data could still be useful to support the formation of various phases in the oxide scales.

#### **3.5.4.2 Cross-Sectional analysis**

To understand the formation of elements, oxides and various other phases across the cross-section of oxidized and corroded samples, FE-SEM/EDS analysis for some of the selected specimens was carried out along their cross-sections using genesis EDAX software. Cross-sectional BSE images and SE images were taken at some points of interest including scale/coating and substrate. The elemental composition (weight %) was carried out by EDS analysis at various points along the cross-section. An approximate distribution of various elements across the thickness of the scales is estimated using these data. In some cases, the oxide scale thickness was also measured from these BSE images.

# CHAPTER 4

## Cr<sub>3</sub>C<sub>2</sub>-NiCr COATING

---

*Characterisation, oxidation and hot corrosion behaviour of Cr<sub>3</sub>C<sub>2</sub>-NiCr coatings deposited on superalloys by Detonation gun spray technique (D-gun) as well as bare superalloys are described in this chapter. The cyclic oxidation and hot corrosion studies were performed at an elevated temperature of 900 °C in air and in Na<sub>2</sub>SO<sub>4</sub>-60%V<sub>2</sub>O<sub>5</sub> and Na<sub>2</sub>SO<sub>4</sub>-25% K<sub>2</sub>SO<sub>4</sub> molten salt environments for 100 cycles, respectively. The specimens were visually examined at the end of each cycle during the course of study. The weight change measurements for each coated superalloy and bare superalloys were made to substantiate its oxidation kinetics through the evaluation of the parabolic rate constants, thereby evaluating the protective nature of the coatings. The microstructural characteristics of the corroded products were analysed by using techniques such as XRD, FE-SEM/EDS and X-ray mapping to understand the mode of oxidation and hot corrosion.*

### 4.1 MICROSTRUCTURES OF THE SUBSTRATE SUPERALLOYS

Optical microstructures of the substrate steels are shown in Fig. 4.0, which are explained with reference to atlas of microstructures for industrial alloys (Metals Handbook, 1972 and ASM Handbook, 1995). The microstructures of superni 75 and superni 718, Fig. 4.0 (a) and (b) respectively can be characterised by a nickel-rich  $\gamma$ -solid solution matrix. In case of superni 75, fine carbide particles are dispersed in the gamma matrix mainly along the grain boundaries. In  $\gamma$  matrix of the superni 718, carbide segregation in the form of stringers is revealed. Whereas the microstructure of the superfer 800H (Fig. 4.0 (c)) consists of a solid solution matrix in which some of the grains are delineated by particles of precipitated carbides at the grain boundaries and by twinning lines (Metals Handbook, 1972).

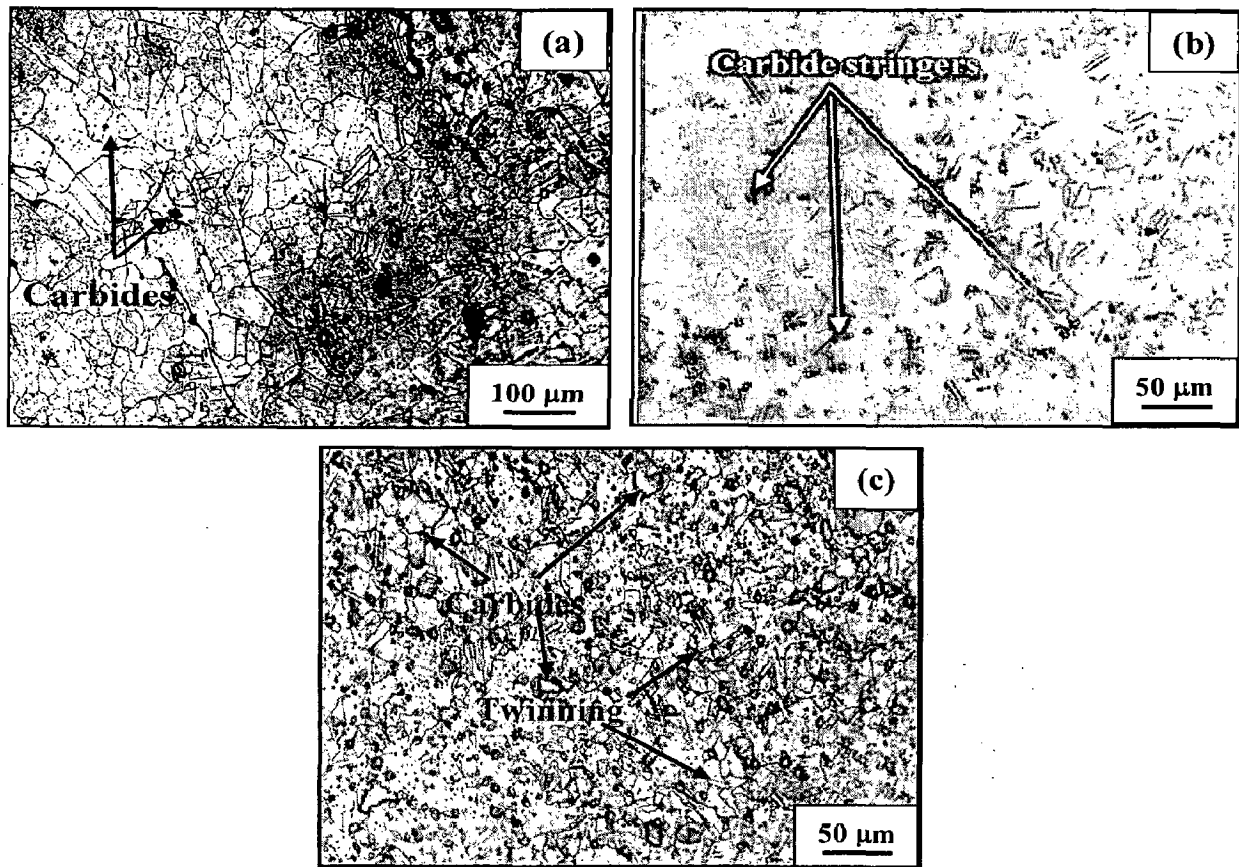


Fig.4.0 Optical micrographs of the substrate superalloys (a) superni 75 (b) superni 718 and (c) superfer 800H.

## 4.2 CHARACTERISATION OF THE COATING

### 4.2.1 Introduction

D-gun spray process is a well established thermal spray technique used for depositing the coatings on materials used in tribological and high temperature applications. The main advantages of this technique are: it can minimize decomposition of the feed powder due to a lower heat enthalpy, high velocity and shorter duration involved in the deposition as compared to plasma and HVOF thermal spray process, higher particle velocity during deposition provides the resulting coatings several advantages, such as lower porosity, good adhesion between the substrate and coating, higher microhardness, bond strength (Hao Du et al., 2007) and lower oxidation of in-flight particles. The cermet coatings have high thermal stability and oxidation

resistance up to 850<sup>0</sup>C, the corrosion resistance is provided by NiCr matrix while the wear resistance is mainly due to the carbide ceramic phase (Guilemany et al., 2006). In general, thermal sprayed coatings are inherently porous with some of pores being interconnected, in such situations; the coating must be deposited without significant oxidation during deposition (Yamada et al., 2002). During HVOF spraying, molten particles are exposed to air and are oxidized in flight to the substrate, oxidation can also occur at the exposed surface of splats prior to the deposition of the subsequent layer (Morimoto et al., 2006). These problems are not manifested in the D-gun process as it offers highest velocity (800–1200ms<sup>-1</sup>) for the sprayed powders that are unattainable by the plasma and HVOF conditions (Hao Du et al., 2005). It also provides coating with compressive residual stress rather than tensile stress (Souza et al., 2007 and Rajasekaran et al., 2008). It is usually considered that the wear resistance of cermet coatings is predominately influenced by their microstructures, e.g., carbide particle size, carbide content and carbide distribution within splats, and porosity, etc (Gang et al., 2006). Splat thickness of D-gun sprayed coating is less, as impact velocity is 2-3 times higher than that of the other thermal spray process (Venkataraman et al., 2006).

The present work has been envisaged to characterize the D-gun sprayed Cr<sub>3</sub>C<sub>2</sub>-25%NiCr coatings on the Ni- and Fe-based superalloys for its high temperature applications such as in thermal power plants and energy conversion systems as there is no reported study so far. The superalloys selected for this study have been procured from the Mishra Dhatu Nigam Limited, Hyderabad (India) and deposited with Cr<sub>3</sub>C<sub>2</sub>-25%NiCr coatings by D-gun process for extending life at the upper end of their performance capabilities. The microstructure, porosity, coating thickness, phase formation and microhardness properties of the coatings have been characterized using the combined techniques of X-ray diffraction (XRD) technique, Field emission scanning electron microscopy/energy-dispersive analysis (FE-SEM/EDS) and X-ray mapping.

#### **4.2.2 Experimental Details**

The details of the substrate material, coating formulation and characterisation of the coating are discussed in chapter 3 (Experimental chapter) of the thesis.

## 4.2.3 Results

### 4.2.3.1 Coating powder

A commercially available  $75\text{Cr}_3\text{C}_2-25(\text{Ni}20\text{Cr})$  powder is used in this study (particle size: 10–38  $\mu\text{m}$ , irregular shape, AMPERIT /584.072). It is evident from the micrograph of the coating powder (Fig.4.1) that the agglomerated and sintered  $\text{Cr}_3\text{C}_2-25\text{NiCr}$  powder showed a clear contrast between the carbide and NiCr matrix phases. The carbide particles are evenly distributed, forming interconnecting networks within each powder particle. Also, the powder particles showed an irregular morphology with the largest particle being  $36\mu\text{m}$  and the smallest one measured  $9\mu\text{m}$  by back scattered electron image (BSEI), which is consistent with the nominal size range provided by the manufacturer

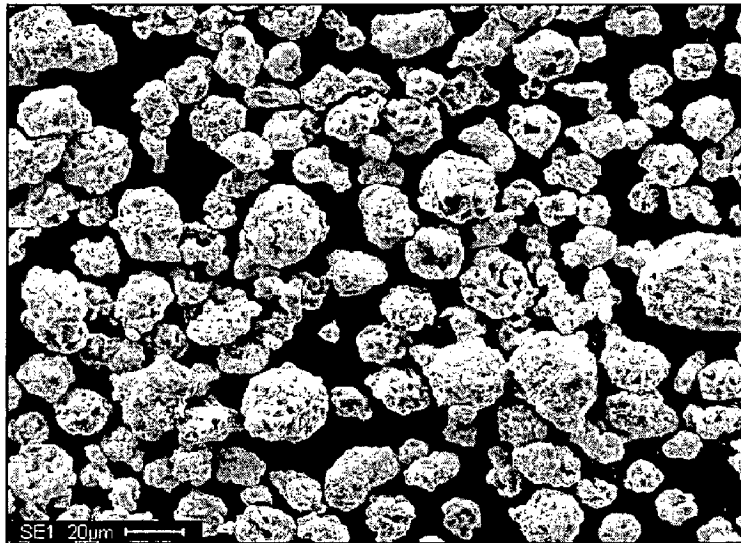
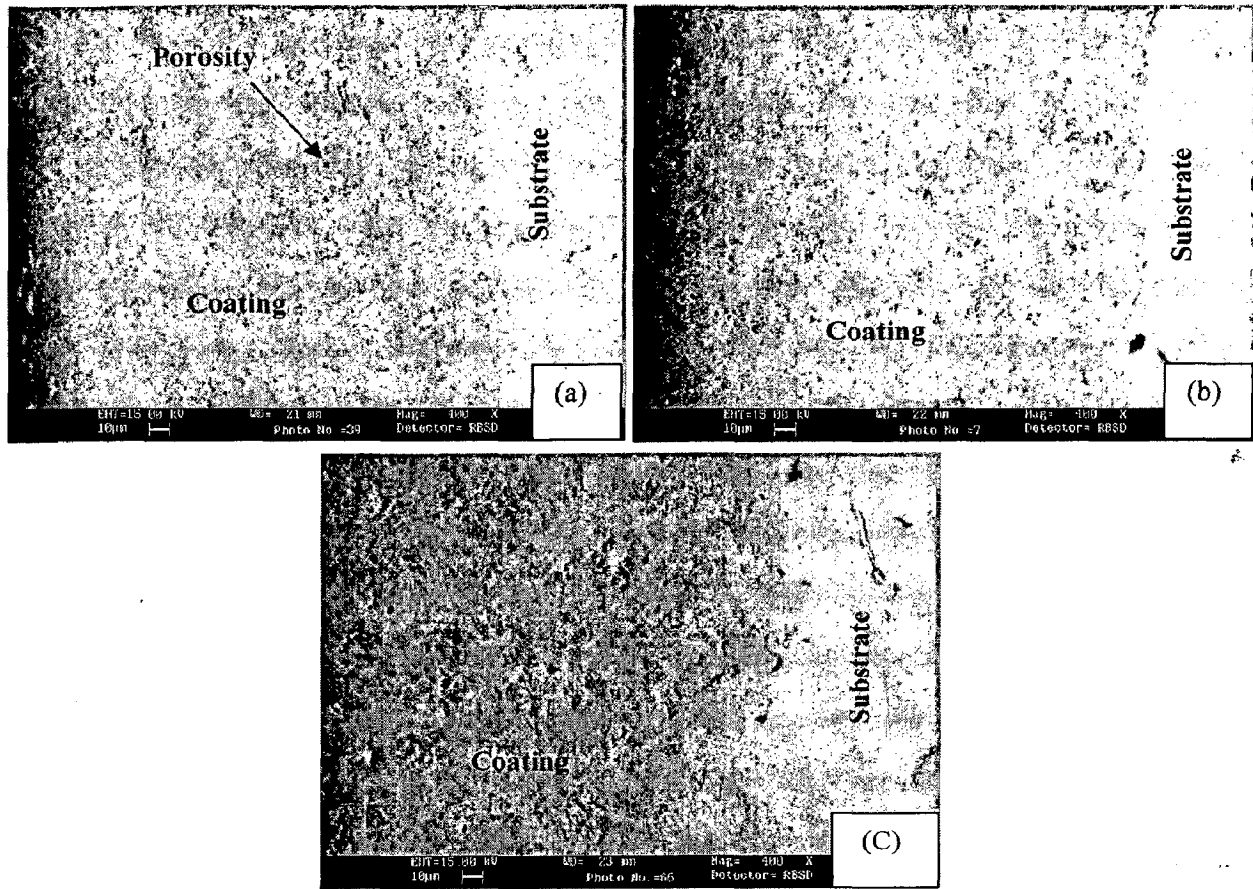


Fig. 4.1 SEM of  $\text{Cr}_3\text{C}_2-25\text{NiCr}$  powder

### 4.2.3.2 Cross Section and surface microstructures of the coating

The BSE images at the cross section of D-gun-sprayed  $\text{Cr}_3\text{C}_2-25\text{NiCr}$  coating is shown in Fig.4.2. It clearly shows the formation of dense, uniform, continuous, and adherent splat like structure. There are no cracks and gaps at the coating–substrate interfaces, which indicate a better adhesion of the coatings on the substrate. SEM micrographs (Fig.4.3 (a-b)) reveal the surface morphology of the as-sprayed and polished surface of the  $\text{Cr}_3\text{C}_2-25\text{NiCr}$  coatings deposited on superni 75.





**Fig. 4.2** BSE Image showing cross section morphology of the D-Gun sprayed  $\text{Cr}_3\text{C}_2$ -25 % NiCr on (a) superni 75, (b) superni 718 and (c) superfer 800H

#### 4.2.3.3 Porosity and coating thickness

Due to the intermittent process during D-gun spraying, few pores and voids occur in D-gun sprayed  $\text{Cr}_3\text{C}_2$ -25%NiCr coatings. The porosity is visible as black contrast regions in the coating and it was less than 0.69 %. Very few micropores are observed in the coatings, which are segregated near the splat boundaries (Fig.4.2). The thickness of the coatings on three superalloys, superni 75, superni 718, superfer 800H, as measured from the BSE images, are 246 $\mu\text{m}$ , 223 $\mu\text{m}$ , and 221 $\mu\text{m}$ , respectively.

#### 4.2.3.4 Microhardness of the coatings

The microhardness data for the coatings is plotted in the Fig.4.4, which show the microhardness profiles along the cross section of the coatings as a function of distance from the coating-substrate interface. The microhardness of the substrates is found to be in the range of

290–494 Hv, and it is in the range of 775–1200Hv along the cross section of the coatings. Further, an increase in microhardness of all the substrates is observed near the coating–substrate interface.

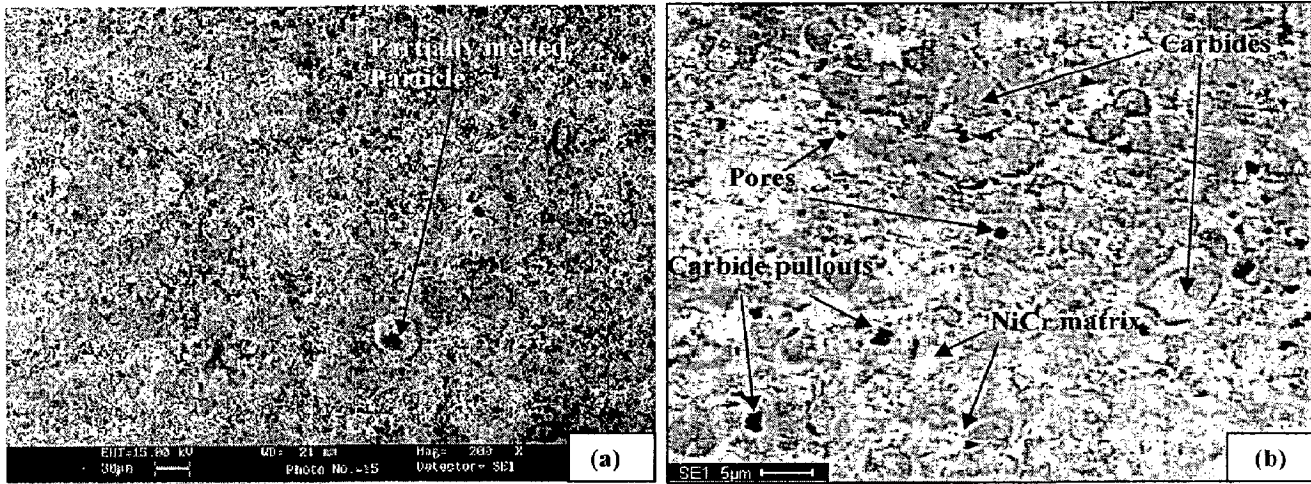


**Fig. 4.3** SEM micrographs showing surface morphology of Detonation gun as-sprayed  $\text{Cr}_3\text{C}_2$ -25%NiCr coating on superalloy superni 75 (a) as-sprayed surface and (b) polished surface

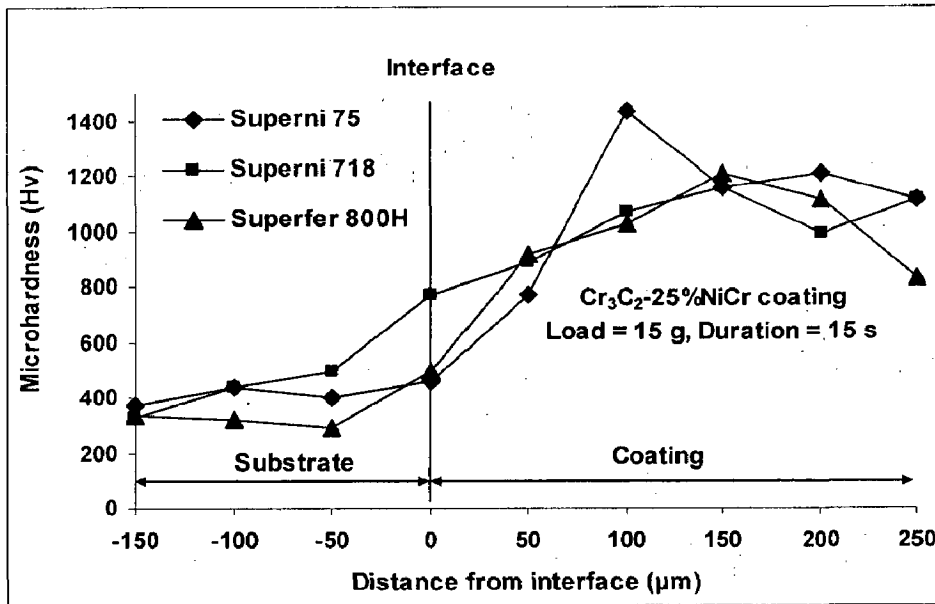


**Fig. 4.4** Microhardness profiles for Detonation-gun sprayed  $\text{Cr}_3\text{C}_2$ -25%NiCr coatings on different superalloys.

#### **4.2.3.5 Surface roughness of the coatings**

The coating surface was very rough in the as-sprayed condition due to the presence of un-melted/partially melted particles and the roughness was found to be in the range of 4.92-6.05 $\mu$ m. The centre line average (CLA) method was used to obtain the Ra values.

#### **4.2.3.6 FE-SEM/EDS analysis**

##### **4.2.3.6.1. Surface morphology of the D-gun as-sprayed coatings**

The FE-SEM micrograph of as sprayed Cr<sub>3</sub>C<sub>2</sub>-NiCr coating is shown in Fig.4.5. Fig.4.5a and b indicates NiCr metallic binder phase corresponds to the white region in the micrograph and the dark grey region is the carbides. The NiCr metallic binder material is present in amorphous/nanocrystalline form, NiCr likely to melt first and dissolve some chromium carbide to form a liquid phase which may be rich in Cr and C, and may become supersaturated. Supersaturated melt may become amorphous or nanocrystalline upon rapid solidification (typically 10<sup>6</sup>-10<sup>7</sup> K/s) during the deposition process (Murthy et al., 2006). Various researchers have also reported that the NiCr acts as a binder phase for the carbide particles (Vuoristo et al., 1994; Guilemany et al., 1998; Takeuchi, 1998). These carbides are clad with the metallic binders, this leads to better binder protection to the coating. The coating has little porosity in the form of black contrast regions in Fig.4.5a. Microstructure of as-sprayed coating, at higher magnification (10,000X, Fig.4.5b) along with EDS spectrum with EDS elemental composition gives various phases present in the coating, which show three types of features (melted, un-melted particles, and NiCr zones). During D-gun process, the incoming powder particles have un-melted core, upon impact on the substrate, the particle freezes rapidly, the coating contains some trapped porosity in which un-melted particle accumulates as reported in the literature (Gledhill et al., 1999; Limin Sun et al., 2003; Khor et al., 2004) as well as in our recent publication (Kamal et al., 2008B). Dense melted chromium carbide (different size) is surrounded by NiCr specks, distributed randomly in the coating. Fractured carbide particle were observed in the coating, which may occur upon impact of powder particle on the substrate under high impact velocities as in D-gun process (Murthy et al., 2007).

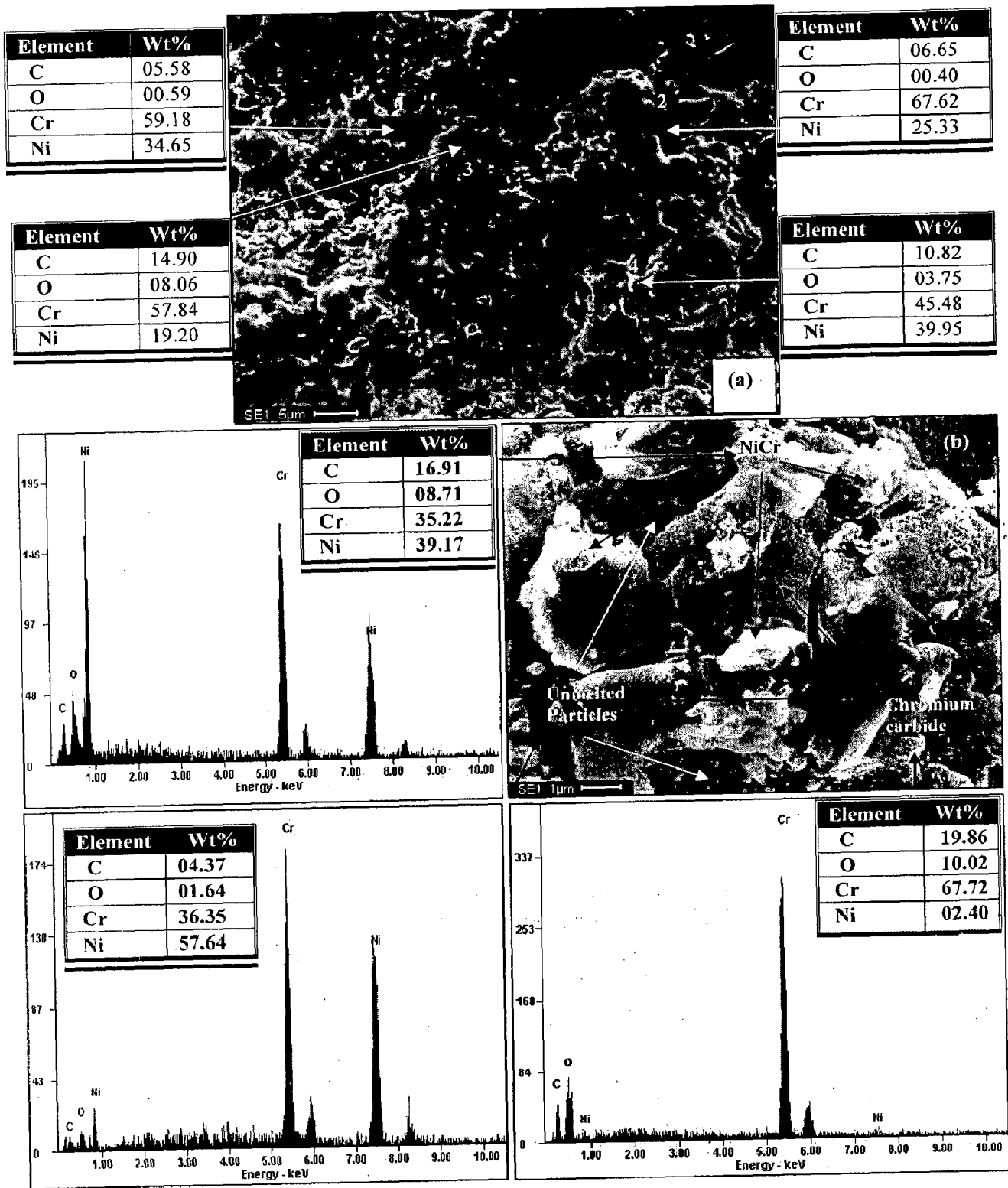


Fig. 4.5 FE-SEM micrographs showing surface morphology of Detonation gun as-sprayed  $Cr_3C_2-25\%NiCr$  coating on superalloy superni 75 (a) at lower magnification 2000 X, (b) at higher magnification 10,000X,

#### 4.2.3.6.2 Cross-sectional analysis

Cross-sectional analysis of the coating was carried out at different points along the cross-section of D-gun sprayed  $\text{Cr}_3\text{C}_2$ -25%NiCr coating on superalloy 75 by FE-SEM/EDS and the results are shown in Fig.4.6. The major portion of  $\text{Cr}_3\text{C}_2$ -25%NiCr coating is covered with chromium carbide, which is found along the nickel rich splats.

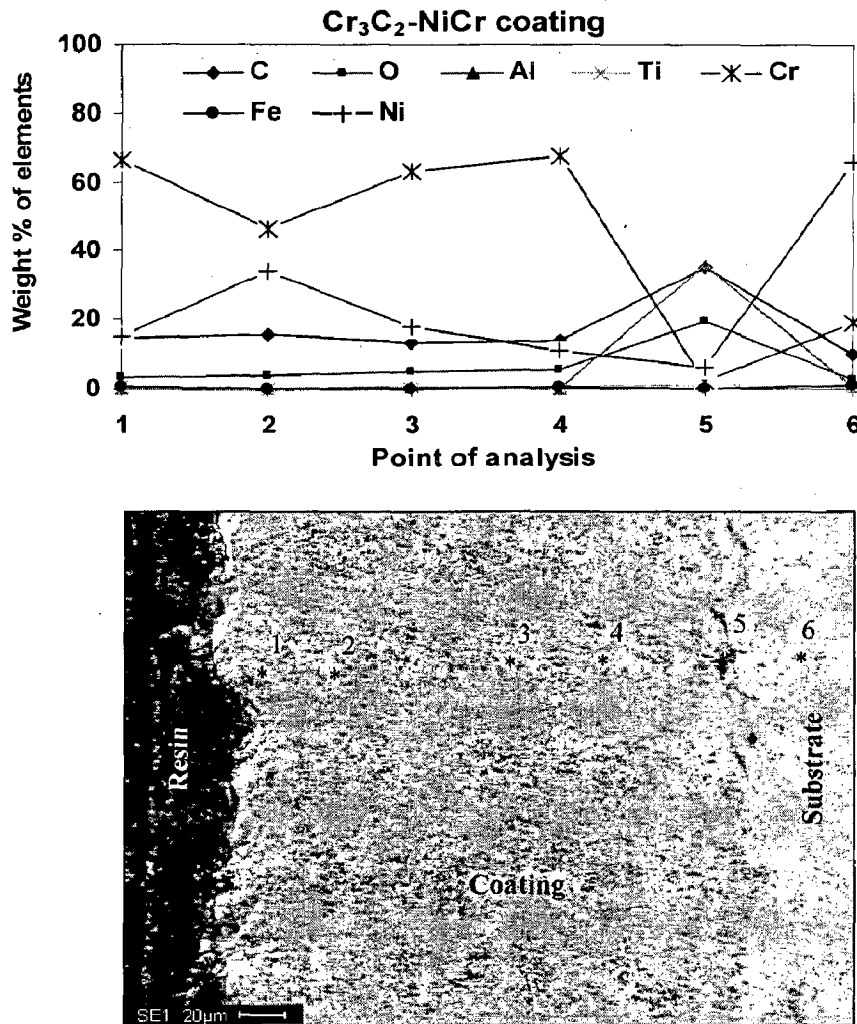


Fig. 4.6. FE-SEM/EDS analysis at the cross-section of as sprayed  $\text{Cr}_3\text{C}_2$ -25%NiCr coating on superalloy 75

#### 4.2.3.7 X-ray diffraction (XRD) analysis

From the XRD results shown in Fig.4.7, it is evident that the powder mainly consists of  $\text{Cr}_3\text{C}_2$ ,  $\text{Cr}_7\text{C}_3$  and Ni, whereas that of  $\text{Cr}_3\text{C}_2$ -NiCr coating (Fig.4.8) contains different superalloys shows  $\text{Cr}_3\text{C}_2$ ,  $\text{Cr}_7\text{C}_3$ , Cr and  $\text{Cr}_{23}\text{C}_6$  as major phases, and Ni, NiC, and SiC as minor phases.

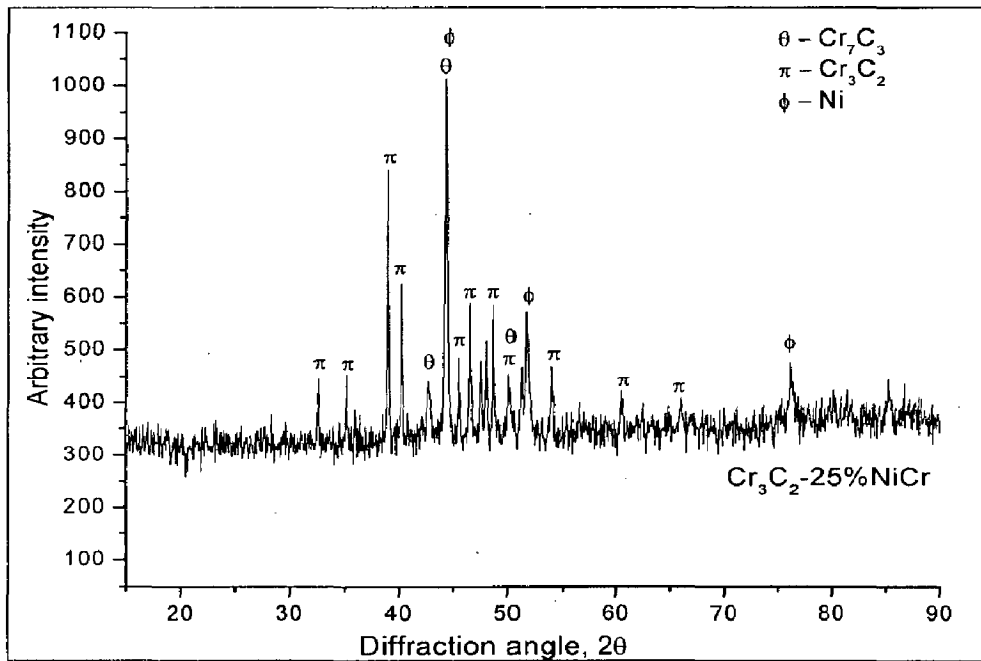


Fig. 4.7 X-ray diffraction for the  $\text{Cr}_3\text{C}_2$ -25%NiCr powder

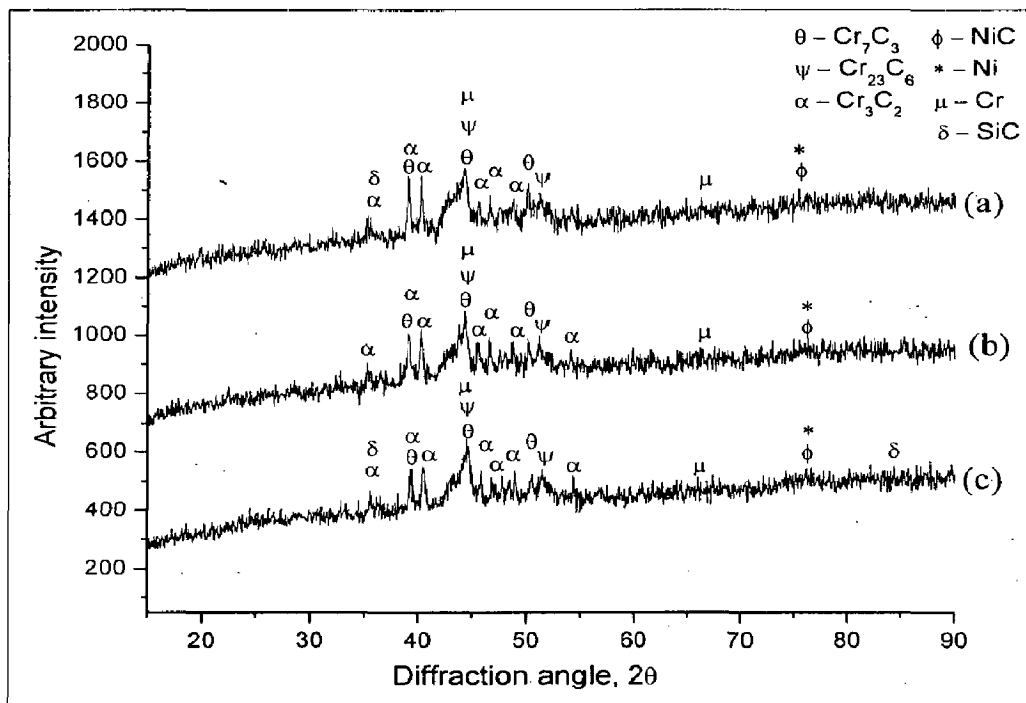


Fig. 4.8 X-ray diffraction for the  $\text{Cr}_3\text{C}_2$ -25%NiCr coating on superalloy (a) superalloy 718, (b) superalloy 75 and (c) superalloy 800H

#### 4.2.3.8 X-ray mapping

D-gun sprayed  $\text{Cr}_3\text{C}_2$ -25%NiCr coated superalloys samples have been cut across the cross-sections and mounted in transoptic mounting resin, mirror-polished and silver pasted between samples and the stub in order to have conductivity. Subsequently, they were gold coated to facilitate X-ray mapping of the different elements present across the coating by FE-SEM/ EDS. Elemental X-ray mappings of the coating show (Fig.4.9-4.11) that the coating area is found to be rich with main elements of the coating powder. Nickel rich splats are surrounded by chromium. Elemental mappings also indicate diffusion of small amount of Ti (Fig.4.9) and Fe (Fig.4.10) from the substrate to the coating. The presence of oxygen at the coating-substrate interface might be due to the in-flight oxidation of coating material, which leads to oxide inclusion in the form of aluminum oxide clearly visible near the coating-substrate interface. It is also believed that some alumina particles might be retained in the asperities during grit blasting of the substrate prior to deposition of the coatings and appeared at the coating-substrate interface as melted alumina oxides.

#### 4.2.4 Discussion

The  $\text{Cr}_3\text{C}_2$ -25%NiCr coating is uniform and no cracks are observed at the surface and edges of the coating. The coated surface is grey in colour. The cross-sectional morphologies shown in Fig.4.2 reveal that the coating exhibits a clear contrast between carbide particles and metallic binder, which are uniformly distributed in the coating. Very few partially melted particles were observed in the microstructure. Further, the coatings possess some porosity, which existed mainly at the interface between flattened particles of melted chromium carbide that corresponds to the non bounding interface area. The porosity is visible in the form of black contrast regions. Dense coatings usually provide better corrosion resistance than the porous coatings. The porosity values of as sprayed  $\text{Cr}_3\text{C}_2$ -25%NiCr coatings are identical with the findings of Murthy et al. (2006). The D-gun sprayed  $\text{Cr}_3\text{C}_2$ -25%NiCr coatings contain less porosity as compared to HVOF sprayed coatings (Wang and Lee, 1997, 2000; Wang and Shui 2002; Wang, 1996 and Hazoor et al., 2006). Low value of porosity may be due to the high impact velocity of the coating particles (Scrivani et al., 2001), which cause high density, and high cohesive strength of individual splats. Seo et al. (2007) suggested that the pores form

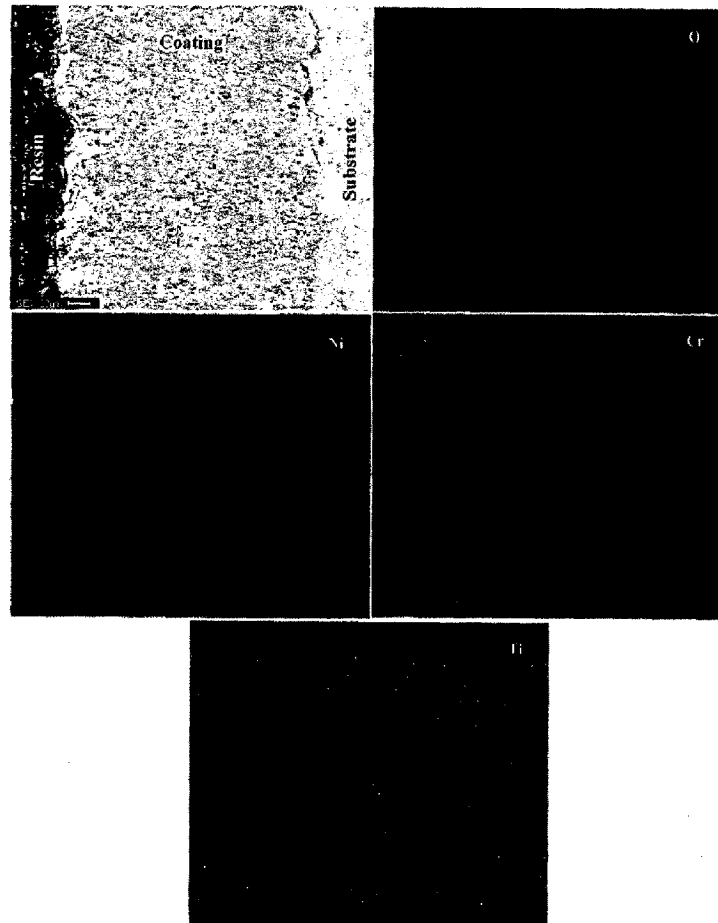


**Fig. 4.9** Composition image (SEI) and X-ray mapping of the cross-section of the as sprayed  $\text{Cr}_3\text{C}_2$ -25%NiCr coating on supemi 75 superalloys



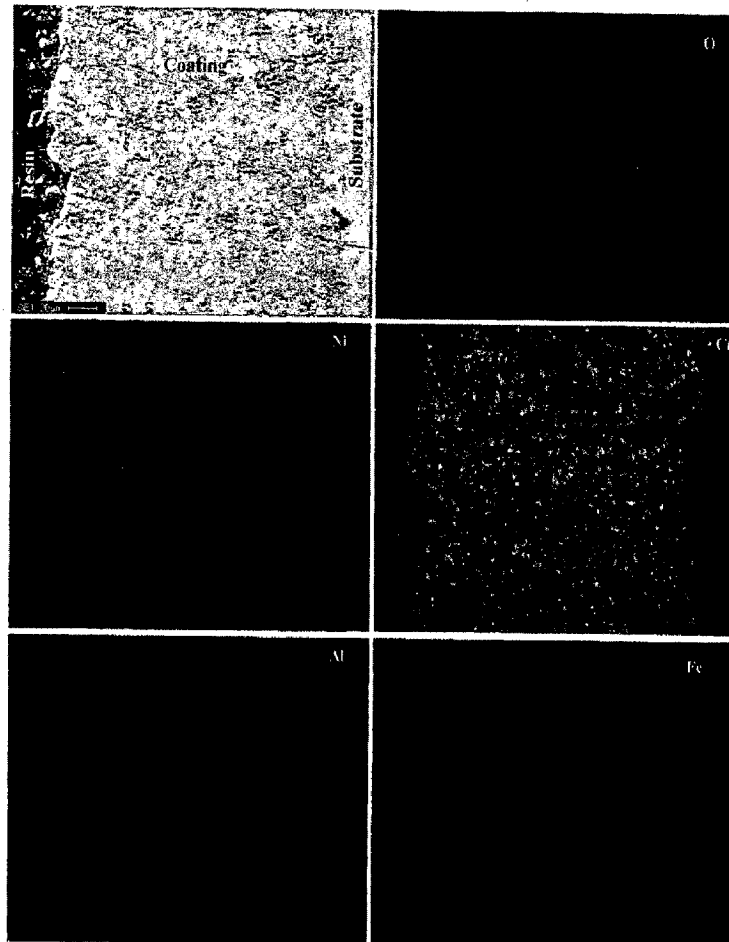


**Fig.4.10** Composition image (SEI) and X-ray mapping of the cross-section of the as sprayed  $\text{Cr}_3\text{C}_2$ -25%NiCr coating on superni 718 superalloys

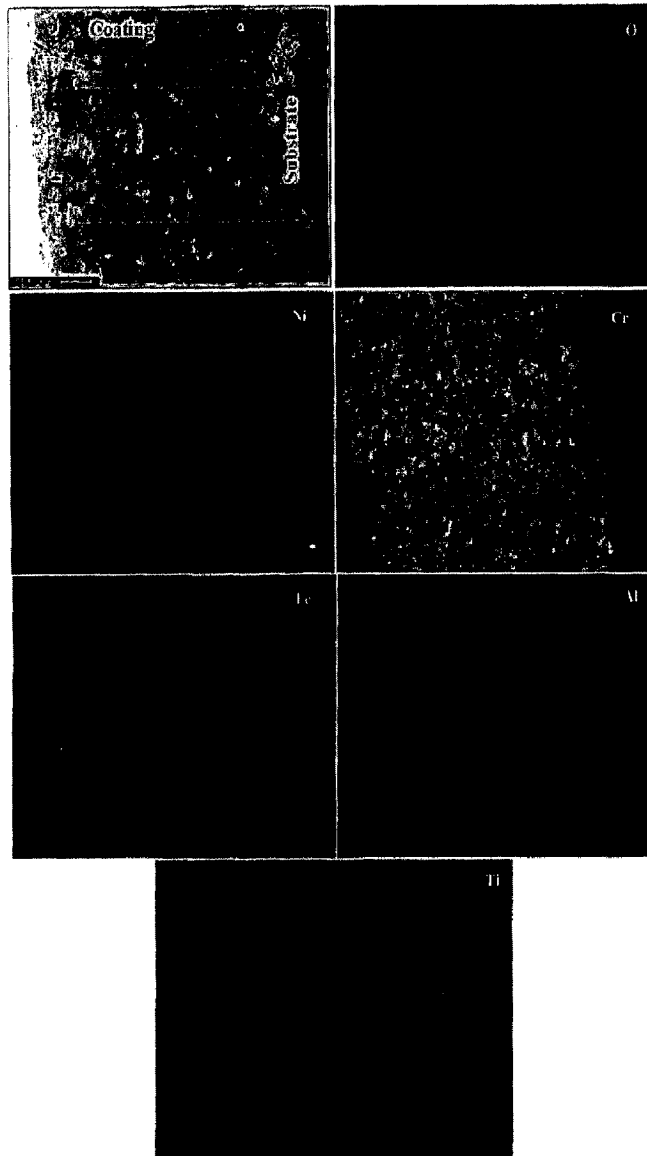


**Fig. 4.11** Composition image (SEI) and X-ray mapping of the cross-section of the as-sprayed  $\text{Cr}_3\text{C}_2$ -25%NiCr coating on superfer 800H superalloys

usually near the splat boundaries. The micropores in the coatings have a significant role to play as far as the corrosion of thermal spray coatings is concerned, as they can provide a pathway to the reactive corrosive elements (Choi et al., 2002) through which the corrosion species can penetrate the coating to reach the substrate and may cause rapid corrosion attack. SEM micrographs corresponding to the surface morphology of as-sprayed and polished surface of the  $\text{Cr}_3\text{C}_2$ -25%NiCr coating are shown in Fig.4.3 (a-b). The as sprayed surface is fairly rough, dense, flat and free of cracks, pores, but shows the presence of partially melted particles (Fig.4.3a), which are identified by its spherical morphology. The polished surface (Fig.4.3b) shows two regions one with the NiCr metallic binder phase corresponds to the white region in the micrograph and the other dark grey region is the carbide (Li et al., 2004), these carbide particles are uniformly and completely clad with the metallic binder and its distribution is uniform due to the lower dissolution of carbides, which leads to a better binder protection in the coating. Also the polished surface showed irregular shaped small pits, although some of the pits are pores, which formed during spraying, it might have also formed due to pullouts of the coating during polishing process (Li et al., 1999). The microhardness of D-gun sprayed  $\text{Cr}_3\text{C}_2$ -25%NiCr coatings has been found to be very high as compared to the superalloy substrates (Fig.4.4). The increase in hardness may also occur due to the decarburisation of  $\text{Cr}_3\text{C}_2$  or oxidation of the binder phase (Matthews et al., 2003). Some variations in hardness values in the coating may be due to the presence of porosity, un-melted and partially melted particles. Wang (1993) showed that D-gun sprayed  $\text{Cr}_3\text{C}_2$ -25%NiCr coating is superior in terms of microhardness and anti wear performance than that of the plasma-sprayed coating. It is observed in the present investigation that the microhardness of D-gun sprayed coating is much higher than that of the HVOF sprayed  $\text{Cr}_3\text{C}_2$ -25%NiCr coating (Hazoor et al., 2006; Wirojanupatump et al., 2001; Hawthorne et al., 1999; and Uusitalo et al., 2002B). Further, near the coating-substrate interface, a slightly higher value of hardness is found as compared to the bare substrates. This increased hardness value near the coating-substrate interface might be due to the work hardening effect of sandblasting of the substrates prior to the coating process (Sundararajan et al., 2005B). Some difference in the microhardness values of the coating on different substrate may be due to minor diffusion of elements from the substrate to coating. For example, the elemental mapping for titanium and iron shows outward diffusion from the substrate to the coating (Fig.4.9-4.10). It shows that the

properties of HVOF sprayed coatings could match well with that of the coatings deposited by other techniques. Fig.4.5a shows the FE-SEM/EDS analysis of phases for  $\text{Cr}_3\text{C}_2$ -25%NiCr coated surface, from which it can be inferred that there is a matrix at point 1 and 2 which contains mainly un-melted particle. There is light gray phase (at point 3) distributed in the coating, which mainly consist of chromium carbide surrounded by NiCr. In the matrix, there is white coloured phase (point 4) distributed randomly in the coating, which mainly consists of Cr and C from  $\text{Cr}_3\text{C}_2$  dissolved in NiCr in varying amounts (Murthy et al., 2007). The microstructure of the as-sprayed coating at higher magnification (Fig.4.5b 10,000X) shows uniform distribution of the carbides (dark grey regions) of different sizes, which also show some fractured carbide particles. The fracturing of carbide particles may occur upon impact on the substrate under high impact velocities as in D-gun process (Murthy et al., 2007).  $\text{Cr}_3\text{C}_2$  particles can be clearly seen with small NiCr rich specks and surrounded by melted aggregate of Ni and Cr along with some amount of un-melted particles distributed in the coating (Guilemany et al., 1996). FE-SEM/EDS analysis of  $\text{Cr}_3\text{C}_2$ -25%NiCr coating along its cross-section are shown in Fig.4.6 EDS analysis of the coating show the top surface (point 1, 3 and 4) contains mainly Cr along Ni rich splats, where as point 2 show the Ni rich splat, point 5 indicates the oxide inclusions of aluminum oxide in the black areas at the coating-substrate interface. It is believed that some alumina particles might have been retained in the asperities during grit blasting of the substrate prior to deposition of the coatings. Sundararajan et al. (2003A) have reported the similar islands of aluminum oxides due to retained alumina powder during polishing. Further, at point 6, it shows the basic elements of substrate. The X-ray diffraction pattern (Fig.4.7) of the coating powder shows the primary phases such as  $\text{Cr}_3\text{C}_2$ ,  $\text{Cr}_7\text{C}_3$  and Ni, which are in accordance with the findings of Murthy et al. (2007). The XRD pattern of as sprayed  $\text{Cr}_3\text{C}_2$ -25%NiCr (Fig.4.8) coating on superalloys indicates that the  $\text{Cr}_7\text{C}_3$  (Matthews et al., 2003) and  $\text{Cr}_{23}\text{C}_6$  carbides are produced by partial decomposition of the initial  $\text{Cr}_3\text{C}_2$  phase during the spraying process, even though  $\text{Cr}_7\text{C}_3$  was also present in the initial powder. Similar findings of the presence of carbide phases in the microstructure of D-gun coatings have been reported by Mohanty et al. (1996).

#### 4.2.5 Conclusions

The D-gun spray technique has been used to deposit  $\text{Cr}_3\text{C}_2$ -25%NiCr coating on three different superalloy substrates and the coatings were characterized for their microstructural features, and hardness in the present work. The following observations were made based on the present study.

1. The coatings on three different superalloy substrates (superni 75, superni 718 and superfer 800H) exhibited a dense structure with the porosity value around 0.69%. The thin splats are observed in the cross section of the coatings. Surface EDS analysis of the coatings showed the similar compositions as found for the initial powder used for deposition of coatings.
2. A good adhesion of the coatings to the substrate was evident from the absence of cracks and gaps at the interfaces as well as due to the uniform distribution of carbide particles along metallic binders.
3. The microhardness of the  $\text{Cr}_3\text{C}_2$ -25%NiCr coatings was found to be in the range of 775 – 1200Hv due to high volume fraction of carbides, dispersed uniformly in the matrix.

## 4.3 OXIDATION STUDIES IN AIR

### 4.3.1 Introduction

Cermet coatings such as WC–Co, CrC, TiC (Kamal et al., 2009A) and SiC (Manoj Kumar et al., 2005) have been developed basically for wear resistant properties. Thermally sprayed  $\text{Cr}_3\text{C}_2$ –NiCr coating is frequently used for a variety of wear resistance applications, in gas turbine, steam turbine and aero-engine to improve the resistance against sliding, abrasive and erosive wear (Rhys-Jones et al., 1990). Recently, these coatings are gaining importance for high temperature wear resistance and corrosion (Matthews et al., 2003) resistance applications in various industrial fields such as power generation, aerospace (Seong et al., 2000; Mann et al., 2000), and the steel industries (Barbezat et al., 1993; Takeuchi, 1998; Kim et al., 1996). In the chromium carbide system, three stable carbides namely  $\text{Cr}_3\text{C}_2$ ,  $\text{Cr}_7\text{C}_3$  and  $\text{Cr}_{23}\text{C}_6$  exist with successive lowering of carbon concentration. Degradation of the cermet composition during thermal spraying occurs through oxidation, decarburisation and carbide dissolution; the effects of which are retained in the as-sprayed coating as a result of the rapid solidification of the material upon impact. Although tribological behavior of D-gun sprayed  $\text{Cr}_3\text{C}_2$ –NiCr is well known in the literature (Murthy et al., 2006; Matthews et al., 2003; Murthy et al., 2007; Mohanty et al., 1996; Wang et al., 1993; Lindgren et al., 1987), but its cyclic oxidation behavior in air at high temperature is not investigated so far. Corrosion/oxidation under cyclic conditions is crucial in land based power generators in industries where frequent power cuts occurs. Also, in short duration flights, the aero engine turbine blades are exposed to harsh environments under cyclic conditions. Various thermal spray processes, such as D-gun spraying, plasma spraying and high velocity oxy-fuel spraying methods are mostly used to apply chromium carbide coating to impart a wear resistance against abrasion and erosion in corrosive environment at high temperature up to 900 °C (Sidhu et al., 2005B). D-gun spray technique can be used successfully to develop protective coatings on the superalloys for combating high temperature oxidation and hot corrosion (Kamal et al., 2009A). Therefore, the present investigation has been focused to investigate the cyclic oxidation behavior of D-gun sprayed  $\text{Cr}_3\text{C}_2$ –NiCr coatings on the selected superalloys in air at 900 °C. The cyclic oxidation behavior of bare superalloys was also investigated and used to assess the performance of coated superalloys.

## 4.3.2 Experimental details

The substrate materials, coating formulation and the oxidation studies are explained in detail in section 3.1, 3.2.3 and 3.4.1.

## 4.3.3 Results

### 4.3.3.3 Visual observations and weight change measurements

Color of oxide scale formed on the bare superalloys superni 75, superni 718 and superfer 800H, after air oxidation for 100 cycles at 900 °C (Fig.4.12 a, c and e), was dark grey. During initial cycles, light lustrous scale were formed, but towards the end of cycles, some greenish tinges were observed on the surface of superni 75 (Fig.4.12a) along with few white spots, a mixture of dark and light grey scale has formed on the surface of superni 718(Fig4.12c), along with brownish grey scale appeared at the edges with few white spots. Whereas in case of superfer 800H (Fig.4.12e), the oxide scale has two regions, with dark and light grey scales, dark grey scale has brownish tinges distributed randomly. On the other hand,  $\text{Cr}_3\text{C}_2$ -NiCr coated superalloys (Fig.4.12 b, d and f) show initially dark grey colour during early cycles, as the oxidation went on, the colour of the oxide scale turned in to greenish on gray background on superni 75 and superni 718(Fig.4.12 b and d), where as coated superfer 800H (Fig.4.12f) shows the blackish green colour on dark gray background. The coatings suffered minor spallation along the corners and edges of the specimens.

Weight gain/unit area ( $\text{mg}/\text{cm}^2$ ) versus number of cycles plots for the bare as well as D-gun sprayed  $\text{Cr}_3\text{C}_2$ - NiCr coated superalloys (superni 75, superni 718 and superfer 800H) oxidised at 900 °C in air up to 100 cycles are shown in Fig.4.13. Bare superalloy superfer 800H shows the maximum weight gain among all the superalloys, where as bare superni 75 and superni 718 shows nearly equal weight gain. The weight gain by superni 75 and superni 718 after 100 cycles is nearly 13% and 16% less than that of superfer 800H. The coated superalloys show much lower weight gain than the bare specimens in the given environment. It is found that 37.3% saving in overall weight gain for  $\text{Cr}_3\text{C}_2$ - NiCr coated superni 75 in comparison with the bare superni 75, whereas  $\text{Cr}_3\text{C}_2$ -NiCr coating on superni 718 and superfer 800H superalloys reduce the weight gain by 26.3% and 19.6% of that gained by the bare superalloys, respectively. All the

coated and bare superalloys followed the parabolic rate law as evident from the Fig.4.14. The values of the parabolic rate constant ( $K_p$ ) are shown in Table 4.1. It is inferred that the  $K_p$  values for the coated superalloys were less than the bare superalloys. The overall weight gain/unit area for the coated and bare superalloys is shown in Fig.4.15.

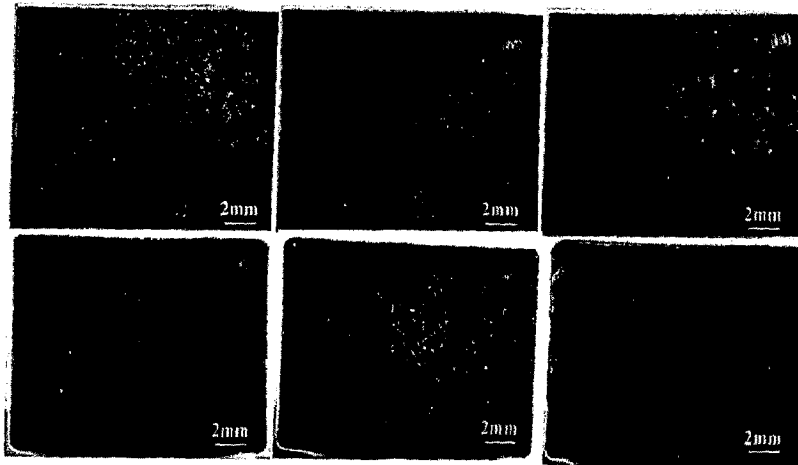


Fig. 4.12 Surface macrograph of  $Cr_3C_2$ -NiCr coated and bare superalloys subjected to cyclic oxidation in air for 100 cycles at 900 °C, (a) Bare superalloy 75, (b) Coated superalloy 75, (c) Bare superalloy 718, (d) Coated superalloy 718, (e) Bare superalloy 800H, (f) Coated superalloy 800H

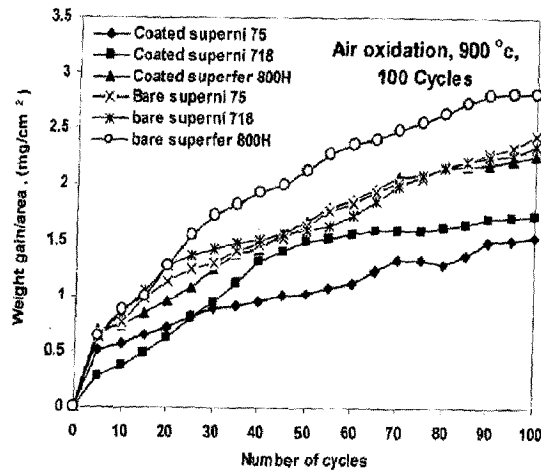


Fig. 4.13 Weight gain/area vs. number of cycles plot for  $Cr_3C_2$ -NiCr-coated and bare



superalloys subjected to cyclic oxidation in air for 100 cycles at 900 °C.

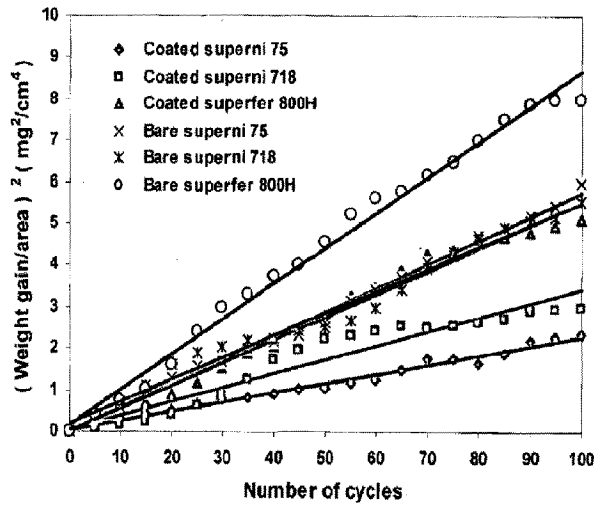


Fig. 4.14 (Weight gain/area)<sup>2</sup> vs. number of cycles plot for Cr<sub>3</sub>C<sub>2</sub>-NiCr-coated and bare superalloys subjected to cyclic oxidation in air for 100 cycles at 900 °C.

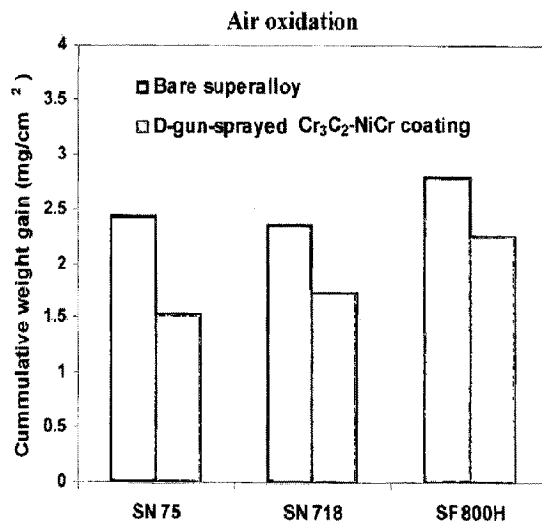


Fig. 4.15 Bar chart showing cumulative weight gain per unit area for bare and Cr<sub>3</sub>C<sub>2</sub>-NiCr-coated superalloys subjected to cyclic oxidation in air for 100 cycles at 900 °C.

#### 4.3.3.4 X-ray diffraction analysis (XRD) analysis

The various phases identified from the X-ray diffraction patterns of the surface oxide formed on un-coated and D-gun sprayed  $\text{Cr}_3\text{C}_2$ -NiCr coated superalloys after cyclic oxidation in air at 900 °C for 100 cycles are shown in Fig.4.16 and 4.17. The main phases identified for the oxidised un-coated superalloys are NiO,  $\text{Cr}_2\text{O}_3$ ,  $\text{Fe}_2\text{O}_3$ ,  $\text{Al}_2\text{O}_3$ , Ni,  $\text{NiFe}_2\text{O}_4$  and  $\text{NiCr}_2\text{O}_4$  (Fig.4.16). The surface oxides on coated superalloys were  $\text{Cr}_2\text{O}_3$ , NiO, NiC,  $\text{Fe}_2\text{O}_3$ ,  $\text{Cr}_3\text{C}_2$ ,  $\text{Cr}_7\text{C}_3$ ,  $\text{Cr}_{23}\text{C}_6$  and  $\text{NiCr}_2\text{O}_4$ . The existence of minor phase such as  $\text{Fe}_2\text{O}_3$  on the surface of oxidised  $\text{Cr}_3\text{C}_2$ -NiCr indicates the diffusion of Fe from the substrate during oxidation at temperature of 900 °C (Fig.4.17)

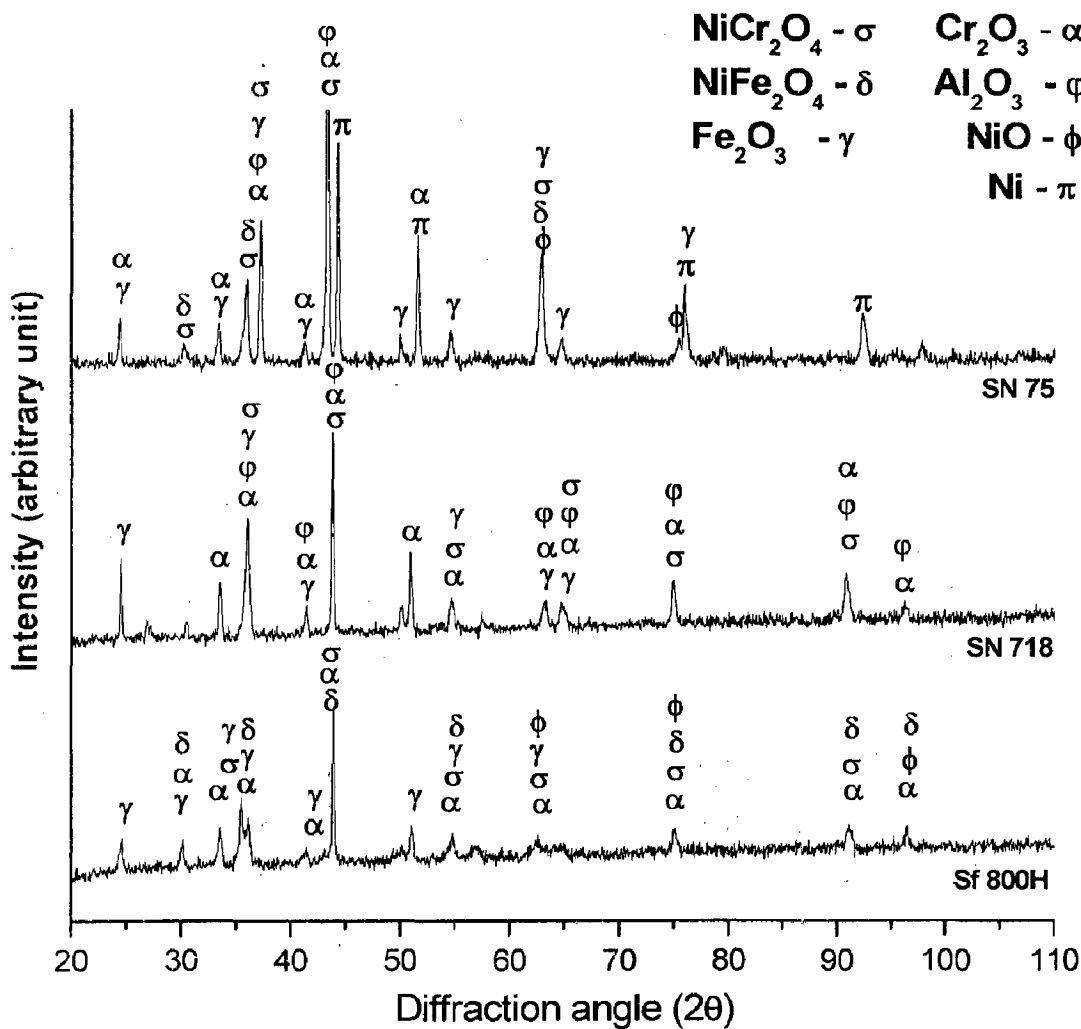


Fig. 4.16 X-ray diffraction patterns for  $\text{Cr}_2\text{C}_3$ -NiCr coated superalloys exposed to cyclic oxidation in air at 900 °C after 100 cycles

### 4.3.3.5 FE-SEM/EDS analysis

#### 4.3.3.5.1 Surface morphology of the scales

FE-SEM micrographs with EDS spectrum reveals the surface morphology of the  $\text{Cr}_3\text{C}_2$ -NiCr coated and bare substrate superalloy specimens after cyclic oxidation in air for 100 cycles at 900 °C as shown in Fig. 4.18-4.19. The surface scale developed on coated superalloy 75 is massive and without any cracks, with globules which are irregularly distributed in the scale. EDS analysis of the scale of  $\text{Cr}_3\text{C}_2$ - NiCr coated superalloy 75 revealed the formation of  $\text{Cr}_2\text{O}_3$  and NiO as a principle phases. In addition,  $\text{Fe}_2\text{O}_3$  and Ti oxides are also present in small amounts (Fig.4.18a). Micrograph of corroded  $\text{Cr}_3\text{C}_2$ -NiCr coated superalloy 718 appears to be dense and continuous. EDS analysis of the scale revealed NiO and  $\text{Cr}_2\text{O}_3$  as major oxide phases, along with small amounts of  $\text{Fe}_2\text{O}_3$ , Mn, Ti, Si, Al, Cu and Ta oxides (Fig.4.18b). Similarly, the scale formed on the coated superalloy 800H is dense with elliptical shaped globules dispersed in the oxidised scale (Fig.4.18c). The EDS analysis clearly indicates the formation of  $\text{Cr}_2\text{O}_3$  and NiO as predominant oxides along with small quantities of minor oxide phases as that of superalloy 718 except Cu and Ta.

**Table 4.1** Parabolic rate constant ( $k_p$ ) values for bare and D-gun sprayed  $\text{Cr}_3\text{C}_2$ -NiCr-coated superalloys subjected to cyclic oxidation in air for 100 cycles at 900 °C

Superalloy substrates	$k_p \times 10^{-12} \text{ g}^2 \text{ cm}^{-4} \text{ s}^{-1}$
Bare Superalloy 75	16.00
Bare Superalloy 718	14.70
Bare Superalloy 800H	23.72
Coated Superalloy 75	06.30
Coated Superalloy 718	09.42
Coated Superalloy 800H	15.33

On the other hand, the oxide scale developed on the surface of bare superalloy 75 is of white contrast region consists of irregular size fine granules, nonuniformly distributed in the matrix having NiO as the principal phase, where as, dark black region depicts the presence of NiO and  $\text{Cr}_2\text{O}_3$  as major phases along with little quantity of Fe and Ti oxides (Fig.4.19a). A homogeneous

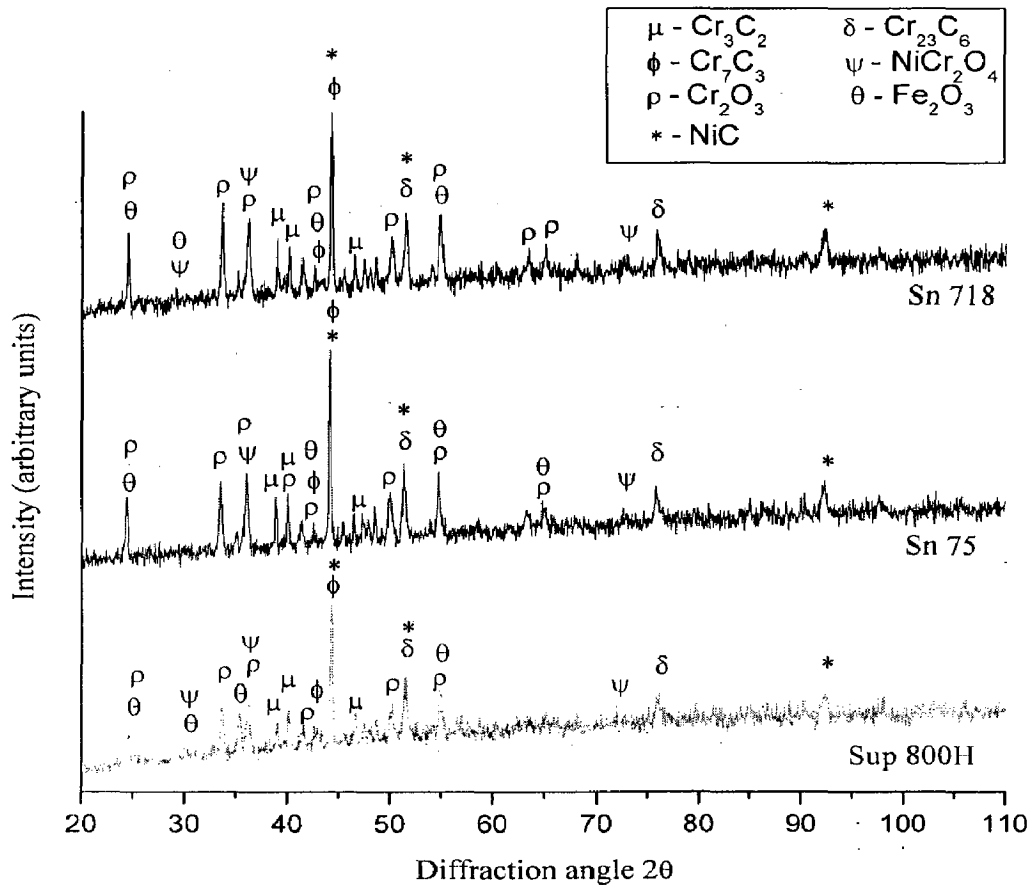


**Fig. 4.17** X-ray diffraction patterns for  $\text{Cr}_2\text{C}_3$ -NiCr coated superalloys exposed to cyclic oxidation in air at 900 °C after 100 cycles.

and continuous surface scale is developed on bare superni 718, which has NiO,  $\text{Fe}_2\text{O}_3$  and  $\text{Cr}_2\text{O}_3$  as the main phases along with minor quantities of Mn, Ti, Si, Al, Cu and Ta (Fig.4.19b). The hemispherical shape protrusion consisting of  $\text{Fe}_2\text{O}_3$ , MnO and  $\text{Cr}_2\text{O}_3$  as predominant phases present on the oxidised surface of bare superfer 800H, while the oxides of MnO,  $\text{TiO}_2$ ,  $\text{SiO}_2$  and  $\text{Al}_2\text{O}_3$  are also found to be present in small amounts (Fig.4.19c).

#### 4.3.3.5.2 Cross-sectional analysis of the scale

Cross-sectional analysis of the scale and the coating was carried out at different points along the cross-section of the air oxidised D-gun  $\text{Cr}_3\text{C}_2$ -NiCr coated superni 75, superni 718 and superfer 800H by FE-SEM/EDS and the results are shown in Fig.4.20. All the oxidised  $\text{Cr}_3\text{C}_2$ -NiCr coating has two regions, one with dark grey patches composed of chromium and the light

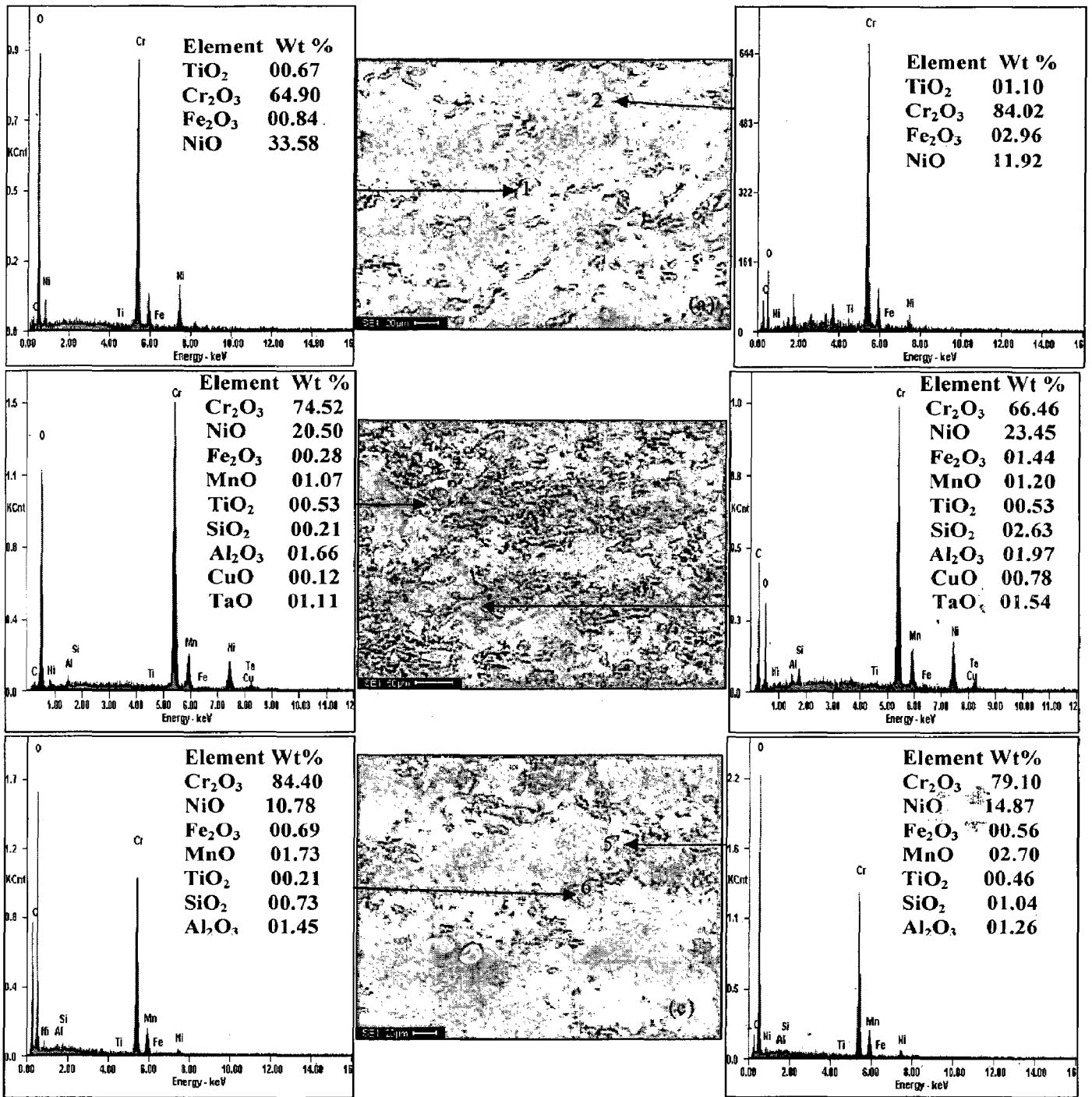


**Fig. 4.18** FE-SEM/EDS analysis along with EDS spectrum for coated superalloys subjected to cyclic oxidation in air at 900 °C after 100 cycles: (a) coated superni 75, (b) coated superni 718 and (c) coated superfer 800H.

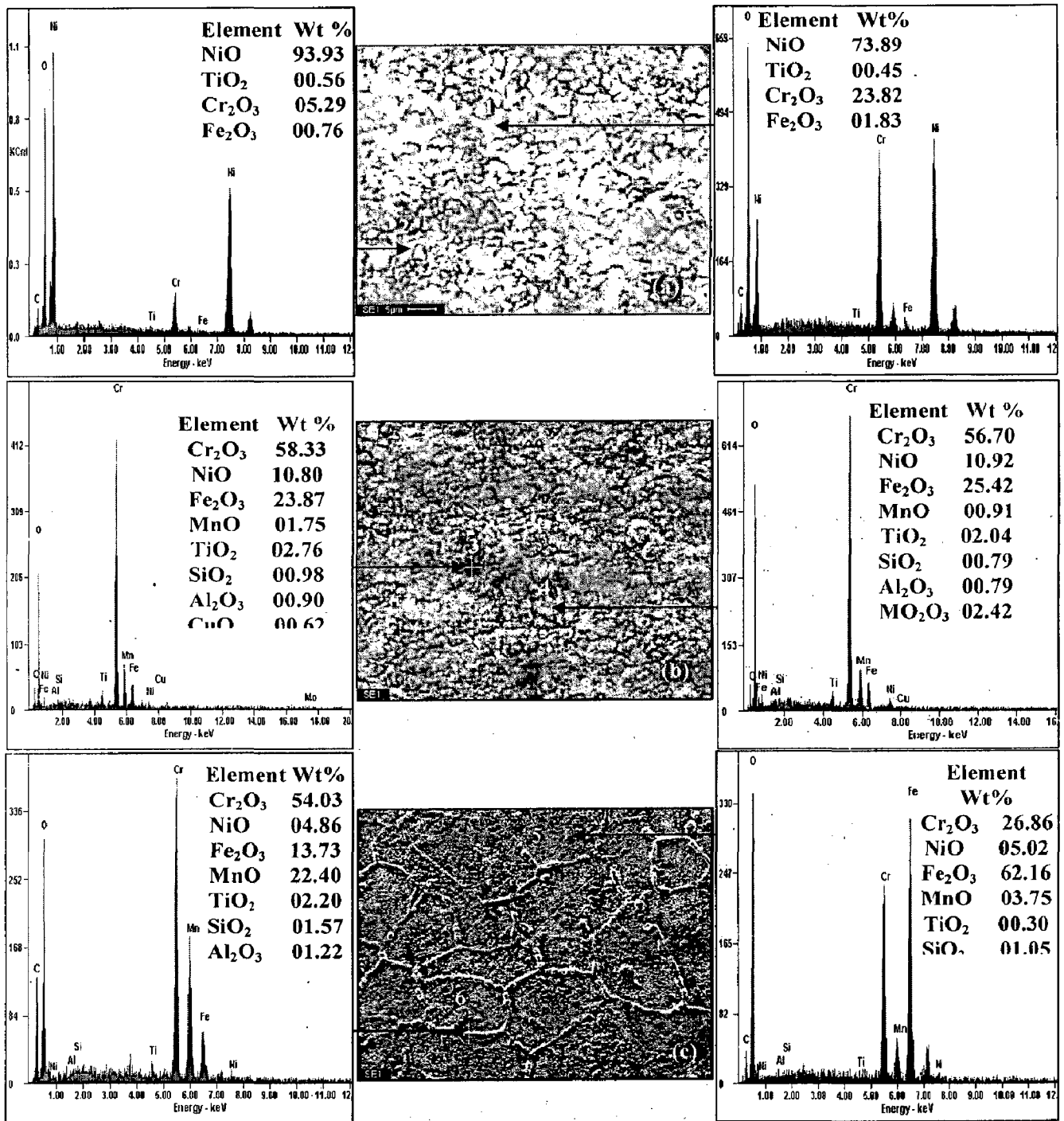


Fig. 4.19 FE-SEM/EDS analysis along with EDS spectrum for the bare superalloys subjected to cyclic oxidation in air at 900 °C after 100 cycles: (a) bare sperni 75, (b) bare sperni 718 and (c) bare sperfer 800H

grey patches show nickel rich splats. FE-SEM image shows the formation of a compact, adherent and continuous oxide scale. Cross-sectional EDS analysis of oxidised coated superni 75 reveals (Fig.4.20a) that the uppermost part of the scale has relatively higher concentration of Cr (point 1 and 2) while Ni rich splats in the subscale region at point 3. Ni starts decreasing towards the substrates at point 4 and 5 but Ni is increasing near the coating-substrate interface (point 6). A location at point 7 in the micrograph depicts the inter diffusion of elements between coating and substrate. Cr<sub>3</sub>C<sub>2</sub>-NiCr coated superni 718 (Fig.4.20b) shows the similar behaviour as that of superni 75, where as superfer 800H (Fig.4.20c) indicates the presence of continuous, adherent and non-uniform oxide scale with variable thickness of chromium oxide (point 1). Ni rich splats are distributed between the inter splats boundaries in the light grey region at point 2 and 3. The dark grey region at point 4 and 5 depicts the presence of chromium rich element. However, at the interface between coating and substrate (point 6), there is a possibility of decarburization of the carbide particle might occur due to the presence of higher amount of oxygen at the black spot. Cr, Ni and Fe have diffused in to the coating from the substrate (point 7).

#### 4.3.3.6 X-ray mapping

The D-gun Cr<sub>3</sub>C<sub>2</sub>-NiCr coated superalloy samples after air oxidation for 100 cycles at 900 °C, were cut across the cross-sections and mounted in transoptic mounting resin, mirror-polished and silver pasted between samples and the stub in order to have conductivity, thereafter, gold coated to facilitate X-ray mapping by FE-SEM/EDS of the different elements present across the scale. FE-SEM/EDS, SE-X-ray mapping of air oxidised Cr<sub>3</sub>C<sub>2</sub>-NiCr coated superni 75 (Fig.4.21) shows very thin oxide scale mainly consisting of chromium in the top scale, in the sub scale region, Ni-rich splats are found mostly at places where Cr is depleted. Oxygen penetration is restricted to the top surface of the coating but its presence at the coating-substrate interface may be either due to the in-flight oxidation of coating material or oxygen might have penetrated during initial cycles of air oxidation run along the intersplat boundaries. The presence of Fe and Ti in the top scale indicates that they might have diffused from the substrate to the top layer of the coating. X-ray mappings for Cr<sub>3</sub>C<sub>2</sub>-NiCr coated superni 718 after 100 cycles of oxidation in air environment at 900 °C (Fig.4.22) indicates that only top surface of the coating has been oxidised (few microns). The oxide scales mainly consist of Cr<sub>2</sub>O<sub>3</sub>, which restrict the penetration of oxidizing species in to the coating. The presence of alumina at the coating-substrate interface

may be due to grit blasting of the substrate prior to the coating. Similarly, X-ray mapping of Cr<sub>3</sub>C<sub>2</sub>-NiCr coated superfer 800H after oxidation at 900 °C for 100 cycles is shown in Fig.4.23, which indicates that the coating has partially oxidized as evident from the oxygen distribution. Chromium is uniformly distributed in entire coating along the Ni rich splat boundaries, silicon has penetrated along the coating-substrate-interface, where as iron has restricted up to the coating-substrate-interface.

#### 4.3.4 Discussion

Weight gain data for D-gun Cr<sub>3</sub>C<sub>2</sub>-NiCr coated and bare superalloys obtained from the oxidation test are plotted in Fig.4.13 and 4.14. These plots clearly indicate that the Cr<sub>3</sub>C<sub>2</sub>-NiCr coated and bare superalloys follow a parabolic rate law up to 100 cycles, the values of parabolic rate constant K<sub>p</sub> ( 10<sup>-10</sup> g<sup>2</sup> cm<sup>-4</sup> s<sup>-1</sup>) were obtained from slope of the linear regression fitted line (Fig.4.14 ) and is given in Table 4.1. Initially the weight gain was higher during first few cycles thereafter, it has increased slowly. Weight gain for the Cr<sub>3</sub>C<sub>2</sub>-NiCr coated superalloys is less than the bare superalloys, which show the protective behaviour of the coating against air oxidation. The cumulative weight gain after 100 cycles of oxidation is plotted in Fig.4.15. The overall weight gain after 100 cycles of air oxidation for Cr<sub>3</sub>C<sub>2</sub>-NiCr coated superni75, superni718, and superfer 800H alloys are 1.53, 1.74, and 2.25 mg/cm<sup>2</sup> respectively. The overall weight gain of 2.44, 2.36, and 2.8 mg/cm<sup>2</sup> was observed for the superni 75, superni 718, and superfer 800H superalloys, respectively. It is found that a 37.3% saving in overall weight gain for Cr<sub>3</sub>C<sub>2</sub>- NiCr coated superni 75 in comparison with the bare superni 75, where as Cr<sub>3</sub>C<sub>2</sub>- NiCr coated superni 718, the weight gain is reduced by 26.3% with reference to bare superni 718. However, superfer 800H could manage only 19.6% saving in over all weight gain with respect to bare superfer 800H. Oxidation of the Cr<sub>3</sub>C<sub>2</sub> (orthorhombic crystal structure) phase leads to decarburisation and formation of Cr<sub>7</sub>C<sub>3</sub> (orthorhombic crystal structure) and Cr<sub>23</sub>C<sub>6</sub> (FCC)) as observed from the XRD analysis of Cr<sub>3</sub>C<sub>2</sub>-NiCr coated superalloys after air oxidation at 900 °C for 100 cycles (Fig.4.17). The carbides follow the stepwise reaction of Cr<sub>3</sub>C<sub>2</sub> with air, which undergoes successive decarburisation reactions to form Cr<sub>2</sub>O<sub>3</sub>, as described by equation (1) (Korablev et al 1988).



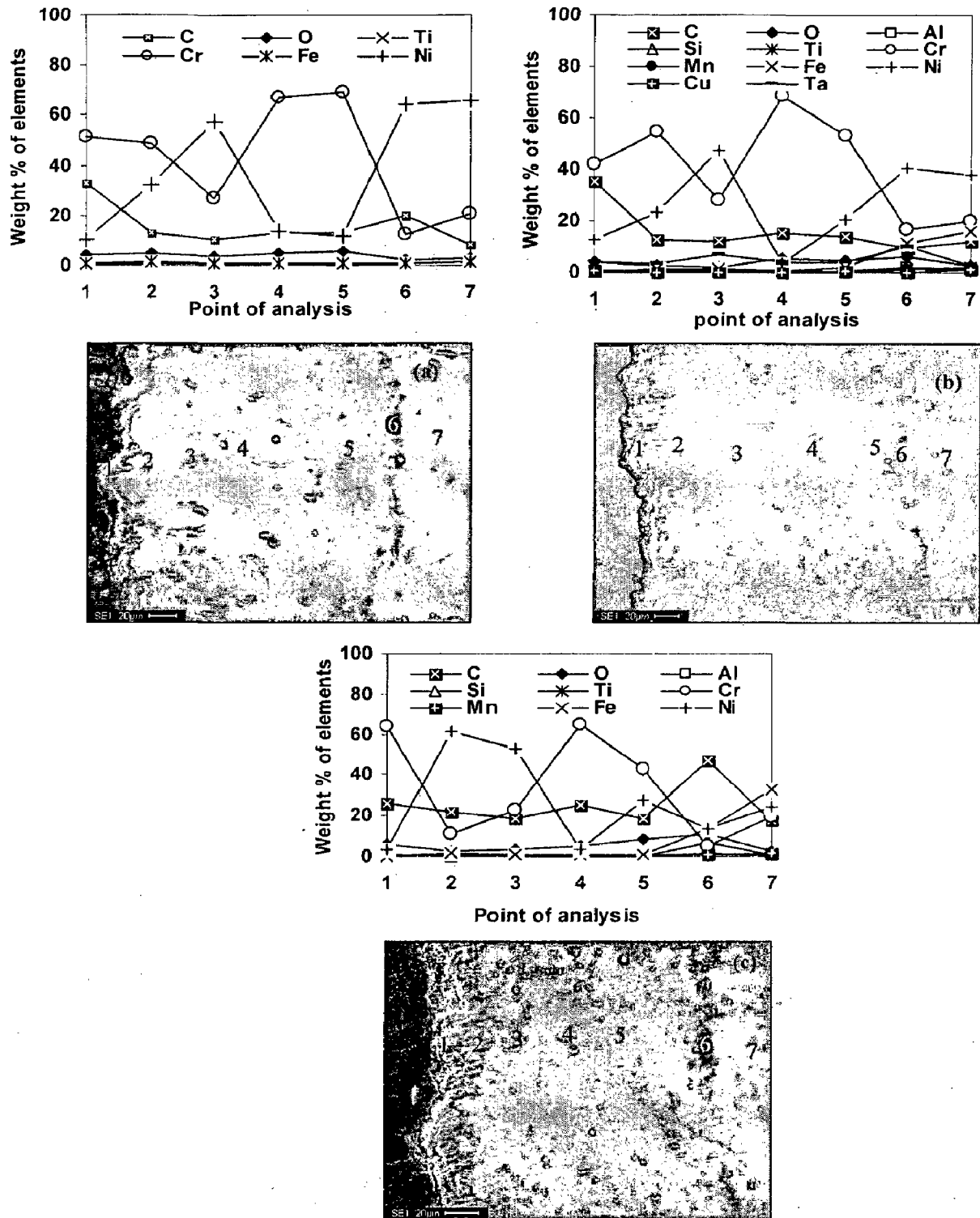


**Fig. 4.20** Morphology of oxide scale and variation of elemental composition across the cross-section of  $\text{Cr}_3\text{C}_2$ -NiCr-coated superalloys subjected to cyclic oxidation at  $900^\circ\text{C}$  in air after 100 cycles: (a) superalloy 75, (b) superalloy 718 and (c) superalloy 800H.

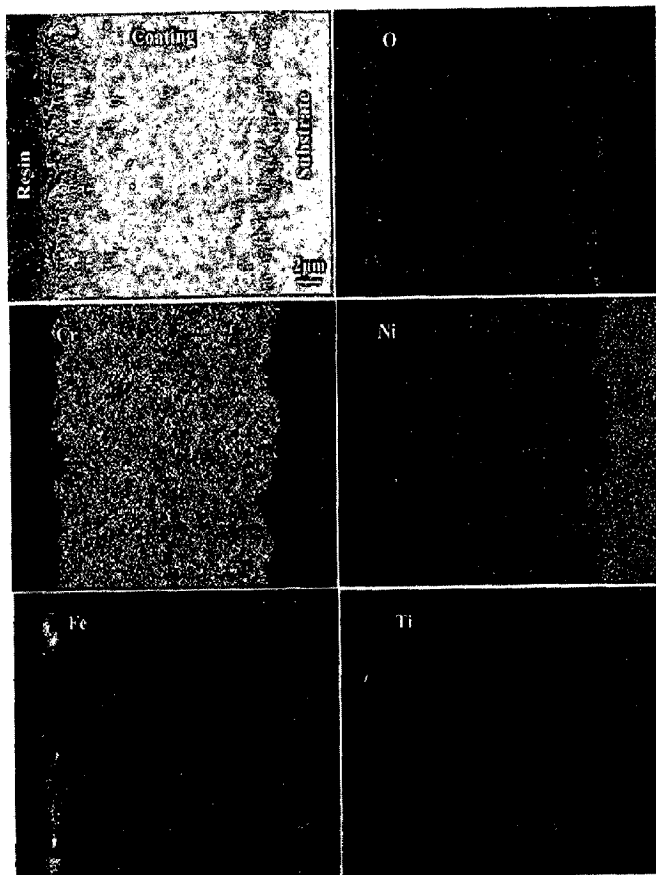


**Fig. 4.21** Composition image (SEI) and X-ray mapping of the cross-section of the  $\text{Cr}_3\text{C}_2$ -NiCr-coated superalloy superalloy superalloy 75 subjected to cyclic oxidation in air at  $900^\circ\text{C}$  after 100 cycles.

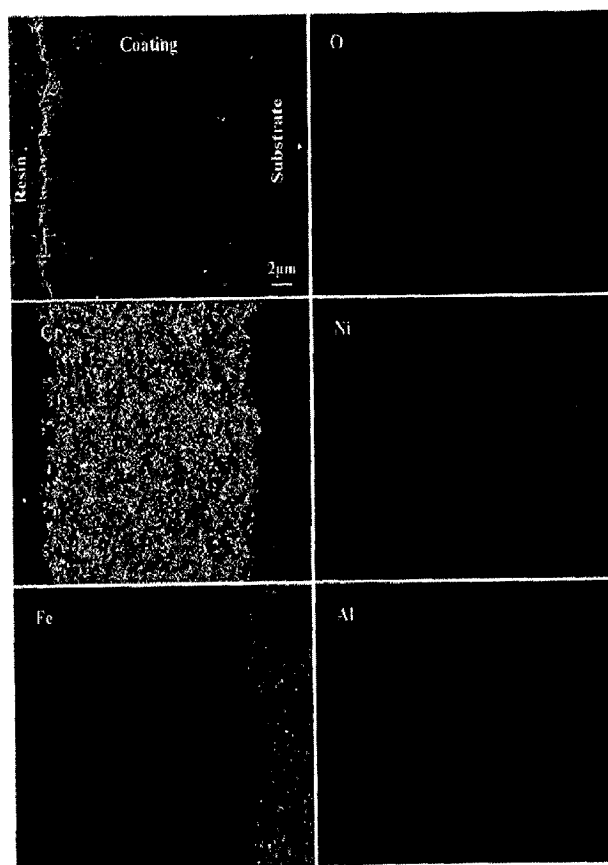


**Fig. 4.22** Composition image (SEI) and X-ray mapping of the cross-section of the  $\text{Cr}_7\text{C}_2$ -NiCr-coated superalloy superalloy 718 subjected to cyclic oxidation in air at  $900^\circ\text{C}$  after 100 cycles.

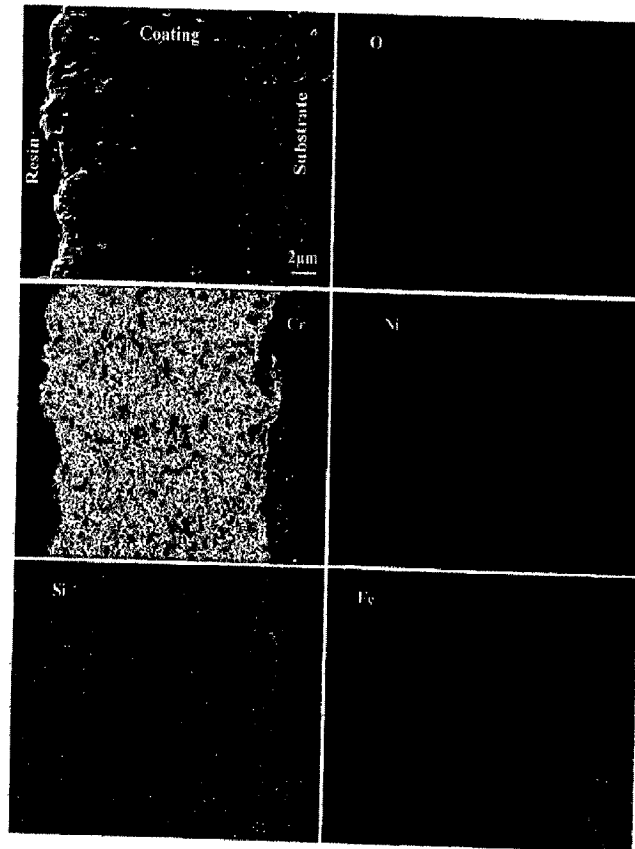
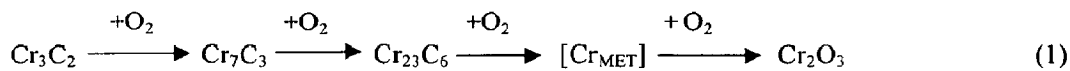


**Fig. 4.23** Composition image (BSEI) and X-ray mapping of the cross-section of the  $\text{Cr}_3\text{C}_2$ -NiCr coated superalloy superfer 800 subjected to cyclic oxidation in air at 900 °C after 100 cycles.



The carbides, namely  $\text{Cr}_7\text{C}_3$  and  $\text{Cr}_{23}\text{C}_6$  were found including  $\text{Cr}_3\text{C}_2$ , based on X-ray diffraction analysis as reported in the literature (Guilemany et al., 1994; Crawmer et al., 1992; Russo et al., 1995). Zimmermann and Kreye (1996) have concluded that the presence of  $\text{Cr}_7\text{C}_3$  and  $\text{Cr}_{23}\text{C}_6$  in the as-sprayed coating cannot be proven solely by X-ray diffraction approach, because their main diffraction peaks coincide with the lines referring to the NiCr and  $\text{Cr}_3\text{C}_2$ . The surface composition analysis of  $\text{Cr}_3\text{C}_2$ -NiCr coated superalloy 75 (Fig.4.18a) indicates 64.90%  $\text{Cr}_2\text{O}_3$  and 33.58% NiO (point 1) and 84.02%  $\text{Cr}_2\text{O}_3$  and 11.92% NiO (at point 2). The weak peaks of EDS spectrum account for 0.84% and 0.296% of  $\text{Fe}_2\text{O}_3$ , and 0.67%-1.10% of  $\text{TiO}_2$ . In case of oxidised coated superalloy 718 (Fig.4.18b), the variations of  $\text{Cr}_2\text{O}_3$  from 74.52% (at point 3) to 66.46% (at point 4), variations of NiO from 23.45% to 20.50% are observed. A very low percentage of other oxides presents on the surface are  $\text{Fe}_2\text{O}_3$ , MnO,  $\text{TiO}_2$ ,  $\text{SiO}_2$ ,  $\text{Al}_2\text{O}_3$ , CuO and TaO. In case of coated superalloy 800H, the amount of  $\text{Cr}_2\text{O}_3$  increase from 79.10% to 84.40%, where as NiO decrease from 14.87% to 10.78% (at point's 5 and 6 (Fig.4.18(c)). The small peaks of EDS spectrum indicates the formation of  $\text{Fe}_2\text{O}_3$ , MnO,  $\text{SiO}_2$  and  $\text{Al}_2\text{O}_3$  on the surface, which clearly reveals the diffusion of these elements from the superalloy substrate to the upper most part of the scale. The predominant phases (Fig.4.19 (a),(b) and (c)) formed on the surface of bare superalloys oxidised at 900 °C in air up to 100 cycles are NiO,  $\text{Cr}_2\text{O}_3$  and  $\text{Fe}_2\text{O}_3$  on superalloy 75 and superalloy 718 and  $\text{Fe}_2\text{O}_3$ , MnO and  $\text{Cr}_2\text{O}_3$  on superalloy 800H, respectively. EDS analysis of the scale of bare superalloy 75 (Fig.4.19a) indicates the presence of 73.89% NiO at point 1 and 93.93% NiO at point 2 as the main phases as indicated by strong peaks of EDS spectrum (Fig.4.19a at point 1 and 2). Fig.4.19 (b) at points 3 and 4 of bare superalloy 718 oxidised at 900 °C show an average of 57%  $\text{Cr}_2\text{O}_3$ , 10.85% NiO and 24%  $\text{Fe}_2\text{O}_3$ . The bare superalloy 800H (Fig.4.19c) show the formation of hemispherical shaped protrusion in entire oxidised surface along the scale grain boundaries. These protrusions mainly consist of  $\text{Fe}_2\text{O}_3$ , MnO and  $\text{Cr}_2\text{O}_3$ . The two different types of hemispherical protrusion are found one rich with formation of  $\text{Fe}_2\text{O}_3$  and  $\text{Cr}_2\text{O}_3$  in white region and other with  $\text{Cr}_2\text{O}_3$  (54.03%) and MnO (22.40%) formation in dark grey region (at point 6), which are clearly visible from the strong peaks of EDS spectrum at point 6 (Fig.4.19c). Further the matrix mainly consists of  $\text{Fe}_2\text{O}_3$  (62.16%) and  $\text{Cr}_2\text{O}_3$  (26.86%) which is evident from the strong peaks of EDS spectrum at point 5 (Fig.4.19c). Cross-sectional EDS analysis of

corroded  $\text{Cr}_3\text{C}_2\text{-NiCr}$  coated samples show that the oxygen has not penetrated in to the alloy substrate (Fig.4.20a, b and c). In case of all superalloys the variation in elemental composition after oxidation studies show the chromium rich elements are present in the uppermost part of coating. Where as nickel rich splats (white) and chromium are present along inter splat region (dark grey), Fe, and Ni have diffused from the substrate in to the coating. Cr has diffused from coating to substrate in case of superalloys 75 and 718 (Fig.4.20 (a) and (b), point 7). But in case of superalloy 800H, the EDS analysis of the corroded  $\text{Cr}_3\text{C}_2\text{-NiCr}$  coated superalloy 800H (Fig.4.20(c) at point 7) in the substrate show that the iron, nickel and chromium decrease from 43.83%, 32.00% and 21.00% in the original alloy to 33.17%, 24.63% and 18.95% respectively, therefore inter-diffusion indicates all the above elements (Fe, Ni and Cr) have diffused from the substrate to the coating. It has also been confirmed from the X-Ray mapping as shown in Fig.4.21, 4.22 and 4.23. The formation of thermodynamically stable chromium oxide scale and it's slow growth as shown in X-Ray mapping analysis (Fig.4.21, 4.22 and 4.23), might have acted as barrier to the inward diffusion of oxygen into the coating. Fe is clearly visible in top surface of the coating, which confirms the diffusion of this element from the substrate to the top coating surface, where as Ti in the coating is found along the intersplat region (Fig.4.21). It is believed that some alumina particles might be retained in the asperities during grit blasting of the substrate prior to deposition of the coatings and appeared at the coating-substrate interface as melted  $\text{Al}_2\text{O}_3$  (Fig.4.22). Si has moved up to the coating-substrate interface (Fig.4.23) and also diffused along the intersplat region of the coating. The life of  $\text{Cr}_3\text{C}_2\text{-NiCr}$  coating in oxygen containing atmosphere at high temperature is dependent upon the formation of a protective oxide scale,  $\text{Cr}_2\text{O}_3$ . The  $\text{Cr}_2\text{O}_3$  phase is thermodynamically stable up to very high temperatures due to its high melting points as well as it forms a dense, continuous and adherent layers that grow relatively slow (Stott, 1988). The scale of this type forms a solid diffusion barrier that inhibits interaction of oxygen with the underlying coating. The reaction rate is rapid initially as oxygen and the reacting elements in the coating are in direct contact. Once the scale grows and becomes continuous, diffusion of either species becomes increasingly difficult due to the growing diffusion barrier. As a result, the rate of mass gain due to oxygen uptake reduces with time. The growth of oxide scale typically displays a parabolic dependence with time and its longevity is dependent upon the concentration of the scale-forming element in the coating material, temperature, oxidising conditions, and alloy microstructure (Kofstad, 1998; Birks and Meier

1983). It may be mentioned based on the present investigation that  $\text{Cr}_3\text{C}_2\text{-NiCr}$  coating can provide a very good oxidation resistance at high temperature although it is traditionally specified for wear and erosion resistance applications. Based on the XRD, FE-SEM/EDS and X-ray mapping analysis, the following oxidation mechanism (Fig.4.24) for the  $\text{Cr}_3\text{C}_2\text{-NiCr}$  coated superalloy superni 75 at  $900^\circ\text{C}$  in air after 100 cycles is proposed.

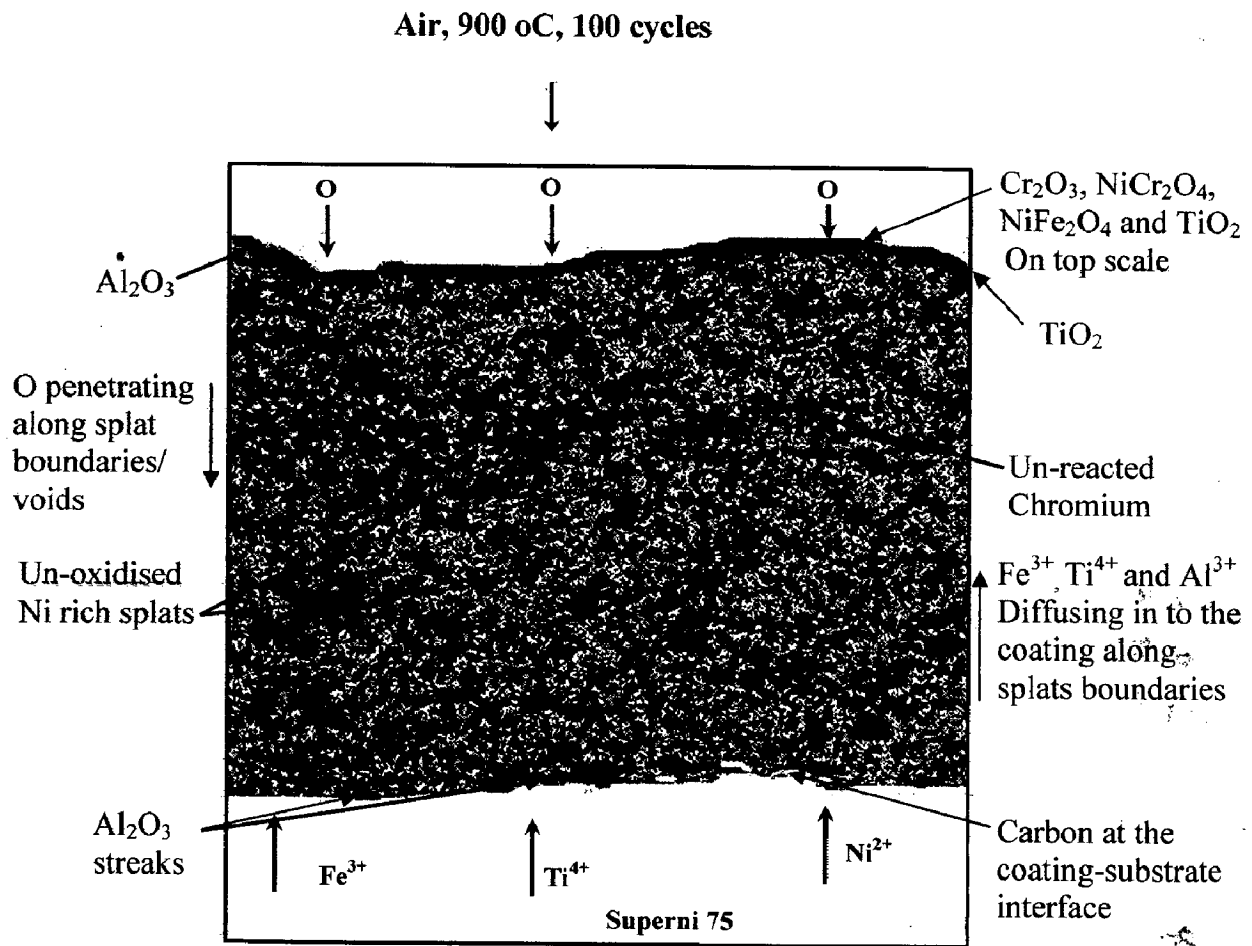


**Fig. 4.24** Schematic of the proposed oxidation mechanism of the  $\text{Cr}_3\text{C}_2\text{-NiCr}$  coated superalloy superni 75 at  $900^\circ\text{C}$  in air after 100 cycles.

### 4.3.5 Conclusions

$\text{Cr}_3\text{C}_2$ -NiCr coating on Ni and Fe based superalloy substrates has been uniformly deposited by D-gun spraying process in the present work and the following conclusions are made

- 1 The coating has shown uniform, adherent and dense structure with alternate layers of splat.
- 2 The D-gun sprayed  $\text{Cr}_3\text{C}_2$ -NiCr coatings on three different superalloys when subjected to cyclic oxidation in air at  $900^\circ\text{C}$  for 100 cycles were found to be successful in maintaining its adherence with the substrate superalloys. The oxide scales were also found to be intact and there is no indication of any spalling in all the cases.
- 3 The weight gain data for all the  $\text{Cr}_3\text{C}_2$ -NiCr coated superalloys indicated a less weight gain compared to bare superalloys. The oxidation behaviour of all  $\text{Cr}_3\text{C}_2$ -NiCr coated and bare superalloys followed a parabolic rate law.
- 4 A saving in overall cumulative weight gain for  $\text{Cr}_3\text{C}_2$ -NiCr coated superalloys 75, superalloy 718 and superalloy 800H with respect to the bare alloys are of the order of 37.3%, 26.3% and 19.6% respectively.
- 5 The  $\text{Cr}_3\text{C}_2$ -NiCr coating after exposure to air oxidation showed the presence of mainly oxides of Cr in the upper region of the scale. In the subscale region, the phases revealed were oxides of Cr and Ni, and their spinels, whereas Ni in the splats remained unoxidised and provided protection on the superalloys against high temperature oxidation, as confirmed from the EDS analysis of the oxidised specimens.



## 4.4 HOT CORROSION STUDIES

### 4.4.1 Na<sub>2</sub>SO<sub>4</sub>-60% V<sub>2</sub>O<sub>5</sub> MOLTEN SALT ENVIRONMENT-I

#### 4.4.1.1 Introduction

Degradation of components in hot sections of gas turbine, boilers, industrial waster incinerators are mainly due to the high temperature oxidation, hot corrosion and erosion. superalloys have been developed for high temperature applications, but they are not able to meet the requirements of both the high-temperature strength and the high- temperature erosion-corrosion resistance simultaneously. HVOF-sprayed Cr<sub>3</sub>C<sub>2</sub>-NiCr and WC-Co coatings are widely studied as regards their wear-resistance behaviour, but now there is an increasing interest being shown in their application for protection against high temperature corrosion (Sidhu et al., 2006). Thermal spray coatings, such as tungsten or chromium carbide coatings seem to be an alternative to chromium plating, mainly when good wear resistance is required (Erning and nestler, 1999; Sahraoui et al., 2004; Savarimuthu et al., 2000; Ko and Robertson, 2002). Cr<sub>3</sub>C<sub>2</sub>-NiCr coatings offer greater corrosion and oxidation resistance, also having a high melting point and maintaining high hardness, strength and wear resistance up to a maximum operating temperature of 900 °C (Beczowskiak et al., 1999; Liu, 1998; Staia et al., 2001B; Loubière et al., 1995). In addition to these features, the coefficient of thermal expansion of Cr<sub>3</sub>C<sub>2</sub>(10.3 x 10<sup>-6</sup>/°C) is nearly similar to that of iron (11.4 x 10<sup>-6</sup>/°C) and nickel (12.8 x 10<sup>-6</sup>/°C) that constitute the base of most high temperature superalloys. This minimizes stress generation through thermal expansion mismatch during thermal cycles. Hence, Cr<sub>3</sub>C<sub>2</sub> based coatings have been applied to a wide range of industrial components, including components used in steam and gas turbines (He et al., 2000; Sahoo, 1993; Takeuchi et al., 1993; Kim et al., 1998; Takeuchi, 1998; Wang et al., 2000; Taylor, 1975; Eroglu and Duran, 1997; Liu and Ding 2000). D-gun spray coating process is a thermal spray process, which gives an extremely good adhesive strength, low porosity and coating surfaces with compressive residual stresses (Rajasekaran et al., 2006). The porosity values of D-gun sprayed coatings are very much lower (< 0.8%) than that of HVOF sprayed Cr<sub>3</sub>C<sub>2</sub>-NiCr coating as reported in the literature (Wang and Lee, 1997, 2000; Wang and Shui, 2002; Wang, 1996; Hazoor et al., 2006). The residual fuel used in heat engines such as gas turbines, boilers, and refinery furnaces contains sodium, vanadium and sulphur as impurities. In the combustion system, Na and S react with each other and forms Na<sub>2</sub>SO<sub>4</sub> (melting point 884°C), V reacts with oxygen to form V<sub>2</sub>O<sub>5</sub> (melting point 670 °C) as well as complex vanadates (Reid,

1971; Luthra and Spacil 1982). These compounds commonly known as ash deposit on the surface of the materials and induce accelerated oxidation (hot corrosion) in energy generation systems. Vanadium compounds are good oxidation catalysts and allow oxygen and other gases in the combustion atmosphere to diffuse rapidly to the metal surface and cause further oxidation (Natesan, 1976). One of the most important problems in the petrochemical industry is the behaviour of materials in an aggressive environment with the presence of hydrogen sulphide, carbon dioxide and sand, which contribute to corrosion, erosion and wear of the surface (Scrivani et al., 2001). Thus, in order to improve the efficiency of a gas turbine engine significantly, the hot corrosion resistance of super alloys is as important as its high temperature strength (Misra, 1987; Kohl et al., 1979). Recent studies showed that the materials used for high temperature strength are highly susceptible to hot corrosion and the surface engineering plays a key role in effectively combating the hot corrosion problem (Gurrappa and Sambasiva Rao, 2006). There is no reported literature on hot corrosion behavior of D-gun spray deposited  $\text{Cr}_3\text{C}_2$ -NiCr coating on superalloy substrates. Therefore, the present work has been focused to study the influence of D-gun sprayed  $\text{Cr}_3\text{C}_2$ -NiCr coating on hot corrosion behaviour of Ni and Fe based superalloys. The kinetics of corrosion of D-gun sprayed  $\text{Cr}_3\text{C}_2$ -NiCr coating and bare superalloy substrates was investigated by measuring weight change of the samples. XRD, SEM and FE-SEM/EDS, and X-Ray mapping were used to characterize the corrosion products of the coated and bare samples in order to render an insight in to the corrosion mechanisms

#### **4.4.1.2 Experimental Details**

The substrate materials, coating formulation and the hot corrosion studies are explained in detail in section 3.1, 3.2.3 and 3.4.3.

#### **4.4.1.3 Results**

##### **4.4.1.3.1 Visual observations and Weight change measurements**

Fig.4.25 shows the macrographs for bare and coated superalloys after hot corrosion studies at 900 °C for 100 cycles in  $\text{Na}_2\text{SO}_4$ -60% $\text{V}_2\text{O}_5$  environment. The fragile porous corrosion products (NiO and  $\text{Cr}_2\text{O}_3$ ) were formed on surface of all the bare superalloys due to spalling/sputtering

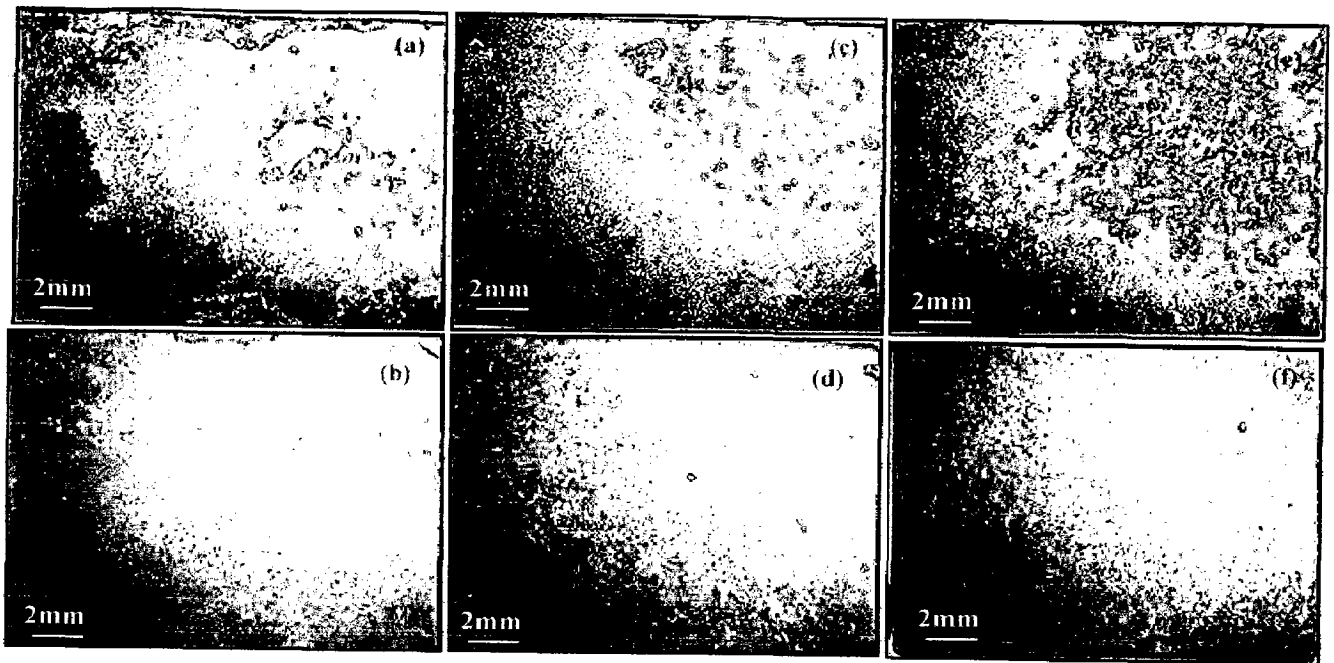


**Fig. 4.25** Surface macrograph of  $\text{Cr}_3\text{C}_2\text{-NiCr}$  coated and bare superalloys subjected to hot corrosion in  $\text{Na}_2\text{SO}_4\text{-60\%V}_2\text{O}_5$  environment at  $900^\circ\text{C}$  for 100 cycles. (a) Bare superalloy 718, (b) Coated superalloy 718, (c) Bare superalloy 75, (d) Coated superalloy 75, (e) Bare superalloy 800H and (f) Coated superalloy 800H

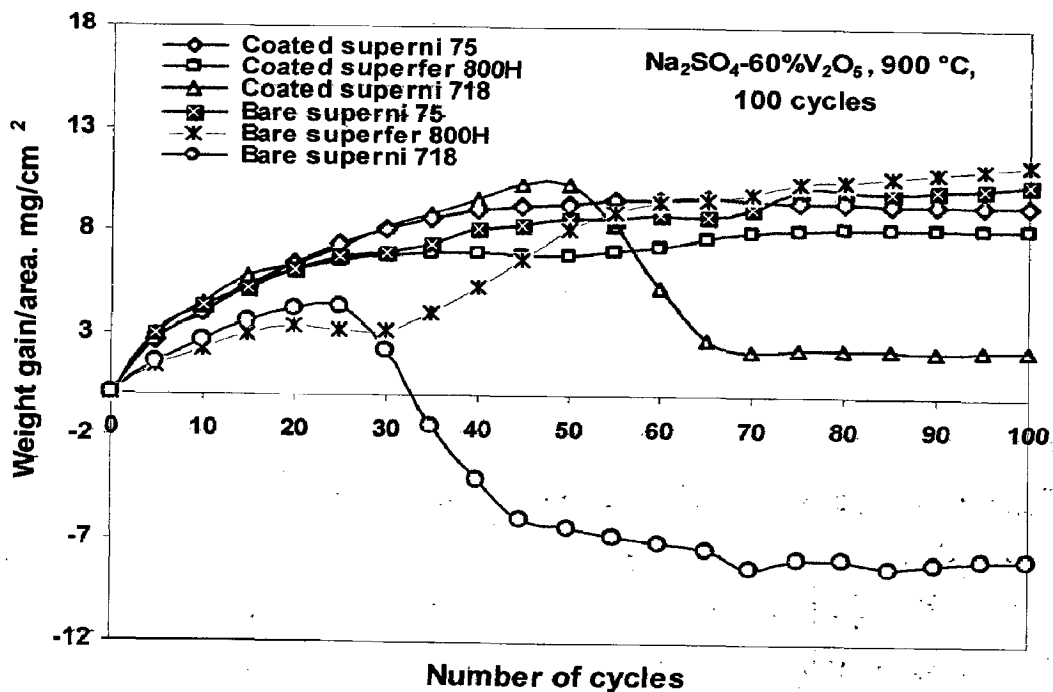


**Fig. 4.26** Weight gain/area vs. number of cycles plot for coated and bare superalloys subjected to cyclic oxidation for 100 cycles in  $\text{Na}_2\text{SO}_4\text{-60\%V}_2\text{O}_5$  at  $900^\circ\text{C}$

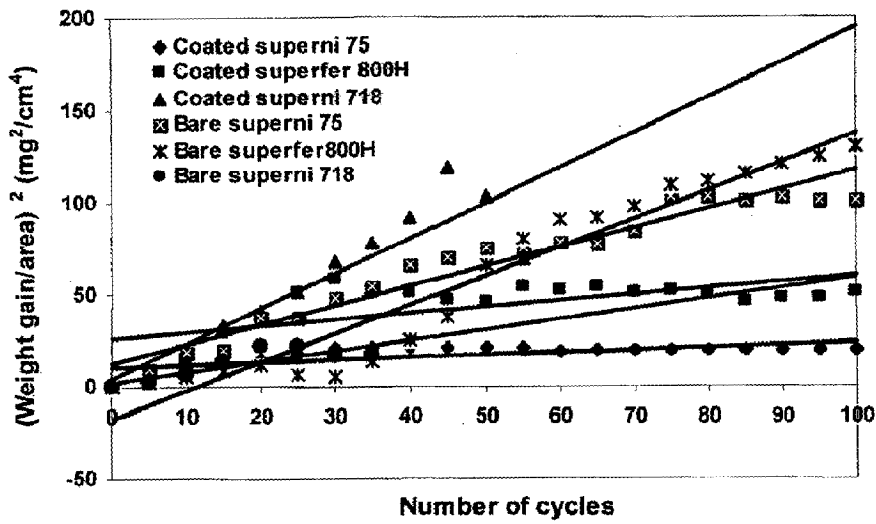


Fig. 4.27 (weight gain/area)² vs. number of cycles plot for coated and bare superalloys subjected to cyclic oxidation for 100 cycles in Na<sub>2</sub>SO<sub>4</sub>-60%V<sub>2</sub>O<sub>5</sub> at 900 °C

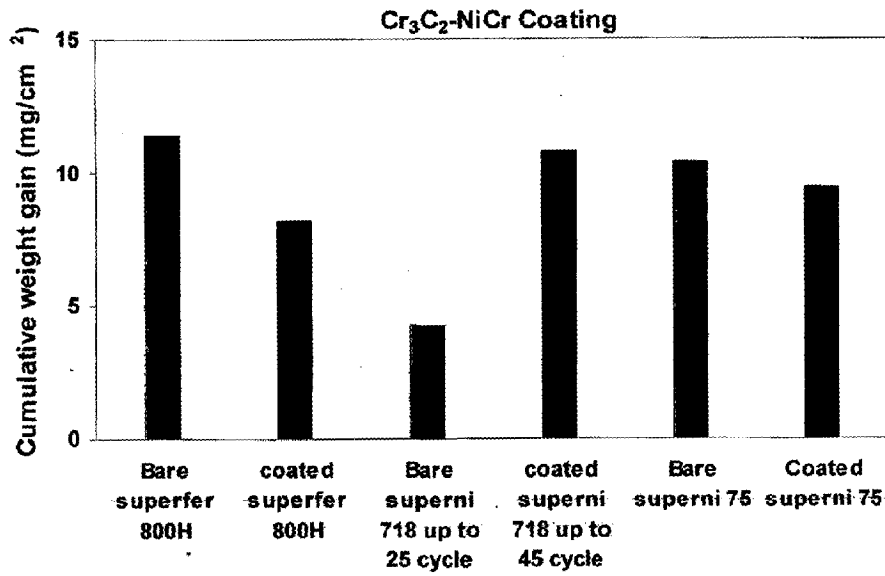


Fig. 4.28 Bar chart showing cumulative weight gain per unit area for coated and bare superalloys subjected to cyclic oxidation for 100 cycles in Na<sub>2</sub>SO<sub>4</sub>-60%V<sub>2</sub>O<sub>5</sub> at 900 °C

right from the initial few cycles which intensified with the progress of study with several corrosion products formed in the boat. The surface became rougher with progressive exposure of time with a uniform pitting observed throughout the surface of the samples. Bare superalloy 718 (Fig.4.25a) in molten salt environment has shown spalling/sputtering behavior from the 5<sup>th</sup> cycle, which intensified with some of the corrosion product started falling outside the boat which has continued up to 70<sup>th</sup> cycle. During initial cycles the colour of the scale was dark grey which turned in to brownish and little greenish with light grey patches around it. The colour of the scale of bare superalloy 75 and bare superalloy 800H (Fig.4.25 c and e) shows dark grey colour during initial few cycles, which subsequently turned to greenish streaks in the form of patches on grey background towards the end of the 100 cycles, which also show some spalled regions on the surface. Whereas Cr<sub>3</sub>C<sub>2</sub>-NiCr coated superalloys (Fig.4.25 b, d and f) show initially dark grey colour and later on it has changed to green colour on grey background. The intensity of green colour is more in case of superalloy 718 (Fig.4.25 b). The coated superalloy 718 and superalloy 800H (Fig.4.25b and f) showed a minor spallation at the edges and corners.

Fig.4.26 shows the weight gain/unit area for the bare and coated superalloys subjected to Na<sub>2</sub>SO<sub>4</sub>-60%V<sub>2</sub>O<sub>5</sub> salt mixture at 900 °C for 100 cycles. The bare superalloy superalloy 800H shows a higher weight gain as compared with coated one, whereas bare and Cr<sub>3</sub>C<sub>2</sub>-NiCr coated superalloy 718 superalloy has shown a parabolic behavior up to 25 and 45 cycles with some spalling/sputtering. In the subsequent cycles, corrosion products started falling outside the boat, there it becomes difficult to monitor actual weight gain. The sputtering continued up to 70 cycles for bare superalloy 718 and 65 cycles for coated superalloy 718, and after that it ceased. Subsequently negligible weight gain was noticed up to 100 cycles, as evident from the Fig.4.26. The weight gain data reveals that the Cr<sub>3</sub>C<sub>2</sub>-NiCr coatings are found to be more hot corrosion resistant than the bare superalloys. It is evident that Cr<sub>3</sub>C<sub>2</sub>-NiCr coated superalloys obey parabolic rate law and exhibit the tendency to act like diffusion barriers to the corroding species. The weight gain square (mg<sup>2</sup>/cm<sup>4</sup>) versus time (number of cycles) plots are shown in Fig.4.27 to establish the rate law for the hot corrosion. It is observed from the graph that all the coatings (except bare superalloy 800H) follow a nearly parabolic rate law. The parabolic rate constant K<sub>p</sub> was calculated by a linear least-square algorithm to a function in the form of  $(W/A)^2 = K_p t$ , where W/A is the weight gain per unit surface area (mg/cm<sup>2</sup>) and 't' indicates the number of cycles represents the time of exposure (Fig.4.27). The parabolic rate constants for bare and coated superalloy

calculated on the basis of 100 cycle data are reported in Table 4.2. Fig.4.28 shows the cumulative weight gain per unit area for coated and bare superalloys.

**Table 4.2** parabolic rate constant ( $K_p$ ) values for D-gun sprayed  $\text{Cr}_3\text{C}_2$ -NiCr-coated and bare superalloys subjected to cyclic oxidation for 100 cycles in  $\text{Na}_2\text{SO}_4$ -60% $\text{V}_2\text{O}_5$  at 900 °C

Description	$K_p$ ( $10^{-10} \text{ g}^2 \text{ cm}^{-4} \text{ s}^{-1}$ )	Oxidation cycles
Bare Superfer 800H	4.311	100
Bare Superni 75	2.93	100
Bare Superni 718	2.29	25
Coated Superfer 800H	1.645	100
Coated Superni 75	2.336	100
Coated Superni 718	6.874	45

#### 4.4.1.3.2 X-ray diffraction analysis (XRD) of scale

The XRD patterns for the corroded surfaces of bare and coated superalloys exposed to  $\text{Na}_2\text{SO}_4$ -60% $\text{V}_2\text{O}_5$  environment at 900 °C after 100 cycles are shown in the Fig.4.29 and 4.30, respectively. The main phases identified for corroded bare superni 75 are NiO,  $\text{TiO}_2$ ,  $\text{Cr}_2\text{O}_3$ ,  $\text{Ni}(\text{VO}_3)_2$ ,  $\text{V}_2\text{O}_4$ ,  $\text{NiFe}_2\text{O}_4$ , and  $\text{NiCr}_2\text{O}_4$ ; where as in the scale of bare superni 718, additional phase,  $\gamma$ - $\text{Fe}_2\text{O}_3$  except  $\text{V}_2\text{O}_4$  is observed. It is also evident from the diffraction patterns that the hot corroded bare superfer 800H has all the above phases except  $\text{V}_2\text{O}_4$ .

In the Fig.4.30, the hot corroded  $\text{Cr}_3\text{C}_2$ -NiCr coated superni 718 indicates the formation of phases like NiO,  $\text{Cr}_2\text{O}_3$ ,  $\text{NiCr}_2\text{O}_4$ ,  $\gamma$ - $\text{Fe}_2\text{O}_3$ ,  $\text{Cr}_{23}\text{C}_6$ ,  $\text{NiVO}_3$ , and  $\text{Ni}_3\text{S}_4$ . Similarly corroded coated superni 75 shows phases like NiO,  $\text{Cr}_2\text{O}_3$ ,  $\text{NiFe}_2\text{O}_4$ ,  $\text{NiCr}_2\text{O}_4$ ,  $\gamma$ - $\text{Fe}_2\text{O}_3$ ,  $\text{NiVO}_3$ , and  $\text{Ni}_2\text{FeVO}_6$  and hot corroded coated superfer 800H reveals the phases like NiO,  $\text{Cr}_2\text{O}_3$ ,  $\text{NiFe}_2\text{O}_4$ ,  $\text{NiCr}_2\text{O}_4$ ,  $\gamma$ - $\text{Fe}_2\text{O}_3$ ,  $\text{Ni}_3\text{S}_4$ , and  $\text{Ni}_2\text{FeVO}_6$ .

#### 4.4.1.3.3 FE-SEM/EDS analysis of the scale

##### 4.4.1.3.3.1 Surface morphology of the scale

FE-SEM/EDS micrographs with EDS spectrum of the coated and bare superalloy specimens showing surface morphology after cyclic hot corrosion in  $\text{Na}_2\text{SO}_4$ -60% $\text{V}_2\text{O}_5$  environment for 100 cycles at 900°C are shown in Fig.4.31 and Fig.4.32, respectively. The EDS analysis of hot corroded  $\text{Cr}_3\text{C}_2$ -NiCr coating scale shows the formation of  $\text{Cr}_2\text{O}_3$  and NiO

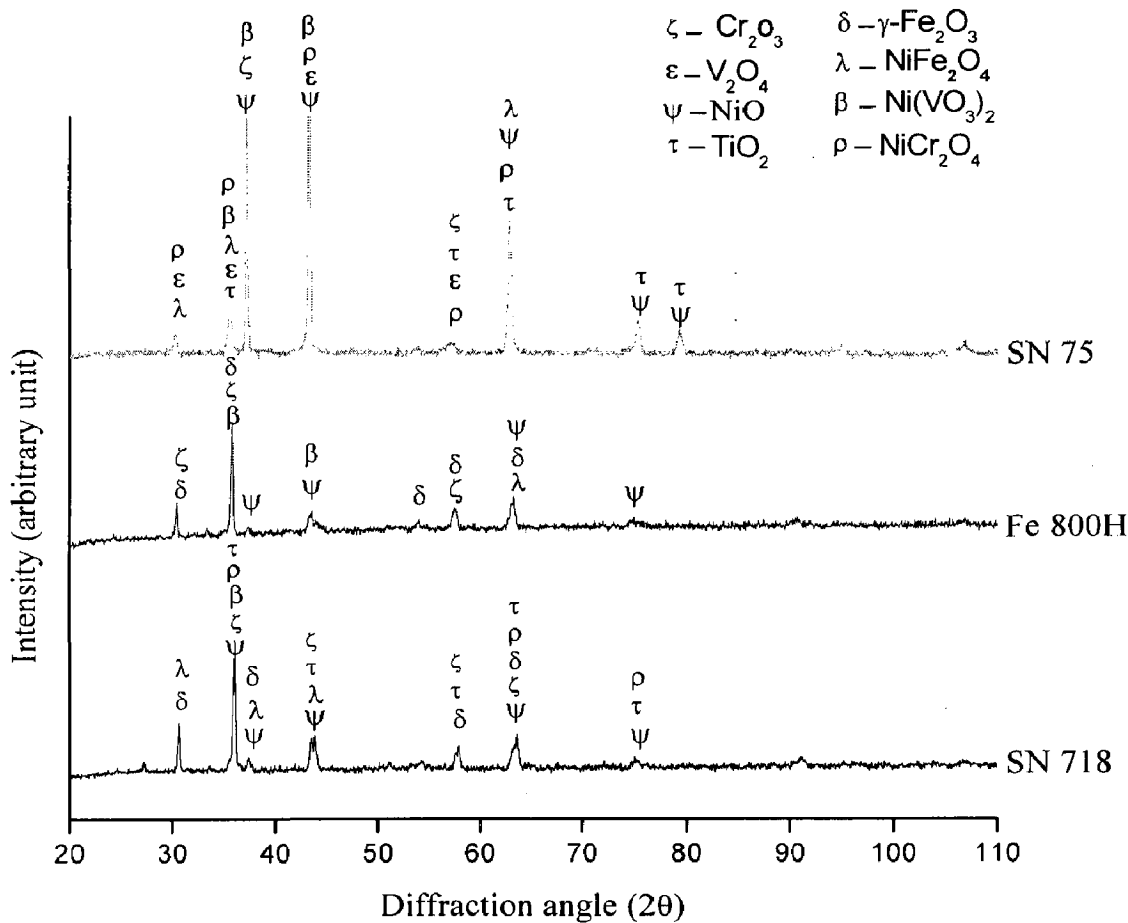


**Fig. 4.29** X-ray diffraction patterns for bare superalloys exposed to cyclic oxidation in  $\text{Na}_2\text{SO}_4\text{-60\%V}_2\text{O}_5$  at  $900^\circ\text{C}$  after 100 cycles.

as major phases on all the superalloys as shown in Fig. 4.31. Superni 75 shows 41%  $\text{Cr}_2\text{O}_3$  with 56% NiO at white region (Fig.4.31a point1) and 60%  $\text{Cr}_2\text{O}_3$  with 38% of NiO in grey region (Fig.4.31a point 2). Superfer 800H (Fig.4.31b) shows more protection by forming the desired protective oxide layer of 68.075%  $\text{Cr}_2\text{O}_3$  and 27.57% NiO at point 3 and 76%  $\text{Cr}_2\text{O}_3$  and 19.29%NiO in point 4, along with small quantities of  $\text{Fe}_2\text{O}_3$ , MnO,  $\text{SiO}_2$ ,  $\text{SO}_3$ ,  $\text{TiO}_2$  and  $\text{V}_2\text{O}_5$  as indicated by weak peaks of EDS spectrum (Fig.4.31b). The presence of these elements on the surface of hot corroded  $\text{Cr}_3\text{C}_2\text{-NiCr}$  coated superfer 800H indicates that these elements may have diffused from the substrate to the uppermost part of the scale during hot corrosion of the specimen at  $900^\circ\text{C}$ . Similarly, superni 718 shows an average of 56%  $\text{Cr}_2\text{O}_3$  with 34%NiO as major phases (Fig.4.31c). The surface micrographs of corroded bare superalloys indicate the

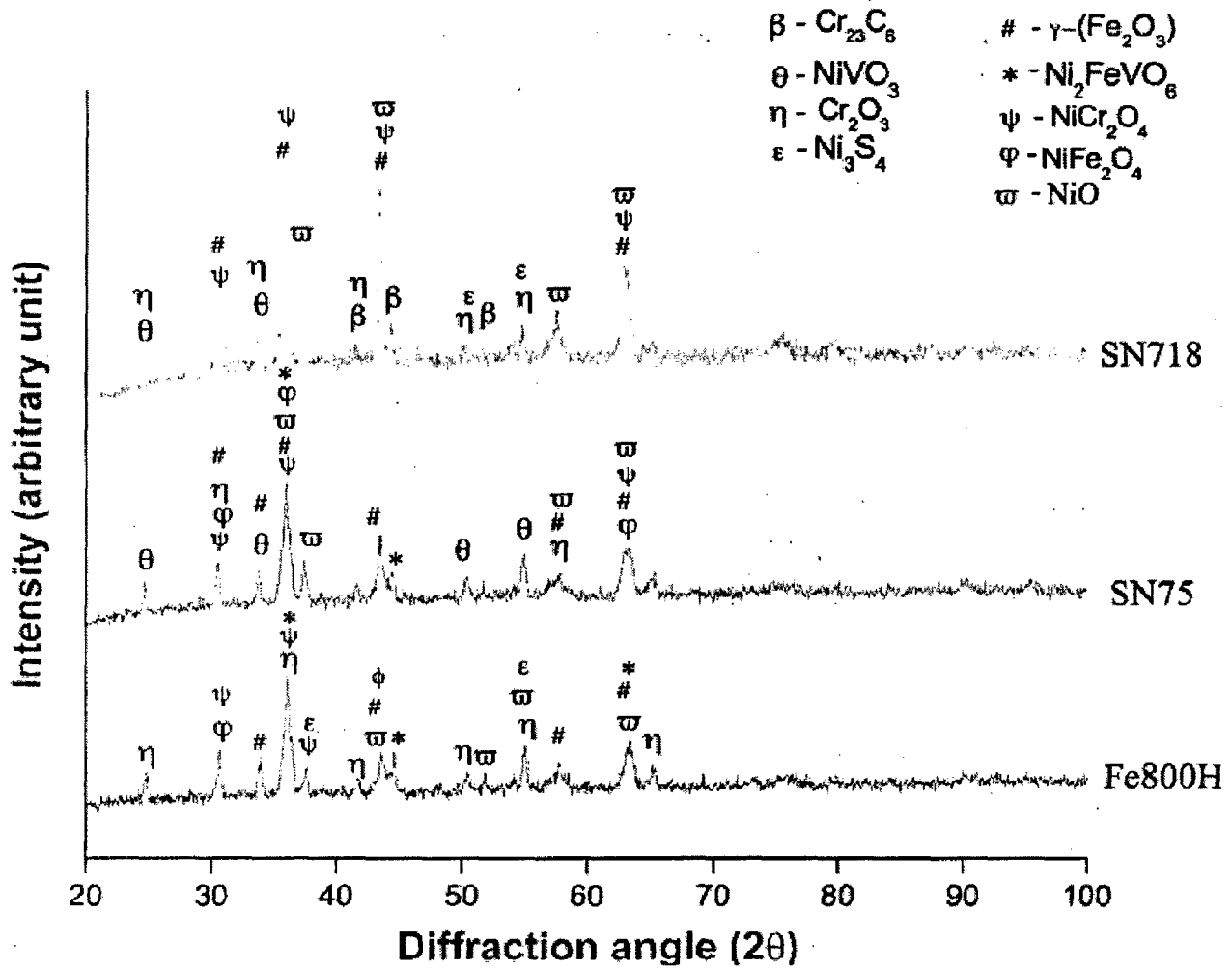


**Fig.4.30** X-ray diffraction patterns for  $\text{Cr}_2\text{C}_3$ -NiCr coated superalloys exposed to cyclic oxidation in  $\text{Na}_2\text{SO}_4$ -60% $\text{V}_2\text{O}_5$  at  $900^\circ\text{C}$  after 100 cycles

spalling behaviour of the scale as shown in Fig.4.32. The EDS analysis of the scale for the corroded bare superalloy 75 (Fig.4.32a) indicates the presence of white granules of 91.94% NiO at point 1 and 96.34% NiO at point 2 as the main phase. In the case of bare superalloy 800H (Fig.4.32b) substrate, the phases such as NiO,  $\text{Fe}_2\text{O}_3$  and  $\text{Cr}_2\text{O}_3$  appear as predominant phases, with small amounts of  $\text{V}_2\text{O}_5$ , MnO and  $\text{SiO}_2$ . It may be noticed that the percentage of  $\text{Cr}_2\text{O}_3$  has increased in the black area (point 3) of the scale. Also, bare superalloy 718 (Fig. 4.32c) shows NiO,  $\text{Cr}_2\text{O}_3$  and  $\text{Fe}_2\text{O}_3$  as principal phases along with very small percentage of MnO,  $\text{SiO}_2$ ,  $\text{SO}_3$ , and  $\text{V}_2\text{O}_5$  as indicated by EDS spectrum. The amount of  $\text{Cr}_2\text{O}_3$  varies from 16 % to 9% at point 5 and 6 respectively.



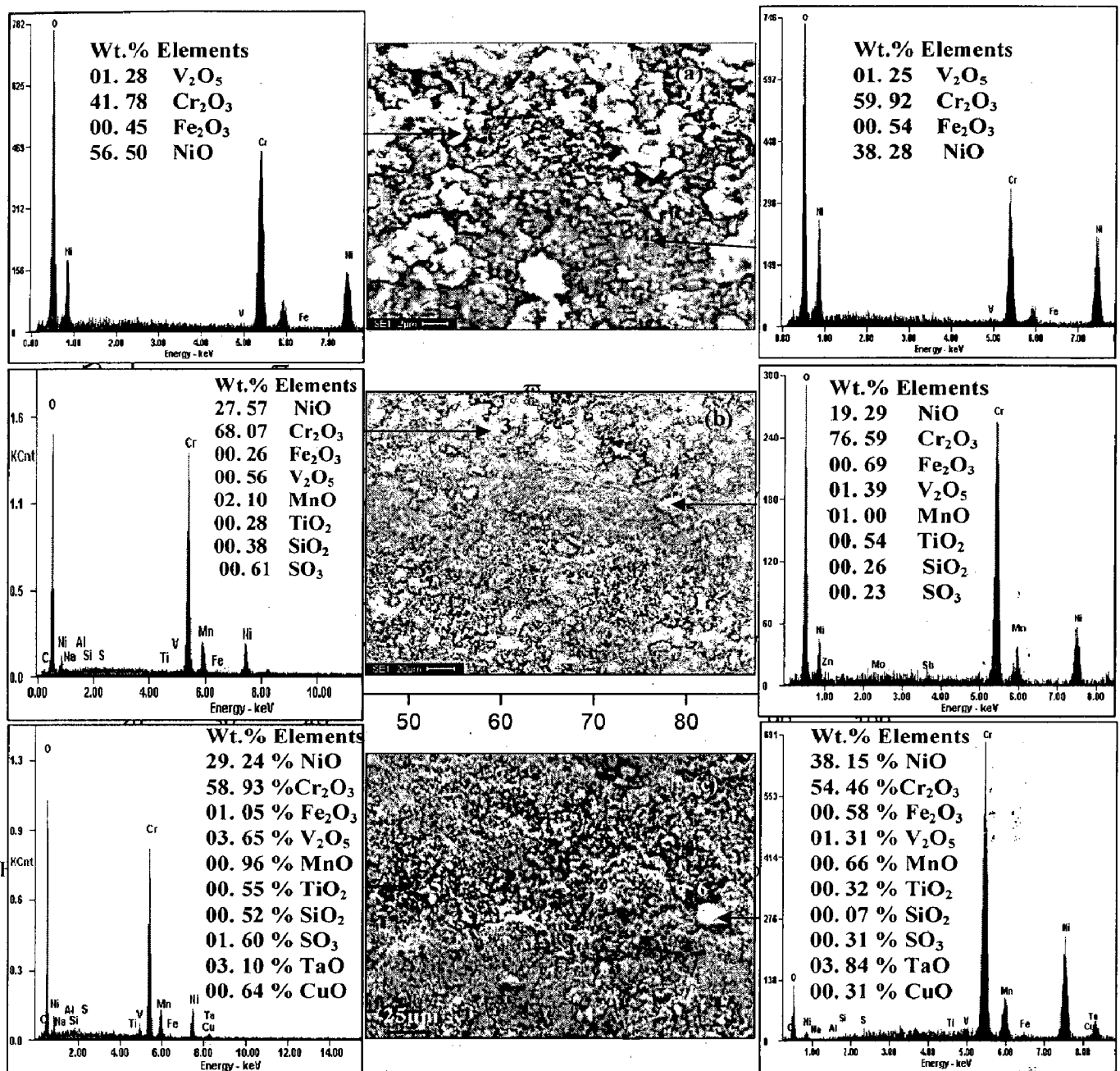


**Fig. 4.31** FE-SEM/EDS analysis along with EDS spectrum for Cr<sub>2</sub>C<sub>3</sub>-NiCr coated superalloys subjected to cyclic oxidation in Na<sub>2</sub>SO<sub>4</sub>-60%V<sub>2</sub>O<sub>5</sub> at 900 °C after 100 cycles (a) superni 75, (b) superfer 800H (c) superni 718

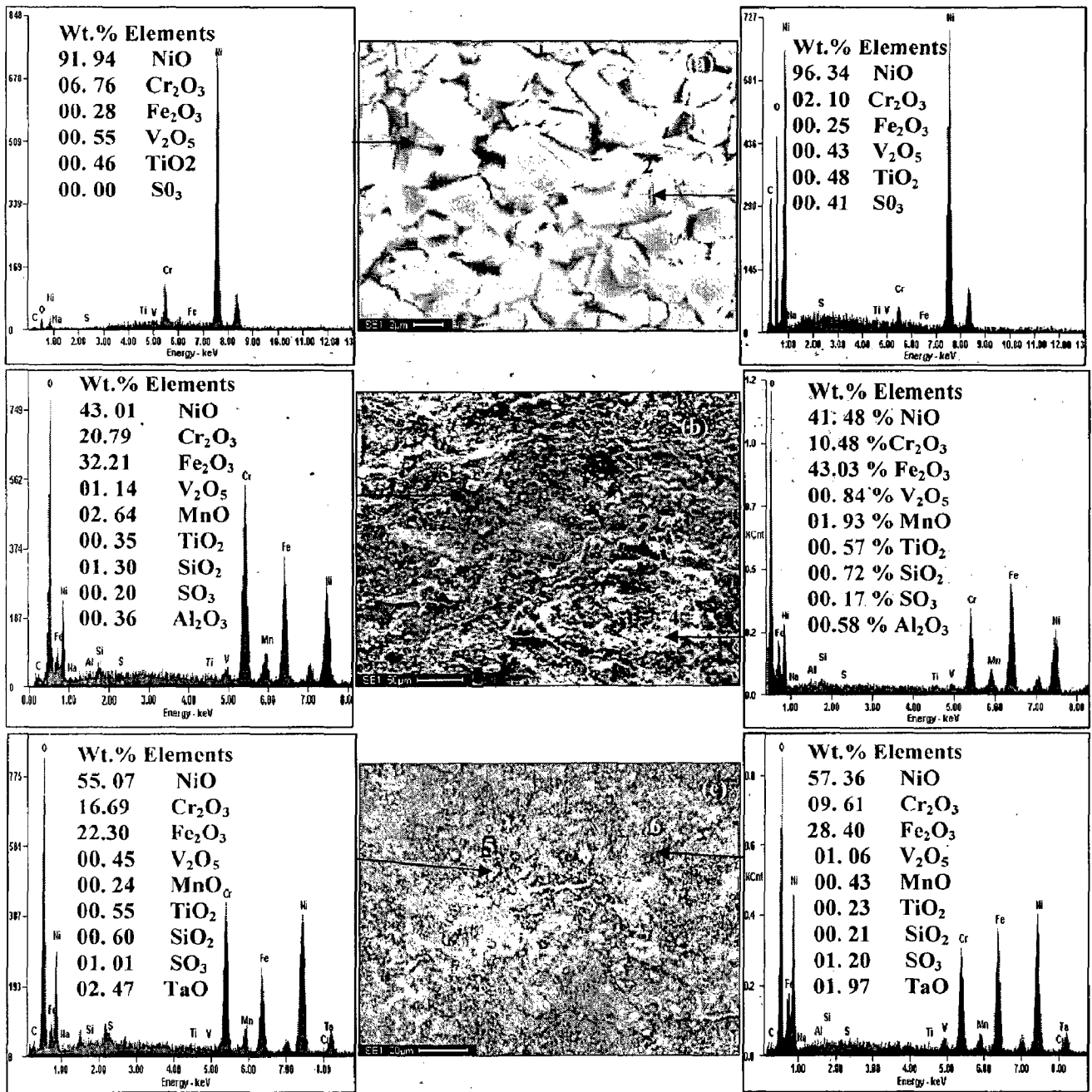


**Fig. 4.32** FE-SEM/EDS analysis along with EDS spectrum for the bare superalloys subjected to cyclic oxidation in Na<sub>2</sub>SO<sub>4</sub>-60%V<sub>2</sub>O<sub>5</sub> at 900 °C after 100 cycles: (a) superni 75 (b) superfer 800H, (c) superni 718.

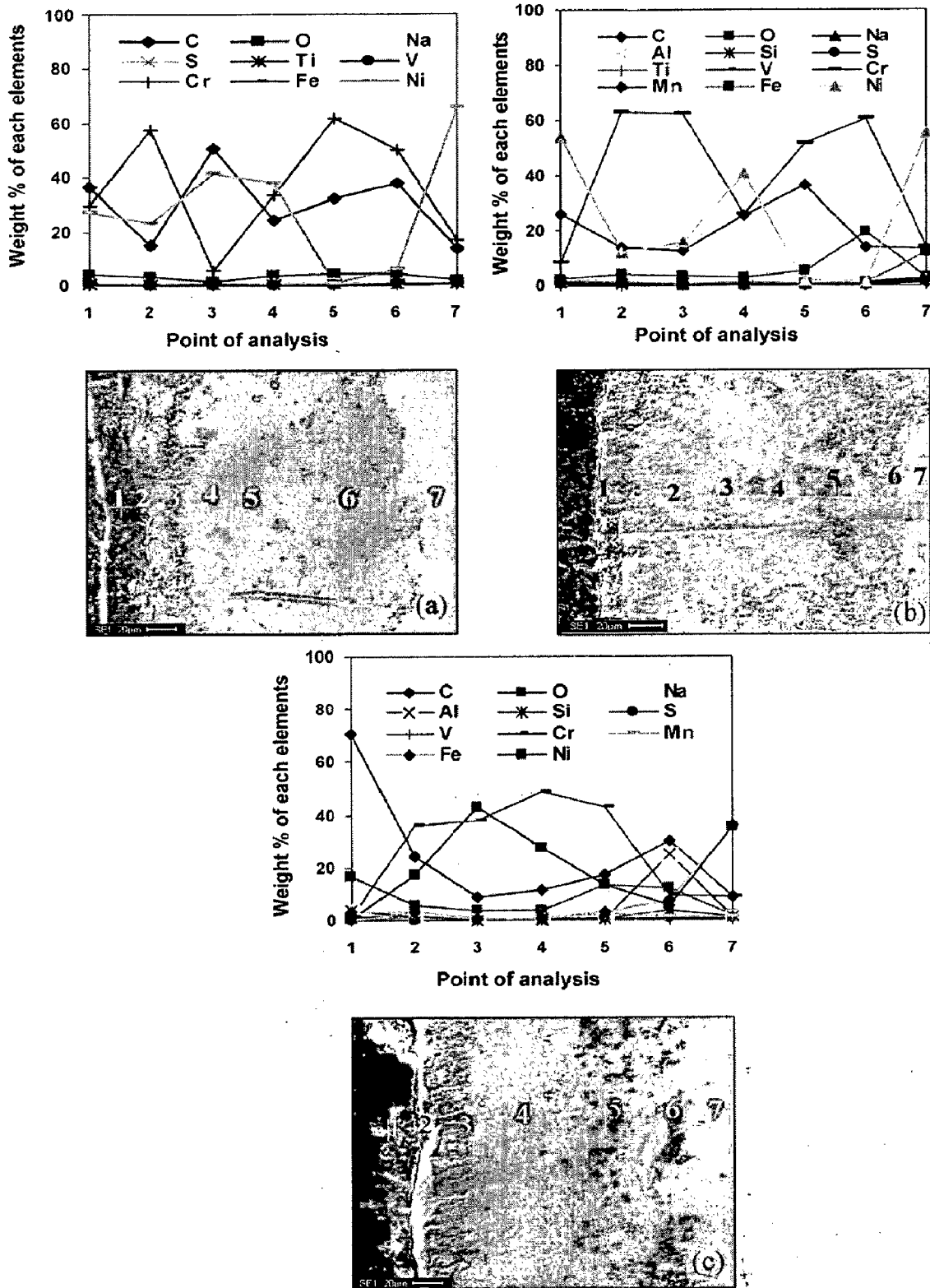


**Fig. 4.33** Oxide scale morphology and variation of elemental composition across the cross-section of  $\text{Cr}_3\text{C}_2\text{-NiCr}$  coated superalloys subjected to cyclic oxidation at  $900^\circ\text{C}$  in  $\text{Na}_2\text{SO}_4\text{-60\%V}_2\text{O}_5$  after 100 cycles (a) superni 75, (b) superni 718 and (c) superfer 800H.

#### **4.4.1.3.3.2 Cross-sectional analysis of the scale**

FE-SEM/EDS analysis was carried out at different points of interest along the cross-section of the hot corroded D-gun  $\text{Cr}_3\text{C}_2$ -NiCr coated superalloys, superalloy 75, superalloy 718 and superalloy 800H and the results are shown in Fig.4.33. A continuous and adherent oxide scale is formed on the coated super alloy, which has retained the dense structure of the as sprayed coatings even after the hot corrosion run for 100 cycles. There is no indication of any crack in the scale, also there is no diffusion of oxygen in to the substrate material in all the three coated superalloys, the presence of oxygen at the coating-substrate interface may be due to the in flight oxidation of coating or oxygen might have penetrated during initial cycles of hot corrosion run along the intersplat boundaries. It is believed that some alumina particles might be retained in the asperities during grit blasting of the substrate prior to deposition of the coatings and appeared at the coating - substrate interface as melted alumina oxides. EDS analysis of corroded  $\text{Cr}_3\text{C}_2$ -NiCr coated superalloy 75 (Fig.4.33a) shows the top surface of the scale (point 1) contains mainly oxides of Cr and Ni, with subsequent splats boundaries shows a layer rich with Cr - 57.66 wt. % (point 2) and Ni - 23.02 wt % and the second layer with Ni - 41.33 wt.% (point 3) and chromium 5.73 wt %. Further, at points 4, 5 and 6, chromium starts increasing with the reducing trend of Ni. Superalloy 718 (Fig.4.33b) shows that the top surface of the coating mostly has a homogeneous, adherent and non-uniform oxide scale with variable thickness of nickel oxide (point 1) scale is formed. At point 2, 3 and 5 Cr rich splats are formed but at point 4, Ni rich splats are observed, presence of 19.55 wt.% oxygen at coating-substrate interface (point 6) indicates a thick band of  $\text{Cr}_2\text{O}_3$ . Cross sectional EDS analysis of superalloy 800H (Fig.4.33c) also shows that the  $\text{Cr}_3\text{C}_2$ -NiCr coating provided the necessary protection against the hot corrosion by forming a  $\text{Cr}_2\text{O}_3$  (at points 2 and 4) scale on the uppermost part of coating and NiO in the subscale region (point 3). The presence of oxygen at points 5 and 6 may be due to the in flight oxidation of coating, which leads to the formation of  $\text{Cr}_2\text{O}_3$ .

#### **4.4.1.3.4 X-ray mapping**

The hot corroded samples were cut across the cross-sections and mounted in transoptic mounting resin, mirror-polished and gold coated to facilitate X-ray mapping by FE-SEM/EDS of the different elements present across the scale. X-ray mapping analyses of the scale formed on  $\text{Cr}_3\text{C}_2$ -NiCr D-gun coated superalloy 75, superalloy 718, and superalloy 800H superalloy after hot

corrosion in  $\text{Na}_2\text{SO}_4$ -60% $\text{V}_2\text{O}_5$  environment at  $900^\circ\text{C}$  for 100 cycles are shown in Fig.4.34-4.36. In all these superalloys, V is found in the entire scale mainly at splat boundaries showing its penetrating nature into the scale. Its penetration is restricted mainly to the upper most part of the scale. Si (except for superni 75) and Fe elements of the substrate superalloy, in general, show their diffusion behaviour from the substrate to the top scale. SEI X-ray mapping of hot corroded  $\text{Cr}_3\text{C}_2$ -NiCr coated superni 75 superalloy shows that the oxide scale exhibits dense structure and mainly consists of Cr in which Ni rich splats is present (Fig.4.34). These Ni-rich splats are present mostly at places where Cr is depleted. A meager amount of iron has diffused from the substrate to the top layer of the coating. Unreacted vanadium is present at the top of the oxide scale, presence of oxygen at the coating-substrate interface indicating the formation of  $\text{Cr}_2\text{O}_3$  band just above the interface between substrate and coating. X-ray mappings for  $\text{Cr}_3\text{C}_2$ -NiCr coated superalloy superni 718 after 100 cycles of hot corrosion in an environment of  $\text{Na}_2\text{SO}_4$ -60% $\text{V}_2\text{O}_5$  at  $900^\circ\text{C}$  (Fig.4.35) indicate the formation of relatively dense scale of  $\text{Cr}_2\text{O}_3$ , NiO and  $\text{NiCr}_2\text{O}_4$ . The upper most part of the scale is primarily shows some traces of Si and Fe, which might have diffused from substrate to the scale; Si is also present along the splat boundaries of coating-substrate interface. Ni-rich splats are present in the entire partially oxidised coating along with Cr present at the intersplat boundaries. Fig.4.36 shows the X-ray mapping of the oxide scale formed on the  $\text{Cr}_3\text{C}_2$ -NiCr coated superfer 800H superalloy. It reveals that the scale mainly consist of Cr in the upper most part of the scale, presence of oxygen in the top scale shows the formation of  $\text{Cr}_2\text{O}_3$  band with NiO layer in the subscale region where Cr is depleted. V, Si, Fe, and Si are found along the splat boundaries, meager amount of S is penetrated in to the substrate also. Some amounts of Fe and Si have diffused from the substrate into the top scale.

#### 4.4.1.4 Discussion

Surface macrograph of bare and coated superalloys (Fig.4.25) after hot corrosion run for 100 cycles in  $\text{Na}_2\text{SO}_4$ -60% $\text{V}_2\text{O}_5$  environment clearly indicates the formation of brownish with light greenish grey patches around it on bare superni 718 and greenish streaks in the form of patches on grey background on bare superni 75 and bare superfer 800H. In case of all coated superalloys, it shows the formation of green colour on grey back ground which represents the formation of oxide of chromium and nickel. The weight gain curves for D-gun sprayed  $\text{Cr}_3\text{C}_2$ -NiCr coated and bare superalloys followed nearly a parabolic behaviour (Fig.4.26). A small deviation from the

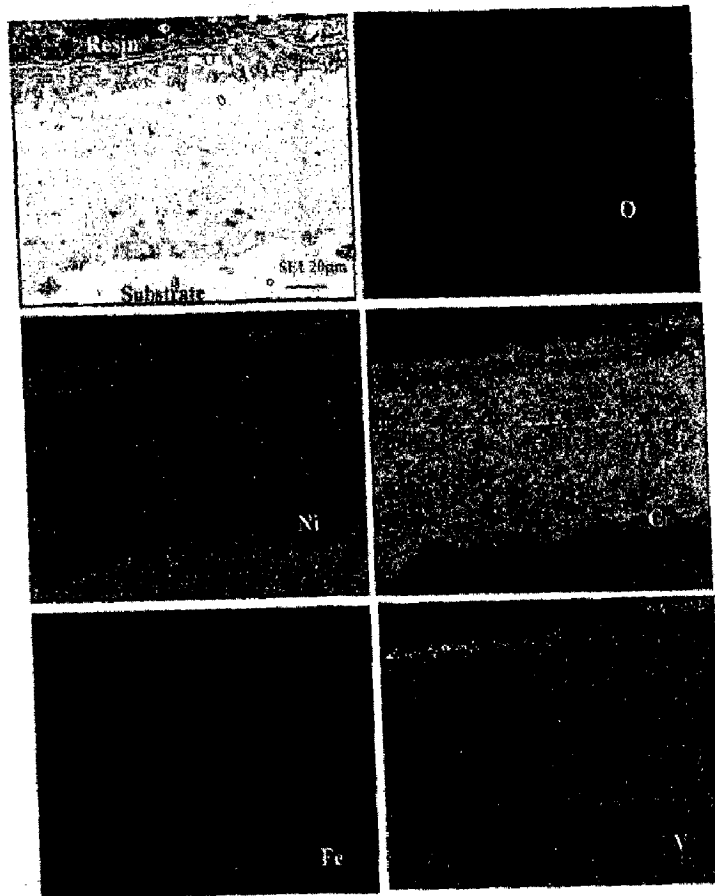


**Fig. 4.34** Composition image (SE) and X-ray mapping of the cross-section of the  $\text{Cr}_3\text{C}_2$ -NiCr-coated superalloy superalloy superalloy 75 subjected to cyclic oxidation at  $900^\circ\text{C}$  in  $\text{Na}_2\text{SO}_4$ -60% $\text{V}_2\text{O}_5$  after 100 cycles.

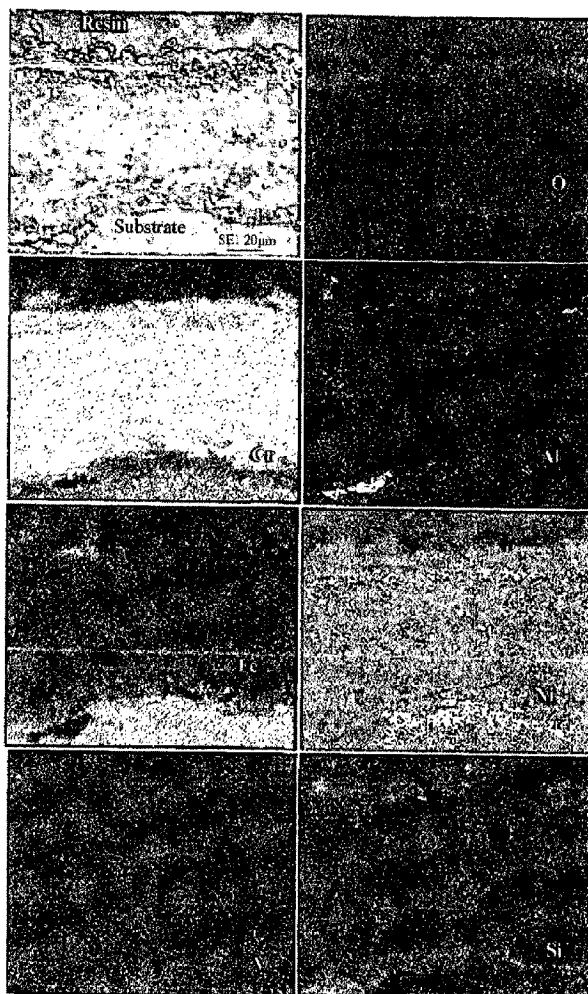


**Fig. 4.35** Composition image (SE) and X-ray mapping of the cross-section of the  $\text{Cr}_3\text{C}_2$ -NiCr coated superalloy superalloy superalloy 718 subjected to cyclic oxidation at  $900^\circ\text{C}$  in  $\text{Na}_2\text{SO}_4$ -60% $\text{V}_2\text{O}_5$  after 100 cycles.

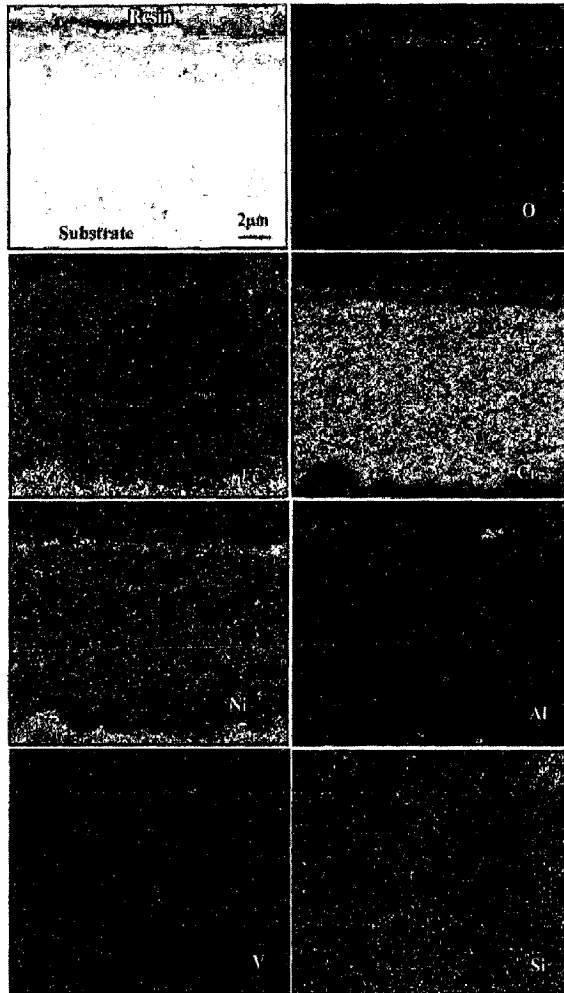


**Fig. 4.36** Composition image (SE) and X-ray mapping of the cross-section of the  $\text{Cr}_3\text{C}_2$ -NiCr coated superalloy superfer 800H subjected to cyclic oxidation at 900 °C in  $\text{Na}_2\text{SO}_4$ -60% $\text{V}_2\text{O}_5$  after 100 cycles



parabolic rate law might be due to cyclic scale growth. The higher weight gain of the specimens during the first few cycles might be due to the rapid formation of oxides at the splat boundaries and within the open pores due to the penetration of the oxidizing species, further the subsequent increase in weight is gradual. Parabolic rate constant for the bare superalloy is found to be greater than the coated superalloy. The parabolic rate constant ( $k_p$  in  $10^{-10} \text{ g}^2 \text{ cm}^{-4} \text{ s}^{-1}$ ) were obtained from the slope of the linear regression fitted line  $(\text{cumulative weight gain} / \text{area})^2$  versus number of cycles (Table 4.2). The nature of fit, parabolic rate law, for hot corrosion experiments are shown in Fig.4.27. The  $\text{Cr}_3\text{C}_2$ -NiCr coated superfer 800H (Fig.4.28) superalloy has shown minimum weight gain, where as coated superfer 75 revealed a higher weight gain which is 12% more than coated superfer 800H.  $\text{Cr}_3\text{C}_2$ -NiCr coating has been found successful in reducing the overall weight gain of superfer 800H by 28% with reference to bare superfer 800H. Where as coated superfer 75 has reduced the overall weight gain by 10% compared to bare superfer 75 (Fig.4.28). Fig.4.29 shows the XRD-analysis of bare superalloy which indicates the formation of NiO,  $\text{Cr}_2\text{O}_3$  and  $\text{Fe}_2\text{O}_3$  as major phases. Oxide scale of corroded  $\text{Cr}_3\text{C}_2$ -NiCr coating indicates the formation of NiO,  $\text{Cr}_2\text{O}_3$  and  $\text{NiCr}_2\text{O}_4$  as major phases on all the superalloys as revealed by XRD-analysis (Fig.4.30). The presence of minor phase such as  $\text{Fe}_2\text{O}_3$  on the surface of hot corroded  $\text{Cr}_3\text{C}_2$ -NiCr indicates the diffusion of Fe from the substrate during hot corrosion of the specimens at temperature about  $900^\circ\text{C}$ . FE-SEM/EDS analysis of corroded  $\text{Cr}_3\text{C}_2$ -NiCr coated superfer 75 shows the two regions, one white rich in nickel oxide(56%) and other grey rich in chromium oxide(60%), as shown in the EDS spectrum (point 1 and 2 of Fig.4.31a). Coated superfer 800H and superfer 718 show (Fig.4.31 b and c) the presence  $\text{Fe}_2\text{O}_3$ , MnO and  $\text{TiO}_2$  on the top surface of the coating which indicates the diffusion of these elements from the substrate to the top scale, as indicated by weak peaks of EDS spectrum at point 3 and 4 of Fig.4.31b. The points 5 and 6 of Fig.4.31c indicate TaO,  $\text{Fe}_2\text{O}_3$ , MnO and  $\text{TiO}_2$ . All three corroded bare superalloys show oxide scales of three different chemical composition on the surface, namely superalloy superfer 75 (Fig.4.32a) shows NiO (96%) in the form of fine irregular shaped crystals as a predominant phase, but superalloy superfer 800H and superfer 718 (Fig.4.32 b and c) show a massive scale with NiO,  $\text{Cr}_2\text{O}_3$  and  $\text{Fe}_2\text{O}_3$  as major phases with differing percentages.

Cross sectional EDS analysis of hot corroded  $\text{Cr}_3\text{C}_2$ -NiCr coated superalloys (Fig.4.33a, b and c) clearly show the inter diffusion of coating and substrate alloy elements. In case of superfer 75 (Fig.4.33(a) at point 7), which lies in the substrate, it can be inferred that the percentage of nickel

decreases from 77.1% in the original alloy to 65.47%, where as chromium decrease from 19.5% to 16.38%, which clearly indicates that Ni and Cr have diffused from substrate to the coating. The EDS analysis of the corroded Cr<sub>3</sub>C<sub>2</sub>-NiCr coated superalloy 718 Fig.4.33 (b) at point 7 in the substrate shows that the nickel increases from 52.37% in the original alloy to 55.07%, and iron decreases from 18.5% to 12.38%, where as chromium decreases from 19% to 14.22%. It is evident that inter diffusion causes iron and chromium move from substrate to the coating where as nickel diffuse from coating to the substrate. Similarly superalloy 800H (Fig.4.33(c) at point 7) in the substrate shows that the iron decreases from 43.8% in the original alloy to 35.78% and chromium decreases from 21% to 8.95%, where as nickel increases from 32% to 35.42%, this also clearly indicates that iron and chromium diffused from substrate to coating where as nickel diffused from coating to substrate.

During hot corrosion studies, initially the corroding species reacts with the top surface of the coating and starts migrating through the inter splat interface and diffusion of elements of substrate for example iron moves upward along this inter splat space at the coating-substrate interface, as the oxidation proceeds elements basically chromium get oxidised and forms a continuous Cr<sub>2</sub>O<sub>3</sub> layer below the top oxide layer. Oxygen and chromium are found along the splat boundaries as revealed by X-ray mapping (Fig.4.34, 4.35 and 4.36), thereby suggesting the formation of Cr<sub>2</sub>O<sub>3</sub>. The continuous band of Cr<sub>2</sub>O<sub>3</sub> in the subscale and Cr<sub>2</sub>O<sub>3</sub> along the splat boundaries will not allow any further transport of the oxidising species and the metallic ions. The presence of these elements at the coating surface will decrease oxygen availability in the underlying alloy and favors the formation of most thermodynamically stable oxide i.e. Cr<sub>2</sub>O<sub>3</sub>. With the passage of time, coating get partially oxidised along the splat boundaries due to which the further oxidation become negligible. This partially oxidised coating provides protection to the substrate. Cr<sub>2</sub>O<sub>3</sub> and NiO nuclei at the coating surface react to form NiCr<sub>2</sub>O<sub>4</sub> spinel, as it is evident from XRD analysis (Fig.4.30). So, the reaction is confined mainly to the top of the coating. Some minor spalling of the oxide scale of coated superalloys especially on the edges and corners (Wang et al., 2004) during cooling periods of the thermal cycles may be due to different values of thermal expansion coefficients of the coatings, substrate and oxides (Niranatlumpong, et al., 2000; Evans, et al., 2001; Sidhu et al., 2005A ). Based on the XRD, FE-SEM/EDS and X-ray mapping analysis, the following oxidation mechanism (Fig.4.37) for the Cr<sub>3</sub>C<sub>2</sub>-NiCr coated superalloy superalloy 75 at 900 °C in Na<sub>2</sub>SO<sub>4</sub>-60%V<sub>2</sub>O<sub>5</sub> molten salt after 100 cycles is proposed.

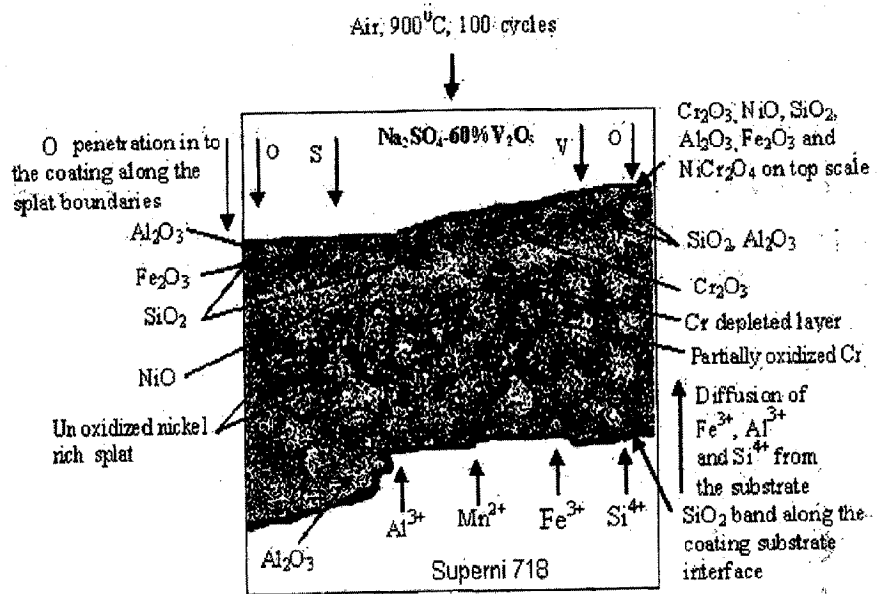


Fig. 4.37 Schematic of the proposed oxidation mechanism of the Cr<sub>3</sub>C<sub>2</sub>-NiCr coated superalloy superni 718 at 900 °C in Na<sub>2</sub>SO<sub>4</sub>-60%V<sub>2</sub>O<sub>5</sub> after 100 cycles.

#### 4.4.1.5 Conclusions

- D-gun spraying process has been successfully used to deposit  $\text{Cr}_3\text{C}_2\text{-NiCr}$  coating on Ni and Fe based superalloy substrates in the range of 200–250  $\mu\text{m}$  thickness, the coating has nearly uniform, adherent and dense microstructure with porosity less than 0.8 %.
- Weight gain data for  $\text{Cr}_3\text{C}_2\text{-NiCr}$  coated superalloys indicated less weight gain compared to bare super alloys, hence the hot corrosion protection of  $\text{Cr}_3\text{C}_2\text{-NiCr}$  coated superalloy is of the order

**Superfer 800H > Superni75 > Superni 718.**

- EDS analysis detected relatively more oxides of nickel in the upper region of the scale of bare superalloy, where as coated superalloys show more oxides of chromium in the upper region of the scale. The oxides of chromium and nickel, and their spinels may be contributing to blocking the transport of degrading corrosive species through the  $\text{Cr}_3\text{C}_2\text{-NiCr}$  coating and thus contributed to hot corrosion resistance.
- The hot corrosion resistance of the coating is also partly attributable to the presence of very low porosity, uniform fine grains and the flat splat microstructure of  $\text{Cr}_3\text{C}_2\text{-NiCr}$  coating obtained by D-gun process.
- Initial spallation and sputtering might be due to the different values of thermal expansion coefficients of the coatings, substrate and oxides. Some elements of the substrate such as Fe, Cr, Si, and Mn showed a tendency of outward diffusion from the substrate to the coating along the inter splat boundaries, which is indicated by depletion of the elements in the alloy substrate.
- However, nickel has shown two distinct inter diffusion behaviour, such as, for  $\text{Cr}_3\text{C}_2\text{-NiCr}$  coated superni 75, nickel has shown outward diffused from substrate alloy to coating. Contrary to this, in case of  $\text{Cr}_3\text{C}_2\text{-NiCr}$  coated superni 718 and superfer 800H, Ni has shown inward diffusion from coating to substrate alloy.

## **4.4.2 Na<sub>2</sub>SO<sub>4</sub>-25%K<sub>2</sub>SO<sub>4</sub> MOLTEN SALT ENVIRONMENT-II**

### **4.4.2.1 Introduction**

The hot corrosion behavior of Cr<sub>3</sub>C<sub>2</sub>-NiCr coatings deposited on the superalloys (namely superni 75, superni 718 and superfer 800H) exposed to Na<sub>2</sub>SO<sub>4</sub>-25%K<sub>2</sub>SO<sub>4</sub> at temperature 900 °C for 100 cycles has been investigated in the present work. The different composition of the salt as compared to the salt composition given in section 4.3.1 has been chosen simulating the variable composition of the salt environment manifested in the actual applications.

### **4.4.2.2 Experimental Details**

The substrate materials, coating formulation and the hot corrosion studies are explained in detail in section 3.1, 3.2.3 and 3.4.3.

### **4.4.2.3. Results**

#### **4.4.2.3.1 Visual observations and Weight change measurements**

Fig.4.38 shows the colour of oxide scale formed on the coated and bare superalloy after hot corrosion studies at 900 °C for 100 cycles in 75 wt. % Na<sub>2</sub>SO<sub>4</sub>-25% K<sub>2</sub>SO<sub>4</sub> environments. Coated superni 75 and superfer 800H (Fig.4.38a and c) show a light grey colour oxide with some tinges of light green colour, where as coated superni 718 (Fig.4.38b) indicates bluish grey patches with greenish tinges. The colour of the scale appeared on the surface of bare superni 75 was dark grey during early cycles, turned to light bluish patches on greenish background towards the end (Fig.4.38d). The presence of green colour scale indicates the formation of NiO as reported by Bornstein et al., (1975). In case of bare superni 718, a silver grey patch on greenish and brownish grey background (Fig.4.38e) was observed. Where as, bare superfer 800H showed spallation behaviour of the oxide scale in the initial few cycles at the edges and corners, but after 10cycles, the sputtering and spalling intensified on the whole surface giving lustrous appearance, which lasted up to 22 cycles. Finally, after 100 cycles, silver grey patches on the bluish and brownish grey back ground are found (Fig.4.38f). The kinetics of hot corrosion was determined from the weight change (mg/cm<sup>2</sup>) versus time plots for the bare and coated three superalloys subjected to hot corrosion in Na<sub>2</sub>SO<sub>4</sub>-25%K<sub>2</sub>SO<sub>4</sub> environment at 900 °C up to 100 cycles as shown in Fig.4.39. The curve shows an initial weight gain in all the cases.

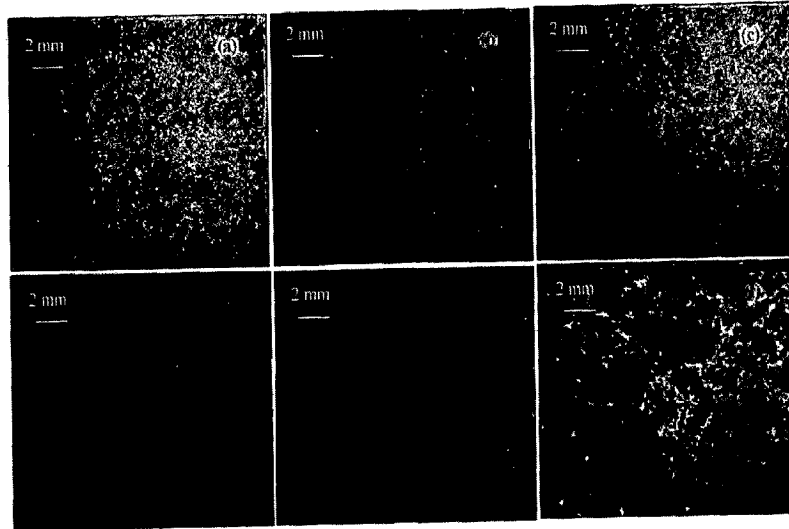


Fig. 4.38 Surface macrograph of  $\text{Cr}_3\text{C}_2\text{-NiCr}$  coated and bare superalloys subjected to hot corrosion in  $\text{Na}_2\text{SO}_4\text{-}25\%\text{K}_2\text{SO}_4$  environment at  $900\text{ }^\circ\text{C}$  for 100 cycles, (a) Coated superalloy 75, (b) Coated superalloy 718, (c) Coated superalloy 800 H, (d) Bare superalloy 75, (e) Bare superalloy 718, (f) Bare superalloy 800 H.

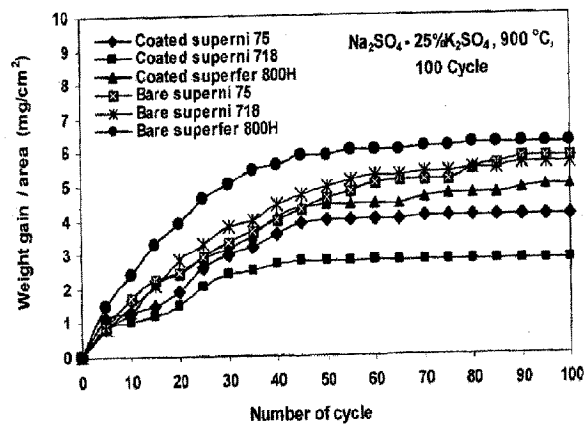


Fig. 4.39 weight gain/area vs. number of cycles plot for  $\text{Cr}_3\text{C}_2\text{-NiCr}$  coated and bare superalloys subjected to cyclic oxidation for 100 cycles in  $\text{Na}_2\text{SO}_4\text{-}25\text{ wt. } \%$   $\text{K}_2\text{SO}_4$  at  $900\text{ }^\circ\text{C}$ ,

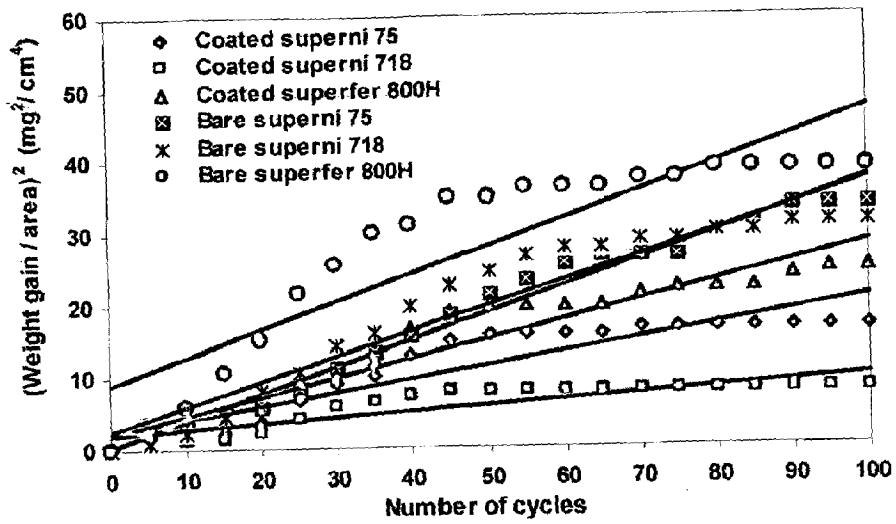


Fig. 4.40 (weight gain/area)<sup>2</sup> vs. number of cycles plot for coated and bare superalloys subjected to cyclic oxidation for 100 cycles in Na<sub>2</sub>SO<sub>4</sub>-25% K<sub>2</sub>SO<sub>4</sub> at 900 °C

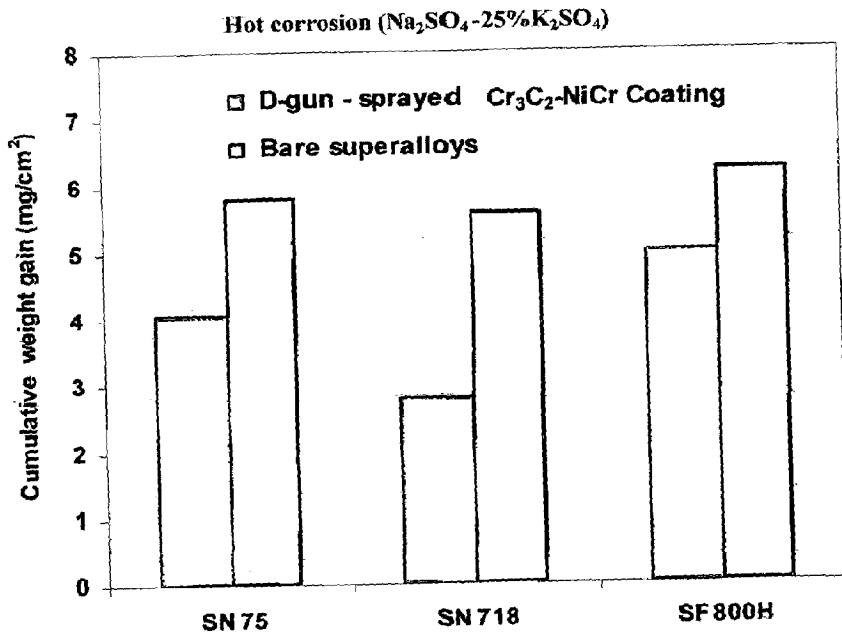


Fig. 4.41 Bar chart showing cumulative weight gain per unit area for coated and bare superalloys subjected to cyclic oxidation for 100 cycles in Na<sub>2</sub>SO<sub>4</sub>-25%K<sub>2</sub>SO<sub>4</sub> at 900°C

**Table 4.3** Parabolic rate constant (kp) and correlation coefficient values for coated and Bare superalloys subjected to cyclic oxidation for 100 cycles in Na<sub>2</sub>SO<sub>4</sub>-25% K<sub>2</sub>SO<sub>4</sub> at 900 °C.

Substrates	Kp X 10 <sup>-10</sup> gm <sup>2</sup> cm <sup>-4</sup> s <sup>-1</sup>	Correlation coefficients values (R <sup>2</sup> )
Bare superni 75	1.025	0.9786
Bare superni 718	0.961	0.9119
Bare superfer 800H	1.059	0.8173
Coated Superni 75	0.509	0.9035
Coated Superni 718	0.221	0.8357
Coated Superfer 800H	0.727	0.9133

The Cr<sub>3</sub>C<sub>2</sub>-NiCr-coated superalloys in all cases show a much lower weight gain than the bare specimens in the given molten salt environment. Coated superni 718 showed the lowest weight gain, whereas bare superfer 800H showed highest weight gain. The weight gain of bare superni 718 and superni 75, after 100 cycles, is nearly three-fifth and four-fifth, respectively, as compared to that of superfer 800H. In general, the oxidation behaviour of both bare and Cr<sub>3</sub>C<sub>2</sub>-NiCr-coated samples follow a parabolic rate law, except for bare superfer 800H and coated superni 718, which slightly deviates compared to uncoated superfer 800H from the parabolic rate, as can be inferred from the square of weight change (mg<sup>2</sup>/cm<sup>4</sup>) versus number of cycle plots (Fig.4.40). The correlation coefficient values, the parabolic rate constants (kp in 10<sup>-10</sup> g<sup>2</sup> cm<sup>-4</sup> s<sup>-1</sup>) for the Cr<sub>3</sub>C<sub>2</sub>-NiCr-coated and bare superalloys after 100 cycles of hot corrosion run are shown in Table 4.3. Cumulative weight gain per unit area for coated and bare superalloys is shown in Fig.4.41.

#### 4.4.2.3.2 X-ray diffraction analysis

The X-ray diffraction analysis profiles for the scale of bare and D-gun sprayed Cr<sub>3</sub>C<sub>2</sub>-NiCr coated superalloy after hot corrosion in Na<sub>2</sub>SO<sub>4</sub>-25%K<sub>2</sub>SO<sub>4</sub> environment for 100 cycles at 900 °C are shown in Fig.4.42 and 4.43. The phases detected at the surface of the bare specimens are Cr<sub>2</sub>O<sub>3</sub>, Fe<sub>2</sub>O<sub>3</sub>, NiO, NiS, CrS, FeS and NiCr<sub>2</sub>O<sub>4</sub>, respectively (Fig.4.42), whereas, the phases detected at the surface of the coated specimens are Cr<sub>2</sub>O<sub>3</sub>, Cr<sub>7</sub>C<sub>3</sub>, Cr<sub>23</sub>C<sub>6</sub>, NiO and NiCr<sub>2</sub>O<sub>4</sub> spinel (Fig.4.43).



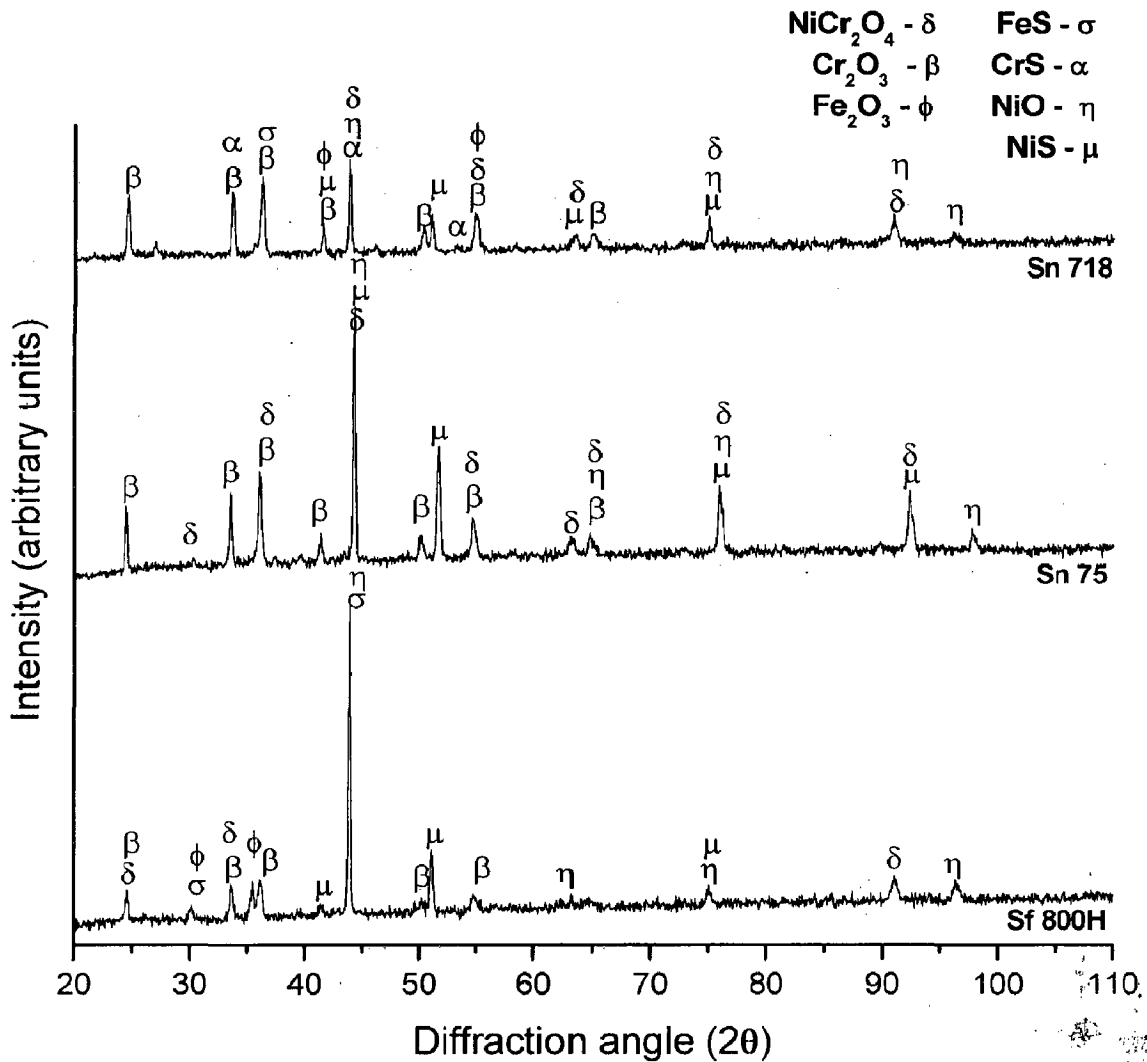


**Fig. 4.42** X-ray diffraction patterns for bare superalloys exposed to cyclic oxidation in  $\text{Na}_2\text{SO}_4$ -25% $\text{K}_2\text{SO}_4$  environment at 900 °C after 100 cycles, (a) superni 718, (b) superni 75 and (c) superfer 800 H.

#### 4.4.2.3.3 FE-SEM/EDS analysis of the scales

##### 4.4.2.3.3.1. Surface scale analysis

FE-SEM micrographs with EDS spectrum reveals the surface morphology of the  $\text{Cr}_3\text{C}_2$ -NiCr coated and bare superalloy specimens after cyclic hot corrosion in molten salt environment ( $\text{Na}_2\text{SO}_4$ -25% $\text{K}_2\text{SO}_4$ ) for 100 cycles at 900 °C as shown in Fig.4.44-4.45 The surface oxide scale developed on coated superalloys is massive, without any cracks, with clusters in which, irregular disc shaped  $\text{Cr}_2\text{O}_3$  distributed throughout the coating. EDS analysis of the scale of  $\text{Cr}_3\text{C}_2$ - NiCr

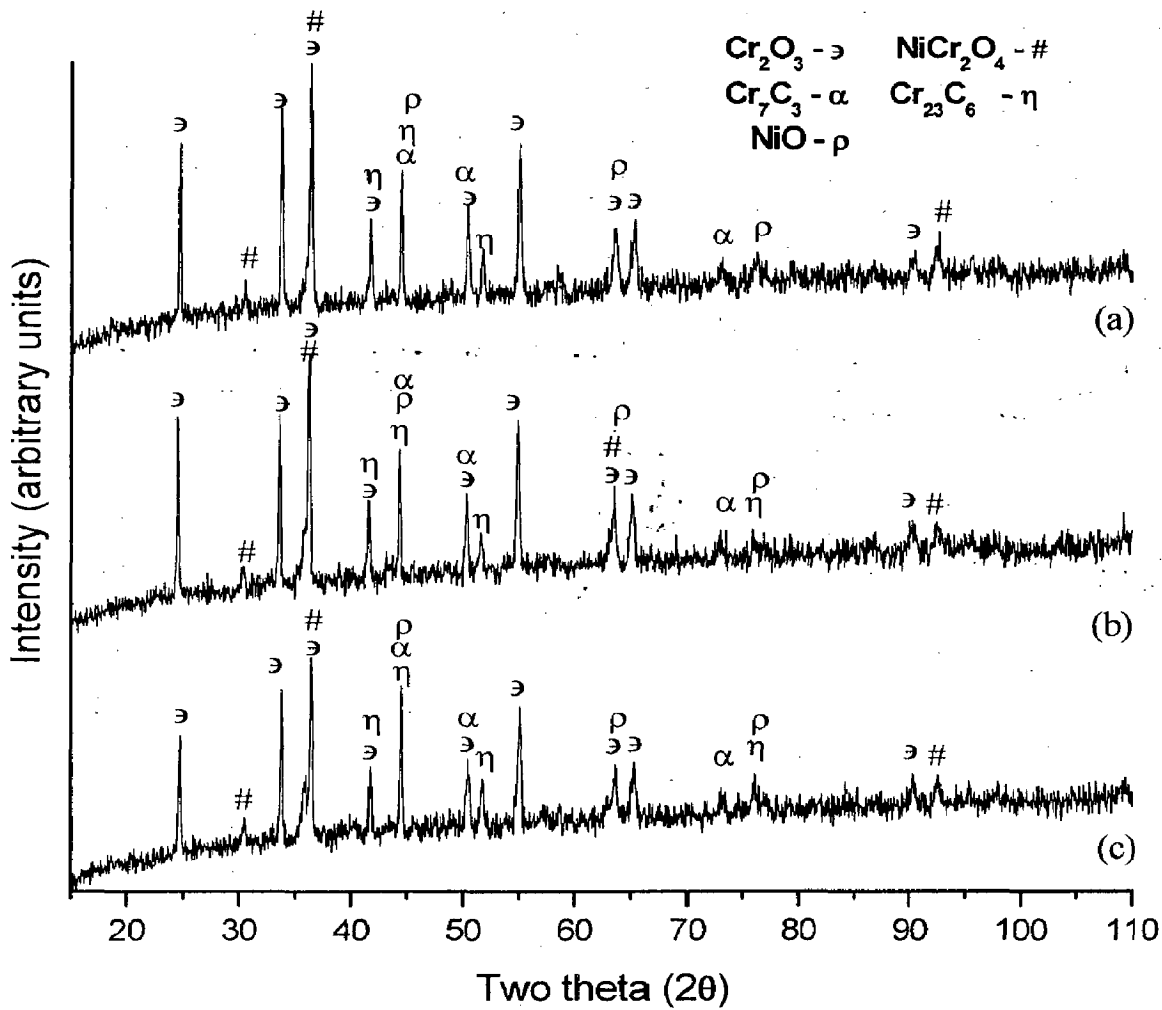


**Fig. 4.43** X-ray diffraction patterns for  $\text{Cr}_2\text{C}_3$ -NiCr coated superalloys exposed to cyclic oxidation in  $\text{Na}_2\text{SO}_4$ -25% $\text{K}_2\text{SO}_4$  environment at  $900^\circ\text{C}$  after 100 cycles, (a) Coated superni 718, (b) Coated superni 75 and (c) Coated superfer 800 H.

coated superni 75 revealed the formation of  $\text{Cr}_2\text{O}_3$  and NiO as a principle phases. In addition,  $\text{Fe}_2\text{O}_3$ , S, Na and Ti oxides are also present in small amounts (Fig.4.44a). The scale on the corroded  $\text{Cr}_3\text{C}_2$ -NiCr coated superni 718 appears (Fig.4.44b) to be dense, EDS analysis of the scale revealed  $\text{Cr}_2\text{O}_3$  as major oxide phase, along with small amounts of NiO,  $\text{Fe}_2\text{O}_3$ , Mn, Ti, Si, Al, Cu and Ta oxides. The presence of these oxides shows the outward diffusion of these elements from the substrate to the top surface of the coating. The globules (at point X in Fig.4.44b) represent the formation of Si and Al oxides as the predominant phase, along with un-

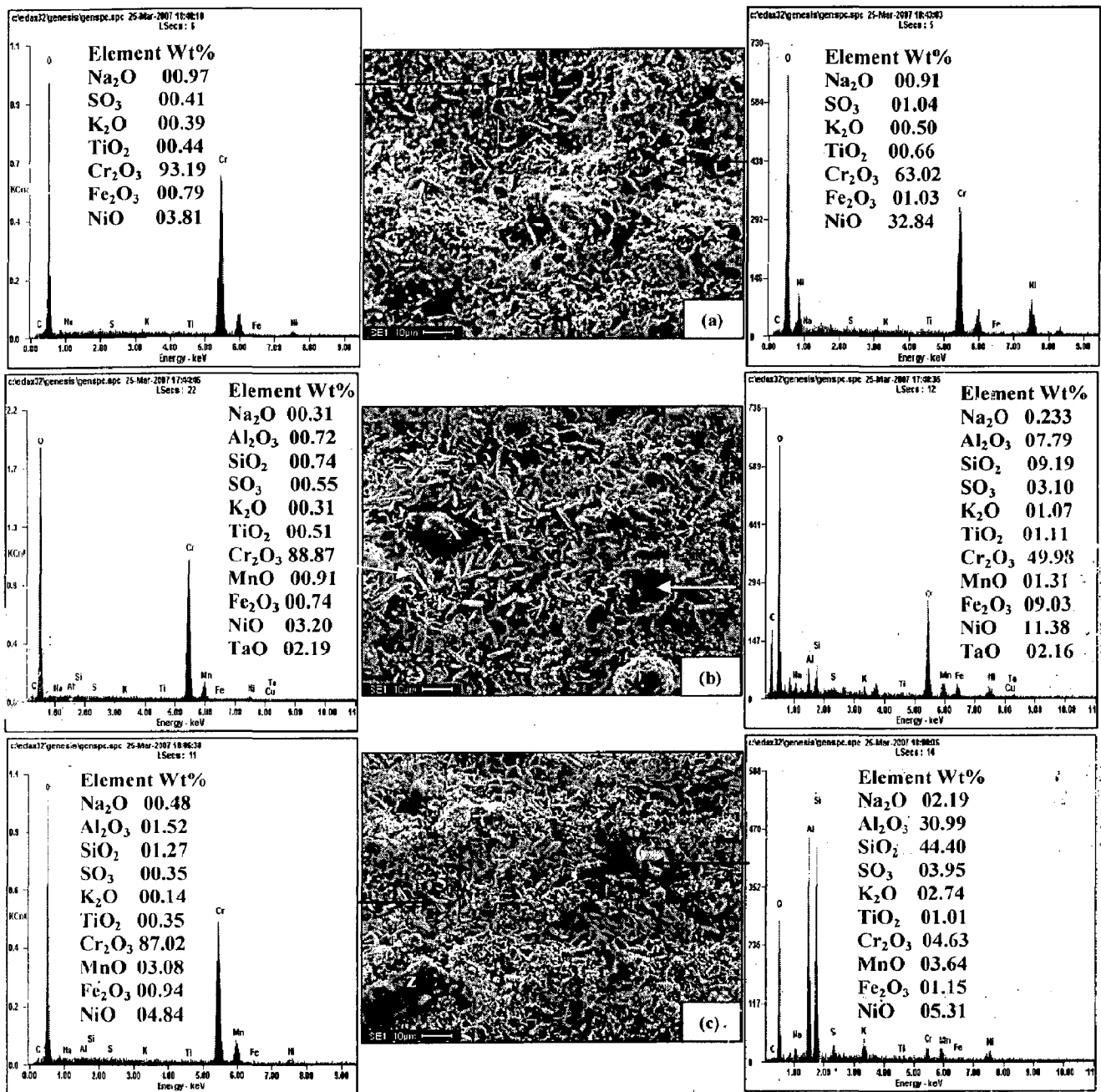


Fig. 4.44 FE-SEM/EDS analysis for coated superalloys subjected to cyclic oxidation in Na<sub>2</sub>SO<sub>4</sub>-25%K<sub>2</sub>SO<sub>4</sub> environment at 900 °C after 100 cycles: (a) Coated superalloy 75, (b) Coated superalloy 718 and (c) Coated superalloy 800 H.

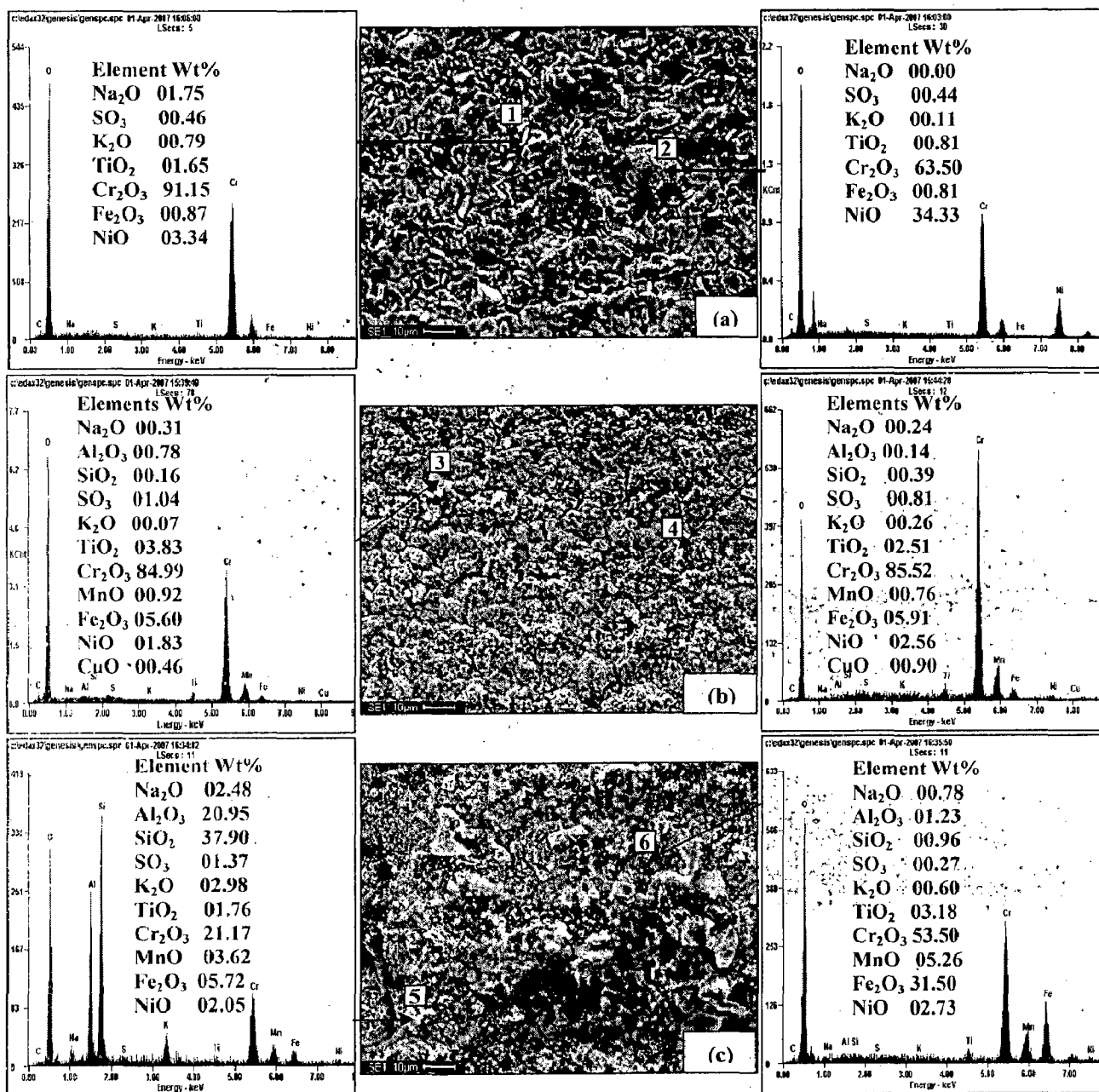


Fig. 4.45 FE-SEM/EDS analysis for bare superalloys subjected to cyclic oxidation in Na<sub>2</sub>SO<sub>4</sub>-25%K<sub>2</sub>SO<sub>4</sub> environment at 900 °C after 100 cycles: (a) superalloy 75, (b) superalloy 718 and (c) superalloy 800 H.

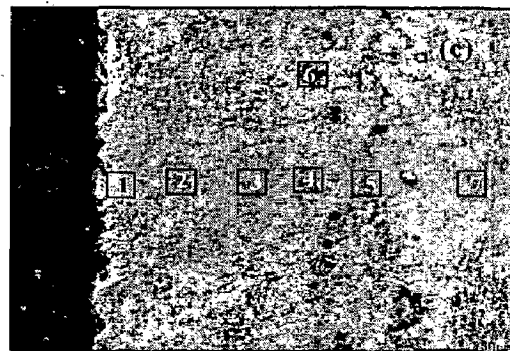
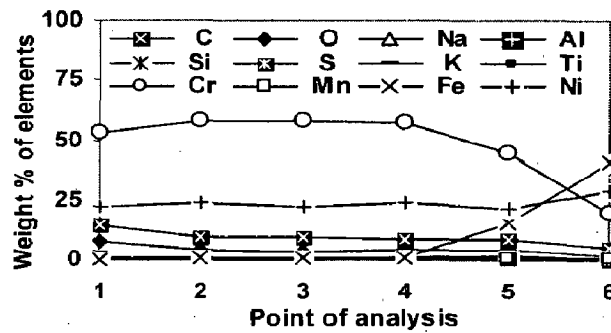
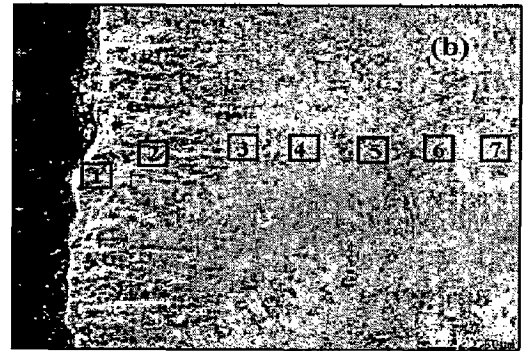
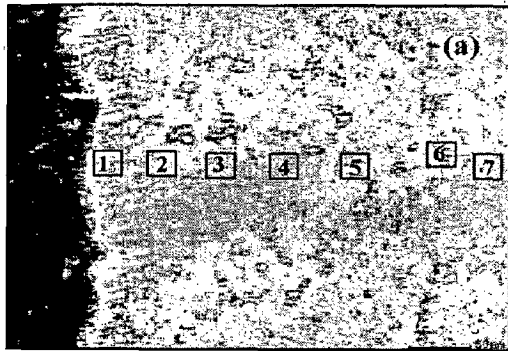
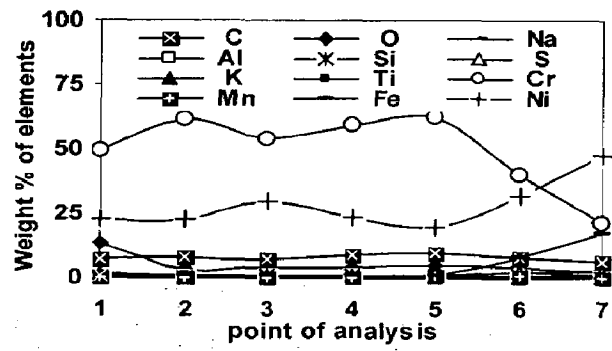
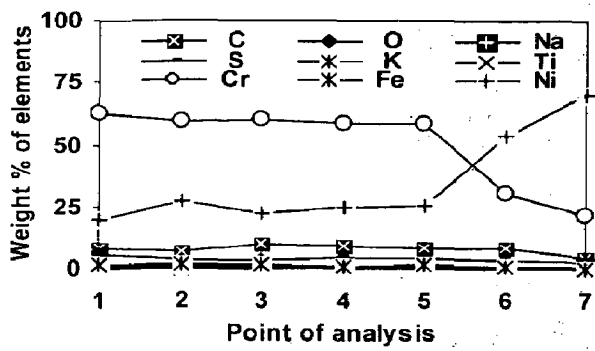


Fig. 4.46

Oxide scale morphology and variation of elemental composition across the cross-section of  $\text{Cr}_3\text{C}_2$ -NiCr coated superalloys subjected to cyclic oxidation at  $900^\circ\text{C}$  in  $\text{Na}_2\text{SO}_4$ -25% $\text{K}_2\text{SO}_4$  environment after 100 cycles (a) superni 75, (b) superni 718 and (c) superfer 800H

melted particles identified in the coating by their spherical morphology. Similarly, the scale formed on the coated superfer 800H (Fig.4.44c) depicts the diffusion Al, Si and Mn from the substrate elements in to the coating. The EDS analysis clearly indicates the formation of  $\text{Cr}_2\text{O}_3$  as predominant oxide. The nodules indicated at point Z (Fig.4.44c) consists mainly oxides of chromium and manganese.

On the other hand, the oxide scale developed on the surface of bare superni 75 after cyclic hot corrosion in molten salt environment ( $\text{Na}_2\text{SO}_4$ -25% $\text{K}_2\text{SO}_4$ ) for 100 cycles at 900 °C is dense with small elongated grains, mainly consisting of  $\text{Cr}_2\text{O}_3$  and NiO as a predominant oxides, along with little amount of Fe and Ti oxides (Fig.4.45a). Where as a homogeneous and continuous small round grain scale is formed on hot corroded bare superni 718, the scale shows  $\text{Cr}_2\text{O}_3$  as the major oxide phase, along with minor quantity of NiO,  $\text{Fe}_2\text{O}_3$ , Mn, Ti, Si, Al, Cu and Ta (Fig.4.45b). SEM micrograph of corroded bare superfer 800H (Fig.4.45c), indicates spallation of oxide scale, diffusion of substrate elements in to the scale, major oxides of Al, Si, Fe, Mn and  $\text{Cr}_2\text{O}_3$  have formed on the surface as evident from the EDS spectrum.

#### **4.4.2.3.3.2. Cross-sectional analysis**

FE-SEM/EDS analysis was carried out at different points of interest along the cross-section of hot corroded coated superni 75, superni 718 and superfer 800H and the results are shown in Fig.4.46. In all the cases, a dense and adherent oxide scale has formed on the coated superalloys, which has retained its dense structure. FE-SEM micrograph across the cross section of  $\text{Cr}_3\text{C}_2$ -25%NiCr-coated superni 75 alloy after 100 cycles at 900 °C in molten salt environment indicates an oxide scale on the top surface (Fig.4.46 (a) point 1) mainly consisting of chromium and nickel rich oxides, further in the subscale region at points 2, 3, 4 and 5 the presence of Cr and Ni rich elements was observed. Inter-diffusion of Cr and Ni have occurred from coating in to substrate and from substrate in to coating, respectively as evident from EDS analysis at point (Fig.4.46a). Corroded coated superni 718 (Fig.4.46b) showed the top surface of the coating mostly consisting of a homogeneous, adherent and non-uniform oxide scale of chromium and nickel (point 1). In the subscale region (point 2) Cr percentage increases where as Ni remains same, but at point 3 Cr decreases and Ni increases, thereby suggesting light grey regions correspond to Ni-rich and dark grey corresponds to Cr-rich areas, this continued further at point 4 and 5. There is interdiffusion of coating and substrate elements across the interface (point 6 and 7). Cross sectional analysis of

the oxidised  $\text{Cr}_3\text{C}_2$ -25%NiCr coated superfer 800H (Fig.4.46c) indicates a scale which mainly consists of oxides of chromium and nickel. There is a constant variation in the composition of Cr and Ni at points 2, 3 and 4. Some carbide is exposed to the surface during polishing, observed as black spots just above the coating-substrate-interface.

#### 4.4.2.3.4 X-ray mapping

X-ray mapping analysis of the different elements present across the scale is shown in Fig.4.47-4.49. In all the cases, a thick band of Ni has formed just below the coating-substrate interface where Cr is depleted. SE X-ray mapping of hot corroded  $\text{Cr}_3\text{C}_2$ -NiCr coated superni 75 showed a thin oxide scale mainly consisting of chromium and nickel (Fig.4.47). Where as X-ray mappings for hot corroded  $\text{Cr}_3\text{C}_2$ -NiCr coated superni 718 after 100 cycles at 900 °C (Fig.4.48) indicates a variation in the thickness of oxide scale mainly consisting of chromium and nickel at the top surface and rest of the coating is partially got oxidized as evident from the oxygen distribution. Aluminum has found along the coating-substrate interface, also a small amount of Al has diffused in to the top surface of coating during initial cycles of hot corrosion run. The presence of aluminum at the coating-substrate interface may be due to entrapped alumina particles, which might be retained in the asperities during grit blasting of the substrate prior to deposition of the coatings. Similarly, X-ray mapping of  $\text{Cr}_3\text{C}_2$ -NiCr-coated superfer 800H after hot corrosion in molten salt environment at 900 °C for 100 cycles (Fig.4.49) indicates the formation of a scale containing mainly of chromium and nickel rich elements. Aluminum has shown its presence in the form of clusters, mainly at the coating-substrate interface, where all other elements are found to be depleted.

#### 4.4.2.4 Discussion

The weight gain graph (Fig.4.39) shows that the weight of bare superalloy increases continuously, where as weight gain of the coated specimens is relatively high during first few cycles of hot corrosion, but subsequently increase in weight gain is found to be gradual for coated superalloys. The initial high oxidation rate of the coated specimens might be attributed due to air which is entrapped during D-gun deposition and sheltered in the pores, since the cooling of the coating was rapid; there is shortage of time for the residual air to react with the surrounding coating alloys. But the coating underwent in situ reaction during high temperature.

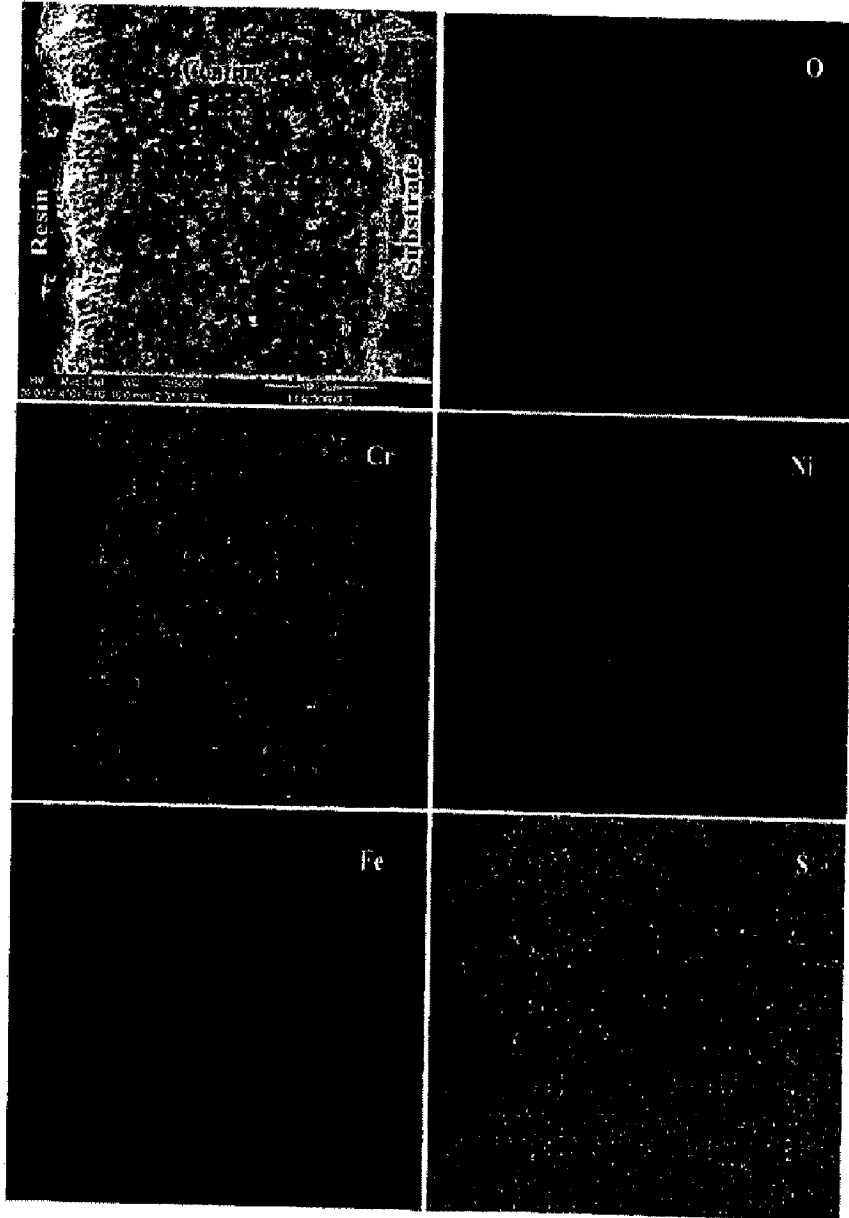


**Fig. 4.47** Composition image (SE) and X-ray mapping of the cross-section of the  $\text{Cr}_3\text{C}_2$ -NiCr-coated superalloy superalloy 75 subjected to cyclic oxidation at  $900^\circ\text{C}$  in  $\text{Na}_2\text{SO}_4$ -25%  $\text{K}_2\text{SO}_4$  after 100 cycles.



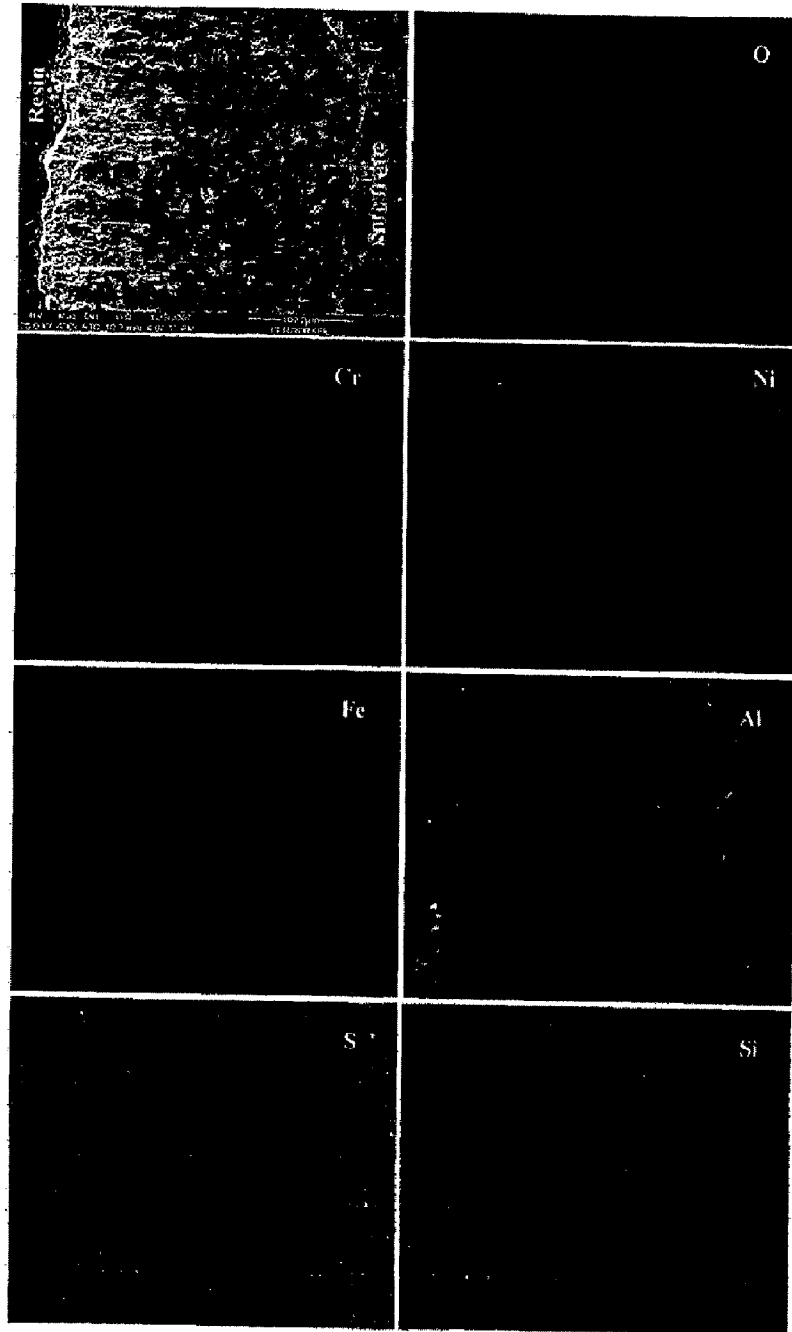


**Fig. 4.48** Composition image (SE) and X-ray mapping of the cross-section of the  $\text{Cr}_3\text{C}_2$ -NiCr-coated superalloy superalloy 718 subjected to cyclic oxidation at  $900^\circ\text{C}$  in  $\text{Na}_2\text{SO}_4$ -25% $\text{K}_2\text{SO}_4$  after 100 cycles.

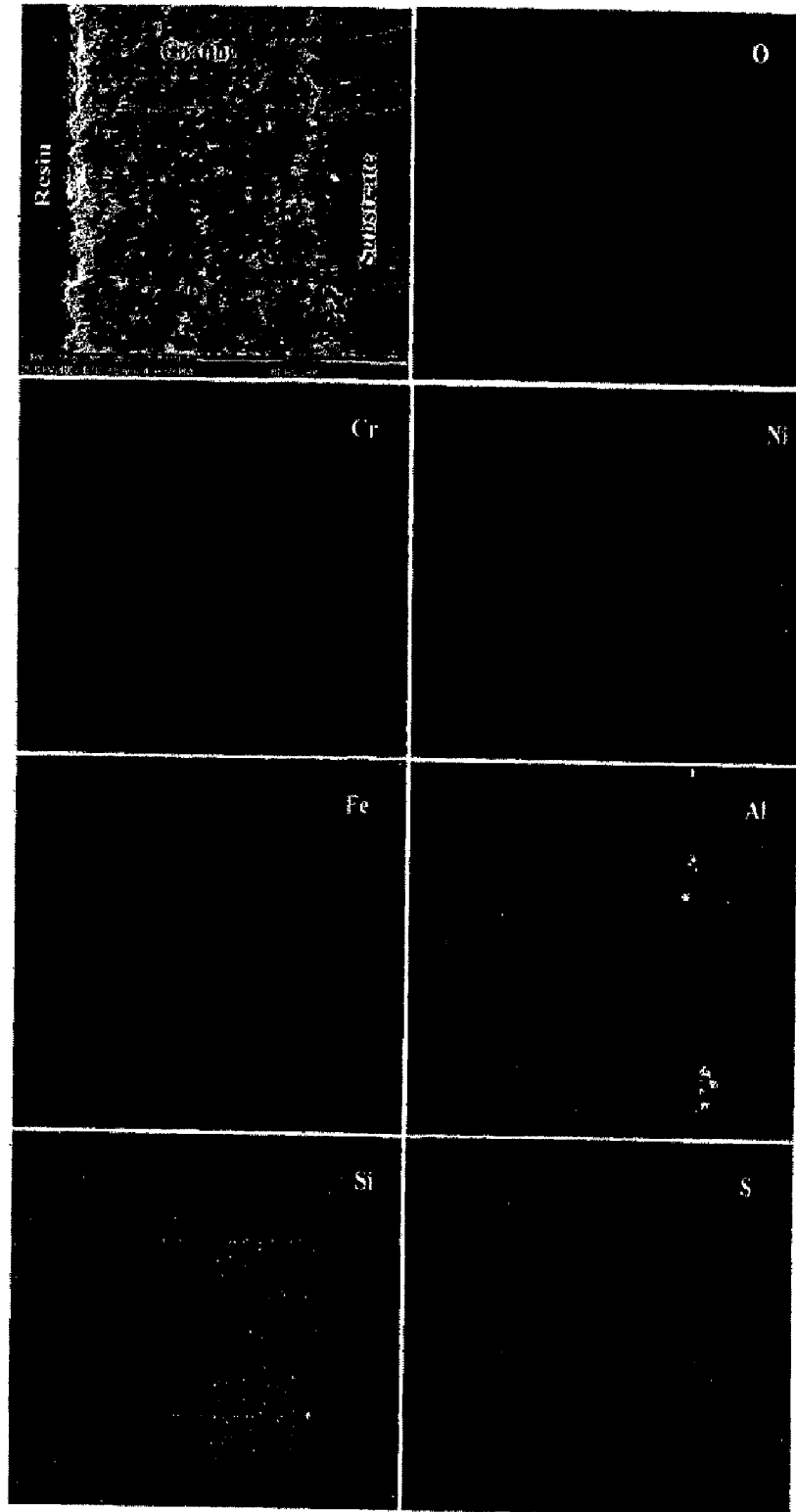


**Fig. 4.49** Composition image (SE) and X-ray mapping of the cross-section of the Cr<sub>3</sub>C<sub>2</sub>-NiCr-coated superalloy superfer 800H subjected to cyclic oxidation at 900 °C in Na<sub>2</sub>SO<sub>4</sub>-25%K<sub>2</sub>SO<sub>4</sub> after 100 cycles.

oxidation (900 °C), leading to partial oxidations of the coating, during the subsequent cycles, the formation of oxides have blocked the pores, and acted as diffusion barriers to the inward diffusion of corrosive species. This leads to slow oxide scale growth. Chromium exhibits higher affinity for oxygen to form  $\text{Cr}_2\text{O}_3$  during the earlier stages of hot corrosion (Singh, 2005). This shows that the oxidation resistance of  $\text{Cr}_3\text{C}_2$ -NiCr coating is solely based on the formation of  $\text{Cr}_2\text{O}_3$ , which acts as a diffusion barrier for the corrosive species as reported by Seiersten and Kofstad (1987). Once the oxides are formed at the places of porosity, the growth of the oxides becomes limited mainly to the surface of the specimens. This would relatively minimize the weight gain and result in the steady state oxidation behavior with the progress of long term high temperature exposure, which are in accordance with the similar observation reported for the plasma sprayed NiCrAlY coatings on Nimonic 80A and SS41 alloy substrates, respectively, by Choi et al. (2002) and Niranatlumpong et al. (2000). Poor corrosion resistance of bare superalloy superfer 800H, is due to intense spallation and sputtering which can be attributed to the severe strain developed as a result of  $\text{Fe}_2\text{O}_3$  precipitation from the liquid phase and the interdiffusion of intermediate layer of iron oxide. Presence of Si, Al Fe, Mn and K phases in a thin layer might have imposed severe strain on the scale, which may result in the spallation, cracking and exfoliation of the oxide scale, the cracks might have allowed the corrosive liquid to reach the metal substrate (Sachs, 1958). The presence of  $\text{Fe}_2\text{O}_3$  in the spalled scale has also been reported to be non-protective by Das et al. (2002) during their hot corrosion study on  $\text{Fe}_3\text{Al}$ -based iron aluminides in  $\text{Na}_2\text{SO}_4$  atmosphere. Sidhu et al. (2006A), (2006B), and (2006C) have evaluated the hot corrosion behaviour of HVOF- sprayed  $\text{Cr}_3\text{C}_2$ -NiCr-coating on Fe- and Ni-based superalloys in a  $\text{Na}_2\text{SO}_4$ -60% $\text{V}_2\text{O}_5$  at 900 °C under cyclic conditions for 50 cycles. The weight gains, reported in their work, were 2 to 3 times higher than that of same coatings, formulated by D-gun process, exposed to  $\text{Na}_2\text{SO}_4$ -25% $\text{K}_2\text{SO}_4$  environment for 100 cycles at the same temperature in the present work. The cumulative weight gain of coated and bare superalloys after 100 cycles of hot corrosion is plotted in Fig.4.41. The overall weight gain for the bare superalloys superni 718, superni 75, and superfer 800H alloys are 5.58, 5.80 and 6.21  $\text{mg}/\text{cm}^2$  respectively. The bare Ni-based superalloys superni 718 and superni 75 showed a better resistance to the hot corrosion and the weight gain was less as compared to bare Fe-based superfer 800H superalloy. The higher weight gain of superfer 800H may be due to the presence of iron oxide which might have diffused in to the coating up to the surface, since the presence of  $\text{Fe}_2\text{O}_3$  in the scale has been

reported to be non-protective as discussed above. An overall weight gain of 2.800, 4.072, and 4.9800 mg/cm<sup>2</sup> was observed for the Cr<sub>3</sub>C<sub>2</sub>-NiCr coated superalloys 718, 75, and superfer 800H superalloys (Fig.4.41), respectively. The Cr<sub>3</sub>C<sub>2</sub>-NiCr coating provides the maximum hot corrosion resistance to superalloy 718 and has been found successful in reducing the weight gain by around 50% of that gained without a coating. Coatings on superalloy 75 and superfer 800H superalloys reduce the weight gain by 30% and 20% of that gained by the bare superalloys, respectively. This may be possibly due to the presence of Cr<sub>2</sub>O<sub>3</sub>, NiO and NiCr<sub>2</sub>O<sub>4</sub> spinel present in the top scales of coated superalloys, as revealed by surface XRD analysis, the major and minor phases detected at the surface of the specimens with the XRD analysis are Cr<sub>2</sub>O<sub>3</sub>, Cr<sub>7</sub>C<sub>3</sub>, Cr<sub>23</sub>C<sub>6</sub>, NiO and NiCr<sub>2</sub>O<sub>4</sub> spinel. Oxidation of the Cr<sub>3</sub>C<sub>2</sub> (Orthorhombic crystal structure) phase leads to decarburisation and results in the formation of Cr<sub>7</sub>C<sub>3</sub> (orthorhombic crystal structure) and Cr<sub>23</sub>C<sub>6</sub> (FCC)) as observed from the XRD analysis of Cr<sub>3</sub>C<sub>2</sub>-NiCr coated superalloys after hot corrosion at 900 °C for 100 cycles (Fig.4.43). The presence of these phases, except carbides, in the scale of coated superalloys is further supported by the surface, cross sectional EDS (Fig.4.44 and 4.46) and X-ray mapping analyses (Fig.4.47-4.49), further it has been observed that the scales formed on the coated superalloy 718 superalloys were observed to be dense and compact, without any spallation/ sputtering or peeling of the scale. This also contributes to the lower weight gain. Chromia is the best oxide to resist hot corrosion in molten sulfates, as it preferentially reacts with O<sup>2-</sup> in molten sulfates to form chromate. The chromate will stabilize the melt chemistry, and consequently prevent the dissolution of the protective oxide scale (Wang et al., 2007). Cross-sectional EDS analysis of corroded Cr<sub>3</sub>C<sub>2</sub>-NiCr-coated samples shows that the oxygen has not been penetrated into the alloy substrate (Fig.4.46a, b and c), in case of all superalloys, the variations in elemental composition after hot corrosion studies show the chromium rich elements are present in the uppermost part of coating. From EDS analysis at point 7 (Fig. 4.46a), which lies in the substrate, it can be inferred that the percentage of nickel decreases from 77.1% in the original alloy to 70.16%, whereas chromium increases from 19.5 to 21.7% which clearly indicates that Ni has diffused from substrate to the coating, Cr on the other hand has diffused from coating to substrate. Similar interdiffusion is found in case of coated superalloy 718 (point 7 in Fig. 4.46b), in case of coated superfer 800H, all the major elements such as Fe, Cr and Ni have diffused into the coating from the substrate (point 6 in Fig.4.46c), this inter-diffusion is mainly due to concentration gradient. The formation of thermodynamically stable chromium oxide scale

and its slow growth as shown in X-ray mapping analysis (Fig.4.47-4.49), might have acted as barrier to the inward diffusion of oxygen into the coating. The formation of spinel of  $\text{NiCr}_2\text{O}_4$  via solid phase reaction between  $\text{NiO}$  and  $\text{Cr}_2\text{O}_3$  in the oxide scales has been reported by Ren et al. (2005), which also helps to develop oxidation resistance as the spinel phase usually has lower diffusion coefficients of the cations and anions than those in their parent oxides (Chatterjee et al., 2001). An oxide scale that contains  $\text{Cr}_2\text{O}_3$  has shown excellent spallation resistance against the cyclic oxidation in molten salt environment, which indicates further effectiveness of the coatings due to the scale spallation resistance as reported by Stott (1992). The similar steady state oxidation studies have been made by Kamal et al. (2008A) for  $\text{Cr}_3\text{C}_2$ -NiCr coated superalloys in the different corrosive environment ( $\text{Na}_2\text{SO}_4$ -60% $\text{V}_2\text{O}_5$ ), which shows different surface morphology than the present corrosive environment ( $\text{Na}_2\text{SO}_4$ -25%  $\text{K}_2\text{SO}_4$ ). Based on the XRD, FE-SEM/EDS and X-ray mapping analysis, the following oxidation mechanism (Fig.4.50) for the  $\text{Cr}_3\text{C}_2$ -NiCr coated superalloy superni 718 at 900 °C in  $\text{Na}_2\text{SO}_4$ -25% $\text{K}_2\text{SO}_4$  molten salt after 100 cycles is proposed

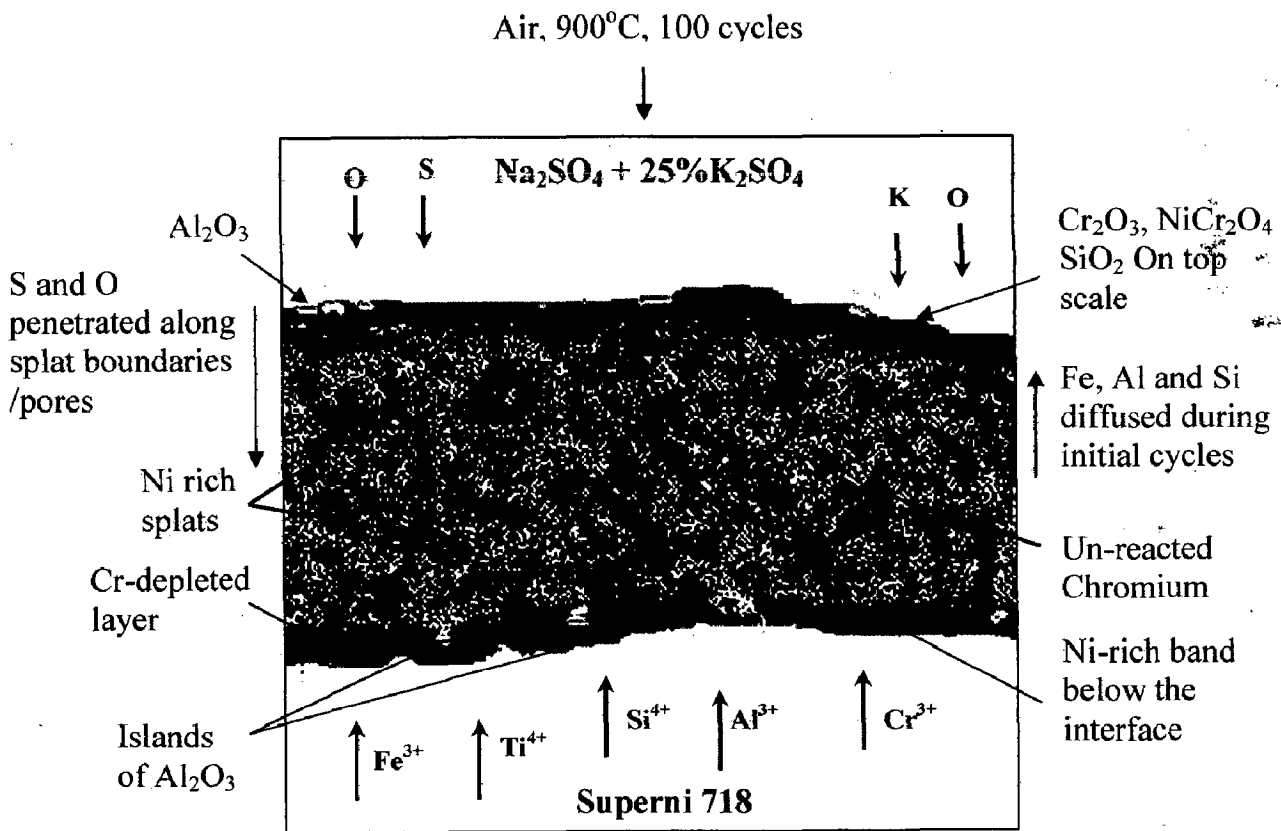


**Fig. 4.50** Schematic of the proposed oxidation mechanism of the  $\text{Cr}_3\text{C}_2$ -NiCr coated superalloy superni 718 at 900 °C in  $\text{Na}_2\text{SO}_4$ -25% $\text{K}_2\text{SO}_4$  after 100 cycles.

#### 4.4.2.5 Conclusions

- $\text{Cr}_3\text{C}_2$ -NiCr coatings, deposited on selected superalloys using the D-gun process, showed a higher hot corrosion resistance in the molten salt environment at  $900^\circ\text{C}$  as compared to the bare superalloys.
- The surface oxide scale developed on coated superalloys is massive, crack free, with dense clusters mainly consisting of oxides of Cr and Ni, in which, irregular disc shaped  $\text{Cr}_2\text{O}_3$  distributed throughout the coating.
- The  $\text{Cr}_3\text{C}_2$ -NiCr-coated superalloys in all cases showed a lower weight gain than that of the bare specimens in the molten salt environment.
- Coated superalloy 718 shows lowest weight gain and parabolic rate constant among the other coated superalloys.
- The better performance of coated superalloy 718 in the given environments has been attributed for its tendency to form protective dense oxides of chromium, nickel and their spinel.

# CHAPTER 5

## NiCrAlY+0.4wt%CeO<sub>2</sub> COATING

---

### 5.1 CHARACTERISATION OF THE COATING

#### 5.1.1 Introduction

Modern industrial gas turbines are operated at gas inlet temperatures up to 1400 °C similar to aircraft engines to achieve the maximum efficiency for satisfying the demands of power industries. The turbine blades used in gas turbines are subjected to the highest thermal and mechanical load at 1400 °C during service conditions (Czech et al., 1995). Currently, only composite material comprising of the base material, usually a Ni-base superalloys, and the coatings based on MCrAlY (M=Co, Ni, or CoNi) provide the necessary mechanical properties and protection against high temperature corrosion, respectively. The coatings are used as either stand-alone protective overlay coatings or as a bond coat for thermal barrier coatings (TBCs), which widely applied to blades and hot section components of gas turbines (Li et al., 2007). Mevrel (1989) has reported that as the operating temperatures of the gas turbines increases, its required service life can not be achieved using diffusion coatings, whereas overlay coatings performed better in aggressive environment at elevated temperature. The deposition of MCrAlY (M is Ni and/or Co) overlays and Pt-aluminide diffusion coatings as typical bond coats over the superalloys to provide protection against oxidation as well as to reduce the mismatch stresses between the top coat and the superalloy has been reported in the literature (Hocking, 1993; Bouhanek et al., 2000; Gurrappa, 2000; Evans and Taylor, 2001; Kim et al., 2002; He, 2002). Sidhu et al., 2004; Sidhu and Prakash 2005 have characterized plasma sprayed NiCrAlY coatings on boiler-tube steels and analysed its suitability for the applications in thermal power plants. Jain et al., (2007) have investigated the adhesion strength of vacuum plasma sprayed NiCrAlY overlay top coat deposited on a Cu-26Cr bond coated GRCop-84 copper alloy substrate and observed that the tensile strength of the coating is higher than that of the substrate.

D-gun spraying technique has been commercially used in the manufacture of wear resistant coatings for its high hardness and low power cost. Due to the low porosity and good adhesion of the DGS coatings, the inward diffusion of oxygen in to the coatings is effectively prevented

(Zhang et al., 2002). The presence of 0.4 Wt %  $\text{CeO}_2$  in MCrAlY coating is found to be beneficial as cerium being a surface-active element reduces the surface tension and the interfacial energy between the crystal nucleus and the melt during the process of solidification, which results in improving the wetting properties and decreasing the contact angle between the melt and a substrate (Tian et al., 2006). In recent years, rare earths (RE) have been successfully applied to modify the surface properties of thermal spray coatings. It has been reported (Zhenyu et al., 2006) that the addition of  $\text{CeO}_2$  could refine and purify the microstructure of coatings, and increase the microhardness and wear resistance of the coatings. Also, the friction coefficient of the ceria added coatings has decreased slightly. Zhang and Li, (2000A) have found that cerium improved the protective efficiency of the aluminide coating against dry sand erosion and corrosion in dilute NaCl and  $\text{H}_2\text{SO}_4$  solution, respectively. In recent studies, it has been shown that the erosion resistance of aluminide coatings can be improved by rare earth elements, for example, yttrium improved the resistance of FeAlCr(Y) coatings to corrosion, corrosive erosion and dry sand erosion, respectively (Zhang and Li, 2000B). Wang et al., (1998, 2003A) and Wang and Yan, (2006) demonstrated that the addition of rare earth elements can increase the wear and corrosion resistance of coatings due to the improved hardness, toughness, bond strength and thermal shock resistance of the coating materials. Initially, research has been focused on the optimization of the general NiCrAlY composition, i.e., the Ni/Co ratio and the correct allocation of the Cr and Al portions (Czech et al., 1994). Later on, ceria has been added to improve the microstructure and corrosive resistance of these coatings. In spite of the progress made so far, a further improvement is required to optimize the oxidation, hot corrosion resistance and mechanical properties of the coatings. There is very little published information on the application of  $\text{CeO}_2$  in NiCrAlY alloy coatings deposited by D-gun. In the present work, the microstructures, porosity, coating thickness, phase formation and microhardness of D-gun sprayed NiCrAlY+RE alloy coatings are studied using the combined techniques of X-ray diffraction (XRD) technique, Field emission scanning electron microscopy/energy-dispersive analysis (FE-SEM/EDS), and X-ray mapping to provide an experimental basis so as to enlarge applications of rare earth oxides in the coatings industries.



## 5.1.2 Experimental Details

The details of the substrate material, coating formulation and characterisation of the coating are explained in chapter 3.

## 5.1.3. Results

### 5.1.3.1 Coating powder

A commercially available NiCrAlY (particle size: 5/45  $\mu\text{m}$ , H.C.Starck - 413.3) powder with the chemical composition of Ni-22Cr-10Al-1Y was chosen for the deposition of coatings. Fig.5.1 shows that the particles are of spherical shape with wide particle size distribution, ranging from 2 to 35 $\mu\text{m}$ , which are nearly consistent with the nominal size range provided by the manufacturer. A mixture of CeO<sub>2</sub> (0.4 wt %) with 99.99% purity and NiCrAlY powder were dry-ball milled in a conventional rotating ball mill with stainless steel balls as a milling/grinding medium for 8 hrs to obtain the homogenous powder for the deposition of coatings.

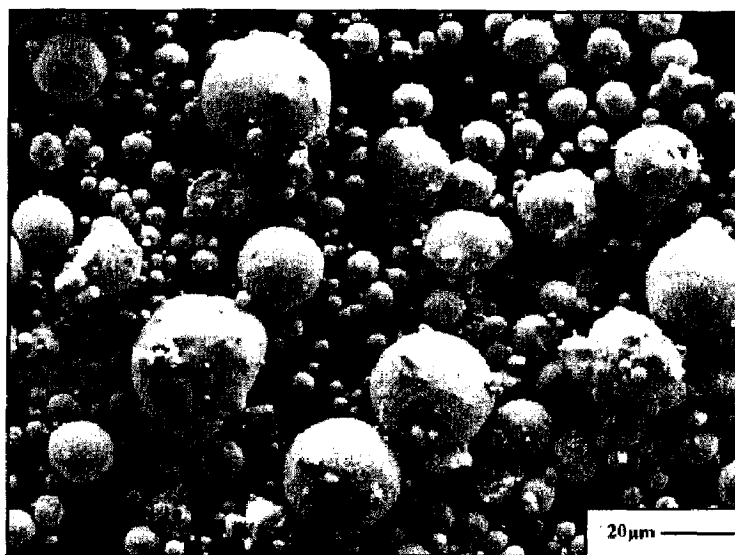
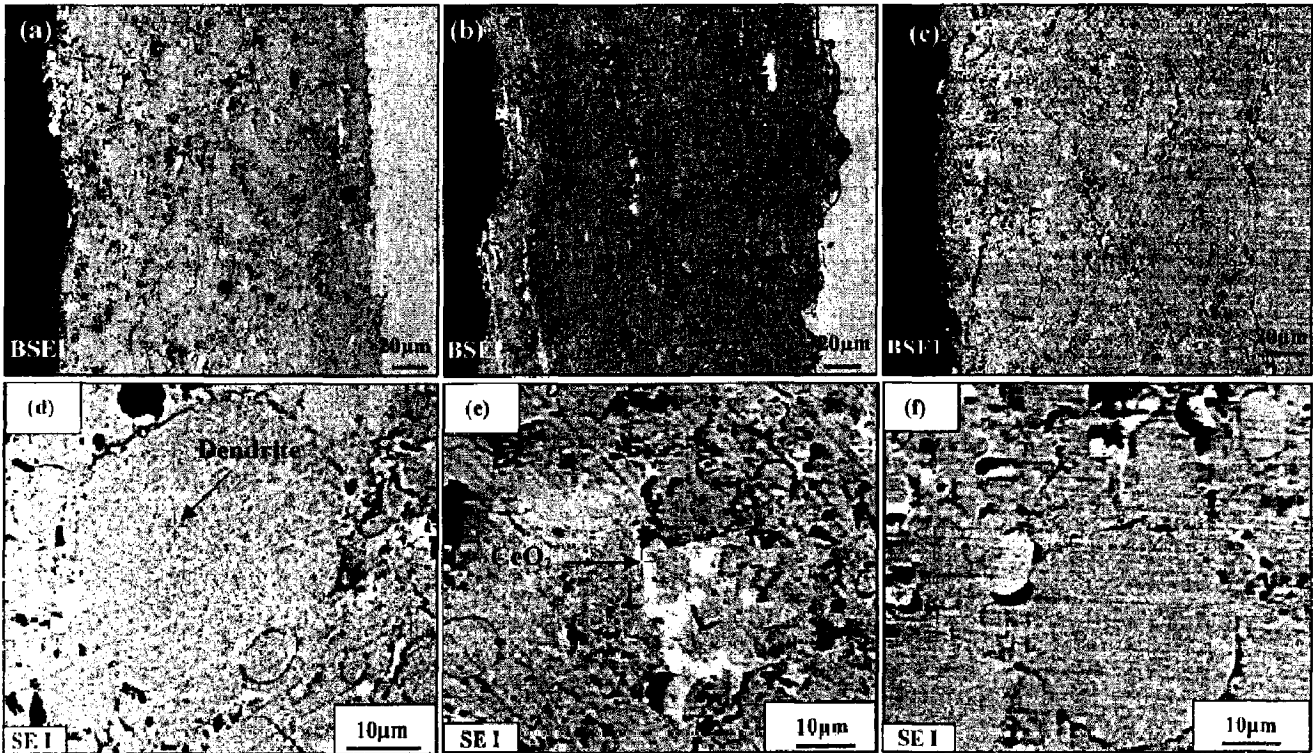


Fig. 5.1 SEM of NiCrAlY + 0.4wt % CeO<sub>2</sub> powder

### 5.1.3.2 Cross-section and surface microstructures of the coating

Fig.5.2 shows the FE-SEM micrographs of NiCrAlY+RE (with 0.4wt% CeO<sub>2</sub>) alloy coating. Along the cross section (Fig.5.2a, b and c), the coating clearly shows the formation of dense, uniform, continuous, adherent splat like structure. Oxides, which are believed to be formed due to the in-flight oxidation of powder particles, appeared as dark areas in the coating. Coating

depicts the absence of cracks and gaps at the coating–substrate interfaces, thereby indicated better adhesion. Surface morphology (Fig.5.2d, e and f) of the as-prayed coating depicts the formation of globular dendritic structure with some traces of cerium oxide.



**Fig. 5.2** SEM micrographs showing as-sprayed cross-sectional and surface morphology of Detonation gun sprayed NiCrAlY + 0.4wt % CeO<sub>2</sub> coating on (a and d) superni 75, (b and e) superni 718 and (c and f) superfer 800H respectively.

### 5.1.3.3 Porosity and coating thickness

Due to the intermittent process during D-gun spraying, few pores are observed in D-gun sprayed coatings (Fig. 5.2). Dense coatings usually provide better corrosion resistance than the porous coatings, as porosities can do harm to the persistent corrosion resistance of the coating (Zhao et al., 2004A, 2005C). The porosity is visible as black contrast regions in the coating and it was less than 0.58 %. Very few micropores are observed near the splat boundaries. The thickness of the coatings was measured from the optical microscope images, taken along the cross section of the mounted samples (Fig.5.2). The thickness of the coatings on three superalloys, superni 75, superni 718 and superfer 800H are 220µm, 250 µm, and 200 µm, respectively (Fig.5.2).

#### 5.1.3.4. Surface roughness (Ra) of the as-sprayed coating

The coating surface was very rough in the as-coated condition due to the presence of un-melted particles and the roughness was found to be in the range of 6.17-6.94 $\mu\text{m}$ . The centre line average (CLA) method was used to obtain the Ra values.

#### 5.1.3.5 Microhardness of the coatings

The microhardness data for the coatings is plotted in the Fig.5.3, which show the microhardness profiles along the cross section of the coatings as a function of distance from the coating-substrate interface. The microhardness of the substrates is found to be in the range of 287-520 Hv and that of coating in the range of 697-920Hv along the cross section. Further, an increase in microhardness of all the substrates is observed near the coating-substrate interface.

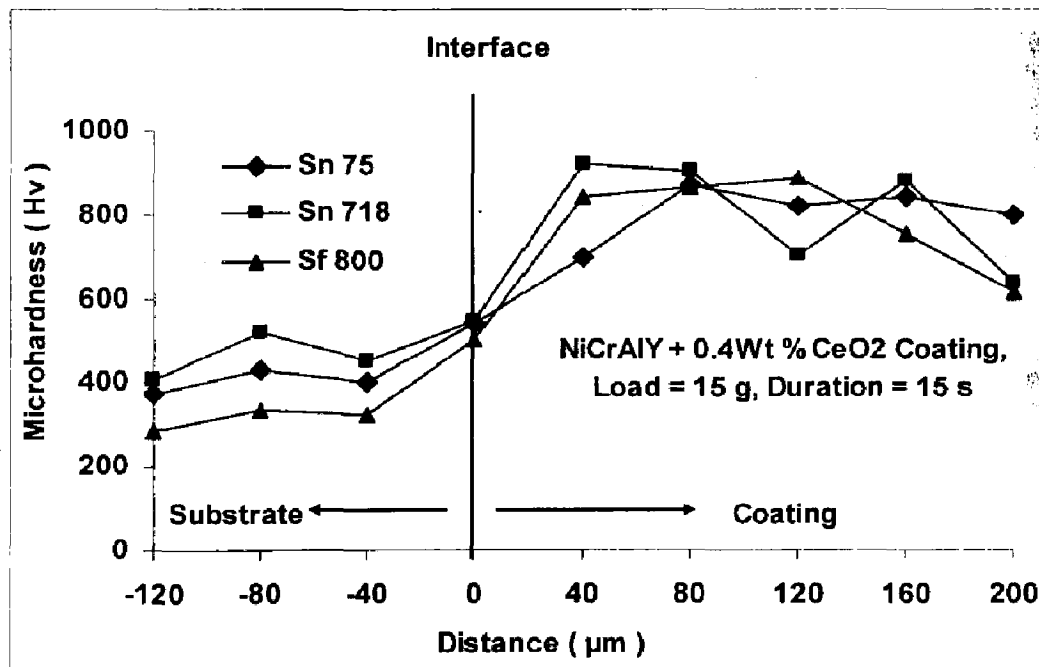


Fig. 5.3 Microhardness profiles for Detonation-gun sprayed NiCrAlY+0.4wt%CeO<sub>2</sub> coating on different superalloys.

#### 5.1.3.6 X-ray diffraction (XRD) analysis

XRD patterns of the NiCrAlY+0.4wt%CeO<sub>2</sub> powder and D-gun sprayed NiCrAlY+0.4wt%CeO<sub>2</sub> coatings are shown in Fig. 5.4. It shows the formation of  $\gamma$ -Ni (nickel solid solution) and  $\gamma'$ -Ni<sub>3</sub>Al as major phases.

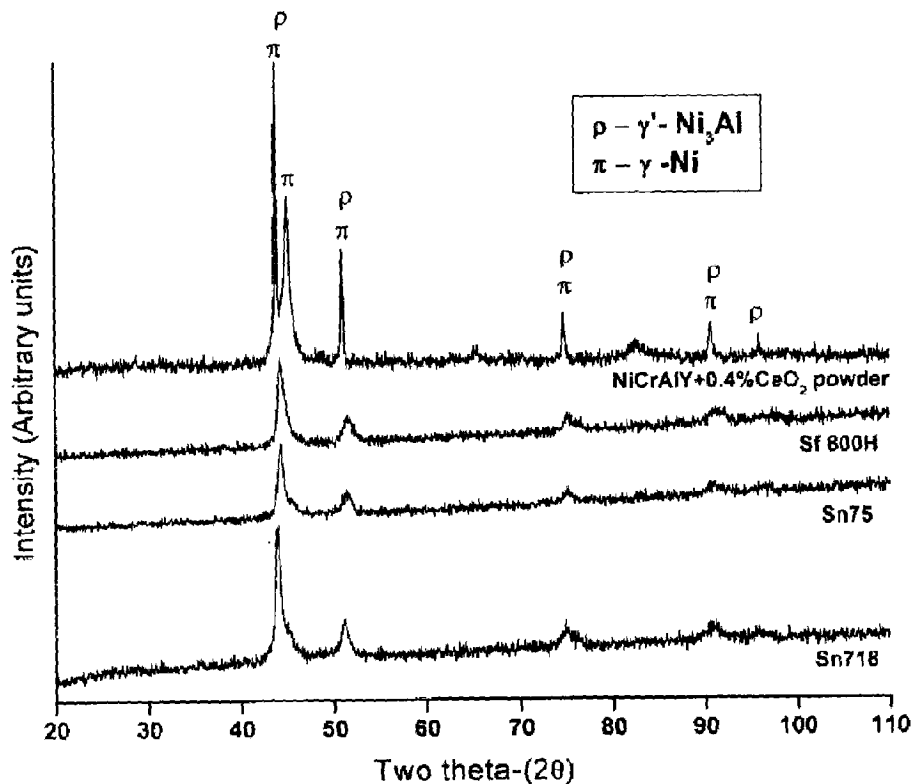


Fig. 5.4 X-ray diffraction for the NiCrAlY+0.4wt%CeO<sub>2</sub> powder and coating on different superalloys

### 5.1.3.7 FE-SEM/EDS analysis

#### 5.1.3.7.1. Surface morphology

FE-SEM micrographs with EDS (Energy Dispersive X-Ray Spectrometry) spectrum reveals the surface morphology of the as-sprayed and polished NiCrAlY+0.4wt%CeO<sub>2</sub> coating on superalloy 75 specimens and shown in Figs.5.5a and b, respectively. As-sprayed surface microstructure of NiCrAlY+0.4wt%CeO<sub>2</sub> coating on superalloy 75 (Fig.5.5a) shows the presence of flat glassy (point 1) and rougher agglomerated zones (point 2). Some traces of cerium oxide distributed along the splat boundary as can be affirmed from white patches in the microstructure (Fig.5.5b at point 3), whereas the dark region at point 4 represents the presence of oxides of Al, also as-sprayed coating depicts the existence of un-melted/or partially melted globular dendritic structure at point 5. The EDS elemental composition at point 1-5 is reported in Table 5.1

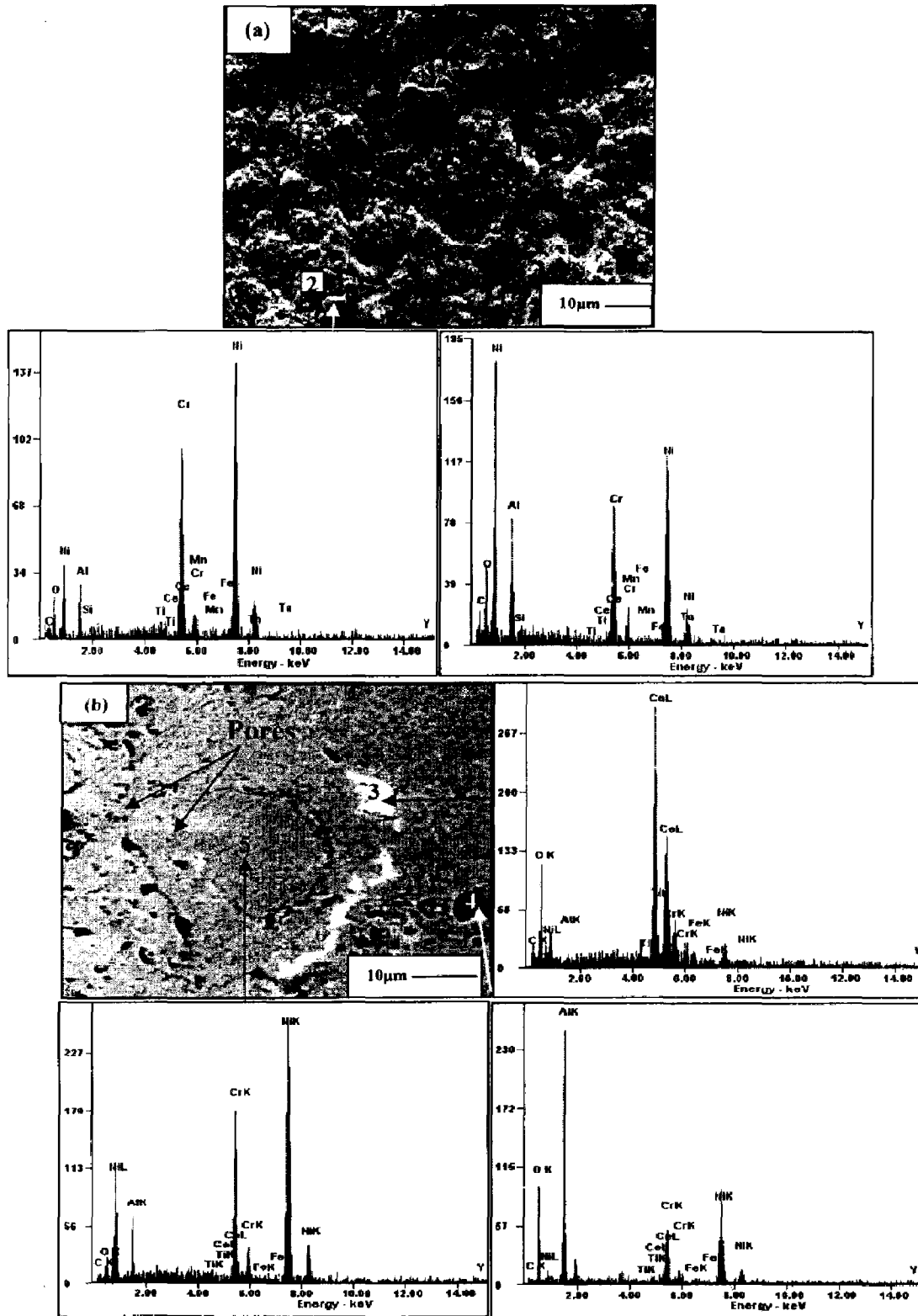


Fig. 5.5 FE-SEM surface micrographs with EDS spectrum of D-gun sprayed NiCrAlY + 0.4 wt%CeO<sub>2</sub> coating (a) as-sprayed superfer 800H and (b) polished superni 75

### 5.1.3.7.2. EDS cross-sectional line analysis

The cross-sectional image and the corresponding EDS point analysis of the NiCrAlY +0.4 wt% CeO<sub>2</sub> coated superalloy superni 718 is shown in Fig. 5.6. It is observed that nickel rich elements predominantly present followed by chromium and aluminum respectively. EDS analysis along the cross-section has detected oxides of Al and Ce along the splat boundaries (Fig. 5.6)

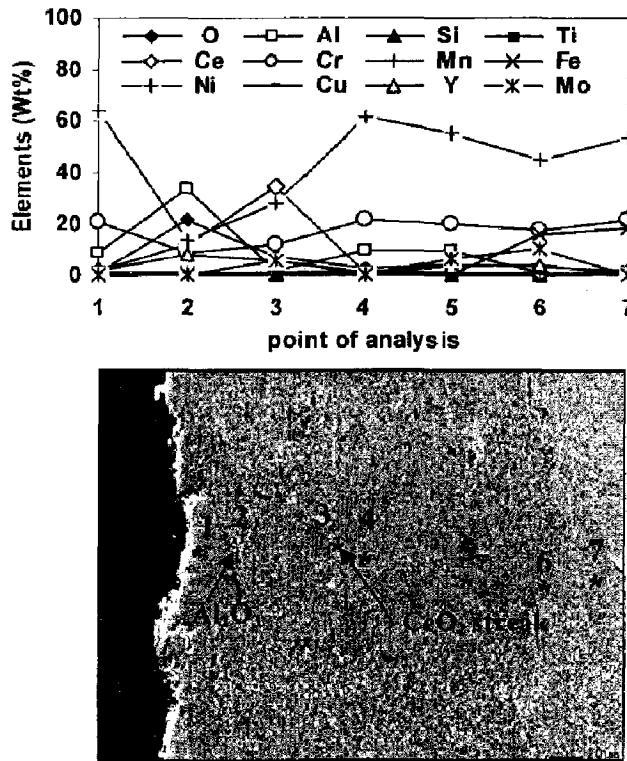


Fig. 5.6 FE-SEM/EDS analysis at the cross-section of as sprayed NiCrAlY+0.4wt% CeO<sub>2</sub> coating on superalloy superni 718

Table 5.1 The EDS elemental composition of the as-sprayed and polished NiCrAlY +0.4 wt% CeO<sub>2</sub> coating on superni 75

Point	1	2	3	4	5
O	11.6	4.4	15.2	21.3	3.0
Al	10.9	9.5	0.7	32.8	9.8
Ce	0.9	2.3	67.4	2.6	0.0
Cr	21.3	20.9	4.9	10.9	21.3
Fe	0.8	0.4	1.2	0.5	0.4
Ni	54.2	62.1	8.6	31.5	62.9
Y	0.0	0.0	1.7	0.0	2.2

### 5.1.3.8 X-ray mapping

The elemental X-ray mappings of the coating show that the coating area indicating the presence of elements of the coating powder. Coated superalloys, Inconel 75, Inconel 718 and Inconel 800H show (Fig. 5.7- 5.9) the Ni rich splats are distributed uniformly throughout the coating, whereas chromium is distributed along Ni rich splat boundaries, Al streaks distributed randomly in the coating. Elemental mapping also show the CeO<sub>2</sub> tinges distributed entire coating along the splat boundaries. Some amount of cerium oxide and chromium diffused into the substrate in all the superalloy substrates.

### 5.1.4 Discussion

D-gun sprayed NiCrAlY+0.4wt%CeO<sub>2</sub> coatings on superalloys, along the cross-section and surface exhibits a dense, adherent and splat like microstructure (Fig.5.2). Little porosity mainly confined to the splat boundaries (Seo et al., 2007). Cerium oxide streaks are present along the splat boundaries (Fig.5.2b and e). Surface morphology of coating depicts the formation of globular dendritic structure composed of Ni and Cr elements. Due to discontinuous powder flow in the D-gun process, several powder particles are attached together and forms big agglomerate. The melting of such joint particles is more difficult than that of small spherical particles, due to which dendritic structure appears in the coating upon partial melting of the powder during D-gun deposition (Fig.5.2d and e). The diameter of the dendrite (Fig.5.2d) is equal to that of original powder particles (Fig.5.1). The agglomerates are not fully melted during spraying; as a result, more un-melted dendritic particles appeared in the coating (Zhang et al., 2003). Porosity measurements were made for the D-gun sprayed coatings, which are found to be less than 0.58%. Due to high velocity and high impact of the sprayed powder particles, the coatings, produced by the D-gun process, exhibit very dense structure with very low porosity. (Yamada et al., 2002) reported that D-gun coatings exhibit extremely low as-deposited porosity. The porosity values of as sprayed coatings are nearly identical with the findings of Mayoral et al., (2008).

Surface roughness is one of the important parameters of the D-gun sprayed NiCrAlY+0.4wt % CeO<sub>2</sub> coatings need to be measured for its better performance in the high temperature applications. For example, in thermal power plants, the coatings employed on the boiler tube components are subjected to solid particle erosion and therefore it is essential to ensure the erosion resistance of the coatings with respect to its surface features such as surface roughness,

adhesive bond strength and morphology of the grain. It may be mentioned that higher surface roughness of the coated component would result in the higher erosion rate, contradictory to this statement the beneficial effect of surface roughness, as reported by Fu et al (2000) and Li et al., 2000, in enhancing fretting fatigue life. During fretting, hard oxide debris formed at the contact surface may cause severe abrasion. However, on a rough surface, the wear debris may escape from the contact area into the adjacent depressions instead of causing abrasion damage. The microhardness of D-gun sprayed coating has been found to be very high as compared to the superalloy substrates (Fig.5.3). Some variations in hardness values across the coating may be due to the presence of micro pores, un-melted and partially melted particles. Hardness is one of the important mechanical properties of the coating need to be measured to ensure its reliability in the actual applications (Tucker et al., 1994). Near the coating-substrate interface, a slightly higher value of hardness is found as compared to the bare substrates. This increased hardness value near the coating-substrate interface might be due to the work hardening effect of sandblasting of the substrates prior to the coating process (Sundararajan et al., 2005B). Hardening of substrate superalloy may also be partly attributed to the high speed impact of the coating particles during D-gun spraying. Similar phenomenon has also been observed in our previous publications (Kamal et al., 2008A and 2008B). Further, the higher values of the hardness of the coatings as compared to the substrate alloys may be partly contributed by the high density and cohesive strength of the individual splats as a result of the high impact velocity of the coating particles as suggested by Rajasekaran et al., 2008; Hao Du et al., 2007 and Park 2007. Ahmed and Hadfield, (1996) analyzed the rolling contact fatigue performance of thermally sprayed (WC-12%Co coatings) rolling element bearing steel balls and reported that the performance of high velocity oxy fuel and D-gun sprayed coatings were superior than that of the plasma sprayed coatings due to their inherent properties such as low porosity, high hardness and compressive residual stresses (Chen et al., 2005). Some difference in the microhardness values on different substrate may be due to minor diffusion of coating elements, such as  $CeO_2$  as evident from the elemental X-ray mapping (Fig.5.7-5.9). Zhenyu et al., (2006) investigated the effects of rare earth oxide  $CeO_2$  on the microstructure and wear resistance of thermal sprayed Fe-Ni-Cr alloy coatings, they compared the results with those for coatings without  $CeO_2$  and observed that the addition of rare earth oxide  $CeO_2$  could refine and purify the microstructure of coatings, and increase the microhardness of the coatings. Zhang et al., (2003) reported the microhardness of D-gun



sprayed NiCrAlY coating as 506Hv, in our present investigation, it is found that the addition of 0.4wt%CeO<sub>2</sub> improved the microhardness of D-gun sprayed NiCrAlY coating, which lies between 697-920Hv. The XRD patterns of as-sprayed coatings reveal the presence of  $\gamma$ -Ni and  $\gamma'$ -Ni<sub>3</sub>Al as a principal phase (Fig.5.4). Similar phases have also been revealed by Zhang et al., (2002 and 2003) for D-gun sprayed NiCrAlY coatings. FE-SEM micrographs with EDS spectrum corresponding to the surface morphology of as-sprayed and polished surface of the coating are shown in Fig. 5.5a and b. The as-sprayed surface is fairly rough, dense and free of cracks, with flat glassy (Fig.5.5a at point 1) represents melted region and partially melted rougher agglomerated zones(Fig.5.5a at point 2) as evident from the results of EDS elemental compositions shown in Table 5.1. The coating has few micropores observed in the dark areas of coating (Fig.5.5b). The polished surface (Fig.5.5b) shows three regions one with the cerium oxide (point 3) phase corresponds to the white patch which is confirmed from EDS analysis as reported in Table 5.1, while dark region shows the presence of Al streaks (point 4) distributed non-uniformly in the coating along the splat boundaries. Chen et al., (2005) and Zhang et al., (2002) have observed similar Al streaks in their studies on air-plasma-sprayed and D-gun sprayed NiCrAlY coating respectively. Further, the light grey region depicts the formation of dendritic structure with basic coating elements (point 5). The presence of Al and Ce oxides in the coatings is supplemented by EDS cross-sectional analysis (Fig.5.6a and b) and X-Ray mapping (Fig.5.7-5.9). The uniform distribution of Ce oxide along the splats relieves the internal stress and purifies the boundaries of grains and phases in the coating as suggested by Tao et al., (2000). Also, the polished surface showed irregular shaped small pits. Although some of the pits are pores, which formed during spraying, these pores might have also got formed due to pullouts of the coating during polishing process. Such type of behaviour was also reported by Li and Ding, (1999)

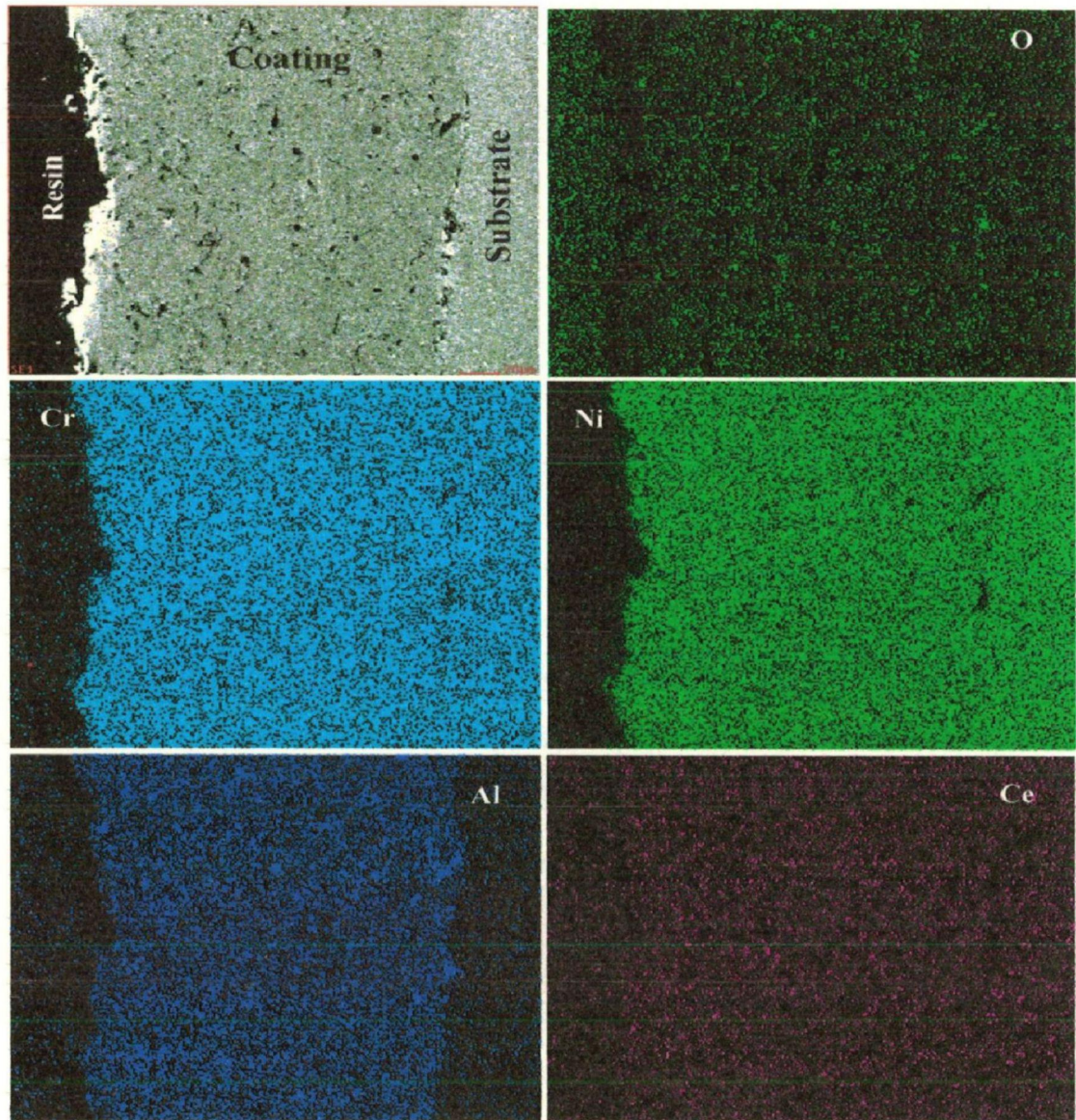


**Fig. 5.7**

Composition image (SEI) and X-ray mapping of the cross-section of the as sprayed NiCrAlY+0.4wt%CeO<sub>2</sub> coated on superni 75 superalloys.



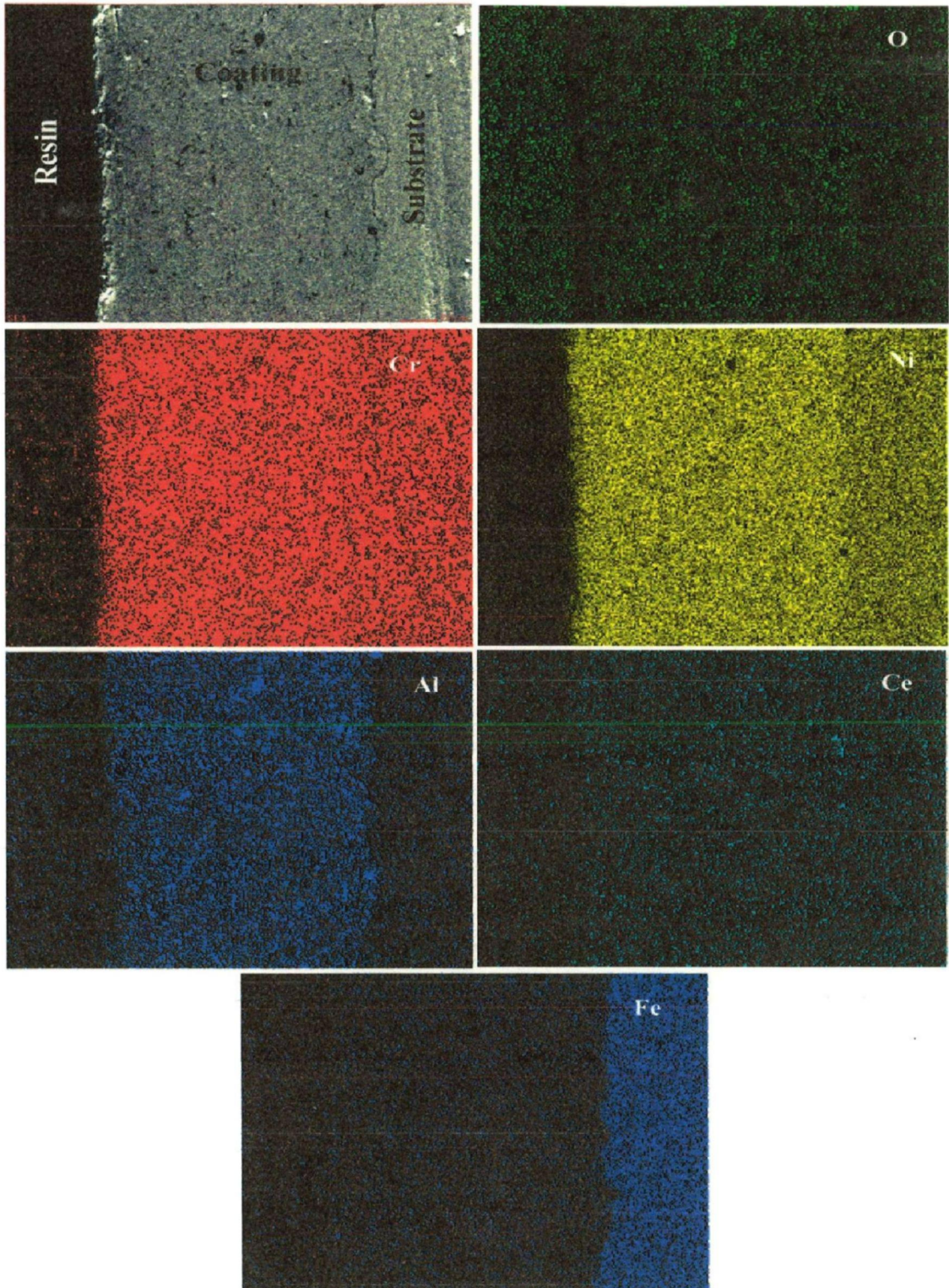


**Fig. 5.8**

Composition image (SEI) and X-ray mapping of the cross-section of the as sprayed NiCrAlY+0.4wt%CeO<sub>2</sub> coated on superni 718 superalloys.



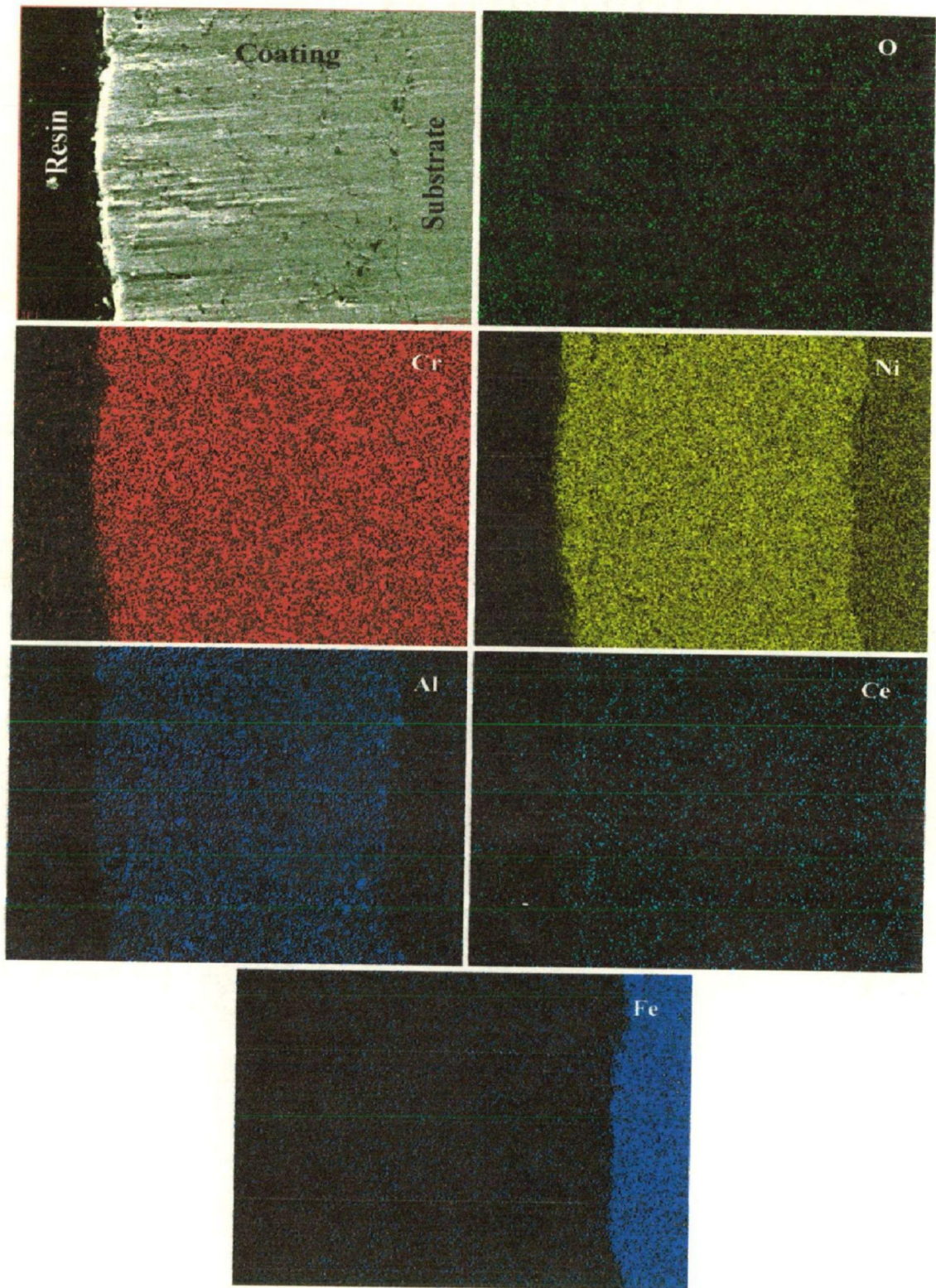


**Fig. 5.9**

Composition image (SEI) and X-ray mapping of the cross-section of the as sprayed NiCrAlY+0.4wt%CeO<sub>2</sub> coated on superfer 800H superalloys.

### 5.1.5 Conclusions

- In the present work, NiCrAlY + RE (with 0.4wt% CeO<sub>2</sub>) coating was deposited on Ni and Fe based superalloys by D-gun spray process.
- The addition of CeO<sub>2</sub> to the NiCrAlY coatings resulted in forming a finer microstructure and a lower percentage of inclusions. Al has been identified as oxide, which appeared along the splat boundaries in the coatings, these oxides are oriented parallel to the substrate surface.
- XRD analysis revealed the presence of  $\gamma$ -Ni or  $\gamma'$ -Ni<sub>3</sub>Al phases in the as-coated NiCrAlY+0.4 wt % CeO<sub>2</sub>.
- Surface morphology of the as-sprayed coating depicts the formation of un-melted particles in the form of globular dendritic structure. The diameter of the dendrites are equal to that of original powder particles. The microhardness of the coating is found to be in the range of 697-920 H<sub>v</sub> and the average porosity was less than 0.58%.
- The thickness of coating ranges from 200-250  $\mu$ m and it showed a good adhesion with the substrate.
- Surface roughness of the coating was found to be in the range of 6.17-6.94  $\mu$ m, respectively.

## 5.2 OXIDATION STUDIES IN AIR

### 5.2.1. Introduction

Thermal spray coatings are frequently used to prevent high temperature oxidation and hot corrosion at elevated temperatures in gas turbines and other equipments (Yamada et al., 2002). The MCrAlY based bond coatings play a significant role in providing rough surface for the application of thermal barrier coatings and to provide protection for the alloy from oxidation and / or hot corrosion, due to proven performance of these coatings for a variety of superalloys for over two decades in different applications (Gurrappa, 2001).  $\text{Cr}_2\text{O}_3$  or  $\text{Al}_2\text{O}_3$  generally regarded as the best protective oxides, with relatively slow diffusion compared to other oxides, many common alloys contain sufficient chromium or aluminum to provide a protective  $\text{Cr}_2\text{O}_3$  or  $\text{Al}_2\text{O}_3$  scale (Sophie Roure et al., 1994). Aluminium concentration less than about 8% were found to be prone to corrosion attack (Rajan Ambat et al., 2000). The addition of small quantities (typically 2% or less) of various elements to high-temperature alloys containing chromium or aluminum (Sophie Roure et al., 1994) and rare earths (Rajan Ambat and Zhou, 2004) has been shown to enhance corrosion resistance. The so-called reactive-element effect has been known for more than 50 years and reactive elements such as Y, Ce, La and Th are commonly used in industry to improve the performance of high-temperature alloys (Sophie Roure et al., 1994). Many metallic components in fuel-conversion or power generating units, invariably, subjected to thermal cycling or thermal fluctuations under the actual service conditions, which frequently lead to failure of protective  $\text{Cr}_2\text{O}_3$  or  $\text{Al}_2\text{O}_3$  layers. It allows more aggressive attack of the metallic components by the environments, which necessitated evaluation of coating properties under non-isothermal oxidation conditions (Mitra, et al., 1993). It is observed that the addition of oxides of the rare earth elements ( $\text{CeO}_2$ ) increases the thermal stability of the porous structure (Mokhnachuk, et al., 2006). Addition of 0.4 Wt % cerium oxides can considerably improve the properties of MCrAlY coating (Tian et al., 2006). It has been demonstrated that when alloys are doped with RE, like ceria, their corrosion resistance at high temperature is improved, this improvement could be attributable to the fact that cerium can enhance the resistance of protective alumina or chromia scale developed during corrosion/oxidation by promoting the adherence and plasticity of the scale as well as reducing its porosity (Zhang and Li. 2000A). It is well known in the literature that, reactive elements such as Y and Ce plays an important role in reducing oxidation rates of alloys and increase oxidation resistance of the fluxing alloy coatings (Zhenyu

et al., 2006). Little information is available in the open literature on high temperature oxidation behaviour of D-gun sprayed NiCrAlY coating with cerium addition on Ni- and Fe-based superalloys. To the authors' knowledge, there is no reported literature on effects of cerium on oxidation behavior of D-gun sprayed NiCrAlY coating. Therefore, the present work has been focused to investigate the cyclic oxidation behaviour of D-gun sprayed NiCrAlY+0.4wt%CeO<sub>2</sub> coatings on three superalloys, in air environment, at 900 °C. The coatings are characterized by XRD, FE-SEM/EDS and X-Ray mapping analysis.

## **5.2.2 Experimental details**

The substrate materials, coating formulation and the oxidation studies are explained in detail in section 3.1, 3.2.3 and 3.4.1

## **5.2.3 Results**

### **5.2.3.1 Visual observations**

Initially the colour of the NiCrAlY+0.4wt%CeO<sub>2</sub>-coated superalloys was light grey, with the progress of oxidation studies, the colour of oxide scale formed on the coated superalloys was dark grey up to 4 cycles. Further, the colour of the oxide scale turned greenish with the progress of oxidation study. For the coated superni 75 and superni 718, high intensity greenish colour is noted on the surface of the specimen, whereas superfer 800H shows light greenish colour on the grey background. Compact and dense scale gradually developed on all the superalloys, although the coatings suffered minor spallation along the corners and near the edges of the specimens as shown in Fig.5.10.

### **5.2.3.2 Weight change measurements**

Weight gain/unit area (mg/cm<sup>2</sup>) versus number of cycles plots for the bare as well as D-gun sprayed NiCrAlY+0.4wt%CeO<sub>2</sub> coated superalloys (superni 75, superni 718 and superfer 800H) oxidised at 900 °C in air for 100 cycles are shown in Fig.5.11. Bare superalloy superfer 800H shows the maximum weight gain than that of the bare superni 75 and superni 718. The weight gain by superni 75 and superni 718 after 100 cycles is nearly 13% and 16% less than that of superfer 800H. The coated superalloys show lower weight gain than the bare specimens in the



given environment. It is found that 13% reduction in overall weight gain for coated superalloys in comparison with the bare superalloys, whereas coated

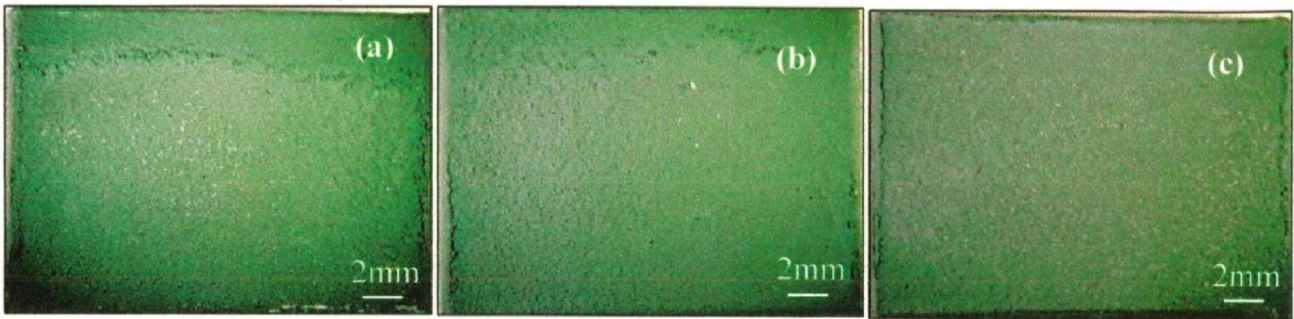


**Fig. 5.10** Surface macrograph of NiCrAlY+0.4wt%CeO<sub>2</sub> coated superalloys subjected to cyclic oxidation in air for 100 cycles at 900 °C, (a) superalloy 75, (b) superalloy 718 and (c) superalloy 800H.

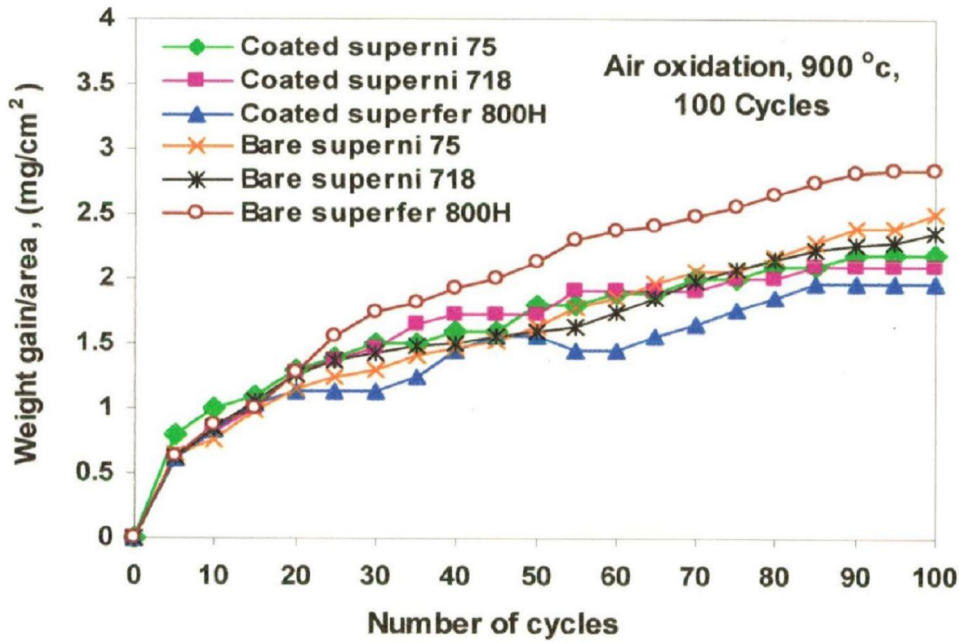


**Fig. 5.11** Weight gain/area vs. number of cycles plot for NiCrAlY+0.4wt%CeO<sub>2</sub> coated and bare superalloys subjected to cyclic oxidation in air for 100 cycles at 900 °C.



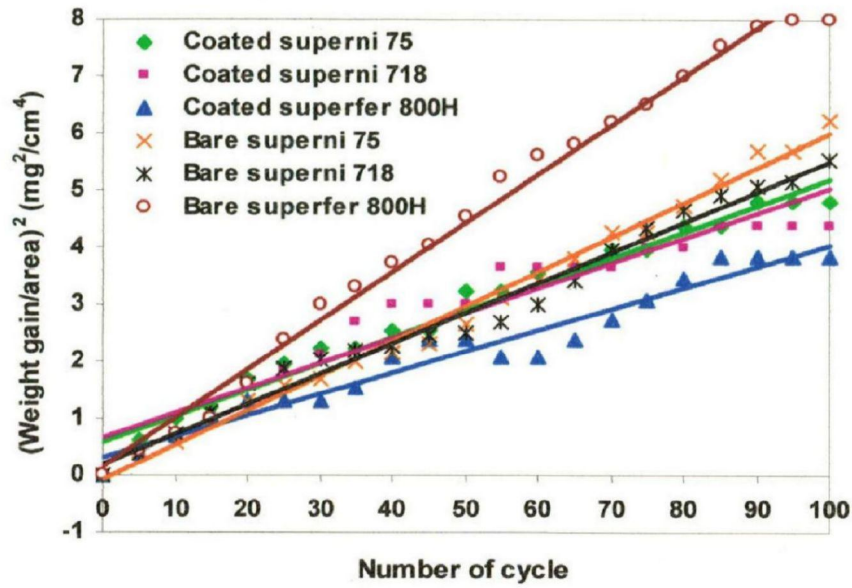


Fig. 5.12

(Weight gain/area)<sup>2</sup> vs. number of cycles plot for NiCrAlY+0.4wt%CeO<sub>2</sub> coated and bare superalloys subjected to cyclic oxidation in air for 100 cycles at 900 °C.

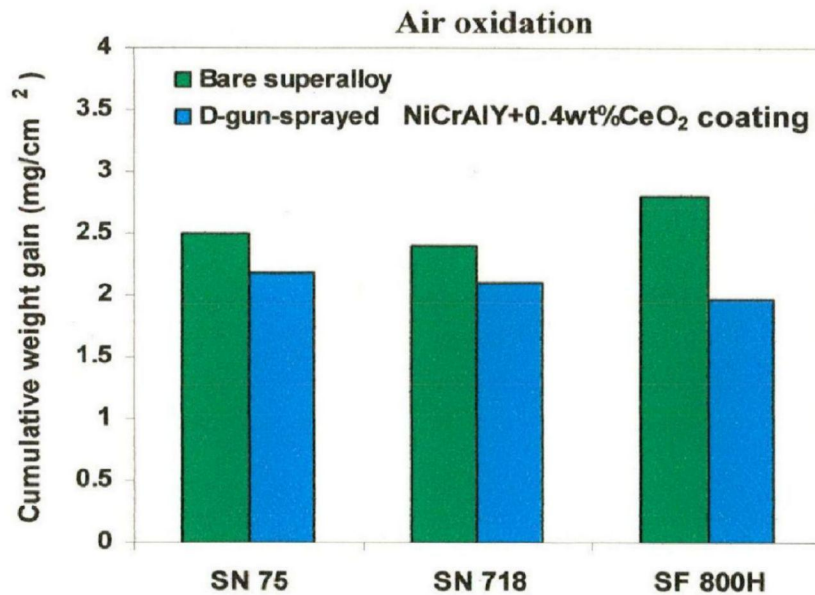


Fig. 5.13

Bar chart showing cumulative weight gain per unit area for bare and NiCrAlY + 0.4Wt%CeO<sub>2</sub>-coated superalloys subjected to cyclic oxidation in air for 100 cycles at 900 °C.

superfer 800H showed 30% reduction in weight gain as compared to bare superfer 800H. All the coated and bare superalloys followed the parabolic rate law except coated superni 718 and superfer 800H, as it slightly deviates from the parabolic law, which is evident from the Fig.5.12. The values of the parabolic rate constant ( $k_p$ ) are shown in Table5.2. It is inferred that the  $k_p$  values for the coated superalloys are less than the bare superalloys. The overall weight gain/unit area for the coated and bare superalloy is shown in Fig.5.13.

**Table 5.2** Parabolic rate constant ( $k_p$ ) values for bare and D-gun sprayed NiCrAlY+0.4wt% CeO<sub>2</sub>-coated superalloys subjected to cyclic oxidation in air for 100 cycles at 900 °C

Superalloy substrates	$K_p \times 10^{-12} \text{ g}^2 \text{ cm}^{-4} \text{ s}^{-1}$
Bare superni 75	16.86
Bare superni 718	16.44
Bare superfer 800H	23.72
Coated superni 75	12.86
Coated superni 718	12.19
Coated superfer 800H	10.44

### 5.2.3.3 X-ray diffraction analysis (XRD) analysis

The various phases identified from the X-ray diffraction patterns of the surface oxide formed on D-gun sprayed NiCrAlY+0.4wt%CeO<sub>2</sub> coated superalloys after cyclic oxidation in air at 900 °C for 100 cycles are shown in Fig.5.14. The surface oxides formed on the coated superalloys indicates the presence of NiCr<sub>2</sub>O<sub>4</sub>, NiAl<sub>2</sub>O<sub>4</sub>,  $\alpha$ -Al<sub>2</sub>O<sub>3</sub>, Ni<sub>3</sub>Al and NiO.

### 5.2.3.4 FE-SEM/EDS analysis

#### 5.2.3.4.1 Surface morphology of the scales

FE-SEM micrographs with EDS spectrum reveals the surface morphology of the NiCrAlY+0.4wt%CeO<sub>2</sub> coated superalloy specimens after cyclic oxidation in air for 100 cycles at 900 °C as shown in Figs.5.15. The surface scale developed on coated superni 75 (Figs.5.15a)

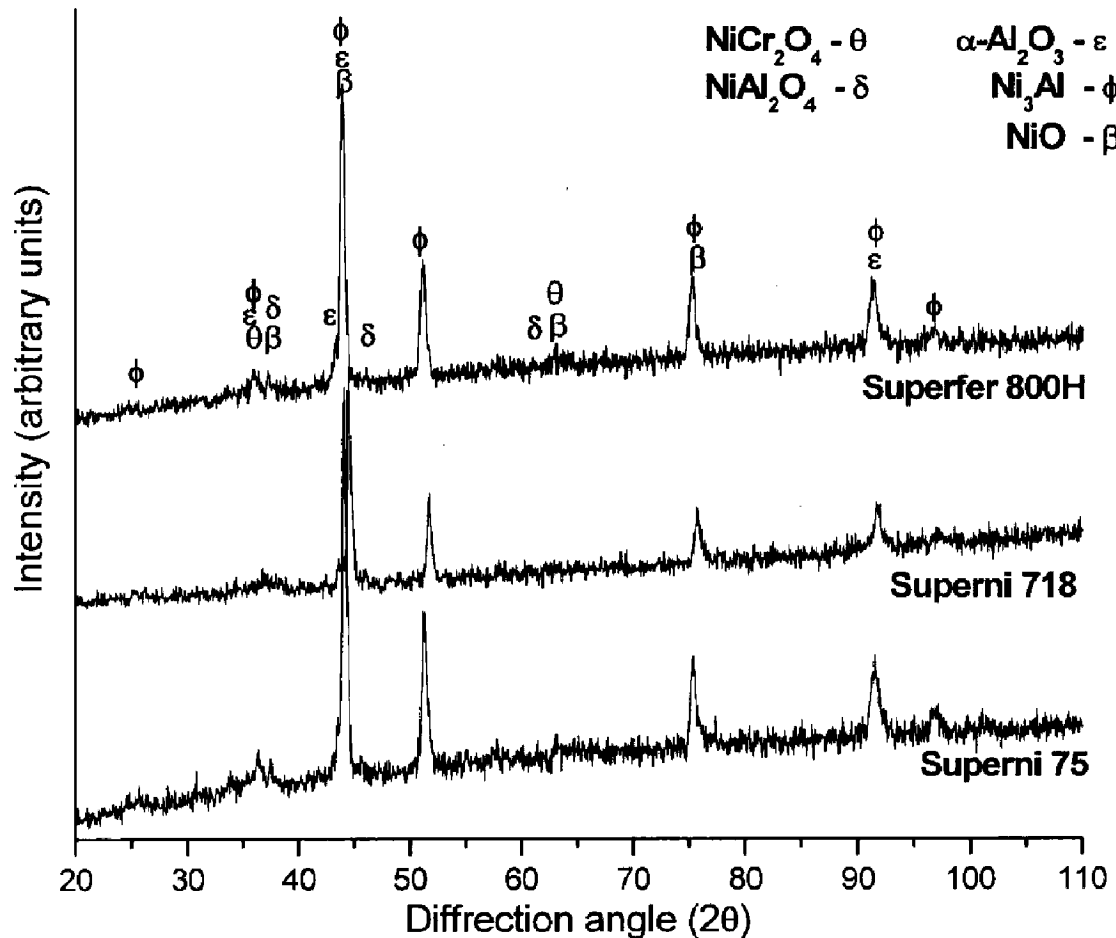


**Fig. 5.14** X-ray diffraction patterns for NiCrAlY+0.4wt%CeO<sub>2</sub> coated superalloys exposed to cyclic oxidation in air at 900 °C after 100 cycles.

is massive and without any cracks. Further, the scale shows globules of different size irregularly distributed in the scale, EDS analysis on these globules shows O, Al, Ni and Cr to be the predominant elements, thereby suggesting the formation of respective oxides and spinels. However, the white phase, mainly consisting of Ni along with Al and Cr which are randomly distributed on these globules. Micrograph of oxidised coated superni 718 appears to be dense and

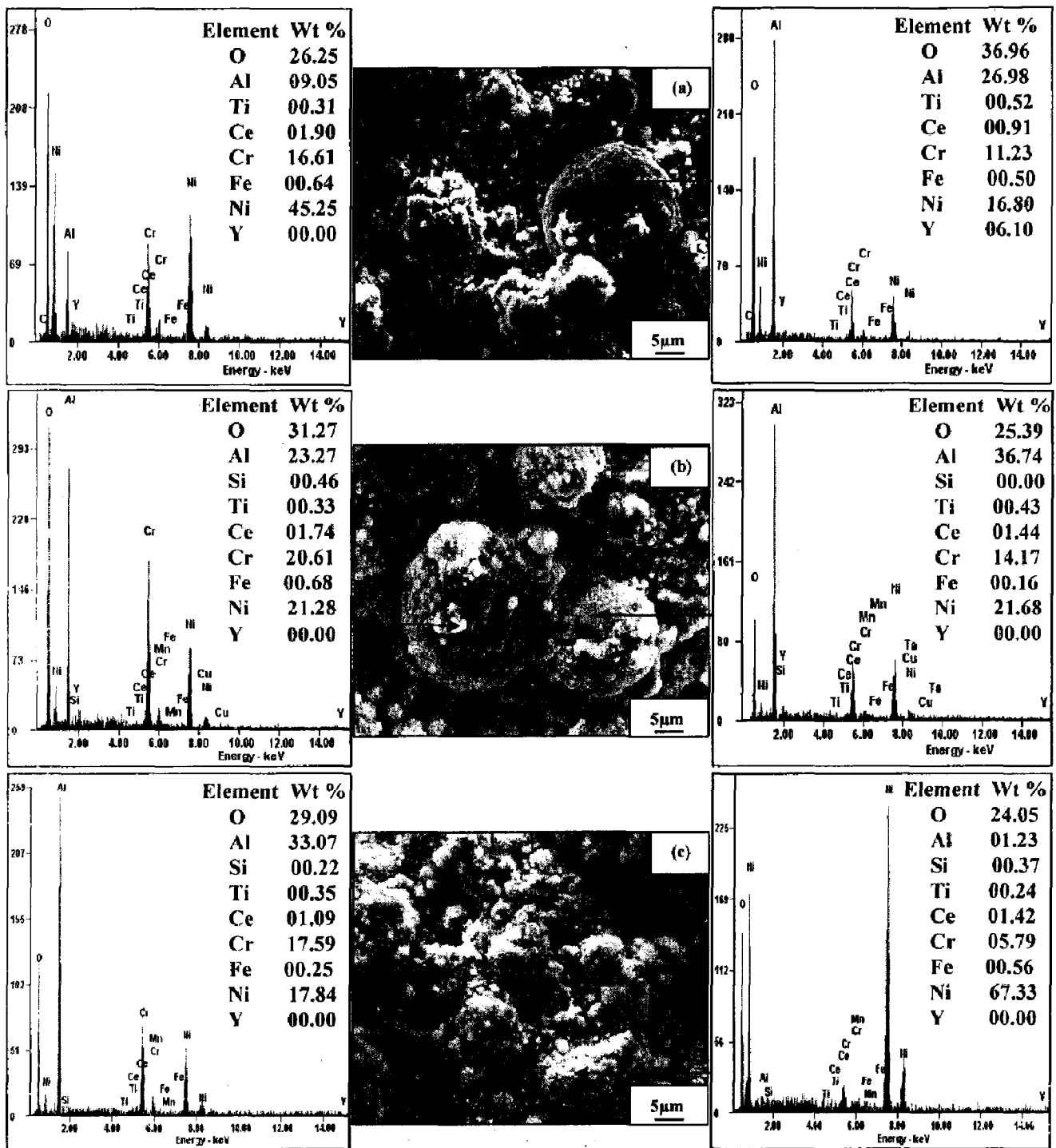


Fig. 5.15 FE-SEM/EDS analysis along with EDS spectrum for NiCrAlY+0.4wt%CeO<sub>2</sub> coated superalloys subjected to cyclic oxidation in air at 900 °C after 100 cycles: (a) superni 75, (b) superni 718 and (c) superfer 800H.

continuous with different size globules (Figs.5.15b), EDS analysis revealed that O and Al are again found to be the predominant element, along with Ni and Cr. Similarly, the scale formed on the coated superfer 800H is dense with major elements of O, Al, Ni and Cr, whereas white region depicts the presence of rich in O and Ni, suggesting the formation of NiO phase (Figs.5.15c).

#### **6.2.3.4.2 Cross-sectional analysis of the scale**

EDS analysis of the scale and the coating was carried out at different points along the cross-section of the air oxidised D-gun NiCrAlY+0.4wt%CeO<sub>2</sub> coated specimens and is shown in Fig.5.16. Cross-sectional EDS analysis of oxidised coated superni 75 reveals (Fig.5.16a) that the uppermost part of the scale has relatively higher concentration of Cr and Ni (point 1), while Al is existing around the Ni rich splats (point 2). Further, point 3, 4 and 5 depict the presence of Ni rich splats. Across the coating-substrate interface (point 6) concentration of Cr increases significantly with depletion of Ni, thereby suggesting the segregation of coating-substrate elements. Inter-diffusion of Cr from coating in to the substrate and Ni from the substrate in to the coating has occurred, as evident from EDS analysis at point 7 (Fig.5.16a). Coated superni 718 (Fig.5.16b) shows the presence of Ni, Cr and Al rich elements in the top most layer, The existence of significant quantity of oxygen at black contrast spot (18.78 wt. % at point 2) along with Al and Ni depicts the formation of Al<sub>2</sub>O<sub>3</sub> and NiO. Further, along the cross-section of coating, (points 3, 4 and 5) Ni-rich splats are found; absence of oxygen at these points suggests that these Ni-rich splats are in the un-oxidised state. The presence of alumina at the coating-substrate interface may be due to grit blasting of the substrate prior to the coating. The possibility of aluminum at the coating-substrate interface may be due to entrapped alumina particles, which might have retained in the asperities during grit blasting of the substrate prior to deposition of the coatings (point 6). Whereas, superfer 800H indicates continuous, adherent oxide scale (Fig.5.16c). Nearly circular Ni-rich splats are distributed in the coating; along these splat boundaries Al is found. Presence of oxygen (point 2) along the splat boundaries indicates the formation of oxides of Al. At point 3, 4 and 5, the concentration of Ni is decreases with the increase in Cr percentage. Further, along the coating-substrate interface (at point 6) concentration of Cr increases significantly with depleted Ni.

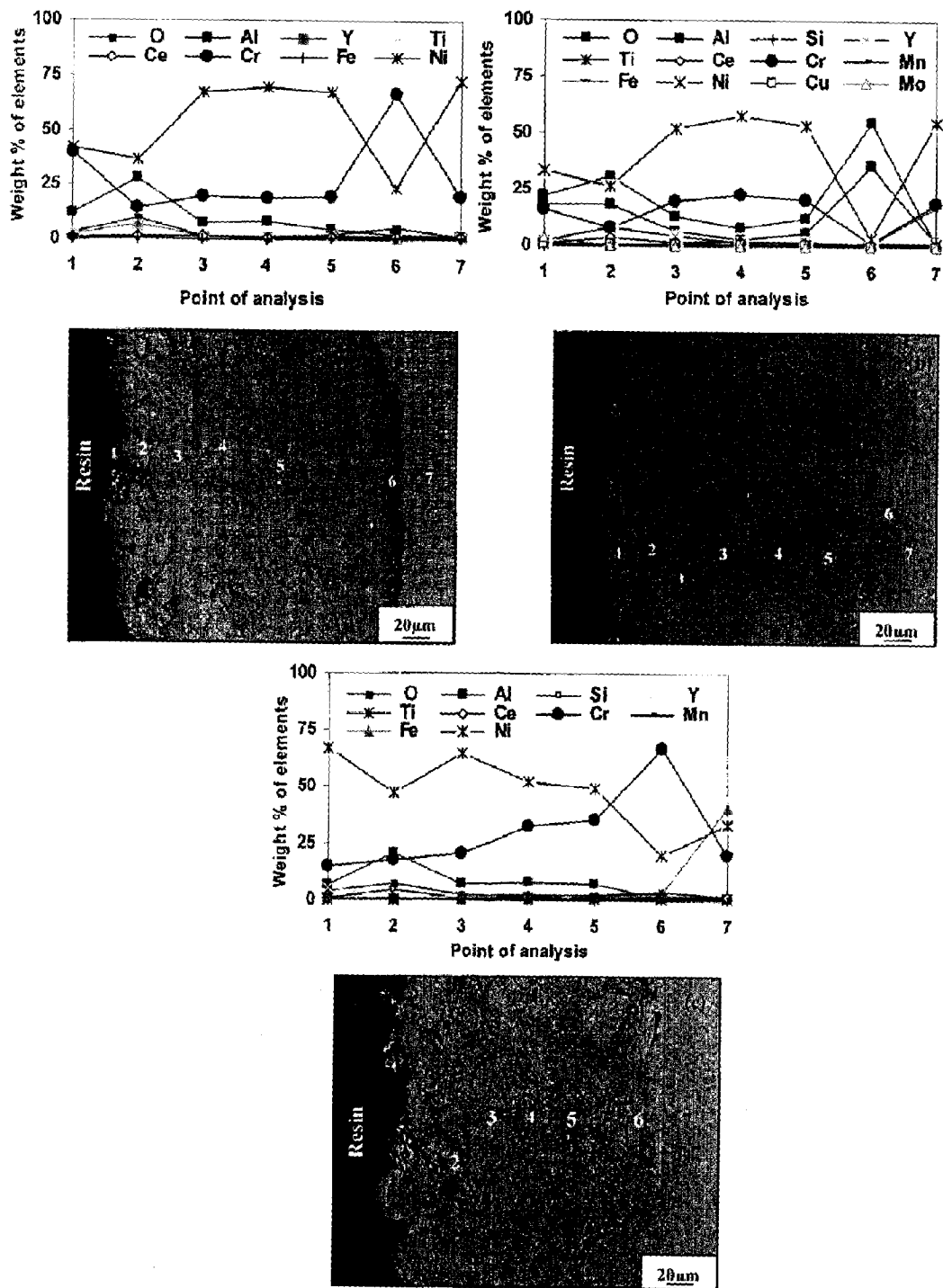


Fig. 5.16 Morphology of oxide scale and variation of elemental composition across the cross-section of NiCrAlY+0.4wt%CeO<sub>2</sub>-coated superalloys subjected to cyclic oxidation at 900 °C in air after 100 cycles: (a) superalloy 75, (b) superalloy 718 and (c) superalloy 800H.

### 5.2.3.5 X-ray mapping

FE-SEM/EDS, BSEI-X-ray mapping of air oxidised NiCrAlY + 0.4 wt% CeO<sub>2</sub> coated superni 75 (Fig.5.17) indicate the formation of a scale containing mainly nickel and chromium, with some traces of aluminum. In the sub scale region, the splats are rich in Ni containing chromium and aluminum at the splat boundaries, black chunks and halfpenny shaped areas are mainly consisting of oxides of Al distributed along the Ni-rich splat boundaries. Chromium shows a tendency to form a thick band along the coating-substrate interface, where all other elements are found to be depleted. The topmost layer of the scale found with traces of iron indicates its diffusion behaviour from the substrate to the coating. X-ray mapping for coated superni 718 after 100 cycles of oxidation in air environment at 900 °C (Fig.5.18) indicates the formation of a dense and thick scale containing mainly oxygen, nickel, chromium and aluminum in the top surface. Below the upper most part of the scale, the coating has, un-reacted Ni-rich splats, whereas Cr and Al have oxidised and distributed along these splat boundaries, as evident from oxygen distribution. Iron shows a relatively higher concentration just above the coating-substrate interface suggesting the diffusion of iron from the substrate to the coating. Tinges of cerium oxide and silicon were found in the coating along splat boundaries. The presence of alumina at the coating-substrate interface may be due to grit blasting of the substrate prior to the coating. Similarly, X-ray mapping of NiCrAlY + 0.4 wt% CeO<sub>2</sub> coated superfer 800H after oxidation at 900 °C for 100 cycles is shown in Fig.5.19. X-ray mapping indicates that the coating has Ni-rich splats. The topmost layer of the scale is found to be rich in nickel, aluminum and chromium. Aluminum and oxygen are distributed along the Ni-rich splat boundaries, thereby suggesting the formation of oxides of Al. Similarly, a band of Cr has formed along the coating-substrate interface. Small amount of silicon has penetrated along the splat boundaries and reached top surface of the coating, whereas iron is restricted up to the coating-substrate-interface.

### 5.2.4 Discussion

The greenish colour (Fig.5.10) scale formed on the coated specimens indicates the presence of NiO as a major phase, which is identical with findings of Singh (2003) and Bornstein et al., (1975). Weight gain data for coated and bare superalloys revealed that (Fig.5.11), initially, the weight gain was higher during first few cycles; further, subsequent increase in weight gain is gradual for coated superalloys, whereas in case of bare superalloys, it increases continuously.



Initial high oxidation rate of coated superalloys might be due to entrapped air during D-gun deposition and sheltered in the voids and splat boundaries. Since the cooling of the coating was rapid, there is shortage of time for the residual air to react with the surrounding coating alloys (Zhang et al., 2002) However, the coating underwent in-situ reaction during high temperature oxidation (900 °C) and were partially oxidised, during the subsequent cycles, the formation of oxides have clogged the voids and splat boundaries and acted as diffusion barriers to the inward diffusion of oxygen. This leads to a slow oxide scale growth; consequently, the weight gain is

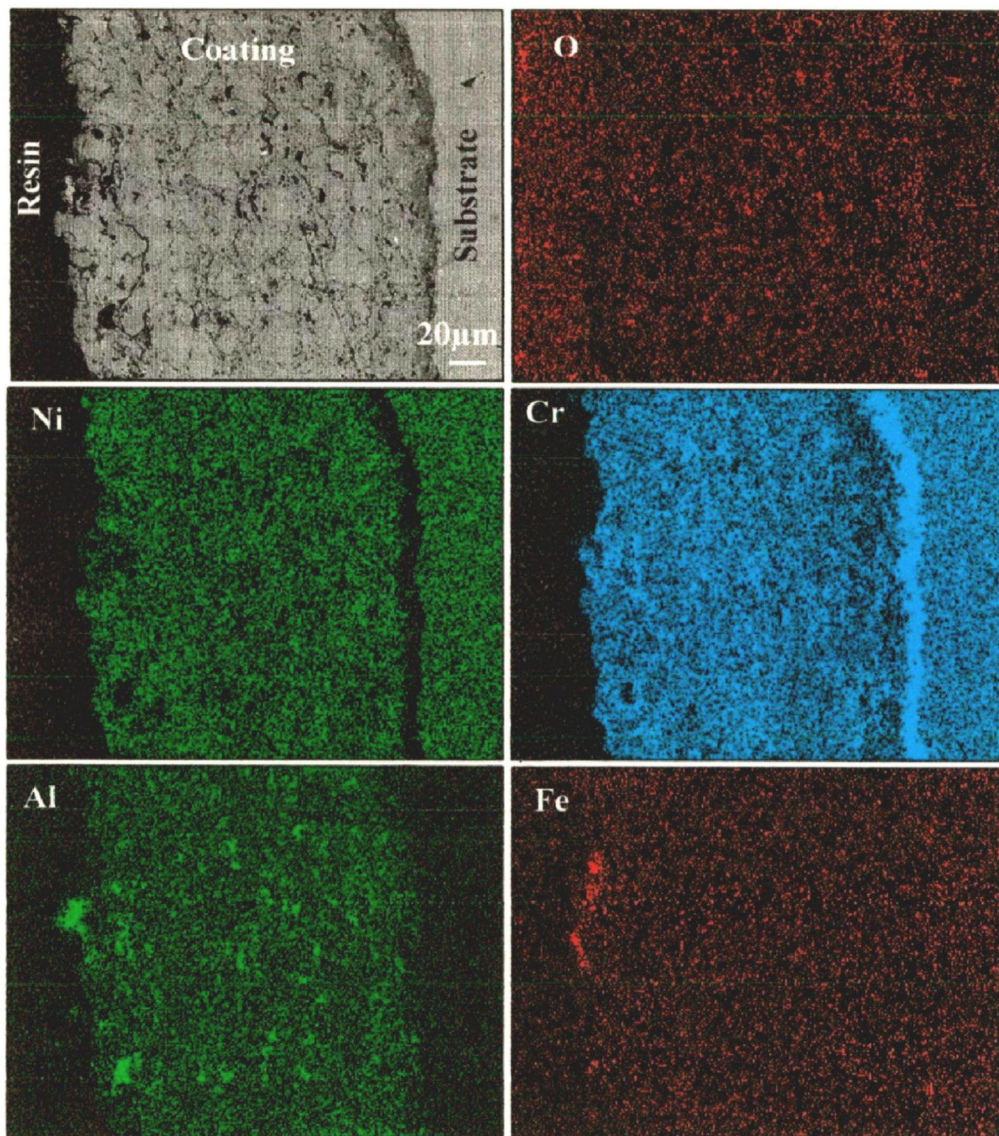


**Fig. 5.17** Composition image (SEI) and X-ray mapping of the cross-section of NiCrAlY+ 0.4 wt %CeO<sub>2</sub>-coated superalloy superalloy superalloy 75 subjected to cyclic oxidation in air at 900 °C after 100 cycles.



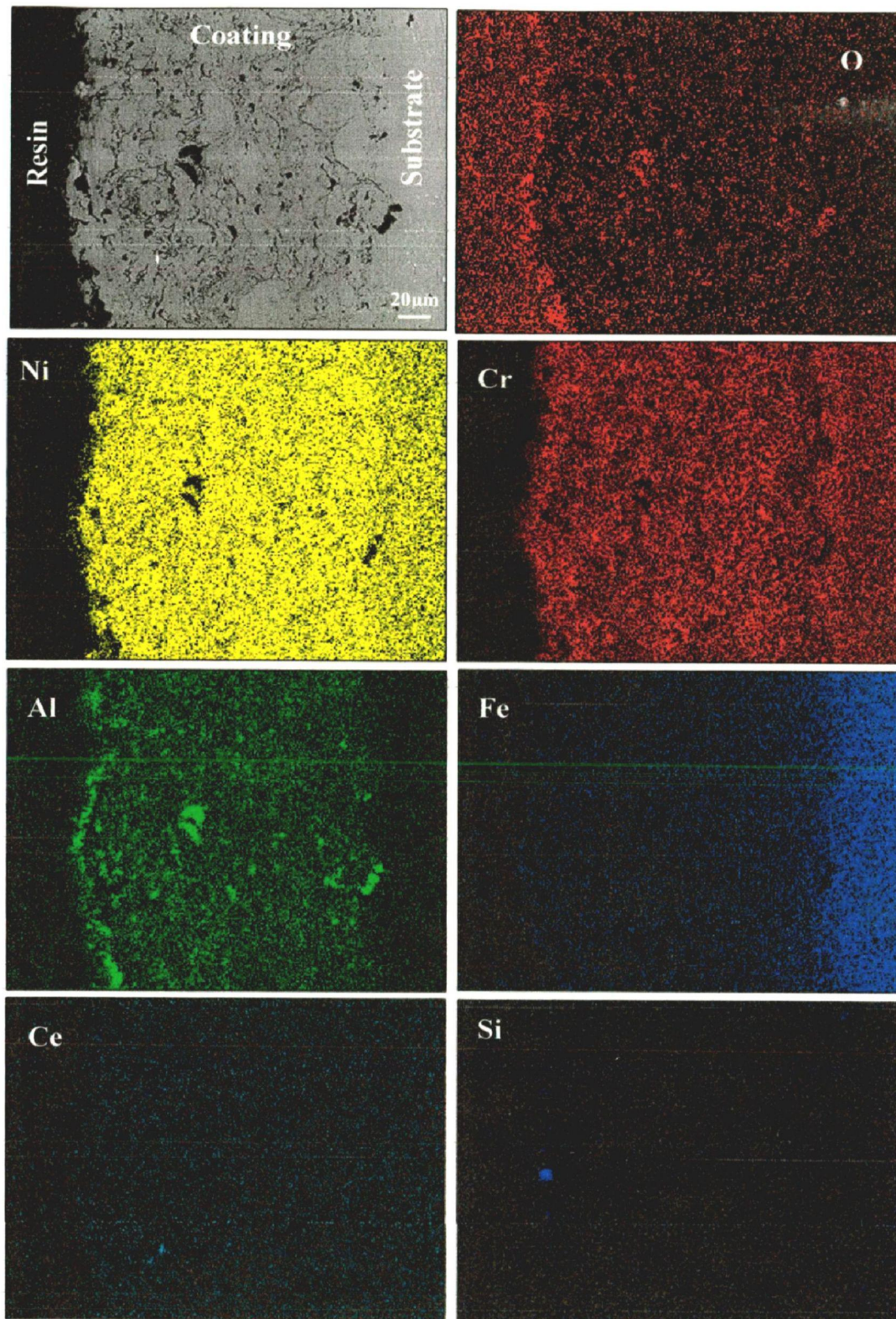


**Fig. 5.18** Composition image (SEI) and X-ray mapping of the cross-section of NiCrAlY + 0.4 wt %CeO<sub>2</sub>-coated superalloy superni 718 subjected to cyclic oxidation in air at 900 °C after 100 cycles.



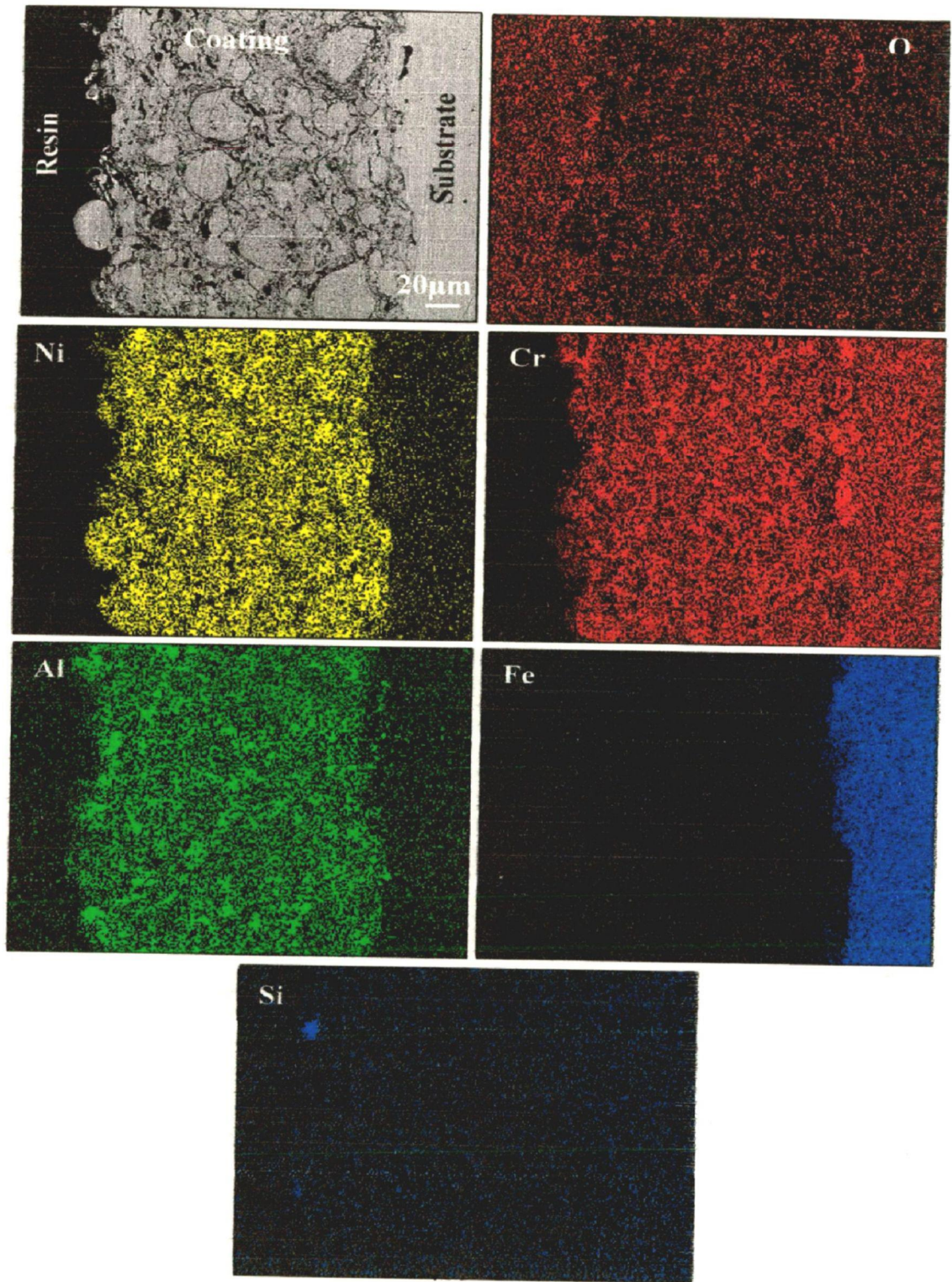


**Fig. 5.19** Composition image (SEI) and X-ray mapping of the cross-section of NiCrAlY + 0.4 wt %CeO<sub>2</sub>-coated superalloy superfer 800H subjected to cyclic oxidation in air at 900 °C after 100 cycles.

low. The weight gain for the coated and bare superalloys (Fig.5.12) follow a parabolic rate law up to 100 cycles, except coated superalloy 718 and superalloy 800H, where it slightly deviates from the parabolic rate law, a small deviation from the parabolic rate law might be due to cyclic scale growth. The values of parabolic rate constant  $k_p$  ( $10^{-10} \text{ g}^2 \text{ cm}^{-4} \text{ s}^{-1}$ ) were obtained from slope of the linear regression fitted line (Fig.5.12) and is shown in Table 5.2. Total weight gain for the coated superalloys is less than for the bare superalloys, which show the protective behaviour of the coating against oxidation. The cumulative weight gain after 100 cycles of oxidation for coated superalloy 75, superalloy 718, and superalloy 800H alloys are 2.19, 2.1 and 1.96  $\text{mg/cm}^2$  respectively (Fig.5.13). The overall weight gain of 2.5, 2.4, and 2.8  $\text{mg/cm}^2$  for bare superalloys superalloy 75, superalloy 718, and superalloy 800H, respectively was observed. The coating provides the maximum oxidation resistance to superalloy 800H as it reduces the weight gain by around 30% of that without a coating. Coatings on superalloy 75 and superalloy 800H superalloys reduce the weight gain by 13% each as compared to the bare superalloys, respectively. The better oxidation resistance shown by the coated superalloy 800H is also indicated by lower weight gain and lower parabolic rate constant ( $10.44 \times 10^{-10} \text{ gm}^2 \text{ cm}^{-4} \text{ s}^{-1}$ ). Further, the scales formed on the coated superalloy 800H superalloys were found to be dense, compact and without any spallation/sputtering or peeling of the scale. Presence of Si,  $\text{NiCr}_2\text{O}_4$ , NiO,  $\alpha\text{-Al}_2\text{O}_3$  and respective spinels might have further contributed to the lower weight gain. During high temperature oxidation, Zhang et al., (2002) reported that aluminum oxide formed in the voids, which increases  $\text{Al}_2\text{O}_3$  concentration along the Ni-rich splat boundaries. Further, he reported that, oxygen, which consumed in this reaction, was not provided by the inward diffusion of the outer air, but the air taken into the coating during deposition and sheltered in the voids. Since the solidification of the coating was so rapid that, there is shortage of time for residual air to react with the surrounding alloy, but there is in situ reaction during high temperature oxidation and formed  $\text{Al}_2\text{O}_3$ . The major and minor phases detected at the surface of coated superalloys specimens with the XRD analysis are  $\text{NiCr}_2\text{O}_4$ ,  $\text{NiAl}_2\text{O}_4$ ,  $\alpha\text{-Al}_2\text{O}_3$ ,  $\text{Ni}_3\text{Al}$  and NiO (Fig.5.14). The spinel phase usually has lower diffusion coefficients of the cations and anions than those in their parent oxides (Chatterjee et al., 2001). Above phases in the oxide scale, further supported by the surface EDS (Fig.5.15), cross-sectional EDS (Fig.5.16) and X-ray mapping analyses (Fig.5.17 to 5.19). Singh (2003), Wu et al. (2001, 2002) reported the formation of similar phases. According to Toma et al. (1999), the oxidation resistance of MCrAlY coating based on the formation of  $\alpha\text{-Al}_2\text{O}_3$  in the steady state of

oxidation as it grows very slowly and is thermodynamically stable. In addition to the oxides of Ni, Cr and Al, presence of  $\text{NiCr}_2\text{O}_4$ ,  $\text{NiAl}_2\text{O}_4$  spinels also develops oxidation resistance. Wang et al. (2002, 2003B) have also reported the formation of  $\text{Cr}_2\text{O}_3$  and  $\text{Al}_2\text{O}_3$  phases for the arc ion plated NiCrAlY coating, when oxidised at 900 °C. Whereas Toma et al., (1999) have reported similar phases for oxidised VPS MCrAlY coatings and Choi et al., (2002) for oxidised air plasma spray NiCrAlY coatings. Goward (1998) and Tawancy and Sridhar (1992) have reported that yttrium got segregated along the grain boundaries of  $\text{Al}_2\text{O}_3$ , and lowers the scale growth rates.  $\text{Cr}_2\text{O}_3$  is also best oxide to resist oxidation, as it prevents the dissolution of the protective oxide scale (Wang et al., 2007). As chromium exhibits higher affinity for oxygen to form  $\text{Cr}_2\text{O}_3$  during the earlier stages of oxidation, which acts as a diffusion barrier for the corrosive species as reported by Kamal et al., 2008C. Once the oxides formed at the place of voids, the growth of the oxides becomes limited mainly to the surface of the specimens. This would relatively minimize the weight gain and result in the steady state oxidation behavior with prolonged exposure to high temperature. These oxides, once formed, plug/seal the splat boundaries and all other possible diffusion paths in the coatings, thereby blocking or slowing the penetration of aggressive species. Schematic of the proposed oxidation mechanism of the NiCrAlY+0.4wt%CeO<sub>2</sub> coated superalloy superfer 800H at 900 °C in air after 100 cycles is shown in Fig.5.20.

### 5.2.5 Conclusions

- The NiCrAlY+0.4wt%CeO<sub>2</sub> coating was found to be successful in maintaining its contact to the substrate superalloys during cyclic oxidation for 100 cycles at 900 °C.
- Chromium shows a tendency to form a thick band along the coating-substrate interface, where all other elements were depleted.
- In case of all three coated superalloys, greenish colour oxide scale has formed after air oxidation for 100 cycles at 900 °C.
- The coating provides the maximum oxidation resistance to superfer 800H as it reduces the weight gain around 30% of that of bare superfer 800H superalloy.
- The coating after exposure to air oxidation showed the presence of oxides mainly consisting of Al, Cr, Ni and their spinels in the upper region of the scale.
- Un-oxidised Ni-rich splats, in the subscale region, surrounded by aluminum and chromium oxides were observed.



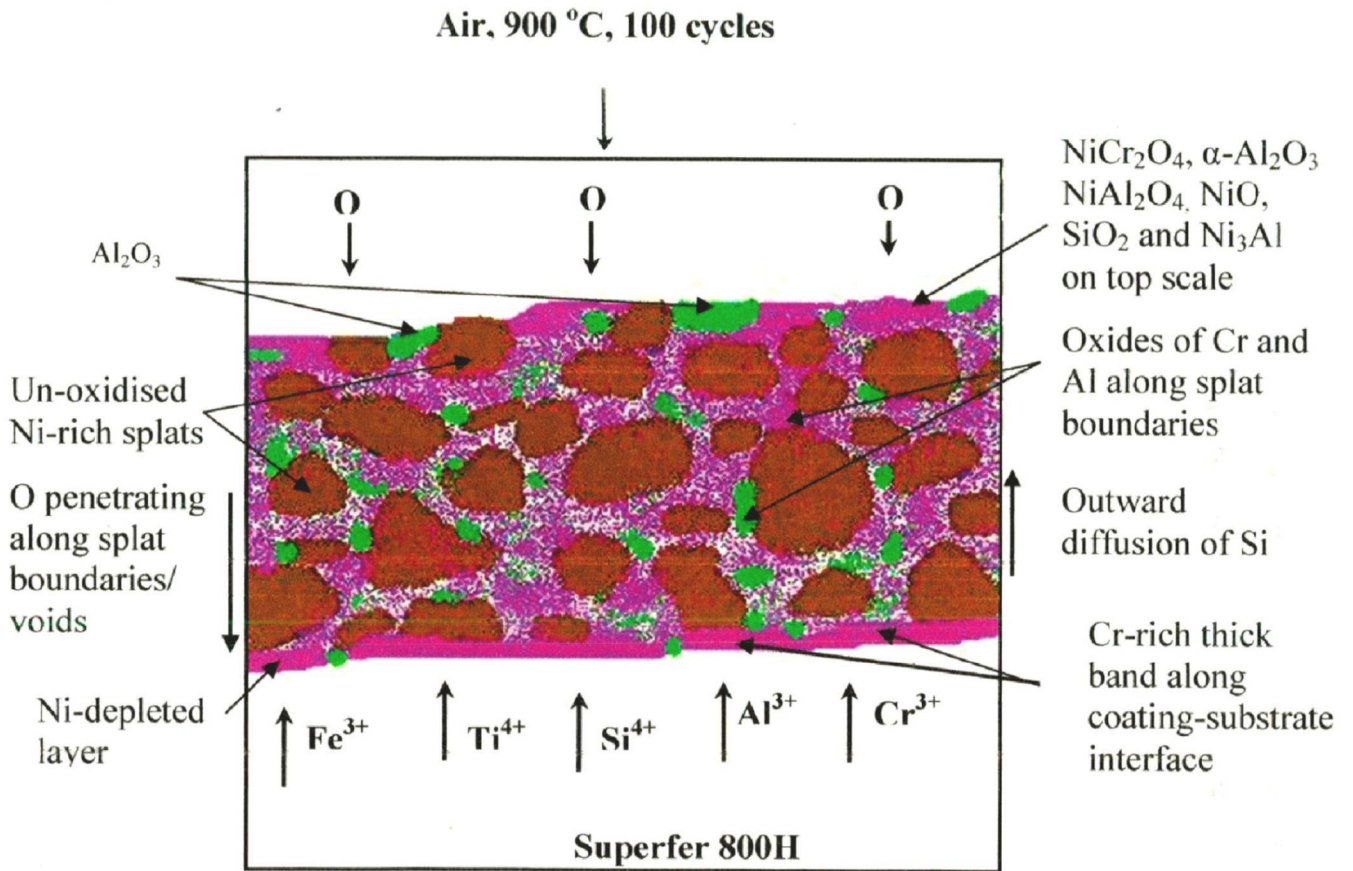


**Fig. 5.20** Schematic of the proposed oxidation mechanism of the  $\text{NiCrAlY}+0.4\text{wt}\%\text{CeO}_2$  coated superalloy superfer 800H at 900 °C in air after 100 cycles.

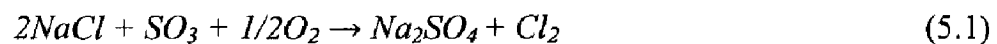
## 5.3 HOT CORROSION STUDIES

### 5.3.1 Na<sub>2</sub>SO<sub>4</sub>–60%V<sub>2</sub>O<sub>5</sub> MOLTEN SALT ENVIRONMENT-I

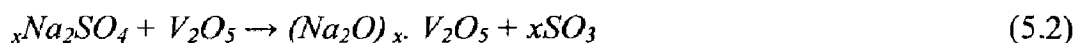
#### 5.3.1.1 Introduction

Superalloys find their largest application in the gas turbine industry, constituting over 50% of the gas turbine weight; these are preferred because of the alloys superior mechanical strength, surface stability, creep and fatigue resistance (Maledi et al., 2006). In utility gas turbines the air and fuel encountered frequently contain corrosive contaminants that can cause serious hot corrosion problems. A wide range of fuel can be used in utility turbines (ranging from clean gas to crude oil) and these fuels can contain sulfur, sodium, potassium, vanadium and lead, as contaminants (Khajavi and Shariat, 2004). Blades within the turbine section of advanced gas turbine engines can operate at temperatures ranging from 650 to 950°C, under highly stressed conditions, and in gas environments which are generally extremely oxidising and which in many cases contain corrosive fuel residues and ingested salts. Therefore new structural materials and coating compositions with improved mechanical properties and greater resistance to high temperature oxidation and hot corrosion, respectively were developed (Tatlock et al., 1987). As these blades are exposed to extremely high temperature, they tend to suffer from significant material degradation during service (Bettge et al., 1995 and Esmaeili et al., 1995).

The corrosion causing elements enter with the air ingested into the turbine inlet and with fuel. For example, turbines operating near the sea coast, on ships, or on aircraft operating close to the ocean surface can ingest Na<sub>2</sub>SO<sub>4</sub> directly as a component of sea water, or NaCl in the sea water can react with the sulfur impurity in the fuel to form Na<sub>2</sub>SO<sub>4</sub> within the engine (Gilbert Santoro et al., 1984) by the following reaction which has been proposed by Khajavi and Shariat, (2004).



Small amount of vanadium may be present in fuel oils, which on combustion forms V<sub>2</sub>O<sub>5</sub>. This may further reacts with Na<sub>2</sub>SO<sub>4</sub> to form low melting sodium vanadates, which are highly corrosive as reported by Sidhu (2006).



During operation, blades and vanes of gas turbines have to withstand both mechanical and thermal loadings as well as chemical attack by oxidation, which increases significantly with temperature. The base material (usually a Ni-base superalloy) provides the necessary mechanical properties and coatings provide a protection against oxidation and corrosion Li et al., (2007).

Recent studies showed that the materials used for high temperature strength are highly susceptible to hot corrosion and the surface engineering plays a key role in effectively combating the hot corrosion and oxidation problems (Kamal et al., 2007A and C). Increasing demands for the high performance superalloy make the surface coatings more favorable than ever, as they offer cost-effective ways to combat degradation resulting from mechanisms such as wear, oxidation and corrosion Zhang et al., (2002 and 2003). Seybolt (1971) studied the role of rare earth additions on the hot corrosion behavior of various Ni based alloys in liquid  $\text{Na}_2\text{SO}_4$  in still air at 1000 °C, and reported that the rate of hot corrosion attack is diminished due to the influence of rare earth, further, it was observed that rare earth addition in the form of oxides are very effective in minimizing the hot corrosion as it forms oxysulfides by combining with sulphur. Gitanjaly (2003) has reported that superficial application of ceria on Fe- and Ni- based superalloys lead to the marked reduction in oxidation rate under aggressive environment of molten salt at 900 °C. She reported that presence of  $\text{CeO}_2$  on the surface led to the possible formation of  $\text{CeVO}_4$ , which may be contributing to the reduction in the corrosion attack, as  $\text{CeVO}_4$  is solid at the reaction temperature of 900 °C. Wang et al., (1998 and 2003A) were the first to introduce rare earth elements to improve wear and corrosion. There is no reported literature so far on the hot corrosion studies of D-gun sprayed NiCrAlY + 0.4wt% $\text{CeO}_2$  coating on the superalloys. The present work, therefore, has been focused to investigate the hot corrosion of NiCrAlY + 0.4wt% $\text{CeO}_2$  coatings deposited on the selected superalloys. Weight change technique has been used to establish the kinetics of hot corrosion of the coated and bare superalloys exposed to molten salt environment,  $\text{Na}_2\text{SO}_4$ -60% $\text{V}_2\text{O}_5$  under cyclic conditions at 900 °C. The microstructural characterizations and phase identifications of the coated samples and corrosion products were carried out by FE-SEM/EDS, X-ray mapping and XRD, respectively, to elucidate the corrosion mechanisms.

### **5.3.1.2 Experimental Details**

The substrate materials, coating formulation and the hot corrosion studies are explained in detail in section 3.1, 3.2.3 and 3.4.3.

### 5.3.1.3 Results

#### 5.3.1.3.1 Visual observations and Weight change measurements

A rough oxide scale with grey colour on thick greenish background has formed on the coated superalloys (Fig.5.21), after hot corrosion studies at 900 °C for 100 cycles in Na<sub>2</sub>SO<sub>4</sub>-60%V<sub>2</sub>O<sub>5</sub> environment. During the course of study, a dense and compact scale gradually developed on all the coated superalloys, salt patches were observed on the background from the 3<sup>rd</sup> cycle onwards which continued up to 21<sup>st</sup> cycle. Surface roughening of the coating was observed from the 17<sup>th</sup> cycle. Colour of the oxide scale formed on the coated superalloy 75 (Fig.5.21a) was dark grey after the first cycle which continued up to 7<sup>th</sup> cycle, after 8<sup>th</sup> cycle, greenish tinges noticed on the surface. But intensity of greenish colour intensified from the 13<sup>th</sup> cycle onwards which continued up to 100 cycles. With the progress of studies, after 15<sup>th</sup> cycle, minor spallation of the scale was noticed near the corners and edges. Grey colour patches on greenish background was noticed in case of coated superalloy 718 (Fig.5.21b), minor spallation of the coating along the sharp corners was observed from the 28<sup>th</sup> cycle onwards. In case of coated superalloy 800H (Fig.5.21c), colour of the oxide scale was dark grey from the initial few cycles, thereafter greenish patches noticed on the surface from 8<sup>th</sup> cycle which intensified from the 13<sup>th</sup> cycle. Spallation in the form of little bulging of the scale was noticed along the edges from 26<sup>th</sup> cycle onwards and towards the end of 100 cycles, coating shows light grey colour on greenish background. The kinetics of hot corrosion was determined from the weight change (mg/ cm<sup>2</sup>) versus time plots for the bare and coated three superalloys subjected to hot corrosion in Na<sub>2</sub>SO<sub>4</sub>-60%V<sub>2</sub>O<sub>5</sub> environment at 900 °C up to 100 cycles as shown in Fig.5.22. The bare superalloy superalloy 800H shows a higher weight gain followed by superalloy 75 as compared with coated one, whereas bare superalloy 718 superalloy has shown a parabolic behavior up to 25 cycles with some spalling/sputtering. With the progress of studies, corrosion products started falling outside the boat; thereby it becomes difficult to monitor actual weight gain. The sputtering continued up to 70 cycles thereafter it has ceased. Further, negligible weight gain was noticed up to 100 cycles. The NiCrAlY+0.4wt%CeO<sub>2</sub> coated superalloys in all cases show a much lower weight gain than the bare specimens in the given molten salt environment. Coated superalloy 800H showed the lowest weight gain, whereas bare superalloy 800H showed highest weight gain. Whereas among coated superalloys superalloy 75 showed highest weight gain followed by superalloy 718 and superalloy 800H respectively. The weight gain by coated superalloy 800H and superalloy 718 after 100 cycles is nearly 45% and 15% less than



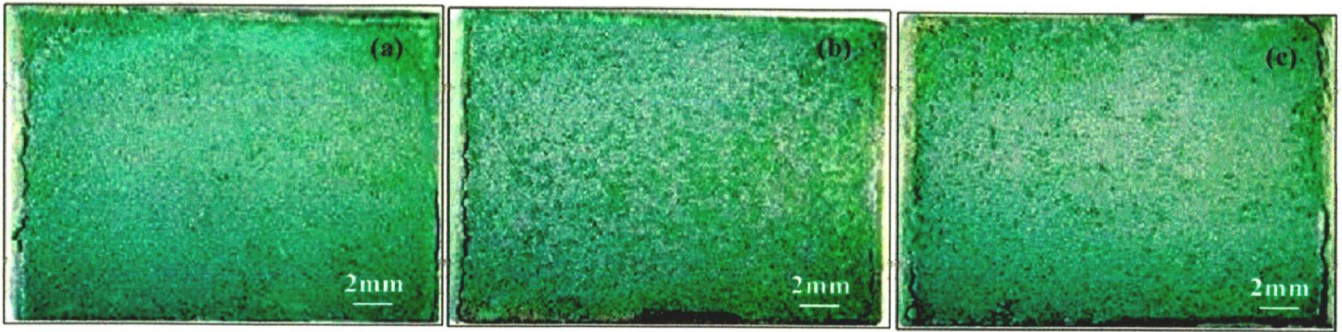


**Fig. 5.21** Surface macrograph of NiCrAlY+0.4wt%CeO<sub>2</sub> coated superalloys subjected to hot corrosion in Na<sub>2</sub>SO<sub>4</sub>-60%V<sub>2</sub>O<sub>5</sub> environment at 900 °C for 100 cycles, (a) Superni 75, (b) Superni 718, (c) Superfer 800H

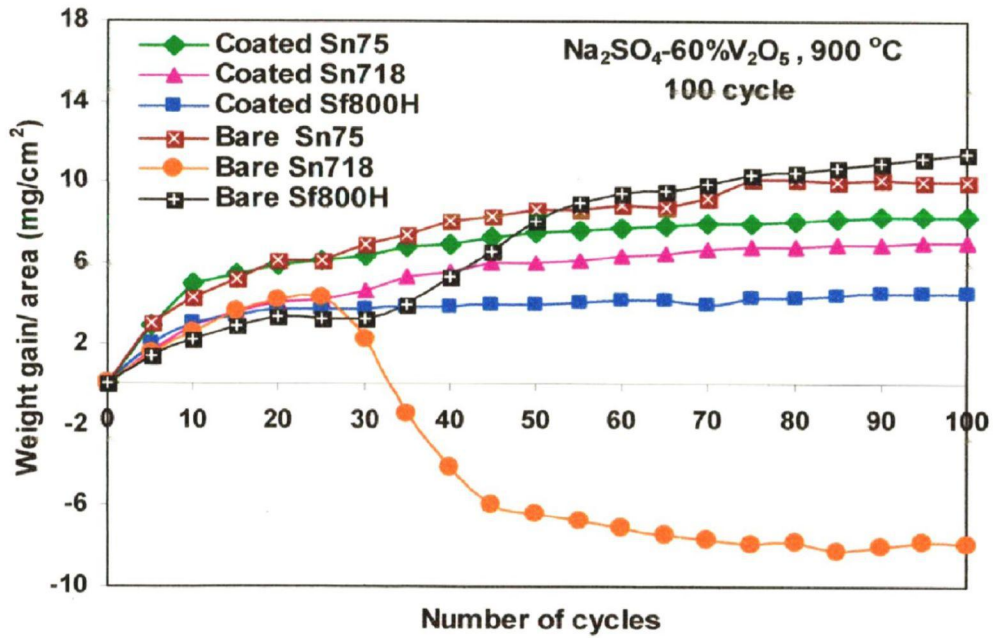


**Fig. 5.22** weight gain/area vs. number of cycles plot for NiCrAlY+0.4wt%CeO<sub>2</sub> coated and bare superalloy subjected to cyclic oxidation for 100 cycles in Na<sub>2</sub>SO<sub>4</sub>-60%V<sub>2</sub>O<sub>5</sub> at 900 °C.

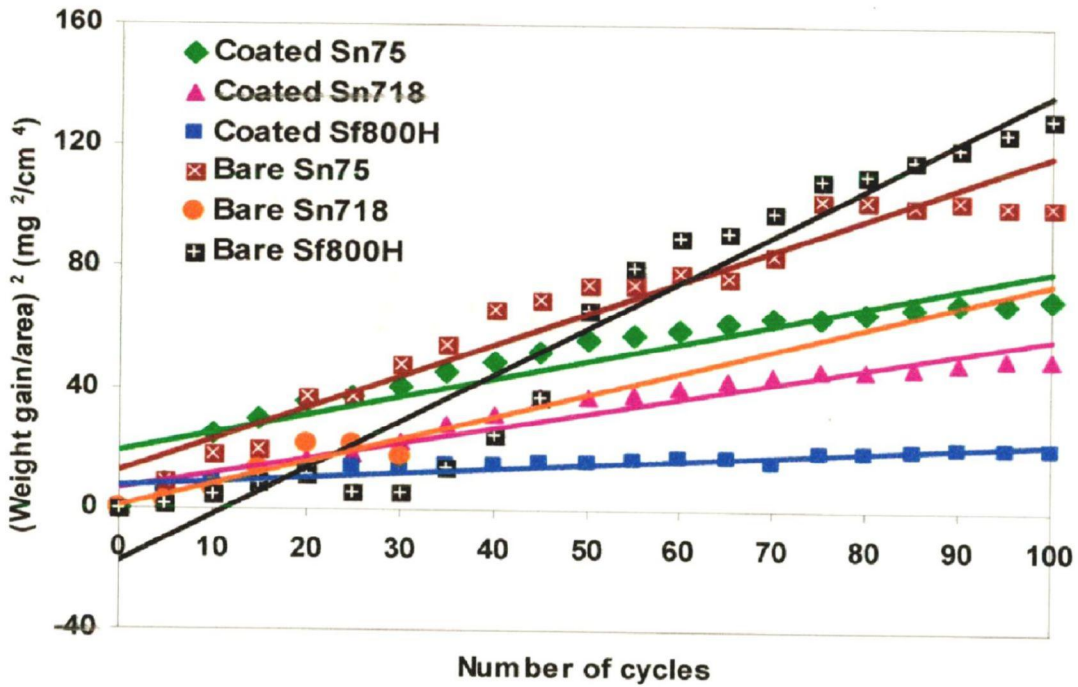


**Fig. 5.23** (weight gain/area)<sup>2</sup> vs. number of cycles plot for NiCrAlY+0.4wt%CeO<sub>2</sub> coated and bare superalloys subjected to cyclic oxidation for 100 cycles in Na<sub>2</sub>SO<sub>4</sub>-60% V<sub>2</sub>O<sub>5</sub> at 900 °C.

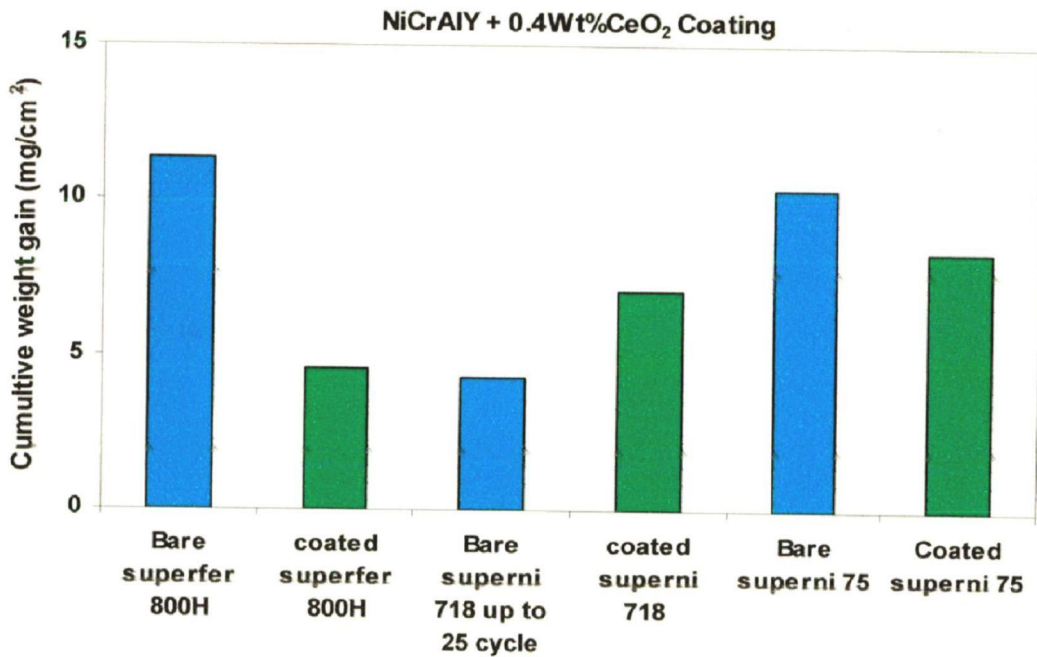


**Fig. 5.24** Bar chart showing cumulative weight gain per unit area for NiCrAlY+0.4wt% CeO<sub>2</sub> coated and bare superalloys subjected to cyclic oxidation for 100 cycles in Na<sub>2</sub>SO<sub>4</sub>-60%V<sub>2</sub>O<sub>5</sub> at 900 °C.

that of coated superalloy 75. It is also found that 60% and 15% saving in overall weight gain for coated superalloy 800H and superalloy 75 in comparison with the bare superalloy 800H and superalloy 75 respectively. In general, the hot corrosion behaviour of both bare and coated samples follow a parabolic rate law, except for bare superalloy 800H, as it slightly deviates from parabolic rate, as can be inferred from the square of weight change ( $\text{mg}^2/\text{cm}^4$ ) versus number of cycle plots shown in Fig.5.23. Table 5.3 shows the values of the parabolic rate constants ( $k_p$  in  $10^{-10} \text{ g}^2 \text{ cm}^{-4} \text{ s}^{-1}$ ) for the coated and bare superalloys for 100 cycles of hot corrosion. Cumulative weight gain per unit area for coated and bare superalloys is shown in Fig. 5.24.

**Table 5.3** Parabolic rate constant ( $k_p$ ) values for D-gun sprayed NiCrAlY+0.4wt%CeO<sub>2</sub>-coated and bare superalloys subjected to cyclic oxidation for 100 cycles in Na<sub>2</sub>SO<sub>4</sub>-60% V<sub>2</sub>O<sub>5</sub> at 900 °C

Superalloys	Parabolic rate constants ( $k_p$ ) ( $10^{-10} \text{ g}^2 \text{ cm}^{-4} \text{ s}^{-1}$ )
Bare superalloy 800H	4.31
Coated superalloy 800H	0.41
Bare superalloy 718	2.10
Coated superalloy 718	1.42
Bare superalloy 75	2.92
Coated superalloy 75	1.68

### 5.3.1.3.2 X-ray diffraction analysis

The X-ray diffraction peaks for the scale of D-gun-sprayed NiCrAlY+0.4wt%CeO<sub>2</sub> coated superalloy after hot corrosion in Na<sub>2</sub>SO<sub>4</sub>-60%V<sub>2</sub>O<sub>5</sub> environment for 100 cycles at 900 °C are as illustrated in Fig.5.25. The major and minor phases detected at the surface of the specimens with the XRD analysis are NiCr<sub>2</sub>O<sub>4</sub>, NiAl<sub>2</sub>O<sub>4</sub>, NiO, Ni, Cr<sub>2</sub>O<sub>3</sub> and Al<sub>2</sub>O<sub>3</sub>.

### 5.3.1.3.3 FE-SEM/EDS analysis of the scales

#### 5.3.1.3.3.1. Surface scale analysis

FE-SEM micrographs with EDS spectrum along with EDS compositional analysis reveals the surface morphology of the NiCrAlY+0.4wt%CeO<sub>2</sub> coated substrate superalloy specimens after cyclic hot corrosion in molten salt environment (Na<sub>2</sub>SO<sub>4</sub>-60%V<sub>2</sub>O<sub>5</sub>) for 100 cycles at 900

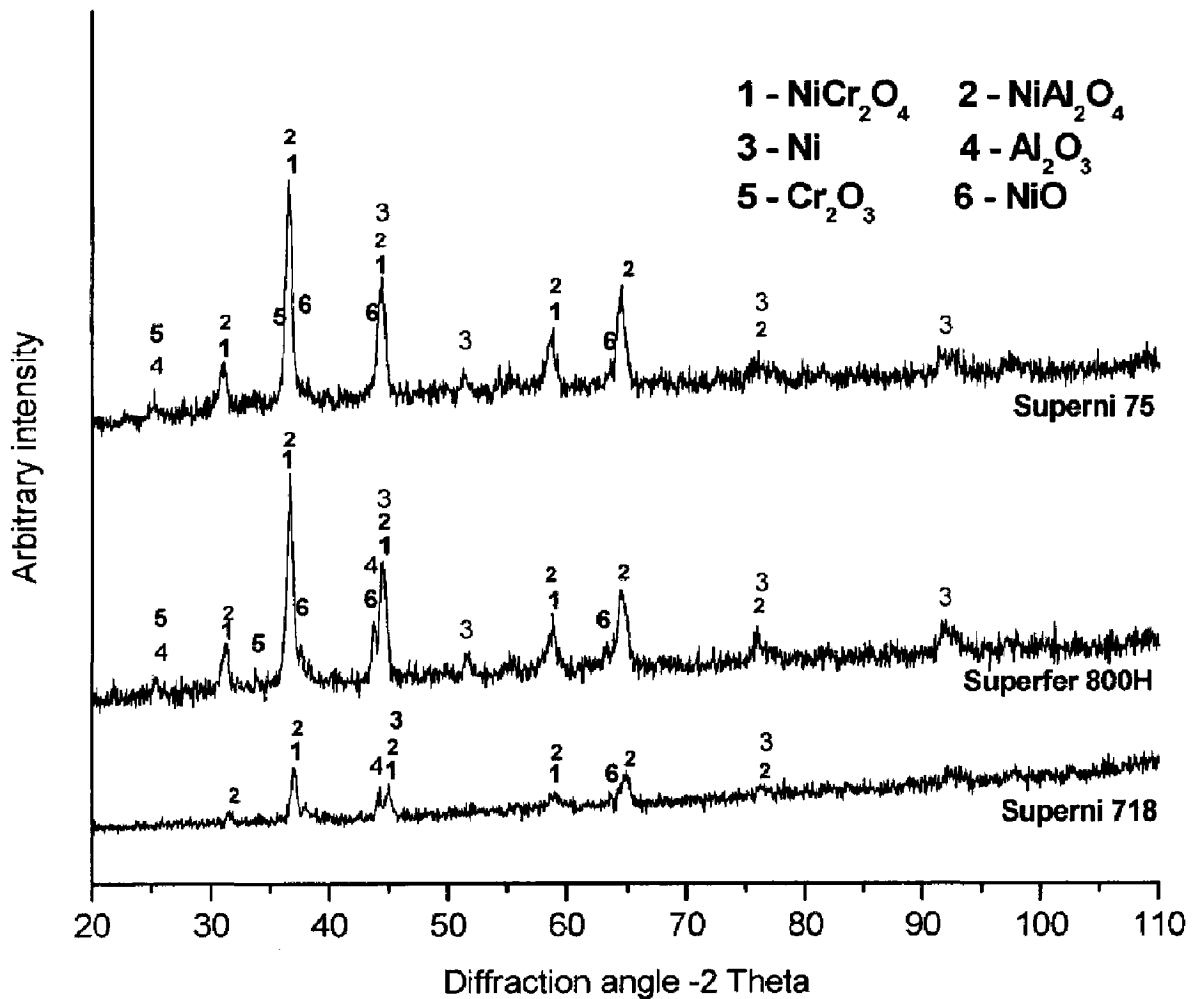


**Fig. 5.25** X-ray diffraction patterns for NiCrAlY+0.4wt%CeO<sub>2</sub> coated superalloys exposed to cyclic oxidation in Na<sub>2</sub>SO<sub>4</sub>-60%V<sub>2</sub>O<sub>5</sub> environment at 900 °C after 100 cycles.

°C are shown in Figs.5.26. The surface scale develop on coated superalloys are dense, adherent with few cracks, the corroded superalloys revealed two regions in the coating; one with dense oxide layer on which irregular shaped group of white NiO granules are non uniformly distributed on the coating surface. The EDS analysis of these white granules shows NiO as a principle phase as evident from the high intensity peaks of EDS spectrum (Fig.5.26a and c). The other region in the coating is of dark with compact and continuous scale, mainly consisting of oxides of Al, Cr and Ni elements of the coatings, as evident from high intensity peaks of EDS spectrum with EDS composition analysis (Fig.5.26a, b and c).

### **5.3.1.3.3.2 Cross-sectional analysis of the scale**

Cross-sectional analysis of the scale and the coating was carried out at different points along the cross-section of the hot corroded D-gun coated superalloys: Inconel 75, Inconel 718 and Inconel 800H by FE-SEM/EDS and the results are shown in Fig.5.27. All the oxidised NiCrAlY+0.4wt%CeO<sub>2</sub> coating on all superalloys show the formation of thin compact, adherent and continuous oxide scale (nearly 10-15µm thick) clearly visible along the cross-section of the coating. EDS analysis of corroded coated Inconel 75 reveals (Fig.5.27a) that the uppermost part of the scale has relatively higher concentration of oxygen along with Ni, Cr and Al (point 1 and 2), suggesting the formation of oxides of Ni, Cr and Al. EDS analysis at point 3 and 5 reveals Ni rich splats, which are in an un-oxidised state due to absence of oxygen at these points. Existence of oxygen at point 4 represents the presence of oxides of Al, non-uniformly distributed in the form of streaks. Thick band of Cr (point 6) concentrated along the coating-substrate interface. Point 7 represents the basic elements of the substrate. Corroded NiCrAlY+0.4wt%CeO<sub>2</sub> coated Inconel 718 (Fig.5.27b) showed the top surface of the coating mostly consisting of a homogeneous, adherent and non-uniform oxide scale with variable thickness, the oxide scale mainly consists of Ni, Cr and Mo (point 1). The white areas (Points 2, 4, 5 and 6) in the coating are found to be Ni-rich splats and absence of oxygen at these points suggests that these Ni-rich splats are in the un-oxidised state. The existence of significant quantity of oxygen at black contrast spot (27.83 wt. % at point 3) along with Al and Y depicts the formation of Al<sub>2</sub>O<sub>3</sub> and Y<sub>2</sub>O<sub>3</sub>. The oxide scale formed on the surface of corroded Inconel 800H (Fig.5.27c) is compact, adherent and uniform. Existence of higher amount of oxygen on the top surface of the scale (point 1) indicates mainly oxides of Ni, Cr and Al, whereas in the sub scale region, point 2, 3 and 5 are identified as un-oxidised Ni-rich splats which are uniformly spread in the coating. The dark area along the splat boundary (point 4) represents higher amount of oxygen thereby suggesting the oxides of Cr, Ni and Al. Along the coating-substrate interface (at point 6), concentration of Cr increases significantly with depleted Ni, thereby suggesting the segregation of coating-substrate elements.

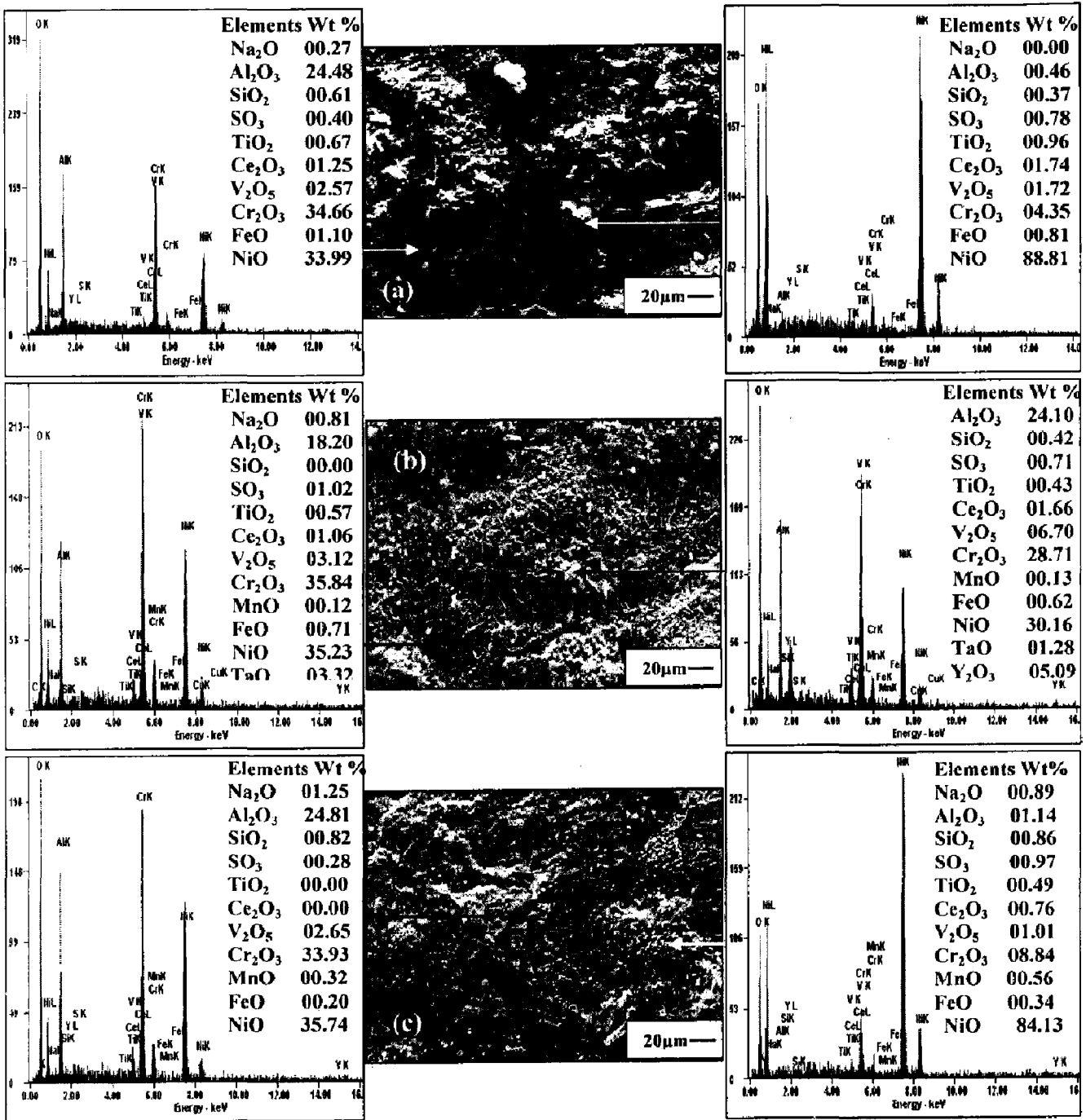


**Fig. 5.26** FE-SEM/EDS analysis along with EDS spectrum for NiCrAlY+0.4wt%CeO<sub>2</sub> coated superalloys subjected to cyclic oxidation in Na<sub>2</sub>SO<sub>4</sub>-60%V<sub>2</sub>O<sub>5</sub> environment at 900 °C after 100 cycles: (a) superni 75, (b) superni 718 and (c) superfer 800H.



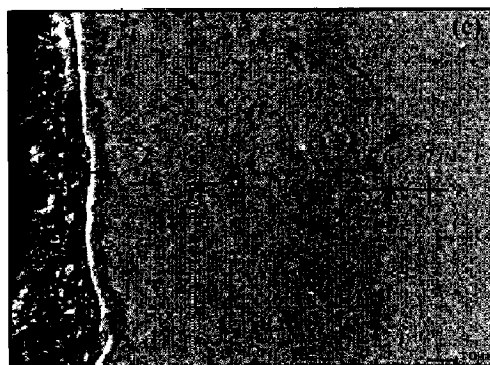
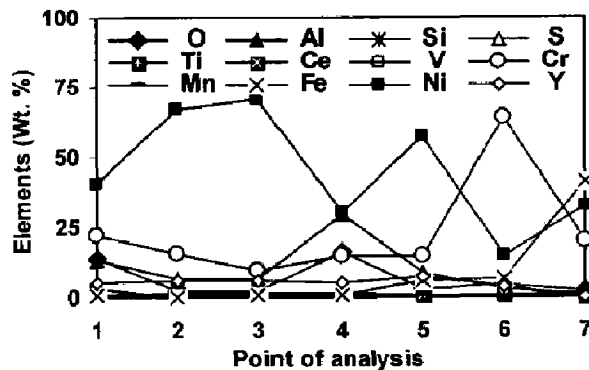
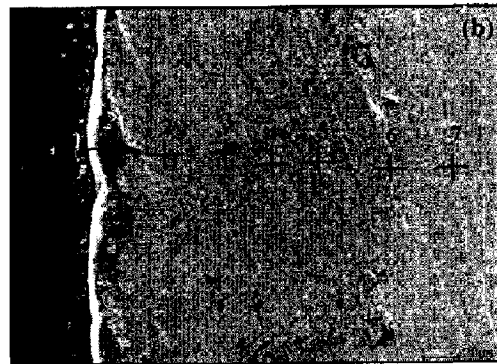
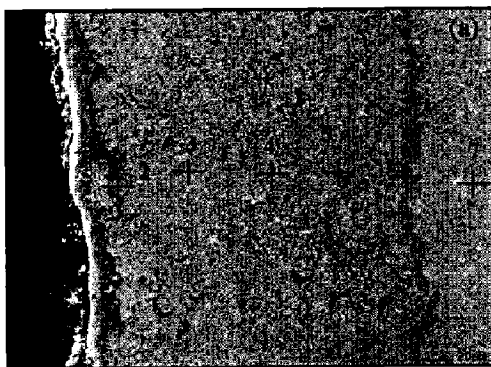
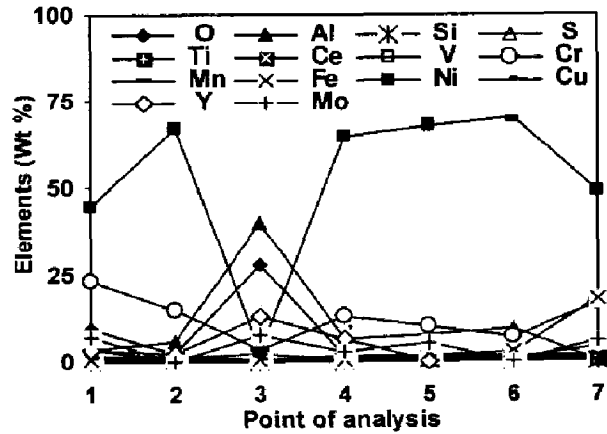
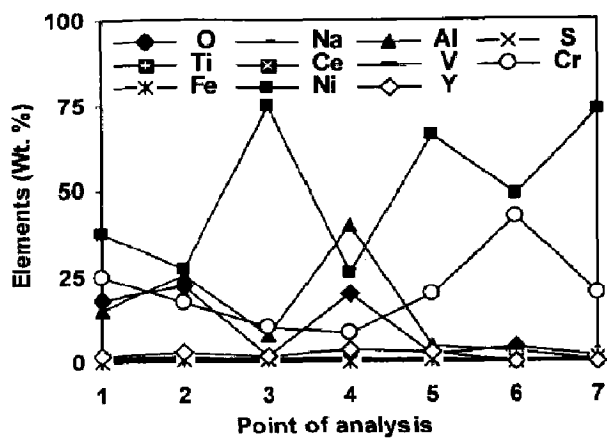


Fig. 5.27

Oxide scale morphology and variation of elemental composition across the cross-section of NiCrAlY+0.4 wt% CeO<sub>2</sub> coated superalloys subjected to cyclic oxidation at 900 °C in molten salt after 100 cycles (a) Superni 75, (b) Superni 718

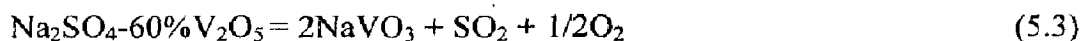
and (c) Superfer 800H.

#### 5.3.1.3.4 X-Ray mapping.

FE-SEM/EDS and SEI X-ray mapping of hot corroded coated superni 75 (Fig.5.28) showed a very thin oxide scale (10-15 $\mu$ m) mainly consisting of chromium in the top scale and Ni-rich splats at sub scale region which partially got oxidised as evident from the oxygen distribution. Al restricted below the Cr oxide layer. The presence of Fe in the top scale as well as along the splat boundaries in the coating indicates that the Fe might have diffused from the substrate to the top layer of the coating during hot corrosion run. Cerium oxide uniformly distributed along the Ni rich splat boundaries, further it diffused in to the substrate (Fig.5.28). Vanadium is restricted to the top surface of the oxide scale. X-ray mappings for hot corroded NiCrAlY+0.4wt%CeO<sub>2</sub> coated superni 718 after 100 cycles at 900 °C (Fig.5.29) indicates a variation in the thickness of oxide scale mainly of chromium at the top surface along with Fe and Si which might have diffused in to the coating from the substrate, Al is present in the sub scale region also. Some traces of Al streaks are distributed along the Ni rich splat boundaries. Similarly. X-Ray mapping of the cross-section of the corroded coated superfer 800H (Fig.5.30) sample exposed to Na<sub>2</sub>SO<sub>4</sub>-60%V<sub>2</sub>O<sub>5</sub> at 900 °C indicates the presence of chromium-rich top scale along with a thick band of silicon and iron. Whereas, aluminum is distributed in the subscale region, some traces of sulphur penetrated in to the coating and substrate, few streaks of vanadium co-existed with the cerium oxide penetrated deep in to the coating.

#### 5.3.1.4 Discussion

The weight gain graph, Fig.5.22, show that the weight gained by bare superalloys increases continuously due to accelerated oxidation in the molten salt environment, whereas the coated superalloys in all cases showed better hot corrosion resistance. The bare and coated Fe-based superfer 800H superalloy showed least and highest resistance to the hot corrosion respectively. The continuous increase in weight of bare superalloys can be attributed to the formation of NaVO<sub>3</sub>, at a temperature of 900 °C, the Na<sub>2</sub>SO<sub>4</sub>-60%V<sub>2</sub>O<sub>5</sub> will combine and form NaVO<sub>3</sub> having a melting point of 610 °C as reported by Sidhu et al., (2006H).





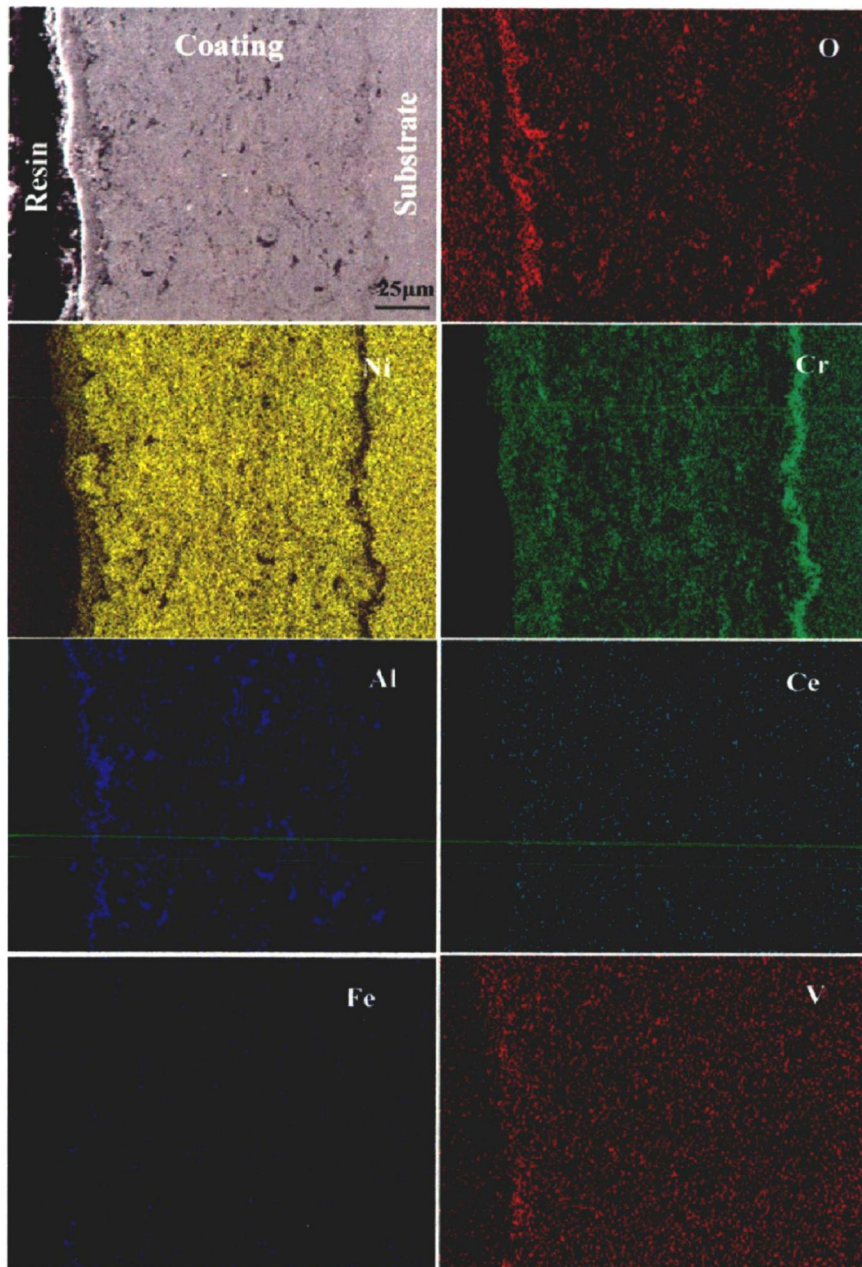


**Fig. 5.28** Composition image (SE) and X-ray mapping of the cross-section of the NiCrAlY + 0.4wt % CeO<sub>2</sub> coated superalloy superalloy superalloy 75 subjected to cyclic oxidation at 900 °C in Na<sub>2</sub>SO<sub>4</sub>-60%V<sub>2</sub>O<sub>5</sub> after 100 cycles.

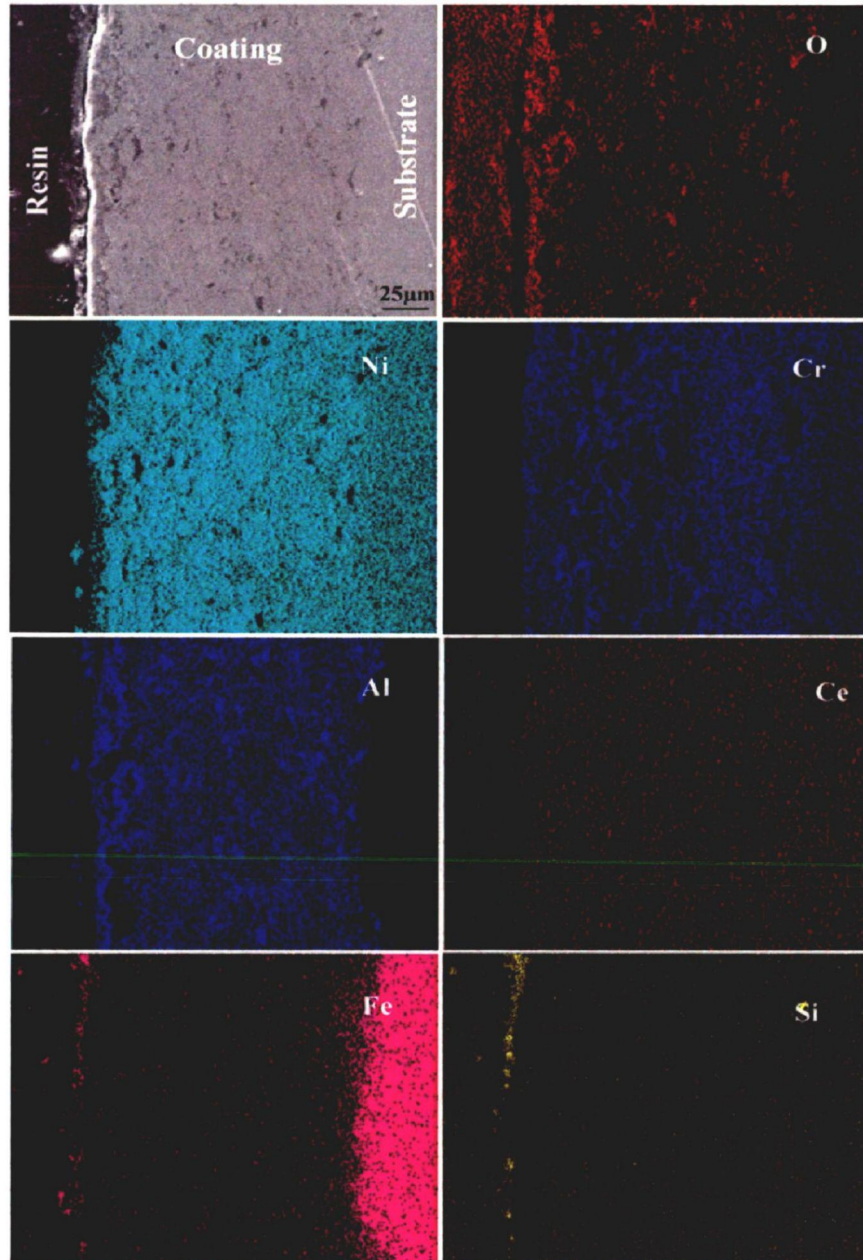


**Fig. 5.29** Composition image (SE) and X-ray mapping of the cross-section of the NiCrAlY + 0.4wt % CeO<sub>2</sub> coated superalloy superni 718 subjected to cyclic oxidation at 900 °C in Na<sub>2</sub>SO<sub>4</sub>-60%V<sub>2</sub>O<sub>5</sub> after 100 cycles.



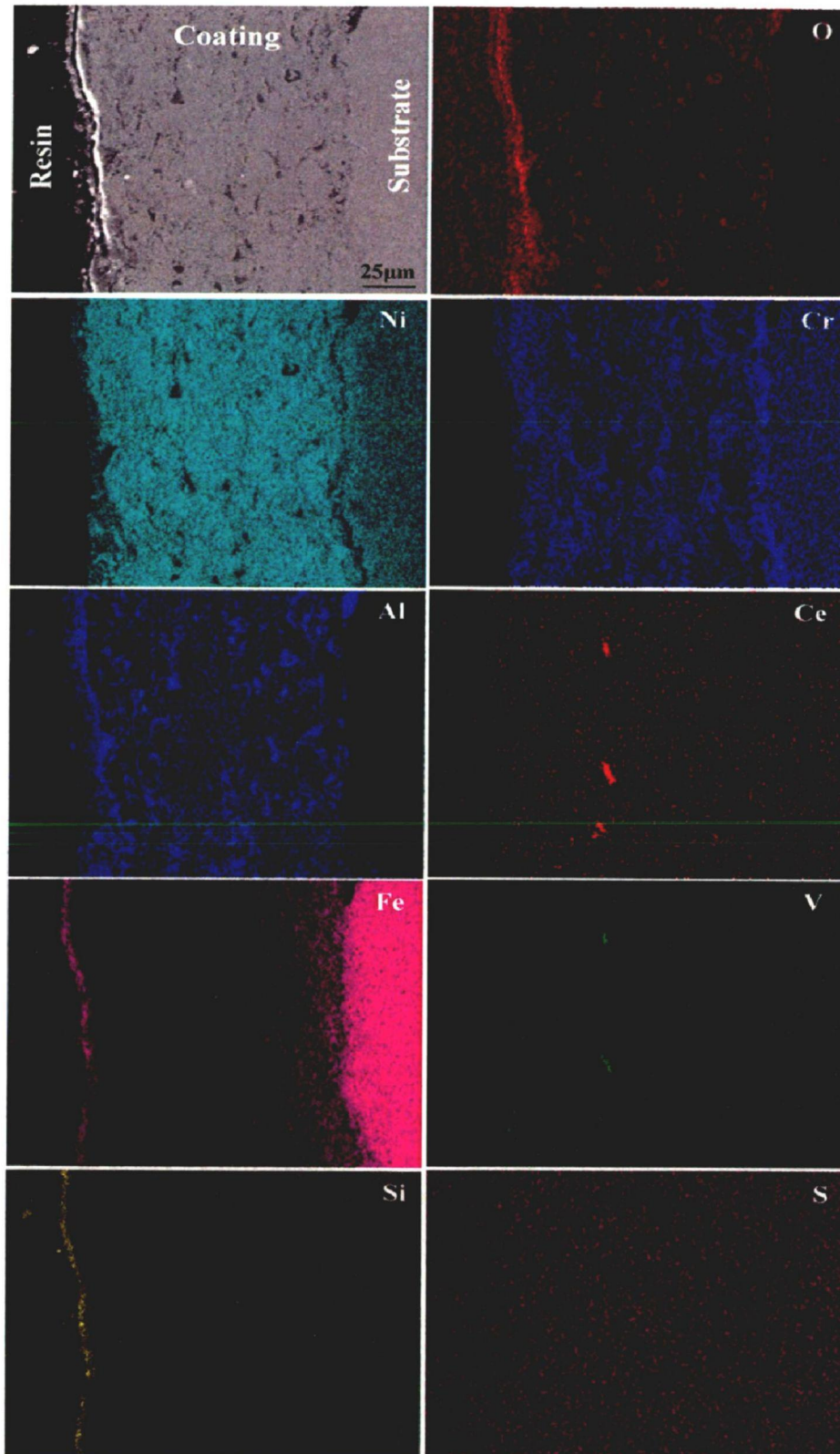


**Fig. 5.30**

Composition image (SE) and X-ray mapping of the cross-section of the NiCrAlY +0.4wt%CeO<sub>2</sub> coated superalloy superfer 800H subjected to cyclic oxidation at 900 °C in Na<sub>2</sub>SO<sub>4</sub>-60%V<sub>2</sub>O<sub>5</sub> after 100 cycles.

The formation of low melting sodium vanadate causes dissolution of protective oxide scale (Gurrappa, 2001) as per the following reaction as suggested by Seiersten and Kofstad, (1987) and Swaminathan et al. (1993)



Fryburg et al., (1984) and Guo et al., (2006B) have suggested that this  $\text{Na}_2\text{CrO}_4$  gets evaporated as a gas. The weight gain of the coated and bare specimens is relatively high during the early cycles of hot corrosion, but subsequently increase in weight gain is found to be gradual. It is because of Ni and Cr on the surface oxidise fast when protective oxides of Al has not been formed. As the oxidation cycle proceeds, the air which is entrapped during D-gun deposition and protected in the porosities, since the cooling of the coating was rapid; there is shortage of time for the residual air to react with the surrounding coating alloys. But, the coating underwent insitu reaction during high temperature (900 °C) oxidation and formed oxides of aluminum ( $\text{Al}_2\text{O}_3$ ) at the splat boundaries and within open pores. During the subsequent cycles, as discussed above, the formation of oxides plug/seal the pores and splat boundaries, and act as diffusion barriers to the inward diffusion of corrosive species, leading to slow oxide scale growth. All the coated superalloys followed parabolic behaviour whereas bare superalloys deviates from the parabolic rate law except bare superni 75, the parabolic rate constant for the bare and coated superalloys are shown in Table 5.3. The overall weight gain of 8.37, 7.077, and 4.53  $\text{mg}/\text{cm}^2$  was observed for the NiCrAlY+0.4wt%CeO<sub>2</sub> coated superni 75, superni 718, and superfer 800H superalloys (Fig.5.24), respectively. The coating provides the maximum hot corrosion resistance to superfer 800H and has been found successful in reducing the weight gain by around 60% of that gained without a coating, which is also evident from the parabolic rate constant ( $k_p = 0.41310^{-10} \text{ g}^2\text{cm}^{-4} \text{ s}^{-1}$ ). Coatings on superni 75 reduce the weight gain by 17% of that gained by the bare superalloys. A comparatively less corrosion resistance shown by coated superni 75 and 718 in comparison with the coated superfer 800H might be due to the presence of less protective bigger and more quantity of oxides (NiO) formed on the surface scale (Fig.5.26 a and b), which allows the penetration of corrosive species through the scale to the coating. This NiO formed in the surface scale is porous due to reprecipitation by fluxing action; also the scale formed on the surface is non uniform (Fig.5.27a and b) due to which the oxygen has penetrated little deep in to the coating as attributed from the X-ray mapping analysis (Fig,5.28-5.30). Better performance of coated superfer 800H might be due to uniform, dense, thick scale formed on the surface mainly

consisting of Cr, Ni and Al, presence of these elements along with oxygen represents the formation of oxides of Cr, Ni, Al and the spinels of  $\text{NiCr}_2\text{O}_4$  and  $\text{NiAl}_2\text{O}_4$  as revealed by XRD analysis (Fig.5.25). The presence of  $\text{CeO}_2$  with vanadium across the coating depicts the formation of  $\text{CeVO}_4$ , which might have further contributed in reducing hot corrosion attack (Fig.5.30). Spinel phase usually has lower diffusion coefficients of the cations and anions than those in their parent oxides Chatterjee et al., (2001). The presence of these phases in the scale of coated superalloys is further supported by the surface (Fig.5.26c), cross-sectional EDS (Fig.5.27c) and X-ray mapping analyses (Fig.5.30). Sidhu (2003), Wu et al., (2001 and 2002) reported the formation of similar phases. Further the coating also revealed the formation of continuous thin oxide scale of Si and Fe on the top surface of coated superfer 800H (Fig.5.30), as these elements have diffused in to the coating through the splat boundaries and open pores, which acts as a channel for the transport of coating and substrate elements during initial cycles of hot corrosion, which further contributed to higher resistance to hot corrosion. Wang et al. (2004) and Grunling and Bauer (1982) reported that presence of silicon can promote the formation of continuous dense scale and improve the adherence of the outer scale to the coating in the subsequent hot corrosion process. Whereas Yttrium was found to be segregated along the grain boundaries of  $\text{Al}_2\text{O}_3$  and lowers the scale growth rates (Goward, 1998 and Tawancy and Sridhar, 1992). RE segregate to oxide grain boundaries, where they can significantly reduce the outward transport of Al, hence decrease the rate of oxidation and contribute to the improved scale adherence and reduced interfacial void formation (Pint, 1996). A schematic diagram of the proposed hot corrosion mechanism of the  $\text{NiCrAlY}+0.4\text{wt}\%\text{CeO}_2$  coated superalloy superfer 800H at  $900^\circ\text{C}$  in  $\text{Na}_2\text{SO}_4-60\%\text{V}_2\text{O}_5$  after 100 cycles is shown in Fig. 5.31.

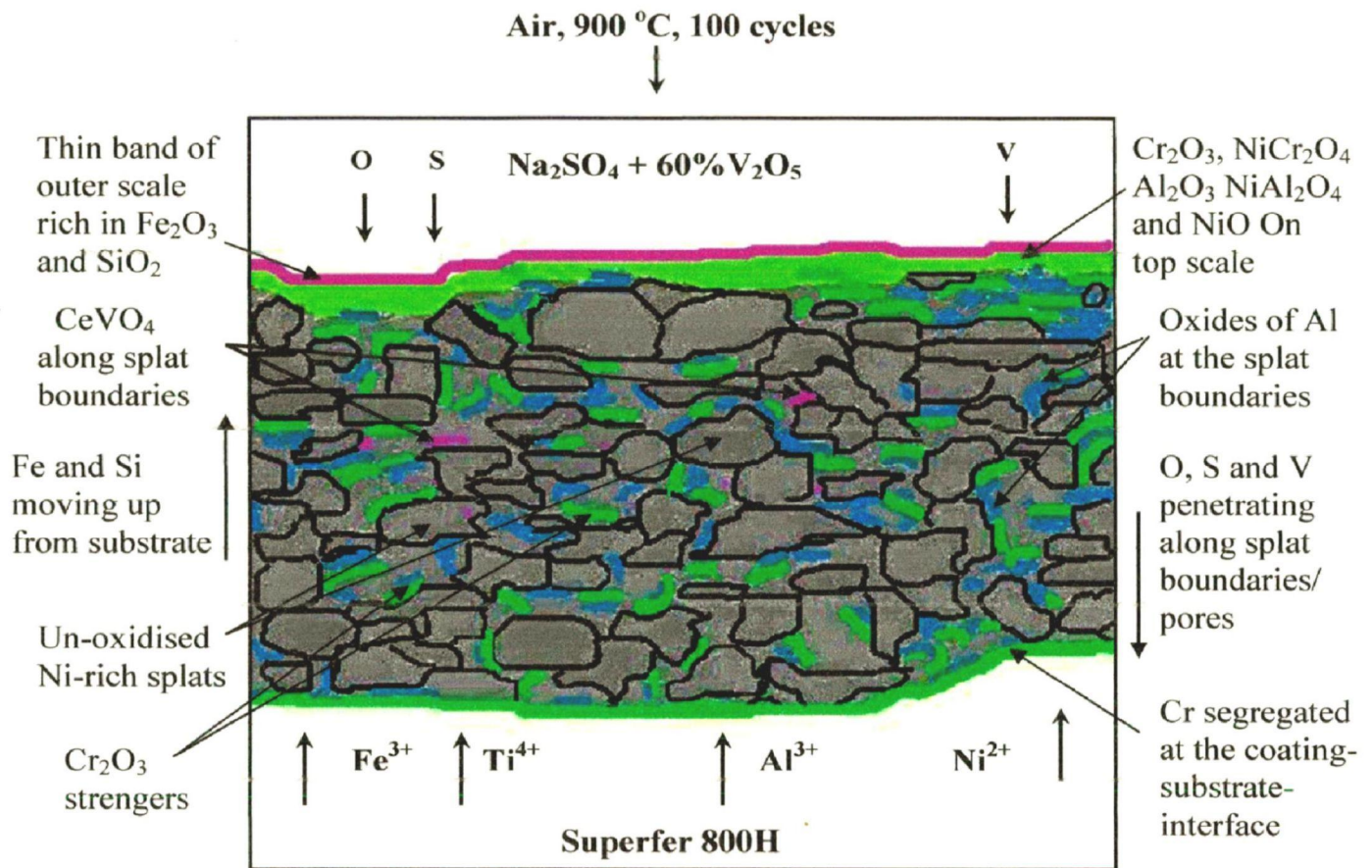


**Fig. 5.31** Schematic diagram of the proposed hot corrosion mechanism of the NiCrAlY+0.4wt%CeO<sub>2</sub> coated superalloy superfer 800H at 900 °C in Na<sub>2</sub>SO<sub>4</sub>-60%V<sub>2</sub>O<sub>5</sub> after 100 cycles.

### 5.3.1.5 Conclusions

NiCrAlY+0.4wt%CeO<sub>2</sub> coating on Ni and Fe based superalloy substrates has been uniformly deposited by D-gun spraying process in the present work and the following conclusions are made.

- Cerium oxide uniformly distributed along the Ni rich splat boundaries, further it diffused in to the substrate. Some traces of Al streaks are distributed along the Ni rich splat boundaries.
- The bare and coated Fe-based superfer 800H superalloy showed least and highest resistance to the hot corrosion, respectively.
- D-gun sprayed NiCrAlY+0.4wt%CeO<sub>2</sub> coating found to be effective in imparting hot corrosion resistance to superfer 800H in the molten salt environment.
- The formation of oxides along the splat boundaries and within open pores of the coatings might have acted as diffusion barrier to the inward diffusion of molten salt
- There are 60% and 15% savings in overall weight gain for NiCrAlY+0.4wt%CeO<sub>2</sub> coated superfer 800H and superni 75 in comparison with the bare superfer 800H and superni 75, respectively,
- A dense oxide scale formed on the coated superalloy and hot corrosion resistance of the coating might be due to the formation of protective phases like NiO, Cr<sub>2</sub>O<sub>3</sub>, Al<sub>2</sub>O<sub>3</sub>, NiCr<sub>2</sub>O<sub>4</sub> and Ni Al<sub>2</sub>O<sub>4</sub>.
- The formation of small amounts of oxides of iron and silicon shows diffusion of these elements from the substrate to the coating.

## **5.3.2 Na<sub>2</sub>SO<sub>4</sub>-25%K<sub>2</sub>SO<sub>4</sub> MOLTEN SALT ENVIRONMENT-II**

### **5.3.2.1 Introduction**

The hot corrosion behavior of NiCrAlY+0.4wt%CeO<sub>2</sub> coatings deposited on the superalloys (namely superni 75, superni 718 and superfer 800H) exposed to Na<sub>2</sub>SO<sub>4</sub>-25%K<sub>2</sub>SO<sub>4</sub> at temperature 900 °C for 100 cycles has been investigated in the present work. The different composition of the salt as compared to the salt composition given in section 5.3.1 has been chosen simulating the variable composition of the salt environment manifested in the actual applications. It is well known in the literature that reactive elements such as Y and Ce play a role in reducing oxidation rates of alloys and increase oxidation resistance of the fluxing alloy coatings (Zhenyu et al., 2006). Mahesh et al. 2008A and Kamal et al. (2009B) have studied the characteristics of HVOF and D-gun sprayed NiCrAlY+0.4wt%CeO<sub>2</sub> coatings on superalloys. However, the coatings with these microstructural characteristics need to be tested for combating hot corrosion problems in various corrosive environments (Na<sub>2</sub>SO<sub>4</sub>-25%K<sub>2</sub>SO<sub>4</sub>), which frequently encountered in the coal fired thermal power plants.

### **5.3.2.2 Experimental details**

The substrate materials, coating formulation and the hot corrosion studies are explained in detail in section 3.1, 3.2.3 and 3.4.3.

### **5.3.2.3 Results**

#### **5.3.2.3.1 Visual observations and weight change measurements**

The colour of oxide scale formed on the coated superalloy superni 75, superni 718 and superfer 800H, after exposure at 900 °C for 100 cycles in Na<sub>2</sub>SO<sub>4</sub>-25%K<sub>2</sub>SO<sub>4</sub> environment (Fig.5.32) shows dark grey during initial hot corrosion run thereafter it starts turning to greenish with un-reacted molten salt layers. The colour of the scale appeared on the surface of coated superni 75 (Fig.5.32a) superalloys were grey during early cycles, which continued up to 15 cycles. Greenish colour in the form of patches observed from the 16<sup>th</sup> cycle onwards, further it was intensified from 19<sup>th</sup> cycle. Some cracks were observed along the corners from 6<sup>th</sup> cycle, which further intensified from 11<sup>th</sup> cycle, during subsequent hot corrosion study corrosion products in the form of fine powder started falling inside the boat which continued up to 32<sup>nd</sup> cycle. For the coated superni 718 (Fig.5.32b), the colour of the oxide scale was grey





**Fig. 5.32** Surface macrograph of NiCrAlY+0.4wt%CeO<sub>2</sub> coated superalloys subjected to cyclic oxidation in Na<sub>2</sub>SO<sub>4</sub>-25%K<sub>2</sub>SO<sub>4</sub> environment at 900 °C for 100 cycles, (a) superni 75, (b) superni 718 and (c) superfer 800H

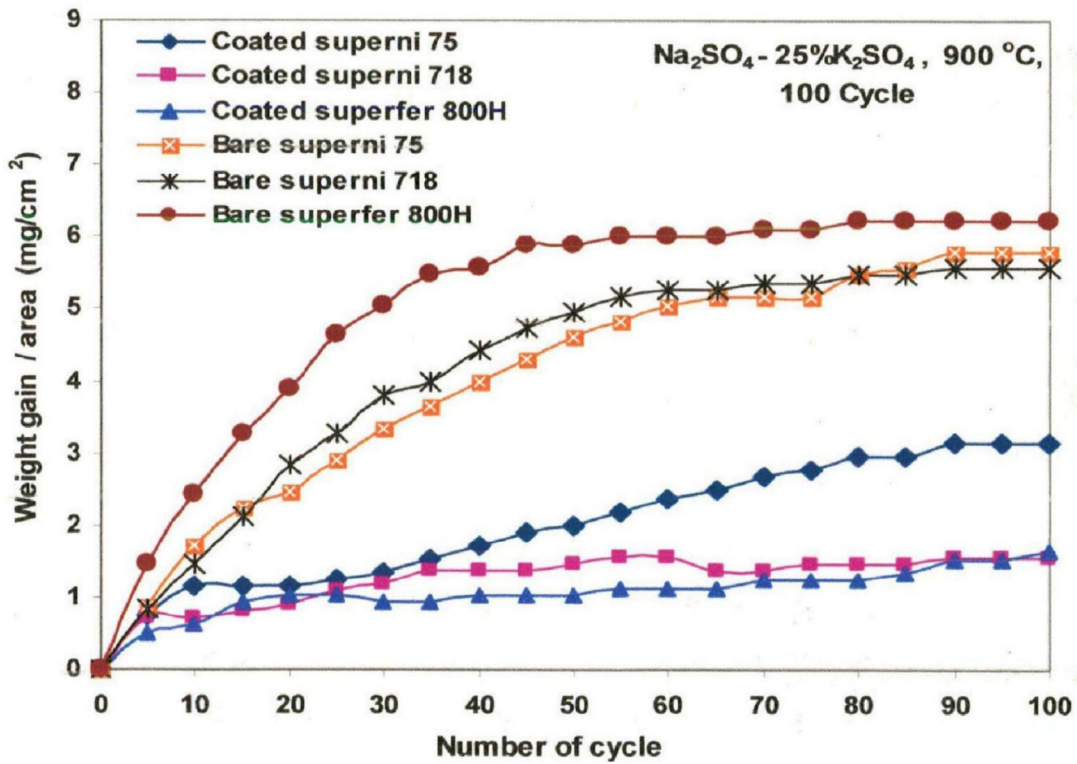


**Fig. 5.33** weight gain/area vs. number of cycles plot for NiCrAlY+0.4wt%CeO<sub>2</sub> coated and bare superalloys subjected to cyclic oxidation for 100 cycles in Na<sub>2</sub>SO<sub>4</sub>-25% K<sub>2</sub>SO<sub>4</sub> at 900 °C.

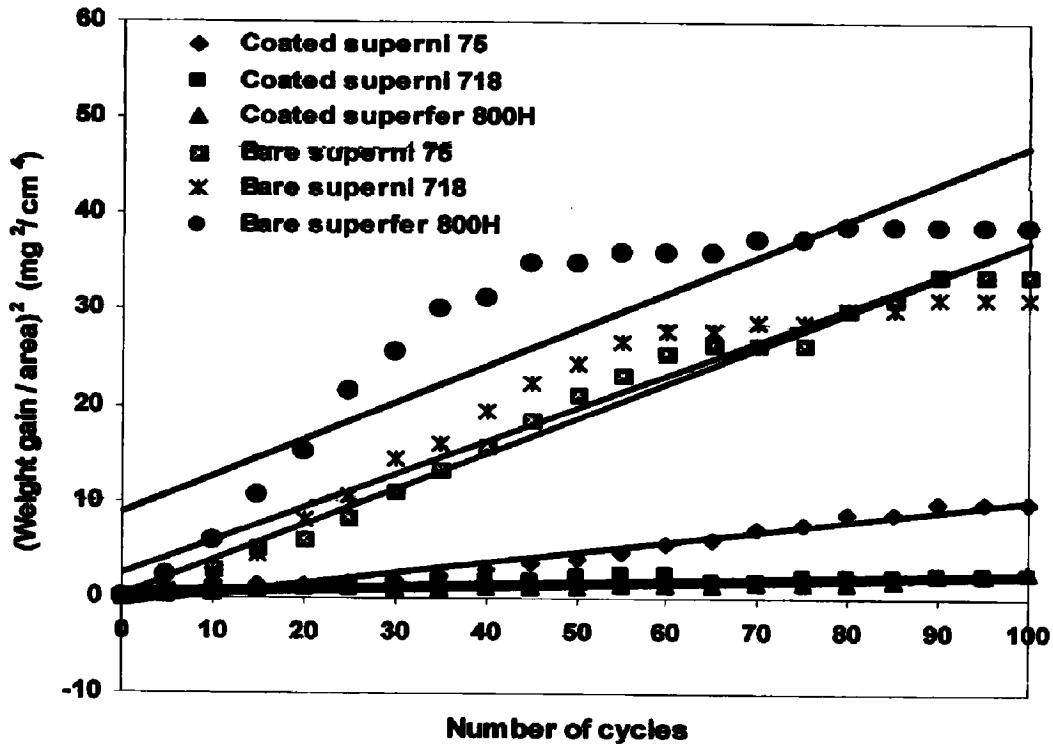


Fig. 5.34

(weight gain/area)² vs. number of cycles plot for NiCrAlY+0.4wt%CeO<sub>2</sub> coated and bare superalloys subjected to cyclic oxidation for 100 cycles in Na<sub>2</sub>SO<sub>4</sub>-25% K<sub>2</sub>SO<sub>4</sub> at 900 °C.

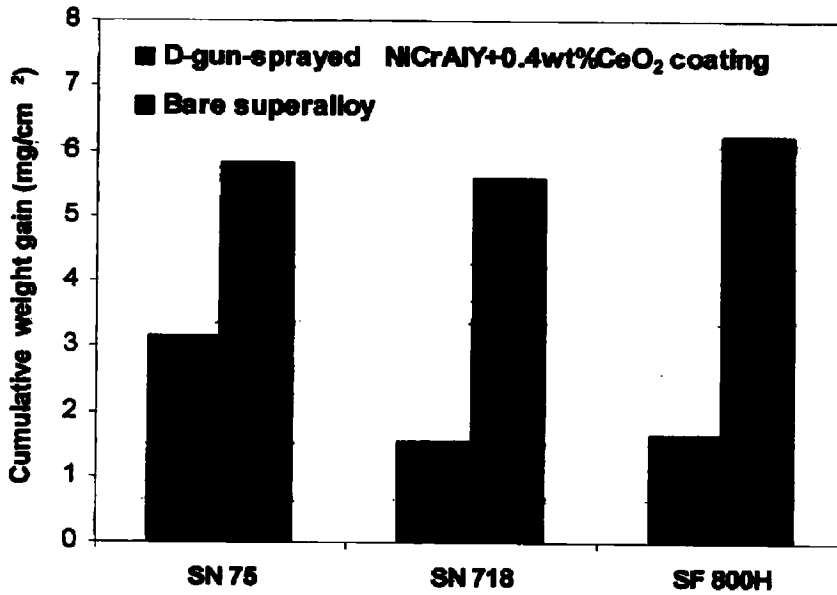


Fig. 5.35

Bar chart showing cumulative weight gain per unit area for NiCrAlY+0.4wt% CeO<sub>2</sub> coated and Bare superalloys subjected to cyclic oxidation for 100 cycles in Na<sub>2</sub>SO<sub>4</sub>-25% K<sub>2</sub>SO<sub>4</sub> at 900 °C.

during early few cycles, further light grey colour patches was observed from 9<sup>th</sup> cycle which turned in to greenish from 19<sup>th</sup> cycle onwards. Further, white colour molten salt patches intensified on greenish background, which was observed from the 25<sup>th</sup> cycle, minor spallation was observed along the edges of the coating. Similar behaviour was observed in case of coated superfer 800H (Fig.5.32c). Weight gain/unit area (mg/cm<sup>2</sup>) versus number of cycles plots for the bare as well as D-gun sprayed NiCrAlY+0.4wt%CeO<sub>2</sub> coated superalloys (superni 75, superni 718 and superfer 800H) oxidised at 900 °C in molten salt environment (Na<sub>2</sub>SO<sub>4</sub>-25%K<sub>2</sub>SO<sub>4</sub>) up to 100 cycles are shown in Fig.5.33. The coated superalloys in all cases showed much lower weight gain as compared to the bare specimens in the given molten salt environment. Coated superni 718 and superfer 800H showed the lowest weight gain, whereas bare superfer 800H showed highest weight gain. The hot corrosion behaviour of NiCrAlY+0.4wt%CeO<sub>2</sub>-coated superalloys follow nearly a parabolic rate law, whereas bare superalloys deviate from the parabolic rate law, as can be inferred from the square of weight change (mg<sup>2</sup>/cm<sup>4</sup>) versus number of cycle plots (Fig.5.34).The parabolic rate constants (kp in 10<sup>-10</sup> g<sup>2</sup> cm<sup>-4</sup> s<sup>-1</sup>) for the NiCrAlY+0.4wt%CeO<sub>2</sub>-coated and bare superalloys after 100 cycles of hot corrosion run is shown in Table 5.4. A cumulative weight gain per unit area for coated and bare superalloys is shown in Fig. 5.35.

**Table 5.4** Parabolic rate constant (kp) for NiCrAlY+0.4wt%CeO<sub>2</sub> coated and bare superalloy subjected to cyclic hot corrosion for 100 cycles in Na<sub>2</sub>SO<sub>4</sub>-25%K<sub>2</sub>SO<sub>4</sub> environment at 900 °C.

Substrate	Kp X 10 <sup>-10</sup> gm <sup>2</sup> cm <sup>-4</sup> s <sup>-1</sup>
Bare superni 75	1.025
Bare superni 718	0.961
Bare superfer 800H	1.09
Coated superni 75	0.3011
Coated superni 718	0.0592
Coated superfer 800H	0.0564

### 5.3.2.3.2 X-ray diffraction analysis (XRD)

The various phases identified from the X-ray diffraction patterns of the surface oxide formed on D-gun sprayed NiCrAlY+0.4wt%CeO<sub>2</sub> coated superalloys after cyclic hot corrosion in 75 wt.% Na<sub>2</sub>SO<sub>4</sub>-25%K<sub>2</sub>SO<sub>4</sub> environment at 900 °C for 100 cycles are shown in Fig.5.36. The surface oxides on corroded coated superalloys are NiCr<sub>2</sub>O<sub>4</sub>, NiAl<sub>2</sub>O<sub>4</sub>, α-Al<sub>2</sub>O<sub>3</sub>, Ni<sub>3</sub>Al and NiO.

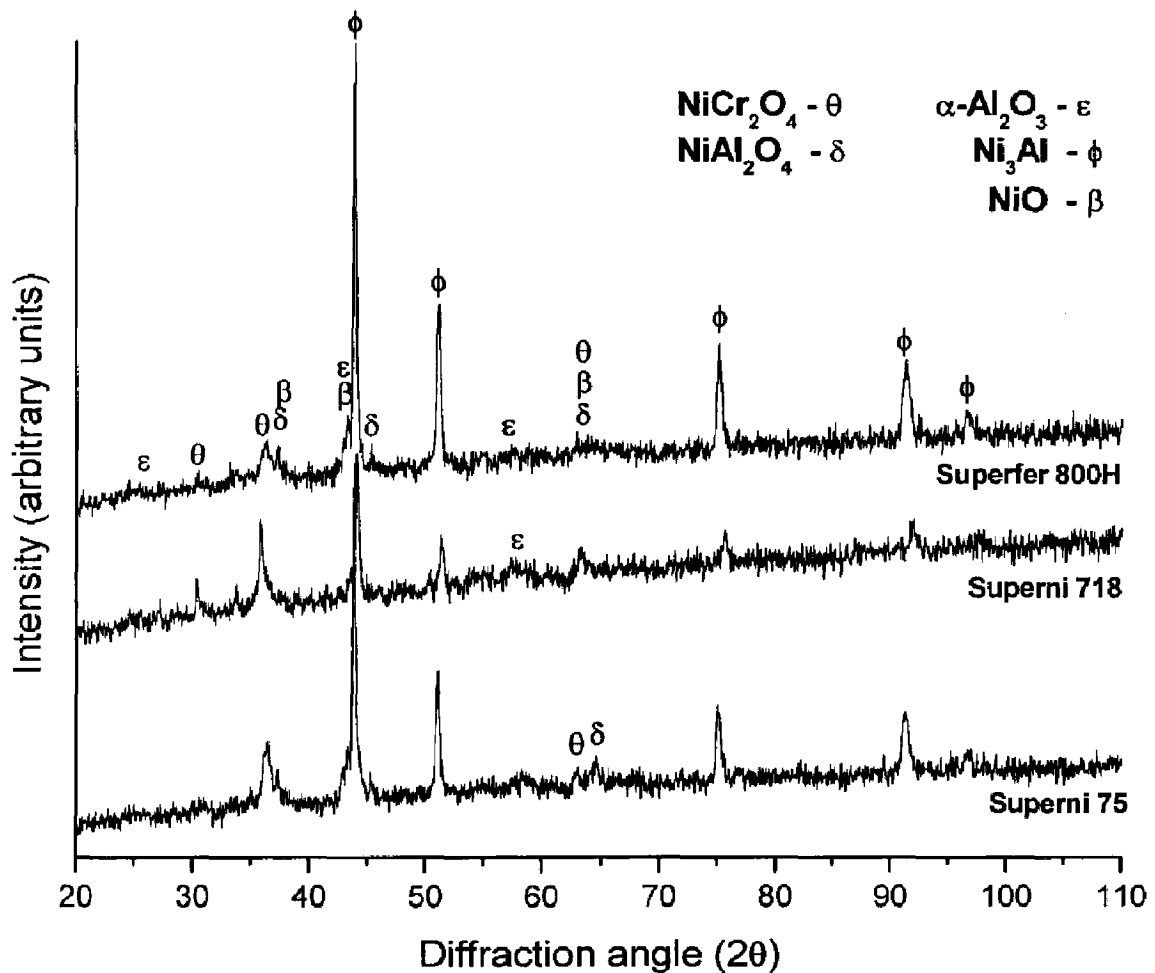


**Fig. 5.36** X-ray diffraction patterns for Cr<sub>2</sub>C<sub>3</sub>-NiCr-coated superalloys exposed to cyclic Oxidation in Na<sub>2</sub>SO<sub>4</sub>-25%K<sub>2</sub>SO<sub>4</sub> environment at 900 °C after 100 cycles, (a) superni 718, (b) superni 75 and (c) superfer 800H.

### **5.3.2.3.3 FE-SEM/EDS analysis**

#### **5.3.2.3.3.1 Surface morphology of the scales**

FE-SEM micrographs with EDS spectrum reveals the surface morphology of the NiCrAlY+0.4wt%CeO<sub>2</sub> coated superalloy specimens after cyclic hot corrosion in molten salt environment (Na<sub>2</sub>SO<sub>4</sub>-25%K<sub>2</sub>SO<sub>4</sub>) for 100 cycles at 900 °C as shown in Fig.5.37. The FE-SEM/EDS analysis of surface scale developed on coated superalloy 75 (Fig.5.37a) is massive, crack free, with dense clusters mainly containing of O, Al, Cr and Ni-rich elements, in which, irregular rectangular shaped discs of Cr<sub>2</sub>O<sub>3</sub> is clearly visible. Micrograph of corroded coated superalloy 718 (Fig.5.37b) also appears to be dense and continuous with smaller size rectangular discs of Cr<sub>2</sub>O<sub>3</sub> as a major phase. Micrograph indicates globular aggregates and rectangular elongated phases. The aggregate are consisting of Ni and Cr. Whereas rectangular crystalline phase is mainly Cr<sub>2</sub>O<sub>3</sub>. Similarly, FE-SEM/EDS analysis revealed the scale formed on the coated superalloy 800H is dense white agglomerated free crystalline granules with major elements of O, Ni followed by Cr, whereas rectangular shaped discs region depicts the presence of O and Cr-rich elements followed by Ni (Fig.5.37c).

#### **5.3.2.3.3.2 Cross-sectional analysis**

EDS analysis of corroded NiCrAlY+0.4wt%CeO<sub>2</sub> coated superalloy 75 reveals (Fig.5.38a) that the uppermost part of the scale has relatively higher concentration of oxygen along with Ni, Cr and Al (point 1), suggesting the formation of oxides of Ni, Cr and Al. Further in the subscale region at points 2, 3, the Ni rich splats are in an un-oxidised state due to absence of oxygen at these points. Existence of oxygen at point 4 represents the presence of oxides of Al and Y; increase in chromium content at point 5 represents the segregation of Cr along the Ni-rich splat boundaries, further along the coating-substrate interface, a thick band of chromium layer is formed. Minor inter-diffusion of coating and substrate has occurred, as evident from EDS analysis at point 7 (Fig.5.38a). Corroded NiCrAlY+0.4wt%CeO<sub>2</sub> coated superalloy 718 (Fig.5.38b) showed the top surface of the coating mostly consisting of a homogeneous, adherent and non-uniform oxide scale with variable thickness. The oxide scale mainly consists of O, Ni, Cr and Al rich elements (Point 1), which depict the formation of respective oxides and their spinels, further presence of these phases supported by XRD analysis (Fig.5.36). Ni-rich splats were found at point 2, 4 and 5 but aluminum and yttrium coexist.

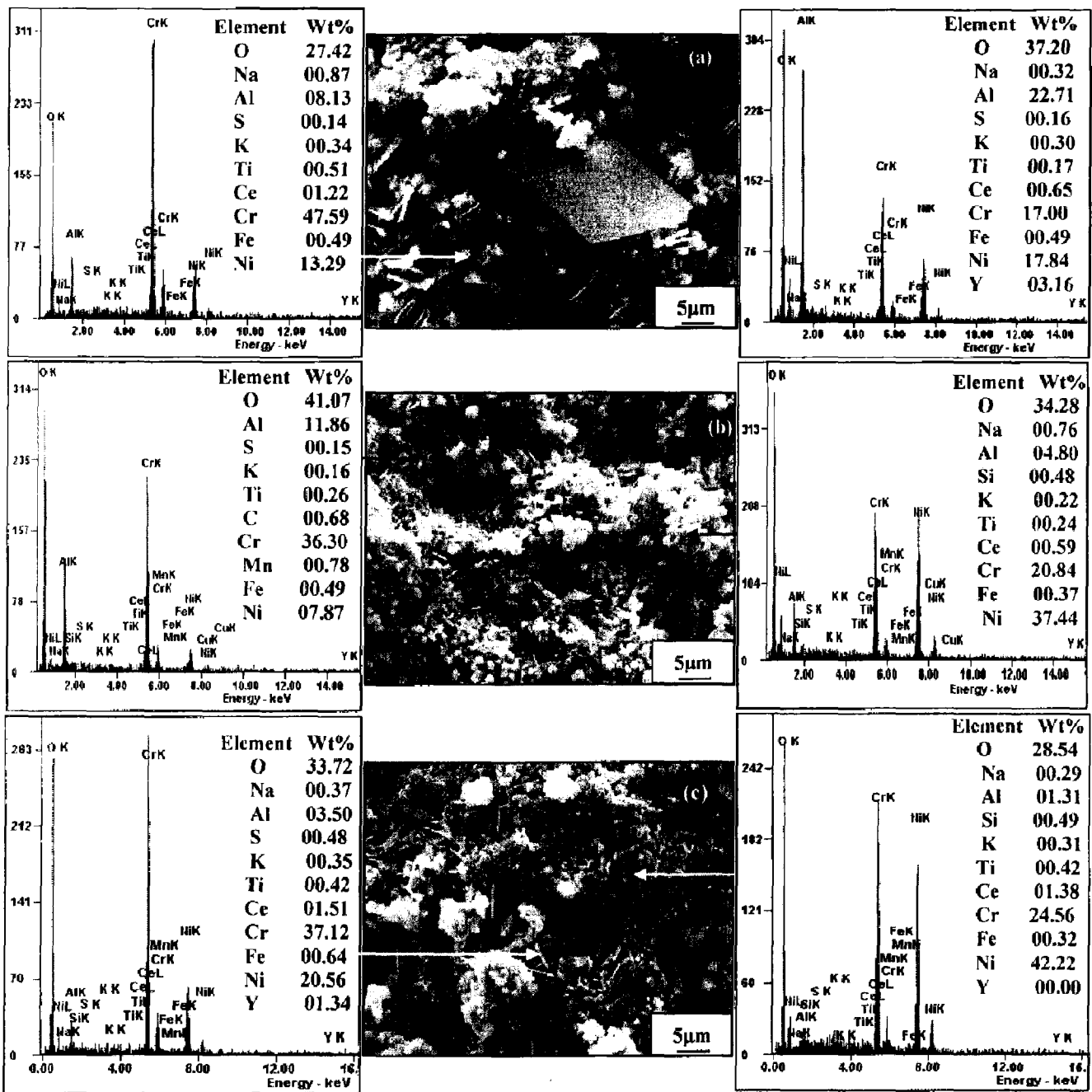


Fig. 5.37 FE-SEM/EDS analysis for NiCrAlY+0.4wt%CeO<sub>2</sub> coated superalloys subjected to cyclic oxidation in Na<sub>2</sub>SO<sub>4</sub>-25%K<sub>2</sub>SO<sub>4</sub> environment at 900 °C after 100 cycles: (a) superalloy 75, (b) superalloy 718 and (c) superalloy 800H.

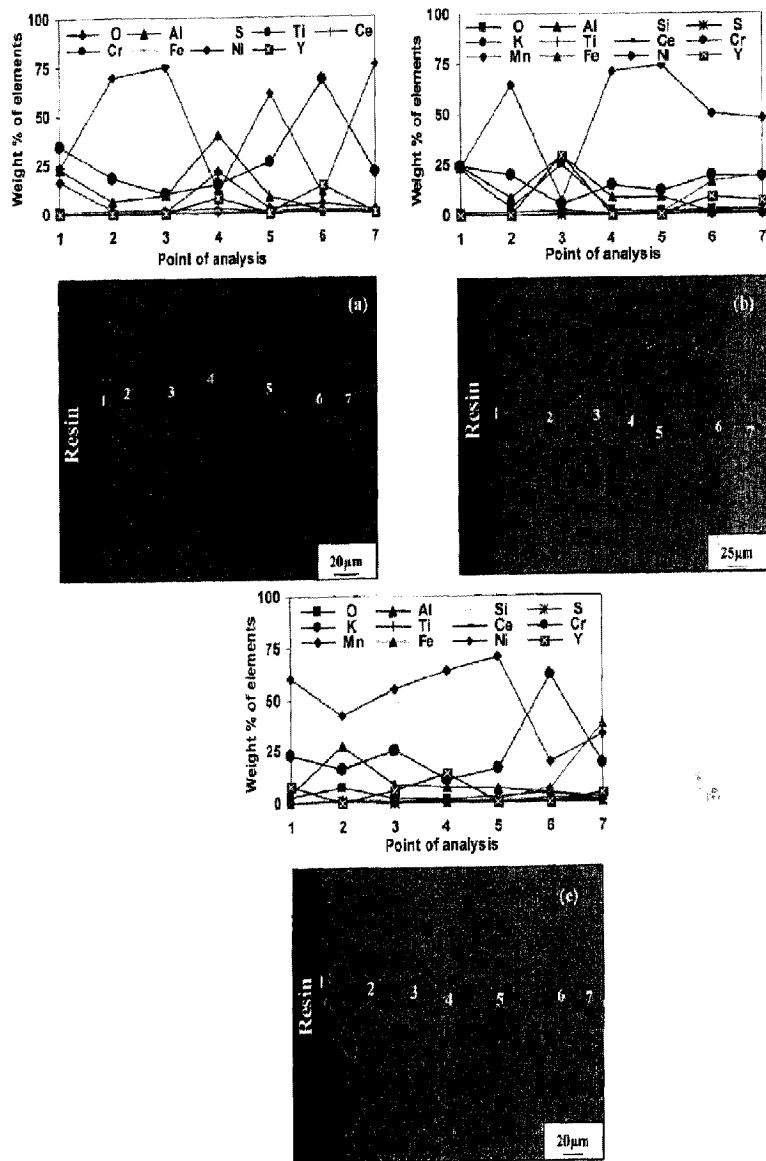


Fig. 5.38 Oxide scale morphology and variation of elemental composition across the cross-section of NiCrAlY+0.4wt%CeO<sub>2</sub> coated superalloys subjected to cyclic oxidation at 900 °C in Na<sub>2</sub>SO<sub>4</sub>-25%K<sub>2</sub>SO<sub>4</sub> environment after 100 cycles (a) superalloy 75, (b) superalloy 718 and (c) superalloy 800H.

with O along the Ni-rich splat boundaries (Points 3) indicating the formation of their oxides. There is segregation of yttrium across the coating-substrate interface (Point 6). Similarly cross sectional analysis of the oxidised NiCrAlY+0.4wt%CeO<sub>2</sub>-coated superfer 800H (Fig.5.38c) indicates that the entire coating has partially oxidised along Ni-rich splat boundaries, as there is no scale formation in the uppermost part of coating (Point 1), presence of Cr, Al and O along the Ni-rich splat boundaries (Point 2), represents the formation of respective oxides. Chromium has also distributed along Ni-rich splat boundaries as evident from EDS analysis at point 3 and 5. Light grey phase in the coating where Ni-rich splats remain in the un-reacted state as O is found to be absent at these places (Point 4). Along the coating-substrate interface (at point 6), concentration of Cr increases significantly with depleted Ni, thereby suggesting the segregation of coating-substrate elements.

#### **5.3.2.3.4 X-ray mapping**

FE-SEM/EDS and BSEI X-ray mapping of hot corroded NiCrAlY+0.4wt%CeO<sub>2</sub> coated superni 75 (Fig.5.39) shows uppermost part of the coating has O, Ni, Cr and Al, which represents the formation of respective oxides and their spinel, whereas in the subscale region, nearly elliptical shaped, Ni-rich splats are distributed in the coating, which is partially oxidised as evident from the oxygen distribution. Al in the form of streaks of Al<sub>2</sub>O<sub>3</sub> is distributed along the Ni rich splat boundaries, which is believed to be oxidised as evident from the oxygen distribution. A thick band of chromium segregated along the coating-substrate interface coexisting with oxygen thereby indicating the formation of Cr<sub>2</sub>O<sub>3</sub> band just above the coating-substrate interface. The X-ray mappings for hot corroded NiCrAlY+0.4wt%CeO<sub>2</sub>-coated superni 718 after 100 cycles at 900 °C (Fig.5.40) indicates a scale mainly consist of oxygen, chromium, aluminum and nickel at the top surface and rest of the coating is only partially oxidised as evident from the oxygen distribution. Below the upper most part of the scale, the coating has un-reacted Ni-rich splats, whereas Cr and Al are distributed along with oxygen around these splat boundaries, indicating formation of their oxides. The elemental mapping for iron showed outward diffusion from the substrate to the coating, the diffusion seems to have almost reached the top surface. Similarly X-ray mappings for NiCrAlY+0.4wt%CeO<sub>2</sub>-coated superfer 800H after 100 cycles of hot corrosion at 900 °C (Fig.5.41) represents that the coating has partially oxidised along Ni-rich splat boundaries, some streaks of Al<sub>2</sub>O<sub>3</sub> are distributed along the Ni rich



splat boundaries. Similarly, a thin irregular band of Cr has formed along the coating-substrate interface. The topmost layer of the scale found with traces of iron and titanium indicates its diffusion behaviour from the substrate to the coating.

#### 5.3.2.4 Discussion

The oxide scale formed on the NiCrAlY+0.4wt%CeO<sub>2</sub>-coated superalloys samples after hot corrosion in molten salt environment (Na<sub>2</sub>SO<sub>4</sub>-25%K<sub>2</sub>SO<sub>4</sub>) for 100 cycles at 900 °C, were greenish in colour (Fig.5.32). Greenish colour might be attributed to the presence of both NiO and Cr<sub>2</sub>O<sub>3</sub> (Khajavi and Shariat, 2004). The weight gain graph, Fig.5.33, show that the weight gained by bare superalloys increases continuously due to accelerated oxidation in the molten salt environment, whereas weight gain of the coated specimens is relatively high during first few cycles of hot corrosion, but subsequently increase in weight gain was found to be gradual. The initial higher oxidation rate of the coated specimens might be attributed to the formation of oxides along the splat boundaries and voids, further they have clogged the pores and acted as diffusion barriers to the inward diffusion of corrosive species. This leads to a slow oxide scale growth; consequently the weight gain is low. Aluminum (Belzunce et al, 2001) and Chromium (Singh et al., 2005C) exhibit higher affinity for oxygen to form Al<sub>2</sub>O<sub>3</sub> and Cr<sub>2</sub>O<sub>3</sub> during the earlier stages of hot corrosion, once the oxides are formed along the splat boundaries and at the places of porosity, the growth of the oxides becomes limited mainly to the surface of the specimens. This would relatively minimize the weight gain and result in the steady state oxidation behavior with the progress of long term high temperature exposure. All the NiCrAlY+0.4wt%CeO<sub>2</sub>-coated superalloys followed parabolic rate law, whereas bare superalloys show a slight deviation due to cyclic scale growth. The values of parabolic rate constant K<sub>p</sub> (10<sup>-10</sup> g<sup>2</sup> cm<sup>-4</sup> s<sup>-1</sup>) were obtained from the slope of the linear regression fitted line (Fig.5.34) and is shown in Table 5.4. Weight gain for the coated superalloys is less than the bare superalloys, which show the protective behaviour of the coating against hot corrosion. The NiCrAlY+0.4wt%CeO<sub>2</sub> coating provides the maximum hot corrosion resistance to superfer 800H and superni 718 as it reduces the weight gain by 74% and 72% of that gained without a coating (Fig.5.35), respectively. Coating on superni 75, reduces the weight gain by 46% of that gained by the bare superni 75. The better hot corrosion resistance shown by the NiCrAlY + 0.4 wt% CeO<sub>2</sub>-coated superfer 800H might be ascribed due to lower weight gain as evident from the lower parabolic rate constant (0.0564 x 10<sup>-10</sup> gm<sup>2</sup> cm<sup>-4</sup> s<sup>-1</sup>), further coating has partially oxidised

along Ni-rich splat boundaries. (Zhang et al 2003) reported that aluminum oxide formed in the voids, which increases  $\text{Al}_2\text{O}_3$  along the Ni-rich splat boundaries. Presence of NiO,  $\alpha\text{-Al}_2\text{O}_3$ ,  $\text{NiAl}_2\text{O}_4$  and  $\text{NiCr}_2\text{O}_4$  spinels in the coating as revealed by XRD analysis (Fig.5.36), contributes to the lower weight gain; the presence of these phases in the scale of coated superalloys is further supported by the surface EDS (Fig.5.37c), cross-sectional EDS (Fig.5.38c) and X-ray mapping analyses (Fig.5.41). The spinel phase usually has lower diffusion coefficients of the cations and anions than those in their parent oxides (Chatterjee et al., 2001). According to Lee and Lin, (2002) there are two possibilities of the formation of spinel phase; it may be through the reaction of Al and Ni with oxygen in the molten salt or through the development of sulphides. Further, they suggested that the  $\text{NiAl}_2\text{O}_4$  may have a better hot corrosion resistance than NiO since its solubility is smaller in the molten salt. In the present study, the co-existence of O, Ni, Cr and Al as shown by EDS analysis (Fig.5.37) may be indicative of formation of the spinel, which is further supported by XRD analysis. Oxides of Al and Cr are relatively much more protective than NiO scales since they are reasonably stoichiometric oxides, with low defect concentrations, and can give effective protection to the alloy in environments of high oxygen activity (Stott, 1987). Bare superalloy superfer 800H shows least corrosion resistance due to intense spallation and sputtering which can be attributed to the severe strain developed as a result of  $\text{Fe}_2\text{O}_3$  precipitation from the liquid phase and the inter-diffusion of intermediate layer of iron oxide. The weight gain of coated superni 718 and superfer 800H after 100 cycles is nearly half as compared to that of coated superni 75. The cumulative weight gain of coated and bare superalloys after 100 cycles of hot corrosion is plotted in Fig.5.35. The overall weight gain for the bare superni 718, superni 75, and superfer 800H alloys are 5.58, 5.80 and 6.21  $\text{mg/cm}^2$  respectively. An overall weight gain of 1.55, 1.64 and 3.14  $\text{mg/cm}^2$  was observed for the  $\text{NiCrAlY}+0.4\text{wt}\%\text{CeO}_2$ -coated superni 718, superfer 800H and superni 75, superalloys, respectively. As per (Toma et al., 1999), the oxidation resistance of MCrAlY coating is based on the formation of  $\alpha\text{-Al}_2\text{O}_3$ , which, grows very slowly and is thermodynamically stable. The chromium-rich intermediate layer between coating-substrate (Fig.5.39 and 5.41) behaves as a diffusion barrier to limit the outward diffusion of the atoms of the substrate alloying elements in to the coating. Schematic of the proposed oxidation mechanism of the  $\text{NiCrAlY}+0.4\text{wt}\%\text{CeO}_2$  coated superalloy superfer 800H at 900 °C in  $\text{Na}_2\text{SO}_4\text{-}25\%\text{K}_2\text{SO}_4$  after 100 cycles is shown in Fig. 5.42.

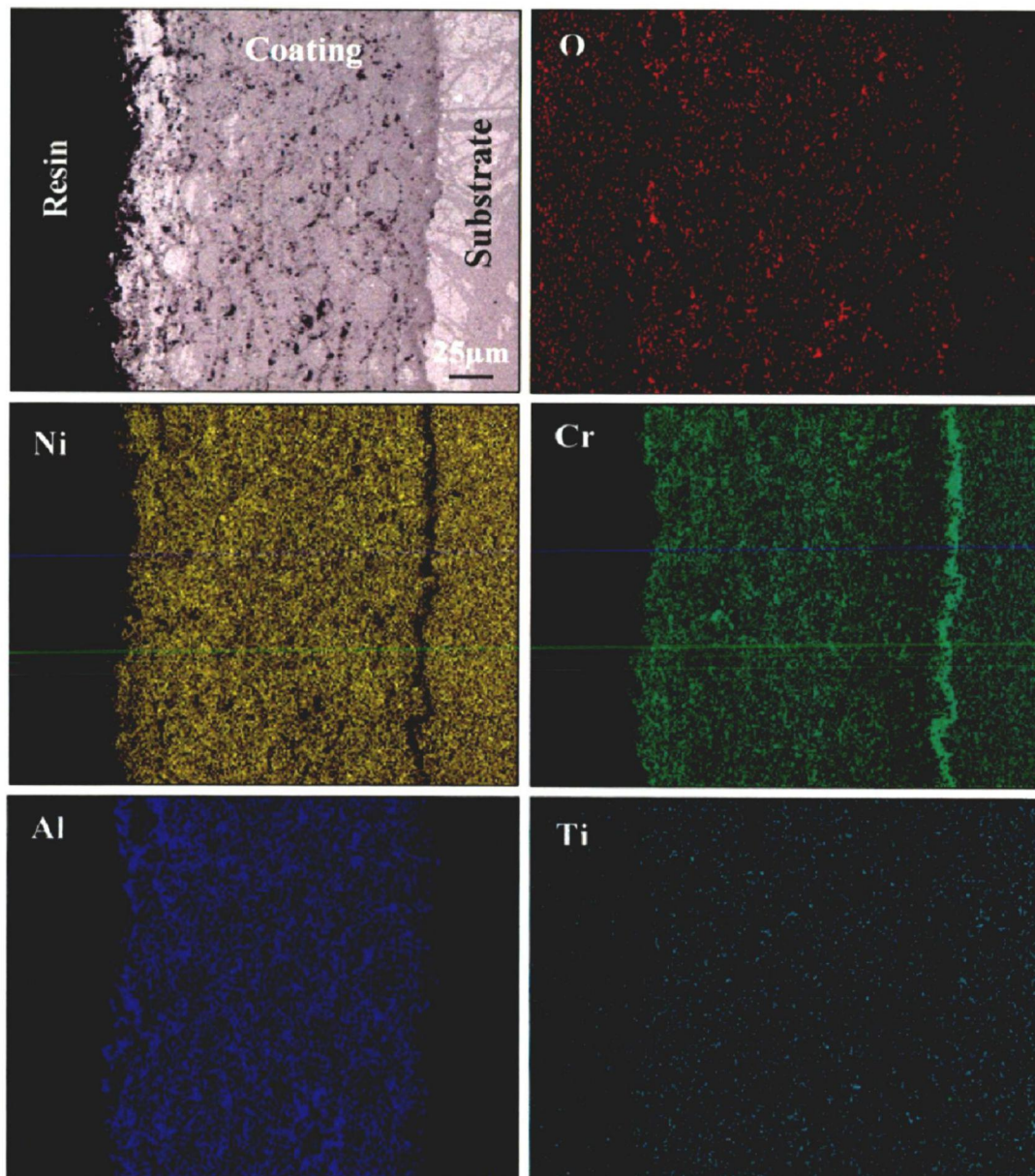


**Fig. 5.39** Composition image (SE) and X-ray mapping of the cross-section of the NiCrAlY +0.4wt%CeO<sub>2</sub> coated superalloy superalloy 75 subjected to cyclic oxidation at 900 °C in Na<sub>2</sub>SO<sub>4</sub>-25%K<sub>2</sub>SO<sub>4</sub> after 100 cycles.



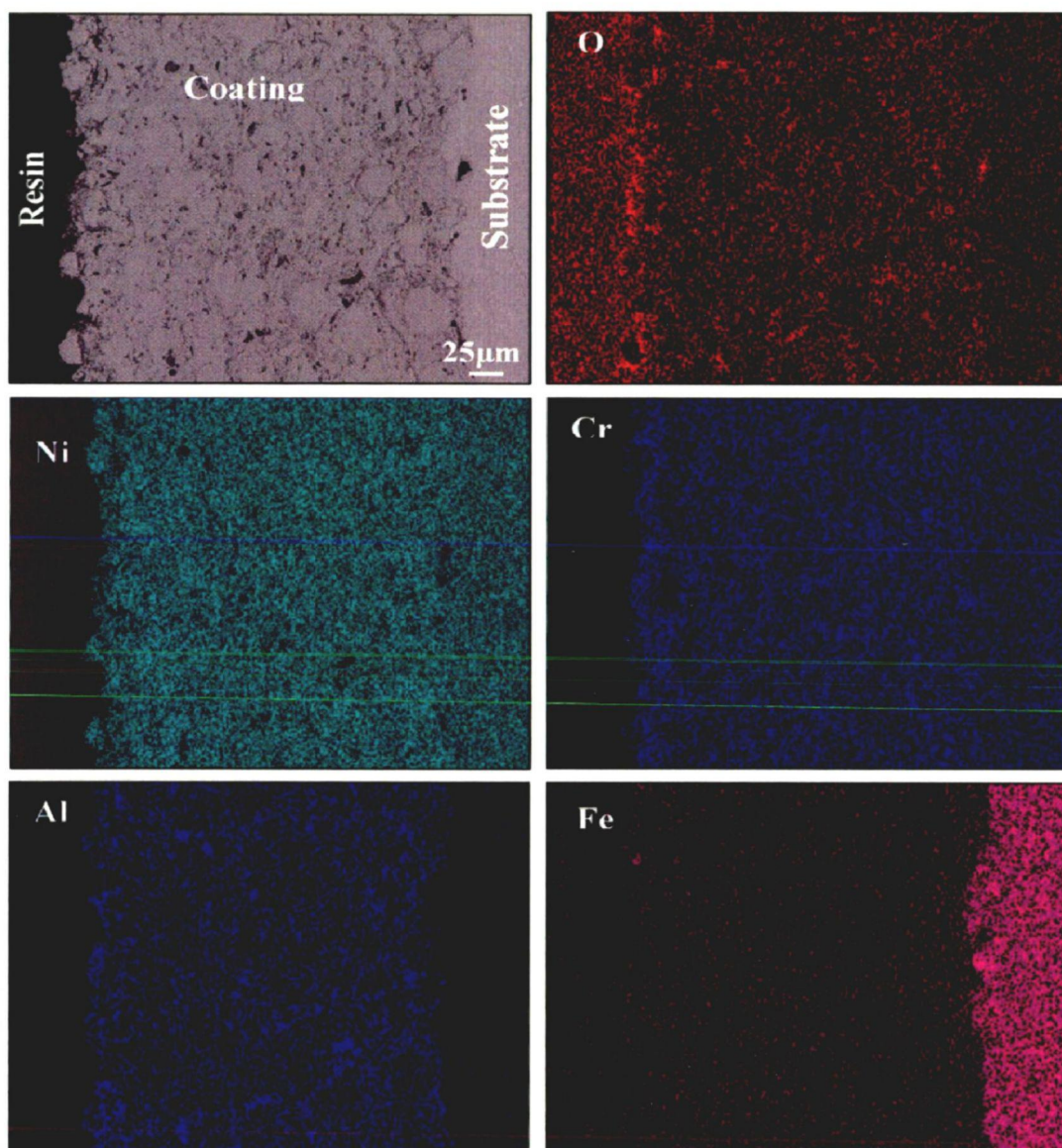


**Fig. 5.40** Composition image (SE) and X-ray mapping of the cross-section of the NiCrAlY +0.4wt%CeO<sub>2</sub> coated superalloy superni 718 subjected to cyclic oxidation at 900 °C in Na<sub>2</sub>SO<sub>4</sub>-25%K<sub>2</sub>SO<sub>4</sub> after 100 cycles.



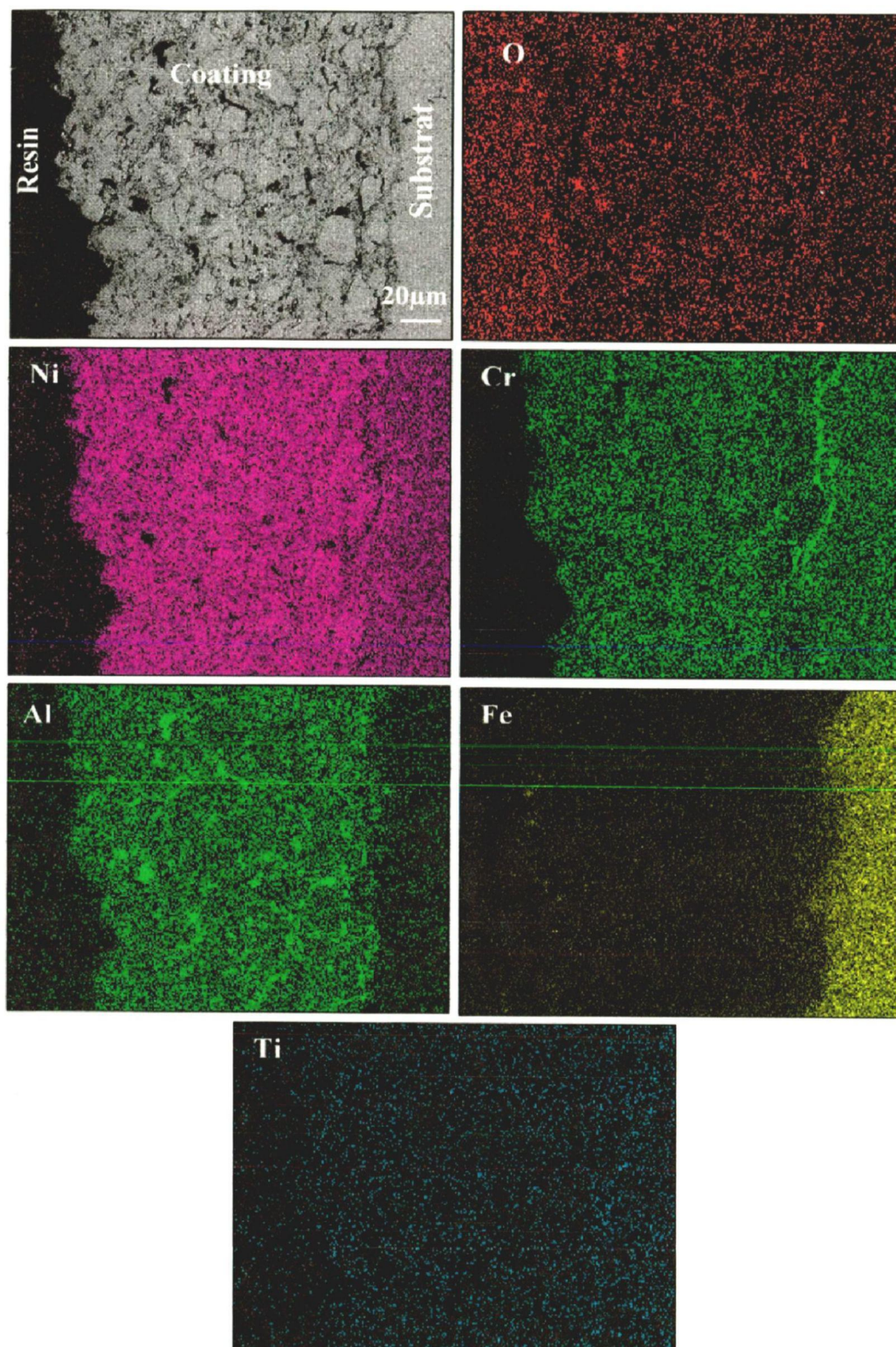


**Fig. 5.41** Composition image (SE) and X-ray mapping of the cross-section of the NiCrAlY + 0.4 wt%CeO<sub>2</sub> coated superalloy superfer 800H subjected to cyclic oxidation at 900 °C in Na<sub>2</sub>SO<sub>4</sub>-25%K<sub>2</sub>SO<sub>4</sub> after 100 cycles.

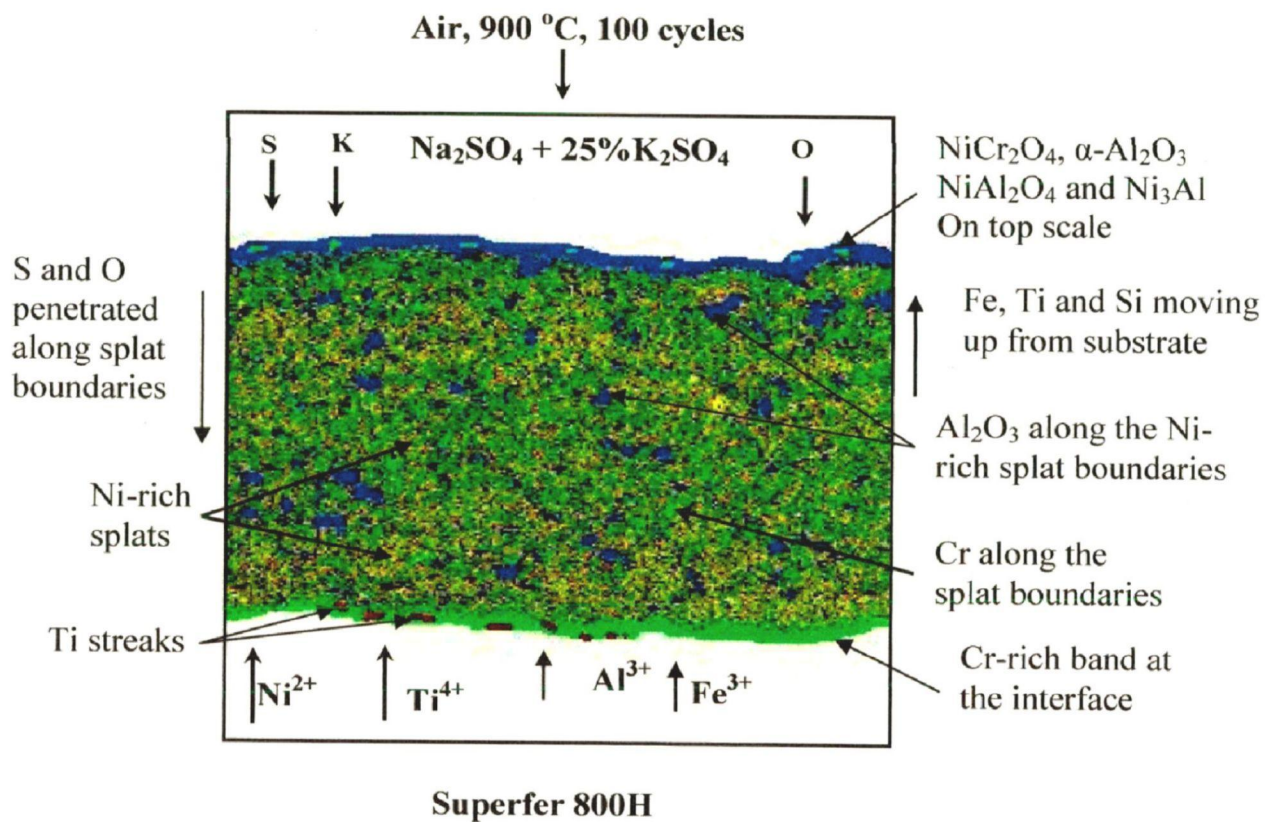


**Fig. 5.42** Schematic of the proposed oxidation mechanism of the NiCrAlY+0.4wt%CeO<sub>2</sub> coated superalloy superfer 800H at 900 °C in Na<sub>2</sub>SO<sub>4</sub>-25%K<sub>2</sub>SO<sub>4</sub> after 100 cycles.

### 5.3.2.5 Conclusions

- Greenish colour oxide scale observed in the coated alloys might be attributed to the presence of oxides of Ni and Cr
- Coated superalloys follow nearly a parabolic rate law, whereas bare superalloys deviates from the parabolic rate law.
- The NiCrAlY+0.4wt%CeO<sub>2</sub> coating provides the maximum hot corrosion resistance to superfer 800H and superni 718 as it reduces the weight gain by 74% and 72% to that of bare superalloys, respectively.
- The various phases identified from the X-ray diffraction patterns are NiCr<sub>2</sub>O<sub>4</sub>, NiAl<sub>2</sub>O<sub>4</sub>, α-Al<sub>2</sub>O<sub>3</sub>, Ni<sub>3</sub>Al and NiO.
- Corroded coating depicts the formation of two regions one with Ni-rich region (white agglomerated crystalline granules) and other with Cr-rich region (rectangular shaped discs).
- EDS analysis for the surface of corroded coated superalloys reveals the uppermost part of the scale has relatively higher concentration of oxygen with Ni, Cr and Al
- Coating has Ni rich splats, along the cross-section, which are mainly in an un-oxidised state.
- Aluminum and yttrium coexist with O along the Ni-rich splat boundaries in the coating.



# CHAPTER 6

## NiCoCrAlYTa COATING

---

### 6.1 CHARACTERISATION OF THE COATING

#### 6.1.1 Introduction

Nickel based superalloys, by virtue of their excellent high temperature properties coupled with corrosion resistance, have been widely used as gas turbine engine components (Sinha et al., 2005). In today's gas turbines, the emphasis is on saving energy and reducing the amounts of pollutants emitted; this can be attained only by designing alloys with higher melting points and the capability to retain mechanical integrity at increased temperatures (Maledi et al., 2006). To meet these demands, the development of nickel based superalloys (NBSAs) has reached its limit, as the alloys are operating at critical temperatures close to their melting points, further increase in the operating temperatures would result in dissolution of the strengthening phases and even melting (Maledi et al., 2006). Structural alloys have been developed for optimal mechanical properties (Aymeric Raffaitin et al., 2006) and coatings have been developed to provide the environmental resistance (Caron and Khan, 1999; Demasi-Marcin and Gupta, 1994). Superalloy components in the hottest sections of gas turbines need the application of overlay coatings like NiCoCrAlY compositions in order to resist effectively the environmental attack by hot gases and deposits (Fritscher et al., 2004). NiCoCrAlY alloys are widely used for high temperature applications due to their outstanding property profile with good ductility, high strength up to 700 °C and excellent oxidation resistance (Brandl et al., 1996; Huang, 1992; Beele et al., 1997; Choquet et al., 1987). For instance, NiCoCrAlY alloys are used as corrosion-resistant coatings applied on various superalloy components and also serve as bond layers for thermal barrier coatings (TBC) on superalloy substrates (Baufeld and Schmqcker, 2005). Sidhu et al., (2004, 2005) have characterized NiCrAlY coating on boiler-tube steels in order to provide some data base regarding their engineering applications. Various researchers have suggested the use of MCrAlY (M is Ni and/or Co) overlays and Pt-aluminide diffusion coatings as typical bond coats to protect the superalloy against oxidation and to reduce the mismatch stresses between the top



coat and the superalloy (Hocking, 1993; Bouhanek et al., 2000; Gurrappa 2000; Evans and Taylor, 2001; Kim et al., 2002; He, et al. 2002;). In the late 1960s, the Pratt and Whitney Company initiated a program to develop coatings with compositions nominally independent of substrates, and with capabilities for tailoring to the wide range of requirements of gas turbine applications (Goward, 1998). D-gun spraying is characterized by the spraying of particles that are accelerated by the D- wave and impact on the substrate surface at a high velocity of 800–1200 m/s (Semenov and Cetegen, 2002; Wagner et al., 1984; Wu et al., 2003), which is higher than that of High Velocity Oxyfuel spraying (HVOF) (about 550-850 m/s) (Stokes and Looney, 2001). As a result, higher particle velocity during deposition provides a minimum decomposition of the feed powder, due to lower heat enthalpy and shorter duration involved in the coating process (Hao Dua, 2007). The study on D- gun sprayed NiCoCrAlYT<sub>a</sub> coatings on superalloy has never been reported to the best of author's knowledge. The aim of this paper is to characterize the D-gun sprayed NiCoCrAlYT<sub>a</sub> alloy coatings on superalloys in relation to microstructure, porosity, coating thickness, phase formation and microhardness by using the combined techniques of optical microscope, X-ray diffraction (XRD) technique, Field emission scanning electron microscopy/energy-dispersive analysis (FE-SEM/EDS) and X-ray mapping to provide an experimental basis so as to enlarge applications of NiCoCrAlYT<sub>a</sub> coatings.

### **6.1.2 Experimental Details**

The details of the substrate material, coating formulation and characterisation of the coating are explained in chapter 3 (Experimental chapter).

### **6.1.3 Results**

#### **6.1.3.1 Coating powder**

A commercially available NiCoCrAlYT<sub>a</sub> (particle size: 5-37 $\mu$ m; shape-spheroidal, gas atomized, sulzer metco (Amdry 997)) powder with chemical composition Ni 23Co 20Cr 8.5Al 4Ta 0.6Y is shown in Fig.6.1.

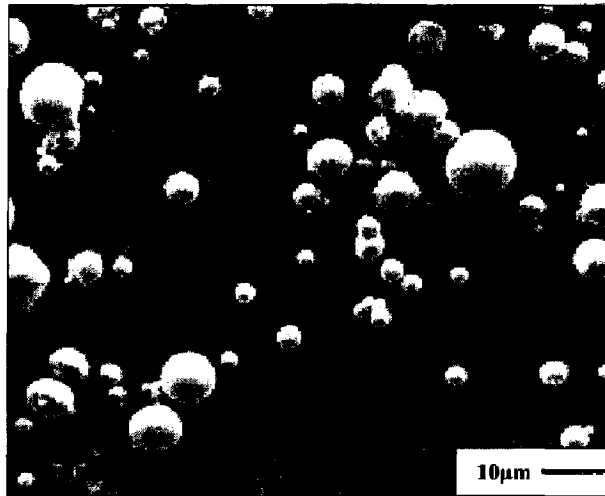


**Fig. 6.1** SEM of NiCoCrAlYTa powder

### **6.1.3.2 Cross-section and surface microstructures of the coating**

Cross-sectional and surface FE-SEM morphology for the D-gun sprayed NiCoCrAlYTa coating on a superalloy 75, superalloy 718 and superalloy 800H superalloy substrates, respectively, is shown in Fig.6.2. Micrograph clearly revealed the presence of porosity; oxide stringers ( $\text{Al}_2\text{O}_3$ ) (Fig.6.2b and c), un-melted and semi-melted particles and oxide inclusions (Fig. 6.2d and f). Un-melted particles are identified in the coating by their size and near-spherical morphology similar to that shown in Fig.6.1. The oxides believed to be formed due to in-flight oxidation of powder particles (Zhang et al., 2002), which are entrapped between successive splats.

### **6.1.3.3 Measurement of thicknesses and porosity of the coatings**

The thickness of the coatings was measured at ten different locations from the optical microscope images, taken along the cross section of the mounted samples (Fig. 6.2). The average thickness of the coatings on three superalloys, superalloy 75, superalloy 718 and superalloy 800H were 250 $\mu\text{m}$ , 200  $\mu\text{m}$ , and 250  $\mu\text{m}$ , respectively (Fig.6.2). During D-gun spraying, high particles velocities can produce a uniform coating with high hardness and strong adhesion to the substrate. The formation of few micro pores and voids along the splat boundaries in the coatings is due to the low torch temperature and very short heating time for the particles during the D-gun spray process (Wu et al., 2003). The porosity is visible as black contrast regions in the coating and it was less than 0.48 % .

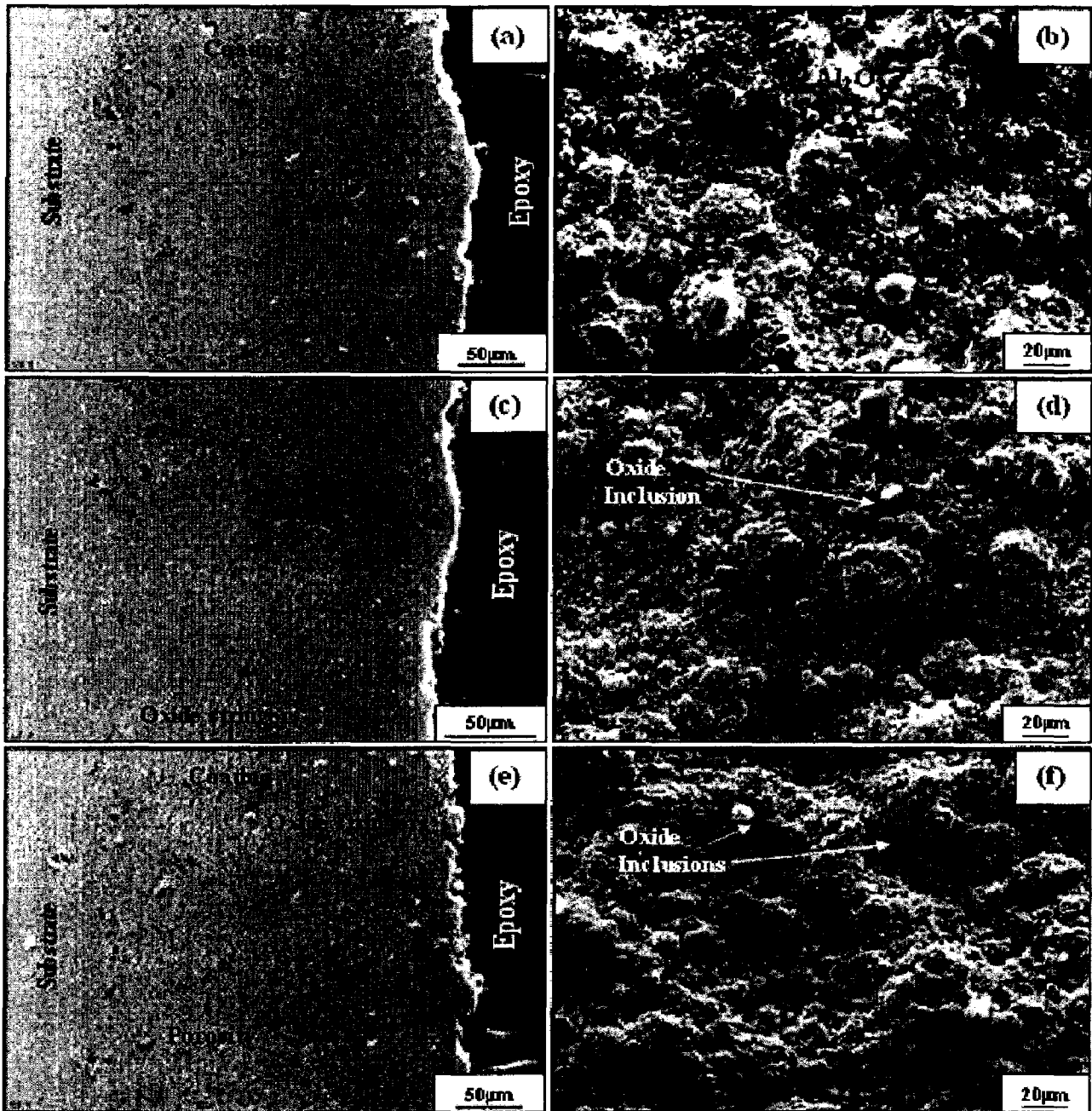


**Fig. 6.2** FE-SEM micrographs showing as-sprayed cross-sectional and surface morphology of D-gun sprayed NiCoCrAlYTa coating on (a and b) superni 75, (c and d) superni 718 and (e and f) superfer 800H respectively.

### 6.1.3.4 Surface roughness (Ra) of the as-sprayed coating

The coating surface was very rough in the as-coated condition due to the presence of unmelted particles and the roughness was found to be in the range of 6.25- 7.48(Ra) $\mu\text{m}$ . The centre line average (CLA) method was used to obtain the Ra values.

### 6.1.3.5 Microhardness of the coatings

The microhardness data for the coatings is plotted in the Fig. 6.3, which show the microhardness profiles along the cross section of the coatings as a function of distance from the coating-substrate interface. The microhardness of the substrates is found to be in the range of 290-395 Hv and it is 385-748Hv along the cross section of the coatings. Further, an increase in microhardness of superni 75 and superfer 800H is observed near the coating-substrate interface.

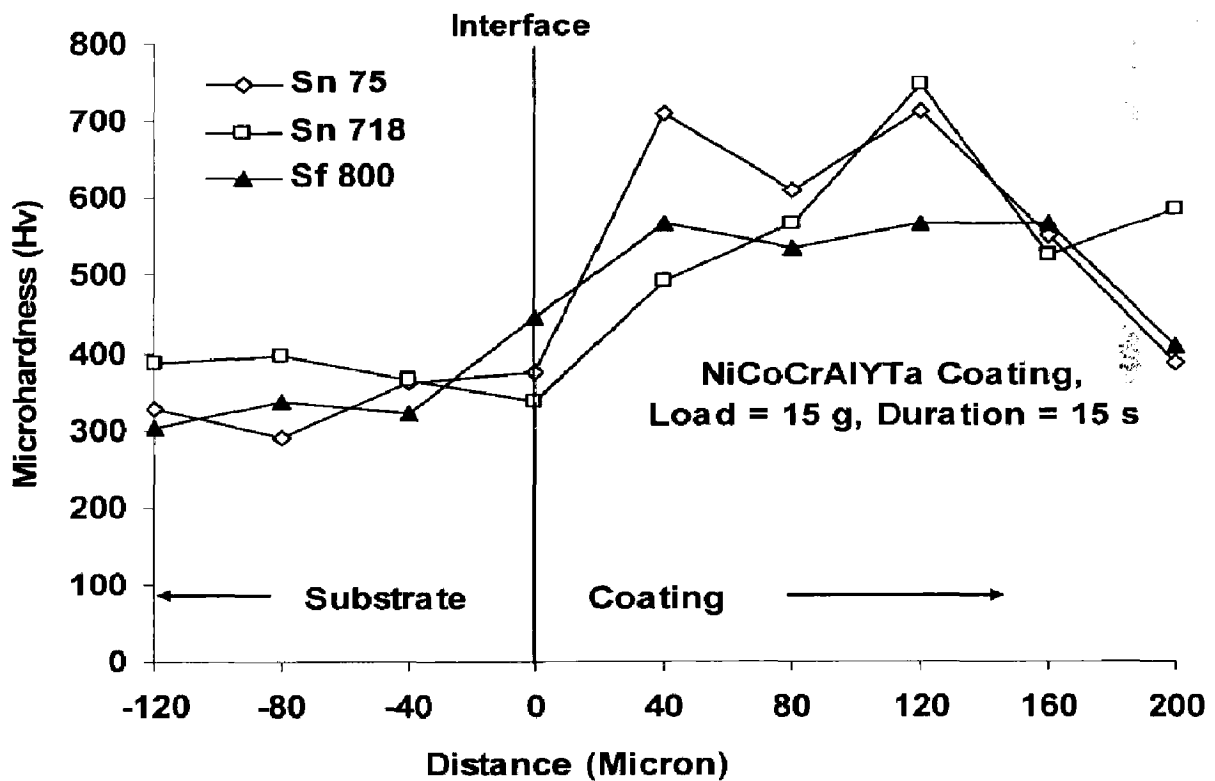


Fig. 6.3 Microhardness profiles for D-gun sprayed NiCoCrAlYTa coatings on three different superalloys.

### 6.1.3.6 X-ray diffraction (XRD) analysis

XRD patterns of the surfaces of the NiCoCrAlYTa powder and D-gun as-sprayed coatings are shown in Fig. 6.4. The NiCoCrAlYTa coated specimen shows the presence of  $\gamma$ -Ni (nickel solid solution) or  $\gamma'$ -Ni<sub>3</sub>Al as major phase.

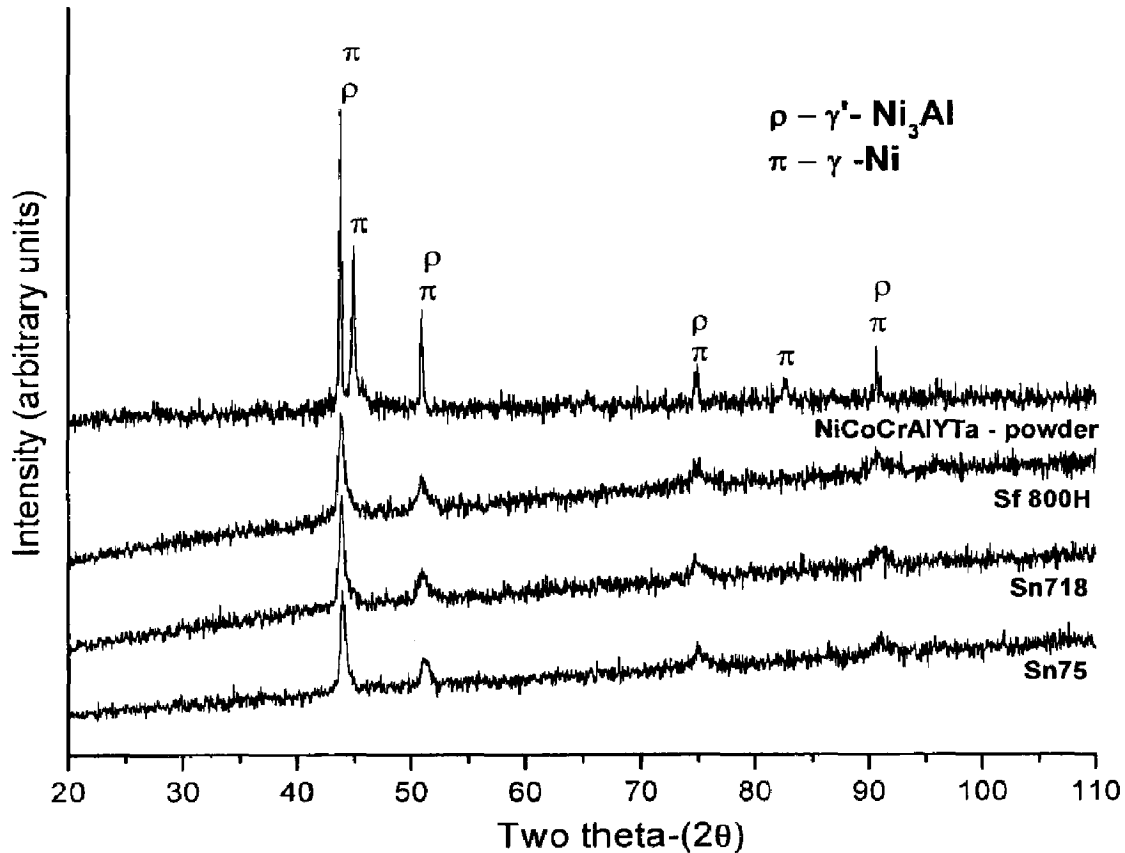


Fig. 6.4 X-ray diffraction pattern of the NiCoCrAlYTa powder and as-sprayed NiCoCrAlYTa coating on different superalloys.

### 6.1.3.7 FE-SEM/EDS analysis

#### 6.1.3.7.1. Surface morphology

FE-SEM micrographs with EDS spectrum reveals the surface morphology of the polished as-sprayed NiCoCrAlYTa coating on three superalloys shown in Fig. 6.5 a, b and c. As-sprayed microstructure of NiCoCrAlYTa coating on superalloy shows the presence of spherical/or elliptical shaped splats, whereas the dark regions represents the presence of oxides of Al, as evident from the EDS spectrum, the coating also show the micro pores along the splat boundaries

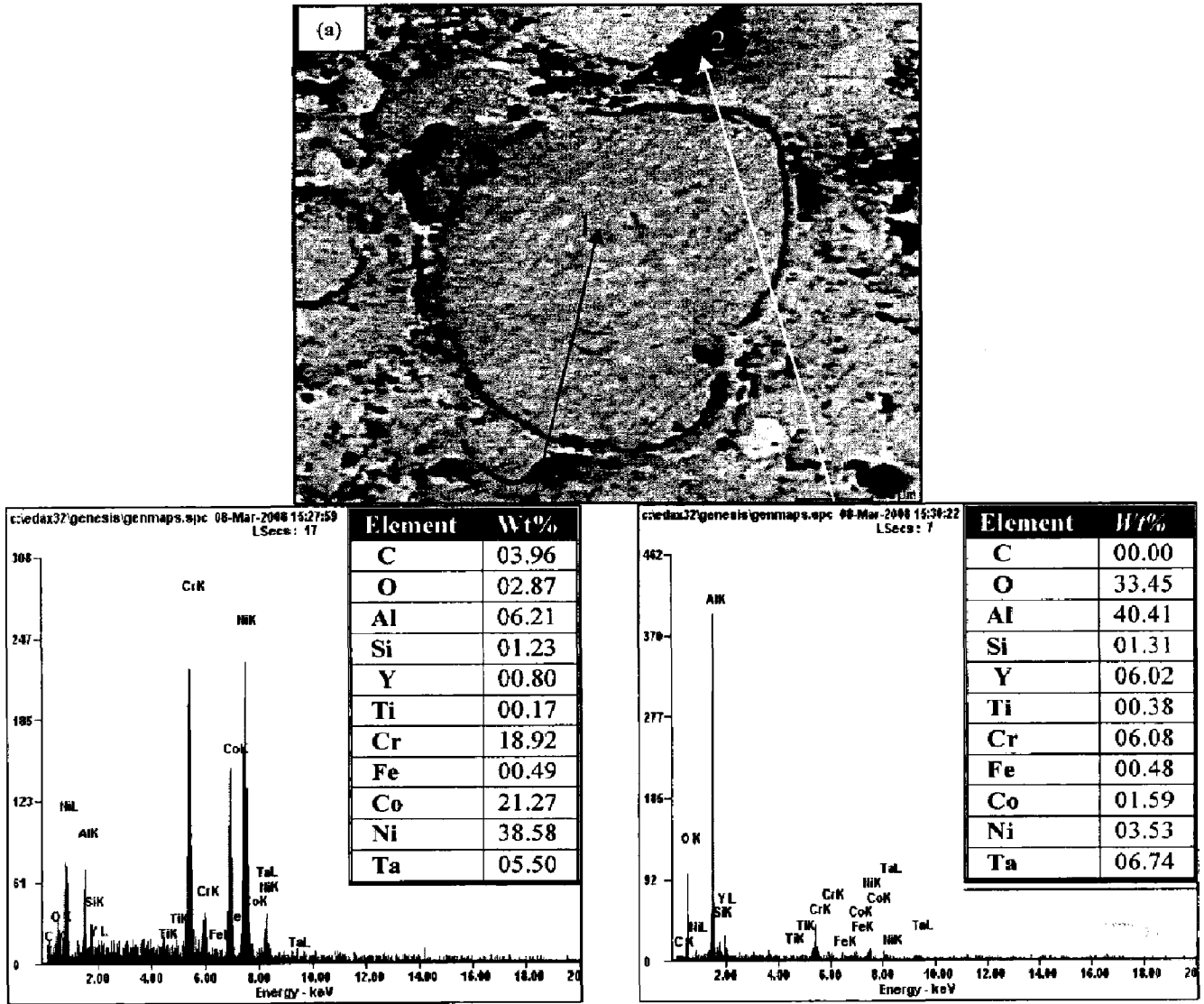
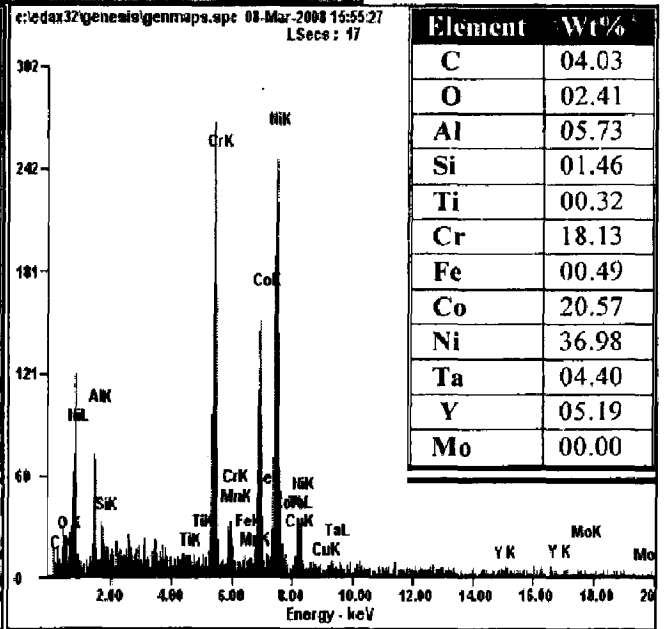
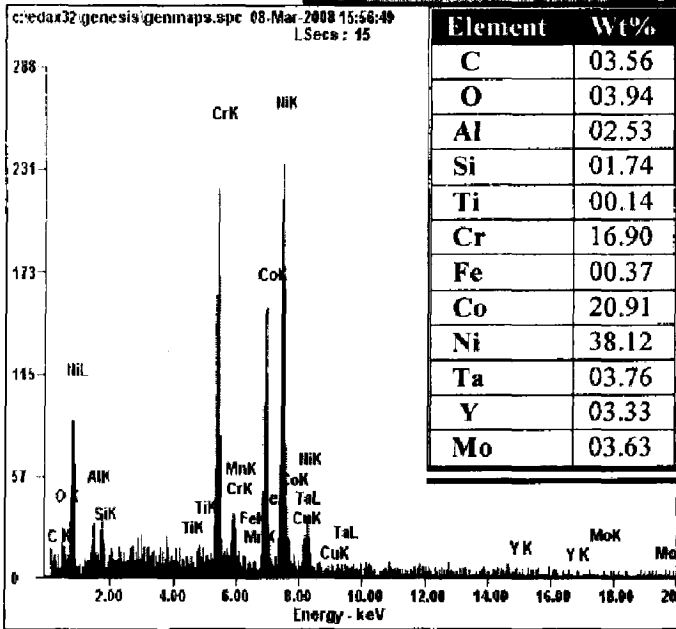
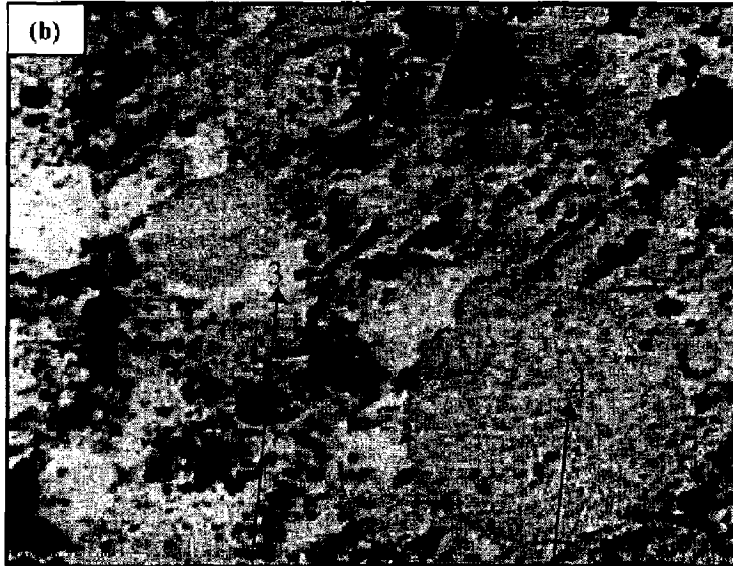
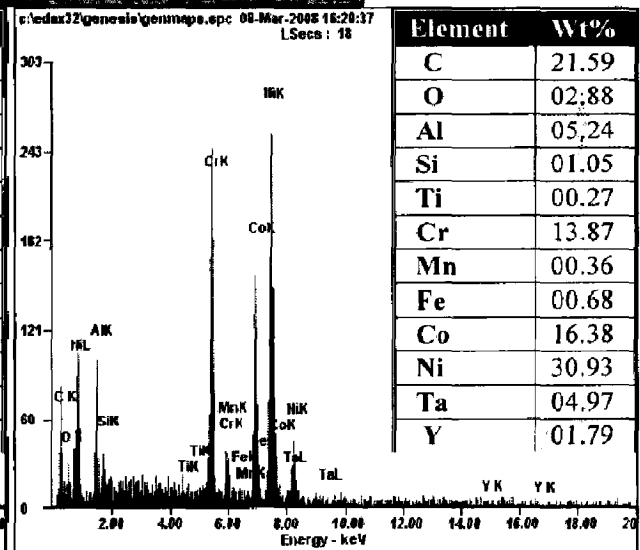
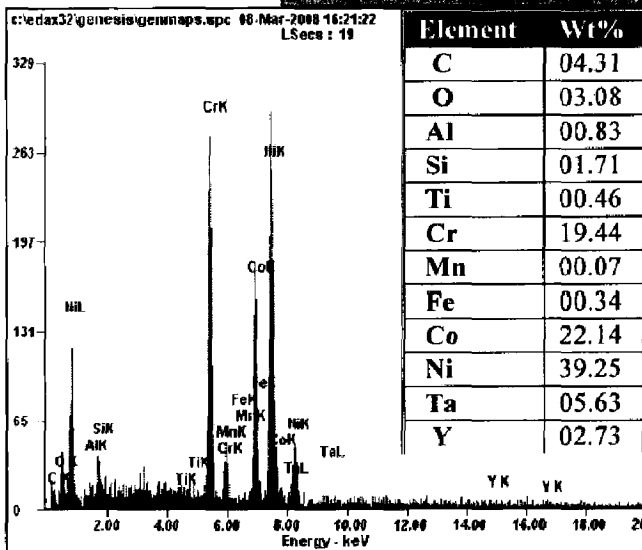


Fig. 6.5 FE-SEM surface micrographs with EDS spectrum along with elemental composition of D-gun sprayed NiCoCrAlYTa coatings on (a) superni 75, (b) superni 718 and (c) superfer 800H.





### 6.1.3.7.2 EDS cross-sectional line analysis

The cross-sectional images and the corresponding EDS line scan of the NiCoCrAlYTa coated superalloys superni 75 shown in Fig. 6.6. It is observed that nickel is mainly present in splat form with chromium and aluminum are distributed along the splat boundaries. EDS analysis has detected oxides of Al along the splat boundaries.



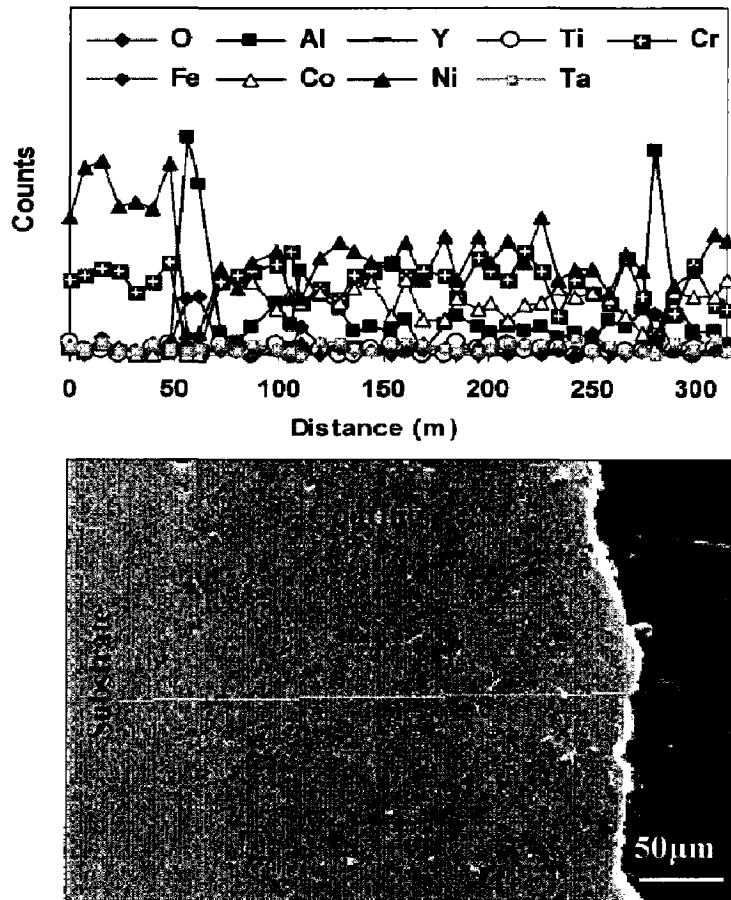
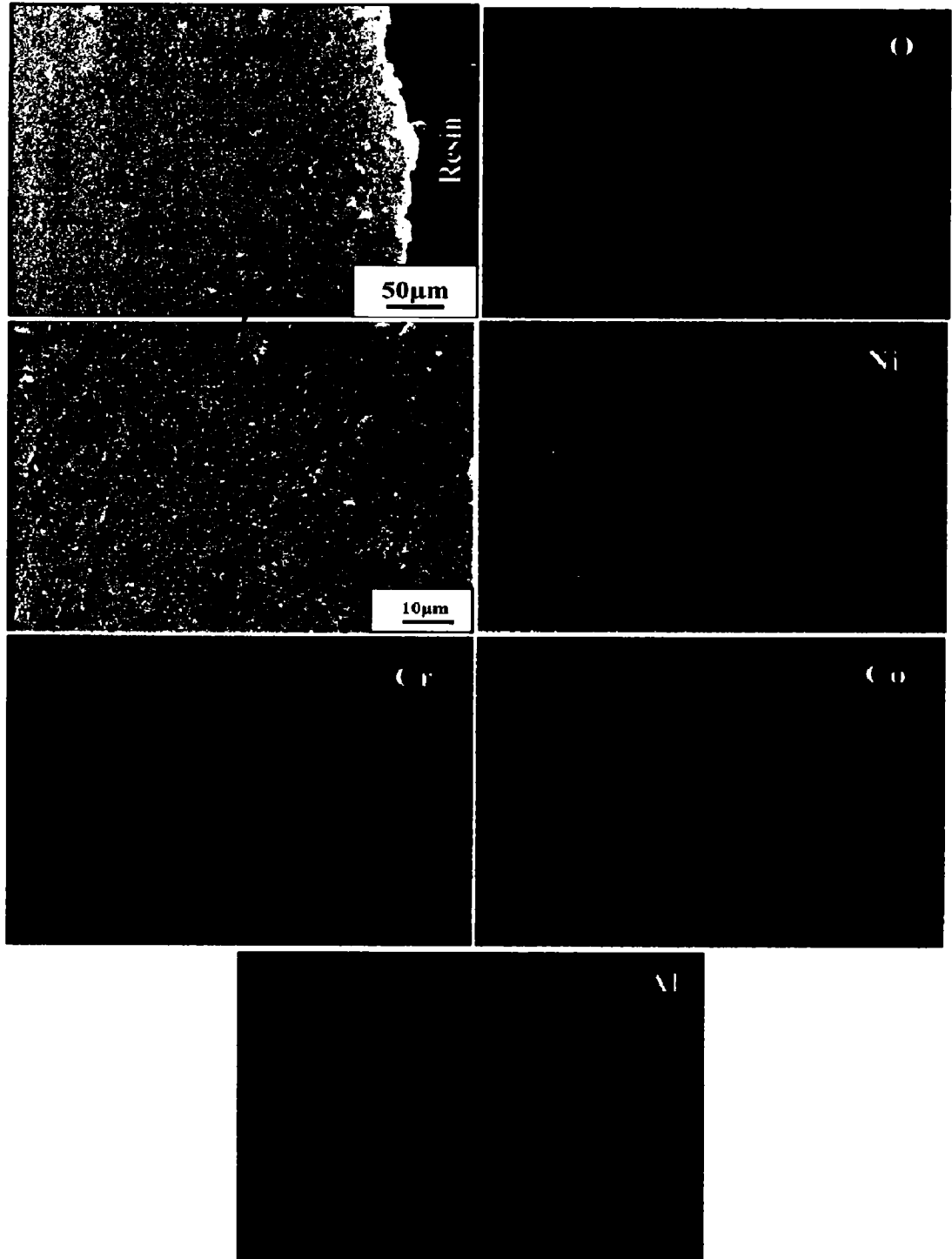


Fig. 6.6 Cross-section morphology of NiCoCrAlYTa coated superalloys in as sprayed condition and cross-section EDS line scan of superni 75.

### 6.1.3.8 X-ray mapping

The elemental X-ray mapping of the coating shows (Fig. 6.7-6.9) the presence of main elements of Ni, Co, Cr and Al, as found in the original coating powder. The coated superalloys shows that the Ni-rich splats distributed uniformly throughout the coating; whereas, chromium, aluminum and cobalt are observed along the splat boundaries. The presence of oxygen in the coating might be due to the in-flight oxidation of coating powder, which leads to oxides streaks in the form of aluminum oxide, which is clearly visible.



**Fig. 6.7** Composition image (SEI) and X-ray mapping of the cross-section of the as-sprayed NiCoCrAlYTa coated on superni 75 superalloys.

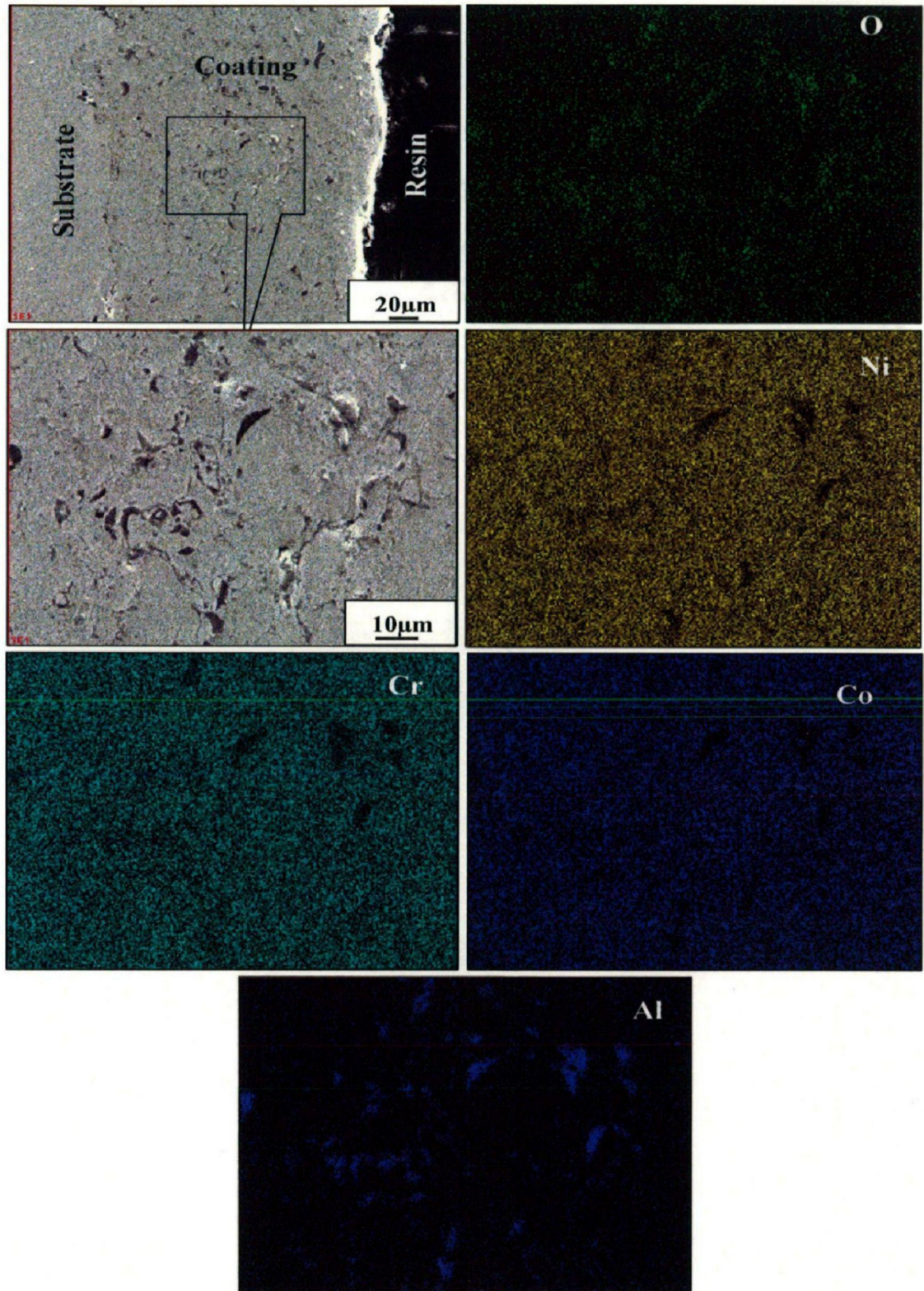


**Fig. 6.8** Composition image (SEI) and X-ray mapping of the cross-section of the as-sprayed NiCoCrAlYTa coated on superni 718 superalloys.



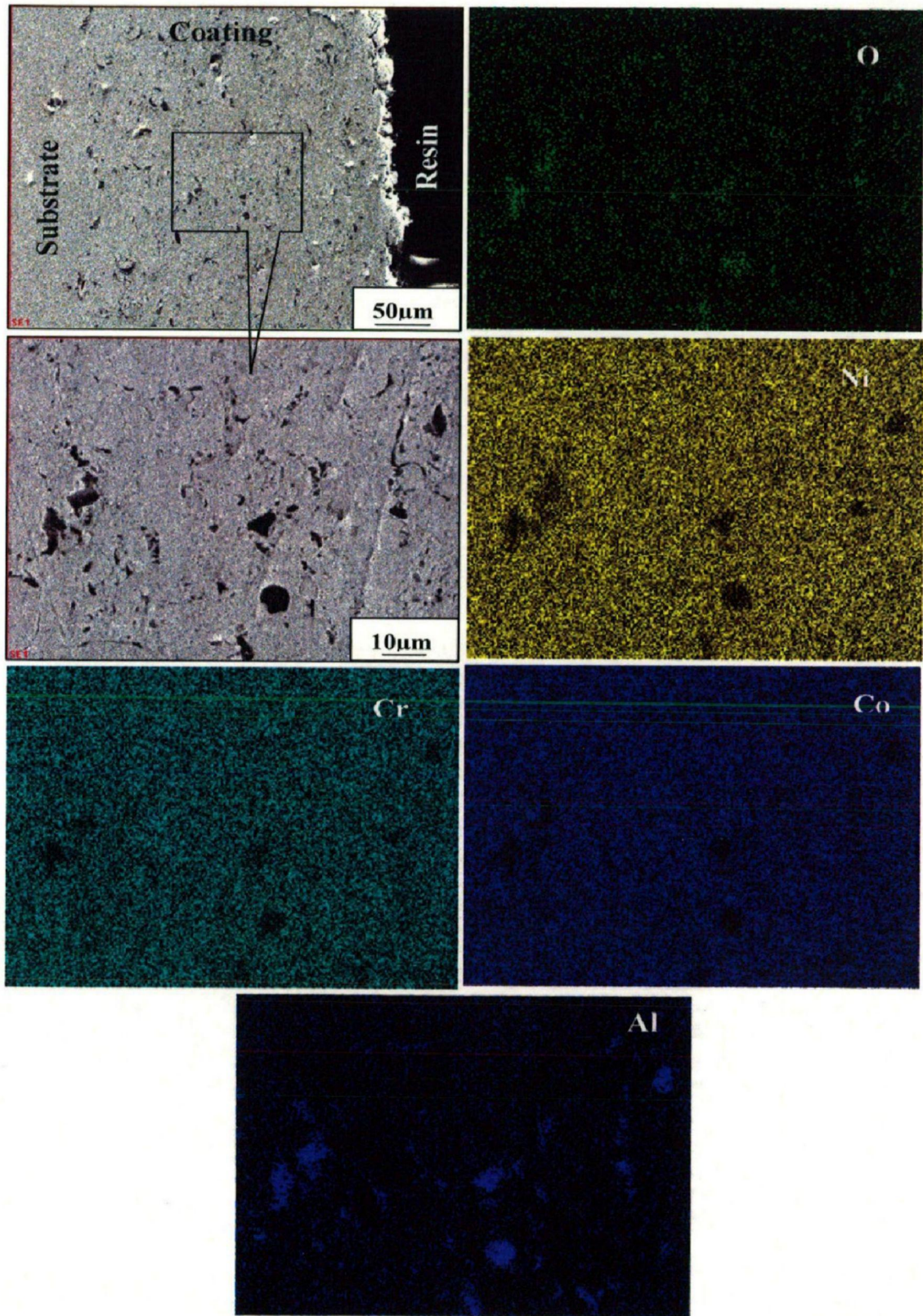


**Fig. 6.9** Composition image (SEI) and X-ray mapping of the cross-section of the as-sprayed NiCoCrAlYTa coated on superfer 800H superalloys.

## 6.1.4 Discussion

NiCoCrAlYT<sub>a</sub> coating on superalloys by D-gun exhibits dense and adherent microstructure. It can be observed that coatings possess porosity, un-melted and semi melted particles and oxide inclusions (Fig.6.2). The thin contrast stringers which appeared in the microstructure are presumably the oxides that are believed to be formed due to the oxidation of in-flight particles. D-gun entraps the air during spraying and micropores acted as the shelters for the residual air (Zhang et al., 2003). It can be deduced that oxidation took place on the surface of the powder droplets during their flight in D-gun spraying. The resulting Al<sub>2</sub>O<sub>3</sub> was then entrapped into the coating and sandwiched between the splats after deposition (Zhang et al., 2002). In-flight oxidation depends strongly upon the amount of air entrapped, particle temperature and nature and turbulence of D- flame. The quantity of air entrained in the D-gun depends strongly upon the jet velocity. Deshpande et al., (2006) proposed that, during in-flight oxidation, a layer of oxide is formed on the molten particle due to chemical reactions between the surface of the liquid phase and oxygen or due to diffusion of oxygen into the liquid. The turbulent mixing of the liquid part of the powder particle during its flight destroys the surface layer of oxides and causes the oxides to be distributed more uniformly through the bulk volume of the particle. However, when temperature of the particle starts dropping during later part of the flight, these oxides tend to solidify and a thin oxide shell would form around the droplet. (Li and Li, 2002) has shown that a decrease in particle radius leads to an increase in the level of oxidation, smaller particles of oxides distributed over the entire particle, whereas with increase in particle size, it is found that the particle develops an oxide coating or shell. Thus, the oxidation of an in-flight particle proceeds from particle surface towards the center. Oxide inclusions along the splat boundaries have also been noted by (Wang et al., 1999). Hence, these oxides have appeared in the form of thin stringers along the splat boundaries (Fig. 6.2c and b). Literature shows that the D-gun coatings have very low porosity levels (< 1%) compared with plasma spray coatings having very high porosity levels of 8–15% (Kharlamov, 1987). The porosity (Fig. 6.2e) values in the present investigation are found to be less than 0.48%. The porosity values of as-sprayed coatings are identical with the findings of Mayoral et al., (2008) and Seo et al., 2007 who have reported that the pores form usually near the splat boundaries.

Surface roughness is one of the important parameters of the D-gun sprayed NiCoCrAlYT<sub>a</sub> coatings need to be measured for its better performance in the high temperature applications. For

example, in thermal power plants, the coatings employed on the boiler tube components are subjected to solid particle erosion and therefore it is essential to ensure the erosion resistance of the coatings with respect to its surface features such as surface roughness, adhesive bond strength and morphology of the grain, etc. The roughness of as-sprayed NiCoCrAlYTa coating, in the present investigation, is higher than the HVOF sprayed NiCoCrAlYTa coating. The roughness of the coatings increases adhesion strength of YSZ top coats in thermal barrier coating systems as reported by Lima and Guilemany, (2007).

Microhardness is one of the important mechanical properties of the coatings need to be measured to ensure its reliability in the actual applications (Tucker, 1974). The microhardness of D-gun sprayed coatings has been found to be very high as compared to the superalloy substrates (Fig. 6.3). Some variations in hardness values in the coating may be due to the presence of micro pores, oxide inclusions, un-melted and partially melted particles. Near the coating–substrate interface, a slightly higher value of hardness is found as compared to the bare substrates. This increased hardness value near the coating–substrate interface might be due to the work hardening effect of sandblasting of the substrates prior to the coating process as reported by our institute research group (Sidhu and Prakash, 2003; Sidhu, et al., 2006H, 2006C; Mahesh, et al., 2008; Sidhu, 2003). Hardening of substrate superalloy may also be partly attributed to the high speed impact of the coating particles during D-gun spraying. Similar phenomenon has also been observed in our previous publications (Kamal et al., 2008A and B). Further, the higher values of the hardness of the coatings as compared to the substrate alloys may be partly contributed by the high density and cohesive strength of the individual splats as a result of the high impact velocity of the coating particles as reported by various researchers (Rajasekaran, et al., 2008; Hao Du et al., 2007). The high hardness values found in the coating could also be due to the severe plastic deformation undergone by partially un-molten material upon impact owing to the high impact velocity of the sprayed particles. Ahmed and Hadfield analyzed the rolling contact fatigue performance of thermally sprayed (WC-12%Co coatings) rolling steel elements and reported that the performance of high velocity oxy fuel and D-gun sprayed coatings were superior than that of the plasma sprayed coatings due to their inherent properties such as low porosity, high hardness and compressive residual stresses (Ahmed and Hadfield, 1996). It can be deduced from the XRD patterns (Fig.6.4) that as-sprayed coatings show  $\gamma$ -Ni (solid solution fcc structure) or  $\gamma'$ -Ni<sub>3</sub>Al as a principal phase. Similar phases have also been reported by Aymeric Raffaitin et al., (2006),

Fernando Juarez et al., (2003) and Frances, et al., (1985) for Praxair Tribomet, Chemical vapor deposition and plasma sprayed NiCoCrAlYTa coatings, respectively.

FE-SEM micrographs with EDS spectrum corresponding to the surface morphology of polished surface of the NiCoCrAlYTa coating are shown in Fig. 6.5 (a, b and c). The coating depicts the formation of globular dendritic structure composed of Ni, Co and Cr elements. Due to discontinuous powder flow in the D-gun process, it is observed that such areas have bigger dendritic agglomerated structure. D-gun coatings are more prone to form agglomerated structure, due to two or more powder particles combined into big agglomerate (Fig.6.5a). The agglomerates are not fully melted during spraying; as a result, un-melted dendritic particles appeared in the coating (Zhang et al., 2003).

As sprayed polished microstructure of NiCoCrAlYTa coatings on superalloy superni 75 (Fig. 6a at point 1) shows the presence of spherical/or elliptical shaped dendrites splats, whereas the dark region at point 2 represents the presence of oxides of Al, as evident from the high peak EDS spectrum along with EDS elemental composition. The diameter of the dendrites is equal to that of original powder particles. The similar microstructural observations were also depicted on other superalloy substrate such as superni 718 and superfer 800H (Fig.6.5b, c), also the surface microstructure show irregular shaped small pits, although some of the pits are pores, which formed during spraying. These pores might have also formed due to pullouts of the coating during polishing process and such type of behaviour has also been reported by Li and Ding, (1999) in the plasma sprayed  $Cr_3C_2$ -NiCr coating.

EDS line scan analysis (Fig.6.6) across the cross-section of the coating had Ni rich elements followed by Cr, Co and Al, respectively. Al streaks in the form of oxides are distributed non uniformly in the coating as evident from high intensity peaks along line, which is further supported by oxygen distribution along these Al streaks as depicted by X-ray mapping (Fig.6.7). Chen, et al., (2005) and Zhang, et al.,(2002) have observed similar Al streaks in their studies on air-plasma-sprayed and D-gun sprayed NiCrAlY coatings, respectively. The X-ray mapping of NiCoCrAlYTa coated superalloys across the cross-section (Fig. 6.7-6.9) depicts that the splats are rich in nickel, whereas Cr, and Co are distributed along these splat boundaries, Al streaks randomly distributed along the splat boundaries.



### 6.1.5 Conclusions

- NiCoCrAlYTa (Amdry 997) coatings were deposited on Ni and Fe based superalloys by D-gun thermal spray process.
- Surface morphology of the as-sprayed coating on all three substrates depicts the formation of un-melted particles in the form of globular dendritic structure. The diameter of the dendrites is equal to that of original powder particles.
- XRD analysis revealed the presence of  $\gamma$ -Ni or  $\gamma'$ -Ni<sub>3</sub>Al as the major phase.
- Surface roughness of the coating was found to be in the range of 6.25-7.48  $\mu\text{m}$ . Microhardness measurements revealed that the coating microhardness varies throughout its section. The microhardness of the coating is found to be in the range of 385-748Hv.
- The thickness of coating ranges from 220-250 $\mu\text{m}$  and it showed a good adhesion with all the substrates due to the absence of cracks and gaps at the interfaces. The measured porosity values are less than 0.48%.



## **6.2 OXIDATION STUDIES IN AIR**

### **6.2.1 Introduction**

Nickel-based superalloys are widely used for high temperature applications, especially for blades in recent advanced gas turbines, due to its good mechanical properties at elevated temperatures (Zhang et al., 1993B; Li and Wahi, 1995; Wang et al., 1995; Chen et al., 1995). Today, numerous Ni-based, Co-based, and Fe-based superalloys serve in all kinds of gas turbine engine applications. Due to the harsh environments in which they are used, it is necessary to protect them with coatings, against heat, oxidation and corrosion (Benoist et al., 2005). The role of the coating, in this case, is to provide a metal surface composition which will react with the environment to produce the most protective scale possible combining corrosion resistance with long term stability and resistance to cracking or spallation under mechanical and thermal stresses induced during the operation of the component (Gurrappa, 2001). Superalloy components in the hottest sections of gas turbines need the application of overlay coatings like NiCoCrAlY compositions in order to resist effectively the environmental attack by hot gases and deposits (Fritscher et al., 2004). D-gun spraying technique has been commercially used in the manufacture of wear resistant coatings for its high hardness and low power cost. Due to the low porosity and good adhesion of the D-gun coatings, the inward diffusion of oxygen in to the coatings is effectively prevented (Zhang et al., 2002). It is possible to achieve temperature as high as 3850 °C in the combustion and highest velocity (800–1200 m s<sup>-1</sup>) for the sprayed powders, in the DGS, which are unattainable by the plasma and HVOF processes (Zhang et al., 2003; Hao Du et al., 2005). There is no reported study on the oxidation behavior of NiCoCrAlYT-Ta-coating on Ni and Fe-based superalloys. Therefore, in the present investigation, an attempt has been made to study the cyclic oxidation behavior of D-gun-sprayed NiCoCrAlYT-Ta-coating on Ni and Fe-based superalloys in air at 900 °C. The cyclic oxidation behavior of bare superalloys was also investigated and used to assess the performance of coated superalloys.

### **6.2.2 Experimental details**

The substrate materials, coating formulation and the oxidation studies are explained in detail in section 3.1, 3.2.3 and 3.4.1.

## 6.2.3 Results

### 6.2.3.1 Visual observations and weight change measurements

The surface micrographs of the coated superalloys after oxidation studies in air, at 900 °C under cyclic conditions are shown in Fig.6.10. The colour of the scale formed on the specimen is dark grey during early cycles, as the oxidation went on, the colour of the oxide scale turned in to greenish. The scale had no cracks and did not show any tendency of spalling during the course of study. The coating was found to be successful in maintaining its contact to the substrate superalloys during cyclic oxidation studies in general, although it suffered minor spallation along or near the edges of the specimens. The kinetics of oxidation was determined from the weight gain/unit area ( $\text{mg}/\text{cm}^2$ ) versus number of cycles plots for the bare as well as D-gun-sprayed NiCoCrAlYTa-coated superalloys (superni 75, superni 718 and superfer 800H) oxidised at 900 °C in air for 100 cycles are shown in Fig.6.11. Bare superalloy superfer 800H shows the maximum weight gain among all the superalloys. The weight gain by bare superni 75 and superni 718 after 100 cycles is nearly 13% and 16% less than that of bare superfer 800H. The coated superalloys show lower weight gain than the bare specimens in the given environment. Coated superni 75 showed the lowest weight gain, whereas bare superfer 800H showed highest weight gain. The weight gain of coated superalloys superni 75 and superni 718 and superfer 800H is nearly half, three-fifth and four-fifth respectively, as compared to that of bare superalloys superni 75 and superni 718 and superfer 800H (Fig. 6.13). The oxidation behaviour of NiCoCrAlYTa-coated superalloys follow nearly a parabolic rate law, except for coated superfer 800H, as it slightly deviates from the parabolic rate, the deviation has been observed after 35 cycles, as can be inferred from the square of weight change ( $\text{mg}^2/\text{cm}^4$ ) versus number of cycle plots (Fig.6.12). The parabolic rate constants ( $k_p$  in  $10^{-10} \text{ g}^2 \text{ cm}^{-4} \text{ s}^{-1}$ ) for the NiCoCrAlYTa-coated and bare superalloys after 100 cycles of hot corrosion run is shown in Table 6.1.

### 6.2.3.2 X-ray diffraction (XRD) analysis

The various phases identified from the X-ray diffraction patterns of the surface oxide formed on D-gun sprayed NiCoCrAlYTa coated superalloys after cyclic oxidation in air at 900 °C for 100 cycles are shown in Fig.6.14. The surface oxides formed on coated superalloys are  $\text{NiCr}_2\text{O}_4$ ,  $\text{Ni}_3\text{Al}$  and Ni.

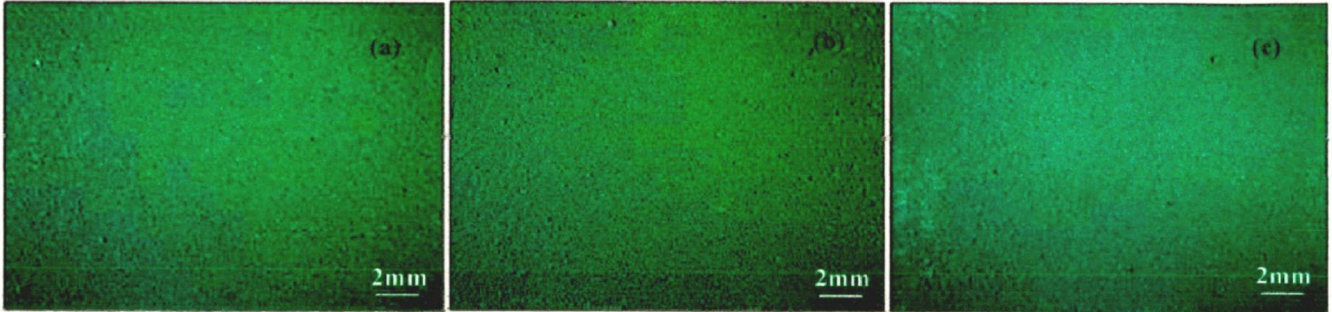


**Fig. 6.10** Surface macrograph of NiCoCrAlYTa coated superalloys subjected to cyclic oxidation in air for 100 cycles at 900 °C, (a) superni 75, (b) superni 718 and (c) superfer 800H.

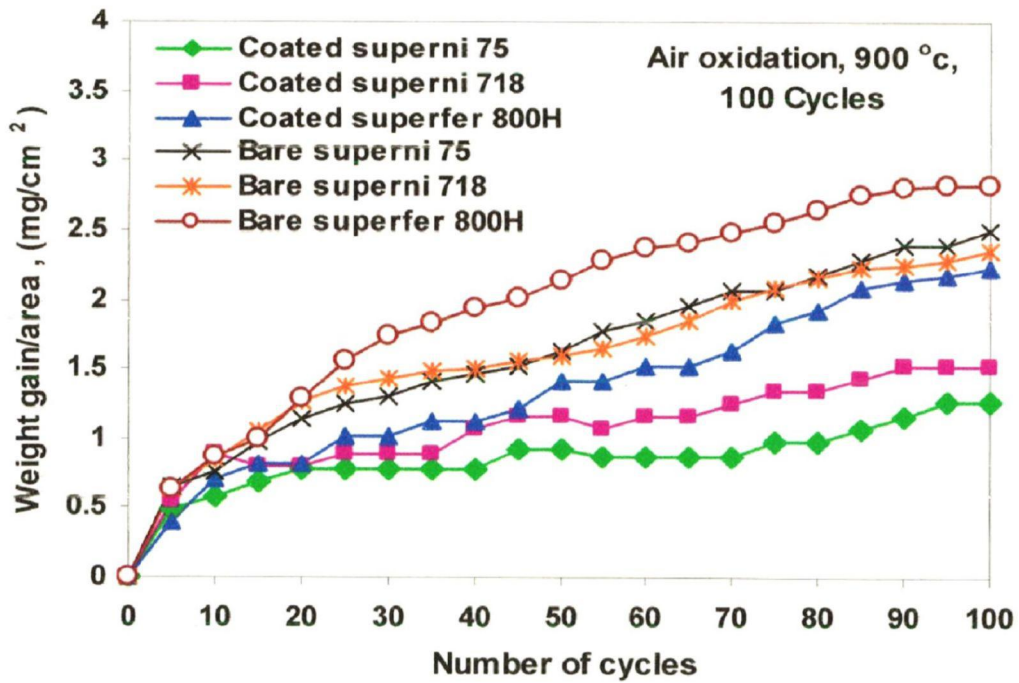


**Fig. 6.11** Weight gain/area vs. number of cycles plot for NiCoCrAlYTa coated and bare superalloys subjected to cyclic oxidation in air for 100 cycles at 900 °C.

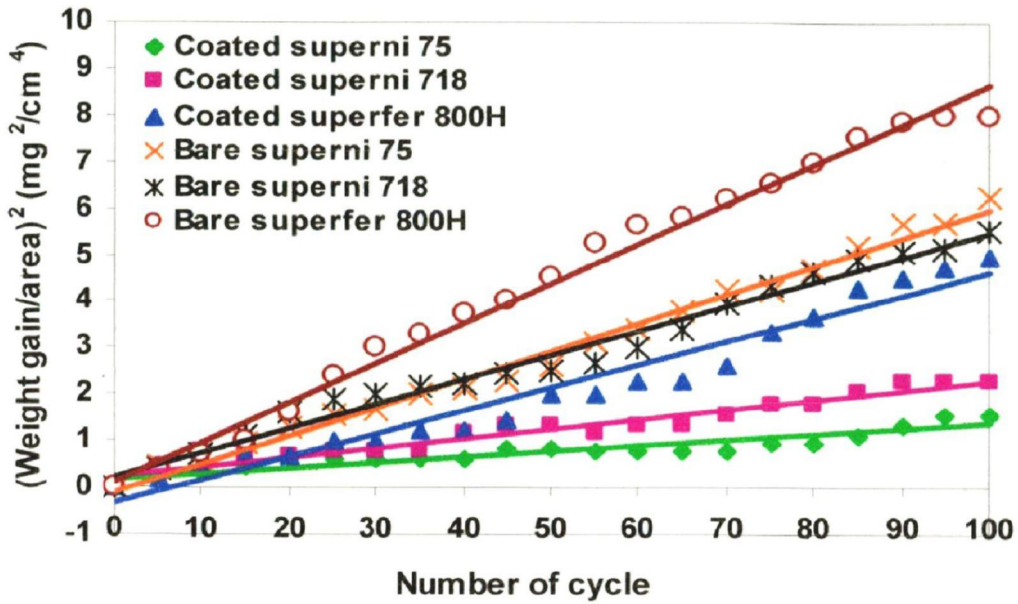


**Fig. 6.12**  $(\text{Weight gain/area})^2$  vs. number of cycles plot for NiCoCrAlYTa coated and bare superalloys subjected to cyclic oxidation in air for 100 cycles at 900 °C.

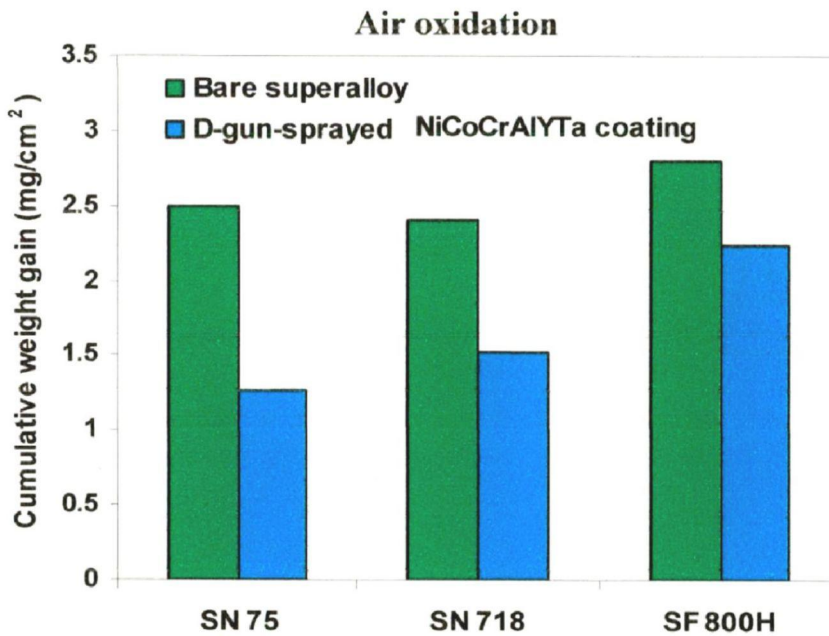


**Fig. 6.13** Bar chart showing cumulative weight gain per unit area for bare and NiCoCrAlYTa coated superalloys subjected to cyclic oxidation in air for 100 cycles at 900 °C.

**Table 6.1** Parabolic rate constant ( $k_p$ ) values for bare and D-gun-sprayed NiCoCrAlYTa-coated superalloys subjected to cyclic oxidation in air for 100 cycles at 900 °C

Superalloy substrates	$K_p \times 10^{-12} \text{ g}^2 \text{ cm}^{-4} \text{ s}^{-1}$
Bare superni 75	16.86
Bare superni 718	16.44
Bare superfer 800H	23.72
Coated superni 75	3.33
Coated superni 718	5.777
Coated superfer 800H	13.80

### 6.2.3.3 FE-SEM/EDS analysis

#### 6.2.3.3.1 Surface morphology of the scales

FE-SEM micrograph with EDS spectrum (Fig. 6.15) reveals the surface morphology of the NiCoCrAlYTa-coated superalloy specimens after cyclic oxidation in air for 100 cycles at 900 °C. The surface scale developed on coated superni 75 (Fig. 6.15a) is massive and dense with O and Al elements whereas white granules are present at some places consisting mainly of Ni, Cr and Co elements along with oxygen indicating the formation of respective oxides and their spinels. Micrograph of oxidised NiCoCrAlYTa-coated superni 718 (Figs. 6.15b), appears to be dense with matrix mainly consisting of oxides of Al, Ni, Cr, and Co, whereas small nodules on the matrix had higher concentration of O and Cr indicating the formation of  $\text{Cr}_2\text{O}_3$ . Similarly, the scale formed on the NiCoCrAlYTa-coated superfer 800H is dense with major elements of O, Al, Ni Co and Cr; whereas white small nodules have O, Cr, Co and Ni elements (Figs. 6.15c).

#### 6.2.3.3.2 Cross-sectional analysis of the scale

Cross-sectional analysis of the scale and the coating is carried out at different points along the cross-section of the air oxidised D-gun NiCoCrAlYTa-coated superni 75, superni 718 and superfer 800H by FE-SEM/EDS and the results are shown in Fig. 6.16. Cross-sectional EDS analysis of air oxidised NiCoCrAlYTa-coated superni 75 reveals (Fig. 6.16a) that the uppermost part of the scale has relatively higher concentration of O, Co, Cr and Ni (point 1), while Al rich element is found by side of Ni rich splats (point 2). Further, at point 3-6 depicts the enrichment

of Ni and depletion of Cr. Inter-diffusion of Cr and Ni from coating in to the substrate and from the substrate in to the coating, respectively, has occurred as evident from EDS analysis at point 7 (Fig.6.16a). NiCoCrAlYTa-coated superalloy 718 (Fig.6.16b) shows the presence of Ni, Cr and Co rich- elements in the top most layer, further, along the cross-section of coating, (Points 2-5), Ni-rich splats found, absence of oxygen at these points suggests that these Ni-rich splats are in the un-oxidised state. The presence of alumina at the coating-substrate interface may be due to grit blasting of the substrate prior to the coating. Whereas, superalloy 800H (Fig.6.16c) indicates a scale which mainly consists of chromium, nickel, cobalt, aluminum and oxygen rich elements. The concentration of Cr, Co and Ni at points 2, 3 and 4, nearly remains unchanged. Presence of O, Al and Y (point 5) along the splat boundaries indicates the formation of oxides of Al and Y

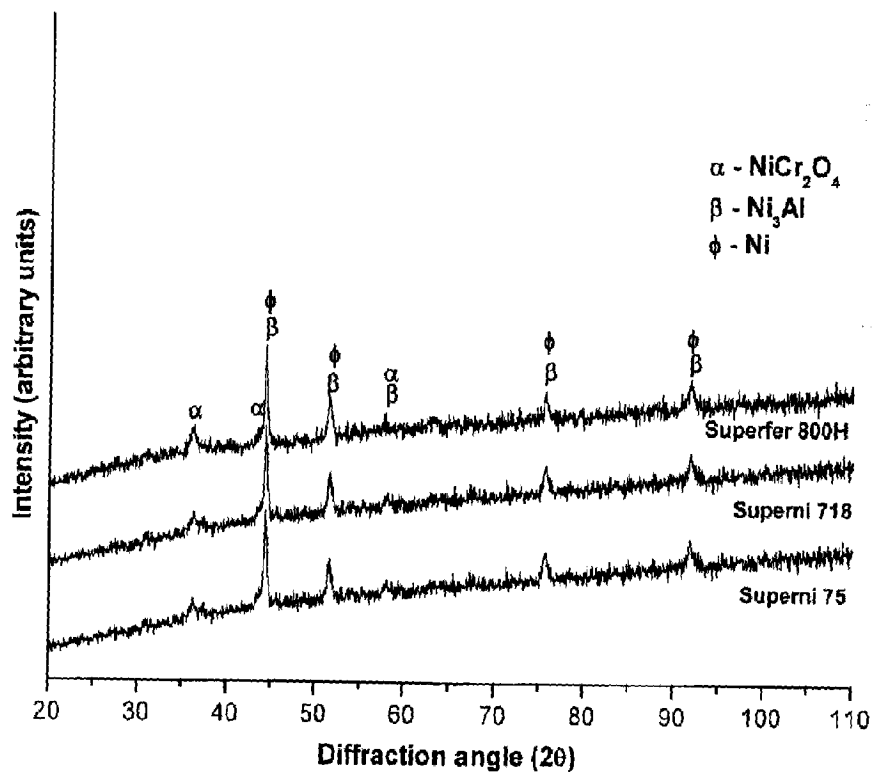


**Fig. 6.14** X-ray diffraction patterns for NiCoCrAlYTa coated superalloys exposed to cyclic oxidation in air at 900 °C after 100 cycles.

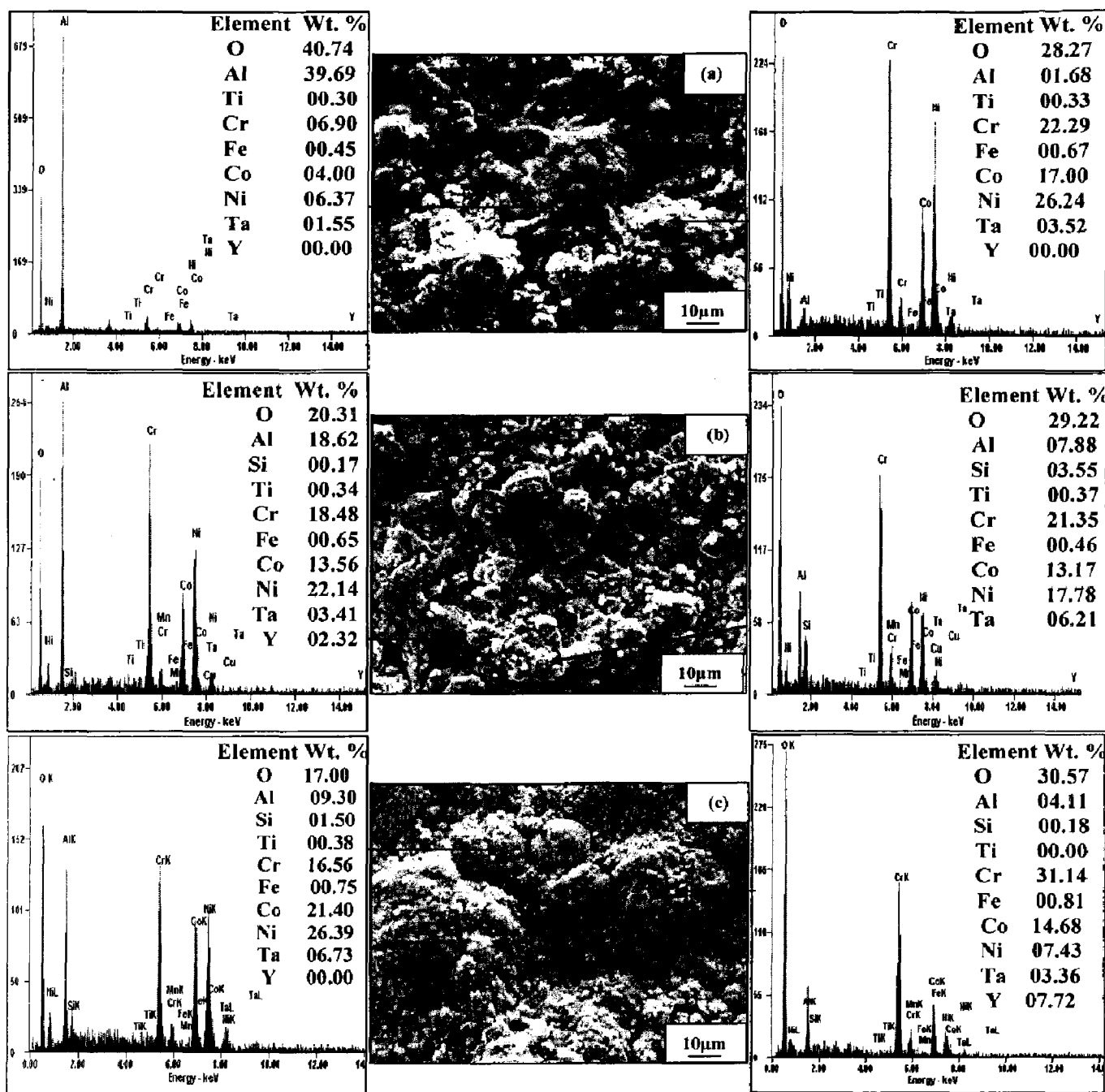
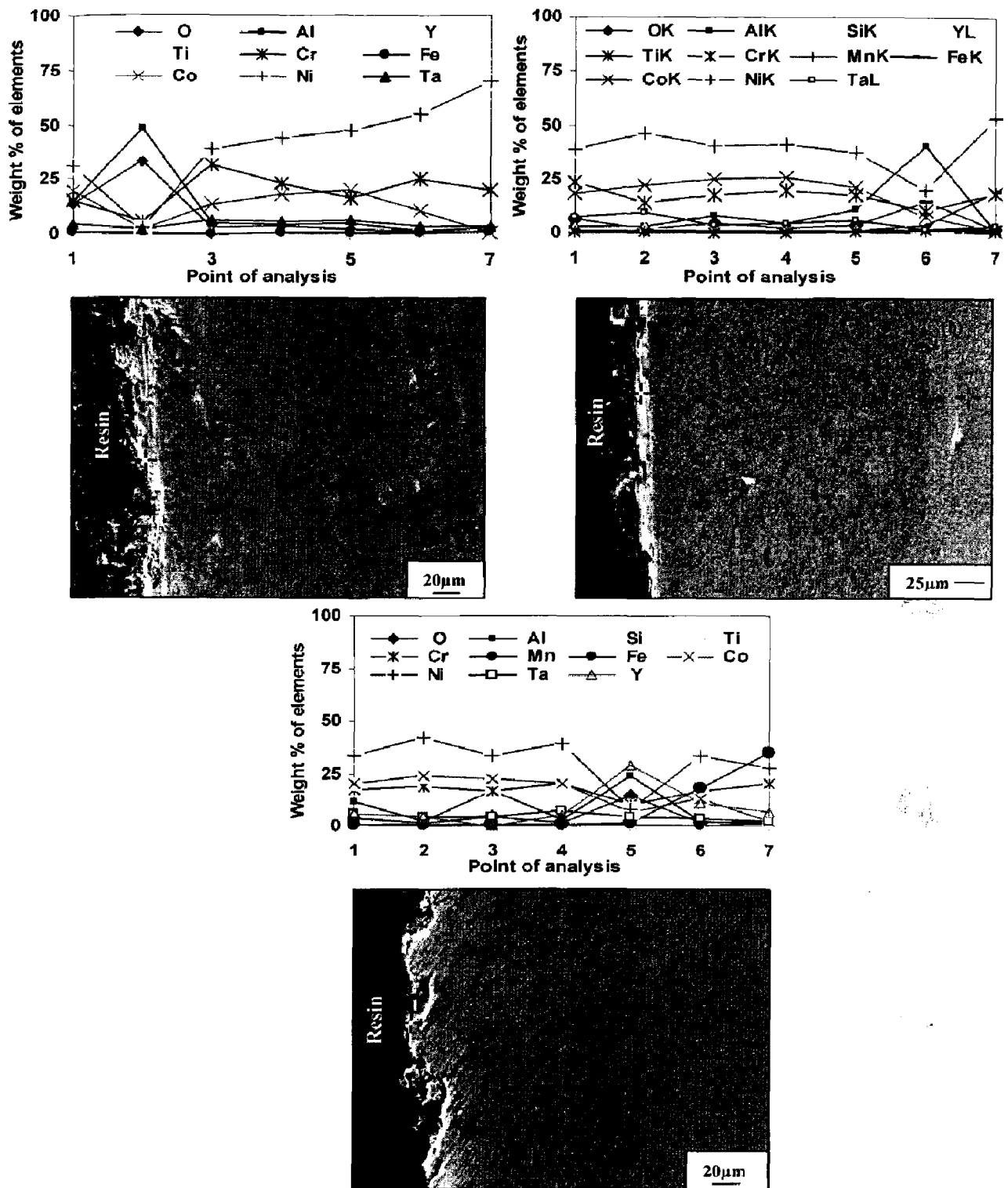


Fig. 6.15 FE-SEM/EDS analysis along with EDS spectrum for NiCoCrAlYTa coated superalloys subjected to cyclic oxidation in air at 900 °C after 100 cycles: (a) superni 75, (b) superni 718 and (c) superfer 800H.



**Fig. 6.16** Morphology of oxide scale and variation of elemental composition across the cross-section of NiCoCrAlYTa-coated superalloys subjected to cyclic oxidation at 900 °C in air after 100 cycles: (a) superni 75, (b) superni 718 and (c) superfer 800H.



#### 6.2.3.4 X-ray mapping

BSE image and X-ray mapping of air oxidised NiCoCrAlYTa-coated superalloy 75 (Fig.6.17) shows very thin oxide scale mainly consisting of O, Ni, Co, Cr and Al in the top scale. Nickel and cobalt-rich splats are present in the subscale containing chromium and aluminum at the splat boundaries. Iron showed outward diffusion from the substrate to the coating, the diffusion seems to have almost reached the top surface. Tantalum shows its distribution in entire coating. The X-ray mappings for oxidised NiCoCrAlYTa-coated superalloy 718 after 100 cycles at 900 °C (Fig.6.18) indicates that only the upper part of the coating has oxidized forming a thick oxide layer of chromium, aluminum, cobalt and nickel along with some traces of silicon, while the underlying coating mainly consists of Ni and Co-rich splats, whereas Cr and Al segregated along these splat boundaries. However, in case of coated superalloy 800H (Fig.6.19), it shows the penetration of oxygen along the splat boundaries in which Al and Cr have oxidised. A small amount of silicon has diffused from the substrate to the top surface of coating, whereas iron restricted just above the coating-substrate interface.

#### 6.2.4 Discussion

D-gun sprayed NiCoCrAlYTa-coated superalloy samples after air oxidation for 100 cycles at 900 °C show greenish colour (Fig.6.10), which might be attributed to the presence of both NiO and Cr<sub>2</sub>O<sub>3</sub> (Khajavi and Shariat, 2004). Un-coated superalloys shows higher weight gain than the coated one, higher weight gain during the initial cycles of oxidation run (Fig.6.11), might be due to the rapid formation of oxides of Ni and Cr where Al oxide has not been formed. It is because of the higher oxidation rate of Ni and Cr than the Al. Further in the subsequent cycles, the entrapped air during D-gun deposition is sheltered in the porosities as well as the coating underwent insitu reaction during high temperature (900 °C) oxidation and formed oxides of aluminum (Al<sub>2</sub>O<sub>3</sub>) at the splat boundaries and within open pores. During the subsequent cycles, as discussed above, the formation of oxides have clogged the pores and splat boundaries, and acted as diffusion barriers to the inward diffusion of oxygen. This would relatively minimize the weight gain and result in the steady state oxidation behavior with the progressive long term high temperature exposure. Coated and bare superalloys follow a parabolic rate law up to 100 cycles, except coated superalloy 800H, as it slightly deviates from the parabolic rate law, small deviation from the parabolic rate law might be due to cyclic scale growth. The values of parabolic rate

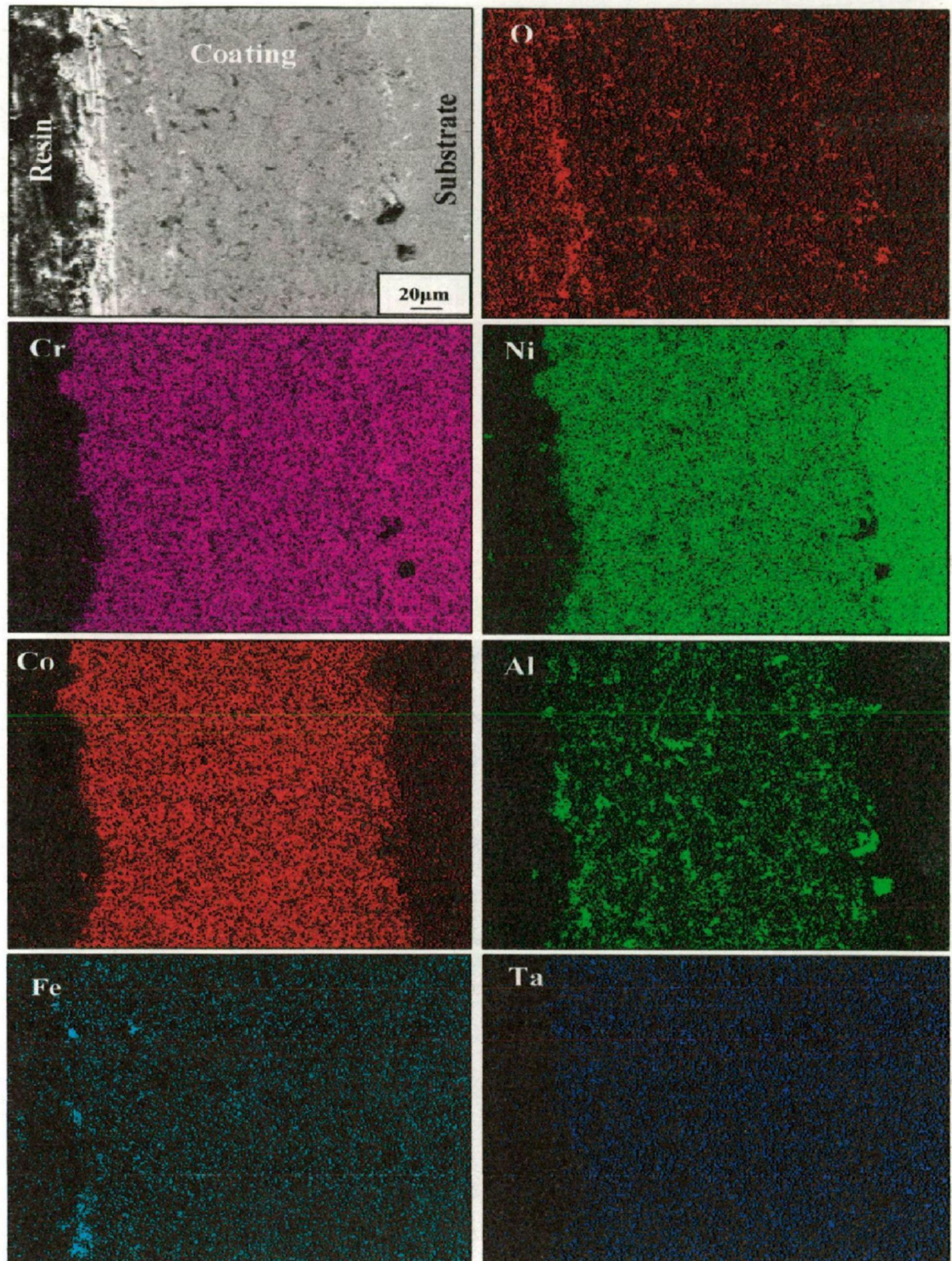


**Fig. 6.17**

Composition image (SEI) and X-ray mapping of the cross-section of NiCoCrAlYTa-coated superalloy superni 75 subjected to cyclic oxidation in air at 900 °C after 100 cycles.



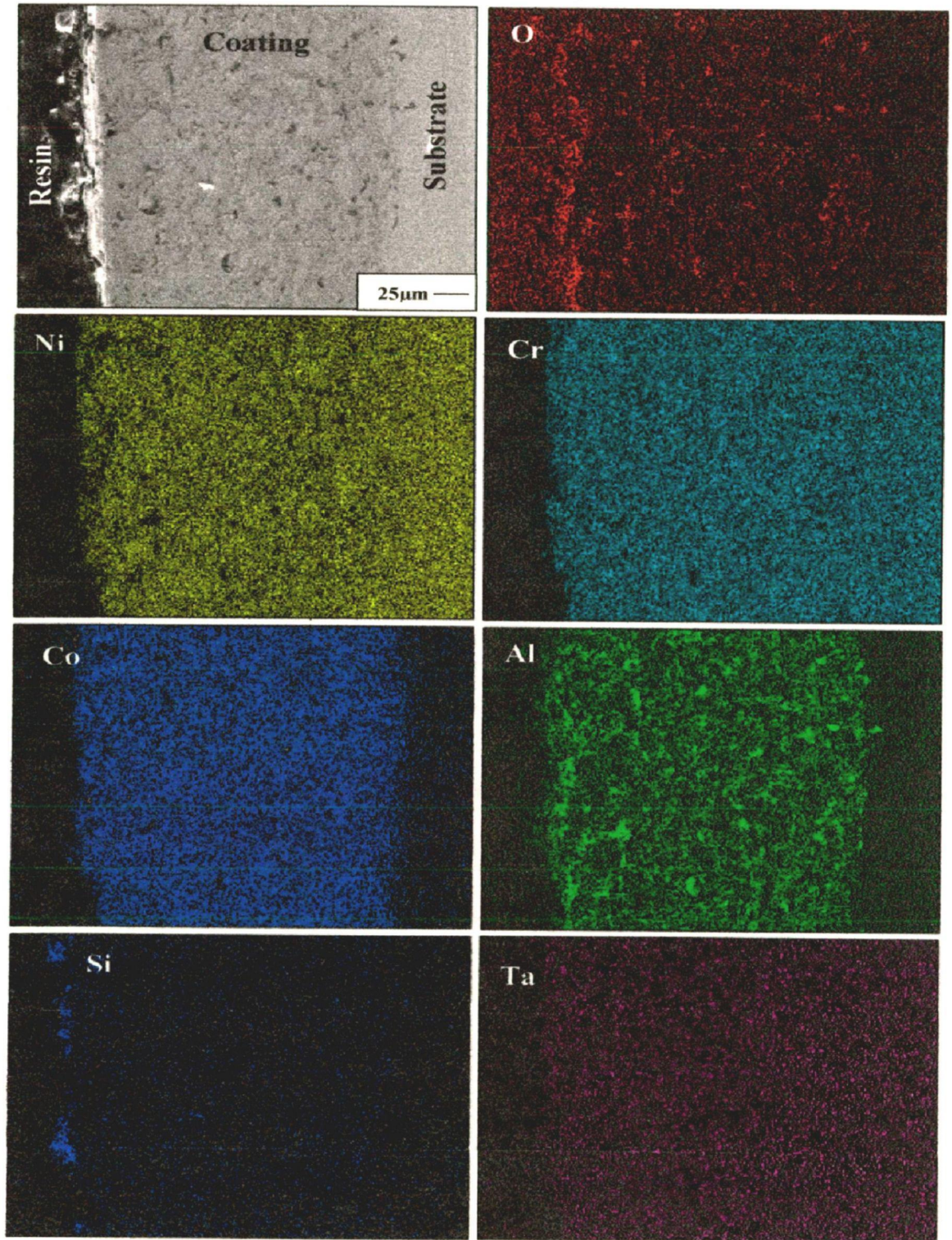


**Fig. 6.18**

Composition image (SEI) and X-ray mapping of the cross-section of NiCoCrAlYTa-coated superalloy superni 718 subjected to cyclic oxidation in air at 900 °C after 100 cycles.



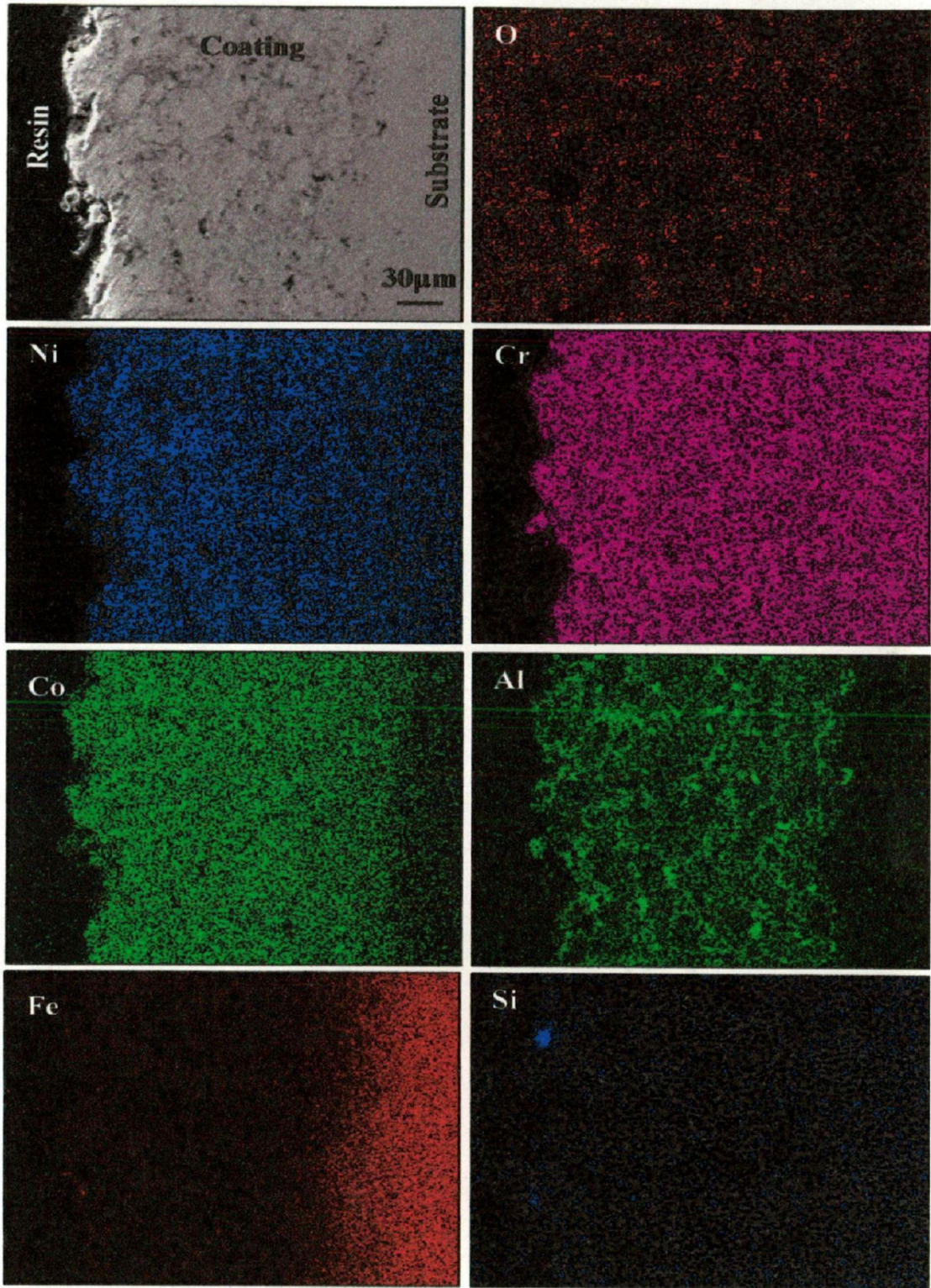


**Fig. 6.19**

Composition image (SEI) and X-ray mapping of the cross-section of NiCoCrAlYTa-coated superalloy superfer 800H subjected to cyclic oxidation in air at 900 °C after 100 cycles.

constant  $K_p$  ( $10^{-10} \text{ g}^2 \text{ cm}^{-4} \text{ s}^{-1}$ ) are obtained from slope of the linear regression fitted line (Fig.6.12) and is given in Table 6.2. Parabolic rate constant, for the coated superalloy is found to be lesser than the bare superalloy. The overall weight gain of 1.25, 1.52 and 2.23  $\text{mg/cm}^2$  is observed for the NiCoCrAlYTa-coated superalloys 75, superalloy 718, and superalloy 800H superalloys (Fig.6.13), respectively. It is found that 21% and 37% saving in overall weight gain for NiCoCrAlYTa-coated superalloy 800H and superalloy 718 in comparison with the superalloy 800H and superalloy 718, respectively (Fig.6.13). The NiCoCrAlYTa coating provides the maximum oxidation resistance to superalloy 75 and has been found successful in reducing the weight gain by around 50% of that gained by the bare superalloy 75 superalloys. Better oxidation resistance shown by the NiCoCrAlYTa-coated superalloy 75 might be ascribed to the formation of oxide of Al, Co, Cr, Ni, thereby suggesting the formation of spinel. Spinel, usually have lower diffusion coefficients of the cations and anions than those in their parent oxides. (Chatterjee et al 2001), Zhang et al., (2003) reported that aluminum oxide is formed in the voids, which increases  $\text{Al}_2\text{O}_3$  along the Ni-rich splat boundaries. Uusitalo et al., (2002B) reported that with strongly flattened splats, the distance from coating surface to coating/substrate interface along the splat boundaries is very long, and thus, high oxidation resistance is expected. Oxides of Al and Cr are relatively much more protective than NiO scales since they are reasonably stoichiometric oxides, with low defect concentrations, and can give effective protection to the alloy in environments of high oxygen activity (Stott, 1987). Further it has been observed that the scales formed on the coated superalloy 75 superalloys are observed to be thin, dense and compact, this also contributes to the lower weight gain as evident from the lower parabolic rate constant ( $3.33 \times 10^{-12} \text{ gm}^2 \text{ cm}^{-4} \text{ s}^{-1}$ ). In the subscale region of coating, Ni and Co remain in the un-reacted state as O is found to be absent at these places. In case of superalloy 800H, chromium, aluminum and yttrium coexist with O at the splat boundaries (Points 5 in Fig. 6.16c), indicating the formation of respective oxides at the splat boundaries, this further contributes to lower weight gain of coated superalloys. Presence of these phases in the scale of coated superalloys is further supported by the surface (Fig.6.15), cross-sectional EDS (Fig.6.16) and X-ray mapping analyses (Fig. 6.17-6.19). The coating also revealed the formation of continuous thin oxide scale of Si and Fe on the top surface of coated superalloys, as these elements have diffused in to the coating through the splat boundaries and open pores. These pores and splats boundaries act as a channel for the transport of coating and substrate elements during initial cycles of oxidation. This has further contributed to increase the

resistance to oxidation. Wang et al., 2004) and Grunling and Bauer, (1992) reported that the presence of silicon can promote the formation of continuous dense scale and improve the adherence of the outer scale to the coating. The formation of thermodynamically stable alumina and chromia scale and its slow growth as shown in X-Ray mapping analysis (Fig. 6.17-6.19), might have acted as barrier to the inward diffusion of oxygen into the coating. The formation of spinel of  $\text{NiCr}_2\text{O}_4$  via solid phase reaction between  $\text{NiO}$  and  $\text{Cr}_2\text{O}_3$  in the oxide scales has been reported by Ren et al., (2005), these oxides, once formed, seal the splat boundaries and all other possible diffusion paths in the coatings, thereby blocking or slowing the penetration of oxygen. Schematic of the proposed oxidation mechanism of the NiCoCrAlYTa coated superalloy superalloy 75 at  $900^\circ\text{C}$  in air after 100 cycles is shown in Fig. 6.20.

### 6.2.5 Conclusions

- Greenish colour oxide scale might be attributed to the presence of oxides of Ni and Cr on the coating.
- Coated and bare superalloys follow nearly a parabolic rate law, whereas coated superalloy 800H slightly deviates from the parabolic rate law.
- NiCoCrAlYTa-coating provides the maximum hot corrosion resistance to superalloy 75 as it reduces the weight gain around 50% of that gained without coating.
- EDS analysis of corroded coated superalloys reveals the uppermost part of the coating has thin oxide scale which consists of mainly oxides of Ni, Cr and Al.
- Iron and silicon showed outward diffusion from the substrate to the coating surface, along the splat boundaries during initial cycles of oxidation.
- Coating has Ni- and Co- rich splats which are in an un-oxidised state.
- Aluminum and yttrium coexist with O along the Ni-rich splat boundaries.



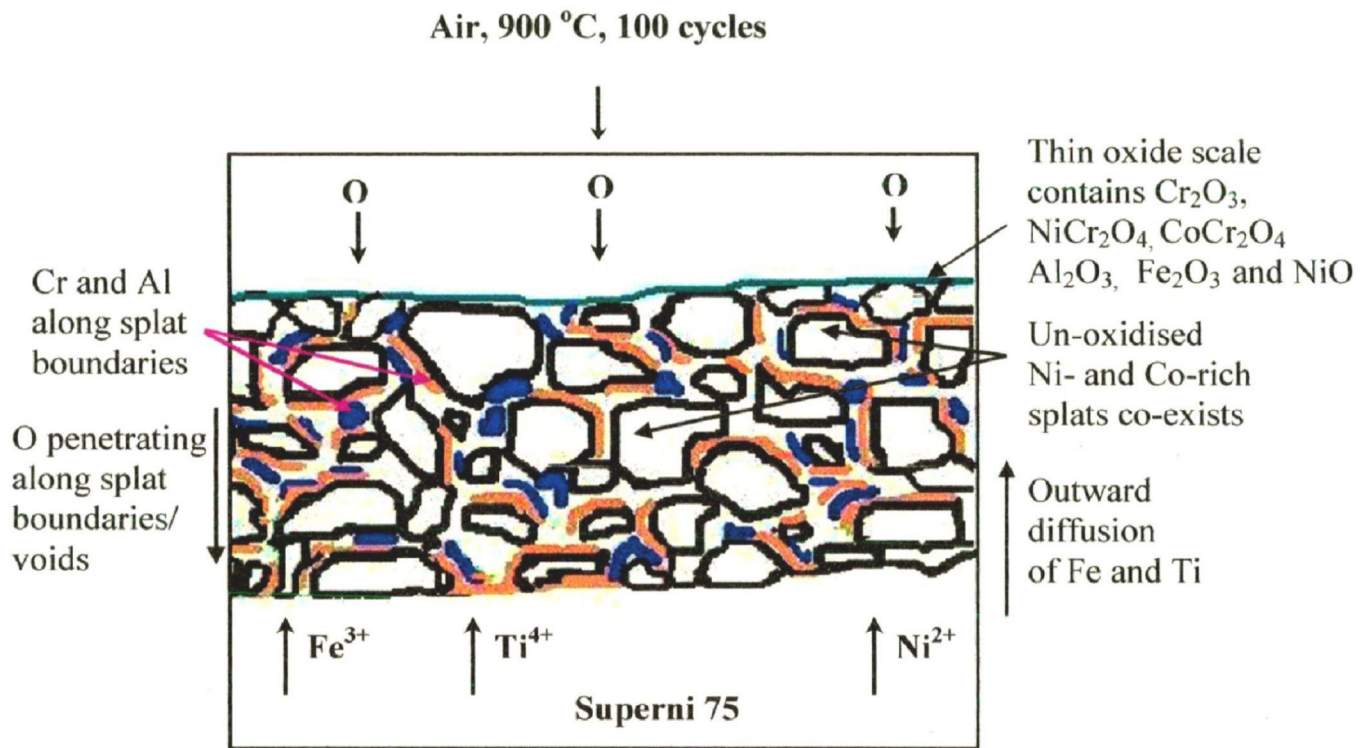


**Fig. 6.20** Schematic of the proposed oxidation mechanism of the NiCoCrAlYTa coated superalloy superni 75 at 900 °C in air after 100 cycles.

## **6.3 HOT CORROSION STUDIES**

### **6.3.1 Na<sub>2</sub>SO<sub>4</sub>–60%V<sub>2</sub>O<sub>5</sub> Molten Salt Environment-I**

#### **6.3.1.1 Introduction**

Frances et al., (1985) studied the hot corrosion behavior of NiCoCrAlYTa coating deposited by low-pressure plasma spray; they reported that hot corrosion rate of the alloy in contact with molten salt mixtures has been reduced. Aymeric Raffaitin et al., (2006) used three different NiCoCrAlYTa coating thicknesses to determine the influence of the Al reservoir on the lifetime of the coated nickel-based single-crystal superalloy MC2, the 110- $\mu\text{m}$  thick NiCoCrAlYTa coating provides a larger Al reservoir, which is beneficial for the formation of a protective alumina scale. The corrosion process can be hindered due to the very slow diffusion rate of oxygen and sulfur into the coating from the molten salt; consequently, the base alloys are protected from hot corrosion attack (Niranatlumpong et al., 2000). Due to the better properties of D-Gun sprayed coatings as discussed earlier in chapters 4, the present work has been focused to study the hot corrosion behavior of NiCoCrAlYTa coatings deposited on superalloys (namely superni 75, superni 718 and superfer 800H) exposed to molten salt (Na<sub>2</sub>SO<sub>4</sub>–60%V<sub>2</sub>O<sub>5</sub>) at 900 °C. The corroded products are analysed to give an insight into the corrosion mechanisms.

#### **6.3.1.2 Experimental details**

The substrate materials, coating formulation and the hot corrosion studies are explained in detail in section 3.1, 3.2.3 and 3.4.3.

#### **6.3.1.3 Results**

##### **6.3.1.3.1 Visual observation and weight change measurements**

Fig.6.21 shows the colour of oxide scale formed on the coated superalloy superni 75, superni 718 and superfer 800H, after hot corrosion studies at 900 °C for 100 cycles in Na<sub>2</sub>SO<sub>4</sub>–60% V<sub>2</sub>O<sub>5</sub> environment. In all the cases, a compact and dense continuous scale gradually developed on all the coated superalloys, but corrosion product in the form of fine powder was observed in the boat. It has formed due to spallation of thin outer most oxide scale by the cyclic corrosion studies, in general the scale was found to be rough and intact, whereas roughening of the exposed coating was observed from the 17<sup>th</sup> cycle onwards.



Initially colour of the coating on superni 75 (Fig.6.21a) was light grey which has changed in to black from the 2<sup>nd</sup> cycle onwards and continued up to 26<sup>th</sup> cycles, white coloured salt patches were noticed on the surface after 5<sup>th</sup> cycle, which continued up to 19<sup>th</sup> cycle. At the end of 16<sup>th</sup> cycle, spallation and cracks were observed only at the edges and corner and subsequently dark green colour started appearing on the surface from 27<sup>th</sup> cycle, which lasted up to 100 cycles. Colour of the oxide scale formed on the coated superni 718 (Fig.6.21b) was dark grey after the first cycle which turned in to black grey during 3<sup>rd</sup> to 25<sup>th</sup> cycles, subsequently, showed the formation of dark green colour on grey background. Spallation of the scale was noticed near the corners and edges after 22<sup>nd</sup> cycle which continued up to 39<sup>th</sup> cycle. The coated superfer 800H (Fig.6.21c) indicated some spallation at the corners and edges from 4<sup>th</sup> cycle onwards. The spallation from these regions mostly confined to the outer layers of the coating. The colour of the scale was dark grey during first cycles which turned to black with the progress of study, after 27<sup>th</sup> cycle, colour of the scale changed from black to dark sea green.

The hot corrosion kinetics was determined from the weight change ( $\text{mg}/\text{cm}^2$ ) versus time plots for the bare and coated three superalloys subjected to hot corrosion in 40% $\text{Na}_2\text{SO}_4$ -60% $\text{V}_2\text{O}_5$  environment at 900 °C up to 100 cycles as shown in Fig.6.22. The bare superfer 800H shows a higher weight gain followed by superni 75 as compared with coated one, but the bare superni 718 superalloy has shown a parabolic behavior up to 25 cycles with some spalling /sputtering. With the progress of hot corrosion run, corrosion products started falling outside the boat, thereby it becomes difficult to monitor actual weight gain. The sputtering has continued up to 70 cycles, thereafter it has ceased. Further, negligible weight gain was noticed up to 100 cycles. The NiCoCrAlYT a coated superalloys in all cases show a lower weight gain than the bare specimens in the given molten salt environment. Coated superfer 800H showed the lowest weight gain, whereas bare superfer 800H showed highest weight gain. Whereas among coated superalloys, superfer 800H showed least weight gain followed by superni 718 and superni 75, respectively. It is revealed that there is over all 37% and 13% saving in overall weight gain for NiCoCrAlYT a coated Superfer 800H and superni 75 in comparison with the bare Superfer 800H and superni 75 respectively, whereas the weight gain by coated Superfer 800H and Superni 718 after 100 cycles is nearly 18% and 6% less than that of coated superni 75. In general, the hot corrosion behaviour of both bare and coated samples follow a parabolic rate law, except for bare superfer 800H, as it slightly deviates from parabolic rate, as can be inferred from the square of



**Fig. 6.21** Surface macrograph of NiCoCrAlYTa coated superalloys subjected to hot corrosion in  $\text{Na}_2\text{SO}_4\text{-60\%V}_2\text{O}_5$  environment at  $900^\circ\text{C}$  for 100 cycles, (a) superni 75, (b) superni 718, (c) superfer 800H.

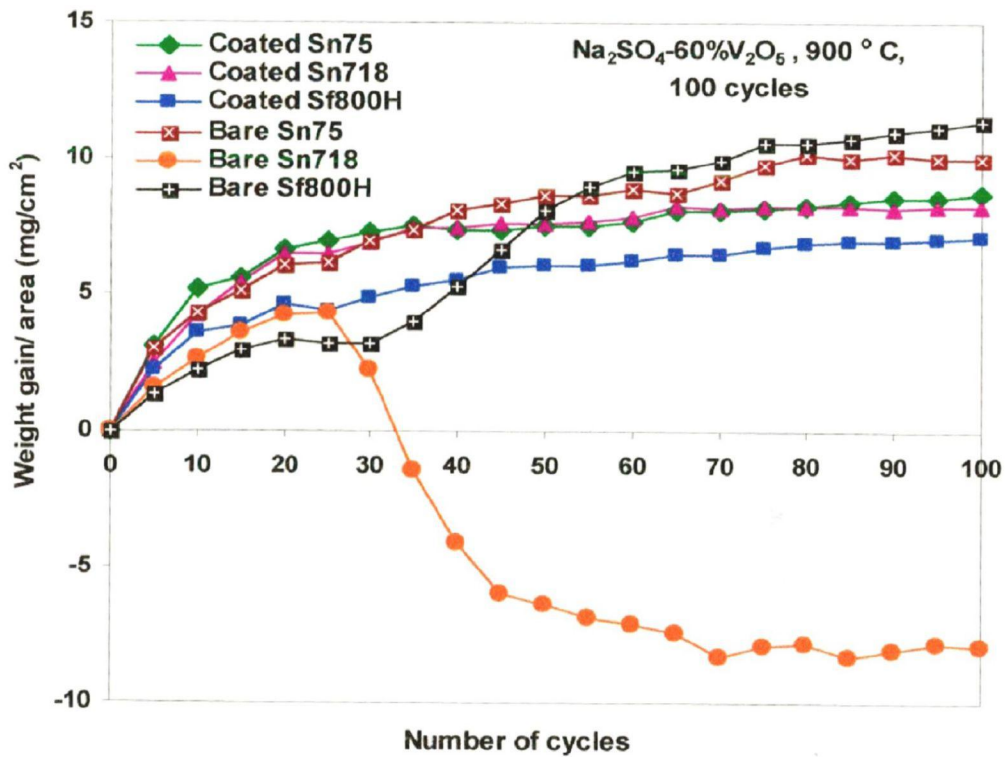


**Fig. 6.22** weight gain/area vs. number of cycles plot for NiCoCrAlYTa coated and un-coated superalloys subjected to cyclic oxidation for 100 cycles in  $\text{Na}_2\text{SO}_4\text{-60\% V}_2\text{O}_5$  at  $900^\circ\text{C}$ .

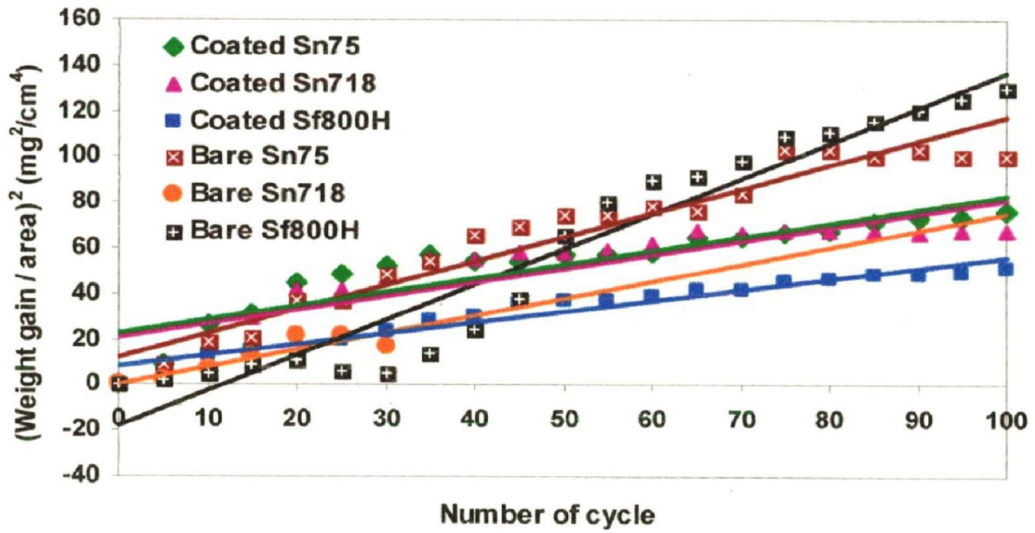


Fig. 6.23

(weight gain/area)<sup>2</sup> vs. number of cycles plot for NiCoCrAlYTa coated and un-coated superalloys subjected to cyclic oxidation for 100 cycles in Na<sub>2</sub>SO<sub>4</sub>-60% V<sub>2</sub>O<sub>5</sub> at 900 °C.

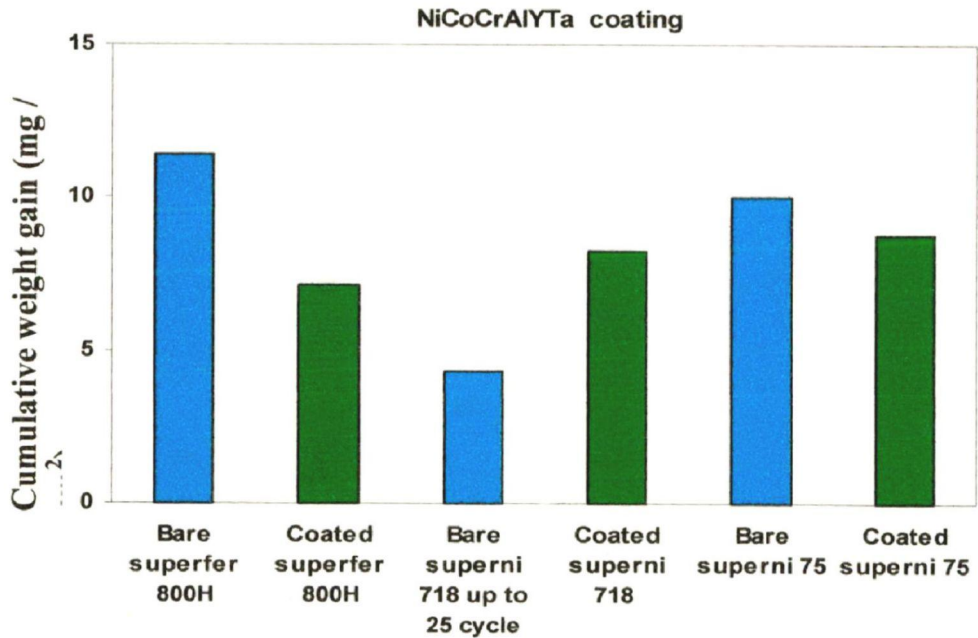


Fig. 6.24

Bar chart showing cumulative weight gain per unit area for NiCoCrAlYTa coated and Un-coated superalloys subjected to cyclic oxidation for 100 cycles in Na<sub>2</sub>SO<sub>4</sub>-60%V<sub>2</sub>O<sub>5</sub> at 900 °C.

**Table 6.2** Parabolic rate constant ( $k_p$ ) values for D-gun sprayed NiCoCrAlYTa-coated and bare superalloys subjected to cyclic oxidation for 100 cycles in  $\text{Na}_2\text{SO}_4$ -60% $\text{V}_2\text{O}_5$  at 900 °C

Superalloys	Parabolic rate constants ( $k_p$ ) ( $10^{-10} \text{ g}^2 \text{ cm}^{-4} \text{ s}^{-1}$ )
Bare superfer 800H	04.31
Coated superfer 800H	1.332
Bare superni 718	02.10
Coated superni 718	01.66
Bare superni 75	02.92
Coated superni 75	01.66

weight change ( $\text{mg}^2/\text{cm}^4$ ) versus number of cycle plots shown in Fig.6.23. Table 6.2 shows the values of the parabolic rate constants ( $k_p$  in  $10^{-10} \text{ g}^2 \text{ cm}^{-4} \text{ s}^{-1}$ ) for the NiCoCrAlYTa coated and bare superalloys for 100 cycles of hot corrosion. Cumulative weight gain per unit area for coated and bare superalloys is shown in Fig.6.24.

### 6.3.1.3.2 X-ray diffraction analysis

The X-ray diffraction peaks for the scale of D-gun-sprayed NiCoCrAlYTa coated superalloy after hot corrosion in  $\text{Na}_2\text{SO}_4$ -60% $\text{V}_2\text{O}_5$  environment for 100 cycles at 900 °C are as illustrated in Fig.6.25. The major and minor phases detected at the surface of the specimens with the XRD analysis are  $\text{NiCr}_2\text{O}_4$ ,  $\text{NiAl}_2\text{O}_4$ ,  $\text{Fe}_2\text{O}_3$ ,  $\text{SiO}_2$ ,  $\text{NiO}$ ,  $\text{Cr}_2\text{O}_3$  and  $\text{Al}_2\text{O}_3$ .

### 6.3.1.3.3 FE-SEM/EDS analysis of the scales

#### 6.3.1.3.3.1 Surface scale analysis

FE-SEM micrographs with EDS spectrum along with EDS elements compositional analysis revealed the surface morphology of the NiCoCrAlYTa coated substrate superalloy specimens after cyclic hot corrosion in molten salt environment ( $\text{Na}_2\text{SO}_4$ -60% $\text{V}_2\text{O}_5$ ) for 100 cycles at 900 °C are shown in Fig.6.26. The surface scale developed on coated superni 75 (Fig.6.26a) is massive with few protruded surfaces, EDS analysis of the scale revealed the presence of higher amount of O, Cr, Ni, Co in white region whereas Ni content is increased in the black area indicating the formation of oxides of Cr, Al, Ni, Co and there spinels. Micrograph of corroded

coated superni 718 (Fig.6.26b) appears to be dense and continuous. EDS analysis of the scale revealed O, Ni, Cr, Co, Al as major elements along with small amount of vanadium, yttrium and tantalum. Similarly, the scale formed on the coated superfer 800H (Fig.6.26c) is dense with major elements of O, Al-rich elements in one region whereas O and Cr-rich elements in other area along with main coatings elements. It confirms the formation of oxides of Cr and Al rich areas as evident from the XRD analysis.

### 6.3.1.3.3.2 Cross-sectional analysis of the scale.

FE-SEM micrograph and EDS analysis at some selected point of interest along the cross section of coated superni 75, superni 718 and superfer 800H corroded in molten salt for 100 cycles at 900 °C are shown in Fig.6.27. A non uniform and adherent thin oxide scale has formed on the three coated superalloys, which has retained its dense structure up to 100 cycles of hot

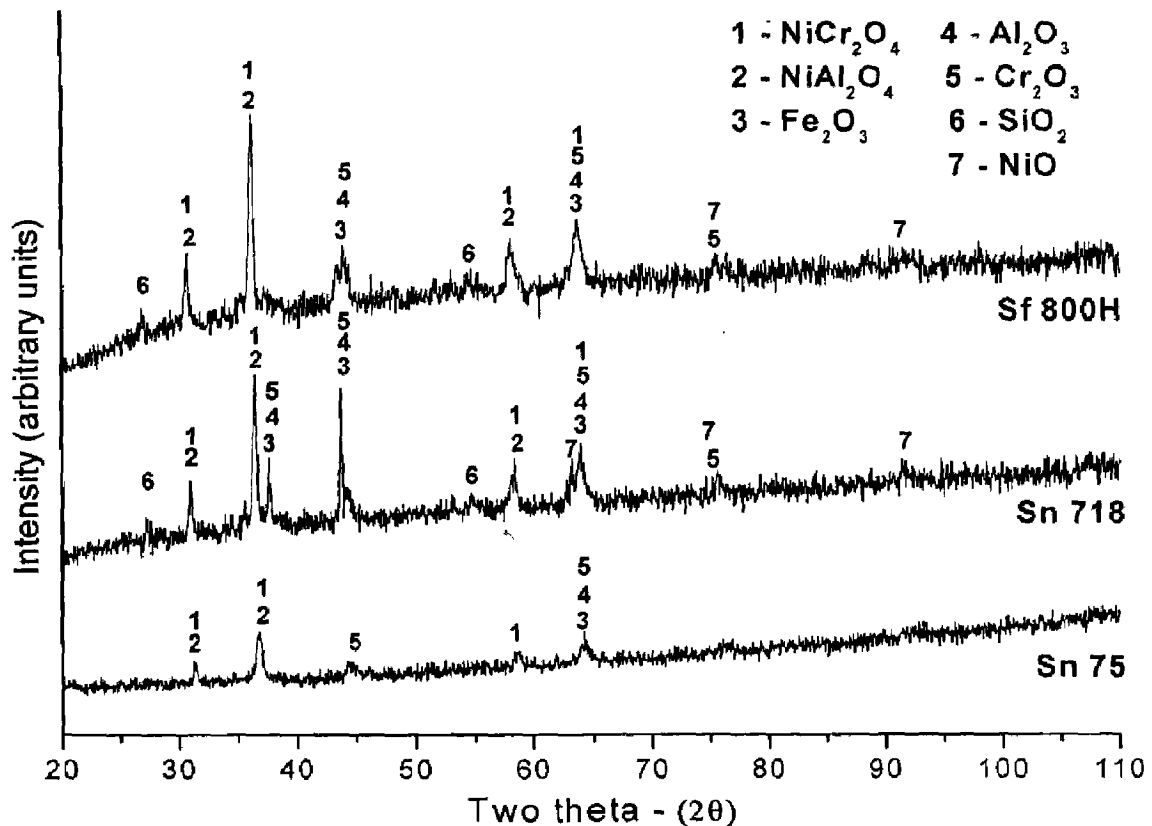


**Fig. 6.25** X-ray diffraction patterns for NiCoCrAlYTa coated superalloys exposed to cyclic oxidation in  $\text{Na}_2\text{SO}_4$ -60% $\text{V}_2\text{O}_5$  environment at 900 °C after 100 cycles.

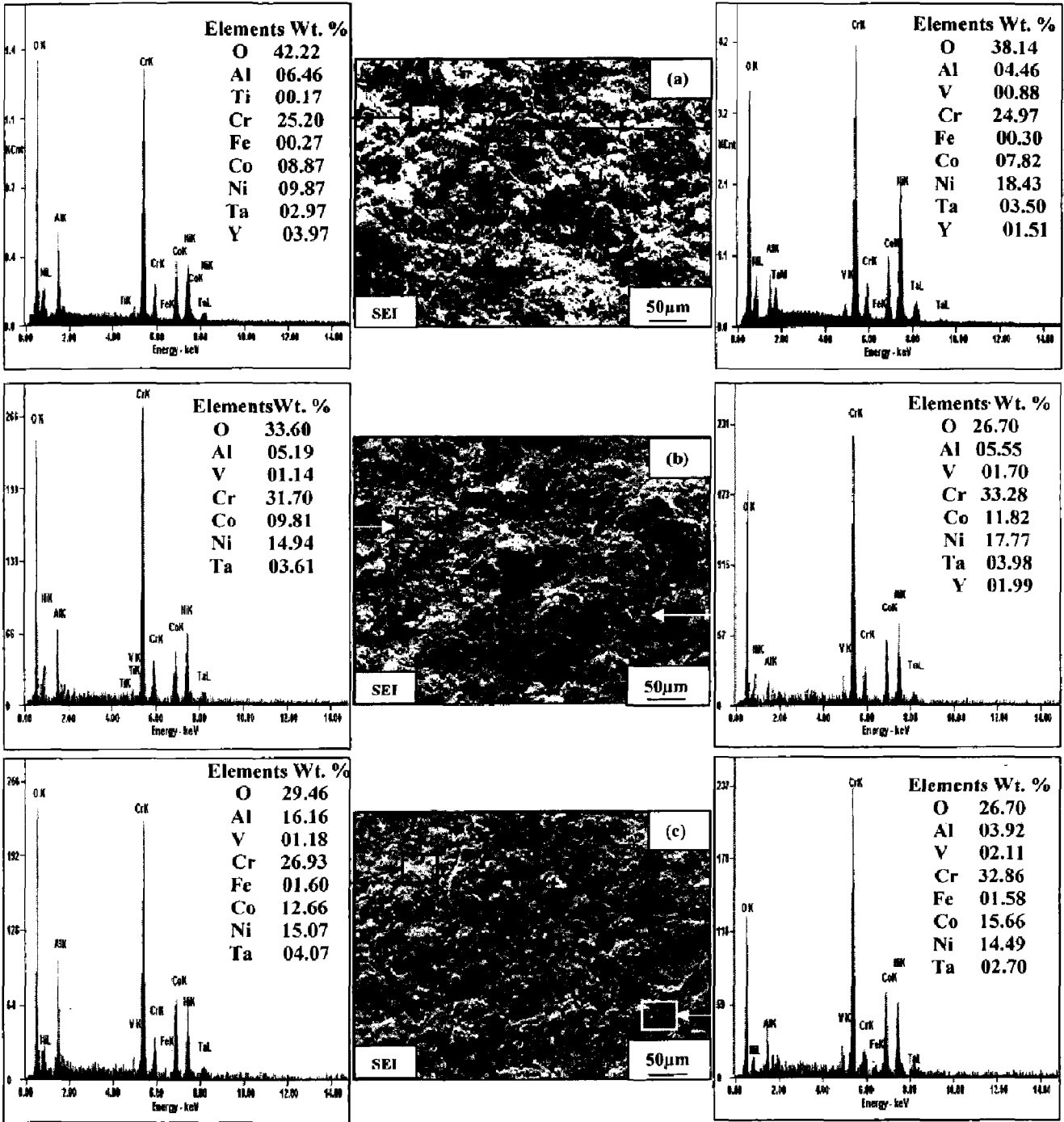


**Fig. 6.26** FE-SEM/EDS analysis along with EDS spectrum for NiCoCrAlYTa coated superalloys subjected to cyclic oxidation in  $\text{Na}_2\text{SO}_4$ -60% $\text{V}_2\text{O}_5$  environment at 900 °C after 100 cycles: (a) superni 75, (b) superni 718 and (c) superfer 800 H.

corrosion run. EDS analysis of hot corroded NiCoCrAlYTaN coated superalloys (Fig.6.27a, b and c) shows that the corrosive species are not present at point 1 which indicates that the substrate superalloy remained unaffected during the hot corrosion runs. Coating-substrate interface (Fig.6.27a at point 3) depicts the presence of higher amount of Al and O which seems to be an inclusion of aluminum oxide. EDS analysis at point 4 and 5 reveals the presence of only basic elements of the coating thereby suggesting major portion of the NiCoCrAlYTaN coating remained unaffected. Aluminum and Chromium, coexist with O at the boundaries of Ni- and Co-rich splats (Points 6) indicating the formation of their oxides at the splat boundaries. The upper most part of the scale mainly consists of oxides of Cr, Ni and Co (Point 7). Cross-section EDS analysis of hot corroded coated superalloy 718 reveals (Fig.6.27b) that the weight percentage of Cr, Co, Al and O increases appreciably at the top of scale (point 7) where Ni decreases substantially signifying that light contrast phase at the top of scale might be rich with oxides of Cr, Co and Al. In the subscale region (point 6), Al and Ni percentage increases but Cr and Co decreases substantially which suggest the formation of respective oxides. The white phase in the scale (point 5, 4 and 2) consisted of coating elements which are presumed to be un-oxidised as oxygen is found to be absent at these points. The stringers along the splat boundaries (point 3) depict the presence of oxygen along with Cr and Al thereby suggesting the formation of respective oxides. In case of coated superalloy 800H (Fig.6.27c), EDS analysis of the corroded coating at point 7 in the substrate show that the nickel and iron decreases from 32% and 44% in the original alloy to 27% and 38% respectively, thereby indicating the diffusion of Ni- and Fe- in to the coating from the substrate during the hot corrosion run. The light grey phases (Points 2, 3, 4 and 6) in the coating consist of mainly Ni-, and Co-rich splats, which are remain in the un-reacted state as O is found to be absent at these places. Presence of oxygen (point 5) along the splat boundaries indicates the formation of oxides of Al, where Ni, Cr and Co decreases substantially. The weight percentage of Cr-, Al- and O increases appreciably at the top of scale (point 7) where Ni and Co decreases substantially signifying that light contrast phase at the top of scale might be rich with oxides of Cr and Al.



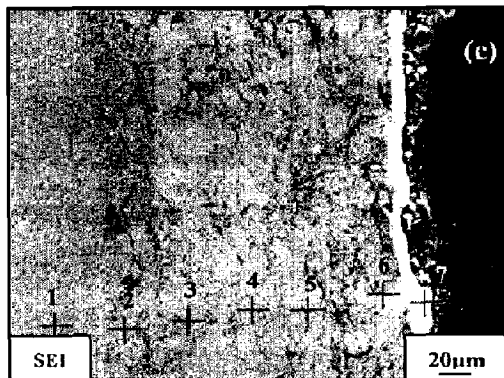
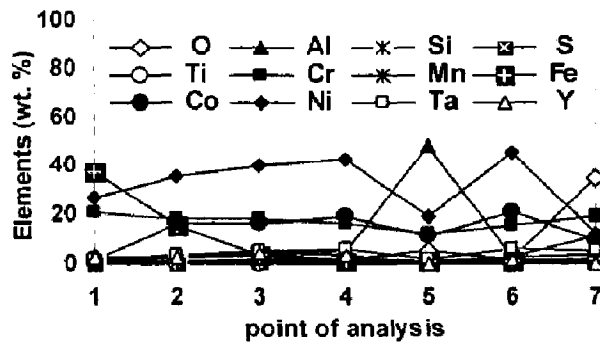
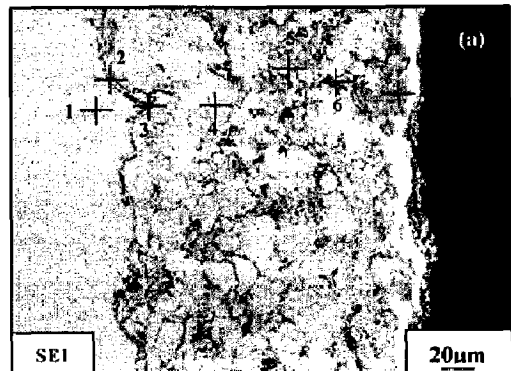
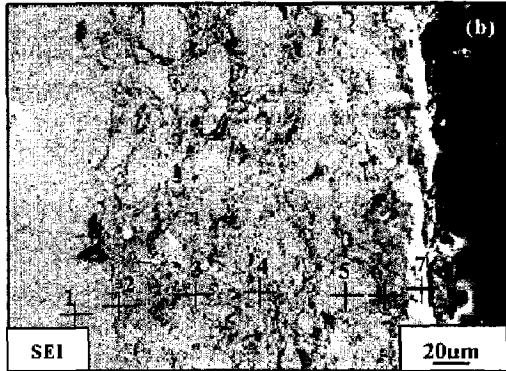
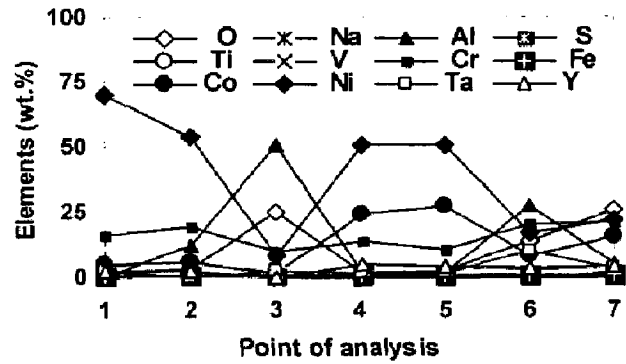
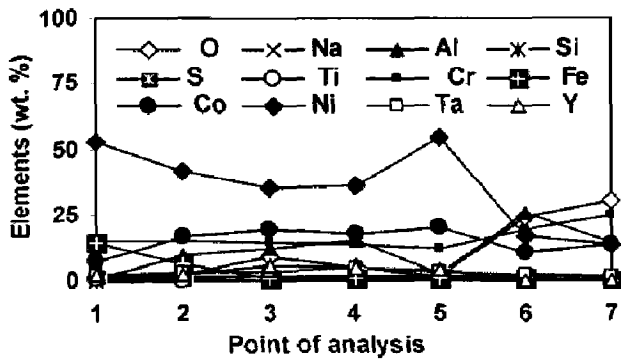


**Fig. 6.27**

Oxide scale morphology and variation of elemental composition across the cross-section of NiCoCrAlYTa coated superalloys subjected to cyclic oxidation at 900 °C in molten salt after 100 cycles (a) superni 75, (b) superni 718 and (c) superfer 800H.

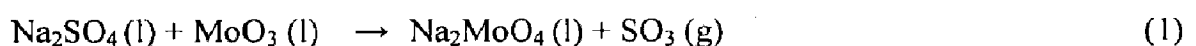


#### 6.3.1.3.4 X-Ray mapping

Elemental X-ray mapping analysis of the scale formed on D-gun coated superalloys after hot corrosion in  $\text{Na}_2\text{SO}_4$ -60% $\text{V}_2\text{O}_5$  environment at 900 °C for 100 cycles is shown in Fig.6.28-6.30. X-ray mappings for the corroded NiCoCrAlYTaNi coated superalloy 75 (Fig.6.28) indicate that the upper most part of the thin scale mainly consist of oxide of Cr as evident from the oxygen and chromium distribution, Cobalt is observed to be relatively less in this chromium-rich topmost scale. Nickel and cobalt-rich splats are present in the subscale containing chromium and aluminum at the splat boundaries. Iron shows its diffusion tendency from the substrate in to the coating, as it could reach to the top surface of the scale. The scale formed on coated superalloy 718 (Fig.6.29) has a thick layer of chromium in the topmost part of the scale, along with Ni at some places. The co-existence of Cr and Ni with O indicates the formation of spinel of Ni and Cr, thereby leaving a chromium-depleted band under it. Below this layer, the coating has un-reacted Ni-and Co-rich splats, with Cr and Al distributed along these splat boundaries. The elemental mapping for silicon and iron showed outward diffusion from the substrate to the coating, the elements have almost reached the top surface. X-ray mappings for coated superalloy 800H (Fig.6.30) after 100 cycles of hot corrosion in given environment at 900 °C indicates that only the upper part of the coating has oxidized forming a thick oxide layer of chromium, along with some traces of nickel, cobalt, iron and silicon, while the underlying oxide layer mainly consists of aluminum. An un-oxidised nickel-and cobalt-rich splats are encircled by oxides of chromium and aluminum.

#### 6.3.1.4 Discussion

Weight change data for the NiCoCrAlYTaNi coated and bare superalloys subjected to hot corrosion test in molten salt ( $\text{Na}_2\text{SO}_4$ -60% $\text{V}_2\text{O}_5$ ) environment are plotted in Fig.6.22. Severe hot corrosion suffered by bare superalloy 718 may be due the presence of Mo (3.05%) in the alloy, shows intense spalling and sputtering of its scale. Usually molybdenum oxidised to  $\text{MoO}_3$  (m.p. 795 °C) which are easily reacts with the sodium sulfate ( $\text{Na}_2\text{SO}_4$ ) to form a low melting phase  $\text{Na}_2\text{MoO}_4$  (Fryburg et al., 1984; Peters et al., 1976) by the following reaction.



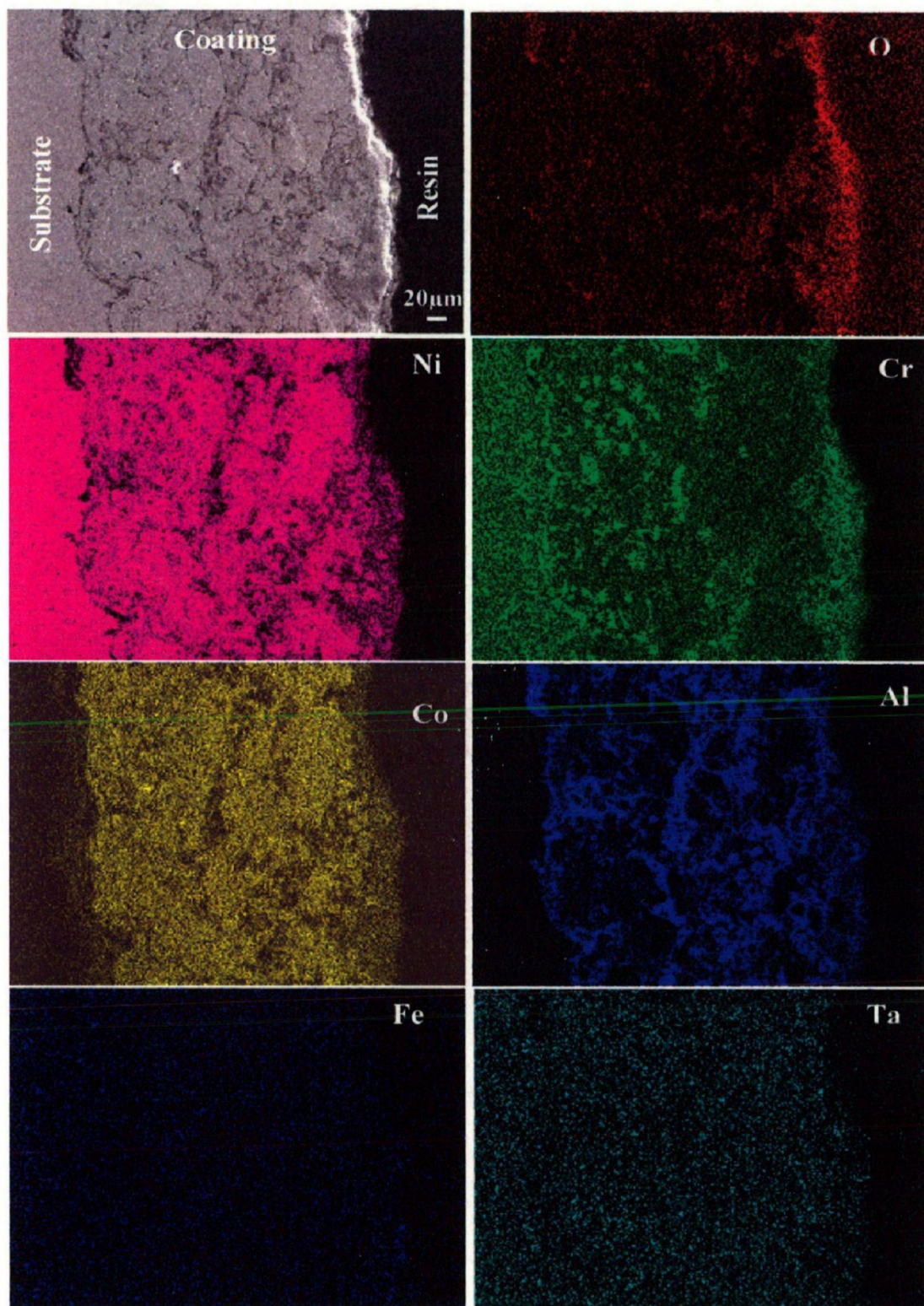


**Fig. 6.28** Composition image (SE) and X-ray mapping of the cross-section of the NiCoCrAlYTa coated superalloy superni 75 subjected to cyclic oxidation at 900 °C in  $\text{Na}_2\text{SO}_4\text{-60}\%\text{V}_2\text{O}_5$  after 100 cycles.



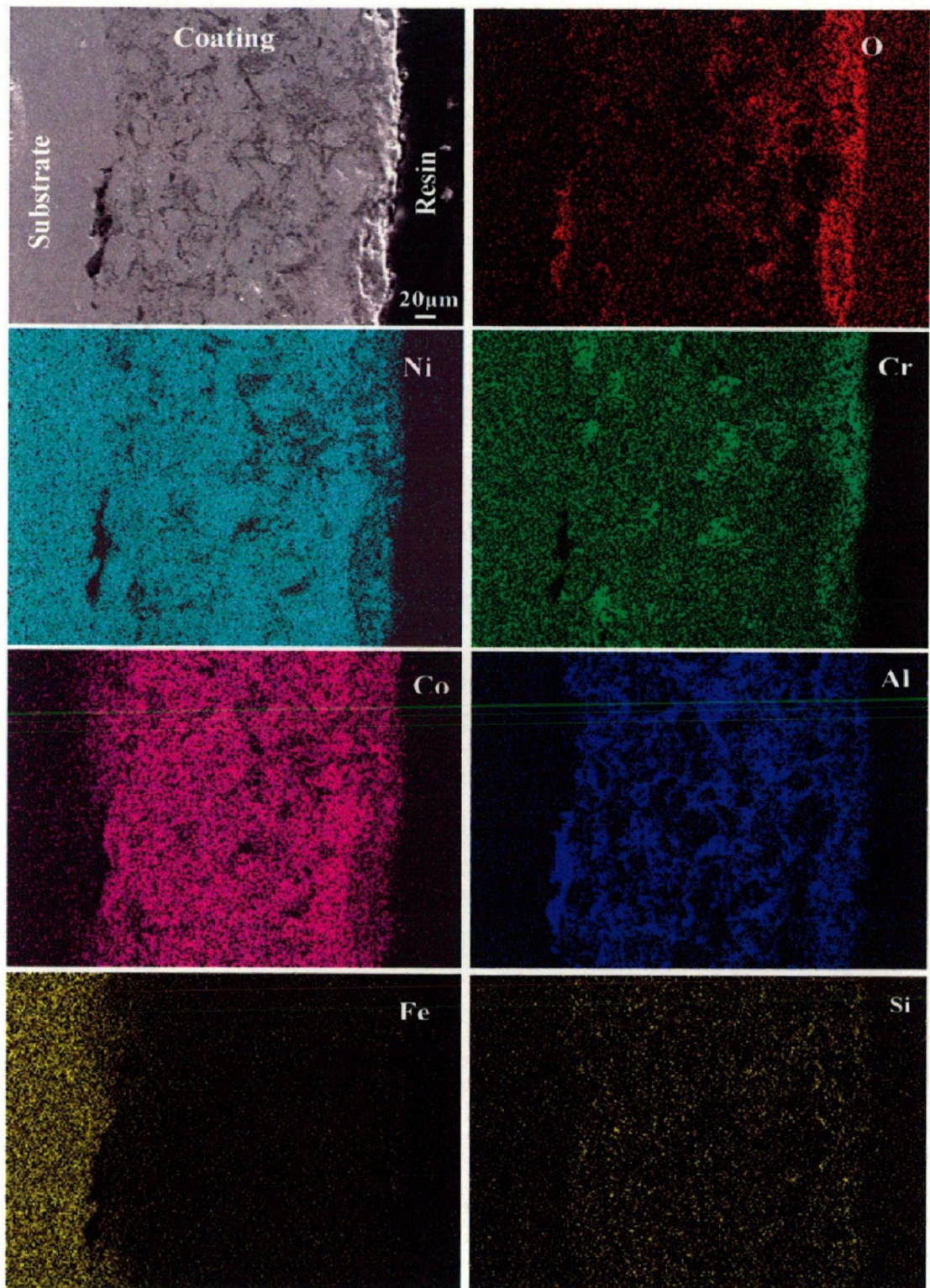


**Fig. 6.29**

Composition image (SE) and X-ray mapping of the cross-section of the NiCoCrAlYTa coated superalloy superni 718 subjected to cyclic oxidation at 900 °C in  $\text{Na}_2\text{SO}_4$ -60% $\text{V}_2\text{O}_5$  after 100 cycles.



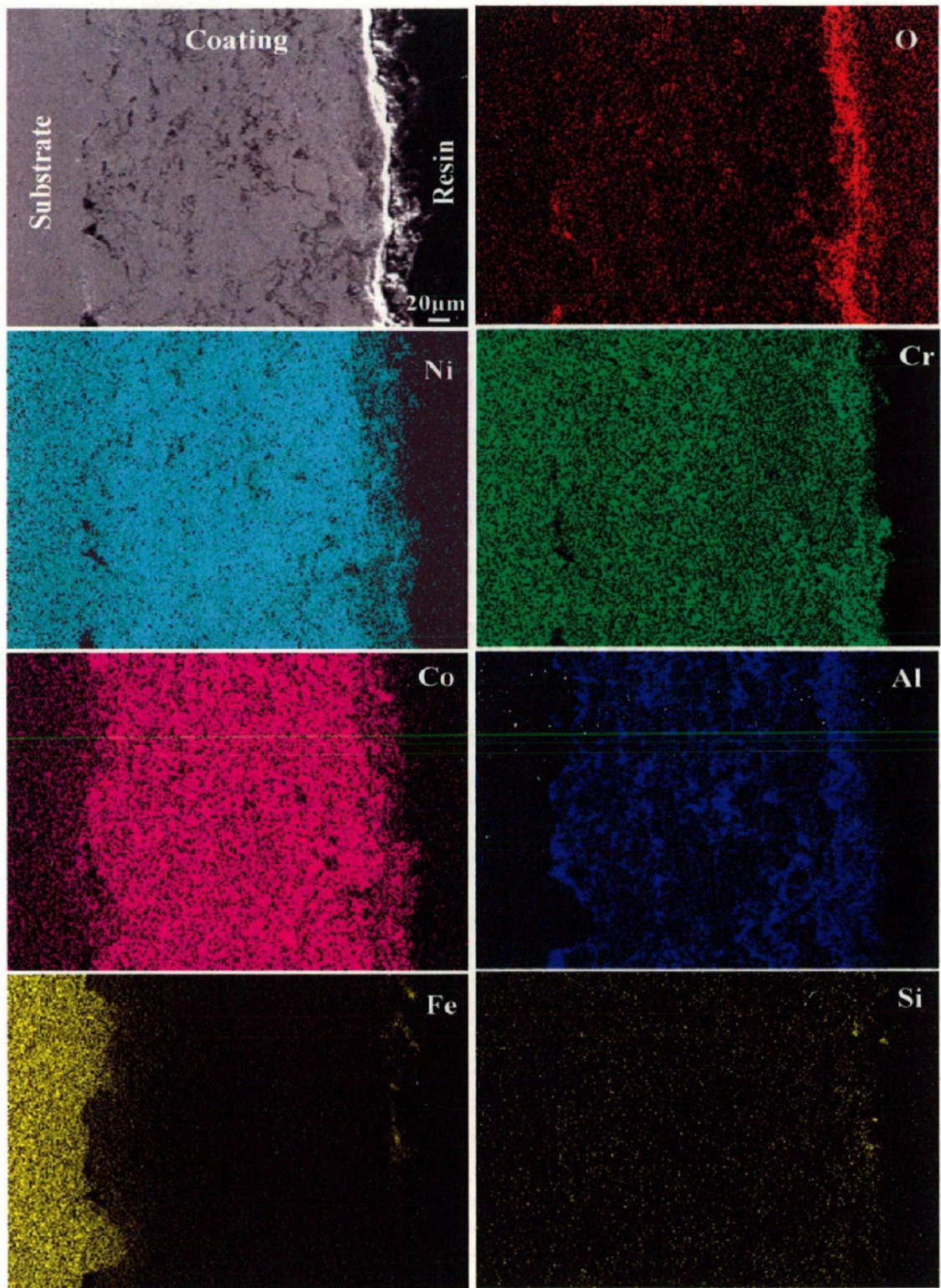


**Fig. 6.30** Composition image (SE) and X-ray mapping of the cross-section of the NiCoCrAlYTa coated superalloy superfer 800 subjected to cyclic oxidation at 900 °C in  $\text{Na}_2\text{SO}_4$ -60% $\text{V}_2\text{O}_5$  after 100 cycles.

They are highly corrosive in nature, causes acidic fluxing of the oxides scale leading to accelerated spallation/sputtering (Pettit and Meier, 1985). Identical findings have also been reported by Misra, (1986), Shih et al., (1989) and Prakash et al., (2005). Catastrophic hot corrosion of the bare superalloy supermi 718 can also be partly attributed to severe strain developed due to the precipitation of  $\text{Fe}_2\text{O}_3$  from the liquid phase and inter-diffusion of intermediate layers of Fe- oxide as reported by Sachs, (1958), further different oxides present in a thin layer might have imposed severe strains on the oxide film, which may result in cracking and exfoliation of the scale. These cracks generates channel for the corrosive liquid phase to reach the metal substrate. Goebel et al., (1973) reported the catastrophic hot corrosion of nickel based alloy containing W and Mo in sodium sulphate environment. Uncoated superalloys shows higher weight gain than the coated one, higher weight gain during the initial cycles of hot corrosion run for coated superalloy, might be due to the rapid formation of oxides of Ni and Cr where Al oxide has not been formed, because oxidation rate of Ni and Cr is higher than Al. Further, in the subsequent cycles, the entrapped air during  $\hat{\text{D}}$ -gun deposition is sheltered in the porosities and since the cooling of the coating was rapid, there is shortage of time for the residual air to react with the surrounding coating alloys (Zhang et al., 2002). The coating has oxidized at high temperature ( $900\text{ }^\circ\text{C}$ ) due to the entrapped air and formed oxides of aluminum ( $\text{Al}_2\text{O}_3$ ) at the splat boundaries and within open pores. During the subsequent cycles, as discussed above, the formation of oxides have blocked the pores and splat boundaries, and acted as diffusion barriers to the inward diffusion of corrosive species. This would relatively minimize the weight gain and result in the steady state oxidation behavior with the progress of long term high temperature exposure, which are in accordance with the similar observation reported for the plasma sprayed NiCrAlY coatings on Nimonic 80A and SS41 alloy substrates, respectively by Choi et al., (2002) and Niranatlumpong et al., (2000). The parabolic rate constant values ( $K_p 10^{-10} \text{ g}^2 \text{ cm}^{-4} \text{ s}^{-1}$ ) were obtained from slope of the linear regression fitted line and is shown in Table 6.2. The nature of fit, parabolic rate law, for hot corrosion experiments are shown in Fig.6.23. The parabolic rate constant for the hot corroded coated superalloys found to be lesser than the bare superalloy. The overall weight gain of 8.75, 8.23, and 7.14  $\text{mg/cm}^2$  was observed for the NiCoCrAlYT<sub>a</sub> coated supermi 75, supermi 718, and superfer 800H superalloys (Fig.6.24),

respectively. The NiCoCrAlYTa coating provides the maximum hot corrosion resistance to superfer 800H and has been found successful in reducing the weight gain by around 37% of that gained without a coating, which is also evident from the parabolic rate constant ( $k_p = 1.332 \cdot 10^{-10} \text{ g}^2 \text{ cm}^{-4} \text{ s}^{-1}$ ). Coatings on superni 75 reduce the weight gain by 13% than that of the weight gained by the bare superni 75. The comparatively less corrosion resistance is shown by coated superni 75 and 718 than the coated superfer 800H might be due to formation of larger quantity of less protective (NiO) oxides, which allows the penetration of corrosive species through the scale to the coating. The NiO formed in the surface scale is porous due to reprecipitation by fluxing action as evident from the cross-sectional EDS analysis (Fig.6.27a and b) due to which oxygen might have penetrated deeper in to the coating as evident from the X-ray

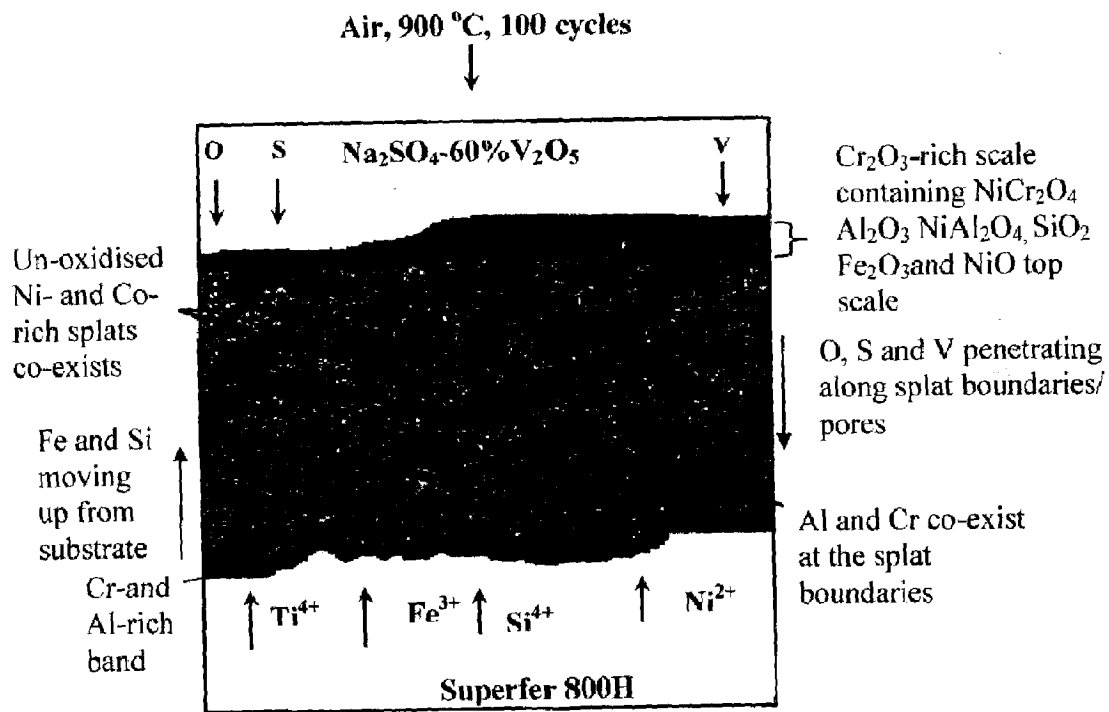


**Fig. 6.31** Schematic of the proposed oxidation mechanism of the NiCoCrAlYTa coated superalloy superfer 800H at 900 °C in Na<sub>2</sub>SO<sub>4</sub>-60%V<sub>2</sub>O<sub>5</sub> after 100 cycles.

mapping analysis (Fig.6.28-6.29), discontinuous formation of oxide scale further propagates oxidising species to the coating. Better performance of coated superfer 800H might be due to uniform, dense, thick scale formed on the surface mainly consisting of Cr and Al, presence of these elements along with oxygen represents the formation of oxides of Cr and Al. A lower amount of NiO is found on the top surface of the coating as observed from the X-ray mapping analyses (Fig 6.30), subscale region mainly consisting of Ni and Co which remain in the unreacted state as O is found to be absent at these places. Chromium and aluminum coexist with O at the boundaries of splats (Points 5 in Fig.6.27c), indicating the formation of their oxides at the splat boundaries.

### **6.3.1.5 Conclusions**

- A compact and dense continuous oxide scale developed on all the coated superalloys.
- Coated superfer 800H showed the lowest weight gain, whereas bare superfer 800H showed highest weight gain. The phases detected at the surface of the specimens with the XRD analysis are  $\text{NiCr}_2\text{O}_4$ ,  $\text{NiAl}_2\text{O}_4$ ,  $\text{Fe}_2\text{O}_3$ ,  $\text{SiO}_2$ ,  $\text{NiO}$ ,  $\text{Cr}_2\text{O}_3$  and  $\text{Al}_2\text{O}_3$ .
- The elemental mapping for silicon and iron showed outward diffusion from the substrate to the coating, the diffusion seems to have almost reached the top surface.
- Severe hot corrosion suffered by bare superfer 718 may be due the presence of Mo (3.05%) in the alloy.
- The NiCoCrAlYTaN coating provides the maximum hot corrosion resistance to superfer 800H and has been found successful in reducing the weight gain by around 37%.
- The formation of oxides along the splat boundaries and within open pores of the coatings might have acted as diffusion barrier to the inward diffusion of corroding species.



## **6.3.2 Na<sub>2</sub>SO<sub>4</sub>-25%K<sub>2</sub>SO<sub>4</sub> MOLTEN SALT ENVIRONMENT-II**

### **6.3.2.1 Introduction**

The hot corrosion behavior of NiCoCrAlYTa coatings deposited on the superalloys (namely supemi 75, supemi 718 and superfer 800H) exposed to Na<sub>2</sub>SO<sub>4</sub>-25%K<sub>2</sub>SO<sub>4</sub> at temperature 900 °C for 100 cycles has been investigated in the present work. The different composition of the salt as compared to the salt composition given in section 6.3.1 has been chosen simulating the variable composition of the salt environment manifested in the actual applications. The objective of this work was to develop an improved understanding of hot corrosion behaviour of D-gun sprayed NiCoCrAlYTa coating on different substrate, further to illustrate the effect of substrate on the coating performance.

### **6.3.2.2 Experimental details**

The substrate materials, coating formulation and the hot corrosion studies are explained in detail in section 3.1, 3.2.3 and 3.4.3.

### **6.3.2.3 Results**

#### **6.3.2.3.1 Visual observations and weight change measurements**

Light greenish oxide scale formed on the coated superalloy supemi 75, supemi 718 and superfer 800H (Fig.6.32), after hot corrosion studies at 900 °C for 100 cycles in 75% Na<sub>2</sub>SO<sub>4</sub>-25%K<sub>2</sub>SO<sub>4</sub> environment. In all the cases, a compact and intact scale gradually developed on all the coated superalloys, roughening of the coating were observed from the 17<sup>th</sup> cycle. Salt patches were observed from the 8<sup>th</sup> cycle onwards. Colour of the oxide scale formed on the coated supemi 75 (Fig.6.32a) was black after the first cycle which continued up to 17<sup>th</sup> cycle, after 18<sup>th</sup> cycle, greenish tinges noticed on the surface in the subsequent cycle. The light greenish colour intensified with the progress of studies. Minor spallation of the scale was noticed near the corners and edges after 20<sup>th</sup> cycle. The similar behaviour was observed on the coated supemi 718 (Fig.6.32b), except it has shown some minor spallation in the form of protrusions along the



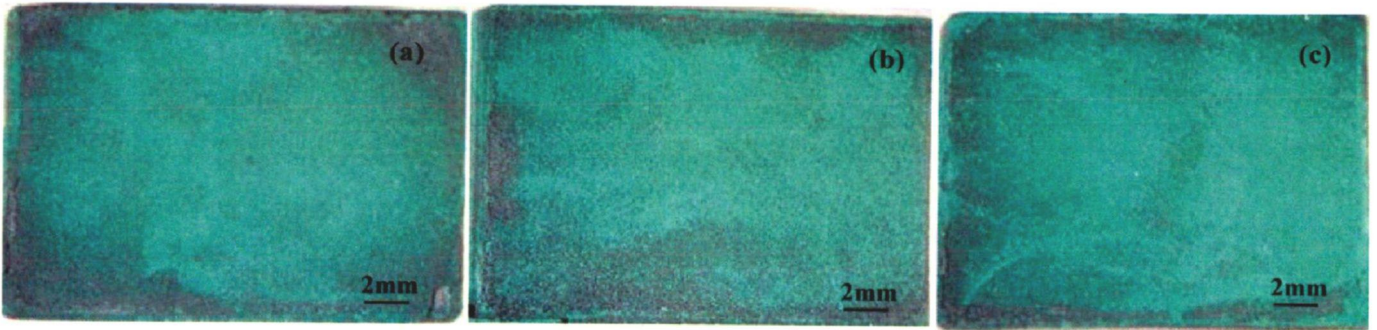


**Fig. 6.32** Surface macrograph of NiCoCrAlYTa coated superalloys subjected to cyclic oxidation in  $\text{Na}_2\text{SO}_4$ -25% $\text{K}_2\text{SO}_4$  environment at 900 °C for 100 cycles, (a) superni 75, (b) superni 718 and (c) superfer 800H

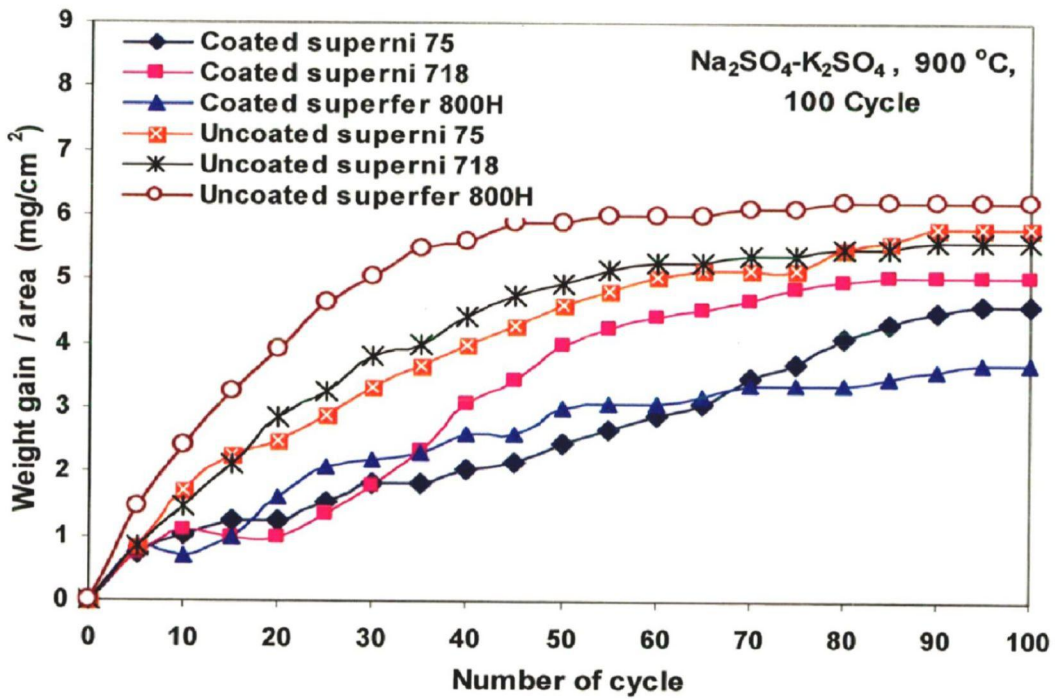


**Fig. 6.33** weight gain/area vs. number of cycles plot for NiCoCrAlYTa coated and un-coated superalloys subjected to cyclic oxidation for 100 cycles in  $\text{Na}_2\text{SO}_4$ -25% $\text{K}_2\text{SO}_4$  at 900 °C.

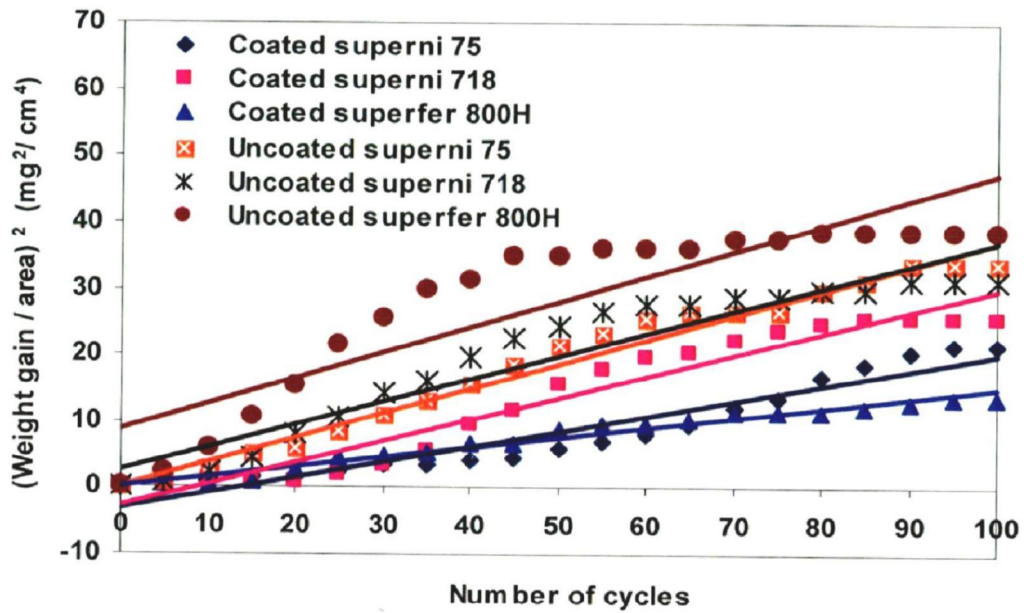


**Fig. 6.34** (weight gain/area)<sup>2</sup> vs. number of cycles plot for NiCoCrAlYTa coated and uncoated superalloys subjected to cyclic oxidation for 100 cycles in Na<sub>2</sub>SO<sub>4</sub>-25%K<sub>2</sub>SO<sub>4</sub> at 900 °C.

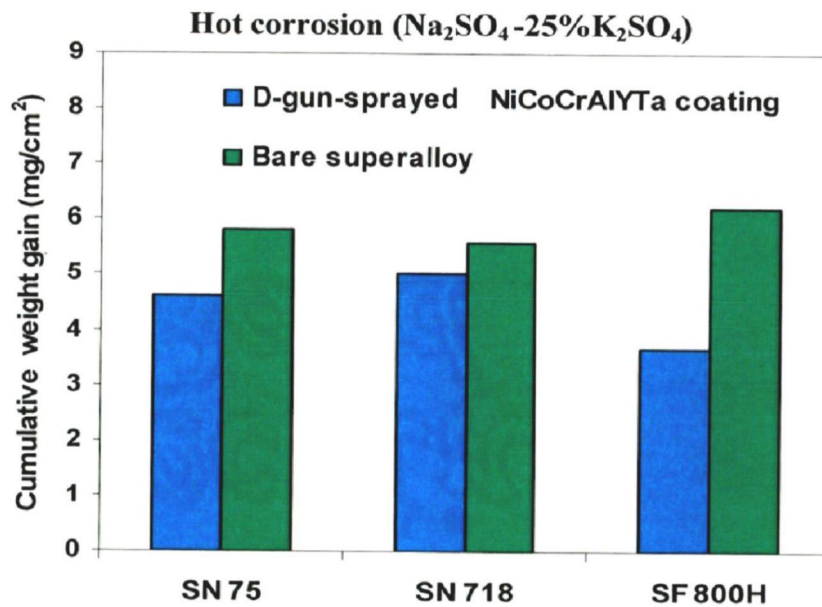


**Fig. 6.35** Bar chart showing cumulative weight gain per unit area for NiCoCrAlYTa coated and uncoated superalloys subjected to cyclic oxidation for 100 cycles in Na<sub>2</sub>SO<sub>4</sub>-25%K<sub>2</sub>SO<sub>4</sub> at 900 °C.

corner. In case of coated superfer 800H (Fig.6.32c), colour of the oxide scale was black from the initial cycles, which went up to 24<sup>th</sup> cycle, thereafter greenish patches were noticed on the surface which further goes on changing to light see green colour lasted up to 100 cycles.

The hot corrosion kinetics was determined from the weight change ( $\text{mg}/\text{cm}^2$ ) versus time plots for the bare and coated superalloys subjected to hot corrosion in  $\text{Na}_2\text{SO}_4$ -25% $\text{K}_2\text{SO}_4$  environment at 900 °C up to 100 cycles as shown in Fig.6.33. The NiCoCrAlYT<sub>a</sub> coated superalloys in all cases show a lower weight gain than the bare specimens in the given molten salt environment. Bare and coated superalloy superfer 800H shows the highest and least weight gain, respectively. Among coated superalloys, superfer 800H showed least weight gain followed by supermi 75 and supermi 718 respectively. In general, the hot corrosion behaviour of both bare supermi 75 and coated superfer 800H followed a parabolic rate law, whereas all other bare and coated superalloys slightly deviated from parabolic rate, as can be inferred from the square of weight change ( $\text{mg}^2/\text{cm}^4$ ) versus number of cycle plots shown in Fig.6.34. Values of the parabolic rate constants ( $k_p$  in  $10^{-10} \text{ g}^2 \text{ cm}^{-4} \text{ s}^{-1}$ ) for the NiCoCrAlYT<sub>a</sub> coated and bare superalloys for 100 cycles of hot corrosion is shown in Table 6.3. Cumulative weight gain per unit area for coated and bare superalloys is shown in Fig.6.35.

**Table 6.3** Parabolic rate constant ( $k_p$ ) for NiCoCrAlYT<sub>a</sub> coated and bare superalloys subjected to cyclic hot corrosion in  $\text{Na}_2\text{SO}_4$ -25% $\text{K}_2\text{SO}_4$  environment for 100 cycles at 900 °C.

Superalloy substrate	$K_p \times 10^{-10} \text{ gm}^2\text{cm}^{-4}\text{s}^{-1}$
Bare supermi 75	1.0
Bare supermi 718	0.9
Bare superfer 800H	1.1
Coated Supermi 75	0.7
Coated Supermi 718	0.9
Coated Superfer 800H	0.4

### 6.3.2.3.2 X-ray diffraction analysis (XRD)

The various phases identified from the X-ray diffraction patterns of the surface oxide formed on D-gun sprayed NiCoCrAlYTb coated superalloys after cyclic hot corrosion in  $\text{Na}_2\text{SO}_4$ -25%  $\text{K}_2\text{SO}_4$  environment at 900 °C for 100 cycles are shown in Fig.6.36. The surface oxides on coated superalloys were  $\text{NiCr}_2\text{O}_4$ ,  $\text{CoCr}_2\text{O}_4$ ,  $\text{Ni}_3\text{Al}$ ,  $\alpha\text{-Al}_2\text{O}_3$  and  $\text{NiO}$ .

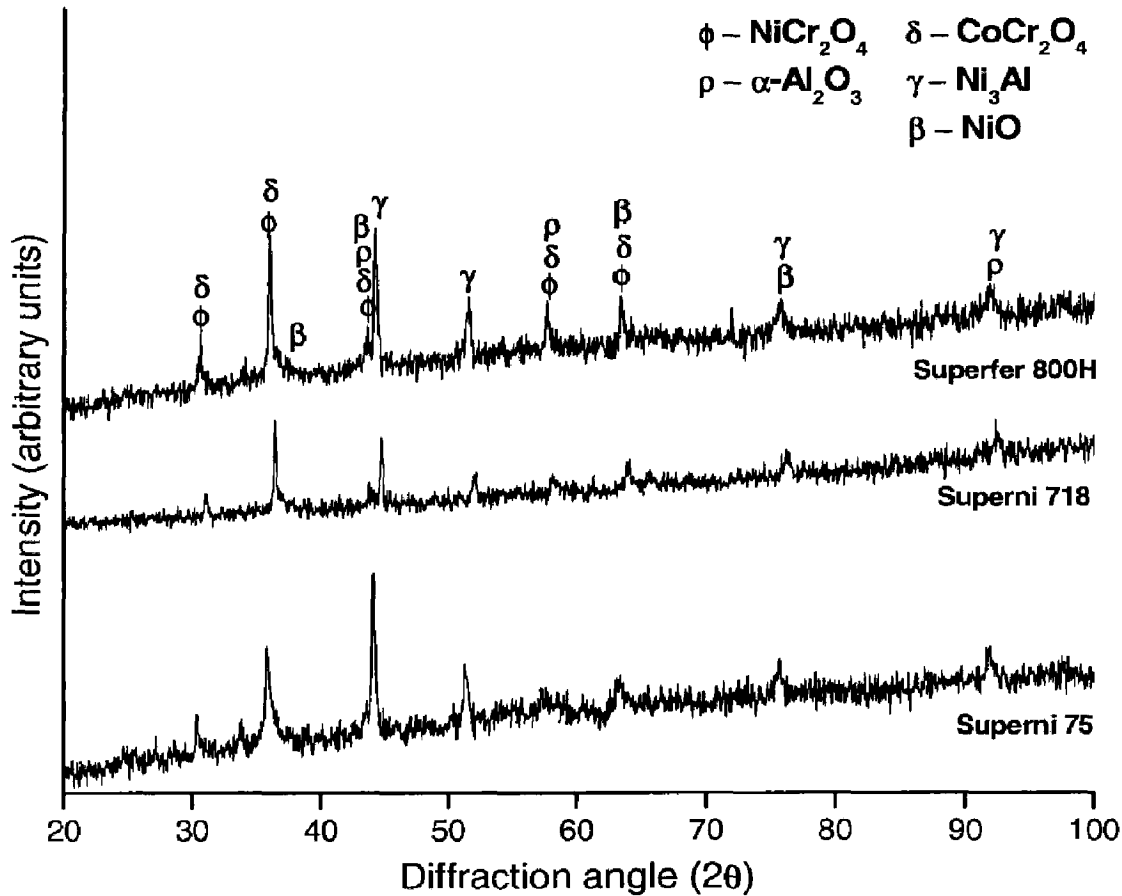


**Fig. 6.36** X-ray diffraction patterns for NiCoCrAlYTb -coated superalloys exposed to cyclic oxidation in  $\text{Na}_2\text{SO}_4$ -25% $\text{K}_2\text{SO}_4$  environment at 900 °C after 100 cycles.

### **6.3.2.3.3 FE-SEM/EDS analysis**

#### **6.3.2.3.3.1 Surface morphology of the scales**

FE-SEM micrographs with EDS spectrum reveals the surface morphology of the NiCoCrAlYTa-coated superalloy specimens after cyclic hot corrosion in molten salt environment ( $\text{Na}_2\text{SO}_4$ -25% $\text{K}_2\text{SO}_4$ ) for 100 cycles at 900 °C as shown in Fig.6.37. Surface scale developed on NiCoCrAlYTa-coated supermi 75 (Fig.6.37a) consisting of dense clusters in which, irregular needles along with white agglomerated crystalline nodules distributed throughout the coating. EDS analysis shows that the surface mainly consisted of O, Al, Co, Cr and Ni elements. FE-SEM micrograph of corroded NiCoCrAlYTa-coated supermi 718 (Fig.6.37b) mainly consisting nodules of O, Cr and Al with white network phase consisting mainly  $\text{Cr}_2\text{O}_3$ . Similarly, FE-SEM micrograph revealed the scale formed on the NiCoCrAlYTa-coated superfer 800H is dense with white agglomerated crystalline granules and needles. EDS analysis of the crystalline granules show O, Ni-rich major elements followed by Cr, whereas needle shaped region depicts mainly the presence of O, Ni and Cr (Figs.6.37c).

#### **6.3.2.3.3.2 Cross-sectional analysis**

Cross-sectional analysis of the scale and the coating was carried out at different points along the cross-section of the D-gun NiCoCrAlYTa-coated supermi 75, supermi 718 and superfer 800H specimens after cyclic hot corrosion in molten salt environment ( $\text{Na}_2\text{SO}_4$ -25% $\text{K}_2\text{SO}_4$ ) for 100 cycles at 900 °C as shown in Fig.6.38.

Cross-sectional EDS analysis of NiCoCrAlYTa-coated Supermi 75 reveals (Fig.6.38a) that the uppermost part of the scale has relatively higher concentration of O, Cr and Al (point 1), while point 2,3 and 5 corresponds to Ni-rich splats which are in un-oxidised state, as evident from the absence of oxygen. Increase in concentration of O and Al around Ni rich splats (point 4) suggest the formation of aluminum oxide at the coating-substrate interface, further the concentration of Cr and Al increases, but Ni and Co decreases. NiCoCrAlYTa-coated supermi 718 (Fig.6.38b) shows the presence of O and Cr rich- elements along with little amount of Al on the top most layers. Further, along the cross-section of coating, (Points 2 and 4), Ni-rich splats are found; absence of oxygen at these points suggests that these Ni-rich splats are in the un-oxidised state. Along the Ni-rich splat boundary (point 3 and 5), Al concentration increases, where all other

elements decreases, further Al is segregated along the coating-substrate interface (point 6). Ni and Cr elements have diffused in to the coating as evident from the EDS analysis

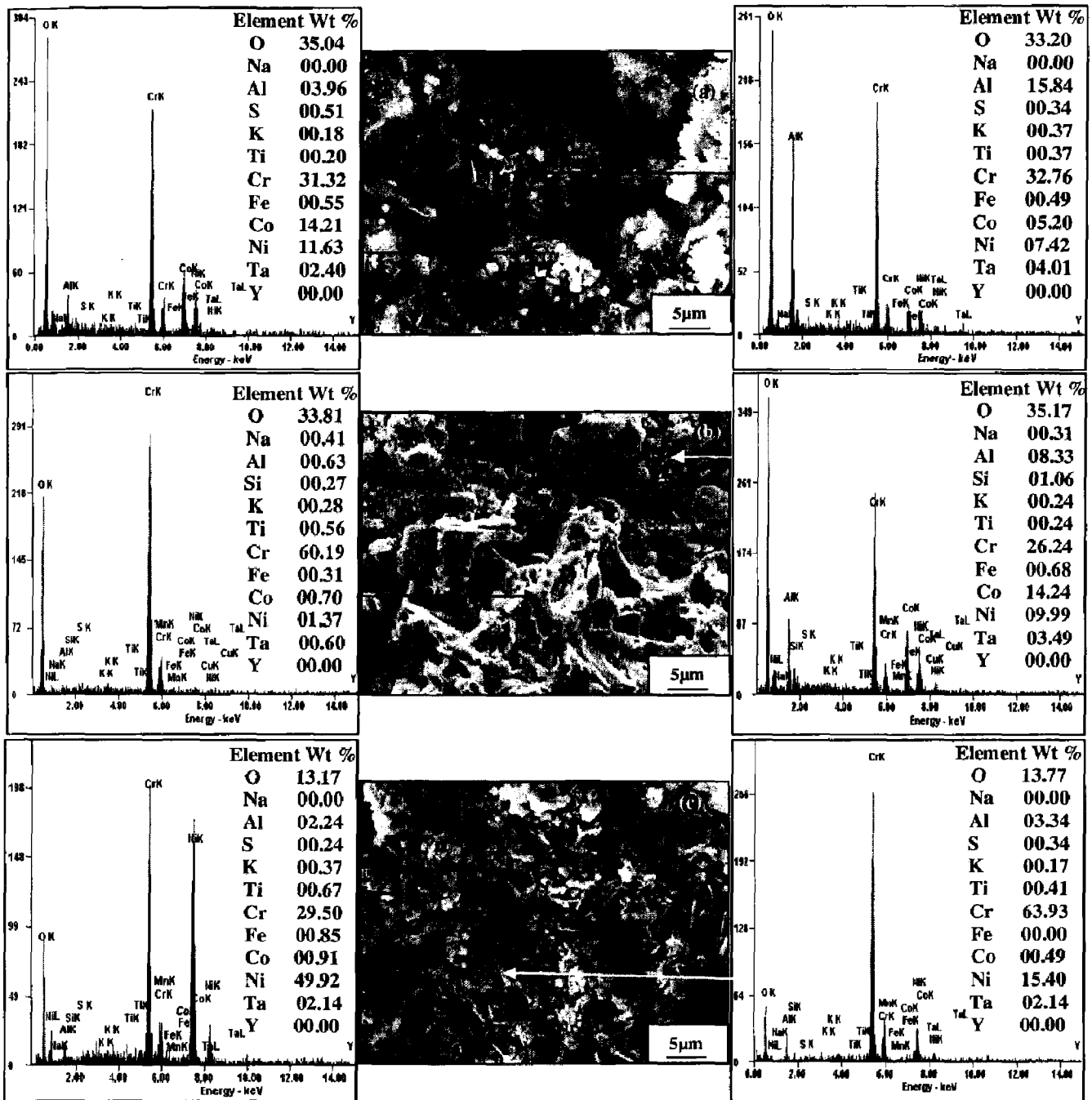
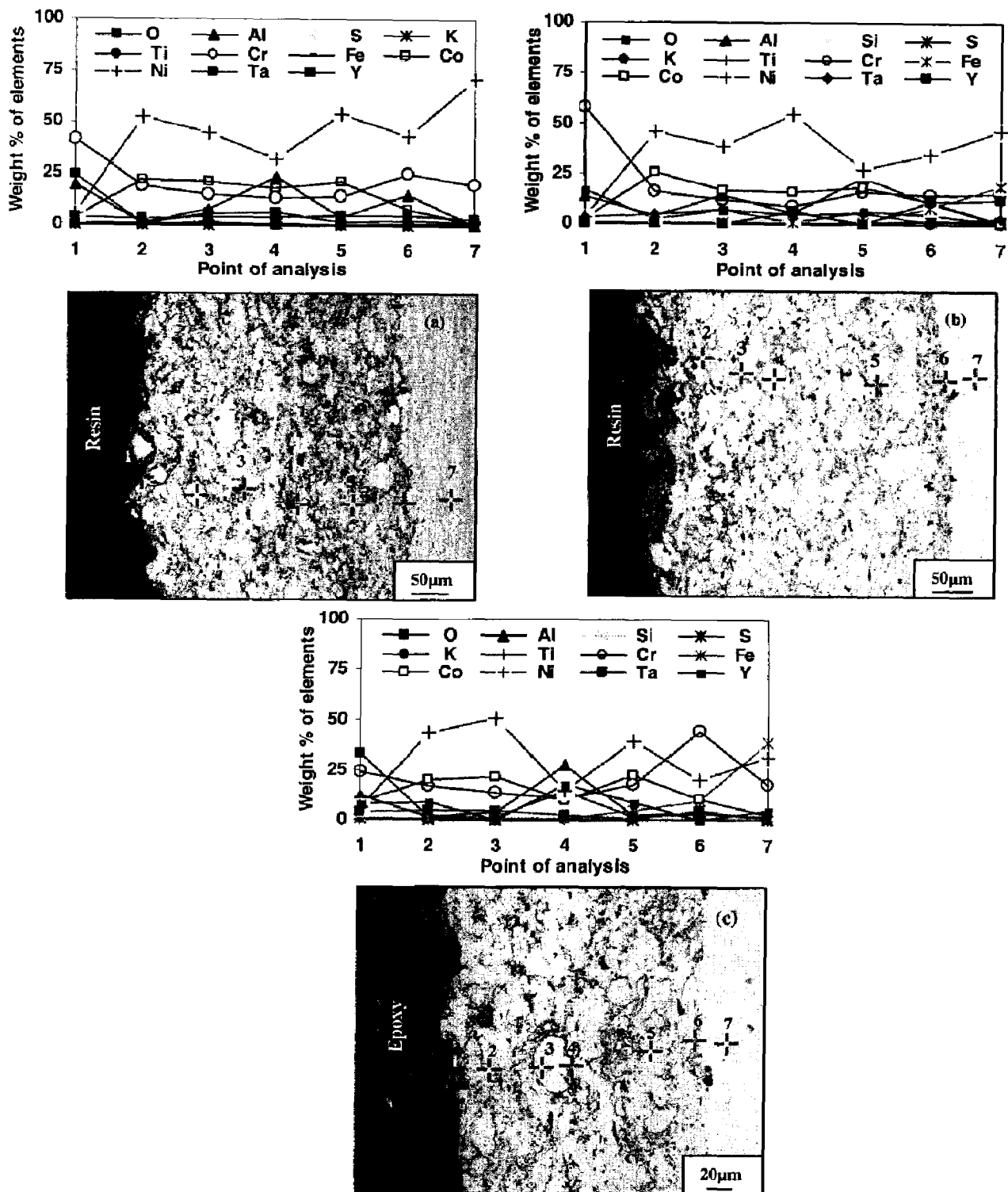


Fig. 6.37 FE-SEM/EDS surface analysis for NiCoCrAlYTa coated superalloys subjected to cyclic oxidation in  $\text{Na}_2\text{SO}_4$ -25% $\text{K}_2\text{SO}_4$  environment at 900 °C after 100 cycles(a) Coated superni 75, (b) Coated superni 718 and (c) Coated superfer 800H.



**Fig. 6.38** Oxide scale morphology and variation of elemental composition across the cross-section of NiCoCrAlYTa-coated superalloys subjected to cyclic oxidation at 900 °C in Na<sub>2</sub>SO<sub>4</sub>-25%K<sub>2</sub>SO<sub>4</sub> environment after 100 cycles (a) supemi 75, (b) supemi 718 and (c) superfer 800H.



at point 7. The superfer 800H (Fig.6.38c) indicates a scale consists of oxides of chromium, white phase in the subscale region (point 2, 3 and 5) contains coating elements which are presumed to be un-oxidised as oxygen is found to be absent at these points. The presence of higher amount of oxygen, along the Ni-rich splat boundary, with chromium and yttrium depicts the formation of respective oxides. Along the coating-substrate interface (at point 6), concentration of Cr increases significantly with Ni gets depleted, thereby suggesting the segregation of coating - substrate elements.

#### **6.3.2.3.4 X-ray mapping**

D-gun sprayed NiCoCrAlYTa-coated superalloy samples after hot corrosion in molten salt environment for 100 cycles at 900 °C is shown in Fig.6.39-6.41. X-ray mapping of hot corroded coated supermi 75 (Fig.6.39) shows uppermost part of the coating has O, Ni, Cr and Al, which represents the formation of respective oxides of Cr, Al, Ni and spinel, whereas in the subscale region, nearly elongated shaped, Ni-rich splats distributed across the coating. Al in the form of streaks is distributed along the Ni rich splat boundaries, which are believed to be oxidised as could be seen from the oxygen distribution. The X-ray mappings for hot corroded NiCoCrAlYTa-coated supermi 718 after 100 cycles at 900 °C (Fig.6.40) indicates a scale mainly consisting of oxygen, chromium and aluminum at the top surface. Below the upper most part of the scale, the coating has un-reacted Ni-rich splats, whereas Cr and Al has oxidised and distributed along these splat boundaries. The elemental mapping for iron showed upward diffusion from the substrate to the coating, the diffusion seems to have almost reached the top surface. Similarly X-ray mappings for NiCoCrAlYTa-coated superfer 800H after 100 cycles of hot corrosion at 900 °C (Fig.6.41) represents that the top surface of coating has thick oxide scale containing mainly of chromium and aluminum rich elements. Oxidised Al streaks are present along Ni-rich splat boundaries, as evident from the oxygen distribution; whereas Ni-rich splats are in un-oxidised state. The topmost layer of the scale found with traces of iron and silicon

#### **6.3.2.4 Discussion**

During initials cycles of hot corrosion run at 900 °C for D-gun sprayed NiCoCrAlYTa-coated superalloy samples, the colour of the oxide scale on the surface was dark, in the subsequent cycles it turned in to light sea green colour (Fig.6.32). Un-coated superalloys shows higher



weight gain with continuous increase, whereas coated show initial increase in weight gain followed by gradual increase (Fig.6.33). The coated superalloys followed a parabolic rate law (Fig.6.34), whereas bare superalloys slightly deviates due to (except bare superni 75) cyclic scale growth. The parabolic rate constant for the bare and coated superalloys are given in Table 6.3. The weight gain of coated superalloys superni 75 and superni 718 and superfer 800H is nearly four-fifth, nine-tenth and three-fifth as compared to that of bare superalloys superni 75

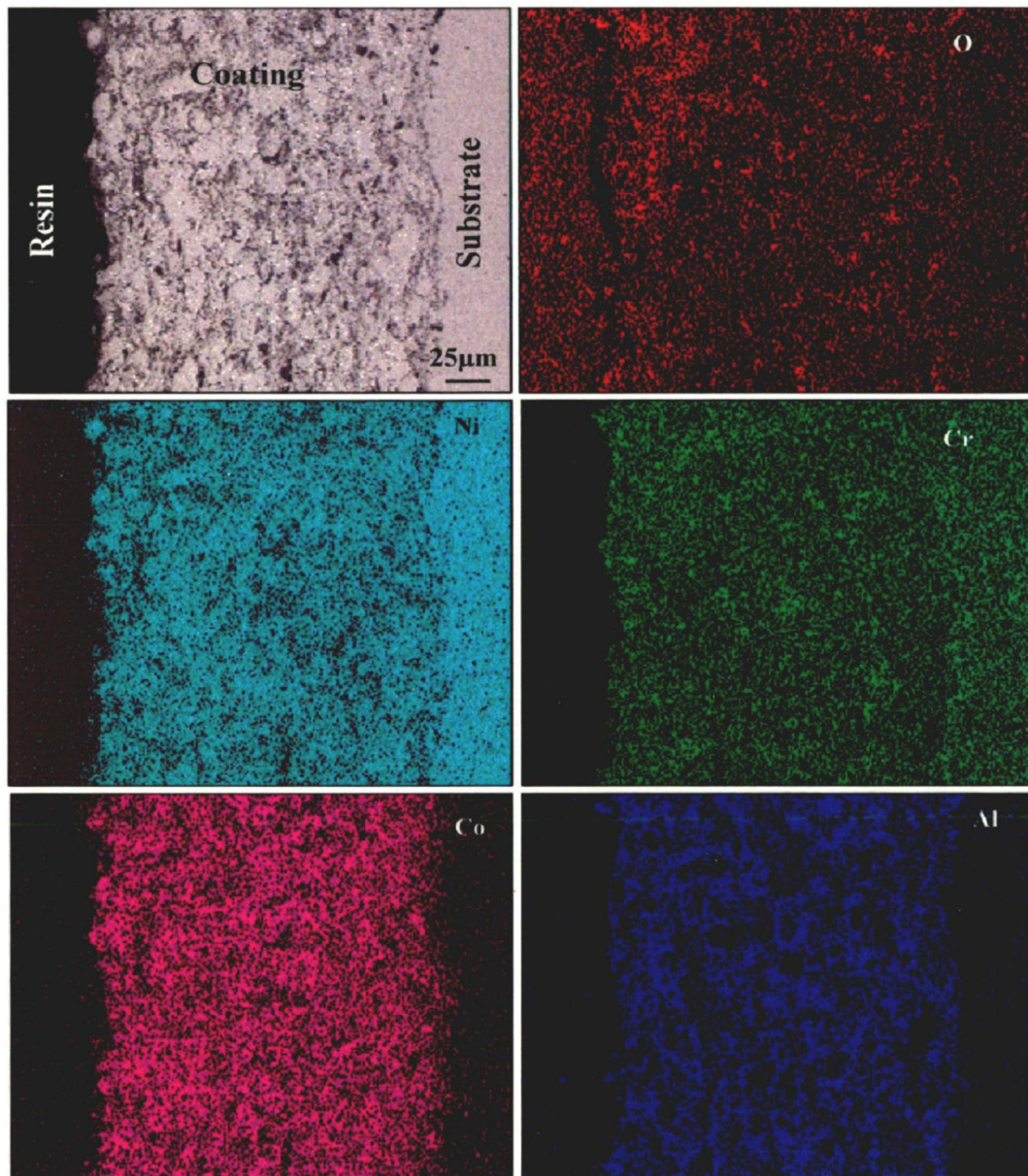


**Fig. 6.39** Secondary electron image (SEI) and X-ray mapping of the cross-section of the NiCoCrAlYTa-coated superalloy superni 75 subjected to cyclic oxidation at 900 °C in  $\text{Na}_2\text{SO}_4$ -25% $\text{K}_2\text{SO}_4$  after 100 cycles.



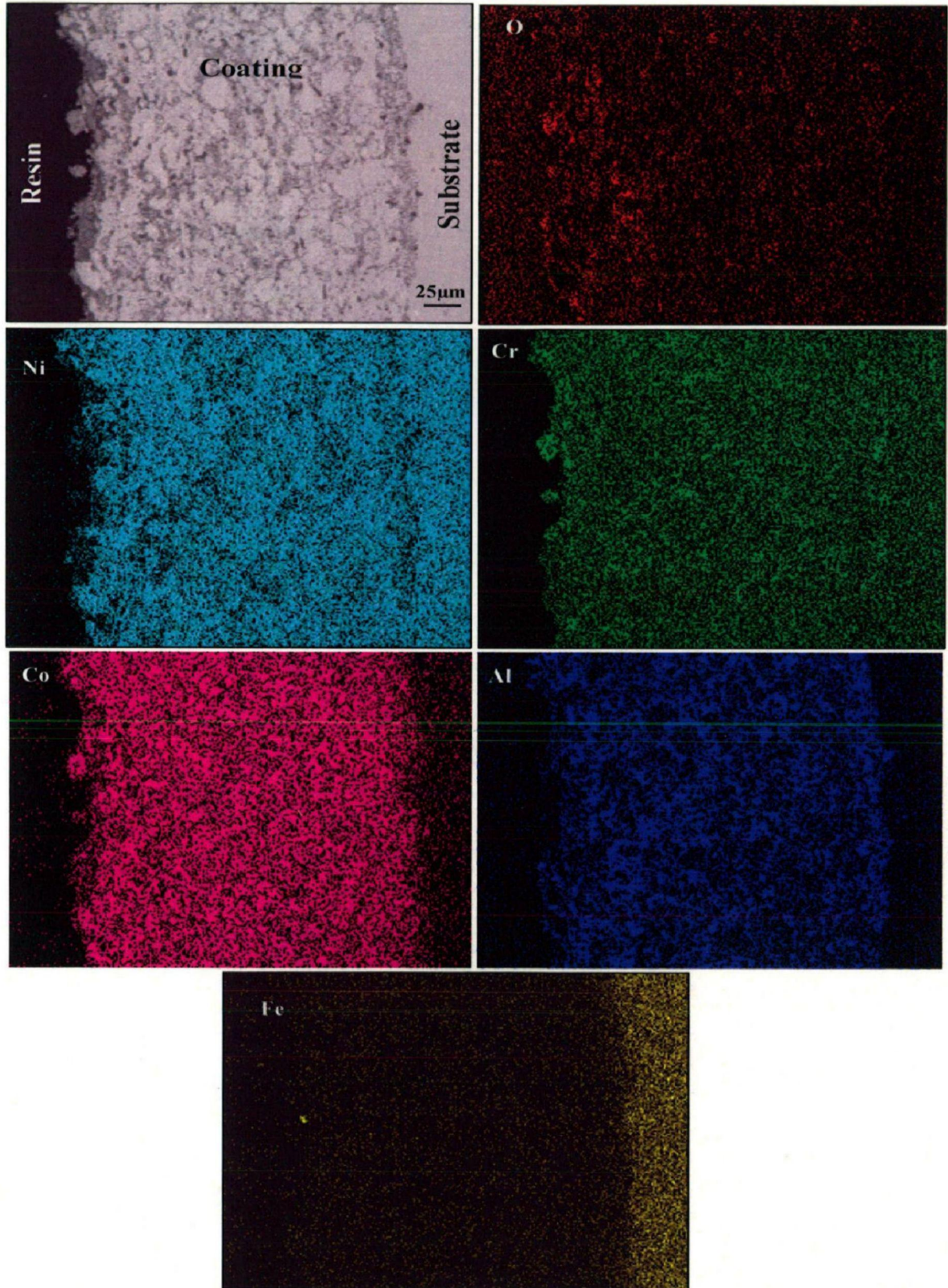


**Fig. 6.40** Secondary electron image (SEI) and X-ray mapping of the cross-section of the NiCoCrAlYTa-coated superalloy superalloy 718 subjected to cyclic oxidation at 900 °C in  $\text{Na}_2\text{SO}_4$ -25% $\text{K}_2\text{SO}_4$  after 100 cycles.



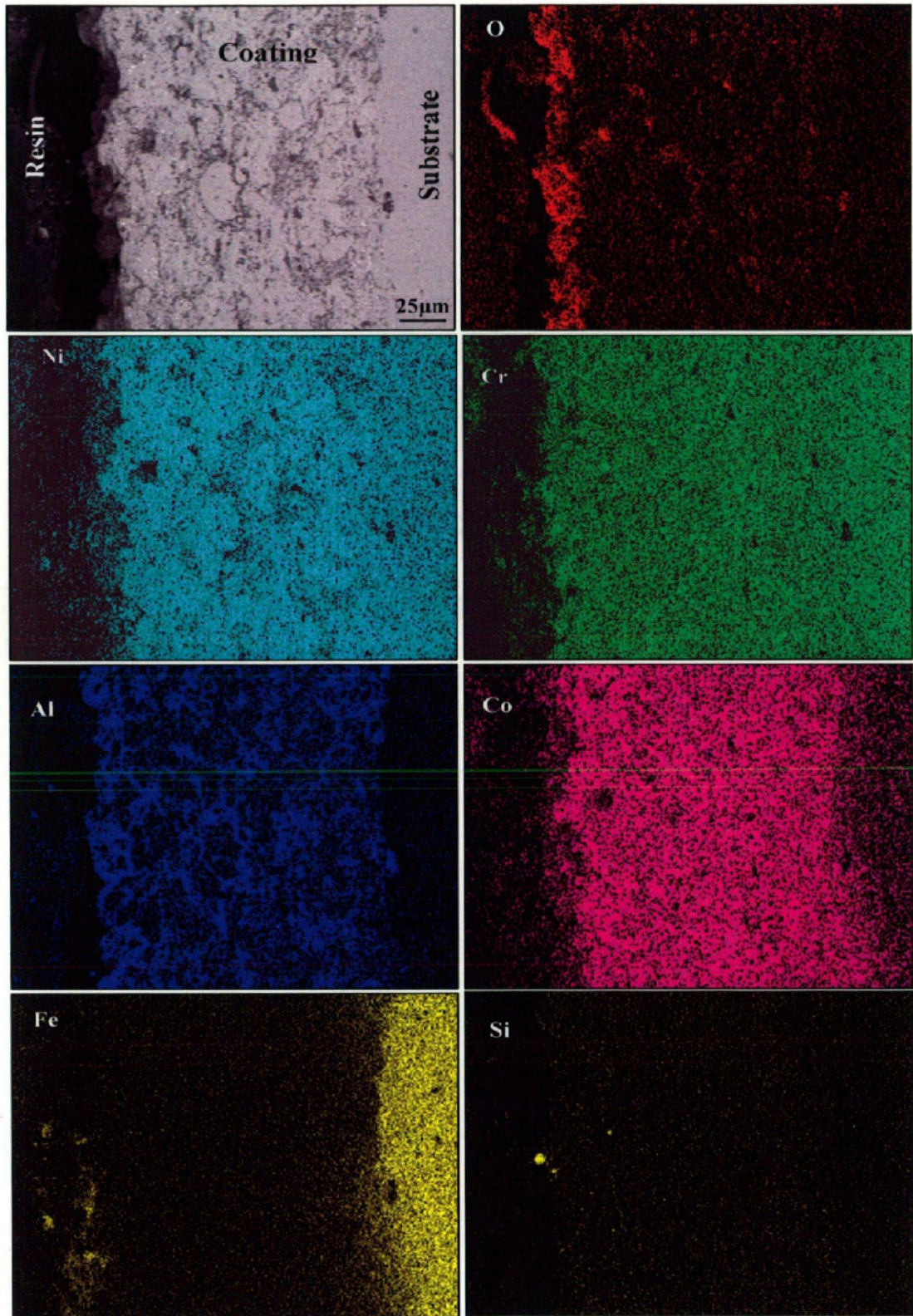


**Fig. 6.41** Secondary electron image (SEI) and X-ray mapping of the cross-section of the NiCoCrAlYTa-coated superalloy superfer 800H subjected to cyclic oxidation at 900 °C in  $\text{Na}_2\text{SO}_4$ -25% $\text{K}_2\text{SO}_4$  after 100 cycles.

and superalloys 718 and superalloy 800H, respectively. Weight gain for the NiCoCrAlYTa-coated superalloys is less than the bare superalloys, which show the protective behaviour of the coating against hot corrosion. Cumulative weight gain of 4.6, 5, and 3.68 mg/cm<sup>2</sup> was observed for the coated superalloys 75, 718, and 800H superalloys, respectively (Fig.6.35). The NiCoCrAlYTa coating provides maximum hot corrosion resistance to superalloy 800H and has been found successful in reducing the weight gain by around 41% of that gained without a coating. Better protection attributed to the formation of thick and adherent oxide scale of Cr and Al on the top surface of coating. In the subscale region, oxides of Cr and Al across the periphery of Ni-rich splat boundaries acted as diffusion barriers to the inward diffusion of corrosive species (Fig.6.41). This would relatively minimize the weight gain and result in the steady state oxidation behavior with the progress of hot corrosion test. Whereas coated superalloy 75 and superalloy 718 superalloys were effective in reducing the weight gain by 21% and 10% that of bare superalloys, respectively. XRD analysis of corroded superalloys revealed the formation of Ni<sub>3</sub>Al,  $\alpha$ -Al<sub>2</sub>O<sub>3</sub> and NiO and spinels (NiCr<sub>2</sub>O<sub>4</sub>, CoCr<sub>2</sub>O<sub>4</sub>) on the coated surface, which might have further contributed in reducing the weight gain (Fig.6.36). These phases in the scale of coated superalloys are further supported by surface EDS analysis (Fig.6.37), Cross-sectional EDS (Fig.6.38) and X-ray mapping analyses (Fig.6.39-6.41). These oxides are more protective than NiO scales since they are reasonably stoichiometric oxides, with low defect concentrations, and can give effective protection to the alloy in environments of high oxygen activity (Stott, 1987). An increase in concentration of O, Cr and Al rich elements around Ni- and Co-rich splats (Fig.6.38) suggest the formation of oxides of Cr and Al, aluminum has higher affinity towards oxygen. Cr<sub>2</sub>O<sub>3</sub> is easier to react with Na<sub>2</sub>SO<sub>4</sub> than Al<sub>2</sub>O<sub>3</sub> to reduce the oxygen ion activity of Na<sub>2</sub>SO<sub>4</sub>. Hence, Al<sub>2</sub>O<sub>3</sub> was protected and formed a continual layer near the alloy (Guo et al., 2006B). These oxides are further effective in reducing the penetrating behaviour of corrosive species towards the substrate. The upper most part of the oxide scale for coated superalloy 800H revealed traces of iron and silicon indicating their diffusion behaviour from the substrate to the coating, during initial cycles of hot corrosion, these elements have diffused along the splat boundaries and interconnected pores. However in the subsequent cycles, the oxide which fills the pores and splat boundaries, suppress further diffusion of substrate elements. Schematic of the proposed oxidation mechanism of the NiCoCrAlYTa coated superalloy superalloy 800H at 900 °C in Na<sub>2</sub>SO<sub>4</sub>-25%K<sub>2</sub>SO<sub>4</sub> after 100 cycles is shown in Fig.6.42.



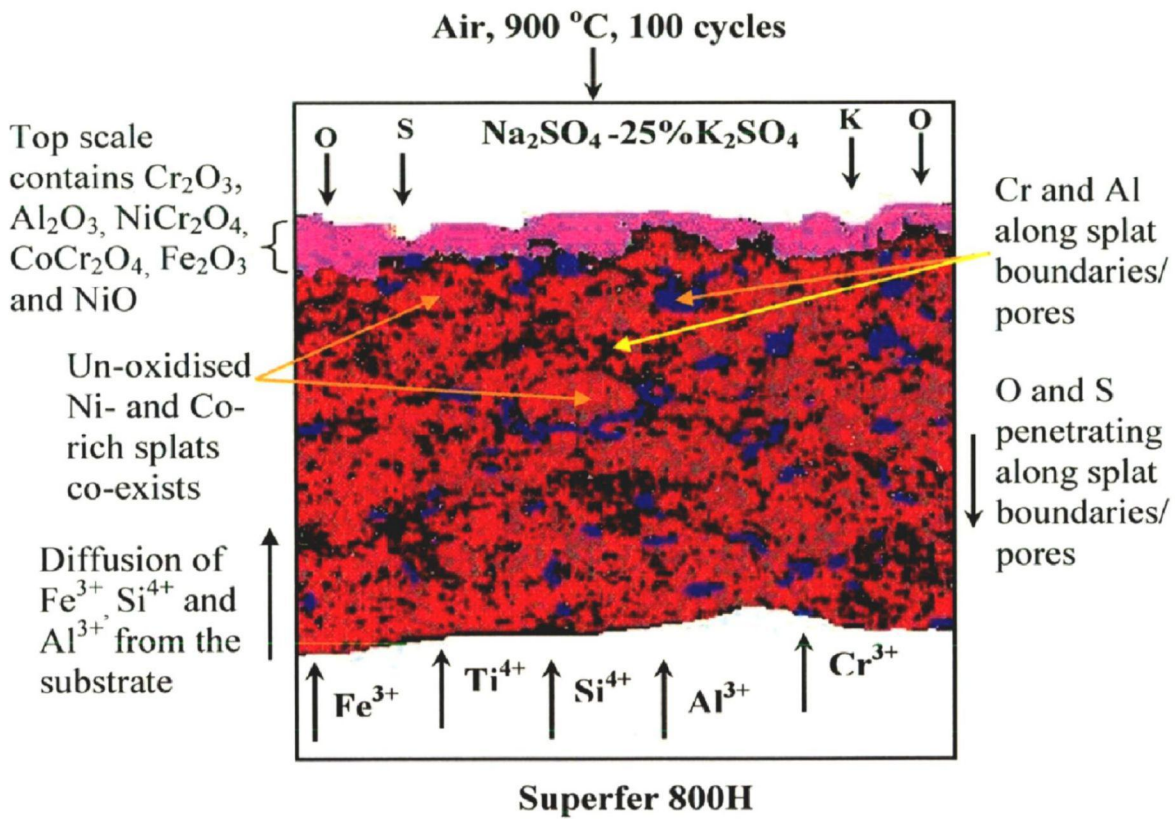


**Fig. 6.42** Schematic of the proposed oxidation mechanism of the NiCoCrAlYTa coated superalloy superfer 800H at 900 °C in  $\text{Na}_2\text{SO}_4$ -25% $\text{K}_2\text{SO}_4$  after 100 cycles.

### 6.3.2.5 Conclusions

- Colour of the oxide scale formed on the coated superalloys after hot corrosion test was black up to 17<sup>th</sup> to 24<sup>th</sup> cycle, which turned to sea green colour towards the end of 10 cycles.
- Thick and dense oxide scale of chromium and aluminum has formed on the top surface of coated superalloy superfer 800H.
- The NiCoCrAlYTaN coating provides maximum hot corrosion resistance to superfer 800H by reducing the weight gain by around 41% of that gained without a coating.
- All the coated superalloys after hot corrosion test revealed the formation of spinels (NiCr<sub>2</sub>O<sub>4</sub>, CoCr<sub>2</sub>O<sub>4</sub>) as predominant phases which might be contributing for reducing the weight gain.
- In all the cases coating partially got oxidised below the top scale where Ni- and Co- rich splats are mostly un-oxidised, along the inter splat region coating show the presence of Cr and Al.

# CHAPTER 7

## CORROSION STUDIES IN INDUSTRIAL ENVIRONMENT OF COAL FIRED BOILER

---

This chapter deals with the study of hot corrosion behaviour of the bare and D-gun coated superfer 800H exposed to low temperature super-heater zone of the coal fired boiler of Guru Nanak Dev Thermal Power Plant, Bathinda, Punjab, India. The specimens were hanged in the platen super-heater of coal fired boiler where the gas temperature was around  $900\text{ }^{\circ}\text{C} \pm 10\text{ }^{\circ}\text{C}$ . Hot corrosion experiments were performed for 10 cycles, each cycle consisting of 100 hours exposure followed by 1 hour cooling at ambient temperature. The specimens were visually examined at the end of each cycle for any change in colour, luster, spalling tendency and other physical changes of the scale if any. Weight change measurements were done at the end of each cycle. The weight change data could not be of much use for predicting hot corrosion behaviour of the coated alloys as spalling and ash deposition also occurred. The extent of corrosion has been evaluated by measuring thickness of the unreacted portion of the samples after the total exposure of 1000 hours. The different phases and their distribution in the hot corroded specimens were analysed with the help of XRD, FE-SEM/EDS and X-ray mapping.

### 7.1 Experimental details

The details of the studies in the industrial environment of bare and D-gun coated specimens are explained in chapter 3.

## 7.2 RESULTS AND DISCUSSION

### 7.2.1 Visual Examination

#### 7.2.1.1 Bare and D-gun coated superfer 800H

The macrographs for the bare superfer 800H and D-gun sprayed  $\text{Cr}_3\text{C}_2\text{-NiCr}$ ,  $\text{NiCrAlY} + 0.4\text{wt}\%\text{CeO}_2$  and  $\text{NiCoCrAlYTaNi}$  coatings on superfer 800H after 1000 hours of exposure to low temperature super-heater zone of the coal fired boiler are shown in Fig.7.1. Light grey coloured scale appeared on the surfaces of bare superfer 800H (Fig.7.1a) after first cycle, which is lasted

up to 3<sup>rd</sup> cycle, ash deposition has started after 4<sup>th</sup> cycle. Greenish and brownish spots appeared on the surface along with white spots of ash deposits, which further intensified towards the end and final scale was of dark brown colour with protrusions. No spalling and cracks were observed in the scale throughout the experimentation. The macrographs of D-gun sprayed coatings on superfer 800H after exposing to the boiler environment are shown in Fig.7.1 (b) to 7.1(d). The macrograph of Cr<sub>3</sub>C<sub>2</sub>-NiCr coated specimen (Fig.7.1b) show the formation of grey colour scale after first cycle, which is lasted up to 2<sup>nd</sup> cycle. After 3<sup>rd</sup> cycle, ash deposition was noticed on the coatings, in the subsequent cycle brownish colour was noticed. Towards the last cycles, the scale was grey in colour with brown patches. In case of NiCrAlY+0.4wt%CeO<sub>2</sub> coated superfer 800H (Fig.7.1c), the colour of scale was initially grey which has turned dark grey with increase in the exposure time (up to 4<sup>th</sup>), ash deposition was noticed after 5<sup>th</sup> cycle. It indicates the formation of light brownish colour on the surface, which has continued up to 10<sup>th</sup> cycles. Even after 1000 hours of exposure, the scale which was light brown in colour was intact and did not show any presence of cracks. In case of NiCoCrAlYTaNi coated superfer 800H (Fig.7.1d), light grey colour

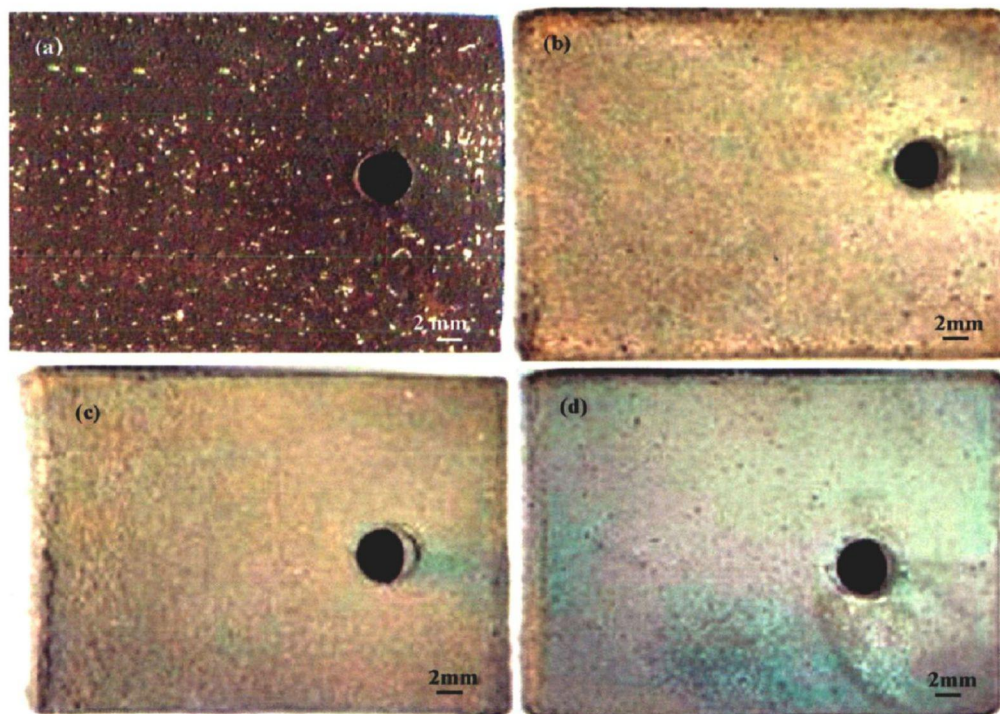


**Fig. 7.1** Macrographs of the (a) bare and D-gun sprayed (b) Cr<sub>3</sub>C<sub>2</sub>-NiCr,(c) NiCoCrAlYTaNi and (d) NiCoCrAlYTaNi coated on superfer 800H after 1000 hours exposure to low temperature super-heater zone of the boiler at 900 °C.



scale was formed on the surface after first cycle. No spallation was observed during the course of the study. Deposition of ash was noticed after 4<sup>th</sup> cycle, further in the subsequent cycles, after 4<sup>th</sup> cycle, colour of the scale was dark grey, which continued up to 10 cycles.

## **7.2.2 Hot Corrosion of bare and coated superfer 800H**

### **7.2.2.1 Corrosion Kinetics**

The weight change per unit area ( $\text{mg}/\text{cm}^2$ ) versus time plot for 1000 hours exposure of bare and D-gun coated  $\text{Cr}_3\text{C}_2$ -NiCr, NiCrAlY+0.4wt%CeO<sub>2</sub> and NiCoCrAlYTaNi on superfer 800H to the boiler environment is shown in Fig.7.2 and Fig.7.3. The weight change in case of coated sample is consisting of the scale formation at the top surface of the coating by reaction and also from the partial oxidation of the coating elements like Cr, Al and Ce at the splat boundaries. The partially oxidised coating remains intact and adherent to substrate, preventing further attack on the substrate superalloy. This partially oxidised coating provides protection against the boiler environment. Bare superfer 800H shows the lowest weight gain, erosion combined with oxide scale spallation is attributed to lower weight gain. Among coated superalloys, D-gun sprayed  $\text{Cr}_3\text{C}_2$ -NiCr coated superfer 800H shows the lowest weight gain, which is around 65% and 54% less than that of NiCrAlY+0.4wt%CeO<sub>2</sub> and NiCoCrAlYTaNi coated superfer 800H, respectively. The  $(\text{weight change}/\text{area})^2$  versus time plot for bare and D-gun coated superfer 800H is shown in Fig.7.3. It is observed that all the coated and bare coated superfer 800H follows the parabolic rate law, except NiCrAlY+0.4wt%CeO<sub>2</sub> coated superalloy. The parabolic rate constants ( $k_p$  in  $10^{10} \text{ g}^2 \text{ cm}^{-4} \text{ s}^{-1}$ ) for the bare and  $\text{Cr}_3\text{C}_2$ -NiCr, NiCrAlY+0.4wt%CeO<sub>2</sub> and NiCoCrAlYTaNi coated superfer 800H was found to be 0.86, 8.1, 46 and 25 respectively.

### **7.2.2.2 Average scale Thickness and Depth of Internal Attack**

The BSE images across the cross-section of the scales formed on bare and D-gun coated superfer 800H are shown in Fig.7.4. The average scale thickness for bare superfer 800H is found to be 52  $\mu\text{m}$ , and that for D-gun sprayed  $\text{Cr}_3\text{C}_2$ -NiCr, NiCrAlY+0.4wt%CeO<sub>2</sub> and NiCoCrAlYTaNi coated superfer 800H are 220, 200 and 190  $\mu\text{m}$ , respectively. The internal corrosion attack is absent in case of D-gun coated superalloy, whereas the bare superfer 800H shows average internal corrosion attack up to 15 $\mu\text{m}$  from the scale-substrate interface. The average gain in scale

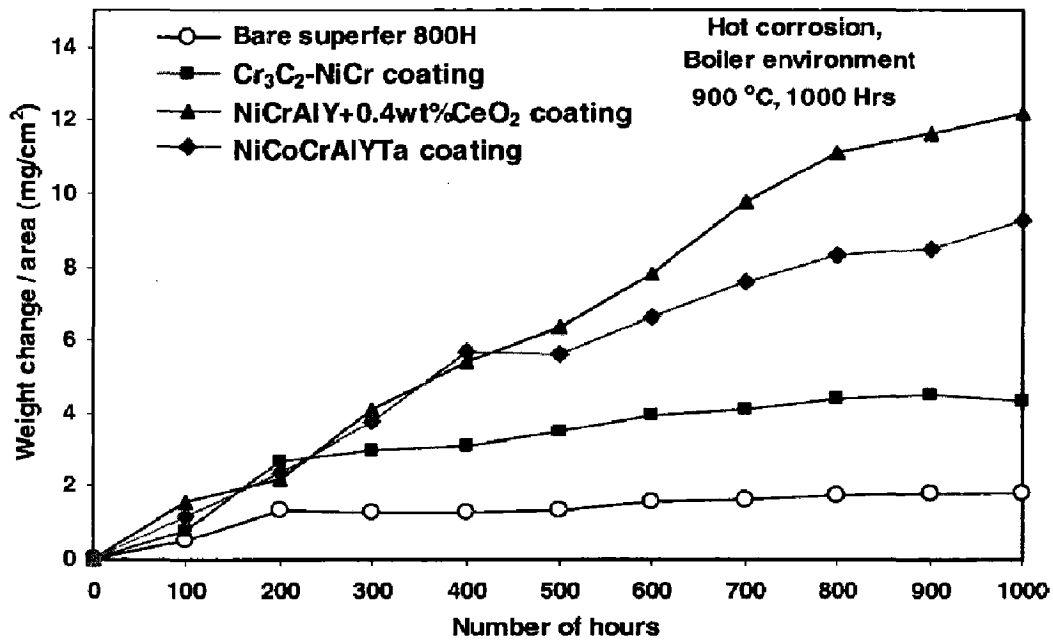


Fig. 7.2 Weight change vs. time plots for the bare and D-gun coated superfer 800H subjected to 1000 hrs cyclic exposure to low temperature super-heater zone of the coal fired boiler at 900 °C.

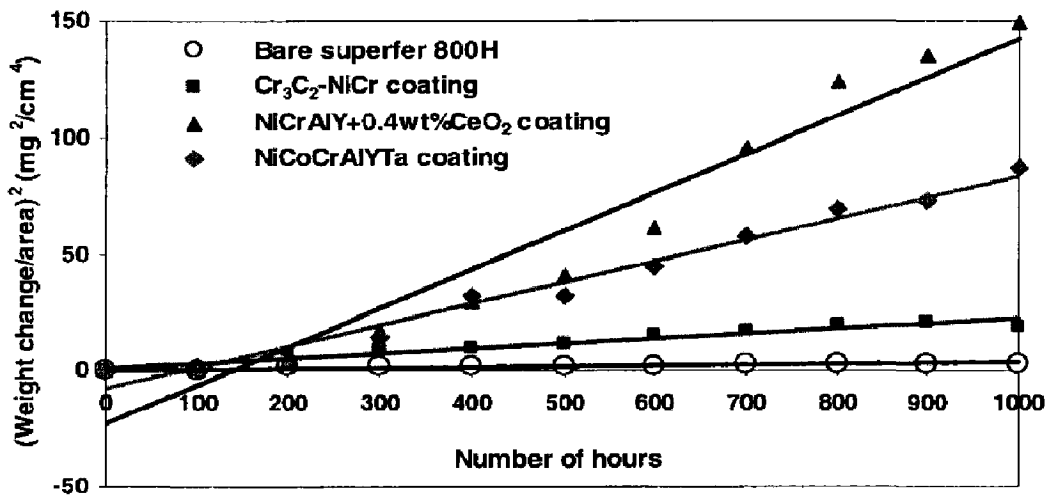


Fig. 7.3 (Weight gain/area)<sup>2</sup> vs. number of hours plots for the bare and D-gun coated superfer 800H subjected to 1000 hrs cyclic exposure to low temperature super-heater zone of the coal fired boiler at 900°C.

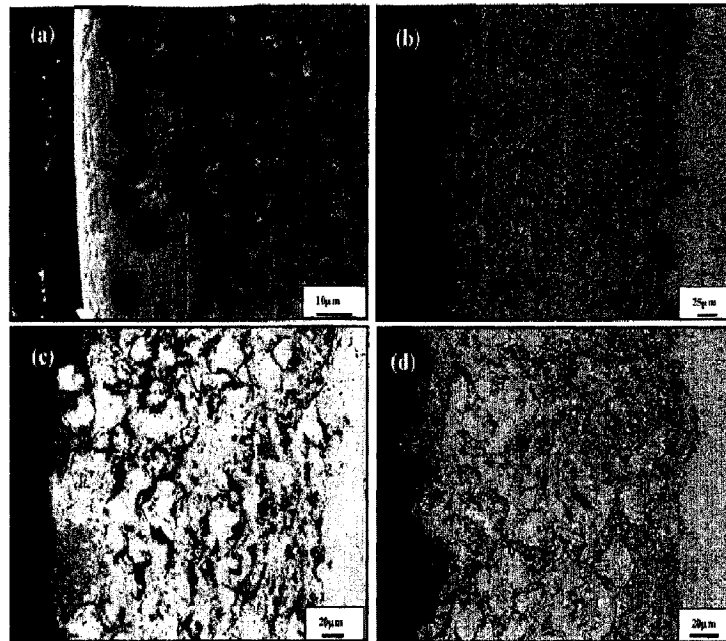


Fig. 7.4 BSE images for the bare and D-gun coated superfer 800H after 1000 hrs exposure to low temperature super-heater zone of the coal fired boiler at 900 °C:(a) Bare superalloy (b)Cr<sub>3</sub>C<sub>2</sub>-NiCr coated (c)NiCrAlY+0.4wt%CeO<sub>2</sub> coated(d) NiCoCrAlYTa coated.

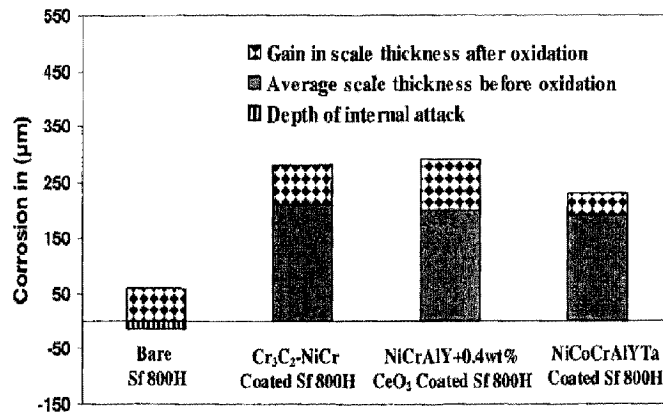
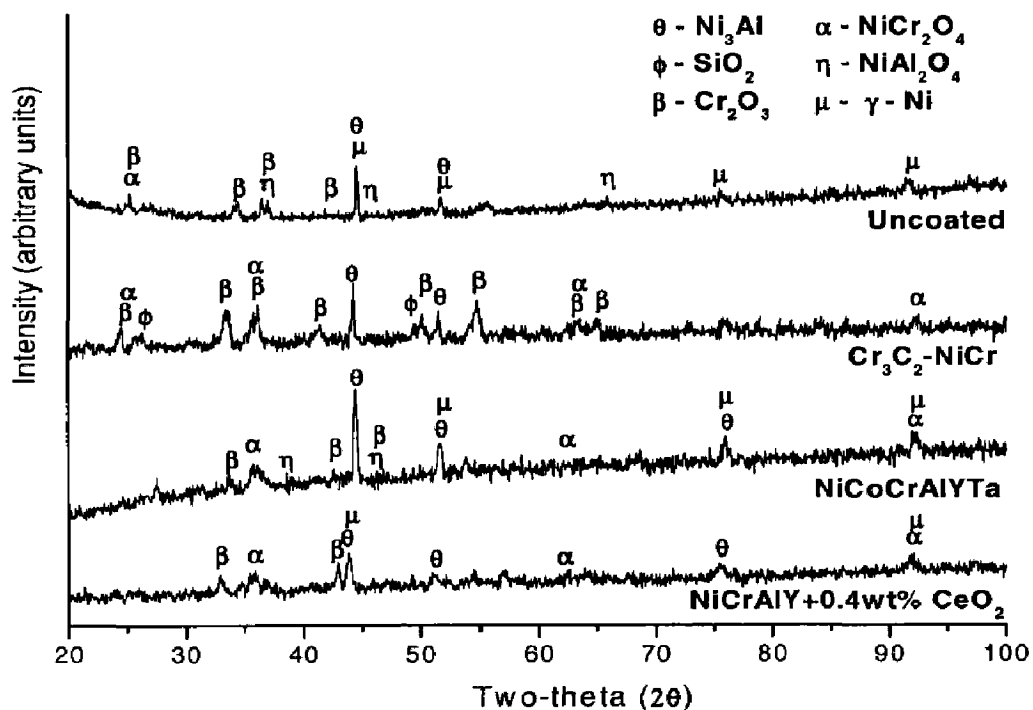


Fig. 7.5 Bar charts indicating the extent of corrosion for the bare and D-gun coated superfer 800H after 1000 hrs exposure to the coal fired boiler at 900 °C.



**Fig. 7.6** X-ray diffraction patterns for the (i) bare and D-gun sprayed (ii)  $\text{Cr}_3\text{C}_2$ -NiCr (iii) NiCrAlY+0.4wt% $\text{CeO}_2$  (iv) NiCoCrAlYTaNiCrAlY+0.4wt% $\text{CeO}_2$  coatings on superfer 800H after 1000 hrs of exposure to low temperature super-heater zone of the coal fired boiler at 900 °C.

thickness of about 60, 70, 90 and 40 $\mu\text{m}$  for bare superfer 800H,  $\text{Cr}_3\text{C}_2$ -NiCr, NiCrAlY+0.4wt%  $\text{CeO}_2$  and NiCoCrAlYTaNiCrAlY+0.4wt% $\text{CeO}_2$  coated superfer 800H, respectively and depth of internal corrosion attack for bare superfer 800H are shown in Fig.7.5.

### 7.2.2.3 X-ray Diffraction Analysis

The X-ray diffraction patterns for the corroded bare and D-gun coated superfer 800H are shown in Fig.7.6. The bare superfer 800H after exposure to the boiler environment for 1000 hrs indicated the presence of  $\text{NiCr}_2\text{O}_4$ ,  $\text{Cr}_2\text{O}_3$ ,  $\text{NiAl}_2\text{O}_4$ ,  $\text{Ni}_3\text{Al}$  and  $\gamma$ -Ni on the surface of the specimen. In case of  $\text{Cr}_3\text{C}_2$ -NiCr coated superfer 800H, the surface scale indicated the presence of  $\text{NiCr}_2\text{O}_4$ ,  $\text{Cr}_2\text{O}_3$ ,  $\text{SiO}_2$  and  $\text{Ni}_3\text{Al}$ . The NiCrAlY+0.4wt% $\text{CeO}_2$  coated superfer 800H indicates

the presence of  $\text{NiCr}_2\text{O}_4$ ,  $\text{Cr}_2\text{O}_3$ ,  $\text{Ni}_3\text{Al}$  and  $\gamma\text{-Ni}$  phases. In case of NiCoCrAlYT<sub>a</sub> coated superfer 800H, the phases formed on the surface consist of  $\text{NiCr}_2\text{O}_4$ ,  $\text{NiAl}_2\text{O}_4$ ,  $\text{Cr}_2\text{O}_3$ ,  $\text{Ni}_3\text{Al}$  and  $\gamma\text{-Ni}$ .

#### **7.2.2.4 FE-SEM/EDS Analysis**

##### **7.2.2.4(a) Surface Analysis**

The FE-SEM micrographs showing surface morphology of the scale formed on bare and D-gun coated superfer 800H are given in Fig.7.7. The oxide scale formed on the bare superfer 800H represents two regions mainly consisting of black and white. The black area on the surface indicates the formation of oxides of chromium, aluminum, silicon and iron (Fig.7.7a). The EDS analysis shows that the white phase of the scale consists mainly of  $\text{SiO}_2$ ,  $\text{Al}_2\text{O}_3$ ,  $\text{Cr}_2\text{O}_3$  and  $\text{Fe}_2\text{O}_3$  with little amounts of  $\text{TiO}_2$ ,  $\text{CaO}$  and  $\text{NiO}$ . It can be inferred that the composition of the white phase is almost similar to ash composition along with some other oxides of the scale. In case of  $\text{Cr}_3\text{C}_2\text{-NiCr}$  coated superfer 800H (Fig.7.7b), uniform and adherent surface scale rich in chromium and iron followed by silica and aluminium is observed in the dark area, whereas, the white area corresponds to the chromium, aluminum and silicon as the major phases along with small amount of Fe, Ti, Ni and Ca. The scale formed on the surface of NiCrAlY+0.4wt%CeO<sub>2</sub> coated superfer 800H (Fig.7.7c) contains higher amount of globular white phase consisting mainly of alumina and silica which indicates the deposition of ash. The EDS analysis of light grey globular areas on the surface also indicates the presence of ash deposition along with oxides of aluminum, nickel, chromium, and silicon. The presence of Ti in the surface scale indicates its outward diffusion from the substrate, whereas presence of Fe in the surface scale is due to diffusion from the substrate and partly due to interaction with ash. Further, the scale formed on the surface of NiCoCrAlYT<sub>a</sub> coated superfer 800H (Fig.7.7d) depicts the presence of uneven surfaces with clusters of ash in the form of white globules. EDS analysis in the dark region reveals mainly of O, Al, Si and Fe. The white globules represent ash deposition which contains oxide of aluminum and silicon.

##### **7.2.2.4 (b) Cross-Section Analysis**

EDS analysis and BSE images at some selected points of interest across the cross-section of corroded bare and D-gun coated superfer 800H are shown in Fig.7.8. Discontinuous oxide scale has formed on the bare superfer 800H (Fig.7.8a). The uppermost part of the scale mainly

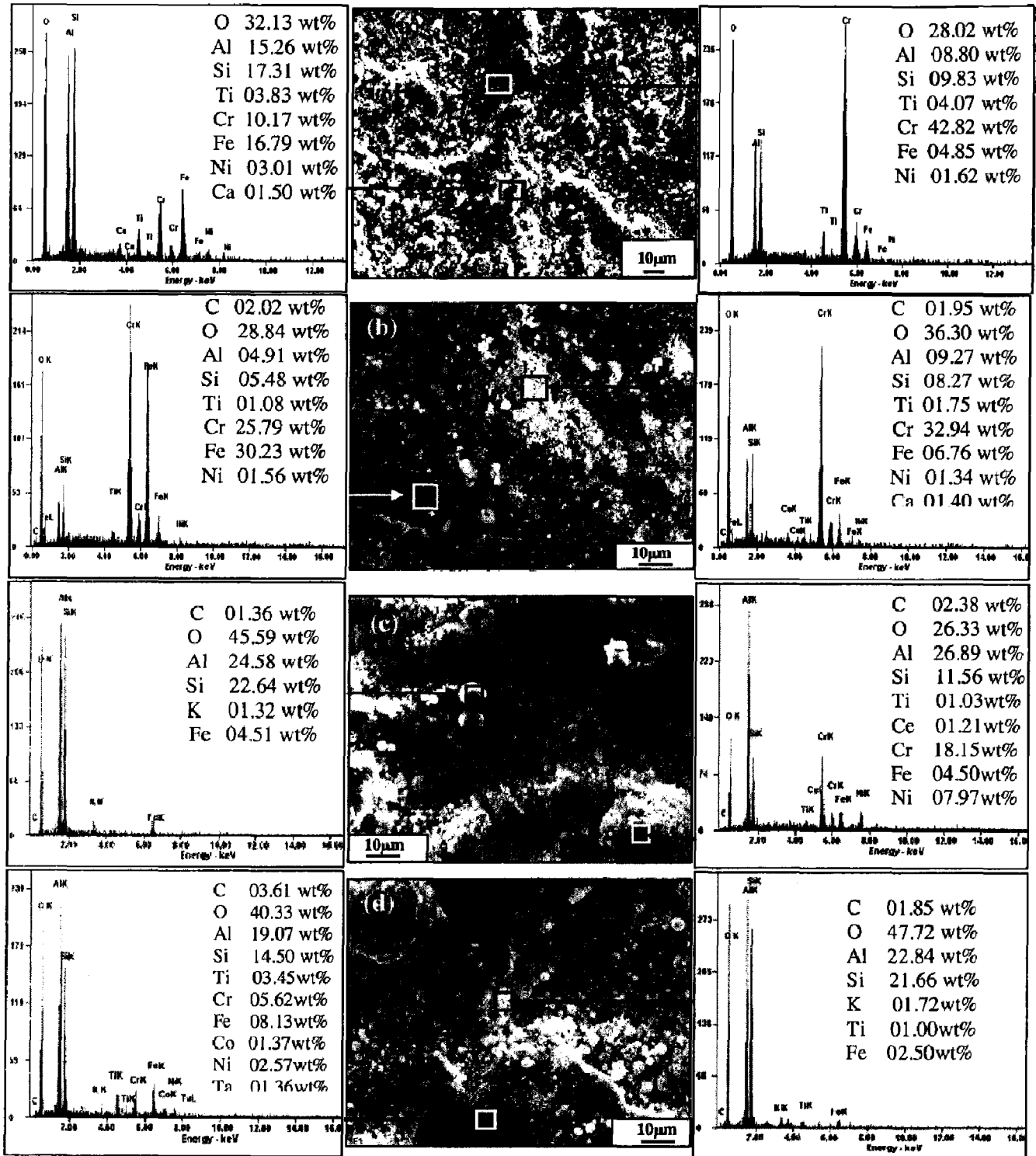
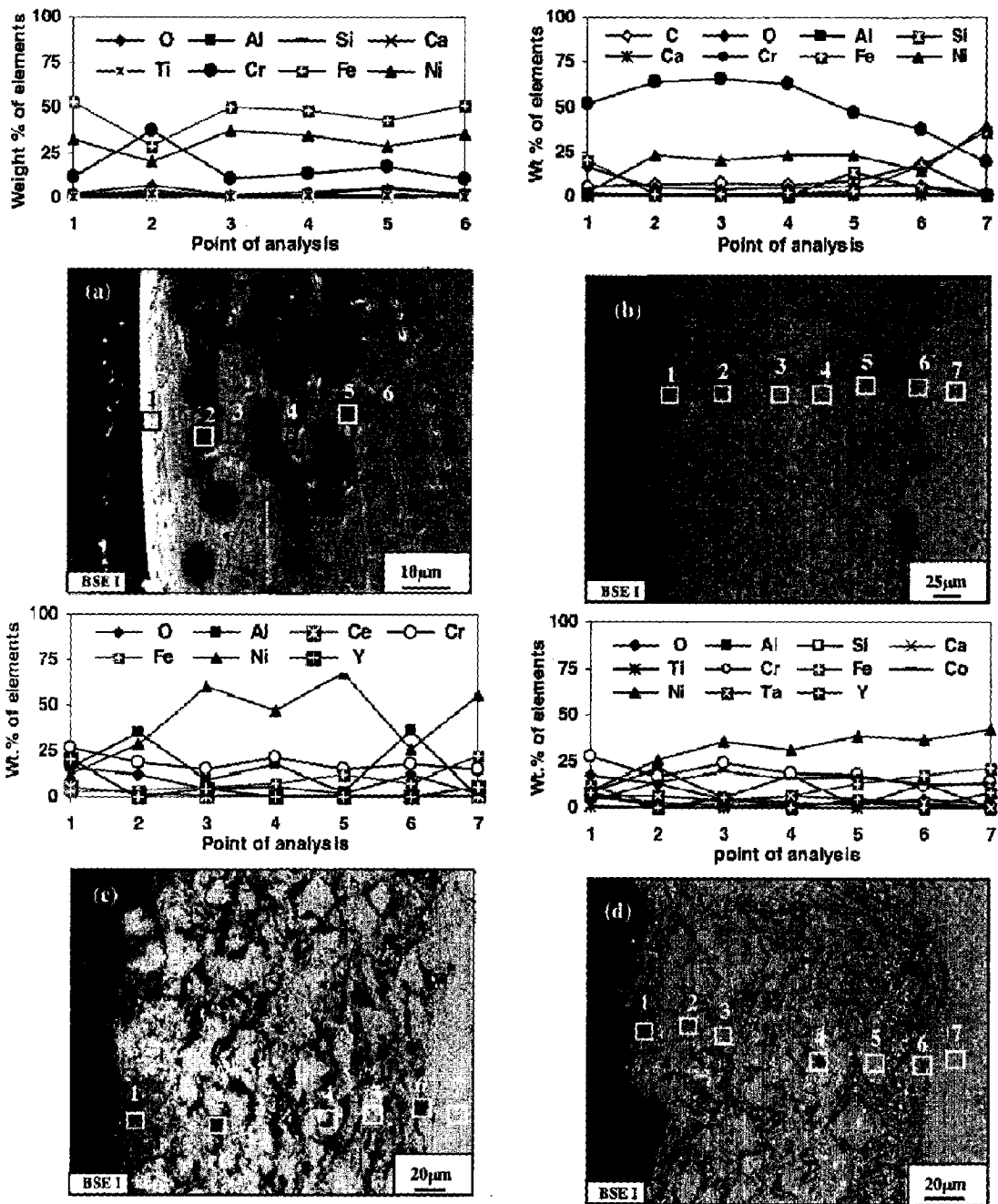


Fig. 7.7 FESEM/EDS analysis showing elemental composition (wt.%) for the bare and D-gun coated superfer 800H after 1000 hrs exposure to low temperature super heater zone of the coal fired boiler at 900 °C: (a) Bare superfer 800H (b) Cr<sub>3</sub>C<sub>2</sub>-NiCr coated (c) NiCrAlY+0.4wt%CeO<sub>2</sub> coated (d) NiCoCrAlYTaNi coated.

consists of iron, nickel and chromium, whereas in the subscale region, the scale has some cracks (point 2) in the black region which is parallel to the top surface, contains mainly chromium oxide as evident from the EDS analysis. Point 3, 4 and 5 depicts the presence of nickel, iron and chromium. Point 6 shows the basic elements of substrate. BSEI image of the corroded  $\text{Cr}_3\text{C}_2$ -NiCr coated superfer 800H (Fig.7.8b) indicates thin adherent and compact oxide scale formed on the top surface of the coating (point 1), below the upper most part of the scale (point 2, 3 and 4), the coating is rich in Cr and Ni. Along the coating-substrate interface (Point 6), the amount of Fe and C increases and Cr and Ni decreases. EDS analysis at point 7 in the substrate indicates the absence of oxygen. The cross sectional BSEI images of corroded NiCrAlY+ 0.4 wt%CeO<sub>2</sub> coated superfer 800H (Fig.7.8c) shows that the scale formed on the top surface mainly consists of oxygen, chromium, aluminum and yttrium, thereby suggesting the formation of respective oxides and spinels. EDS analysis at point 2 indicates the formation of oxide of Al and Cr along the splat boundaries of nickel. Light grey regions (Point 3 and 5) in the coating show nickel rich splats with small amount of Al, Fe and Cr, absence of oxygen at these points suggests that these nickel rich splats are in unoxidised state. Half penny shaped regions in the coating (point 4) distributed along the splat boundaries depicts the presence of Al and Cr, where Ni decreases substantially. The dark area (Point 5) near the coating-substrate-interface is rich in aluminum and chromium along with oxygen thereby suggesting the formation of Al<sub>2</sub>O<sub>3</sub> and Cr<sub>2</sub>O<sub>3</sub>. The absence of oxygen (Point 7) shows that the coating has prevented the penetration of oxygen into the substrate superalloy. The oxide scale formed on the surface of corroded NiCoCrAlYTa coated superfer 800H (Fig.7.8d) consist mainly of oxides of Cr, Fe and Y. Oxygen, chromium and aluminum along the Ni-rich splat boundaries (point 2 and 4) represents the formation of oxides stringers of Al and Cr. Ni-rich splats (point 3 and 5) in the coating are in un-oxidised state as oxygen seems to be absent. Along the coating-substrate interface (Point 6), concentration of iron and aluminum increases, whereas chromium decreases. Point 7 in the substrate shows the absence of oxygen indicating the protective behaviour of the coating.

#### 7.2.2.5 X-ray mapping analysis

BSEI images and elemental X-ray mapping for the bare and D-gun coated superfer 800H after 1000 hours of exposure to low temperature super-heater zone of the coal fired boiler at 900 °C is shown in Fig.7.9 to 7.12. The BSE images of the bare superfer 800H show uppermost part of the



**Fig. 7.8** Oxide scale morphologies and variations of elemental composition (wt%) across the cross section of (a) bare and D-gun sprayed (b)  $\text{Cr}_3\text{C}_2\text{-NiCr}$ , (c)  $\text{NiCrAlY}+0.4\text{wt}\% \text{CeO}_2$  and (d)  $\text{NiCoCrAlYTaNi}$  coating on superfer 800H after 1000 hours exposure to the coal fired boiler at  $900^\circ\text{C}$ .



scale consisting mainly iron, nickel, chromium (Fig.7.9). In the subscale region, the scale has cracked which mainly consist of  $\text{Cr}_2\text{O}_3$  and  $\text{SiO}_2$  as evident from the O distribution. During the course of study, oxygen might have penetrated deep in to the substrate along the cracks of weak oxide scale. Oxygen, silicon and chromium are existing mainly in the black region of the scale, where all other elements are depleted. Tinges of Al and Ti have also been observed in the scale. Elemental X-ray mapping analysis of the scale formed on D-gun sprayed  $\text{Cr}_3\text{C}_2$ -NiCr coated superfer 800H (Fig.7.10) indicates that the scale formed on the surface is adherent and continuous. The topmost layer of the scale is found to be enriched with oxides of Ni, Fe, Si, Al and Cr. In the subscale region, the coating has Ni-rich splats which are in un-oxidised state, whereas Cr has partially oxidised along the Ni-rich splat boundaries. An aluminum and silicon oxide is found along the coating-substrate interface; also a small amount of Si has diffused in to the top surface of coating during initial cycles of hot corrosion run. Another possibility of aluminum at the coating-substrate interface may be due to entrapped alumina particles, which might be retained in the asperities during grit blasting of the substrate prior to deposition of the coatings. Iron has diffused in to the coating and formed a band just above the coating-substrate interface. Also some traces of iron in the topmost layer of the scale indicate its diffusion behaviour from the substrate to the coating. The NiCrAlY+0.4wt%CeO<sub>2</sub> coated superfer 800H forms a discontinuous and adherent oxide scale after exposure to boiler environment for 1000 hours at 900°C (Fig.7.11). The scale mainly consists of non-uniformly distributed oxides of Cr and Al in the top most layers. The coating has irregular shaped splats rich in Ni, in the subscale region Ni is in un-oxidised state. Al and Cr are found along the splat boundaries and exist with oxygen. Iron has shown its diffusion behaviour in to the coating. Elemental X-ray mapping analysis for the scale formed on the NiCoCrAlYT<sub>a</sub> coated superfer 800H (Fig.7.12) after 1000 hours of exposure to the boiler environment shows uppermost part of the oxide scale mainly consisting of O, Ni, Cr, Fe and Al. Below the upper most part of the scale, the coating has, un-reacted Ni-and Co-rich splats, whereas Cr and Al have oxidised and distributed along these splat boundaries, as evident from oxygen distribution. The topmost layer of the scale is found with traces of iron which indicates its diffusion behaviour from the substrate to the coating. Cobalt has diffused in to the substrate and formed a thick band below the coating-substrate interface. Cr and Al have segregated along the coating-substrate interface, where Ni and Co have depleted.

### 7.3 Summary of Results

Results obtained after 1000 hours of exposure of bare and coated (D-gun) superfer 800H to the low temperature super-heater zone of the coal fired boiler at  $900\pm 10$  °C are summarised in Table 7.1.

### 7.4 Comprehensive Discussion

The lower weight gain of bare superfer 800H than its coated counterpart might be attributed to spallation of the oxide scale in the actual environment of the coal fired boiler and fluxing action of the molten salt along with erosion of oxide scale. The most common deposit found on boiler super heaters is sodium vanadyl vanadate,  $\text{Na}_2\text{O} \cdot \text{V}_2\text{O}_4 \cdot 5\text{V}_2\text{O}_5$ , which melts at a relatively low temperature, 550 °C, above the melting point, this ash material corrodes metals by long-term contact (Sidhu and Prakash, 2006). The accumulation of low melting-point salts from flue-gas on the fire side surface of boiler tubes induces hot corrosion and is considered a root cause for the severe wastage of tube materials used for super heaters and reheaters in “advanced” steam-generating system (Sidhu et al, 2005C). The interaction of ash ( $\text{Na}_2\text{O}$ ,  $\text{K}_2\text{O}$  etc.) with the boiler gas ( $\text{SO}_2$ ,  $\text{SO}_3$ ,  $\text{O}_2$  etc.) results in the formation of alkali sulphates ( $\text{K}_2\text{SO}_4$ ,  $\text{Na}_2\text{SO}_4$ ). These alkali sulphates react with iron oxides (present in the scale or in the ash itself), in presence of  $\text{SO}_3$  in the gas, to form alkali-ion trisulphates ( $\text{Na}$ ,  $\text{K}$ ) $_3\text{Fe}(\text{SO}_4)_3$ , these alkali-iron trisulphates are molten at the operating temperature of the boiler due to their low melting temperatures: 624°C for  $\text{Na}_3\text{Fe}(\text{SO}_4)_3$ , 618°C for  $\text{K}_3\text{Fe}(\text{SO}_4)_3$  and 552°C for the mixed compound ( $\text{Na}$ ,  $\text{K}$ ) $_3\text{Fe}(\text{SO}_4)_3$  (Srivastava et al, 1997; Weulersse-Mouturat et al., 2004). These molten compounds can flux the scale or react with the alloy to form internal sulphides. Therefore, the alkali-iron trisulphides are responsible for the degradation of super-heater in the coal-fired plants.

#### 7.4.1 Bare Superalloys

Bare superfer 800H shows that the top scale consisting mainly of oxides of Cr, Fe, Al, Si and Ti as evident from the EDS analysis (Fig.7.7). The higher amount of Al and Si is found in the ash. There is continuous formation of thin oxide scale with subsequent depletion by spallation and erosion under cyclic test conditions. The top surface may contains inclusions, which leads to vertical cracks through which the corrosive species might have penetrated along the crack and between the metallic layers. The cracks and oxide layer have propagated parallel

**Table 7.1** Summary of the results obtained for bare and coated superfer 800H exposed to low temperature super-heater zone of the coal fired boiler at  $900\pm 10$  °C for 1000 hours.

Bare super alloy	Coating	Weight gain mg/cm <sup>2</sup>	$k_p \times 10^{-10}$ g <sup>2</sup> cm <sup>-4</sup> s <sup>-1</sup>	Extent of Corrosion $\mu$ m	Major XRD phases	Minor XRD phases	Remarks
Superfer 800H	Bare	1.8	0.86	52	Ni <sub>3</sub> Al, Cr <sub>2</sub> O <sub>3</sub> , and $\gamma$ -Ni	NiCr <sub>2</sub> O <sub>4</sub> NiAl <sub>2</sub> O <sub>4</sub>	Greenish and brownish spots appeared on the surface along with white spots of ash deposits
	Cr <sub>3</sub> C <sub>2</sub> -NiCr	4.3	8.1	210	NiCr <sub>2</sub> O <sub>4</sub> , Cr <sub>2</sub> O <sub>3</sub> and Ni <sub>3</sub> Al	SiO <sub>2</sub>	Grey colour noticed after first cycle. Towards the end, the scale was grey in colour with brown patches
	NiCrAlY+ 0.4 wt%CeO <sub>2</sub>	12.2	46	200	Cr <sub>2</sub> O <sub>3</sub> Ni <sub>3</sub> Al and $\gamma$ -Ni	NiCr <sub>2</sub> O <sub>4</sub>	The scale indicates the formation of light brownish colour on the surface, the scale was intact and did not show any presence of cracks.
	NiCoCrAlYTa	9.3	25	190	NiCr <sub>2</sub> O <sub>4</sub> Ni <sub>3</sub> Al and $\gamma$ -Ni	NiAl <sub>2</sub> O <sub>4</sub> Cr <sub>2</sub> O <sub>3</sub>	Light grey colour scale formed on the surface after first cycle, towards end, dark grey colour noted No spallation was observed.

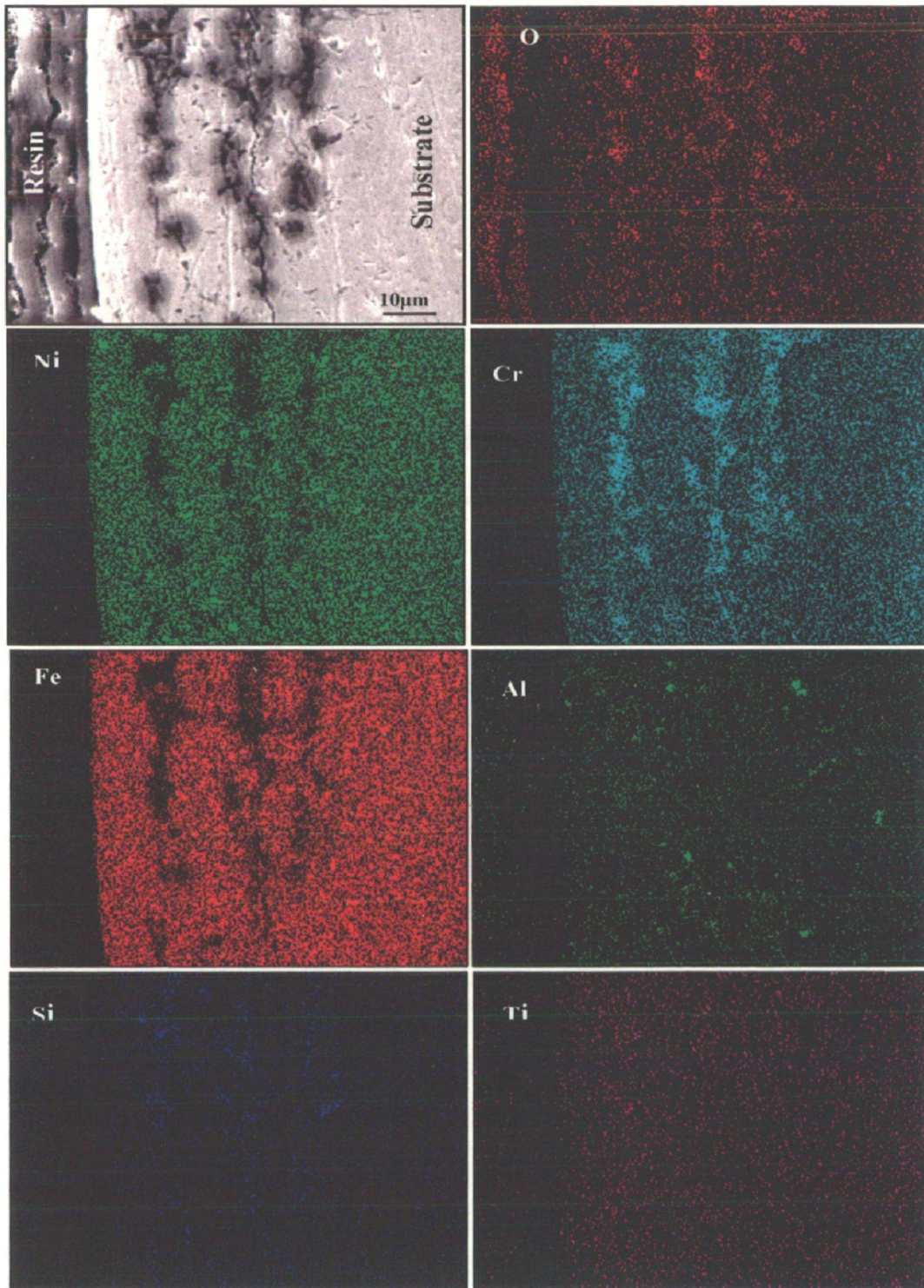


**Fig. 7.9**

Composition image (BSEI) and X-ray mappings across the cross-section of bare superfer 800H after 1000 hrs of exposure to low temperature super heater zone of the coal fired boiler at 900 °C.



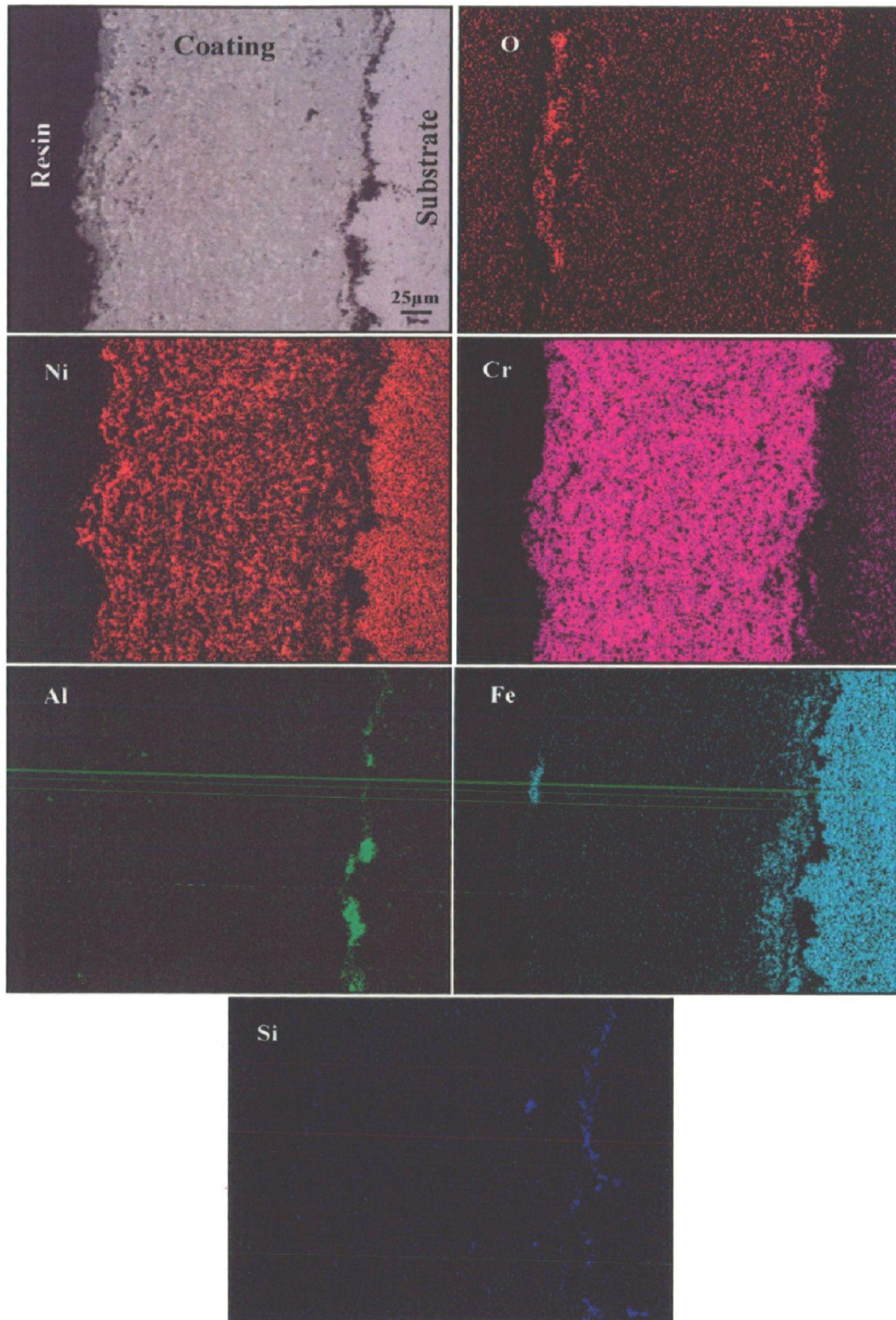


**Fig. 7.10** Composition image (BSEI) and X-ray mappings across the cross-section of D-gun sprayed  $\text{Cr}_3\text{C}_2$ -NiCr coated superfer 800H after 1000 hrs of exposure to low temperature super heater zone of the coal fired boiler at 900 °C.



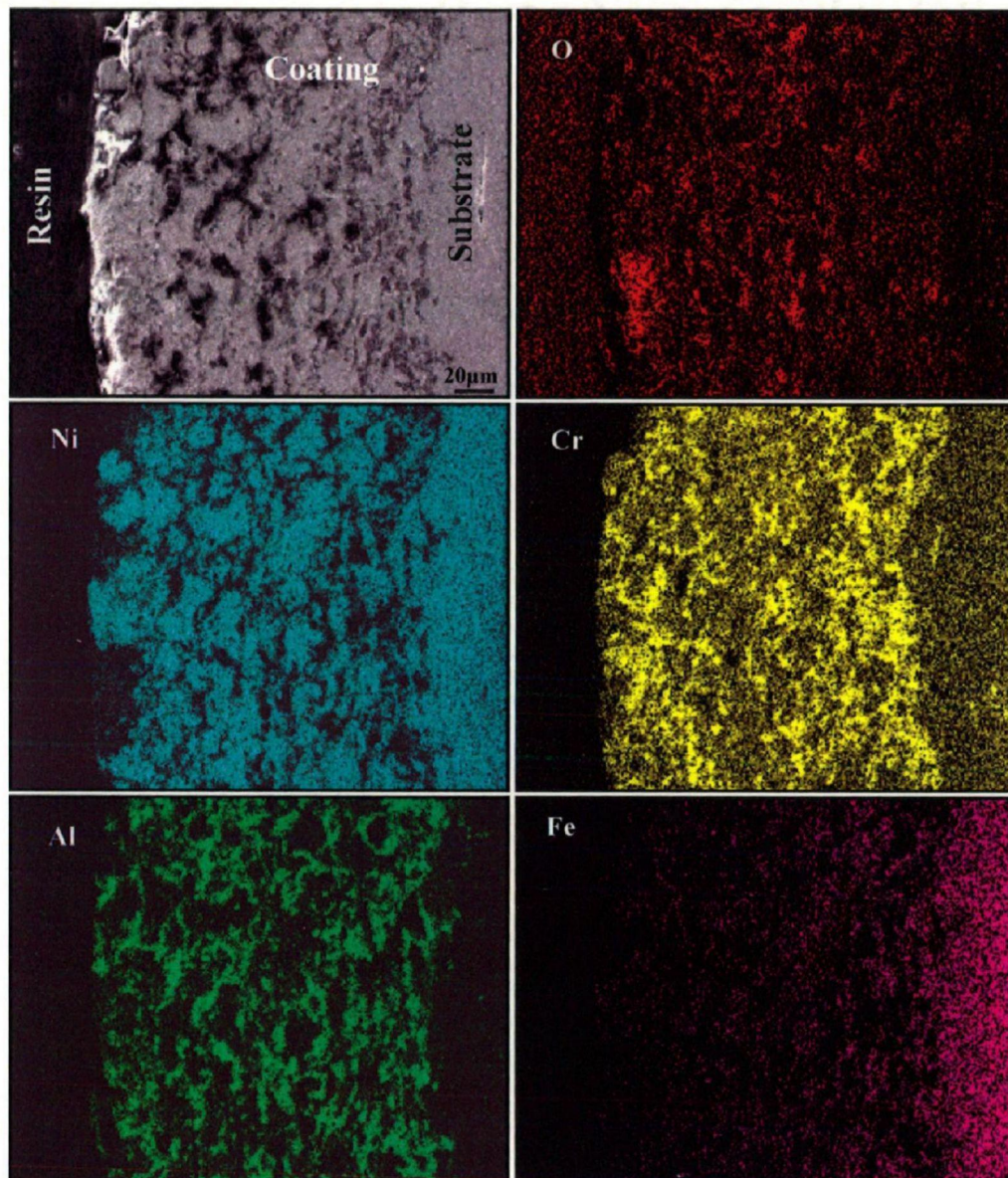


**Fig. 7.11** Composition image (BSEI) and X-ray mappings across the cross-section of D-gun sprayed NiCrAlY+0.4wt%CeO<sub>2</sub> coated superfer 800H after 1000 hrs of exposure to low temperature super heater zone of the coal fired boiler at 900 °C.



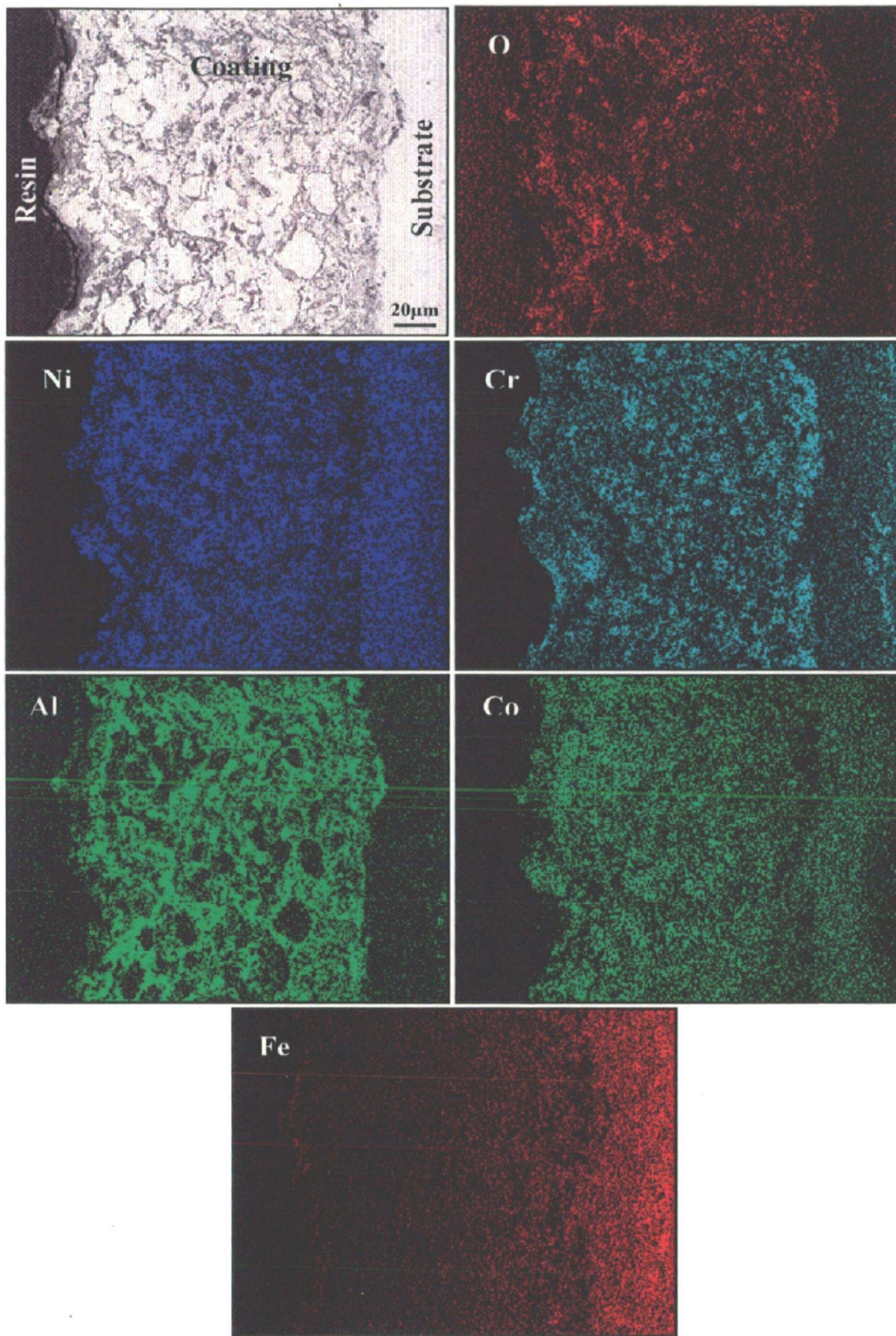


**Fig. 7.12**

Composition image (BSEI) and X-ray mappings across the cross-section of D-gun sprayed NiCoCrAlYTa coated superfer 800H after 1000 hrs of exposure to low temperature super heater zone of the coal fired boiler at 900 °C.

to the top surface. An average, internal corrosion attack seems to be of 15 $\mu$ m from the scale-substrate interface (Fig.7.5). An average gain in scale thickness reported to be of 40 $\mu$ m, due to deposition of ash. The XRD analysis of the corroded bare superfer 800H did not indicate the presence of the sulphides in the oxide scale. This may be due to the formation of very thin oxide scale on the surface. Weulersse-Mouturat et al. (2004) reported that due to their low content, alkali-iron-trisulphates were not identified in the scale. In general, bare samples follow a parabolic rate law, as can be inferred from the square of weight change ( $\text{mg}^2/\text{cm}^4$ ) versus number of cycle plots shown in Fig.7.3. Surface EDS analysis of the scale of dark region revealed the oxides of Cr, Al, Fe and Si.

## **7.4.2 D-gun Coated Superfer 800H**

### **7.4.2.1 Cr<sub>3</sub>C<sub>2</sub>-NiCr Coating**

The weight change data and the corrosion rate show that the Cr<sub>3</sub>C<sub>2</sub>-NiCr coating provides relatively higher protection to the base alloy in the given boiler environment as compared to other coatings under study. The maximum corrosion resistance of Cr<sub>3</sub>C<sub>2</sub>-NiCr coated superfer 800H has been attributed to the formation of thin chromium oxide rich scale. The coating is in intimate contact with the substrate as evident from the BSEI micrograph shown in Fig.7.4b. The chromium exhibits higher affinity for oxygen to form Cr<sub>2</sub>O<sub>3</sub> during the earlier stages of oxidation, which acts as a diffusion barrier for the corrosive species as reported by (Kamal et al, 2008C). Once the oxides formed at the place of voids, the growth of the oxides becomes limited mainly to the surface of the specimens. This is supported by the cross-sectional EDS (Fig.7.8b) and X-ray mapping analysis (Fig.7.10). This would relatively minimize the weight gain and result in the steady state oxidation behaviour with prolonged exposure to high temperature. These oxides, once formed, plug/seal the splat boundaries and all other possible diffusion paths in the coatings, thereby blocking or slowing the penetration of aggressive species. The corroded surface of D-gun coated superalloy after 1000 hours of exposure shows the formation of thick oxide scale consisting mainly of Cr, Al, Si, Ni and Fe. The presence of higher amount of Al and Si indicate the composition of the ash. The XRD analysis indicates the formation of NiCr<sub>2</sub>O<sub>4</sub>, Cr<sub>2</sub>O<sub>3</sub>, SiO<sub>2</sub> and Ni<sub>3</sub>Al. The Ni<sub>3</sub>Al phase is similar to the as-sprayed condition of the coating. It is believed that the scale formed on the surface is very thin and X-rays penetrated deep into the coating, indicating the phases of as-sprayed coating. The EDS analysis of the corroded surface



after 1000 hours of exposure show the presence of higher amount of aluminum, silicon and oxygen, indicating the composition of the ash. The cross sectional EDS analysis shows that the chromium and aluminum oxide formed along the splat boundaries is responsible for blocking the transport of degrading species through Cr<sub>3</sub>C<sub>2</sub>-NiCr coating. Iron has diffused just above the coating-substrate interface by forming a band and presence of aluminum oxide along the coating-substrate interface. It might be attributed due to grit blasting and possible diffusion from the substrate and from the ash, as evident from the X-ray mapping analysis, which is in tandem with the results of cross-sectional EDS analysis.

#### **7.4.2.2 NiCrAlY+0.4wt%CeO<sub>2</sub> Coating**

The NiCrAlY+0.4wt%CeO<sub>2</sub> coated superfer 800H indicates the formation of discontinuous oxide scale on the top surface mainly consisting of O, Ni, Cr, Al and Fe, subscale region of coating represents the presence of oxides of Cr and Al along the Ni-rich splat boundaries, which are in un-oxidised state in the coating, thereby suggesting the partial oxidation of coating, as revealed by cross-sectional EDS (Fig.7.8c). The partially oxidised coating is in intimate contact with the substrate as evident from the BSEI micrograph (Fig.7.4c). The absence of oxygen below the scale-substrate interface indicates that the NiCrAlY+0.4wt%CeO<sub>2</sub> coating provided the necessary protection to the superfer 800H in the actual working environment of the boiler. The formation of these oxides is supported by X-ray mapping analysis (Fig.7.11). The presence of oxygen in the coating might be attributed to the penetration of some oxidising species through the discontinuous oxide scale on the top surface, open pores and along the splat boundaries of the coating during the initial period of exposure. The cross sectional EDS analysis show that oxides of aluminum and chromium existing along the nickel rich splat boundaries responsible for blocking the transport of degrading species through the NiCrAlY+0.4wt%CeO<sub>2</sub> coatings. The X-ray mapping analysis is further supported by the EDS results. Once the protective layer is formed on the surface, the penetration of the corroding species is stopped. The identical findings have been reported by Belzunce et al (2001) who have observed internal oxidation during earlier stages of the study and suggested the penetration of oxidising species into the coatings through the open pores until all the accessible internal surfaces got oxidised. Niranatlumpong et al. (2000) also opined that internal oxidation takes place due to porosity in the thermal spray coatings. The main phases identified by the X-ray diffraction analysis on

NiCrAlY+0.4wt%CeO<sub>2</sub> coated superfer 800H after exposure to boiler environment are NiCr<sub>2</sub>O<sub>4</sub>, Cr<sub>2</sub>O<sub>3</sub>, Ni<sub>3</sub>Al and  $\gamma$ -Ni. The phases Ni<sub>3</sub>Al and  $\gamma$ -Ni are similar to the as-sprayed condition of the coating. It is believed that the scale formed on the surface is very thin and X-rays penetrated deep into the coating. The surface EDS analysis indicated the white phase of the scale mainly consisting of alumina and silica along with small amounts of Fe<sub>2</sub>O<sub>3</sub>, and K<sub>2</sub>O.

#### 7.4.2.3 NiCoCrAlYT<sub>a</sub>

The weight gain plots (Fig.7.2) clearly indicate that the NiCoCrAlYT<sub>a</sub> coated superalloy superfer 800H follow a parabolic rate law up to 10 cycles of 1000 hours. The values of parabolic rate constant  $k_p$  ( $25 \cdot 10^{-10} \text{ g}^2 \text{ cm}^{-4} \text{ s}^{-1}$ ) were obtained from slope of the linear regression fitted line (Fig.7.3). The surface EDS analysis (Fig.7.7d) shows that the dark and white phase of the scale composed mainly of O, Si, Al, Fe, Cr and little amounts of Ti, Co, Ta and K. It is inferred that the composition of the white phase is almost similar to ash composition along with some other oxides of the scale, hence it suggests the formation of oxides of Cr, Al, Ni and spinels, formation of these oxides are further supported by XRD analysis (Fig.7.6). The BSE images of the coated superfer 800H show that the coating partially got oxidised with intimate contact with the substrate and indicate the absence of oxygen at the substrate (Fig.7.8d). The presence of oxygen in the coating indicates the penetration of oxygen during the initial exposure to the boiler environment. Oxide stringers of chromium and aluminum have formed along the splat boundaries. Oxides of Al and Cr along nickel- and Co- rich splat boundaries have plugged/sealed the pores and inter splat boundaries and acted as diffusion barriers to the inward diffusion of corrosive species through the NiCoCrAlYT<sub>a</sub> coatings. The presence of these phases in the scale of coated superalloy is supported by cross-sectional EDS (Fig.7.8d) and X-ray mapping analyses (Fig.7.12). Oxygen elemental maps for the coated superalloy confirm that the diffusion of oxygen is restricted to scale-substrate interface and substrate alloy indicates no sign of oxidation. Therefore, it is concluded that the NiCoCrAlYT<sub>a</sub> coating has provided necessary protection to superfer 800H alloy in the coal fired boiler environment.

# CHAPTER 8

## COMPARATIVE DISCUSSION

---

*In this chapter, the performance of the superalloys and D-gun spray coatings deposited on the superalloys subjected to high temperature air oxidation, aggressive environments such as  $\text{Na}_2\text{SO}_4$ -60% $\text{V}_2\text{O}_5$ ,  $\text{Na}_2\text{SO}_4$ -25% $\text{K}_2\text{SO}_4$ , and in actual boiler environments, under cyclic conditions, is compared.*

### 8.1 Oxidation in air

The bar charts showing the overall weight gains in air at 900°C after 100 cycles for the coated and bare superalloys are presented in Fig. 8.1. From the bar charts, it can be inferred that the bare superalloys exhibit lower oxidation resistance than the coated superalloys. The bare superfer 800H shows a least oxidation resistance among bare superalloys whereas NiCoCrAlYTa coating exhibits a highest oxidation resistance among the coatings. D-gun sprayed NiCoCrAlYTa coating deposited on superni 75 provides the maximum oxidation resistance and is found successful in reducing the weight gain by around 50% of that gained by the bare superni 75 superalloy. It is due to the formation of oxides of Al, Co, Cr, Ni, and spinel on the NiCoCrAlYTa coatings. Spinel, usually has lower diffusion coefficients of the cations and anions than those in their parent oxides (Chatterjee et al. 2001). Coating has Ni- and Co-rich splats which are in an un-oxidised state, whereas aluminum and yttrium coexist with O along these splat boundaries. The as-sprayed coating seems to have good adhesion with the substrate as no cracks and gaps are seen at the interface. Zhang et al., (2003) reported that alumina is formed in the voids, which increases the formation of  $\text{Al}_2\text{O}_3$  along the Ni-rich splat boundaries. Further, the scales formed on the coated superni 75 superalloy are observed to be thin, dense and compact (Fig.6.17), which contributes to the lower weight gain as evident from the lower parabolic rate constant ( $3.33 \times 10^{-12} \text{ gm}^2 \text{ cm}^{-4} \text{ s}^{-1}$ ). In the subscale region of coating, Ni and Co remain in the un-reacted state as O is found to be absent at these places (Fig.6.16a). In case of NiCrAlY+0.4wt% $\text{CeO}_2$  coating, the bigger size oxides globules in the surface oxides allows penetrations of oxygen little deeper in to the coating, where the coating got oxidised along the Ni-rich splat boundaries. Further Cr shows a tendency to form a thick band along the coating-substrate interface, where all other elements were depleted. Comparatively a lower oxidation resistance of  $\text{Cr}_3\text{C}_2$ -NiCr might be

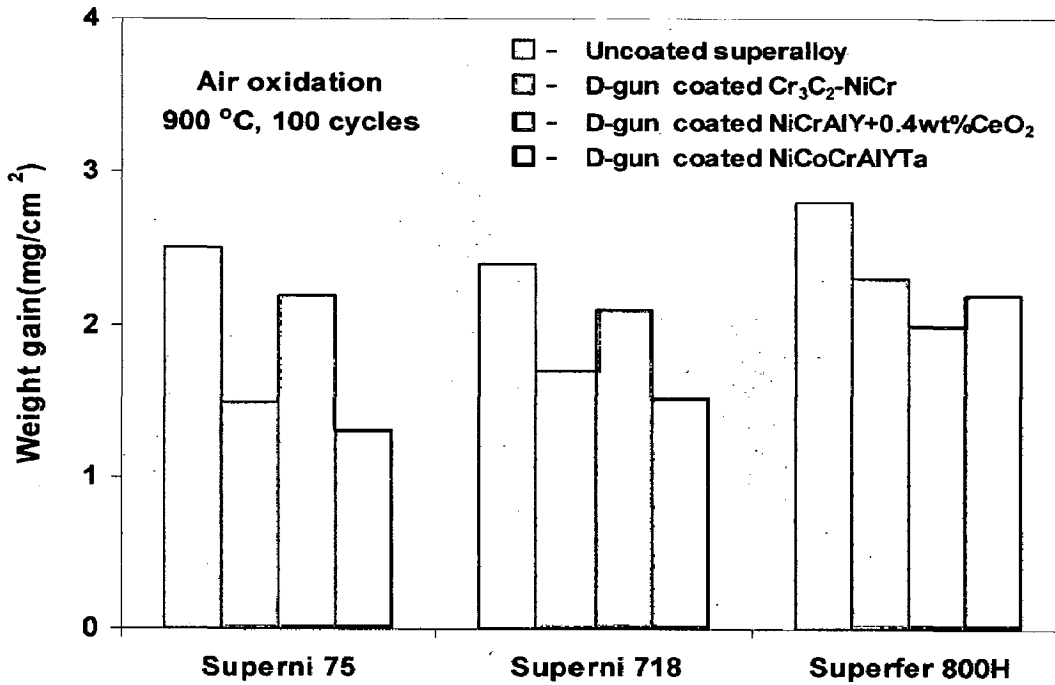
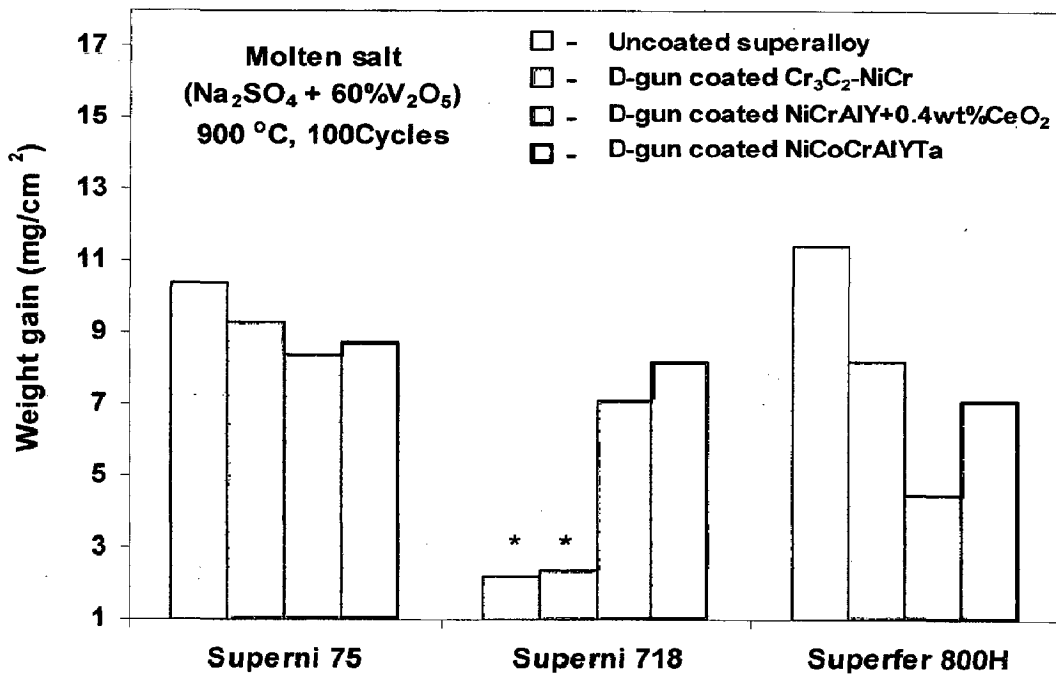


**Fig. 8.1** Bar chart showing cumulative weight gain (mg/cm<sup>2</sup>) for the bare and coated superalloys subjected to cyclic oxidation in air at 900 °C for 100 cycles



\* Extensive spalling made it difficult to monitor the weight gain

**Fig. 8.2** Bar chart showing cumulative weight gain (mg/cm<sup>2</sup>) for the bare and coated superalloys subjected to cyclic oxidation in Na<sub>2</sub>SO<sub>4</sub>-60%V<sub>2</sub>O<sub>5</sub> environment at 900 °C for 100 cycles

attributed to the presence of less protective NiO. The oxidation behaviour of all the coatings follow nearly a parabolic rate law, except for bare superfer 800H, as it slightly deviates after 35 cycles, as shown in Fig.6.12.

## 8.2 Na<sub>2</sub>SO<sub>4</sub>–60% V<sub>2</sub>O<sub>5</sub> Molten Salt Environment-I

The bar chart showing the overall weight gain for bare and coated superalloys after 100 cycles in molten (Na<sub>2</sub>SO<sub>4</sub>–60%V<sub>2</sub>O<sub>5</sub>) salt environment is presented in Fig. 8.2. It is evident that the bare superalloys show a higher weight gain as compared to coated superalloys under cyclic conditions. The bare superalloy superfer 800H exhibits a lower resistance to the molten salt environment, as evident from the higher parabolic rate constant ( $4.311 \times 10^{-10} \text{ g}^2 \text{ cm}^{-4} \text{ s}^{-1}$ ) as well as higher weight gain (Fig. 8.2). While bare superni 718 suffered accelerated hot corrosion, in the form of intense spalling and sputtering of the scale, the cumulative weight gain of it could be determined up to only 25 cycles of the study. The accelerated corrosion of the alloy superni 718 might be attributed to presence of 3.05% Mo content in the basic composition of this alloy as has already been discussed in chapter 4. Among D-gun coated superalloys, NiCrAlY+0.4wt%CeO<sub>2</sub> coating (on all substrates) provides the maximum hot corrosion resistance to superfer800H and has been found successful in reducing the weight gain by around 60% of that gained without a coating, which is also evident from the lower parabolic rate constant ( $k_p = 0.41310^{-10} \text{ g}^2 \text{ cm}^{-4} \text{ s}^{-1}$ ). A comparatively less corrosion resistance is shown by Cr<sub>3</sub>C<sub>2</sub>–NiCr coated superni 75 than the NiCrAlY+0.4wt%CeO<sub>2</sub> coated superfer 800H. It might be due to the presence of less protective and higher amount of oxides (NiO) formed on the surface scale (Fig.5.25 a), which allows the penetration of corrosive species through the scale to the coating. This NiO formed in the surface scale is porous due to reprecipitation by fluxing action; also the scale formed on the surface is non uniform (Fig.5.26a) due to which the oxygen has penetrated little deep in to the coating as attributed from the X-ray mapping analysis (Fig,5.27). Comparatively little lower hot corrosion resistance of NiCoCrAlYT a coated superalloys might be attributed to the formation of less protective oxides of Fe and Ni which allows oxygen penetration for fluxing action of oxide scale. The better performance of NiCrAlY+0.4wt%CeO<sub>2</sub> coated superfer 800H might be due to uniform, dense, thick scale formed on the surface mainly consisting oxides of Cr, Ni, Al and the spinels of NiCr<sub>2</sub>O<sub>4</sub> and NiAl<sub>2</sub>O<sub>4</sub>, in which Cr<sub>2</sub>O<sub>3</sub> is in

the form of needles have increased the surface area. It had provided a better adhesion of the scale. Further, the coating also revealed the formation of continuous thin oxide scale of Si and Fe on the top surface of coated superfer 800H (Fig. 5.29), which has further contributed to higher resistance to hot corrosion. The rare earths ( $\text{CeO}_2$ ) segregate along the grain boundaries of the coatings, where they can significantly reduce the outward transport of Al and decrease the rate of oxidation as observed in the present work. It also contributes to the improved scale adherence and reduced interfacial void formation as reported in the literature (Pint (1996)).

### 8.3 $\text{Na}_2\text{SO}_4$ –25% $\text{K}_2\text{SO}_4$ Molten Salt Environment-Ii

The aggressiveness of  $\text{Na}_2\text{SO}_4$ –25% $\text{K}_2\text{SO}_4$  molten salt is comparatively less than the  $\text{Na}_2\text{SO}_4$ –60% $\text{V}_2\text{O}_5$  due to less degradation of coating in the former as evident from Fig. 8.3. All the coated superalloys follow a parabolic rate law, whereas bare superalloys deviates from the parabolic rate law, which is due to cyclic scale growth. Further, it is observed again that the bare superalloy superfer 800H has shown higher weight gain in the molten salt environment. However, D-gun sprayed NiCrAlY+0.4wt% $\text{CeO}_2$  coating on superalloy superni 718 and superfer 800H exhibit the lowest weight gain and lower parabolic rate constants in the given molten salt environment, its protection against hot corrosion is due to the formation of NiO,  $\alpha$ - $\text{Al}_2\text{O}_3$ ,  $\text{NiAl}_2\text{O}_4$  and  $\text{NiCr}_2\text{O}_4$  spinels in the coating as revealed by XRD analysis (Fig.5.34). Further, it has been observed in the present work that the surface morphology of the oxide scale formed on the coated surface in  $\text{Na}_2\text{SO}_4$ –25% $\text{K}_2\text{SO}_4$  environment indicates two regions in the coating, one with dense white agglomerated free crystalline granules with major elements of O, Ni followed by Cr. On the other region, rectangular shaped discs region depicts the presence of O and Cr-rich elements followed by Ni. Further in the subscale region, coating has partially got oxidised along Ni-rich splat boundaries but Ni rich splats along the cross-section are mainly in the un-oxidised state. Some streaks of  $\text{Al}_2\text{O}_3$  are also distributed along the Ni rich splat boundaries. Similarly, a thin irregular band of Cr has formed along the coating-substrate interface where it might be blocking penetration of oxidising species in to the substrate. Zhang et al., (2003) reported that aluminum oxide is formed in the voids, which increases  $\text{Al}_2\text{O}_3$  along the Ni-rich splat boundaries of NiCrAlY coating. Aluminum (Belzunce et al, 2001) and chromium (Singh et al., 2005C) exhibit higher affinity for oxygen to form  $\text{Al}_2\text{O}_3$  and  $\text{Cr}_2\text{O}_3$  during earlier stages of hot corrosion. Once the oxides are formed along the splat boundaries and at the places of porosity, the growth of the

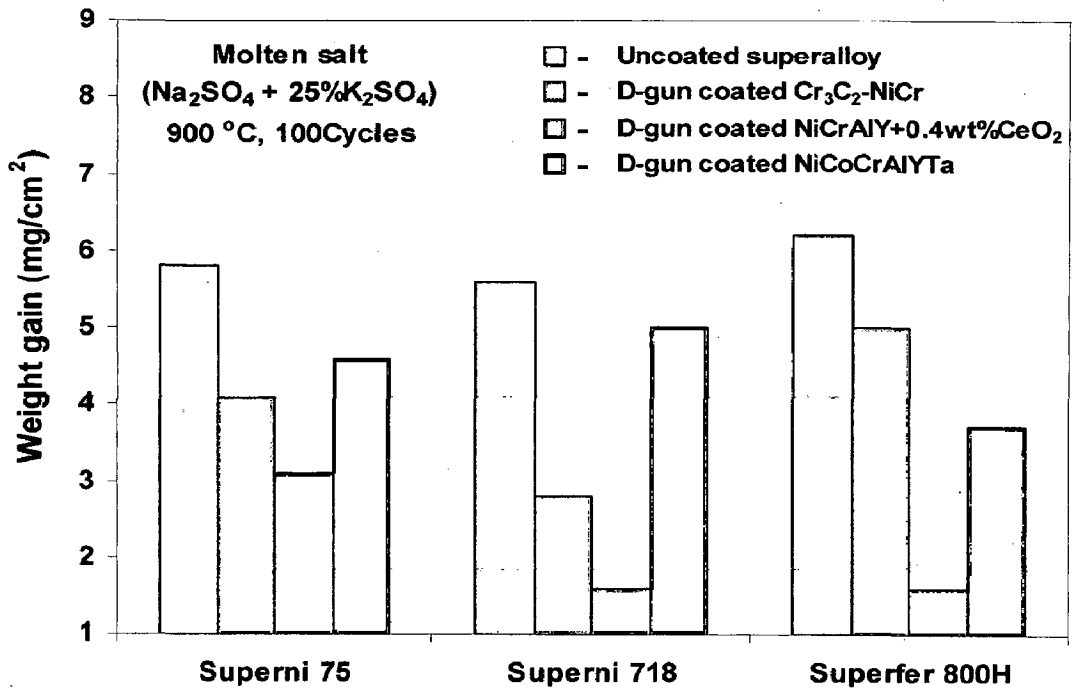


**Fig. 8.3** Bar chart showing cumulative weight gain ( $\text{mg}/\text{cm}^2$ ) for the bare and coated superalloys subjected to cyclic oxidation in  $\text{Na}_2\text{SO}_4$ -25% $\text{K}_2\text{SO}_4$  environment at 900 °C for 100 cycles.

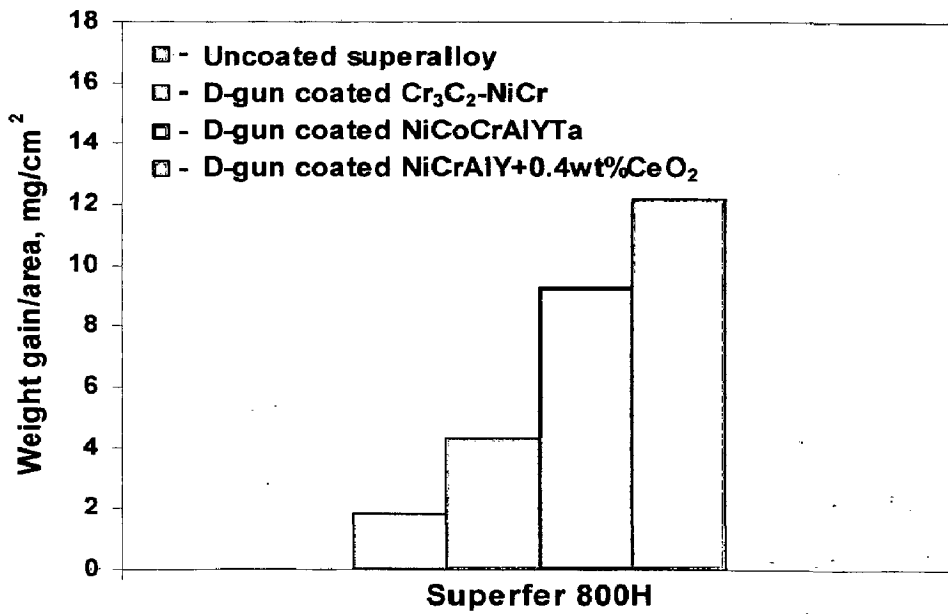


**Fig. 8.4** Bar chart showing net weight change ( $\text{mg}/\text{cm}^2$ ) for the bare and coated superalloys after exposure to platen super-heater zone of the coal fired boiler at 900 °C for 1000 hours.

oxides becomes limited mainly to the surface of the specimens. It relatively minimizes the weight gain and result in the steady state oxidation behavior with the progress of long term high temperature exposure. As regards, the comparison of performance of a particular coating in the different environments is concerned; coatings have shown more cumulative weight gains in the two molten salts than those in the air in all the cases as is obvious from Figs. 8.1, 8.2 and 8.3. The effect of molten salts induced oxidation was relatively high in case of  $\text{Cr}_3\text{C}_2$ -NiCr coating, followed by NiCoCrAlYTa and NiCrAlY+0.4wt%CeO<sub>2</sub> coatings on the basis of ratio of the overall weight gain in two different molten salt atmospheres to the weight gain in air oxidation. NiCrAlY+0.4wt%CeO<sub>2</sub> coating may be recommended as the best coating for the superalloys, as far as hot corrosion resistance is concerned, based upon the findings of the current study. This coating was also successful in maintaining integrity with its respective substrates throughout the exposure time to both the environments of the study, without any significant spalling of its oxide scales. However, while selecting a particular coating for a specific application, various other factors such as substrate compatibility, adhesion, porosity, the possibility of repair or recoating, inter-diffusion, the effect of thermal cycling, resistance to wear and cost should also be considered (Sidky and Hocking, 1999).

#### **8.4 Actual Industrial Coal Fired Boiler Environment**

All the coatings have shown good hot corrosion resistance in the boiler environment consisting of actual working conditions of the coal-fired boiler. The bare superfer 800H has suffered hot corrosion, erosion and ash deposition with internal corrosion attack in the coal fired boiler environment at 900 °C. Erosion combined with oxide scale spallation attributed to lower weight gain of bare superfer 800H, with an average internal corrosion attack up to 15µm from the scale-substrate interface. All the D-gun coated superfer 800H shows a better adhesion to the substrate during entire 1000 hrs of exposure (Fig.7.4) in the following order NiCrAlY +0.4 wt% CeO<sub>2</sub> > NiCoCrAlYTa > Cr<sub>3</sub>C<sub>2</sub>-NiCr. All the D-gun coated superfer 800H has shown weight gain due to the formation of the oxides scale and ash deposition as evident from increase in scale thickness (Fig.7.5). The fluctuation in weight gain data (Fig.7.2) during the experiment can be attributed to the fly ash deposition and rapid thermal cycling, which leads to falling off scale due to erosion and the regeneration of the ash deposit and the oxide scale. The (weight gain/area)<sup>2</sup> plot (Fig.7.3) for the D-gun sprayed NiCrAlY +0.4 wt%CeO<sub>2</sub> coating on superfer 800H shows a slight deviation from the parabolic rate law due to rapid weight change, spalling and erosion of the oxide scale during experiment. The



bar chart indicates a cumulative increase in weight gain for bare and D-gun coated superfer 800H after 1000 hrs of exposure to low temperature super-heater zone of the coal fired boiler. In general, all the coatings which are partially oxidised under study show no internal corrosion attack, whereas bare superfer 800H shows internal corrosion attack. The NiCrAlY+0.4wt%CeO<sub>2</sub> coated superfer 800H shows the highest weight gain due to the formation of discontinuous and adherent oxide scale after exposure to boiler environment for 1000 hours at 900 °C (Fig. 7.8c). A non-uniform oxide scale allows corrosive species to enter in to the coating along the splat boundaries; iron shows its diffusion behaviour in to the coating during initial cycles of hot corrosion run. The better performance of D-gun sprayed Cr<sub>3</sub>C<sub>2</sub>-NiCr coating has been attributed to the formation of adherent, continuous and thin oxide scale of chromium. In the subscale, coating has partially got oxidised and the oxidised chromium is distributed along the splat boundaries leaving behind un-oxidised Ni-rich splats in the coating. It has provided relatively higher protection to the base alloy in the give boiler environment as compared to other coatings under study. The partially oxidised coating is in intimate contact with the substrate as evident from the BSEI micrograph shown in Fig. 7.4b. The hot corrosion resistance of NiCoCrAlYT<sub>a</sub> coated superfer 800H may be ascribed to the formation of oxide of Ni, Cr and Al, and the un-reacted Ni and Co-rich splats found in the subscale region. The oxides of Al and Cr are distributed along the splat boundaries and they have sealed the pores and splat boundaries and acted as diffusion barriers to the inward diffusion of corrosive species through the NiCoCrAlYT<sub>a</sub> coatings.

## CHAPTER 9 CONCLUSIONS

---

*The conclusions from the present investigation regarding oxidation and hot corrosion behaviour of  $\text{Cr}_3\text{C}_2\text{-NiCr}$ ,  $\text{NiCrAlY+0.4wt\%CeO}_2$  and  $\text{NiCoCrAlYTaNi}$  coatings formulated by D-gun spray process on three types of superalloys namely superni 75, superni 718 and superfer 800H are presented in this chapter. The oxidation studies were conducted in air as well as in two molten salt ( $\text{Na}_2\text{SO}_4\text{-60\%V}_2\text{O}_5$  and  $\text{Na}_2\text{SO}_4\text{-25\%K}_2\text{SO}_4$ ) environments under cyclic conditions in a laboratory furnace at an elevated temperature of  $900^\circ\text{C}$  for an oxidation run of 100 cycles in all the cases. In addition to the laboratory tests, an attempt has been made to evaluate the performance of these coating in actual environment of coal fired boiler of Guru Nanak Dev Thermal Power Plant, Bathinda, Punjab, INDIA. All the coating powders were commercially available except  $\text{NiCrAlY+0.4wt\%CeO}_2$ , which was prepared by mixing  $\text{CeO}_2$  (0.4 wt %) 99.99% purity with  $\text{NiCrAlY}$  powder using a conventional rotating ball mill. The salient conclusions from the present investigation are summarised as follows.*

### 9.1 AS-SPRAYED D-GUN COATINGS

- 1) D-gun spraying process has been successfully used to deposit  $\text{Cr}_3\text{C}_2\text{-NiCr}$ ,  $\text{NiCrAlY+0.4wt\%CeO}_2$ , and  $\text{NiCoCrAlYTaNi}$  coatings on superalloys namely superni 75, superni 718 and superfer 800H.
- 2) All the coatings were dense, uniform, continuous, and adherent and had a splat like structure. The thickness of coating was in the range of 200-250  $\mu\text{m}$  for the  $\text{Cr}_3\text{C}_2\text{-NiCr}$ ,  $\text{NiCrAlY+0.4wt\%CeO}_2$  and 220-250 $\mu\text{m}$  for  $\text{NiCoCrAlYTaNi}$  coating.
- 3) Average porosity values for  $\text{Cr}_3\text{C}_2\text{-NiCr}$ ,  $\text{NiCrAlY+0.4wt\%CeO}_2$ , and  $\text{NiCoCrAlYTaNi}$  coating on three superalloys were 0.69%, .58%, and 0.48%, respectively.
- 4) As-sprayed surface roughness of these coatings on three superalloys lies in the range of 4.92-6.05 $\mu\text{m}$ , 6.17-6.94  $\mu\text{m}$  and 6.25-7.48 $\mu\text{m}$ . for  $\text{Cr}_3\text{C}_2\text{-NiCr}$ ,  $\text{NiCrAlY+0.4wt\%CeO}_2$ , and  $\text{NiCoCrAlYTaNi}$  coatings, respectively.

- 5) The higher hardness values were observed for all the coatings than that of the substrates. The  $\text{Cr}_3\text{C}_2$ -NiCr coating showed a maximum hardness in the range of 775-1200Hv, followed by 697-920 Hv for NiCrAlY+0.4wt%CeO<sub>2</sub> coating, whereas NiCoCrAlYTaNi coating exhibited the lowest hardness in the range of 385-748Hv. There is some noticeable variation in the hardness across the coating thickness in all the coatings, which might be due to porosity, oxide inclusion, un-melted and partially melted particles.
- 6) The FE-SEM micrograph of as-sprayed  $\text{Cr}_3\text{C}_2$ -NiCr indicates NiCr metallic binder phase corresponded to the white region in the micrograph and the dark grey region was the carbides, some fractured carbide particle were also observed in the coating at very high magnification.
- 7) In case of NiCrAlY+0.4wt%CeO<sub>2</sub> coating, some stringers of cerium oxide were observed on the polished surface and also across the cross-section along the splat boundaries whereas the dark region represents the presence of oxides of Al. The surface of as-sprayed coating showed the existence of un-melted/or partially melted globular dendritic structure. The diameter of the dendrites was equal to that of original powder particles.
- 8) FE-SEM micrographs of as-sprayed polished NiCoCrAlYTaNi coating on three superalloys depicts the presence of spherical/or elliptical shaped splats, whereas the dark regions represents the presence of oxides of Al. The coating also had the micro pores along the splat boundaries.

## 9.2 OXIDATION STUDIES IN AIR

- 9) Based on the overall weight gain after exposure of 100 cycles in air environment at 900 °C, the oxidation resistance of the bare superalloys studied in the present investigation has been found to be in the following order.

**Superni 718 > Superni 75 > Superfer 800H**

- 10) The superior oxidation resistance of the Ni-based superalloys may be attributed to the development of homogeneous and continuous surface scale consisting of oxides of Ni and Cr
- 11) Poor oxidation resistance of superfer 800H might be due to formation of continuous growth of oxides along the scale grain boundaries consisting of Fe<sub>2</sub>O<sub>3</sub>, MnO and Cr<sub>2</sub>O<sub>3</sub>.

12) All the coatings under study have imparted resistance to oxidation in the given air environment based on the weight gain data. The overall protective behaviour of the coatings in the present study has been found to be in the following sequence:



13) Better performance of NiCoCrAlYTa coating is mainly due to the formation of thin, dense and compact oxide scale consisting of Al, Co, Cr, Ni, and spinels. Spinels usually have lower diffusion coefficients of the cations and anions than those in their parent oxides.

14) Comparatively little higher oxidation resistance of the Cr<sub>3</sub>C<sub>2</sub>-NiCr as compared to NiCrAlY+0.4wt%CeO<sub>2</sub> coating has been attributed to the presence of thermodynamically stable chromium oxide scale. Its slow growth might have acted as a barrier to the inward diffusion of oxygen into the coating.

15) In case of NiCrAlY+0.4wt%CeO<sub>2</sub> coating, during initial high temperature oxidation run, coating might have allowed oxygen to penetrate along the splat boundaries and open pores in the coating, due to which the whole coating got partially oxidised leading to increase in early weight gain. The oxidised coating also revealed the presence of Si and Fe on the top surface of coated superalloys, as these elements might have diffused across the coating along the splat boundaries and open pores. These pores and splats boundaries might have acted as a channel for the transport of coating and substrate elements during initial cycles of oxidation

### 9.3 Na<sub>2</sub>SO<sub>4</sub>-60% V<sub>2</sub>O<sub>5</sub> MOLTEN SALT ENVIRONMENT-I

16) Based on the overall weight gain after 100 cycles in the above environment at 900 °C of bare superalloys it could be arranged in the following order.



17) The superior hot corrosion resistance of the superni 75 superalloys may be attributed to the development of a scale consisting of oxides of nickel in the form of white crystalline granules and to the formation of refractory nickel vanadates, as revealed by XRD analysis.

18) Superni 718 suffered accelerated hot corrosion in the given molten salt environment in the form of intense spalling and sputtering of its scale, which may be ascribed to the presence of 3.05% molybdenum in its basic alloy composition, which might have caused severe hot

corrosion by acidic fluxing, which is in tandem with the published work in the literature (Peters et al, 1976; Fryburg et al, 1984; Prakash et al., 2005 and Pettit and Meier, 1985).

- 19) All the coatings under study have imparted resistance to hot corrosion in the given ( $\text{Na}_2\text{SO}_4$ - $60\%\text{V}_2\text{O}_5$ ) molten salt environment. Based on the weight gain data, the sequence for the overall protective behaviour of coatings on different superalloys, except on superalloy 718, has been observed to follow the sequence as given below:



- 20) Higher weight gain was observed in the early cycles of the study in the given environments for all types of coatings, which may be attributed to the fact that during transient period of oxidation, the oxidizing species might have penetrated in to the coating along the interconnected network of pores and splat boundaries to cause rapid oxidation. However, once all these possible diffusion paths are blocked by the formation of the oxides, the oxidation then becomes limited mainly to the surface of the coatings, thereby entering into a steady state condition.
- 21) D-gun sprayed  $\text{NiCrAlY}+0.4\text{wt}\%\text{CeO}_2$  coating has provided a maximum resistance against hot corrosion in molten ( $\text{Na}_2\text{SO}_4$ - $60\%\text{V}_2\text{O}_5$ ) salt environment. The better performance of  $\text{NiCrAlY}+0.4 \text{ wt}\%\text{CeO}_2$  coated superalloy 800H might be attributed to the formation of uniform, dense, thick scale on the surface mainly consisting oxides of Cr, Ni and Al, the spinels of  $\text{NiCr}_2\text{O}_4$  and  $\text{NiAl}_2\text{O}_4$ , and a thin oxide scale of Si and Fe on the top surface (Fig. 5.29), which might have further contributed to the increase in resistance against hot corrosion. Further  $\text{CeO}_2$  segregated to splat boundaries, where it reacted with vanadium leading to the possible formation of  $\text{CeVO}_4$ , which might have significantly reduced rate of hot corrosion. It might have also contributed to the improved scale adherence and reduced interfacial void formation.
- 22) Comparatively, a lower corrosion resistance of the  $\text{Cr}_3\text{C}_2$ -NiCr coating as compared to the  $\text{NiCrAlY}+0.4\text{wt}\% \text{CeO}_2$  and  $\text{NiCoCrAlYTaNi}$  coatings in the molten salt environment might be ascribed to observed micro spallation and sputtering of the oxide scale of  $\text{Cr}_3\text{C}_2$ -NiCr coated superalloy especially along the edges and corners during cooling periods of the thermal cycles.

## 9.4 Na<sub>2</sub>SO<sub>4</sub>-25%K<sub>2</sub>SO<sub>4</sub> MOLTEN SALT ENVIRONMENT-II

23) All the coatings used in the present investigation have provided resistance to hot corrosion in the above molten salt environment in the following order



It has been observed that the weight gain in above environment is less than that for Na<sub>2</sub>SO<sub>4</sub>-60%V<sub>2</sub>O<sub>5</sub> molten salt. D-gun sprayed NiCrAlY+0.4wt% CeO<sub>2</sub> coating on superalloy superfer 800H showed the lowest weight gain and lowest parabolic rate constants in the above molten salt environment. The better protection against hot corrosion of NiCrAlY+0.4wt%CeO<sub>2</sub> coating might be attributed to formation of thin scale mainly consisting of NiO, α-Al<sub>2</sub>O<sub>3</sub>, NiAl<sub>2</sub>O<sub>4</sub> and NiCr<sub>2</sub>O<sub>4</sub> spinels. The morphology of the oxide scale shows that, Cr is in the form of rectangular discs of Cr<sub>2</sub>O<sub>3</sub>, which are firmly embedded in the matrix consisting mainly of oxides of Al and Ni. The relatively higher weight gain in case of Cr<sub>3</sub>C<sub>2</sub>-NiCr coating as compared to NiCrAlY+0.4 wt% CeO<sub>2</sub> coating may be attributed to the presence of higher amount of chromium which leads to the formation of Cr<sub>2</sub>O<sub>3</sub> around the Ni-rich splats. Higher weight gain of NiCoCrAlYTaNi coating in comparison with the NiCrAlY+0.4 wt% CeO<sub>2</sub> coating might be due to the presence of iron oxide which might have formed by diffusion of Fe through the coating to surface, which might be contributing to lower resistance to hot corrosion.

## 9.5 ACTUAL INDUSTRIAL ENVIRONMENT OF COAL FIRED BOILER

- 24) Greenish and brownish spots appeared on the surface along with white spots of ash deposits on the bare superfer 800H, spallation and erosion under cyclic test condition after 1000 hours exposure at 900 °C in coal fired boiler environment leads to internal corrosion attack up to few microns.
- 25) Similarly, oxide scale developed on the surface of Cr<sub>3</sub>C<sub>2</sub>-NiCr coated superfer 800H was grey in colour with brown patches. In case of NiCoCrAlYTaNi and NiCrAlY+0.4 wt %CeO<sub>2</sub> coated superfer 800H indicating the formation of scales of dark grey and light brownish colour on the surface, respectively was observed.
- 26) All the coatings on the superfer 800H used in the present investigation have provided

resistance to corrosion in coal fired boiler environment at platen super-heater zone when exposed for 1000 hours for 10 cycles at 900 °C and have shown the following trend of resistance to corrosion



- 27) D-gun sprayed  $\text{Cr}_3\text{C}_2\text{-NiCr}$  coating has provided a better protection against erosion and corrosion in above environment. The  $\text{Cr}_3\text{C}_2\text{-NiCr}$  coated superalloy has shown better corrosion resistance than the  $\text{NiCoCrAlYTaNi}$  and  $\text{NiCrAlY+0.4wt\%CeO}_2$  coated superalloy. Since both  $\text{NiCoCrAlYTaNi}$  and  $\text{NiCrAlY+0.4wt\%CeO}_2$  coating partially got oxidised up to coating-substrate interface along the splat boundaries/pores, which remains intact and adherent to substrate, whereas in case of  $\text{Cr}_3\text{C}_2\text{-NiCr}$  coating, mainly upper portion of the coating got oxidised and the remaining portion of the coating appears similar to original as-sprayed coating.
- 28) The coatings have shown ash deposition on the surface, final thickness of coating is contributed by scale formation, erosion and ash deposition. The better corrosion resistance of the  $\text{Cr}_3\text{C}_2\text{-NiCr}$  coated superalloy may be ascribed to the formation of thin band of oxides of chromium and nickel, respectively.
- 29) D-gun sprayed coatings showed low porosity, high bond strength, low oxide content and high hardness, which might have also contributed to enhanced oxidation, hot corrosion and erosion resistance. These desired features of coatings are essential to combat high temperature oxidation and hot corrosion. As compared to other thermal spraying process the impact velocity of D-gun type spraying is at least 2–3 times larger resulting in smaller splat thicknesses (Venkataraman et al., 2006). The distance from the coating surface to coating-substrate interface along the splat boundaries increases significantly in case of smaller splat thicknesses.
- 30) D-gun spraying process has been successfully used to deposit  $\text{Cr}_3\text{C}_2\text{-NiCr}$ ,  $\text{NiCrAlY+0.4wt\%CeO}_2$ , and  $\text{NiCoCrAlYTaNi}$  coatings on Ni- and Fe- based superalloys. All the coatings have protected the substrate in oxidising, molten salt and in boiler environment. These coating can be used on all those surfaces which are facing the fire side corrosion such as in internal combustion engines, industrial waste incinerators, fluidized beds, gas turbine or steam turbines, to provide protection against degradation in these environments.

## SUGGESTIONS FOR FUTURE WORK

---

With respect to present investigation, some of the recommendations for future work are as follows

1. All the investigated coatings have been found to be successful in maintaining continuous surface contact with their respective substrate superalloys during oxidation in air as well as in molten salt; however the adhesive strength of the coatings should be evaluated. The detailed bonding study can help to predict the behaviour of these coatings for different erosive-corrosive environments.
2. High temperature erosion behaviour of the coatings may also be investigated.
3. Hot stage microscopy may be used to understand the development of the scale as well as mechanism of transport of species during the oxidation and hot corrosion runs.
4. Studies may be conducted to investigate the oxidation and hot corrosion behaviour of the thermal spray coatings developed by some other processes such as high-velocity oxy-fuel and plasma spray processes.
5. Cost effectiveness analysis should be done for different types of coatings.
6. Attempts can be made to estimate the useful life of these coated superalloys by using mathematical modeling based on the experimental data.
7. Some efforts should be made to eliminate the porosity of these coatings so as to enhance their corrosion resistance. In this regard post coating treatments should be explored.
8. Some other coatings with different compositions should be formulated and evaluated especially by alloying the coating powders with rare earth elements such as Hf, La, Th etc.



**Table A.1** Summary of oxidation of Fe-, Ni- & Co- base alloys in Air, Na<sub>2</sub>SO<sub>4</sub> and V<sub>2</sub>O<sub>5</sub> environments

Material	Environment	Brief Details
<b>Oxidation in air</b>		
Iron	Gas mixtures containing Ar, O <sub>2</sub> and Cl <sub>2</sub> , 1100 and 1200K	The rate of oxidation of iron was significantly inhibited by the presence of chlorine in the environment, which has been attributed to the formation of a dense layer of Fe <sub>2</sub> O <sub>3</sub> on the outside of the oxide scale formed in the presence of chlorine (Lee and McNallan, 1990).
Inconel 718	Isothermal oxidation in air at 900°C	The oxidation led to the formation of a layer of a rhombohedral phase Cr <sub>2-x</sub> M <sub>x</sub> O <sub>3</sub> high in Cr. They observed that rapid Mn and Ti diffusion across this scale contributed to the formation of a spinel phase and TiO <sub>2</sub> crystals on the surface of the scale. Nb was observed to be rapidly diffusing along the grain boundaries of the alloy in the very first stages of the oxidation. This formed an oxide on the surface of the alloy which was suggested to be CrNbO <sub>4</sub> . For longer oxidation times, the rapid formation of a chromia scale led to the development of a Cr depleted zone in the substrate. This zone was observed to be affected by an inter-granular oxidation of Ti near the interface and of Al deep in the alloy. Further the rate of the oxide scale growth, the depth of the inter-granular oxide penetration and the depth of Cr and Ti depletion were all lower than those obtained under the same conditions on Inconel X and Incoloy 800 (Delaunay et al., 2000)
Ni-10Cr and Ni-20Cr alloys	in air for 50 hours at 1000°C	Ul-Hamid (2002) pointed out that the grain boundaries intersecting the alloy surface in Ni-10Cr exhibited no oxidation, whereas the alloy formed a thick (60µm) oxide layer inwardly. Further it was observed by him that the Ni-20Cr cross-section revealed preferential oxidation at a depth of 65µm at the alloy grain boundaries intersecting its surface, while the oxide at the surface was a few micrometers thick. He noted that the extent to which the grain-boundary oxidation differs from the alloy surface oxidation depends on the Cr content of the alloy. Further during the isothermal oxidation of Ni-20Cr binary alloy at 750 and 1000°C in air, he observed formation of α-Cr <sub>2</sub> O <sub>3</sub> , NiCr <sub>2</sub> O <sub>4</sub> and NiO phases (Ul-Hamid, 2003).
Thin films of Fe-20Cr-Al	Thermal-cycling conditions, 11500C	The films were found to be very susceptible to breakdown oxidation after short periods of exposure to air, due to exhaustion of aluminium in the substrate arising from the large surface area to volume ratio (Stott and Hiramatsu, 2000). It was further observed that when the aluminium concentration in the alloy drops below a critical level, a layer of chromia was able to develop and grow at the alumina-alloy substrate interface. This eventually was suggested to cause breakaway oxidation and formation of iron-rich oxides on the specimen
Fe-15 wt %Cr-4% wt Al	Isothermal as well as cyclic oxidation, 1000-1300°C	The effect of zirconium and yttrium alloying on the high temperature oxidation of Fe-15 wt %Cr-4% wt Al was investigated. It was observed that the yttrium addition decreased the oxidation rate appreciably at 1000°C in O <sub>2</sub> -H <sub>2</sub> O atmosphere where it did not affect oxidation rate in O <sub>2</sub> . Whereas under similar conditions 1% Zr addition increased the weight gain both in O <sub>2</sub> and air but in O <sub>2</sub> -H <sub>2</sub> O weight gain was much less as compared to that of the base alloy. At a temperature of 1200°C in air, the effect of Zr concentration on the oxidation of the alloy was to increase the oxidation rate. Further lower concentration of Zr i.e. 0.2% was found to be beneficial in improving the oxidation resistance under cyclic

		conditions with reduced spalling of the scale. Alloying with 1% Y was also observed to be equally effective in improving the oxidation resistance at 1200°C (Pandey, 1983).
Ni-10Cr-5Al, Ni-20Cr-5Al and Ni-30Cr-5Al alloys	Isothermal oxidation in Air, 1000°C	The oxide formed adjacent to the alloy was $\alpha$ -Al <sub>2</sub> O <sub>3</sub> such that the higher was the Cr content of the alloy the easier was its formation. The Ni-30Cr-5Al alloy formed a complete layer of $\alpha$ -Al <sub>2</sub> O <sub>3</sub> in the initial stages of oxidation through 'oxygen gettering' by Cr. Further a decrease in scale thickness and an increase in scale adherence were observed with an increase in Cr content from 10 to 30% (Ul-Hamid, 2004).
304 L stainless steel	In steam as well as in air, 1000-1375°C	The oxidation by steam was fast as compared to that by air. The diffusion through Fe-Ni-Cr spinel layer was suggested as the parabolic rate controlling process in case of oxidation by steam. Whereas, in case of oxidation by air the formation of Cr <sub>2</sub> O <sub>3</sub> was reflected as a reason for slow oxidation (Bittel et al, 1969).
Austenitic stainless steel (AISI-316, -321 and -304)	Linear heating rate 6 K min <sup>-1</sup> up to 1150°C and the isothermal holding at 1000°C, with and without superficially applied CeO <sub>2</sub>	In the bare condition 321-grade steel was reported to exhibit best performance whereas in the presence of coatings the performance of 316 and 321 grades was identical (Seal et al, 1994). Roy et al (1995) have also studied the role of the similar type of coatings on AISI 347 and reported identical results.
AISI 316 stainless steel	Under non-isothermal heating followed by isothermal holding at 1423 K	The influence of alloy surface preparation as induced by mechanical polishing and electro polishing on the oxidation behaviour has been reported. The mechanically polished surfaces exhibited a shorter incubation period but better oxidation resistance during isothermal holding as compared to electro polished surfaces. This was attributed to enhanced outward diffusion of Cr favouring formation of continuous band of Cr-rich layers (Kuiry et al, 1994).
Laser surface engineered composite boride coating on plain carbon steel	In air, at 600, 800 and 1000°C for 10, 30 and 50 hours	The effect of long duration exposure at high temperature was investigated (Agarwal et al, 2000). They used thermogravimetric technique to study the kinetics of oxidation at elevated temperature. Oxidation rate for all the samples was observed to be parabolic in nature and oxidation kinetic rate constant was reported to increase with increasing temperature of exposure.
<b>Na<sub>2</sub>SO<sub>4</sub> Induced Hot Corrosion</b>		
Pure Iron & Fe-5Cr Alloy, and Fe-13Cr Alloy	Atmosphere of oxygen, 900°C	Pure iron did not undergo accelerated oxidation, which has been attributed to the thickening of the scale too rapidly for sulphur to penetrate the oxide and interact directly with the metal. Authors further reported an immediate acceleration in oxidation rate of Fe-5Cr alloy in the presence of Na <sub>2</sub> SO <sub>4</sub> deposits this was attributed to sulphide formation mechanism which initially restricted spinel formation (Trafford & Whittle, 1980A). In their study conducted on Fe-13% Cr alloy, Na <sub>2</sub> SO <sub>4</sub> coating markedly enhanced the oxidation rate and resulted in the formation of thick, compact and stratified scales. They postulated that formation of sulphides in the alloy substrate and mechanical failure of scale was responsible for the enhanced oxidation (Trafford & Whittle, 1980 B).

Pure iron, chromium and manganese and Chromium	Gas mixture, containing O <sub>2</sub> (3.6%), SO <sub>2</sub> (0.25%) and N <sub>2</sub> (bal), 600-800°C	The enhanced corrosion phenomenon was interpreted in terms of low melting liquid sulphates formation. Further the corrosion rate of pure chromium was not appreciably affected by the salt deposit (Nanni et al, 1987).
Pure Iron	Simulated combustion gas containing SO <sub>3</sub> , 600-800°C	The accelerated reaction observed in the presence of Na <sub>2</sub> SO <sub>4</sub> deposits was attributed to the formation of a liquid salt solution between Na <sub>2</sub> SO <sub>4</sub> and the sulphates of the corroded metal with the production of duplex scales consisting of a mixture of metal oxides and sulphides (Gesmundo & Viani, 1988).
Iron	In oxygen, 750°C	The accelerated oxidation of iron in the presence of deposits of Na <sub>2</sub> SO <sub>4</sub> was attributed to the formation of abundant sulphide which had a highly defected lattice and allowed rapid diffusion of a liquid phase. The liquid phase was eutectic melt of Na <sub>2</sub> SO <sub>4</sub> and Na <sub>2</sub> O. Further it was concluded that the accelerated oxidation had most of the characteristics common with usual low temperature hot corrosion except that it occurred under basic conditions developed by the removal of sulphur from the sulphate deposits instead of the usual acidic conditions established by the SO <sub>3</sub> in the atmosphere (Shi, 1993).
Pure Iron and Fe-Al Alloys	Na <sub>2</sub> SO <sub>4</sub> deposit, O <sub>2</sub> -rich atmospheres containing SO <sub>2</sub> -SO <sub>3</sub> at 650-700°C	The accelerated oxidation of pure iron beneath Na <sub>2</sub> SO <sub>4</sub> deposit was believed to be induced by the formation of eutectic melt of Na <sub>2</sub> SO <sub>4</sub> -iron sulphate. The growth of oxide has been reported to predominant although fluxing contributed a little to the corrosion. In alloys containing Al, fluxing proceeded at a considerable rate in the early stages due to the different oxygen pressure at the oxide/melt interface. Reduction of SO <sub>3</sub> released SO <sub>2</sub> , which caused the formation of sulphides in the scale. Sulphides were supposed to contribute considerably to the acceleration due to their high defect concentration (Shi et al, 1993).
Pure Ni and Al and Fe-Cr, Ni-Cr and Fe-Al alloys	In oxygen and air, 750°C	Shi (1995) studied the possibility of Na <sub>2</sub> SO <sub>4</sub> -Na <sub>2</sub> O eutectic melt formation on the metals deposited with Na <sub>2</sub> SO <sub>4</sub> . In case of Ni, Co, Al, Cr and their alloys he could not detect formation of Na <sub>2</sub> SO <sub>4</sub> -Na <sub>2</sub> O. In case of iron base alloy with high Cr or Al content, where Cr <sub>2</sub> O <sub>3</sub> or Al <sub>2</sub> O <sub>3</sub> were formed, again Na <sub>2</sub> SO <sub>4</sub> -Na <sub>2</sub> O eutectic was not observed. However, at lower Cr or Al content this eutectic melt was suggested to be the possible cause for accelerated rate of corrosion.
Pure Iron	Na <sub>2</sub> SO <sub>4</sub> , Na <sub>2</sub> SO <sub>4</sub> +NaCl, Na <sub>2</sub> SO <sub>4</sub> +V <sub>2</sub> O <sub>5</sub> , combustion gas, 600°C	Iron suffered low temperature hot corrosion in the presence of salt deposits at 600°C. The additions of NaCl and V <sub>2</sub> O <sub>5</sub> to Na <sub>2</sub> SO <sub>4</sub> changed the corrosion kinetics significantly and modified the scale structure (Li et al, 1996).
Binary Iron Aluminate (Fe <sub>3</sub> Al)	In pure oxygen, 1100 K, 1225 K and 1330K	The faster kinetics observed in the initial stages of oxidation was related to the formation of θ-Al <sub>2</sub> O <sub>3</sub> and slower kinetics in the later stages of oxidation to the formation of α-Al <sub>2</sub> O <sub>3</sub> . The overall rate of hot corrosion was higher than that of oxidation at all temperatures. The presence of α-Fe <sub>2</sub> O <sub>3</sub> in addition to alumina was indicated by XRD. Cross-sectional microscopy revealed that the metal-scale interfaces were pitted in hot corrosion conditions and the pits contained aluminium sulphide. Sulphides were also detected along grain boundaries in the intermetallic near the scale-metal interface (Das et al, 2002).

Ferritic Steels containing Cr, Al & Ti	Fused salt mixture containing $\text{Na}_2\text{SO}_4$ at $927^\circ\text{C}$ and gas mixture $\text{CO}$ , $\text{CO}_2$ , $\text{CH}_4$ , $\text{H}_2\text{O}$ , $\text{H}_2$ and $\text{H}_2\text{S}$ at $600^\circ\text{C}$	The presence of Ti with 12 % Cr and 3% Al increased the proportion of Fe, which diffused to the outer layer of the scale. The excellent behaviour of steels at temperatures above $600^\circ\text{C}$ was explained by the increase in Al diffusion coefficient with temperature (Coze et al, 1989).
310 Stainless Steel	Various ratios of $\text{Na}_2\text{SO}_4/\text{NaCl}$ deposit, in air at $750^\circ\text{C}$	The weight gain kinetics in simple oxidation was found to follow a steady state parabolic rate law after 3 hours, while the kinetics with the salt deposits displayed a multi-stage growth rates. The most severe corrosion took place with 75% NaCl mixtures. Uniform internal attack was the morphology of NaCl-induced hot corrosion, while the extent of intergranular attack was more pronounced as the content of $\text{Na}_2\text{SO}_4$ in the mixture was increased (Tsaour et al, 2005).
Pure Nickel and Udimet 700	In a high velocity burner rig, $900^\circ\text{C}$	Corrosion of Ni in the burner rig produced a relatively compact NiO scale along with some internal grain boundary corrosion. Corrosion of Udimet 700 was observed to occur in two stages. During the first stage, the corrosion proceeded by the reaction of $\text{Cr}_2\text{O}_3$ scale with the $\text{Na}_2\text{SO}_4$ and evaporation of the $\text{Na}_2\text{CrO}_4$ reaction product from the surface of the corroding sample. Cr depletion in the alloy occurred and sulphide particles were formed in the Cr depletion zone. Extensive sulphidation occurred during the second stage of corrosion and a thick scale was formed (Misra, 1987).
Pre-oxidised Nickel	In an $\text{SO}_2\text{-O}_2$ gas atmosphere at $900^\circ\text{C}$	Chromate anion suppressed the sulphidation of Ni probably by precipitating solid $\text{Cr}_2\text{O}_3$ from the melt. Vanadate anions enhanced the onset of the hot corrosion and sulphidation probably via rapid dissolution of the protective oxide scale at cracks/defects or grain boundaries (Otsuka & Rapp, 1990).
Pure Nickel	Under $\text{SO}_3 + \text{SO}_2 + \text{O}_2$ gas mixture & $\text{SO}_2$ and $\text{O}_2$ atmospheres, $900^\circ\text{C}$	The corrosion loss in mixed atmosphere containing $\text{SO}_3$ was reported to be larger than those observed in pure $\text{SO}_2$ and $\text{O}_2$ atmospheres. The corrosion loss was found to correspond to the thickness of the oxide layers. High corrosion losses were attributed to the fact that $\text{SO}_3$ strongly acted as an oxidizing agent for the corrosion process (Hara et al 1991).
Ni-23.1 Nb-4.4Al and Ni-19.7Nb-6.0 Cr-2.5Al	Dean rig test, $900^\circ\text{C}$ and $1100^\circ\text{C}$	Below the outer layer, mainly of $\text{NiNb}_2\text{O}_6$ , high proportion of $\text{Al}_2\text{O}_3$ has been reported to be present. Internal oxidation of the metal producing $\text{Al}_2\text{O}_3$ and $\text{Cr}_2\text{O}_3$ was believed to occur before the development of external $\text{Al}_2\text{O}_3$ layer. In some isolated regions the alloy was found to be much more severely attacked, the pit contained $\text{NiNb}_2\text{O}_6$ , $\text{NbCrO}_4$ and Ni. At $1100^\circ\text{C}$ , more uniform corrosion was observed, the outer layer was mainly $\text{NiCr}_2\text{O}_4$ and beneath it a layer of $\text{Cr}_2\text{O}_3$ containing particles of $\text{NbCrO}_4$ was observed. Internal oxides were mainly $\text{Al}_2\text{O}_3$ and there were massive Ni-rich sulphides ahead of oxidation front (Johnson et al, 1978).
Ni-30Cr and Co-30Cr	$600\text{-}900^\circ\text{C}$	The rapid rate of attack was explained on the basis of sulphation of the transient surface oxides (Ni or Co oxides) and the dissolution of these transition metal sulphates into $\text{Na}_2\text{SO}_4$ to yield a liquid phase (Luthra and Shores, 1980).

B-1900	Na <sub>2</sub> SO <sub>4</sub>	Na <sub>2</sub> SO <sub>4</sub> interacted with the alloy to form sodium and sulphur compounds, rapid removal of sulphur from the Na <sub>2</sub> SO <sub>4</sub> by un-retarded diffusion of sulphur and precipitation of Cr-rich sulphide phases promoted the formation of Na <sub>2</sub> O. The catastrophic oxidation observed during sulphidation was due to interactions between Na <sub>2</sub> O and the substrate (Bornstein and DeCrescente, 1970).
Ni-base superalloys and seven binary Ni-base alloys	Pure O <sub>2</sub> , 825-1000°C	Based upon the results, it was concluded that the reduction of the oxide ion content of Na <sub>2</sub> SO <sub>4</sub> was a necessity, but not sufficient condition for sulphidation inhibition. The addition of Mo or V to nickel imparted sulphidation resistance in it because their oxides reacted with and decreased the oxide ion content of Na <sub>2</sub> SO <sub>4</sub> . The disagreement in the literature regarding the effect of Molybdenum on hot corrosion was suggested to be largely due to differences in testing techniques and differences in whether the investigators have been more concerned with the initiation or with propagation modes of hot corrosion (Bornstein et al, 1973).
Ni-base industrial superalloys	Static deposits of Na <sub>2</sub> SO <sub>4</sub> or NaCl or both in still air, 850-1000°C	The susceptibility to hot corrosion was found to be correlated to the type of scale produced during simple oxidation. Alloys forming an Al <sub>2</sub> O <sub>3</sub> scale were found to be susceptible to Na <sub>2</sub> SO <sub>4</sub> deposits, independent of their Cr content. The quantity of the Na <sub>2</sub> SO <sub>4</sub> deposits dictated the nature of attack and, under certain conditions, the refractory element alloy additions appeared to play an essential role. Alloys containing Cr <sub>2</sub> O <sub>3</sub> or TiO <sub>2</sub> in the simple oxidation scale proved to be sensitive to NaCl attack (Bourhis and John, 1975).
Ni-15Cr-Mo (Peters et al), Fe-, Ni- and Co-base alloys	900°C (Peters et al), 600°C and above (Petit and Meier), 975°C in oxygen (Fryburg et al)	The effect of Mo on the hot corrosion of superalloys has also been reported by Peters et al (1976), Petit and Meier (1985) and Fryburg et al (1984). The alloy containing Mo suffered catastrophic degradation. It has been reported that the MoO <sub>2</sub> reacted with Na <sub>2</sub> SO <sub>4</sub> to produce an acid (SO <sub>2</sub> -rich) salt, leading to acidic fluxing. The MoO <sub>3</sub> incorporated into the Na <sub>2</sub> SO <sub>4</sub> via the formation of compounds such as Na <sub>2</sub> MoO <sub>4</sub> , Na <sub>2</sub> MoO <sub>4</sub> .MoO <sub>3</sub> and Na <sub>2</sub> MoO <sub>4</sub> .2MoO <sub>4</sub> . All these phases were liquid and left a high solubility for Al <sub>2</sub> O <sub>3</sub> and Cr <sub>2</sub> O <sub>3</sub> . Peters et al (1976) added that there is threshold amount of molybdenum below which catastrophic attack is not encountered, e.g. for Ni- 15% Cr threshold has been reported to be between 3-4%.
Ni-base Superalloys, B-1900 and NASA-TRW IVA	In pure O <sub>2</sub> , 900°C	After an induction period of little corrosion, local basic fluxing attack of the Cr <sub>2</sub> O <sub>3</sub> / Al <sub>2</sub> O <sub>3</sub> scale distributed to cover the surface and generated catastrophic linear kinetics. During catastrophic attack of B-1900, the sulphate ions reacted to release SO <sub>2</sub> and formed sulphides in the alloy and salt was converted to Na <sub>2</sub> MoO <sub>4</sub> (Fryburg et al, 1982).
Fe-, Ni- and Co-base alloys	Atmospheres containing O <sub>2</sub> , N <sub>2</sub> and SO <sub>2</sub> , 729-1076°C	The corrosion rate was lowest when the chromium content of the alloy was highest. Further Mo and Cu were found to increase the corrosion rate. The main corrosion products formed in air were NiO and Cr <sub>2</sub> O <sub>3</sub> . In hot corrosion tests NiS and Cr <sub>5</sub> S <sub>8</sub> were found (Pehkonen et al, 1987).

Ni and Ni-base Alloy EI 867 with the Aluminate and Cr-Al Diffusion Coatings	Pure Na <sub>2</sub> SO <sub>4</sub>	Low alloyed aluminate and Cr-Al coatings showed very poor resistance to oxidation. After 24 hrs, these had been almost completely removed. Modification of highly alloyed aluminate coatings with Cr resulted in uniform and relatively slow degradation of the coating. Cr enriched zone is supposed to act as a barrier to the oxidation of refractory metals such as Mo, W and V thus preventing the onset of catastrophic corrosion (Godlewski and Godlewska, 1987).
Ni-16Cr-2Nb, IN 738, Ni-16Cr and Superalloy 537	900 and 1000°C	Na <sub>2</sub> SO <sub>4</sub> coated coupons of Ni-16Cr-2Nb and Ni-16Cr developed dense, protective oxide scales and exhibited good hot corrosion resistance. Alloys 537 and IN 738 experienced a shift from basic fluxing to acidic fluxing and as the temperature was increased, the rate of attack increased significantly (Zho et al, 1987).
Inconel 600 and Incolloy 825	Ar +1% O <sub>2</sub> , 940°C	Inconel 600 was able to form a protective layer of chromia in Ar +1% O <sub>2</sub> with or without a thin layer of Na <sub>2</sub> SO <sub>4</sub> at a temperature of 940°C, whereas Incolloy 825 was not able to form chromia in the same environment. This was attributed to the formation of nickel and chromium molybdates due to 3.22% Mo present in the alloy. When O <sub>2</sub> content was only 300ppm, sodium sulphate layer strongly enhanced the corrosion of Inconel 600 and Incolloy 825 (Santorelli et al, 1989).
Review (Shih)	Low-temperature corrosion	Some superalloys containing molybdenum are subjected to sub-melting point hot corrosion when covered with a sulphate, which is associated with the formation of a molybdenum-containing melt resulting from the reaction of MoO <sub>3</sub> with the sulphate (Shih, 1989).
Superalloys HA-188, S-57, IN-617 and TD-NiCrAl	Mach 0.3 burner rig at various temperatures, sea salt concentrations and salt compositions.	Accelerated corrosion of the specimens has been reported in the temperature zones above the calculated dew points of Na <sub>2</sub> SO <sub>4</sub> . It was believed that the corrosion occurred by small amount of salt deposit on those temperature zones during heat-up following each cooling cycle or by small amounts of salt migrating from deposits at cooler zones via a wetting action. Large deposits of salt appear to inhibit corrosion that is why less corrosion was noticed at 900°C when flame was doped with 10 ppm sea salt than when it was doped with 5 ppm sea salt (Santoro, 1979).
Nimonic 105	At 900°C	Hot corrosion did not seem to be very detrimental towards the superalloy. It was concluded that SO <sub>3</sub> pressures below 5x10 <sup>-3</sup> atm did not affect the electrokinetic behaviour, but pressures greater than 5x10 <sup>-3</sup> atmospheres produced higher corrosion rates which was attributed to the acid fluxing by the sulphate melt. Addition of NaCl to the molten Na <sub>2</sub> SO <sub>4</sub> resulted in increased dissolution of Nimonic 105 (Sequeira and Hocking, 1981).
Nimonic 105, 75, 80A and 90	With and without Cr <sub>2</sub> (SO <sub>4</sub> ) <sub>3</sub> , NiSO <sub>4</sub> or CoSO <sub>4</sub> additions, 650-1000°C	Upto 800°C, the lower oxidation rates for Na <sub>2</sub> SO <sub>4</sub> coated alloys were attributed to a scale morphology consisting of inner scales of Cr <sub>2</sub> O <sub>3</sub> acting as a protective oxide film and external scales of NiO. This morphology was observed to be maintained at high temperatures (Maik and Ahmad, 1983).

Alloys B1900 and IN 100 (Al <sub>2</sub> O <sub>3</sub> -formers), Inconel 600, 690, Incoloy 800, IN 738, Nimonic 80A, 100, and 105 (Cr <sub>2</sub> O <sub>3</sub> -formers)	In the presence of Na <sub>2</sub> SO <sub>4</sub> (s) and NaCl (s) separately, and in combination, air, 850 and 1000°C	The Cr <sub>2</sub> O <sub>3</sub> formers got attacked more aggressively by NaCl (s) than Na <sub>2</sub> SO <sub>4</sub> (s). Al <sub>2</sub> O <sub>3</sub> -formers and to some extent NiO-formers were more resistant to NaCl attack than Cr <sub>2</sub> O <sub>3</sub> formers. While Na <sub>2</sub> SO <sub>4</sub> induced corrosion preceded by fluxing and sulphidation reactions, the NaCl induced corrosion was observed to follow a reaction path of fluxing, chloridation and oxidation. The Na <sub>2</sub> SO <sub>4</sub> -NaCl induced corrosion involved combination of reactions occurring in the presence Na <sub>2</sub> SO <sub>4</sub> and NaCl separately (Malik et al, 1988).
Single-crystal Ni-base superalloys and DS Mar M 200	704 and 900°C	All the alloys were severely degraded at 900 and 704°C. There was no significant difference between the hot corrosion of these alloys when tested in air or in oxygen with SO <sub>3</sub> , provided a liquid deposit was present in both cases. It was concluded that all the superalloys under study require a coating if they were to be exposed to any of the hot-corrosion conditions at temperatures of 704°C or higher (Levy et al, 1989).
Inconel 740	850 - 1000°C	The kinetics curves of the alloy at 950°C without Na <sub>2</sub> SO <sub>4</sub> deposit and at 850°C with Na <sub>2</sub> SO <sub>4</sub> deposit obeyed the parabolic law, whereas the uniform parabolic growth behaviour of oxide was not followed at 1000°C without Na <sub>2</sub> SO <sub>4</sub> deposit and at 950°C with Na <sub>2</sub> SO <sub>4</sub> deposit due to oxide spallation at 1000°C and the evaporation of Na <sub>2</sub> CrO <sub>4</sub> melt at 950°C, respectively. The oxide scales were found to be consisting of Cr <sub>2</sub> O <sub>3</sub> , (Ni, Co) Cr <sub>2</sub> O <sub>4</sub> , TiO <sub>2</sub> and Al <sub>2</sub> O <sub>3</sub> and internal oxide scales at all temperatures. The internal sulphidation was suggested to take place due to the existence of Na <sub>2</sub> SO <sub>4</sub> deposit. The complex layered structure of the oxide scales was reported to be in favour of the resistance to oxidation. The accelerated oxidation of the alloy in the presence of Na <sub>2</sub> SO <sub>4</sub> deposit was attributed to the dissolution of Cr <sub>2</sub> O <sub>3</sub> induced by basic fluxing in molten Na <sub>2</sub> SO <sub>4</sub> (Zhao et al, 2004B).
nickel-based superalloy, INCONEL alloy 740,	Simulated pulverized coal-fired environment as coal ash plus flue gas. At 550 and 700 °C	They reported the formation of thin oxide scale on the samples corroded at 550 °C. The hot corrosion, which was characterized by a pitting attack with no internal sulphidation and alloy depletion, resulted from sulphidation mechanism. The corrosion products consisted of Cr <sub>2</sub> O <sub>3</sub> , CrS, NiO, and Ni <sub>3</sub> S <sub>2</sub> . They further reported that the hot corrosion of the alloy at 700 °C consisted of two stages. The oxidation and sulphidation of alloy took place in the initial stage, during which the fluxing of oxide scale did not occur. The compact and protective Cr <sub>2</sub> O <sub>3</sub> scale was formed and Al <sub>2</sub> O <sub>3</sub> , TiO <sub>2</sub> , CrS, and Ti/Nb-sulphide precipitated at the interface of scale/alloy and in Cr-depletion zone. Due to the oxidation of cobalt on the surface of oxide scale, the hot corrosion proceeded to the propagation stage during which stable CoSO <sub>4</sub> melt formed by inward migration of SO <sub>3</sub> and the outward migration of cobalt, and the internal sulphidation reaction proceeded as well. The porous outer layer of oxide scale consisted of CoCr <sub>2</sub> O <sub>4</sub> , Fe (Cr, Al) <sub>2</sub> O <sub>4</sub> , and NiCr <sub>2</sub> O <sub>4</sub> spinels. The inner layer of scale consisted of Cr <sub>2</sub> O <sub>3</sub> , Al <sub>2</sub> O <sub>3</sub> , TiO <sub>2</sub> , and internal sulphides formed, in the initial stage, at the interface and in Cr-depletion zone (Zhao et al., 2005B)

Co-Cr, Co-Al and Co-Cr-Al Alloys.	In $O_2$ - $SO_2$ - $SO_3$ , 600 to 750°C	Co-Cr and Co-Cr-Al alloys reacted non-uniformly, usually in the form of pits and Co-Al alloys suffered broad frontal attack. Under all conditions, a thin sulphur-rich band containing sulphides was observed at the alloy/scale interface and cobalt dissolved near the interface and formed $Co_3O_4$ /or $CoSO_4$ (S) (Luthra, 1982).
Co-Cr, Co-Al and Co-Cr-Al Alloys	In $O_2$ -0.15% ( $SO_2$ + $SO_3$ ), 750°C	Accelerated oxidation tests at 750°C showed that the corrosion resistance of binary Co-Cr and Co-Al alloys increased with the Cr and Al content of alloys. This protection was offered by the rapid growth of $CoCr_2O_4/Cr_2O_3$ and $CoAl_2O_4/Al_2O_3$ oxides in comparison to CoO and $Co_3O_4$ . At high enough Cr ( $\geq 40\%$ ) and Al ( $\geq 15\%$ ) concentrations, the growth rates were so fast that liquid did not even form, consequently the corrosion rates were very low. Tests on Co-Cr-Al alloys indicated that simultaneous presence of Cr and Al was deleterious to the resistance against low temperature hot corrosion (Luthra, 1985).
Metal oxides such as $Co_3O_4$ , NiO, $Al_2O_3$ , $Cr_2O_3$ , $Fe_2O_3$ and $SiO_2$	627-927°C (Malik and Mobin) and 827-927°C (Mobin et al) in $O_2$	The interaction of the metal oxides with $Na_2SO_4$ has been studied. As suggested, the high temperature reaction products usually contain 3-phase structure namely, $Na_2O$ - $MO$ - $M_2O_3$ and metal sulphide and or metal sulphate. The formation of $Na_2O$ - $M_2O$ was further reported to be dependent upon the solid state solubility of metal oxide in the molten salt at high temperature and under limited solubility conditions $Na_2O$ - $M_2O$ was invariably formed, but as soon as conditions got relaxed the oxide $M_2O_3$ precipitated and was observed to form a separate phase (Malik and Mobin, 1987 and Mobin et al, 1996).
<b><math>V_2O_5</math> Induced Hot Corrosion</b>		
Gas-turbine alloys	750°C and above	Vanadium pentaoxide coatings had a deleterious effect throughout the useful temperature range of all the alloys up to 1120 hrs in 70-hr cycles. The effect was reported to be more pronounced for iron base alloys at temperatures above 750°C (Harris et al, 1955).
Technical note (Fairman) Review (Pantony & Vasu)	-----	Fairman (1962) reported that the accelerated oxidation due to $V_2O_5$ is most likely to be the consequence of the catalytic action of vanadium pentoxide. It results in splitting the oxygen molecule at the metal surface, so cause rapid corrosion. Pantony & Vasu (1968A) concluded from the theoretical survey of fireside corrosion of boilers and gas-turbines that in residual fuel ash, $V_2O_5$ can be the most serious cause of "catastrophic" corrosion.



<p>Pure metals such as iron, cobalt, nickel, molybdenum, titanium, tungsten and 99.5% vanadium rods, and single crystals of chromium</p>	<p>Immersion in the melt, in O<sub>2</sub></p>	<p>A diffusion controlled corrosion process given by equation below hold good for the initial stages of vanadic corrosion of all metals under study except nickel and chromium.</p> $\Delta w = Kt$ <p>where <math>\Delta w</math> is the weight change per cm<sup>2</sup> at time <math>t</math>, and <math>k</math> is the velocity constant. Whereas nickel obeyed a logarithmic rate law. The velocity constant was found to be inversely proportional to the depth of melt. On the basis of comparison of activation energies of the various rate processes, a single mechanism underlying the corrosion processes of iron, cobalt, vanadium, titanium, tungsten and molybdenum was suggested, which involves an inward diffusion of oxygen (or other active species) and a sequential outward diffusion of the corrosion products. In case of nickel and chromium, the existence of a coherent corrosion layer separating the slag from nickel and chromium was revealed, which was named as protective barrier for these metals and was found to be absent for other metals under study (Pantony &amp; Vasu, 1968B).</p>
<p>Iron, nickel and several alloys containing iron, nickel, and chromium</p>	<p>liquid vanadates</p>	<p>The rates of corrosion were found to depend on temperature, oxygen partial pressure, the composition, amount and turbulence of the liquid vanadates, composition of the metal or alloys in contact with the liquid vanadates and duration of the corrosion tests. They observed that the corrosion scales present on Armcro iron specimens after cooling consisted of a thick, porous, outer oxide scale and a compact, slightly porous, inner oxide scale. (Kerby and Wilson, 1973).</p>
<p>High temperature alloys</p>	<p>vanadate deposit</p>	<p>Vanadate-induced corrosion of high temperature alloys has been studied by thermogravimetric in laboratory furnaces (using a limited amount of vanadate deposit), in burner rigs (where small amounts of vanadates are continually being deposited on the surface), or by immersion of specimens in crucibles with molten salt. The reaction products formed during exposure in laboratory furnaces and in burner rigs were qualitatively the same, but the kinetics and reaction rates were differing considerably. The mechanisms were found to be complex (Beltran and Shores, 1972).</p>
<p>50Cr-50Ni alloy</p>	<p>In pure V<sub>2</sub>O<sub>5</sub> and sodium vanadates, 750-950°C in a rotating disk apparatus</p>	<p>In pure V<sub>2</sub>O<sub>5</sub> at 810°C, a Cr<sub>2</sub>O<sub>3</sub> scale has been observed on the alloy which subsequently got dissolved slowly into the liquid melt and was thus proposed as a barrier layer by them. In case of NV<sub>6</sub> this barrier layer was not observed. The increased basic character of the melt and its consequently greater fluxing ability toward acidic oxides was thought to be a more important part process than the increased ionic conductivity of NV<sub>6</sub> over V<sub>2</sub>O<sub>5</sub> at this temperature. At 950°C the corrosion in terms of both dissolution rate and corrosion rate was reportedly greater in V<sub>2</sub>O<sub>5</sub> than in NV<sub>6</sub> (Dooley and Wilson, 1975).</p>

<p>Nickel base superalloy Nimonic 80A</p>	<p>flue gas atmosphere containing Na, S, V at 600-700 °C under tensile stress</p>	<p>Sulphur reacts with chromium to form CrS at 600 °C which decomposes into Cr<sub>2</sub>O<sub>3</sub> and SO<sub>2</sub> and then SO<sub>2</sub> escapes into atmosphere. In case of vanadium, large quantities of oxides such as NiO, Cr<sub>2</sub>O<sub>3</sub>, Ni(VO<sub>3</sub>)<sub>2</sub>, NiO.Cr<sub>2</sub>O<sub>3</sub> were formed. Cr<sub>2</sub>O<sub>3</sub> formed a non-protective sodium chromate (yellow stains) and hence further oxidation of nickel took place and the scale spalled off. They suggested that the mechanism was not self sustaining at 600 °C and attack of S was not very severe. They further reported that a eutectic of Ni-Ni<sub>3</sub>S<sub>2</sub> formed at 650 °C penetrated along the grain boundaries at 700 °C and caused severe self sustaining attack. (Iyer et al, 1987).</p>
<p>Nickel base superalloys Nimonic 80A, Hastelloy C-276 and Superni 600</p>	<p>coated with different amounts of V<sub>2</sub>O<sub>5</sub> for a period of 100 hrs In air, 923, 973 and 1023 K</p>	<p>The hot corrosion kinetics obeyed a parabolic law with two regions at 973 and 1023 K, the corrosion rate falling with the formation of a solid Ni<sub>3</sub>V<sub>2</sub>O<sub>8</sub> layer. The acid-base fluxing mechanism and a second mechanism by which nickel vanadate was precipitated from a nickel vanadium compound located in the short circuit diffusion path has been assumed to be occurring in the growing oxide. The corrosion rate for these alloys got decreased with the formation of a compact solid vanadate layer (Swaminathan et al, 1993).</p>

## REFERENCES

---

1. **Agarwal, A., Katipelli, L. R. and Dahotre, N. B.,** (2000), "Elevated Temperature Oxidation of Laser Surface Engineered Composite Boride Coating on Steel," *Meta. Mater. Trans. A*, Vol. 31A, No. 2, pp. 461-473.
2. **Ahmed, R. and Hadfield, M.** (1996), "Rolling Contact Fatigue Behaviour of Thermally Sprayed Rolling Elements," *Surf. Coat. Technol.*, Vol.82, pp.176-186.
3. **Almeraya, C. F., Martinez, V. A. and Gonzalez, R. J. G.,** (1998B), "Electrochemical Studies of Hot Corrosion of Type 347H Stainless Steel," *Brit. Corros. J.*, Vol. 33, No. 4, pp. 288-291.
4. **Almeraya, C. F., Martinez, V. A., Gaona, C., Romero, M.A. and Malo, J.M.,** (1998A), "Hot Corrosion of the Steel SA213-T22 and SA213-TP347H in 80% V<sub>2</sub>O<sub>5</sub>-20% Na<sub>2</sub>SO<sub>4</sub> Mixture," *Revista de Metalurgia*, Vol. 34, No. 1, pp. 11-17.
5. **Aymeric Raffaitin, Fabrice Crabos, Eric Andrieu, and Daniel Monceau,** (2006), "Advanced Burner-Rig Test For Oxidation-Corrosion Resistance Evaluation of MCrAlY/Superalloys Systems," *Surf. Coat. Technol.*, Vol. 201, pp. 3829-3835.
6. **Backman, R., Hupa, M. and Uppstu, E.,** (1987), "Fouling and Corrosion Mechanisms in the Recovery Boiler Superheater Area," *Tappi Journal*, Vol. 70, pp.123-127.
7. **Bai, C. Y., Luo, Y. J. and Koo, C. H.,** (2004), "Improvement of High Temperature Oxidation and Corrosion Resistance of Superalloy IN-738LC by Pack Cementation," *Surf. Coat. Technol.*, Vol. 183, No. 1, pp. 74-88.
8. **Barbezat, G., Nicoll, A.R. and Sickinger, A.,** (1993), "Abrasion, Erosion and Scuffing Resistance of Carbide and Oxide Ceramic Thermal Sprayed Coatings For Different Applications," *Wear*, Vol.162-164, pp.529- 537.
9. **Barbooti, M. M., Al-Madfai, S. H. and Nassouri, H. J.,** (1988), "Thermochemical Studies on Hot ash Corrosion of Stainless Steel 304 and Inhibition by Magnesium Sulphate," *Thermochemical Acta*, Vol. 126, pp. 43-49.
10. **Baufeld, B. and Schmqcker, M.,** (2005), "Microstructural Evolution of a NiCoCrAlY Coating on an IN100 Substrate," *Surf. Coat. Technol.*, Vol199, pp.49- 56.
11. **Beczkiwiak, L., Keller, H. and Schwier, G.,** (1999), "Carbide Materials for HVOF Applications - Powder and Coating Properties," H.C. Starck GmbH and Co: Germany.

12. **Beele, W.**, Czech, N., Quadackers, W.J and Stamm, W., (1997), "Long Term Oxidation Tests on Re-Containing MCrAlY- Coating," *Surf. Coat. Technol.*, Vol. 94–95, pp. 41-45.
13. **Beltran, A.M.** and Shores, D.A., (1972), "Ch. 11: Hot Corrosion," in 'The Superalloys,' Eds. Sims, C.T. and Hagel, W.C., Wiley Publ., John Wiley and Sons, N. Y.
14. **Belzunce, F.J.**, Higuera, V. and Poveda, S., (2001), "High Temperature Oxidation of HFPD Thermal-Sprayed MCrAlY Coatings," *Mater. Sci. Engg. A*, Vol. 297, No. 1-2, pp. 162-167.
15. **Benoist, J.** Badawi, K.F. Malie, A. and Ramade, C., (2005), "Microstructure of Pt Modified Aluminide Coatings on Ni-based Superalloys without Prior Pt Diffusion," *Surf. Coat. Technol.* Vol.194, pp.48–57.
16. **Bettge, D.**, Osterle, W. and Ziebs, J., (1995), "Temperature Dependence of Yield Strength and Elongation of the Nickel-base Superalloy IN738LC and the Corresponding Microstructural Evolution," *Z. Metallkd*, Vol. 86-3, pp.190-197.
17. **Bhushan, B.** and Gupta, B. K. (1991), 'Handbook of Tribology: Materials, Coatings and Surface Treatments,' McGraw-Hill, New York.
18. **Birks, N.** and Meier, G.H., (1983), "Introduction to High Temperature Oxidation of Metals", London: Edward Arnold.
19. **Bittel, J.T.**, Sjordahl, L.H. and White, J.F., (1969), "Oxidation of 304L Stainless Steel by Steam and by Air," *Corros.*, Vol. 25, No. 1, pp. 7-14.
20. **Blackwood, D.J.** Balakrisnan, B. Huang, Y.Z. and. Tan, C.K., (2001), "Influence Of The Chemical Composition Of The Plating Solution on The Ability of Nickel Coatings To Protect Nd<sub>2</sub>Fe<sub>14</sub>b Magnets Against Corrosion," *J. M. M. Materials*, Vol. 223, pp. 103-111.
21. **Blum, R.**, (1997), "Advance (700 °C) PF Power Plant," EC Contact No Sf/1001/97/DK
22. **Bluni, S. T.** and Mardar, A. R., (1996), "Effects Of Thermal Spray Coating Composition And Microstructure on Coating Response and Substrate Protection At High Temperatures," *Corrosion*, Vol.52, No. 3, pp. 213–218.
23. **Bornstein, N. S.** and DeCrescente, M.A., (1969), "Relationship Between Compounds of Sodium and Sulfur and Sulfidation," *Met. Soc. AIME-Trans.*, Vol. 245, No. 9, pp. 1947-1952.
24. **Bornstein, N. S.** and DeCrescente, M.A., (1970), "The Role of Sodium and Sulfur in the Accelerated Oxidation Phenomena-Sulphidation," *Corros.*, Vol. 26, No. 7, pp. 209-214.
25. **Bornstein, N. S.**, Decrescente, M. A. and Roth, H. A., (1975), "Effect of Vanadium and Sodium Compounds on the Accelerated Oxidation of Nickel Base Alloys," *Proc. Conf. on*

Gas Turbine Mater. in the Marine Environment, MMIC-75-27, Columbus, Ohio, USA, pp. 115-160.

26. **Bornstein, N.S., DeCrescente, M.A. and Roth, H.A., (1973), "The Relationship Between Relative Oxide Ion Content of  $\text{Na}_2\text{SO}_4$ , the Presence of Liquid Metal Oxides and Sulfidation Attack," Metall. Trans., Vol. 4, pp. 1799-1810.**
27. **Bouhanek, K., Adesanya, O. A., Stott, F. H., Skeldon, P., Lees, D. G. and Wood, G. C., (2000), "Isothermal and Thermal Cyclic Oxidation Behaviour of Thermal Barrier Coatings: Pt Aluminide Bond Coats," Mater. High Temp., Vol. 17, No. 2, pp. 185-196.**
28. **Bourhis, Y. and John C. St., (1975), " $\text{Na}_2\text{SO}_4$ - and  $\text{NaCl}$ -Induced Hot Corrosion of Six Nickel-Base Superalloys," Oxid. Met., Vol. 9, No. 6, pp. 507-528.**
29. **Brandl, W., Grabke, H.J. Toma, D. and Krueger, J., (1996), "The Oxidation Behaviour of Sprayed MCrAlY Coatings," Surf. Coat. Technol., Vol.86-87, pp.41-47.**
30. **Caron, P and Khan, T., (1999), "Evolution of Ni-Based Superalloys for Single Crystal Gas Turbine Blade Applications," Aero. Sci. Technol., Vol. 3, pp. 513-523.**
31. **Castello, P., Guttman, V., Farr, N. and Smith, G., (2000), "Laboratory-Simulated Fuel-Ash Corrosion Of Superheater Tubes In Coal Fired Ultra Supercritical-Boiler" Meter. corros., 51, No.11, pp.786-790.**
32. **Chatterjee, U. K., Bose, S. K. and Roy, S. K., (2001), "Environmental Degradation of Metals," Pub., Marcel Dekker, 270 Madison Avenue, New York.**
33. **Chattopadhyay, B. and Wood, G.C., (1970), "Transient Oxidation of Alloys" Oxid. Met., Vol 2, No. 4, pp. 373-399.**
34. **Chen, H., Chen, W., Mukherji, D., Wahi, R.P. and Wever, H., (1995), "Cyclic Life of Superalloy IN738LC Under In-phase and Out-of-phase Thermo-mechanical Fatigue Loading," Z. Metalkd., Vol.86-6, pp.423-427.**
35. **Chen, W.R., Wu, X. Marple, B.R. and Patnaik, P.C., (2005), "Oxidation and Crack Nucleation /growth in an Air-Plasma-Sprayed Thermal Barrier Coating with NiCrAlY Bond Coat," Surf. Coat. Technol., Vol.197, pp.109-115.**
36. **Choi, H., Yoon, B., Kim, H. and Lee, C., (2002), "Isothermal Oxidation of Air Plasma Spray NiCrAlY Bond Coatings," Surf. Coat. Technol., Vol. 150, No. 2-3, pp. 297-308.**
37. **Choquet, P. Indrigo, C. and Mevrel, R., (1987), "Microstructure of oxide scales formed on cyclically oxidized M-Cr-Al-Y Coatings," Mate. Sci. Eng. Vol.88, pp.97-101.**

- coatings in the Platen superheater of coal-fired boilers,” *Meta. Mate. Trans. A*, Vol.37A, pp.1927-1930.
38. **Colot, D., Petelot, D., Hoch, P. and Beranger, G.,** (1997), “Mechanisms of Hot Corrosion in Coal Fired Boilers Gas T91 and EM12 Steels,” *Mater. Sci. Forum*, Vol. 251-254, pp. 641-48.
  39. **Conner, J. A. and Connor W. B.,** (1994), “Ranking Protective Coatings: Laboratory Vs. Field Experience,” *JOM*, December, pp. 35-38.
  40. **Coze, L. J., Franzoni, U., Cayla, O., Devisme, A. and Lefort, A.,** (1989), “The Development of High-Temperature Corrosion-Resistant Aluminium-Containing Ferritic Steels,” *Mater. Sci. Eng. A-Struct.*, Vol.120, pp. 293-300.
  41. **Crawmer, D.C., Krebsbach, J.D. and Riggs, W.L.,** (1992), in: C.C. Berndt (Ed.), *Proceedings of the International Thermal Spray Conference and Exposition*, ASMInternational, Materials Park, Ohio, pp.127.
  42. **Cuevas-Arteaga, C., Porcayo-Calderon, J., Izquierdo, G., Martinez-Villafane, A. and Gonzalez-Rodriguez, J.G.,** (2001), “Study of Hot Corrosion of Alloy 800 using Linear Polarization Resistance and Weight Loss Measurement,” *Mater. Sci. Technol.*, Vol.17, No. 7, pp. -885.
  43. **Czech, N., Schmitz, F. And Stamm, W.,** (1994), “Improvement of MCrAlY coatings by addition of rhenium,” *Surf. Coat. Technol.*, Vol. 68/69, pp.17-21.
  44. **Czech, N., Schmitz, F. And Stamm, W.,** (1995), “Microstructural Analysis of The Role of Rhenium In Advanced MCrAlY Coatings,” *Surf. Coat. Technol.*, Vol.76-77, pp.28.-33.
  45. **Das, D., Balasubramaniam, R. and Mungole, M. N.,** (2002), “Hot Corrosion of Carbon-Alloyed Fe<sub>3</sub>Al-Based Iron Aluminides,” *Mater. Sci. Eng. A.*, Vol.338, No.1-2, pp. 24-32.
  46. **Deb, D, Iyer, S. R. and Radhakrishnan, V. M.,** (1996), “A Comparative Study of Oxidation and Hot Corrosion of a Cast Nickel Base Superalloy in Different Corrosive Environments,” *Mater. Letters*, Vol. 29, pp. 19-23.
  47. **Delaunay, F., Berthier, C., Lenglet, M. and Lameille, J. M.,** (2000), “SEM-EDS and XPS Studies of the High Temperature Oxidation Behaviour of Inconel 718,” *Mikrochim. Acta*, Vol. 132, pp 337-343.
  48. **DeMasi-Marcin, J. T. and Gupta, D. K.,** (1994), “Protective Coatings in The Gas Turbine Engine,” *Surf. Coat. Technol.*, Vol. 68-69, pp. 1-9.

49. **Deshpande, S., Sampath, S. and Zhang, H.,** (2006), "Mechanisms of Oxidation and its Role in Microstructural Evolution of Metallic Thermal Spray Coatings—Case Study For Ni–Al," *Surf. Coat. Technol.*, Vol.200, pp.5395–5406.
50. **Dieter, L.,** (2007), "Corrosion and Surface Chemistry of Metals," EPFL Press, Lausanne, Switzerland
51. **Dooley, R. B. and Wilson, J. R.,** (1975), "The Corrosion of 50Cr-50Ni Alloy in Liquid Vanadate Systems in the Temperature Range 750-950<sup>0</sup>C," *Trans. ASME*, July, pp. 422-428.
52. **Du, H.L., Kipkemoi, J., Tsipas, D.N. and Datta, P.K.,** (1996), "The High Temperature Corrosion Behaviour of Hf Modified Chrome-Aluminised Coatings Produced By A Single Step Process," *Surf.Coat. Technol.* Vol. 86-87, pp. 1-8.
53. **Eliasz, N., Shemesh, G. and Latanision, R.M.,** (2002), "Hot Corrosion in Gas Turbine Components," *Eng. Fail. Anal.*, Vol. 9, pp. 31-43.
54. **Erning, U. and Nestler, M.,** (1999), "HVOF Coatings for Hard-Chrome Replacement-Properties And Applications," in: *Proceedings of United Thermal Spray Conference (UTSC 99)*, Dusseldorf, Marzo, pp. 462–466.
55. **Eroglu, S. and Duran, C.,** (1997), "Processing and Properties of a 85% Cr<sub>3</sub>C<sub>2</sub>-10.5%Ni-4.5%Fe Cermet," *Scripta Materialia*, Vol.37, No.7, pp. 991-997.
56. **Esmaeili, S., Engler-Pinto Jr., C.C., Ilschner, B. and Rezai-Aria, F.,** (1995), "Interaction Between Oxidation and Thermo-Mechanical Fatigue in IN738LC Superalloy," *Scripta Meta. Mate.*, Vol.33-11, pp.1777-1781.
57. **Evans, H. E. and Taylor, M. P.,** (2001), "Diffusion Cells and Chemical Failure of MCrAlY Bond Coats in Thermal-Barrier Coating Systems," *Oxid. Met.*, Vol. 55, No. 1-2, pp. 17-34.
58. **Fairman, L.,** (1962), "Technical Note: Mechanism of Accelerated Oxidation by Vanadium-Containing Fuel Ash," *Corros. Sci.*, Vol. 2, pp. 293-296.
59. **Fernando Juarez, Daniel Monceau, Daniel Tetard, Bernard Pieraggi and Constantin Vahlas,** (2003), "Chemical Vapor Deposition of Ruthenium on NiCoCrAlYTa Powders Followed by Thermal Oxidation of the Sintered Coupons," *Surf. Coat. Technol.*, Vol.163 –164, pp.44–49.
60. **Frances, M. Steinmetz, P., Steinmetz, J., Duret, C. and Mevrel, R.,** (1985), "Hot Corrosion Behavior of Low Pressure Plasma Sprayed NiCoCrAlY + Ta Coating on Nickel Based Superalloys," *J. vacuum sci. Technol. A*, Vol. 3(6), pp.2537-2544.

61. **Fritscher, K., Leyens, C. and Schulz, U., (2004), "Investigation of an As-Sprayed NiCoCrAlY Overlay Coating. A Thermoanalytical Approach,"** *Mate. Sci. Engg. A*, Vol.369, pp. 144–150.
62. **Fryburg, G. C., Kohl, F. J. and Stearns, C. A., (1984), "Chemical Reactions Involved in the Initiation of Hot Corrosion of IN-738,"** *J. Electrochem. Soc.*, Vol. 131, No. 12, pp. 2985-2987.
63. **Fryburg, G. C., Kohl, F. J., Stearns, C. A. and Fielder, W. L., (1982), "Chemical Reactions Involved in the Initiation of Hot Corrosion of B-1900 and NASA-TRW VIA,"** *J. Electrochem. Soc.*, Vol. 129, No. 3, pp. 571-585.
64. **Fu, Y., Wei, J. and Batchelor, A.W., (2000), "Some Considerations on the Mitigation of Fretting Damage by the Application of Surface-Modification Technologies,"** *J. Mate. Proc. Technol.* Vol. 99, pp.231-245.
65. **Gang, C. J., Chang-Jiu Li, Yu-Yue Wang and Wen-Ya Li, (2006), "Microstructural Characterization and Abrasive Wear Performance of HVOF Sprayed Cr<sub>3</sub>C<sub>2</sub>-NiCr Coating,"** *Surf. Coat. Technol.*, Vol. 200, pp. 6749–6757.
66. **Gesmundo, F. and Viani, F., (1988), "The Mechanism of Low-Temperature Corrosion of Pure Iron and Manganese at 600-800°C,"** *Mater. Chem. Phys.*, Vol. 20, pp.513-528.
67. **Giggins, C. S and Prttit, F.S. (1971), "The oxidation of TD NiC (Ni<sub>20</sub>Cr-2 Vol pct ThO<sub>2</sub>) between 900 and 1200 °C,"** *Meta. Trans.*, Vol.2, pp1071-1078
68. **Gilbert Santoro, J., Kohl, J.F., Carl Stems, A., Siileyrnan Gokoglu, A. and Daniel Rosner, E., (1984), "Experimental and Theoretical Deposition Rates From Salt-Seeded Combustion Gases of a Mach 0.3 Burner Rig,"** *NASA Technical Paper*, Vol. 222(5), pp.1- 45.
69. **Gitanjaly and Prakash, S., (1999), "Review on Effect of Additives on the Hot Corrosion,"** 5<sup>th</sup> *NACE Proc.*, New Delhi, India, 22-24<sup>th</sup> Nov., pp. 174-182.
70. **Gitanjaly, (2003), "Role of Inhibitors on Hot Corrosion of Superalloys in Na<sub>2</sub>SO<sub>4</sub>-V<sub>2</sub>O<sub>5</sub> Environment,"** Ph. D. Thesis, Met. and Mat. Engg. Deptt., IIT, Roorkee, India.
71. **Gitanjaly, Prakash, S. and Singh, S., (2002), "Effects of MgO and CaO on Hot Corrosion of Fe Base Superalloy Superfer 800H in Na<sub>2</sub>SO<sub>4</sub>-60%V<sub>2</sub>O<sub>5</sub> Environment,"** *Brit. Corros. J.*, Vol. 37, No. 1, pp. 56-62.



72. **Gledhill, H.C., Turner, I.G. and Doyle, C., (1999),** "Direct Morphological Comparison Of Vacuum Plasma Sprayed and Detonation Gun Sprayed Hydroxyapatite Coatings for Orthopedic Applications," *Biomaterials*, Vol. 20, pp.315-322.
73. **Godlewski, K. and Godlewska, E., (1987),** "The Effect of Chromium on the Corrosion Resistance of Aluminide Coatings on Nickel and Nickel-Based Substrates," *Mater. Sci. Eng.*, Vol. 88, pp. 103-109.
74. **Goebel, J. A. and Pettit, F. S., (1970A),** "Na<sub>2</sub>SO<sub>4</sub> - Induced Accelerated Oxidation (Hot Corrosion) of Nickel," *Metall. Trans.*, Vol. 1, pp. 1943-1954.
75. **Goebel, J. A. and Pettit, F. S., (1970B),** "The Influence of Sulphides on the Oxidation Behaviour of Nickel-base Alloys," *Metall Trans*, Vol.1, pp.3421-3429.
76. **Goebel, J. A., Pettit, F. S. and Goward, G. W., (1973),** "Mechanisms for the Hot Corrosion of Nickel-Base Alloys," *Metall. Trans.*, Vol. 4, pp. 261-275.
77. **Goward, G.W., (1998),** "Progress in Coatings for Gas Turbine Airfoils," *Surf. Coat. Technol.*, Vol. 108-109, pp.73-79.
78. **Greene, G.A. and Finfrock, C.C., (2001),** "Oxidation of Inconel 718 in Air at High Temperatures," *Oxid. Met.*, Vol. 55, No. 5-6, pp. 505-521.
79. **Grunling, H.W. and Bauer, R., (1992),** "The Role of Silicon in Corrosion-Resistant High Temperature Coatings," *Thin Solid Films*, Vol.95, pp.3-20.
80. **Guilemany, I. M., Calero, J.A., Sudarshan, T.S., Jeandin, M. and Khor, K.A., (1998), (Eds.),** "Surf. Modi. Technol., Vol. XI, The Institute of Materials, London, pp.81.
81. **Guilemany, J.M, Espallargas, N., Suegama, P.H. and Benedetti A.V., (2006),** "Comparative study of Cr<sub>3</sub>C<sub>2</sub>-NiCr coatings obtained by HVOF and hard chromium coatings," *Corro. Sci.*, 48, pp. 2998-3013.
82. **Guilemany, J.M, Nutting, J. and Llorca-Isern, N., (1994),** "Characterisation of Cr<sub>3</sub>C<sub>2</sub>-NiCr Cermet Powder for High Velocity Oxyfuel Spraying," *Powder Metallurgy*, Vol. 37(4), pp. 289-292.
83. **Guilemany, J.M., Nutting, J. and Llorca-Isern, N., (1996),** "Microstructural Examination of HVOF Chromium Carbide Coatings for High-Temperature Applications," *J. Therm. Spray Technol.*, Vol.5(4), pp.483- 489.

84. **Guo, M.H., Wang, Q.M. Ke, P.L., Gong, J. Sun, C., Huang, R.F. and Wen, L.S., (2006B),** “The Preparation and Hot Corrosion Resistance of Gradient NiCoCrAlYSiB Coatings,” *Surf. Coat. Technol.* Vol.200 pp.3942– 3949.
85. **Guo, M.H., Wang, Q.M., Gong, J., Sun, C., Huang, R.F. and Wen, L.S., (2006A),** “Oxidation and Hot Corrosion Behavior Of Gradient NiCoCrAlYSiB Coatings Deposited by a Combination of Arc ion Plating and Magnetron Sputtering Techniques,” *Corro. Sci.*, Vol.48, pp.2750–2764.
86. **Gurrappa, I. and Sambasiva Rao, A., (2006),** “Thermal Barrier Coatings for Enhanced Efficiency as Turbine Engines,” *Surf. Coat. Technol.*, Vol. 201, No. 6, pp 3016-3029.
87. **Gurrappa, I., (1999),** “Hot Corrosion Behavior of CM 247 LC Alloy in Na<sub>2</sub>SO<sub>4</sub> and NaCl Environments,” *Oxid. Met.*, Vol. 51, No. 5, pp. 353-382.
88. **Gurrappa, I., (2000),** “Hot Corrosion of Protective Coatings,” *Mater. Manuf. Process.*, Vol. 15, No. 5, pp. 761-773.
89. **Gurrappa, I., (2001),** “Identification of Hot Corrosion Resistant MCrAlY Based Bond Coatings for Gas Turbine Engine Applications,” *Surf. Coat. Technol.*, Vol.139, pp. 272-283.
90. **Gurrappa, I., (2003),** “Influence of Alloying Elements on Hot Corrosion of Superalloys and Coatings: Necessity of Smart Coatings for Gas Turbine Engines,” *Mate. Sci.and Technol.*, Vol. 19, no.2. pp. 178-183.
91. **Hancock, P., (1987),** “Vanadic and Chloride Attack of Superalloys,” *Mater. Sci. Technol.*, Vol. 3, pp. 536-544.
92. **Hao Du, Chao Sun, Weigang Hua, Tiegang Wang, Jun Gong, Xin Jiang and Soo Wohn Lee, (2007),** “Structure, Mechanical and Sliding Wear Properties of WC–Co/MoS<sub>2</sub>–Ni Coatings by Detonation Gun Spray ,”*Mater. Sci. Eng A*, Vol.445–446, pp.122-134.
93. **Hao Du, Weigang Hua, Jiengang Liu, Jun Gong, Chao Sun and Lishi Wen, (2005),** “Influence of Process Variables On The Qualities Of Detonation Gun Sprayed WC–Co Coatings”, *Mate. Sci. Eng. A.*, Vol.408, pp. 202–210.
94. **Hara, M., Hisaichi, T., Itoh, K. and Shinata, Y., (1991),** “Effects of SO<sub>3</sub>, SO<sub>2</sub> and O<sub>2</sub> Gasses on Hot Corrosion of Ni and Ni-Cr Alloys in Molten Na<sub>2</sub>SO<sub>4</sub>,” *J. Jpn. I. Met.*, Vol. 55, No. 11, pp. 1207-1215.

95. **Harris, G.T., Child, H.C. and Kerr, J.A.,** (1955), "Effect of the Composition of Gas-Turbine Alloys on Resistance to Scaling and to Vanadium Pentaoxide Attack," *ISIJ Int.*, Vol. 179, pp. 342-347.
96. **Haugsrud, R.,** (2001), "On the High-Temperature Oxidation of Fe, Co, Ni and Cu-based Alloys with Addition of a Less Noble Element," *Mater. Sci. Eng. A-Struct.*, Vol. 298, pp. 216-226.
97. **Haugsrud, R.,** (2003), "On the High-Temperature Oxidation of Nickel," *Corros. Sci.*, Vol. 45, No.1, pp.211-235.
98. **Hawthorne H.M., Arsenault B., Immarigeon J.P., Legoux J.G. and Parameswaran V.R.,** (1999), "Comparison of Slurry and Dry Erosion Behaviour of Some HVOF Thermal Sprayed Coatings," *Wear*, Vol. 225-229, pp. 825-834.
99. **Hazoor, S. S, Sidhu, B.S and Prakash, S.,** (2006), "Mechanical and Microstructural Properties of HVOF Sprayed WC-Co and Cr<sub>3</sub>C<sub>2</sub>-NiCr Coatings on the Boiler Tube Steels Using LPG as the fuel gas," *J. Mate. Pro. Technol.*, Vol.171, pp. 77-82.
100. **He, J. L., Yu, C. H., Leyland, A., Wilson, A. D. and Matthews, A.,** (2002), "A Comparative Study of the Cyclic Thermal Oxidation of PVD Nickel Aluminide Coatings," *Surf. Coat. Technol.*, Vol. 155, No. 1, pp. 67-79.
101. **He, J., ice, M. and Lavernia, E.,** (2000), "Synthesis of Nanostructured Cr<sub>3</sub>C<sub>2</sub>-(Ni20Cr) Coatings," *Meta. Mate. Trans. A*, Vol.31A, pp. 555-564.
102. **Heath, G. R., Heimgartner, P., Irons, G., Miller, R. and Gustafsson, S.,** (1997), "An Assessment of Thermal Spray Coating Technologies for High Temperature Corrosion Protection," *Mater. Sci. Forum*, Vol. 251-54, pp. 809-816.
103. **Herman, h.,** "Plasma Sprayed Coatings," (1988), *Scientific American*, Vol. 259, No. 3, pp.78-83.
104. **Hocking, M. G. and Sidky, P.S.,** (1987), "The Hot Corrosion of Nickel-Based Ternary Alloys and Superalloys for gas Turbine Applications-II. The Mechanism of Corrosion in SO<sub>2</sub>/O<sub>2</sub> Atmospheres," *Corro. Sci.*, Vol. 27, No. 2, pp.205-214.
105. **Hocking, M. G.,** (1993), "Coatings Resistant to Erosive/Corrosive and Severe Environments," *Surf. Coat. Technol.*, Vol. 62, pp. 460-466.

106. **Huang, N.K.**, (1992), "X-ray Photoelectron Spectroscopy Studies on the Surface of NiCoCrAlY Coatings Before and After High-Temperature Oxidation," Surf. Coat. Technol., Vol.53, pp.65-69.
107. **Huang, Y. Wang, Y. and D.J. Blackwood**, (2000), "The Effect of Temperature on Electrochemical Behavior for Cu-Al-O Coatings Prepared by CVD," Vacuum, Vol. 58, pp.586-593.
108. **Hussain, N., Shahid, K.A., Khan, I.H. and Rahman, S.**, (1994), "Oxidation of High-Temperature Alloys (Superalloys) at Elevated Temperatures in Air: I," Oxid. Met., Vol. 41, No. 3-4, pp. 251-269.
109. **Hwang, Y. S. and Rapp., R. A.**, (1989), "Thermochemistry and Solubilities of Oxides in Sodium Sulfate-Vanadate Solutions," Corrosion, Vol. 45, No. 11, pp. 933-37.
110. **Iyer, S. R., Iyer, K. J. L. and Radhakrishnan, V. M.**, (1987), "High Temperature Corrosion of a Ni-Base Superalloy by Vanadium," Proc. of 10<sup>th</sup> ICMC, Madras, India, Vol. IV, pp. 3665-3670.
111. **Iyer, S. R., Iyer, K.J.L. and radha krishnan, V. M.**, (1987), "Hot Corrosion Cracking of Nimonic 80A," High Temp. Technol.; Vol. 5, No.3, pp. 145-150.
112. **Jain, P., Raj, S.V., Hemker, K. J.**, (2007), "Characterization of NiCrAlY Coatings for a High Strength, High Conductivity GRCop-84 copper alloy," Acta Mater. Vol.55, pp.5103-5113.
113. **Jena, A.K. and Chaturvedi, M.C.**, (1984), "Review the Role of Alloying Elements in the Design of Nickel-Base Superalloys," J. Mater. Sci., Vol.19, pp.3121-3139.
114. **Jia, C., Li, Z. and Xie, Z.**, (1999), "A Research on Detonation Gun Coating With Fe-SiC Composite Powders Mechanically Activated," Mater. Sci. Engg. A, Vol.263, pp.96-100.
115. **Johnson, D. M., Whittle, D. P. and Stringer, J.**, (1978), "The Hot Corrosion of Directionally Solidified Ni-Cr-Nb-Al ( $\gamma/\delta$ ) Eutectic Alloys," Oxid. Met., Vol. 12, No. 3, pp. 273-291.
116. **Kadyrov, E. and Kadyrov, V.**, (1995), "Gas Detonation Gun for Thermal Spraying," Adv. Mat.Pro, Vol. 148, No. 2, pp. 21-24.
117. **Kai, W., Leu, C. J. and Wu, Y. J.**, (1998), "Effects of Mo and Al Additions on the Sulfidation Behavior of 310 Stainless Steel," Oxid. Met. Vol.50, pp.89-122.
118. **Kamachi Mudali, U., Bhuvaneshwaran, N., Shankar, P and Baldev Raj**, (2004), "corrosion behaviour of intermetallic aluminide coatings on nitrogen-containing austenitic stainless steels," Vol.46, pp 2867-2892.

119. **Kamal, S., Jayaganthan, R. and Prakash, S., (2008B),** "Characterisation of Detonation Gun Sprayed  $\text{Cr}_3\text{C}_2$ -25NiCr Coatings on Ni and Fe Based Superalloys," Surf. Engg., in press.
120. **Kamal, S., Jayaganthan, R. and Prakash, S., (2008C),** "High Temperature Oxidation Studies Of Detonation-Gun-Sprayed  $\text{Cr}_3\text{C}_2$ -NiCr Coating on Fe- and Ni-Based Superalloys in air Under Cyclic Condition at 900 °C," J Alloys Comp., in press.
121. **Kamal, S., Jayaganthan, R. and Prakash, S., (2008D),** "Mechanical and Microstructural Characterisations of NiCoCrAlYTa Coatings on Superalloys Deposited by Detonation Gun Technique," Surf. Engg. in press.
122. **Kamal, S., Jayaganthan, R. and Prakash, S., (2009A),** "Evaluation of Cyclic Hot Corrosion Behaviour of Detonation Gun Sprayed  $\text{Cr}_3\text{C}_2$ -25%NiCr Coatings on Nickel- and Iron-Based Superalloys," Surf. Coat. Technol., Vol.203, pp.1004-1013.
123. **Kamal, S., Jayaganthan, R. and Prakash, S., (2009B),** "Evaluation of Mechanical and Microstructural Characteristics of Detonation Gun Sprayed NiCrAlY+0.4wt%CeO<sub>2</sub> Coatings on Superalloys" J. Therm. Spray Technol., communicated.
124. **Kamal, S., R. Jayaganthan, S. Prakash and Sanjay Kumar, (2008A),** "Hot Corrosion Behavior of Detonation Gun Sprayed  $\text{Cr}_3\text{C}_2$ -NiCr Coatings on Ni and Fe-based Superalloys in Na<sub>2</sub>SO<sub>4</sub>-60% V<sub>2</sub>O<sub>5</sub> Environment at 900 °C," J Alloys Comp., Vol. 463, pp.358-372.
125. **Kawase, R. and Nakano, A., (1996),** "Production of Heat and Corrosion-Resistant Plastic Coating," proc of the 9<sup>th</sup> national thermal spray conference, Cincinnati, Ohio, pp: 257-262.
126. **Kerby, R. C. and Wilson J. R., (1973),** "Corrosion of Metals by Liquid Vanadium Pentoxide and the Sodium Vanadates," Trans. ASME, January, pp. 36-44.
127. **Kerby, R.C. and Wilson J.R., (1972),** "Electrical Conduction Properties of Liquid Vanadates. II. The Sodium," Canadian journal of chemistry, Vol. 58, pp. 2871-2876.
128. **Khajavi, M.R. and Shariat, M.H., (2004),** "Failure of First Stage Gas Turbine Blades," Eng. Fail. Anal., Vol.11, pp.589-597.
129. **Khalid, F.A., Hussain, N. and Shahid, K.A., (1999),** "Microstructure and Morphology of High Temperature Oxidation in Superalloys," Mater. Sci. & Eng. A- Struct., Vol. 265, pp.87-94.
130. **Khanna, A. S. and Jha, S. K., (1998),** "Degradation of Materials Under Hot Corrosion Conditions," T. Indian I. Metals, Vol. 51, No. 5, pp. 279-290.

131. **Kharlamov, Y.A.**, (1987), "Materials Engineering Forum Detonation Spraying of Protective Coatings," *Mate. Sci. Eng.*, Vol. 93, pp.1-37.
132. **Kharlamov, Y.U.**, (1974), "Impact Interaction of the Particles with the Substrate in Detonation Spray-Deposition," *P. Meta. Met. Ceramic*, Vol.13, No.10, pp. 820-824.
133. **Khor, K.A.**, Li, H. and Cheang, P., (2004), "Significance of Melt-Fraction in HVOF Sprayed Hydroxyapatite Particles, Splats and Coatings," *Biomaterials*, Vol.25, pp.1177–1186.
134. **Kim, D.Y.**, Han, M.S. and Youn, J.G., (1998), "Characterisation of Erosion Resistant Cr<sub>3</sub>C<sub>2</sub> - NiCr Plasma Sprayed Coatings," in *Thermal Spray: Practical Solutions for Engineering Problems*. ASM International.
135. **Kim, D.Y.**, Han, M. S.and Youn, J. G., (1996), in: C.C. Berndt Ed.*Thermal Spray: Practical Solutions for Engineering Problems*, ASM International, Materials Park, Ohio,USA, pp.123-128.
136. **Kim, G. M.**, Yanar, N. M., Hewitt, E. N., Pettit, F. S. and Meier, G. H., (2002), "The Effect of the Type of Thermal Exposure on the Durability of Thermal Barrier Coatings," *Scripta Materialia*, Vol. 46, pp. 489-95.
137. **Klimenko, V. S.**, (1979), "Detonation Spray-Deposition of Alumina of Various Degrees of Filling of The Barrel With Carrier Gas," *Poroshkovaya Metallurgiya*, No. 10, pp. 47–49.
138. **Knotek, O.**, (2001), "Chapter 3: Thermal Spraying and Detonation Spray Gun Processes," in 'Handbook of Hard Coatings: Deposition Technologies, Properties and Applications,' Ed. Bunshah, R. F., Noyes Pub. Park Ridge, New Jersey, U. S. A./William Andrew Publishing, LLC, Norwich, New York, U.S.A., pp. 77-107.
139. **Ko, P.L.** and Robertson, M.F., (2002), "Wear Characteristics of Electrolytic Hard Chrome and Thermal Sprayed WC–10 Co–4 Cr Coatings Sliding Against Al–Ni–Bronze in Air at 21°C and at -40 °C," *Wear*, Vol. 252, pp. 880–893.
140. **Koch, G. H.**, Brongers, M. P. H., Thompson, N. G., Virmani, Y. P. and Payer, J. H., (2002), "Historic Congressional Study: Corrosion Costs and Preventive Strategies in the United States," *Supplement to Mater. Perfor.*, July, pp. 1-11.
141. **Kofstad, P.** (1966), "Ch.1: General Introduction" in 'High Temperature Oxidation of Metals,' John Wiley & Sons Inc. USA.
142. **Kofstad, P.**, (1988), "Chapter 14" in 'High Temperature Corrosion,' Elsevier Applied Science, London & New York, pp. 465.

143. **Kofstad, P.**, (1990), "High Temperature Corrosion of Metals," Proc. of Conf. on Microscopy of Oxidation, London, pp. 1-9.
144. **Kofstad, P.**, (1998), High Temperature Corrosion. London: Elsevier Applied Science, pp. 257.
145. **Kohl, F.J.**, Stearns, C.A. and Fryburg, G.C., (1979), "The Role of NaCl in Flame Chemistry, in the Deposition Process, and its Reaction With Protective Oxides", Proc. 4<sup>th</sup> US/UK Navy Conf. on Gas Turbine Materials in a Marine Environment, Vol. II, U.S. Naval Sea Command, Annapolis, MD, pp. 565.
146. **Kolta, G. A.**, Hewaidy, L. F. and Felix, N. S., (1972), "Reactions Between Sodium Sulphate and Vanadium Pentoxide," Thermochim. Acta, Vol. 4, pp. 151-164.
147. **Korablev, S.F.**, Lysenko, A.V. and Filipchenko, S.I., (1988), "Chemical and Kinetic Peculiarities of the Oxidation of Powdery Chromium Carbide," Soviet Powder Metall. Met. Ceramics, Vol. 27, No. 7, pp. 584-587.
148. **Korpiola, K.** and Vuoristo, P., (1996), "Effect of HVOF Gas Velocity and Fuel-to-Oxygen Ratio on the Wear Properties of Tungsten Carbide Coating," In: Bernt, C. C. (ed.). Thermal Spray: Practical Solutions for Engineering Problems. Cincinnati, USA. 11 - 17 October. ASM.
149. **Krishna, B. V.** and Sidhu, R. K., (2002), "Pitting Corrosion of Steel Tubes in an Air Preheater, Practical Failure Analysis," ASM Int., Vol. 2, No. 5, pp. 61-66.
150. **Kuiry, C.**, Seal, S., Bose, S. K. and Roy, S. K., (1994), "Effect of Surface Preparation on the High-Temperature Oxidation Behaviour of AISI 316 Stainless Steel," ISIJ Int., Vol. 34, No. 7, pp. 599-606.
151. **Kuroda, S.**, Kawakita, J., Makoto Watanabe and Hiroshi Katanoda, (2008), "TOPICAL REVIEW Warm spraying—a Novel Coating Process Based on High-Velocity Impact of Solid Particles," Sci. Technol. Adv. Mater., Vol.9, pp.1-17.
152. **Lambert, P.**, Champagne, B. and Arseneault, B., (1991), "Oxidation and Hot Corrosion in Na<sub>2</sub>SO<sub>4</sub>-10%V<sub>2</sub>O<sub>5</sub> of Ni-17Cr-6Al-0.5Y and Ni-16Cr-5.7Al-0.47Y-5Si, MCrAlY Alloys at 700<sup>o</sup>C," Can. Metall. Quart., Vol. 30, No. 2, pp. 125-130.
153. **Lee, S.Y.** and McNallan, M.J., (1990), "Inhibition of Oxidation of Iron in Environments Containing Chlorine at 1100 and 1200 K," J. Electrochem. Soc., Vol. 137, No. 2, pp. 472-479.

154. Lee, W. H. and Lin, R. Y., (2002), "Hot Corrosion Mechanism of Intermetallic Compound Ni<sub>3</sub>Al," Mater. Chem. Phys., Vol. 77, pp. 86-96.
155. Levy, A. V.,(1993),"The Erosion-Corrosion of Tubing Steels in Combustion Boiler Environments ," Corros. Sci., Vol. 35, No. 5-8, pp. 1035-43.
156. Levy, M., Huie, R. and Pettit, F., (1989), "Oxidation and Hot Corrosion of Some Advanced Superalloys at 1300 to 2000°F (704 to 1093 °C),"Corros., Vol. 45, No. 8, pp. 661-674.
157. Li J. F., Wang X. Y., Liao H., Ding C. X. and Coddet, C., (2004), "Indentation Analysis of Plasma-Sprayed Cr<sub>3</sub>C<sub>2</sub>-NiCr Coatings," J. mate. Sci. letters, Vol.39, pp.7111 – 7114.
158. Li, C. J and Ohmori, A, (1996), "The Lamellar Structure of a Detonation Gun Sprayed Al<sub>2</sub>O<sub>3</sub> Coating," Surf. Coat. Technol., Vol. 82, pp. 254- 258.
159. Li, C. X., Sun, Y. and Bell, T., (2000), "Shot Peening of Plasma Nitrided Steel for Fretting Fatigue Strength Enhancement," Mate. Sci. Technol., Vol 16, pp.1067-1072.
160. Li, C.J., and Li, W.Y., (2002), "Effect of Sprayed Powder Particle Size On The Oxidation Behavior of MCrAlY Materials During High Velocity Oxygen-Fuel Deposition,"Surf. Coat. Technol., Vol.162, pp.31-41.
161. Li, J. and Wahi, R.P., (1995), "Investigation of Lattice Mismatch in the Polycrystalline Nickel-Base Superalloy IN738LC: Influence of Heat Treatment and Creep Deformation," Acta Metall. Mater., Vol.43-2, pp.507-517..
162. Li, J. F. and Ding, C. X., (1999), "Polishing-induced Pull Outs Of Plasma Sprayed Cr<sub>3</sub>C<sub>2</sub>-NiCr Coating ,"J. Mate. Sci. Lett., Vol.18, pp.1719-1721.
163. Li, L., Zhu, R. and Gesmundo, F., (1996), "Hot Corrosion of Iron in the Presence of Salt Mixture Deposit containing NaCl and V<sub>2</sub>O<sub>5</sub> at 600<sup>0</sup>C," J. Mater. Sci. Technol., Vol. 12, No. 6, pp. 445-451.
164. Li, M. H., Sun, X. F., Jin, T., Guan, H.R. and Hu, Z.Q., (2003B), "Oxidation Behaviour of a Single-Crystal Ni-Base Superalloy in Air-II: At 1000, 1100, and 1150<sup>0</sup>C," Oxid. Met., Vol. 60, No.1-2, pp.195-210.
165. Li, M. H., Sun, X. F., Li, J. G., Zhang, Z. Y., Jin, T., Guan, H.R. and Hu, Z. Q., (2003A), "Oxidation Behaviour of a Single-Crystal Ni-Base Superalloy in Air-I: At 800 and 900<sup>0</sup>C," Oxid. Met., Vol. 59, No. 5-6, pp.591-605.



166. Li, M., Sun, X., Hu, W. and Guan, H., (2007) "Microstructural Changes and Elemental Diffusion of Sputtered NiCrAlY Coating on a Ni-base SC Superalloy Subjected to High Temperature," *Mate. Lett.*, Vol.61, pp.5169-5172.
167. Li, Y., Yuan, C., Guo, J. T. and Yang, H. C., (2003C), "Oxidation Kinetics of Cast Ni-Base Superalloy K35," *J. Northeastern Uni.*, Vol. 24, No. 1, pp. 75-78.
168. Li, Y.S., Spiegel, M. and Shimada, S., (2005), "Corrosion Behaviour Of Various Model Alloys With NaCl-KCl Coating," *Maters. Chem. Phys.*, Vol.93, pp.217-223.
169. Lima, C. R. C. and Guilemany, J.M., (2007), "Adhesion Improvements of Thermal Barrier Coatings With HVOF Thermally Sprayed Bond Coats," *Surf. Coat. Technol.*, Vol. 201, pp.4694-4701.
170. Limin Sun, Christopher, Berndt, C. Clare, P. and Grey, (2003), "Phase, Structural and Microstructural Investigations of Plasma Sprayed Hydroxyapatite Coatings," *Mate. Sci.Eng. A*, Vol. 360, pp. 70-84.
171. Lin, T. L., Zhang, Y. H. and Yang, H.W, (1984), "Influence of Hot Corrosion on the Creep Strength of the Nickel-base Superalloy GH37," *Mater. Sci. Eng.*, Vol.62, pp.17-24.
172. Lindgren, J. R. and Johnson, W.R., (1987), "Friction and Wear Behavior of Chromium Carbide Coatings," *Surf. Coat. Technol.*, Vol. 32, pp. 249-260.
173. Liu, G., Li, M., Zhou, Y. and Zhang, Y., (2006), "Influence of Pre-Oxidation on The Hot Corrosion of  $Ti_3SiC_2$  in the Mixture of  $Na_2SO_4$ -NaCl melts," *Corro. Sci.*, Vol.48, pp.650-661.
174. Liu, J. and Ding, C., (2000), "Improvement in the Properties of Plasma-Sprayed Chromium Carbide Coatings Using Nickel-Clad Powders," *Surf. Coat. Technol.*, Vol.130, pp. 15-19.
175. Liu, M., (1998), "Study on the Spray Processes and Characteristics of  $Cr_3C_2$ /NiCr Coating," In *Thermal Spray: Meeting the Challenges of the 21<sup>st</sup> Century*, Nice, France: ASM International, Materials Park, OH-USA.
176. Liu, P. S., Liang, K. M., Zhou, H. Y., Gu, S. R., Sun, X. F., Guan, H. R., Jin, T. and Yang, K. N., (2001), "Cyclic Oxidation Behavior of Aluminide Coatings on the Co-Base Superalloy DZ40M," *Surf. Coat. Technol.*, Vol. 145, pp. 75-79.
177. Loubiere, S, Bonino, J.P., Laurent, C., Rousset, A., Loubiere, S. and Laurent, C., (1995), "Elaboration, Microstructure and Reactivity of  $Cr_3C_2$  Powders of Different Morphology," *Mate. Res. Bull.*, Vol.30, No. 12, pp. 1535-1546.

178. **Luthra, K. L.** and Shores, D.A., (1980), "Mechanism of  $\text{Na}_2\text{SO}_4$  Induced Corrosion at 600-900 °C," J. Electrochem. Soc., Vol. 127, No. 10, pp. 2202-2210.
179. **Luthra, K. L.**, (1982), "Low Temperature Hot Corrosion of Cobalt-Base Alloys: Part I. Morphology of the Reaction Product," Metall. Trans. A, Vol. 13A, pp.1843-1852.
180. **Luthra, K. L.**, (1985), "Kinetics of the Low Temperature Hot Corrosion of Co-Cr-Al Alloys," J. Electrochem. Soc., Vol. 132, No. 6, pp. 1293-1298.
181. **Luthra, K.L.** and Spacil, H.S., (1982), "Impurity Deposits in Gas Turbines from Fuels Containing Sodium and Vanadium," J. Ele. Society, Vol.129, No. 3, pp 649-656.
182. **Ma, X. Q.**, Rhyim, Y.M., Jin, H.W., Park, C.G. and Kim M.C, (1999), "Application of Fractal Dimension to Optimum Deposition of NiCrAlY Coating by D-Gun spray," Mate. Manuf. Pro., Vol. 14, No.2, pp. 195 – 204.
183. **Madhu Chittora**, Project Monitor, Economic Research India Ltd, January 28 - February 3, (2008).
184. **Mahesh, R.A.**, Jayaganthan, R. and Prakash, S., (2008), "Characterisation of HVOF Sprayed NiCrAlY-0.4 wt-% $\text{CeO}_2$  Coatings on Superalloys," Surf. Engg., Vol.24, N0.5, pp.366-373.
185. **Mahesh, R.A.**, Jayaganthan, R. and Prakash, S., (2008A), "Microstructural Characteristics And Mechanical Properties of HVOF Sprayed NiCrAl Coating on Superalloys," J. alloys compounds, (2008) in press.
186. **Maledi, N.B.**, Potgieter, J.H., Sephton, M. Cornish, L.A., Chown, L. and Suss, R., (2006), "Hot Corrosion Behaviour of Pt-Alloys for Application in the Next Generation of Gas Turbines ," International Platinum Conference 'Platinum Surges Ahead', the Southern African Institute of Mining and Metallurgy, 2006, pp. 81-90.
187. **Malik, A. U.** and Ahmad, S., (1983), " $\text{Na}_2\text{SO}_4$ -Induced Corrosion of Some Nimonic Alloys at 650 to 1000°C," Metallkd., Vol. 74, No. 12, pp. 819-824.
188. **Malik, A. U.** and Mobin, M., (1987), "Studies on Some Solid State Reactions Relevant to Hot Corrosion," Proc. of 10<sup>th</sup> ICMC, Madras, India, Vol. IV, pp. 3345-3365.
189. **Malik, A.U.**, Asrar, N., Ahmad, S. and Siddiqi, N. A. B., (1988), "Hot Corrosion Behaviour of Some Industrially Important Nickel-base Alloys in Presence of  $\text{Na}_2\text{SO}_4(\text{S})$  and  $\text{NaCl}(\text{S})$ ," Metallkd., Vol. 79, No.5, pp. 285-295.

190. **Mann, B.S. and Prakash, B.,** (2000), "High Temperature Friction And Wear Characteristics of Various Coating Materials for Steam Valve Spindle Application," *Wear*, Vol. 240, pp.223-230.
191. **Manoj Kumar, B.V., Bikramjit Basu, Murthy, V.S.R., Manoj Gupta,** (2003), "The Role of Tribochemistry on Fretting Wear of Mg–SiC Particulate Composites," *Composites: Part A* 36 (2005) 13–23.
192. **Marceau, J.A. and Adjorlolo, A.A.,** (1995), "Commercial Aircraft," in ASM, "Corrosion Tests and Standards; application and Interpretation." American society for testing and material society, (1995), pp.574-578.
193. **Matthews S. J.,** (2004) "Erosion-Corrosion of Cr<sub>3</sub>C<sub>2</sub>-NiCr High Velocity Thermal Spray Coatings," Ph.D. Thesis, The University of Auckland.
194. **Matthews S., Hyland M. and James B.,** (2003), "Microhardness Variation in Relation to Carbide Development in Heat Treated Cr<sub>3</sub>C<sub>2</sub>-NiCr Thermal Spray Coatings," *Acta Materialia*, Vol.51, pp. 4267–4277.
195. **Mayoral, M. C., Andrés, J.M., Bona, M.T., Higuera, V. and Belzunce, F.J.,** (2008), "Aluminium Depletion in NiCrAlY Bond Coatings by Hot Corrosion as a Function of Projection System," *Surf. Coat. Technol.* 202, p. 1816-1824.
196. **Meier, G.H.,** (1989), "A Review of Advances in High-temperature Corrosion", *Mate. Sci. Engg. A*, Vol. 120, pp. 1-11.
197. **Metals Handbook,** (1975), 'Failure Analysis and Prevention,' Vol.10, ASM Publication, Metals Park OH, USA.
198. **Metals Handbook,** (1990), "Properties and Selection; Iron, Steel and High Performance Alloys, 10<sup>th</sup> Edition," Vol.1, ASM Publication, Metals Park Ohio. pp.981.
199. **Mevrel, R.,** (1989), "State of the Art on High-temperature Corrosion-resistant Coatings," *Materials Mater. Sci. Engg. A*, Vol. 120, pp. 13-24.
200. **Misra, A. K.,** (1986), "Mechanism of Na<sub>2</sub>SO<sub>4</sub>-Induced Corrosion of Molybdenum Containing Nickel-Base Superalloys at High Temperatures," *J. Electrochem. Soc.*, Vol. 133, No. 5, pp. 1029-1037.
201. **Misra, A.K.,** (1987), "Hot Corrosion of Nickel and Cobalt Base Alloys at Intermediate Temperatures," *Proc. of X<sup>th</sup> Intl. Congress on Metallic Corrosion*, Oxford and IBH publishing co. Pvt. Ltd., New Delhi, Vol. 4, pp. 3533-3553.

202. **Mitra, S.K, Roy, S.K and Boset, S.K.,** (1993), "Influence of Superficial Coating of CeO<sub>2</sub> on the Oxidation Behavior of AISI 304 Stainless Steel," *Oxid. Met*, Vol. 39(3/4), pp.22-229.
203. **Mobarra, R., Jafari, A.H. and Karaminezhaad, M.,** (2006), "Hot Corrosion Behavior of MCrAlY Coatings on IN738LC," *Surf. Coat. Technol.* Vol.201, No. 6, pp.2202-2207.
204. **Mobin, M., Malik, A. U., Ahmad, S., Hasan, S. K. and Ajmal, M.,** (1996), "Studies on the Interactions of Metal Oxides and Na<sub>2</sub>SO<sub>4</sub> at 1100 and 1200 K in Oxygen," *Bull. Mater. Sci.*, Vol. 19, No. 5, pp. 807-821.
205. **Mohanty, Smith, R.W., De Bonte, M., Celis, L.P. and Lugscheider E.,** (1996), "Sliding Wear Behavior of Thermally Sprayed 75/25 Cr<sub>3</sub>C<sub>2</sub>/NiCr Wear Resistant Coatings," *Wear*, Vol. 198, pp. 251-266.
206. **Mokhnachuk, O.V., Solov'ev, S. A., Il'in, V. G. and Yaremov, P. S.,** (2006), "Influence of Oxides of the Rare Earth Elements (La<sub>2</sub> O<sub>3</sub> , CeO<sub>2</sub> ) on the Thermal Stability of Highly Dispersed Aluminum Oxide," *Theore. Experi. Chemi.*, Vol. 42(5), pp.327-333.
207. **Morimoto, J., Yoh Sasaki, Shinji Fukuhara, Nobuyuki Abe and Masahiro Tukamoto,** (2006), "Surface Modification of Cr<sub>3</sub>C<sub>2</sub>-NiCr Cermet Coatings by Direct Diode Laser," *Vacuum*, Vol.80, pp.1400-1405.
208. **Moujahid, S. E.,** (1987), "High Temperature Corrosion of Cast Iron Chains by Coal Ash," *Proc. of 10<sup>th</sup> ICMC, Madras, India*, Vol. I, pp. 857-60.
209. **Murthy, J.K.N. and Venkataraman, B.,** (2006), "Abrasive Wear Behaviour of WC-CoCr and Cr<sub>3</sub>C<sub>2</sub>-20(NiCr) Deposited by HVOF and Detonation Spray Processes," *Surf. Coat. Technol.*, Vol.200, pp. 2642-2652.
210. **Murthy, J.K.N., Bysakh, S., Gopinath, K. and Venkataraman, B.,** (2007), "Microstructure Dependent Erosion in Cr<sub>3</sub>C<sub>2</sub>-20(NiCr) Coating Deposited by a Detonation-Gun," *Surf. Coat. Technol.*, Vol. 202, No. 1, pp. 1-12.
211. **Nanni, P., Buscaglia, V., Asmundis, C. D. and Roy, S. K.,** (1987), "Sodium Sulphate Induced Hot Corrosion of Pure Fe, Mn and Cr in Combustion Gas," *Proc. of 10<sup>th</sup> ICMC, Madras, India*, Vol. IV, pp. 3413-3422.
212. **Natesan, K.,** (1976), "Corrosion-Erosion Behavior of Materials in a Coal-Gasification Environment," *Corros.*, Vol. 32, No. 9, pp. 364-370.
213. **Natesan, K.,** (1985), "High-Temperature Corrosion in Coal Gasification Systems," *Corros.*, Vol. 41, No. 11, pp. 646-655.

214. **National Materials Advisory Board**, (1996), "Coatings for High-Temperature Structural Materials: Trends and Opportunities," National Academy Press Washington D.C., <http://www.nap.edu/openbook/0309053811/html>, pp 1-85.
215. **Nelson**, H. W., Krause, H. H., Ungar, E. W., Putnam, A. A., Slunder, C. J., Miller, P. D., Hummel, J. D. and Landry, B. A., (1959), "A Review of Available Information on, Corrosion and Deposits in Coal- and Oil-Fired Boilers and Gas Turbines," Report of ASME Research Committee on Corrosion and Deposits from Combustion Gases, Pub. Pergamon Press and ASME, New York.
216. **Nerz**, J.E.; Kushner B.A., Jr. Rotolico, A.J., (1992), "Microstructural Evaluation of Tungsten Carbide-Cobalt Coatings," ASM International (USA), pp.115-120.
217. **Nicholls**, J. R. and Stephenson, D.J., (1995), "Ch. 22: High-Temperature Coatings for Gas Turbines," in 'Intermetallic Compounds, Principles and Practice, Vol. 2-Practice,' Eds. Westbrook, J.H. and Fleischer, F.L., Pub. John Wiley & Sons Ltd., England.
218. **Nicholls**, J. R., Simms, N. J., Chan, W. Y. and Evans, H. E., (2002), "Smart Overlay Coatings- Concept and Practice," Surf. Coat. Technol., Vol. 149, pp. 236-44.
219. **Nicholls**, J.R., (2000), "Designing Oxidation-Resistant Coatings," JOM, January, pp. 28-35.
220. **Nickel**, H., Quadackers, W. J. and Singheiser, L., (2002), "Analysis of Corrosion Layers on Protective Coatings and High Temperature Materials in Simulated Service Environments of Modern Power Plants Using SNMS, SIMS, SEM, TEM, RBS and X-ray Diffraction Studies," Anal. Bioanal. Chem., Vol. 374, pp. 581-587.
221. **Nicoll**, A. R., (1984), "Chapter 13: The Production and Performance Evaluation of High Temperature Coatings," in 'Coatings and Surface Treatment for Corrosion and Wear Resistance,' Eds. Strafford, K. N., Datta, P. K. and Googan, C. G., (1984), Institution of Corros. Sci. and Technol., Birmingham, Pub. Ellis Horwood Ltd., Chichester.
222. **Niranatlumpong**, P., Ponton, C. B. and Evans, H. E., (2000), "The Failure of Protective oxides on Plasma-Sprayed NiCrAlY Overlay Coatings," Oxid. Met, Volume 53, Nos. 3/4, pp. 241-258.
223. **Otero**, E., Merino, M. C., Pardo, A., Biezma, M. V. and Buitrago, G., (1987), "Study on Corrosion Products of IN657 Alloy in Molten Salts," Proc. of 10<sup>th</sup> ICMC, Madras, India, Vol. IV, pp. 3583-3591.

224. **Otero, E., Pardo, A., Hernaez, J. and Perez, F. J.,** (1990), "The Hot Corrosion of IN-657 Superalloy in Na<sub>2</sub>SO<sub>4</sub>-V<sub>2</sub>O<sub>5</sub> Melt Eutectic," *Corros. Sci.*, Vol. 30, pp. 677-683.
225. **Otero, E., Pardo, A., Hernaez, J. and Perez, F. J.,** (1992), "The Corrosion of Some Superalloys (At 1000 K) in Molten Eutectic Mixture 60% V<sub>2</sub>O<sub>5</sub>-40% Na<sub>2</sub>SO<sub>4</sub>: The Influence of the Oxygen and Carbon Residues," *Corros. Sci.*, Vol. 34, pp. 1747-1757.
226. **Otsuka, N,** (2002), "Effects of Fuel Impurities on the Fireside Corrosion of Boiler Tubes in Advanced Power Generating Systems-A Thermodynamic Calculation of Deposit Chemistry," *Corros. Sci.*, Vol 44, No, pp.265-283.
227. **Otsuka, N. and Rapp, R.A.,** (1990), "Effects of Chromate and Vanadate Anions on the Hot Corrosion of Pre oxidized Ni by a Thin Fused Na<sub>2</sub>SO<sub>4</sub> Film at 9000C," *J. Electrochem. Soc.*, Vol. 137, No. 1, pp. 53-60.
228. **Pandey, J. L.,** (1983), "Effect of Zirconium and Yttrium Alloying on High Temperature Oxidation of Fe-15wt%Cr-4wt%Al," University of Roorkee, Dept. of Chemistry, Roorkee, India.
229. **Pantony, D.A. and Vasu, K. I.,** (1968A), "Studies in the Corrosion of Metals under Melts-1," *J. Inorg. Nucl. Chem.*, Vol. 10, pp. 423-432.
230. **Pantony, D.A. and Vasu, K.I.,** (1968B), "Studies in the Corrosion of Metals under Melts-III," *J. Inorg. Nucl. Chem.*, Vol. 10, pp. 755-779.
231. **Park, S.Y., Kimb, M.C. and Park, C.G.,** (2007), "Mechanical Properties and Microstructure Evolution of the Nano WC-Co Coatings Fabricated by Detonation gun Spraying with Post Heat Treatment," *Mate. Sci. Engg. A*, Vol. 449-451, pp.894-897.
232. **Pehkonen, A., Tikkanen, M. H., Ylasaari, S. and Forsen, O.,** (1987), "Behaviour of Some Super Alloys in Different High Temperature Atmospheres," *Proc. of 10<sup>th</sup> ICMC, Madras, India*, Vol. IV, pp. 3781-3787.
233. **Peters, K. R., Whittle, D. P. and Stringer, J.,** (1976), "Oxidation and Hot Corrosion of Nickel-Based Alloys Containing Molybdenum," *Corros. Sci.*, Vol. 16, pp. 791-804.
234. **Pettit, F. S. and Giggins, C. S.,** (1987), "Hot Corrosion, Ch. 12," in 'Superalloys II,' Eds. Sims, C. T., Stolof, N. S. and Hagel, W. C., Pub. Wiley Pub., N. Y.
235. **Pettit, F. S. and Meier, G. H.,** (1984), "Oxidation and Hot corrosion of Superalloys," *Superalloys (1984)*, M. Gell, C. S. Kartovich, R. H. Bricknel, W. B. Kent, J. F. Radovich (Eds.), The Met. Soc. of AIME, Warrendale, Pennsylvania, pp. 651-687.

236. **Pettit**, F. S. and Meier, G. H., (1985), "Oxidation and Hot corrosion of Superalloys," Superalloys 85, Eds. Gell, M., Kartovich, C. S., Bricknel, R. H., Kent W. B. and Radovich, J. F., Met. Soc. of AIME, Warrendale, Pennsylvania, pp. 651-687.
237. **Pettit**, F.S., (1977), Design of Structural With High Temperature Corrosion Resistance, Fundamental Aspects of Structural Alloy Design, New York: Plenum press. pp. 597-621
238. **Pettit**, F.S., Goebel, J. A. and Goward, G.W, (1969), Thermogravimetric Analysis of the Simultaneous Attack of Some Metals and Alloys by Two Oxidants, Corrosion Science, v9
239. **Pint**, B.A., (1996), "Experimental Observations in Support of the Dynamic-Segregation Theory to Explain the Reactive-Element Effect," Oxid. Met., Vol. 45, pp.1-37.
240. **Porcayo-Calderon**, J., Gonzalez-Rodriguez, J.G. and Martinez, L., (1998), "Protection of Carbon Steel against Hot Corrosion using Thermal Spray Si- and Cr-Base Coatings," J. Mater. Eng. Perform., Vol. 7, pp. 79-87.
241. **Prakash**, S., Puri, D. and Singh, H., (2005), "Hot Corrosion Behaviour of Plasma Sprayed Coating on Ni-Based Superalloys in  $\text{Na}_2\text{SO}_4$ -60% $\text{V}_2\text{O}_5$  Environment," ISIJ Int., Vol: 45, No.6, pp.886-895.
242. **Prakash**, S., Singh, S., Sidhu, B. S. and Madeshia, A., (2001), "Tube Failures in Coal Fired Boilers," Proc. National Seminar on Advances in Material and Processing, Nov., 9-10, IITR, Roorkee, India, pp. 245-253.
243. **Priyantha**, N., Jayaweera, P., Sanjurjo, A., Lau, K., Lu, F. and Krist, K., (2003), "Corrosion-Resistant Metallic Coatings for Applications in Highly Aggressive Environments," Surf. Coat. Technol., Vol. 163-64, pp. 31-36.
244. **Psyllaki**, P.P, Jeandis, M. and Pantelis, D.I., (2001), "Microstructure and Wear Mechanisms of Thermal-Sprayed Alumina Coatings," Mater Lett., Vol.47, pp.77-82.
245. **Rajan Ambat** and Zhou, W., (2004), "Electroless nickel-plating on AZ91D magnesium alloy: effect of substrate microstructure and plating parameters," Surf. Coat. Technol. Vol.179, pp.124-134.
246. **Rajan Ambat**, Naing Naing Aung and Zhou, W., (2000), "Evaluation of microstructural effects on corrosion behaviour of AZ91D magnesium alloy," Corrosion Science, Vol.42 pp.1433-1455.
247. **Rajasekaran B.**, Ganesh Sundara Ramana S., Joshi S.V. and Sundararajan G., (2008)," Performance of Plasma Sprayed and Detonation Gun Sprayed Cu-Ni-In Coatings on Ti-6Al-

- 4V Under Plain Fatigue and Fretting Fatigue Loading,” *Mate. Sci. Engg. A*, Vol. 479, pp. 83-92.
248. **Rajasekaran, B., Ganesh Sundara Raman, S., Joshi, S.V. and Sundararajan, G.,** (2006), “Effect of Detonation Gun Sprayed Cu–Ni–In Coating on Plain Fatigue and Fretting Fatigue Behaviour of Al–Mg–Si alloy,” *Surf. Coat. Technol.*, Vol. 201, Issues 3-4, pp.1548-1558.
249. **Rao, K., Somerville, D. A, and Lee, D. A,** (1986), “Properties and Characterization of Coating Made Using Jet Kote Thermal Spray Technique in”, *Proceeding of the 11<sup>th</sup> international thermal spray conference, Montreal, Canada: Welding Institute of Canada*, pp. 873-882.
250. **Rapp, R. A. and Goto, K. S.,** (1981), “The Hot Corrosion of Metals by Molten Salts,” *Sympos. Fused Salts*, Eds. Braunstein, J. and Selman, J. R., *The Electrochem. Soc., Pennington, N. J.*, pp.159.
251. **Rapp, R. A.,** (1986), “Chemistry and Electrochemistry of the Hot Corrosion of Metals,” *Corros.*, Vol. 42, No. 10, pp. 568-577.
252. **Rapp, R. A.,** (2002), “Hot Corrosion of Materials: A Fluxing Mechanism,” *Corros. Sci*, Vol. 44, No. 2, pp. 209-221.
253. **Rapp, R. A., Devan, J. H., Douglass, D. L., Nordine, P. C., Pettit, F. S. and Whittle, D. P.,** (1981), “High Temperature Corrosion in Energy Systems,” *Mater. Sci. Engg.*, Vol. 50, pp. 1-17.
254. **Ravindra, T., Raghavan, S. and Kamaraj, M.,** (2007), “Hot Corrosion and Oxidation Behaviour of a Directionally Solidified Nickel Base Superalloy,” *Trans .Indian Inst .Met.*, Vol.60, pp.385-392.
255. **Reid, W.T.,** (1971), “External Corrosion and Deposits—Boilers and Gas turbines,” *Elsevier, New York*, pp.115-143.
256. **Ren, X. and Wang, F.,** (2006), “High-temperature Oxidation and Hot-Corrosion Behavior of A Sputtered NiCrAlY Coating With and Without Aluminizing,” *Surf. Coat. Technol.*, Vol. 201, pp.30–37.
257. **Ren, X., Wang, F. and Wang, X.,** (2005), “High-temperature Oxidation and Hot Corrosion Behaviors of the NiCr–CrAl Coating on a Nickel-based Superalloy,” *Surf. Coat. Technol.*, Vol.198, pp. 425-431.



258. **Rhys-Jones, T.N.**, (1990), "Thermally Sprayed Coating Systems for Surface Protection and Clearance Control Applications in Aero Engines," *Surf. Coat. Technol.*, Vol. 43/44, pp. 402-415.
259. **Rocca, E, Steinmetz, P. and Moliere, M.**, (2003), "Revisiting the Inhibition of Vanadium-Induced Hot Corrosion in Gas Turbines," *J. Eng. Gas Turbines and Power*, Vol. 125, PP. 1-9.
260. **Roy, K., Bottino, C., Rakesh, V. R., Kuiry, S. C. and Bose, S. K.**, (1995), "Improved High Temperature Oxidation Behaviour of AISI 347 Grade Stainless Steel by Superficial Coating of CeO<sub>2</sub>," *ISIJ Int.*, Vol. 35, No. 4, pp. 433-442.
261. **Russo, L. and Dorfmann, L.** In: **Ohmori, A. (Ed.)**, (1995), *Thermal Spraying, Current Status and Future Trends*, Japan High Temperature Society, Osaka, pp. 681-686.
262. **Sachs, K.**, (1958), "Accelerated High Temperature Oxidation due to Vanadium Pentoxide," *Metallurgia*, Apr., pp. 167-173.
263. **Sadique, S. E., Mollah, A. H., Islam, M. S., Ali, M. M., Megat, M. H. H. and Basri, S.**, (2000), "High-Temperature Oxidation Behavior of Iron-Chromium-Aluminum Alloys," *Oxid. Met.*, Vol. 54, Nos. 5-6, pp. 385-400.
264. **Sahoo, P.**, (1993), "High Performance Wear Coatings - The Quest Continues," *PMI*, Vol. 25, No. 2, pp. 73-78.
265. **Sahraoui, T., Guessasma, S., Fenineche, N.E., Montavon, G. and Coddet, C.**, (2004), "Friction and Wear Behaviour Prediction of HVOF Coatings and Electroplated Hard Chromium Using Neural Computation," *Mate. Letters*, Vol. 58, pp. 654-660.
266. **Salmenoja, K., Makela, K., Hupa, M. and Backman, R.** (1996), "Superheater Corrosion in Environments Containing Potassium and Chlorine," *J. Inst. Energy*, Vol.69, pp.155-162.
267. **Santorellit, R. Sivieri, E and Cristina reggiani, R.**, (1989), "High-temperature Corrosion of Several Commercial Fe-Cr-Ni Alloys Under a Molten Sodium Sulphate Deposit in Oxidizing Gaseous Environments," *Mater. Sci. Engg. A*, Vol.120, pp. 283-291.
268. **Santoro, G. J.**, (1979), "Hot Corrosion of Four Superalloys: HA-188, S-57, IN-617 and TD-NiCrAl," *Oxid. Met.*, Vol. 13, No. 5, pp. 405-435.
269. **Saravanan, P., Selvarajan, V., Rao, D.S., Joshi, S.V. and Sundararajan, G.**, (2000), "Influence of Process Variables on the Quality of Detonation Gun Sprayed Alumina Coatings," *Surf. Coat. Technol.*, Vol. 123, pp. 44-54.

270. **Saunders**, S. R. J., Gohil, D. D., Banks, J. P., Sheriff, M. U., Tortorelli, P. F., Van, J. H. D. and Wright, I. G., (1997), "Behaviour of FeCr alloy and Iron Aluminides Alloys in Coal Gasification Atmospheres Containing HCl," *Mater. Sci. Forum*, Vol. 251-254, pp. 583-90.
271. **Savarimuthu**, A.C., Megat, I., Taber, H.F., Shadley, J.R., Rybicki, E.F., Emery, W.A., Nuse, J.D. and Somerville, D.A., (2000), "Sliding wear behaviour as a criterion for replacement of chromium electroplate by tungsten carbide (WC) thermal spray coatings in aircraft applications," in: *Proceedings of 1<sup>st</sup> International Thermal Spray Conference (ITSC 2000)*, Canada, pp. 1095-1104.
272. **Scrivani** A., Ianelli S., Rossi A., Groppetti R., Casadei F. and Rizzi G., (2001), "A Contribution to the Surface Analysis and Characterisation of HVOF Coatings for Petrochemical Application," *Wear*, Vol.250, pp.107-113.
273. **Seal**, S., Bose, S. K. and Roy, S. K., (1994), "Improvement in the Oxidation Behaviour of Austenitic Stainless Steels by Superficially Applied, Cerium Oxide Coatings," *Oxid. Met.*, Vol. 41, No. 1-2, pp. 139-178.
274. **Seiersten**, M. and Kofstad, P., (1987), "The Effect of SO<sub>3</sub> on Vanadate-Induced Hot Corrosion," *High Temp. Technol.*, Vol. 5, No. 3, pp. 115-122.
275. **Semenov**, S. Y. and Cetegen, B. M., (2002), "Experiments and modeling of the deposition of nano-structured alumina-titania coatings by detonation waves," *Mate. Sci. Eng.A*, Vol. 335, pp. 67-81.
276. **Seo** D., Ogawa K., Tanno. M., Shoji T. and Murata S., (2007), "Influence of Heat Exposure Time on Isothermal Degradation of Plasma Sprayed CoNiCrAlY Coatings," *Surf. Coat. Technol.*, Vol. 20, pp. 7952-7960.
277. **Seong**, B.G., Hwang, S.Y. and Kim, K.Y., (2000), "High-temperature Corrosion of Remunerator Used In Steel Mills," *Surf. Coat. Technol.*, Vol. 126, pp. 256-265.
278. **Sequeira**, C.A.C. and Hocking, M.G., (1981), "Hot Corrosion of Nimonic 105 in Sodium Sulfate-Sodium Chloride Melts," *Corros.*, Vol. 37, No. 7, pp. 392-406.
279. **Seybolt**, A.U., (1968), "Hot Corrosion Mechanism," *Trans. TMS. AIME*, Vol.242, pp.1955-1961.
280. **Seybolt**, A.U.,(1971), "Role of Rare Earth Additions in the Phenomenon of Hot Corrosion," *Corros. Sci.*, Vol. 11, pp. 751-756.

281. **Sharma, R. N.**, (1996), "Hot Corrosion Behaviour of Iron- and Nickel-Base Superalloys in Salt Environments at Elevated Temperatures," Ph. D. Thesis, Met. Mat. Engg. Deptt., University of Roorkee, Roorkee, India.
282. **Shi, L.**, (1993), "Accelerated Oxidation of Iron Induced by Na<sub>2</sub>SO<sub>4</sub> Deposits in Oxygen at 750<sup>0</sup>C- A New Type Low-Temperature Hot Corrosion," *Oxid. Met.*, Vol. 40, No. 1-2, pp. 197-211.
283. **Shi, L.**, (1995), "On the Possibility of a Na<sub>2</sub>SO<sub>4</sub>-Na<sub>2</sub>O Eutectic Melt Developing on Metals Coated with Na<sub>2</sub>SO<sub>4</sub> Deposit in Oxygen/Air at Intermediate Temperatures," *Corros. Sci.*, Vol. 37, No. 8, pp. 1281-1287.
284. **Shi, L.**, Zhang, Y. and Shih, S., (1992), "The Effect of K<sub>2</sub>SO<sub>4</sub> Additive in Na<sub>2</sub>SO<sub>4</sub> Deposits on Low Temperature Hot Corrosion of Iron-Aluminum Alloys," *Oxid. Met.*, Vol.38, pp.385-405.
285. **Shi, L.**, Zhang, Y. and Shih, S., (1993), "The Low Temperature Hot corrosion of Iron and Iron-Aluminium Alloys," *Corros. Sci.*, Vol. 33, No, 9, pp.1427-1438.
286. **Shifler, David A.**, (2004), "substrate-coating interactions and their effects on hot corrosion resistance," *Proc. Electrochemical society*, v PV 2004-16, high temperature corrosion and material chemistry V-international symposium, electro chemical society Inc., pennington, NJ08524-2896 united state, Oct 3-8, 2004, pp.294-305.
287. **Shih, S.**, Zhang, Y. and Li, X., (1989), "Sub-Melting Point Hot Corrosion of Alloys and Coatings," *Mater. Sci. Eng. A.*, Vol. 120, pp. 277-282.
288. **Shirvani, K.**, Saremi, M., Nishikata, A. and Tsuru, T., (2003), "Electrochemical Study on Hot Corrosion of Si-modified Aluminide Coated In-738LC in Na<sub>2</sub>SO<sub>4</sub>-20wt.% NaCl melt at 750 °C," *Corrosion Science*, Vol.45, pp.1011-1021.
289. **Sibi, M. P.** and Zong, Z., (2003), "Determination of Corrosion on Aluminum Alloy under Protective Coatings Using Fluorescent Probes." *Progress in Organic Coatings*, Vol:47, pp.8-15.
290. **Sidhu, B.**, (2003), 'Studies on the Role of Coatings in Improving Resistance to Hot Corrosion and Degradation,' Ph.D. Thesis, Met. & Mat. Eng. Deptt., Indian Institute of Technology Roorkee, Roorkee.

291. **Sidhu, B.S** and Prakash, S., (2005), "High-Temperature Oxidation Behavior of NiCrAlY Bond Coats and Stellite-6 Plasma-Sprayed Coatings," *Oxid. Met.*, Vol. 63, Nos. ¾, pp.241-259.
292. **Sidhu, B.S** and Prakash, S., (2006), "Evaluation of the Behavior of Shrouded Plasma Spray
293. **Sidhu, B.S.** and Prakash, S., (2003), "Evaluation of the Corrosion Behaviour of Plasma-Sprayed Ni<sub>3</sub>Al Coatings on Steel in Oxidation and Molten Salt Environment at 900<sup>0</sup>C," *Surf. Coat. Technol.*, Vol. 166, No. 1, pp. 89-100.
294. **Sidhu, B.S.**, Puri, D. and Prakash, S., (2004), "Characterisations of Plasma Sprayed and Laser Remelted NiCrAlY Bond Coats and Ni<sub>3</sub>Al Coatings on Boiler Tube Steels," *Mater. Sci. Eng. A-Struct.*, Vol. 368, No. 1-2, pp. 149-158.
295. **Sidhu, B.S.**, Puri, D. and Prakash, S., (2005A), "Mechanical and Metallurgical Properties of Plasma Sprayed and Laser Remelted Ni-20Cr and Stellite-6 Coatings," *J. Mater. Process. Technol.*, Vol. 159, No. 3, pp. 347-355.
296. **Sidhu, H.S.**, Sidhu, B.S. and Prakash, S. (2006A), "The role of HVOF Coatings in Improving Hot Corrosion Resistance of ASTM-SA210 GrA1 Steel in the Presence of Na<sub>2</sub>SO<sub>4</sub>-V<sub>2</sub>O<sub>5</sub> salt Deposits," *Surf. Coat. Technol.*, Vol. 200, pp. 5386-94.
297. **Sidhu, T.S.** Prakash, S. and Agrawal, R.D., (2005B), "Studies on the properties of high-velocity oxy-fuel thermal spray coatings for higher temperature applications," *Mate.Sci.*, Vol.41, No. 6, pp. 805-823.
298. **Sidhu, T.S.** Prakash, S. and Agrawal, R.D., (2006F), "Performance of High Velocity Oxy Fuel -Sprayed Coating on an Fe-Based Superalloy in Na<sub>2</sub>SO<sub>4</sub>-60% V<sub>2</sub>O<sub>5</sub> Environment at 900 °C Part II: Hot Corrosion Behaviour Of Coating," *J Mate. Engg. Perf.*, Vol. 15, pp.130-138.
299. **Sidhu, T.S.** Prakash, S. and Agrawal, R.D., (2006G), "Hot corrosion studies of HVOF sprayed Cr<sub>3</sub>C<sub>2</sub>-NiCr and Ni-20Cr coatings on nickel-based superalloy at 900 °C," *Surf. Coat. Technol.*, Vol. 201, No.3-4, pp.792-800.
300. **Sidhu, T.S.**, (2006), "Studies on the Hot corrosion Behaviour of HVOF Coatings on Some Ni-and Fe- Based Superalloys," Ph.D Thesis, Dept. of Met. & Mat. Engg. Dept., Indian Institute of Technology Roorkee, Roorkee.
301. **Sidhu, T.S.**, Prakash, S. and Agrawal R.D., (2006H), "Hot Corrosion Behaviour of HVOF-Sprayed NiCrBSi Coatings on Ni and Fe-based Superalloys in Na<sub>2</sub>SO<sub>4</sub>-60% V<sub>2</sub>O<sub>5</sub> Environment at 900 °C," *Acta Materialia*, Vol.54, pp. 773-784.

302. **Sidhu**, T.S., Prakash, S. and Agrawal R.D., (2007), "Study of Molten Salt Corrosion of High Velocity Oxy-Fuel Sprayed Cermet and Nickel-Based Coatings at 900 °C," *Meta. Mate. Trans. A*, Vol. 38, pp. 77-85.
303. **Sidhu**, T.S., Prakash, S. and Agrawal, R.D. (2006B), "Hot Corrosion Studies of HVOF NiCrBSi and Stellite-6 Coatings on a Ni-based Superalloy in an Actual Industrial Environment of a Coal Fired Boiler," *Surf. Coat. Technol.*, Vol. 201 Nos 3/4, pp. 1602-1612
304. **Sidhu**, T.S., Prakash, S. and Agrawal, R.D. (2006C), "Characterisation of NiCr Wire Coatings on Ni- and Fe-Based Superalloys by the HVOF process," *Surf. Coat. Technol.*, Vol. 200, pp. 5542-5549.
305. **Sidhu**, T.S., Prakash, S. and Agrawal, R.D. (2006D), "Studies of the Metallurgical and Mechanical Properties of High Velocity Oxy-Fuel Sprayed Stellite-6 Coatings on Ni- and Fe-Based Superalloys," *Surf. Coat. Technol.*, Vol. 201 Nos 1/2, pp. 273-281.
306. **Sidhu**, T.S., Prakash, S. and Agrawal, R.D. (2006E), "Characterisations of HVOF Sprayed NiCrBSi Coatings on Ni- and Fe-based Superalloys and Evaluation of Cyclic Oxidation Behaviour of Some Ni-based Superalloys in Molten Salt Environment," *Thin Solid Films*, Vol. 575 No.1, pp.95-105.
307. **Sidhu**, T.S., Prakash, S. and Agrawal, R.D., (2005C), "Hot Corrosion Performance of a NiC Coated Ni-based alloy," *Scripta Materialia*, Vol. 55, pp.179 –182.
308. **Sidhu**, T.S., Prakash, S. and Agrawal, R.D., (2006I), "Evaluation of Hot Corrosion Resistance of HVOF Coatings on a Ni-based Superalloys in Molten Salt Environment," *Mater. Sci Eng. A.*, Vol. **430**, No.2, pp. 64-78.
309. **Sidhu**, T.S., Prakash, S. and Agrawal, R.D., (2006J), "Hot Corrosion and Performance of Nickel-Based Coatings," *current sci.*, Vol. 90, No. 1, pp.41-47.
310. **Sidky**, P.S. and Hocking, M.G., (1987), "The Hot Corrosion of Ni-Based Ternary Alloys and Superalloys for Application in Gas Turbines Employing Residual Fuels," *Corros. Sci.*, Vol. 27, No. 5, pp. 499-530.
311. **Sidky**, P.S., Hocking, M.G., (1999), "Review of Inorganic Coatings and Coating Processes For Reducing Wear and Corrosion," *Brit. Corros. J.*, Vol. 34, No. 3, pp. 171-183.
312. **Simons**, E.L. Browning, G.V. and Liebhatzky, H.A., (1955), *Corrosion*, Vol.11, pp.505.

313. **Singh, H.**, (2005), "Hot Corrosion Studies of Plasma Sprayed Coatings Over Some Ni- and Fe-Based Superalloys," Ph.D. Thesis, Met. & Mat. Eng. Dept., Indian Institute of Technology Roorkee, Roorkee (2005).
314. **Singh, H.**, Prakash, S. and Puri, D. (2006), "Some observations on the high temperature oxidation behaviour of plasma sprayed Ni<sub>3</sub>Al coatings," Mater. Sci. Engg. A, Vol. 444, pp.242-250.
315. **Singh, H.**, Puri, D. and Prakash, S., (2005C), "Some Studies on Hot Corrosion Performance of Plasma Sprayed Coatings on a Fe-Based Superalloy," Surf. Coat. Technol., Vol. 192, No. 1, pp. 27-38.
316. **Singh, H.**, Puri, D. and Prakash, S., (2005D), "Corrosion Behaviour of Plasma Sprayed Coating on Ni-Based Superalloys in Na<sub>2</sub>SO<sub>4</sub>-60%V<sub>2</sub>O<sub>5</sub> Environment at 900°C," ISIJ Int., Vol. 45, No.6, pp. 886-895.
317. **Sinha, O. P.**, Chatterjee. M., Sarma, V. V.R. S. and Jha, S. N., (2005), "Effect of residual elements on high performance nickel base superalloys for gas turbines and strategies for manufacture," Bull. Mater. Sci., Vol. 28(4), pp.379–382.
318. **Smeggil, J. G.** and Bornstein, N. S., (1983), "Study of Interdiffusion Effects on Oxidation/Corrosion Resistant Coatings for Advanced Single Crystal Superalloys," Proc. sympos. High-Temperature Protective Coatings, March 7-8, Atlanta, GA, USA, Ed. Singhal, S.C., Pub. Metall. Soc of AIME, Warrendale, PA, USA, pp. 61-74.
319. **Smialek, J.L** and Meier, G.M. (1987), "High Temperature Oxidation" Superalloys II, Eds Sims, C.T., Stoloff, N.S., and Hagel, W.C., John Wiley & Sons, Inc. pp. 291-326.
320. **Smith, C.D.**, Patel, S.J., Farr, N.C. and Hoffmann, M., (1999), "The Corrosion Resistance of Nickel Containing Alloys In Coal Fired Boiler Environments [A]," Corrosion 99[C] NACE International, Houston, pp.12.
321. **Sobolev, V.V.**, Guilemany, J.M. and Nutting, J., (2004), "HVOF spraying," B0655, Maney, IOM3, pp.5.
322. **Sophie Roure**, Frank Czerwinski, and Anthony Petric, (1994), "Influence of CeO<sub>2</sub>-Coating on the High-Temperature Oxidation of Chromium," Oxid. Met., Vol.42, pp.75-102.
323. **Souza V.A.D.** and Neville A, (2007), "Aspects of Microstructure on the Synergy and Overall Material Loss of Thermal Spray Coatings in Erosion–Corrosion Environments," Wear, Vol. 263, pp. 339–346.

324. **Srivastava, S.C., Godiwalla, K.M. and Banerjee, M.K., (1997), "Fuel ash Corrosion of Boiler and Superheater Tubes," Jour. Mater. Sci., Vol. 32, pp. 835-849.**
325. **Staia, M. H., Valente, T, Bartuli, C, Lewis, D.B, Constable, C.P, Roman, A., Lesage, J, Chicot, D, and Mesmacque, G., (2001B), "Part II: Tribological Performance of Cr<sub>3</sub>C<sub>2</sub>-25% NiCr Reactive Plasma Sprayed Coatings Deposited at Different Pressures," Surf. Coat. Technol., Vol.146-147, pp. 563-570.**
326. **Staia, M.H., Valente, T, Bartuli, C, Lewis, D.B, Constable, C.P., (2001A), Part I: Characterisation of Cr<sub>3</sub>C<sub>2</sub>-25% NiCr Reactive Plasma Sprayed Coatings Produced at Different Pressures, Surf. Coat. Technol., Vol.146-147, pp. 553-562.**
327. **Stokes, J. and Looney, L., (2001), "HVOF System Definition to Maximise the Thickness of Formed Components," Surf. Coat. Technol., Vol. 148, pp.18-24.**
328. **Stott, F. H. and Hiramatsu, N., (2000), "Breakdown of Protective Scales During the Oxidation of thin Foils of Fe-20Cr-5Al Alloys at High Temperature", Mater. High Temp., Vol. 17, No. 1, pp. 93-99.**
329. **Stott, F. H. Chong, F. M. and Stifling, C. A. in M. F. Rothman (ed.), (1985), "High Temperature Corrosion in Energy Systems," AIME, Warrendale, PA, p. 253.**
330. **Stott, F. H., (1987), "The Protective action of Oxide Scales in Gaseous Environments at High Temperature" Rep. Prog. Phys., Vol.50, pp.861-913.**
331. **Stott, F. H., (1992), "Developments in Understanding the Mechanisms of Growth of Protective Scales on High-Temperature Alloys," Mater. Charact., Vol. 28, No. 3, pp. 311-325.**
332. **Stott, F. H., Wet, D. J. De and Taylor, R., (1994), "The Degradation Resistance of Thermal Barrier Coatings to Molten Deposits at Very High Temperatures," Trans. Mater. Res. Soc. Jpn., Vol. 14A, pp. 135-40.**
333. **Stott, F.H., (1988), "Principles of Growth and Adhesion of Oxide Scales, in the Role of Active Elements in the Oxidation Behaviour of High Temperature Metals and Alloys, E. Lang, Editor. Elsevier Applied Science: London.**
334. **Stringer, J., (1972), "The Functional Form of Rate Curves for the High-Temperature Oxidation of Dispersion-Containing Alloys Forming Cr<sub>2</sub>O<sub>3</sub> Scales," Oxid. Met., Vol.5 (1), pp.49-58.**

335. **Stringer, J.**, (1977), "Hot Corrosion of High Temperature Alloys," *Ann. Rev. Mater. Sci.*, Vol. 7, pp. 477-509.
336. **Stringer, J.**, (1987), "High Temperature Corrosion of Superalloys," *Mater. Sci. Technol.*, Vol. 3, No. 7, pp. 482-493.
337. **Stringer, J.**, (1998), "Coatings in the Electricity Supply industry: Past, Present, and Opportunities for the Future," *Surf. Coat. Technol.* Vol.108–109, pp.1–9.
338. **Stroosnijder, M. F.**, **Mevrel, R.** and **Bennet, M. J.**, (1994), "The Interaction of Surface Engineering and High Temperature Corrosion Protection," *Mater. High Temp.*, Vol. 12, No. 1, pp. 53-66.
339. **Suito, H.** and **Gaskell, D. R.**, (1971), "The Thermodynamics of Melts in the System  $\text{VO}_2\text{-V}_2\text{O}_5$ ," *Metall. Trans.*, Vol. 2, pp. 3299-3303.
340. **Sundararajan T.**, **Kuroda S.** and **Abe F.**, (2005B), "Steam Oxidation of 80Ni-20Cr High-Velocity Oxyfuel Coatings on 9Cr-1Mo Steel: Diffusion-Induced Phase Transformations in the Substrate Adjacent to the Coating," *Meta. Mate. Trans. A*, Vol.36A, pp. 2165- 2174.
341. **Sundararajan, T.**, **Kuroda, S.**, **Itagaki, T.** and **Abe F.**, (2003A), "Steam Oxidation Resistance of Ni-Cr Thermal Spray Coatings on 9Cr-1Mo Steel. Part 1: 80Ni-20Cr," *ISIJ Int.*, Vol. 43, No.1, pp. 95-103.
342. **Sundararajan, T.**, **Kuroda, S.** and **Abe, F.**, (2005A), "Steam Oxidation Resistance of Two-Layered Ni-Cr and Al APS Coating for USC Boiler Applications," *Corros. Sci.*, Vol. 47, No. 5, pp. 1129-1147.
343. **Sundararajan, T.**, **Kuroda, S.**, **Itagaki, T.** and **Abe F.**, (2003B), "Steam Oxidation Resistance of Ni-Cr Thermal Spray Coatings on 9Cr-1Mo Steel. Part 2: 50Ni-50Cr," *ISIJ Int.*, Vol. 43, No.1, pp. 104-111.
344. **Sundararajan, T.**, **Kuroda, S.**, **Nishida, K.**, **Itagaki, T.** and **Abe, F.**, (2004), "Behaviour of Mn and Si in the Spray Powders During Steam Oxidation of Ni-Cr Thermal Spray Coatings," *ISIJ Int.*, Vol. 44, No.1, pp. 139-144.
345. **Swaminathan, J.** and **Raghavan, S.**, (1992), "Effect of Vanadic Corrosion on Creep-Rupture Properties of Superni-600 at 650-750<sup>o</sup>C," *Mater. High Temp.*, Vol. 10, No. 4, pp. 242-250.
346. **Swaminathan, J.** and **Raghavan, S.**, (1994), "Vanadic Hot Corrosion-Creep Interaction of Superni-C 276 in the Temperature Range 650-750<sup>o</sup>C," *High Temp. Mater. Processes*, Vol. 13, No. 4, pp. 277-297.



347. **Swaminathan, J.**, Raghavan, S. and Iyer, S. R., (1993), "Studies on the Hot Corrosion of Some Nickel-Base Superalloys by Vanadium Pentoxide," *T. Indian I. Metals*, Vol. 46, No. 3, pp. 175-181.
348. **Takeuchi, J.**, (1998), "An Improvement of  $\text{Cr}_3\text{C}_2$ -NiCr Sprayed Coatings Followed by Chromium Diffusion Treatment," in *Thermal Spray: Meeting the Challenges of the 21<sup>st</sup> Century.*, Nice, France: ASM International, Materials Park, OH-USA, pp.1425-1430.
349. **Takeuchi, J.**, Nakahira, A. and Barbezat, G., (1993), " $\text{Cr}_3\text{C}_2$ -NiCr Cermet Coatings Using Some HVOF, APS and VPS Process," in *TS93: Thermal Spraying Conference (Thermischespritzkonferenz)* Deutscher Verlag für Schweißtechnik DVS-Verlag GmbH,
350. **Tao Z**, Xun C, Shunxing W, Shian Z, (2000), "Effect of CeO on Microstructure and Corrosive Wear Behavior of Laser-Cladded Ni WC Coating," *Thin Solid Films*, Vol.379, pp.128-132.
351. **Tatlock, G. J.**, Hurd, T. J. and Punni, J. S., (1987), "High Temperature Degradation of Nickel Based Alloys a Consideration of the Role of platinum," *Platinum Metals Rev.*, Vol.31, No.1, pp.26-31.
352. **Tawancy, H. M.** and Sridhar, N, (1992), "High-Temperature Oxidation Behavior of Ni-Cr-Al-Fe-Y Alloy," *Oxid. Met.*, Vol. 37(3/4), pp.143-166.
353. **Taylor, M.P.** and Evans, H. E., (2001), "The Influence of Bond Coat Surface Roughness and Structure on the Oxidation of a Thermal Barrier Coating System," *Mater. Sci. Forum*, Vol. 369-372, pp.711-717.
354. **Taylor, T.**, (1975), "Phase Stability of Chrome-Carbide NiCr Coatings in Low Oxygen Environments," *J. Vacu. Sci. Technol.*, Vol.12, No. 4, pp. 790-794.
355. **Thilkan, H.R.**, Lahiri, A.K. and Banerjee, T., (1967), "Studies on the residue of alloy steels against oil ash corrosion-part I," *NML technical Journal*, May, pp.20-25.
356. **Tian, Y.S.**, Chen, C.Z., Chen, L.X. and Huo, Q.H., (2006), "Effect of RE oxides on the Microstructure of the Coatings Fabricated on Titanium Alloys by Laser Alloying Technique," *Scripta Materialia*, Vol.54, pp.847-852.
357. **Tiwari, S. N.** and Prakash, S., (1996), "Hot Corrosion Behaviour of an Iron-Base Superalloy in Salt Environment at Elevated Temperatures," *Proc. of Sympos. Metals and Materials Research*, Indian Institute of Technology Madras, Madras, 4-5<sup>th</sup> July, pp. 107-117.

358. **Tiwari, S. N. and Prakash, S.**, (1997), "Studies on the Hot Corrosion Behaviour of Some Superalloys in  $\text{Na}_2\text{SO}_4\text{-V}_2\text{O}_5$ ," Proc. of SOLCEC, Kalpakkam, India, 22-24<sup>th</sup> Jan., Paper C33.
359. **Tiwari, S. N. and Prakash, S.**, (1998), "Literature Review-Magnesium Oxide as Inhibitor of Hot Oil Ash Corrosion," Mater. Sci. Technol., Vol. 14, pp. 467-172.
360. **Tiwari, S. N.**, (1997), "Investigations on Hot Corrosion of Some Fe-, Ni- and Co-Base Superalloy in  $\text{Na}_2\text{SO}_4\text{-V}_2\text{O}_5$  Environment under Cyclic Conditions," Ph. D. Thesis, Met. Mat. Engg. Deptt., University of Roorkee, Roorkee, India.
361. **Toma, D., Brandl, W. and Koester, U.**, (1999), "Studies on the Transient Stage of Oxidation of VP Sand HVOF Sprayed MCrAlY Coatings," Surf. Coat. Technol., Vol.120-121, pp.8-15.
362. **Trafford, D. N. H. and Whittle, D. P.**, (1980A), "The Salt Induced Corrosion Behaviour of Fe-Cr Alloys at Elevated Temperatures-I. Alloys Dilute in Chromium," Corros. Sci., Vol. 20, pp. 497-507.
363. **Trafford, D. N. H. and Whittle, D. P.**, (1980B), "The Salt Induced Corrosion Behaviour of Fe-Cr Alloys at Elevated Temperatures-II. Alloys Rich in Chromium," Corros. Sci., Vol. 20, pp. 509-530.
364. **Tsaur, C.C., James C. R. and Chang, Y.Y.**, (2005), "The effect of NaCl deposit and thermal cycle on an aluminide layer coated on 310 stainless steel," Mater. Chem. Phys., Vol. 91, pp. 330 –337.
365. **Tucker, Jr., R. C.**, (1994), "Ch. 11: Advanced Thermal Spray Deposition Techniques," in 'Handbook of Deposition Technologies for Films & Coatings,' Eds. R.F. Bunshah, Noyes Pub. Park Ridge, New Jersey, U. S. A./William Andrew Publishing, LLC, Norwich, New York, U.S.A, pp. 591.
366. **Tucker, R.C.**, (1974), "Structure Property Relationships in Deposits Produced by Plasma Spray and Detonation Gun Technique," J. Vacu. Sci. Technol., Vol. 11, No.4, pp. 725–734.
367. **Tzvetkoff, T. and Gencheva, P.**, (2003), "Mechanism of Formation of Corrosion Layers on Nickel and Nickel-based Alloys in Melts Containing Ox anions-A Review," Mater. Chem. Phys., Vol. 82, No. 3, pp. 897-904.
368. **Ul-Hamid, A.**, (2002), "A Microstructural Study of Preferential Oxidation at the Grain Boundaries of Ni-Cr Alloys," Oxid. Met., Vol. 57, No. 3-4, pp. 217-230.

369. **Ul-Hamid, A.**, (2003), "Diverse Scaling Behavior of the Ni-20Cr Alloy," *Maters. Chem. Phys.*, Vol. 80, pp. 135-142.
370. **Ul-Hamid, A.**, (2004), "A TEM Study of the Oxide Scale Development in Ni-Cr-Al Alloys," *Corros. Sci.*, Vol. 46, No. 1, pp. 27-36.
371. **Uusitalo, M.A.** Vuoristo, P.M. J. and Mantyla, T.A., (2002B), "High Temperature Corrosion of Coatings and Boiler Steels in Reducing chlorine-Containing Atmosphere," *Surf. Coat. Technol.* 161(2002), p. 275-285.
372. **Uusitalo, M.A.**, Vuoristo P.M.J. and Mantyla T.A., (2002A)," Elevated Temperature Erosion-Corrosion of Thermal Sprayed Coatings in Chlorine Containing Environments," *Wear*, Vol. 252, pp.586-594.
373. **Uusitalo, M.A.**, Vuoristo, P.M.J. and Mantyla, T.A., (2003), "High Temperature Corrosion of Coatings and Boiler Steels in Oxidizing Chlorine-containing Atmosphere," *Mater. Sci. Eng. A-Struct.*, Vol. 346, No. 1-2, pp. 168-177.
374. **Uusitalo, M.A.**, Vuoristo, P.M.J. and Mantyla, T.A., (2004), "High Temperature Corrosion of Coatings and Boiler Steels below Chlorine-containing Salt Deposits," *Corros. Sci.*, Vol. 46, No. 6, pp. 1311-1331.
375. **Valdes, C.J.**, Dooley, R.B. and Wilson, J.R., (1973), "The Corrosion of A.I.S.I 446 Stainless Steel in Molten Vanadates in the Temperature Range 700-900<sup>0</sup>C," Report Defense Research Board Canada, Grant No. 7535-14.
376. **Venkataraman R.**, Ravikumar B., Krishnamurthy R. and Das D.K., (2006), "A study on Phase Stability Observed in as Sprayed Alumina-13 wt.% Titania Coatings Grown by Detonation gun and Plasma Spraying on Low Alloy Steel Substrates ,"*Surf. Coat. Technol.* Vol. 201, pp. 3087-3095.
377. **Vuoristo, P.**, Niemi, K., Makela, A. and Mantyla, T., (1994), Proceedings of the 7<sup>th</sup> National Thermal Spray Conference, 20-24 June 1994. Boston, Massachusetts, pp. 21.
378. **Wagner, N.**, Gnadie K., Kreye, H. and Kronewetter, H., (1984), "Particle Velocity in Hypersonic Flame Spraying of WC-Co," *Surf. Coat. Technol.*, Vol. 22, pp. 61-71.
379. **Wang B.** and Lee S.W., (2000), "Erosion-Corrosion Behaviour of HVOF NiAl-Al<sub>2</sub>O<sub>3</sub> Intermetallic-Ceramic Coating," *Wear*, Vol.239, pp. 83-90.
380. **Wang B.**, (1996), "Erosion-Corrosion of Thermal Sprayed Coatings in FBC Boilers," *Wear*, Vol. 199, pp. 24-32.

381. **Wang B.Q.** and Lee S.W., (1997), "Elevated Temperature Erosion of Several Thermal-Sprayed Coatings Under the Simulated Erosion Conditions of in-Bed Tubes in a Fluidized Bed Combustor," *Wear*, Vol. 203–204, pp. 580–587.
382. **Wang B.Q.** and Shui Z.R., (2002), "The Hot Erosion Behavior of HVOF Chromium Carbide-Metal Cermet Coatings Sprayed With Different Powders," *Wear*, Vol. 253, pp. 550–557.
383. **Wang Y.**, (1993), "Friction and Wear Performances Sprayed Ceramic and Cermet Hard Coatings Under Dry Friction of Detonation-Gun- and Plasma-Sprayed Ceramic and Cermet Hard Coatings Under Dry Friction," *Wear*, Vol.161, pp. 69-78.
384. **Wang, B.**, Gong, J., Sun, C., Huang, R.F. and Wen, L.S., (2003B), "The Behavior of MCrAlY Coatings on Ni<sub>3</sub>Al-base Superalloy," *Mater. Sci. Eng. A-Struct.*, Vol. 357, No. 1-2, pp. 39-44.
385. **Wang, B.**, Gong, J., Wang, A. Y., Sun, C., Huang, R. F. and Wen, L. S., (2002), "Oxidation Behavior of NiCrAlY Coatings on Ni-Based Superalloy," *Surf. Coat. Technol.*, Vol. 149, No. 1, pp. 70-75.
386. **Wang, C.J.** and Pan J.Y., (2003), "Corrosion of Carbon Steel With NaCl Coating in an Atmosphere Produced by Burning Emulsified Diesel Oil," *Mater. Chem. Phys.* Vol. 82, pp. 965–973.
387. **Wang, F.**, (1997), "The Effect of Nano Crystallization on the Selective Oxidation and Adhesion of Al<sub>2</sub>O<sub>3</sub> Scales," *Oxid. Met.*, Vol. 48, Nos. 3/4, pp.215-214.
388. **Wang, F.**, Tian, X., Li, Q., Li, L. and Peng, X., (2007), "Oxidation and Hot Corrosion Behavior of Sputtered Nanocrystalline Coating of Superalloy K52," *Thin. Solid Films*, Vol.516, No.16, pp.5740-5747.
389. **Wang, J.**, Zhang, L., Baode Sun and Yaohe Zhou., (2000), "Study of the Cr<sub>3</sub>C<sub>2</sub>-NiCr Detonation Spray Coating," *Surf. Coat. Technol.*, Vol.130, pp.69-73.
390. **Wang, Q.M.**, Wu, Y.N., Ke, P.L. Cao, H.T., Gong, J., Sun, C. and Wen, L.S., (2004), "Hot Corrosion Behavior of AlP NiCoCrAlY(SiB) Coatings on Nickel Base Superalloys," *Surf. Coat. Technol.*, Vol. 86, pp. 389–397.
391. **Wang, X.**, Heberlein, J., Pfender, E. and Gerberich, W., (1999), "Effect of Nozzle Configuration, Gas Pressure, and Gas Type on Coating Properties in Wire Arc Spray," *J. Therm. Spray Technol.*, Vol.8 No. 4, pp.565-575.

392. **Wang, Y.** and Yan, M., (2006), "The effect of CeO<sub>2</sub> on the Erosion and Abrasive Wear of Thermal Sprayed FeAl Intermetallic Alloy Coatings," *Wear*, Vol.261, pp.1201–1207.
393. **Wang, Y.**, Chen,W. and Wang, L., (2003A), "Micro-Indentation and Erosion Properties of Thermal Sprayed NiAl Intermetallic-Based Alloy Coatings," *Wear*, Vol.254, pp.350–355.
394. **Wang, Y.**, Mukherji, D., Chen, W., Kuttner, T. Wahi R.P.and Wever, H., (1995), "The Cyclic Creep Behavior of Nickel-Base Superalloy IN738LC," *Z. Metalkd.*, Vol.86(5), pp.365-370.
395. **Wang, Y.**, Radovan Kovacevic, R. and Liu. J., (1998), "Mechanism of Surface Modification of CeO in Laser Remelted Alloy Spray Coatings," *Wear*, Vol.221, pp.47–53.
396. **Weulersse-Mouterat, K.**, Moulin, G., Billard, P. and Pierotti, G., (2004), "High Temperature corrosion of superheater tubes in wast incinerators and coal-fired plants," *Mater. Sci. Forum*, Vol. 461-464, pp. 973-980.
397. **Whittle, D.P.**, (1983), "Oxidation Mechanisms for alloys in Single Oxidant Gases," *High Temp. Corro. Ed. Rapp.R.A.*, Houston: NACE, pp 171-183.
398. **Wirojanupatump, S.**, Shipway P.H. and McCartney D.G., (2001), "The Influence of HVOF Powder Feedstock Characteristics on the Abrasive Wear Behaviour of Cr<sub>x</sub>C<sub>y</sub>-NiCr coatings," *Wear*, Vol. 249, pp.829–837.
399. **Wright, I.G.**, (1987), "High-Temperature Corrosion," in 'Metals Handbook,' Vol. 13, 9<sup>th</sup> Ed., Metals Park, ASM, pp. 97-103.
400. **Wu, X.**, Weng, D., Chen, Z. and Xu, L., (2002), "Effects of Plasma-Sprayed NiCrAl/ZrO<sub>2</sub> Inter-mediate on the Combination Ability of Coatings," *Surf. Coat. Technol.*, Vol.140, pp.231– 237.
401. **Wu, Y.N.** Zhang, G. Feng, Z.C. Zhang, B.C. Liang, Y. and Liu, F.J., (2001), "Oxidation Behavior of Laser Remelted Plasma Sprayed NiCrAlY and NiCrAlY-Al<sub>2</sub>O<sub>3</sub> coatings," *Surf. Coat. Technol.*, Vol. 138, pp.56– 60.
402. **Wu, Y.N.**, Wang, F.H., Hua, W.G., Gong, J., Sun, C.and Wen, L.S., (2003), "Oxidation Behavior of Thermal Barrier Coatings Obtained by Detonation Spraying," *Surf. Coat. Technol.*, Vol.166, pp. 189–194.
403. **Yamada, K.**, Tomono, Y., Morimoto, J., Sasaki, Y. and Ohmori, A., (2002), "Hot Corrosion Behavior of Boiler Tube Materials in Refuse Incineration Environment," *Vacuum*, Vol. 65, No. 3-4, pp. 533-540.

404. **Yedong, H.** and Stott F. H., (1994), "The Selective Oxidation of Ni-15%Cr and Ni-10%Cr Alloys Promoted by Surface-Applied Thin Oxide Films," *Corros. Sci.*, Vol. 36, No. 11, pp. 1869-1884.
405. **Yoshiba, M.**, (1993), "Effect of Hot Corrosion on the Mechanical Performances of Superalloys and Coating Systems," *Corros. Sci.*, Vol. 35, No. 5-8, pp. 1115-1124.
406. **Zhang, J.S.**, Hu, Z.Q., Murata, Y., Morinaga, M. and Yukawa, N., (1993B) "Design and Development of Hot Corrosion-Resistant Nickel-Base Single-Crystal Superalloys by the d-  
Electrons Alloy Design Theory: Part I. Characterization of the Phase Stability", *Metallurgical Transactions A*, Vol. 24A, pp.2443-2450.
407. **Zhang, J.S.**, Hu, Z.Q., Murata, Y., Morinaga, M. and Yukawa, N., (1993), "Design and Development of Hot Corrosion-Resistant Nickel-Base Single Crystal Superalloys by the d-  
Electron Alloy Design Theory; II: Effects of Refractory Metals Ti, Ta, and Nb on Microstructures and Properties," *Metall. Trans. A*, Vol. 24, No. 11, pp. 2451-2464.
408. **Zhang, T** and Li, D.Y., (2000A), "Effects of Cerium on Dry Sand Erosion and Corrosive Erosion of Aluminide Coating on 1030 Steel," *J. mate. Sci. letters*, Vol. 19, pp. 429- 432.
409. **Zhang, T** and Li, D.Y., (2000B), "Effects of Yttrium on Corrosive Erosion and Dry Sand Erosion of FeAlCr (Y) Diffusion Coatings On 1030 Steel," *J. Mater. Sci. Eng. A*, Vol.277, pp.18-24.
410. **Zhang, Y.J.**, Sun, X.F., Heng-Rong Guan, Zhuang-Qi Hu, (2002), "1050°C Isothermal Oxidation Behavior of D-gun Sprayed NiCrAlY Coating," *Surf. Coat. Technol.*, Vol.161, pp. 302-305.
411. **Zhang, Y.J.**, Sun, X.F., Zhang, Y.C., Jin, T., Deng, C.G., Guan, H.R. and Hua, Z.Q., (2003), "A Comparative Study of DS NiCrAlY Coating and LPPS NiCrAlY Coating," *Mater. Sci. Eng A*, Vol. 360, pp.65-69.
412. **Zhang, Y.S.** and Rapp, R.A., (1987), "Solubilities of CeO<sub>2</sub>, HfO<sub>2</sub> and Y<sub>2</sub>O<sub>3</sub> in Fused Na<sub>2</sub>SO<sub>4</sub>-30 mol% NaVO<sub>3</sub> and CeO<sub>2</sub> in Pure Na<sub>2</sub>SO<sub>4</sub> at 900 °C," *Corros.*, Vol. 43, No. 6, pp. 348-352.
413. **Zhang, Y.S.** and Rapp, R.A., (1994), "Solubilities of CeO<sub>2</sub>, in Molten Na<sub>2</sub>SO<sub>4</sub>-10 mol% NaVO<sub>3</sub> Salt Solution 900 °C, Corros" proceeding of the ninth international symposium on molten salts, electrochem. Soc., May 1994.

414. **Zhao, L.**, Maria Parco and Erich Lugscheider, (2004B) "High Velocity Oxy-Fuel Thermal Spraying of a NiCoCrAlY alloy," *Surf. Coat. Technol.*, Vol.179. pp. 272–278.
415. **Zhao, S.**, Dong, J., Zhang, M. and Xie, X., (2005A), "Oxidation Behaviour of New Ni-Based Superalloy at 950<sup>0</sup>C and 1000<sup>0</sup>C," *Rare Metal Mater. Eng.*, Vol. 34, No. 2, pp. 208-211.
416. **Zhao, S.**, Xie, X., Smith, G. D. and Patel, S.J., (2005B), "The Corrosion of INCONEL alloy 740 in Simulated Environments for Pulverized Coal-Fired Boiler," *Mater.Chem.Phy.* Vol.90, pp. 275–281.
417. **Zhao, W.M.**, Wang, Y., Han, T., Dong, L.X., Wu, K.-Y. and Xue, J., (2005C), "Corrosion Mechanism of NiCrBSi Coatings Deposited by HVOF," *Surf. Coat. Technol.* Vol.190, pp.293-298.
418. **Zhao, W.M.**, Wang, Y., Han, T., Wu, K.-Y. and Xue, J., (2004A), "Electrochemical Evaluation of Corrosion Resistance of NiCrBSi Coatings Deposited by HVOF," *Surf. Coat. Technol.*, Vol.183, pp.118.-125.
419. **Zheng, D.**, Zhu, S. and Wang, F., (2006) "Oxidation and Hot Corrosion Behavior of a Novel Enamel-Al<sub>2</sub>O<sub>3</sub> Composite Coating on K38G Superalloy," *Surf. Coat. Technol.*, Vol.200, pp.5931–5936.
420. **Zhenyu Z.**, Zhiping Wang, Bunv Liangb, Peiqing La, (2006), "Effects of CeO<sub>2</sub> on Friction and Wear Characteristics of Fe –Ni –Cr Alloy Coatings," *Tribo. Inter.*, Vol.39, pp. 971-978.
421. **Zho, Y.**, Zhu, R. and Guo, M., (1987), "Hot Corrosion of Some Nickel-Base Superalloys Containing Niobium," *Corros. NACE*, Vol. 43, No. 1, pp.51-55.
422. **Zimmermann, S.** and Kreye, H., In: Berndt, C.C., (Ed.), (1996), Chromium Carbide Coatings Produced with various HVOF Spray Systems, *Thermal Spray: Practical Solution for Engineering Problems*, Proceedings of the 9<sup>th</sup> National Thermal Spray Conference, ASM International, Materials Park, Ohio, USA, pp. 147.